The effects of ultrasonic waves application during extrusionon the processing parameters and the properties of polyethylene

A thesis submitted for the degree of

Doctor of Philosophy

By

Amir Khamsehnezhad

Wolfson Centre for Materials Processing,

Brunel University,

Uxbridge, UK.

June, 2014

Abstract

The application of polymers in daily life has increased recently, where extensive energy costs are always an issue to consider during the manufacturing. Competitive markets in plastic industry require regular research and development of the materials and the manufacturing process. This thesis addresses the application of the ultrasonic vibrations in the polymer extrusion with the aim of reducing power consumption of the extrusion process. The effective penetration depth of the ultrasonic vibrations in the polymer melt was determined and used in the design of the ultrasonic horn and the housing block.

Two different grades of polyethylene was extruded using a 25mm extruder to investigate the effects of ultrasonic vibrations on the polymer melt during the extrusion of polyethylene strips at 5 different screw speeds. The extruder barrel pressure, die entrance pressure decreased when processing with ultrasonic vibrations and when compared to conventional extrusion. The extruded products' properties were systematically investigated using tensile, DMA and DSC tests. The results indicated that the power consumption of the extrusion process reduced by the application of ultrasonic vibrations without any adverse effect on the extruded products' properties.

A 50mm extruder with second generation ultrasonic horn was used to study the effects of ultrasonic vibrations on the processing parameters and properties of the strips and pipes. The extrusion trials were carried out using two grades of polyethylene for production of the strips and four different grades of polyethylene for production of pipes. Processing with ultrasonic vibrations showed lower barrel and die entrance pressure when compared to the conventional extrusion. The consumed power for extrusion of the strips and pipes was reduced by application of ultrasound in comparison with conventional extrusion. The mechanical, thermal and rheological properties of the strips and pipes did not change by the application of ultrasonic vibrations.

The third generation ultrasonic horn was designed to allow ultrasonic assisted extrusion of pipes using a 90mm industrial extruder. The trials were not successful as a result of ultrasonic horn and generator failure due to change in the horn design characteristics at processing temperatures. New key factors involved in sonotrode design were identifies and

raised and based on these factors, the suggestions to improve the performance of the horn was made.

As a result of this work, various theories are discussed to explain the effects of ultrasonics on the melt. The lack of change in mechanical, thermal and rheological properties indicated that any modification of the polyethylene structure by this research could be dismissed. Thus, the most possible explanation for the observed effect on the process is that high frequency vibrations could increase temperature locally or reduce friction between polymer melt and the ultrasonic horn. It leads again to the key conclusion that with the correct horn design, total power consumption can be reduced without negatively affecting the polymer and product properties.

Acknowledgments

I am deeply grateful to the following people who all assisted me on completing this work.

I am dedicating this work to my loving parents and brother whom throughout many years gave me the support and encouragement to achieve my goals and ambitions of which this thesis is a part of.

I would also like to thank my supportive partner for all her help, support and encouragement during completion of this work.

Table of Contents

List of Figures

Chapter 1

Chapter 2

Chapter 3

Chapter 4

Chapter 5

List of Tables

Chapter 2

Chapter 3

Chapter 4

List of Abbreviations

MWD…………………………………..…………………….Molecular weight distribution

Mw…………………………………...………………………….………..…..Molecular weight

USEP………………………………………………………..Ultrasonic Extrusion process

CEP…………………………….……………...…………Conventional extrusion process

USV…………………………………………………………..………Ultrasound vibrations

US………………………………………………………………………...…Ultrasonics

DSC……………………………………………………...Differential Scanning Calorimetry

DMA…………………………………………………...…Dynamic Mechanical Analysis

List of Publications

2010-'Raman Scattering from Industrially Processed Plastic Pipes'

A. Khamsehnezhad, A. Ahmadnia, J. Silver, R. Withnall, P. Allan and *K. Tarverdi*

Published in XXII INTERNATIONAL CONFERENCE ON RAMAN SPECTROSCOPY. AIP Conference Proceedings, Volume 1267, pp. 566-567 (2010)

2010-'The Effect of Ultrasonic Vibrations on Structure of Polyethylene Extrudates'

L. Anguilano, A. Khamsehnezhad, P. Allan, R. Withnall, J. Silver and K. Tarverdi

Poster submitted in Industry & Impact Conference, Experimental Techniques Centre, Brunel University.

2009-'Effect of Ultrasonic Vibrations on Processing of Polyethylene and Thermal and Mechanical Properties of Extrudate'

Amir Khamsehnezhad, R. Withnall, P. Allan, K. Tarverdi, J. Silver, A. Ahmadnia

Accepted as Extended Abstract and presented in ResCon'09 22-24 June, Brunel University, UK.

2009-'Mechanical Properties of High Density Polyethylene Compound for Pipes Extruded Under the Influence of Ultrasound'

Robert Withnall, A. Ahmadnia, A. Khamsehnezhad, J. Silver, P. Allan and K. Tarverdi

Accepted as Extended Abstract and has been presented in The Seventeenth Annual International Conference on COMPOSITES/NANO ENGINEERING

(ICCE – 17) 26 July - 1 August 2009 in Hawaii, USA.

2009-'Effect of Ultrasonic Vibrations on Processing of Polyethylene and Thermal and Mechanical Properties of Extrudate'

Amir Khamsehnezhad, R. Withnall, P. Allan, K. Tarverdi, J. Silver, A. Ahmadnia

Poster submitted and presented in ResCon'09 22-24 June, Brunel University, UK.

2009-'Mechanical Properties of High Density Polyethylene Compound for Pipes Extruded Under the Influence of Ultrasound'

Robert Withnall, A. Ahmadnia, A. Khamsehnezhad, J. Silver, P. Allan and K. Tarverdi

Accepted as Extended Abstract and published in World Journal of Engineering (WJOE).

Chapter 1

Introduction

1.1 Introduction to Polyethylene

1.1.1 Structure of Polyethylene

Polyethylene is possibly the thermoplastic with the widest range of applications because of its properties. The popularity and use of polyethylene to produce plastic pipes has increased because of its light weight, corrosion resistance and environmental friendly nature. Polyethylene is a thermoplastic material composed of carbon and hydrogen atoms bonded together forming high molecular weight polyethylene as shown in Figure 1-1. The flexibility of the C-C bonds in polyethylene leads to very low temperatures of glass transition (-130°C to -60°C) [1].
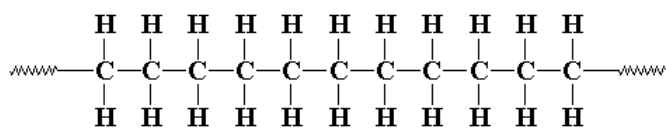
Figure 1-1: Polyethylene molecular chain.

The melting temperature of commercial semi-crystalline polymers is usually in the range of 108°C-145°C [2, 3], where the exact value of melting temperature depends on the molecular structure. In the structure of polyethylene around 50-60% of the material is arranged in a crystal structure while the rest of the material is bound together with Van der Waals forces. It is the structure of the crystal phase compared to the amorphous phase that gives linear polyethylene its characteristic properties.

Commercial polyethylenes vary in their molecular weight (MW), molecular weight distribution (MWD) and their structure (short/long branched or linear). Differences in molecular weight like branching will give rise to variations in properties. The higher the molecular weight, the greater will be the entanglements between polyethylene molecules. Therefore a difference in the MW will affect the properties related to large movements of polymer chains such as tensile strength/elongation and the melt viscosity. Furthermore changes in the chain structure such as short branching will affect the crystallinity of the system and the properties involved with small deformations in the solid form such as Young's modulus.

1.1.2 Mechanical properties of Polyethylene

The mechanical properties of polymers are dependent on the strain rate, temperature, molecular weight and the degree of chain branching. The effect of molecular weight and crystallinity on the tensile properties and stress strain behaviour of polyethylene is shown in Figure 1-2 [4]. It can be seen that by increasing the molecular weight the tensile strength and strain hardening of the samples increase and the yield point becomes more well defined compared to lower molecular weight samples [4]. The increase in the crystallinity has a significant effect on the yield strength while the elongation at break and the strain hardening rate does not seem to be affected significantly by increasing crystallinity.
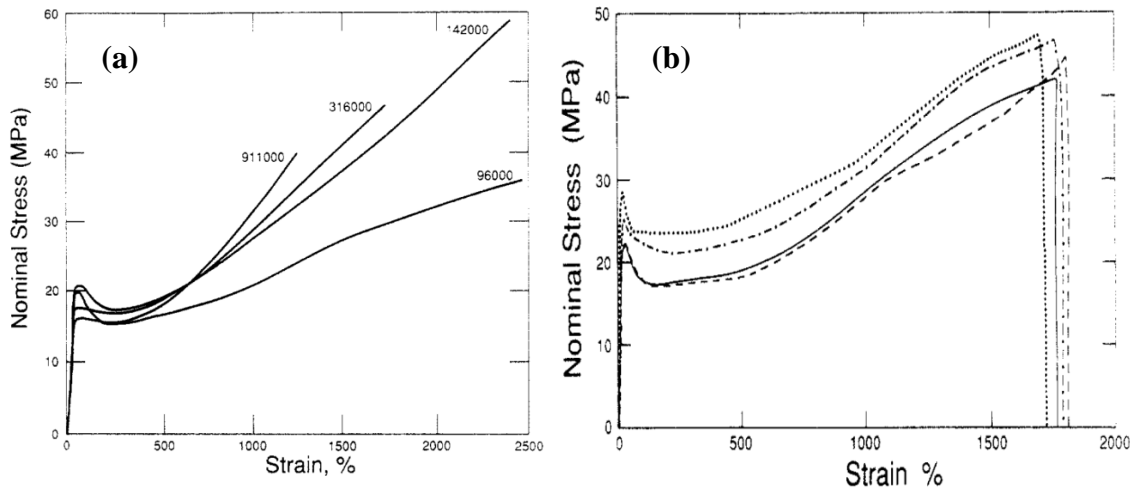
Figure 1-2: Stress-strain curves for linear polyethylene as a function of Mw (a) and different crystallinity levels (b) ($\cdots$) X_C=0.64; (-·-·) X_C=0.55; (—) X_C= 0.44; (-----)X_C=0.46 [4].

The general effects of changing the tensile testing rate and temperature on the stress strain behaviour are shown schematically in Figure 1-3. It can be seen that by increasing the strain rate or decreasing the test temperature the yield point becomes more noticeable.
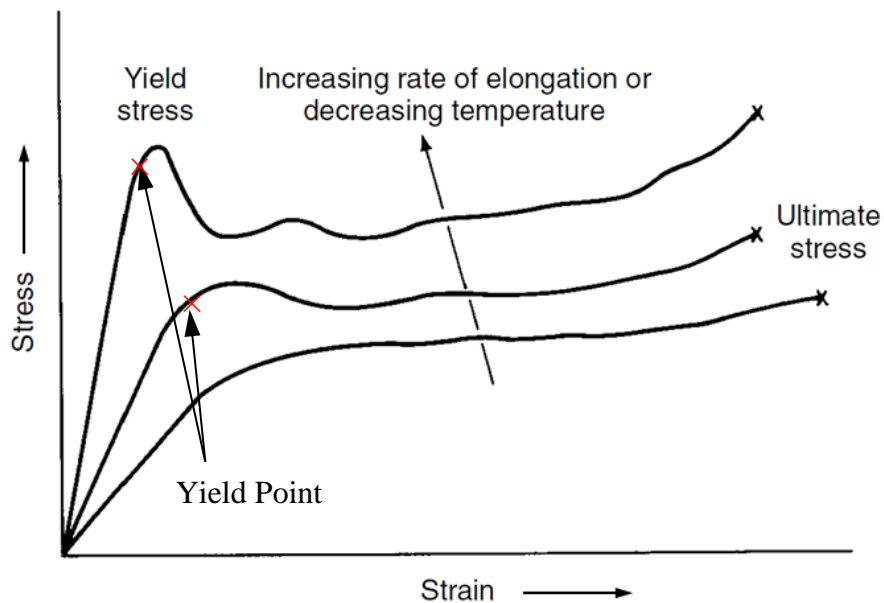
Figure 1-3: Effect of tensile strain rate and temperature on stress strain curves [5, 6].

Deformations up to the yield point are recoverable where the polymer shows almost Hookean behaviour (stress is a linear function of strain). Necking occurs at the yield point

and cold drawing of the sample begins after the yield point where strain hardening can be observed.

1.1.3 Thermal properties

Most of thermoplastic polymer properties such as mechanical, rheological and structural are dependent of test temperature. This could be explained by the fact that, increasing the temperature softens the thermoplastic polymer by allowing movements of chains. On the other hand cooling of the thermoplastic polymers reduces and restricts the movement of the chains. This change of properties by the variation of temperature urges a deeper investigation of the thermal properties of the polyethylene such as glass transition temperature, melting and crystallisation temperature.

Several factors can affect the glass transition temperatures in polymers and these are:

- Molecular weight: high molecular weight polyethylenes compared to low molecular weight polyethylenes have less 'chain ends' in a given volume. Chain ends are less restrained and increase mobility of the polymer leading to lower glass transition temperatures [7, 8].

- Bonding between chains: cross linking or bonding between chains decreases the mobility of the chain and therefore increases T_g [9, 10].

- Stiffness of the back bone: polymers with stiffer backbone (i.e. double bonds instead of single C-C bond) will have higher glass transition temperature as the energy to rotate will increase. Also attachment of side chains will increase the T_g, for instance polypropylene compared to polyethylene has a higher T_g as a result of side chains [11].

Melting temperature is one of the thermal properties that is related to the crystalline phase of the polymer. Melting temperature is the temperature that the crystallite melts and it can be affected by modifying the crystalline phase and structural properties of the polymer. The melting temperature depends on the molecular weight distribution and the degree of crystallinity [12]. It increases by increasing the molecular weight, the stiffness of the

backbone, side groups and presence of intermolecular forces. Reported values of melting temperature for polyethylenes are normally around 140°C [13].

Theoretically, polyethylene could be 100% crystalline as a result of its simple structure and the chain. However in reality this is almost impossible, as presence of random ethylene propylene copolymer results in rubbery material and a phase which leads to a decrease in the degree of crystallinity of the system and forming a semi-crystalline structure. This is also related to the thermodynamics of the system that forces the polymer chains to fold many times in the formation of the crystals. The fold surface has a lower level of crystallinity than the straight chain segments. Crystallisation temperature for polyethylene is normally between 115-132°C and 5-10°C lower than melting point [14].

1.2   Extrusion of Polymers

Extrusion is one of the most important processing methods for plastics. The two main reasons that make the extrusion process different from other processing methods are:

- Its wide range of applications such as blow moulding, profile extrusion, film extrusion and etc.
- The continuous and not cyclic (such as injection moulding, compression moulding and rotational moulding) nature of the extrusion process.

1.2.1 Basic principles of polymer extrusion

The extruder is the heart of the extrusion process, where the plastic which, normally in granular form, is fed through the hopper into the extruder barrel (Figure 1-4). The granules inside the barrel are conveyed forward by the screw while being heated by conduction and shear and then the melt is pumped up to the die. At the end of the extruder the molten polymer is pushed through the die to form into desired shape. In general the plastic extrusion processes consist of three phases:

- Production of well plasticated melt
  Polymer powder/granules conveyed through the extruder and heated to produce the polymer melt. The melt mixed and compacted toward the end of the extruder.

- Forming of the product

  Produced melt by the extruder is pushed through the die to form into the desired shape.

- Cooling of the product so it retains its shape

  The extrudate exiting the die in the shape of the product is still in molten state and it should be cooled to keep the shape.
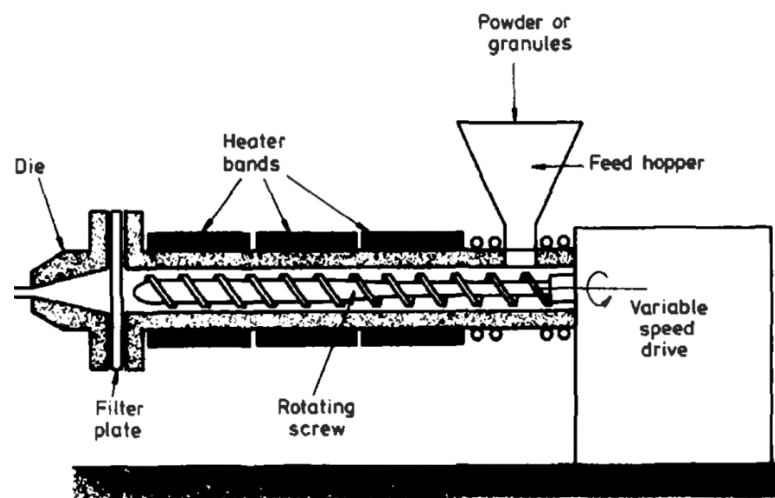
Figure 1-4: A typical single screw extruder[15].

A typical extruder screw consists of three zones which are shown in Figure 1-5. The first is the feed zone where the polymer granules are preheated and conveyed forward to the second zone, the screw depth in this section is constant.

The second zone is the transition or compression zone where the depth of the flight decreases gradually to push back any trapped air to the feed zone and compact the material delivered from feed zone. The melting of the granules by conduction and shear heating occurs in this section. The shear heating is the main process used to melt and homogenise the polymer where the conductive heating is only used to start the process off.

The third zone is the metering zone. It is characterized by its constant flight depth which is comparatively lower than that of the screw in the feed section. In this zone the molten polymer is homogenized in terms of the temperature and consistency and delivered into the die.
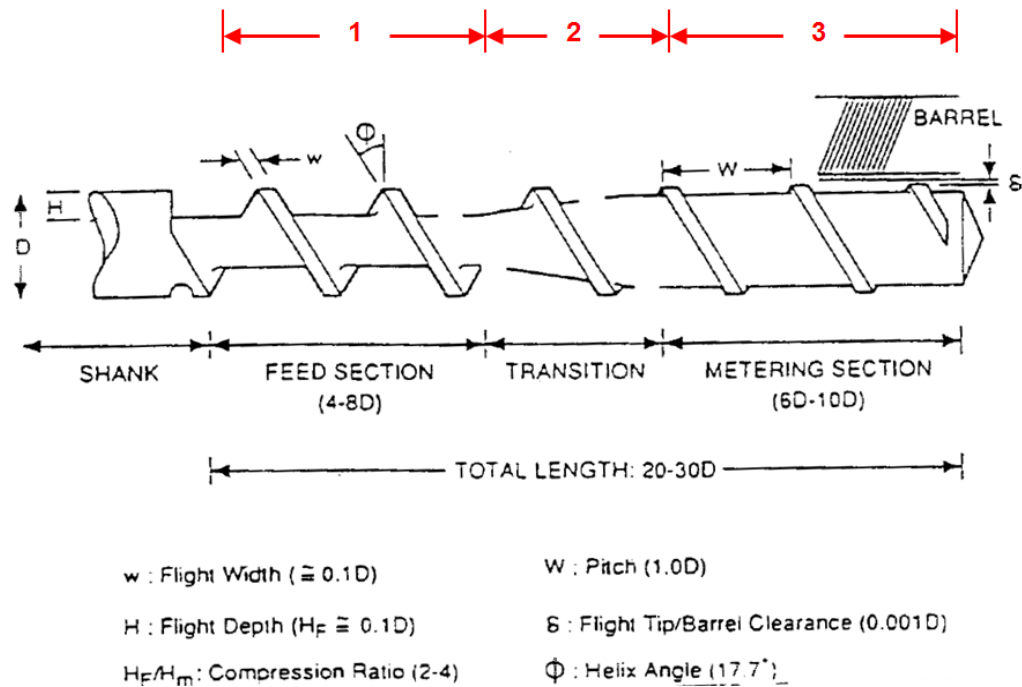
Figure 1-5: Typical plasticating screw geometry[16]. The three typical zones have been labelled above the barrel.

1.2.2 Extrusion of pipes

For the manufacturing of pipes an extruder is needed to provide the molten polymer for shaping and forming the final product. At the end of the extruder different dies can be fitted to produce a variety of product range. As the main objective of this study is pipe processing, a description of a typical pipe die follows.

Figure 1-6 shows a pipe die with spider legs for the alignment of the mandrel. The polymer melt enters the right end of the die where it is of a bigger cross sectional area than the exit of the die. The melt is then distributed evenly on the torpedo shaped mandrel and pushed toward the exit of the die. The mandrel is aligned in the centre of the die to ensure uniform thickness of the extrudate leaving the die. The molten polymer leaves the die in tubular form and enters the cooling/calibration system.
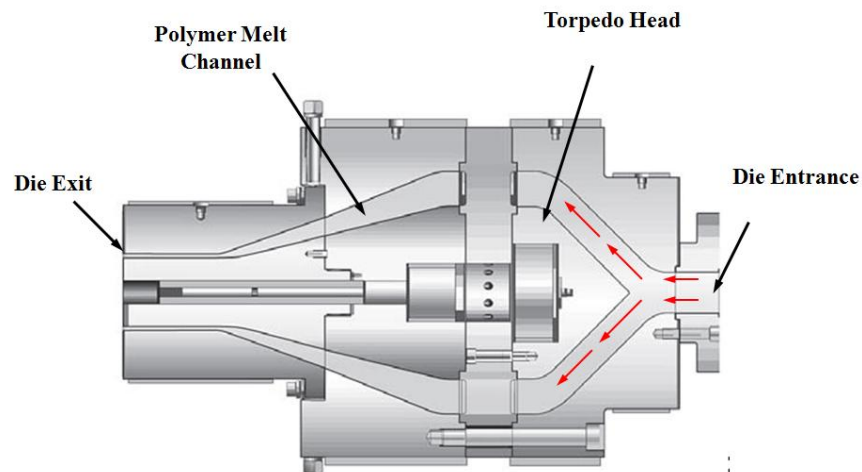
Figure 1-6: A typical pipe die showing the entrance and the exit of the die. The die benefits from spider leg design for the centring of the mandrel [17].

The die is externally heated and has a flow channel which changes shape smoothly from the extruder barrel to the product. The output rate of an extruder die depends on the pressure drop across the die. By increasing the pressure at the end of the extruder barrel and the entrance of the die (increasing screw speed) the output will increase. However, high pressures will cause reduction of material delivery from the metering zone as a result of pressure flow. Therefore it is necessary to match the screw and die design to optimize the overall throughput performance of the extruder.
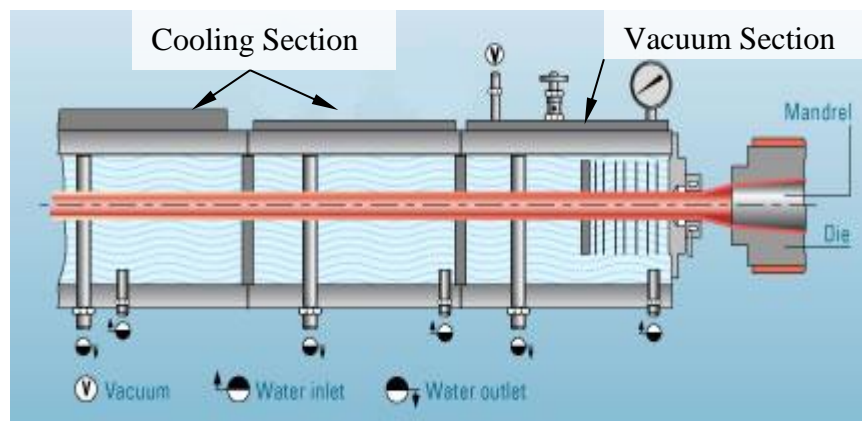
Figure 1-7: A typical Vacuum and cooling tank for manufacturing of polymer pipes.

In order to retain the shape and dimensions the extrudate needs to be calibrated and cooled quickly. A sizing operation is applied to the extrudate immediately after the melt leaves the die to hold the dimensions of the pipe while it is cooled and solidified.

This is accomplished by drawing the extrudate into a sizing sleeve which is fitted to the end of a cooling tank. The extrudate is pulled into the internal walls of the sleeve either by applying the vacuum within the tank or by the air pressure from inside of the extrudate (Figure 1-7). After exiting the vacuum sizing tank the pipe moves through the spray cooling tank where water is sprayed onto the pipe to complete the cooling process.

To pull the extrudate from the die into the vacuum/cooling tank and to maintain a constant draw down ratio of the melt a puller or haul-off is used. Normally the haul-off is equipped with special pads on the belt to increase the grip on the pipe and also avoid a change of shape caused by the load applied to grip the pipe.

The last element of a pipe manufacturing line is a cutter or saw which cuts the manufactured pipes into standard lengths.

1.3 Ultrasonic waves and their applications

Ultrasonics is a branch of acoustics that deals with vibration waves of higher frequency than the hearing range and it is often considered as vibrations with frequencies higher than 20 KHz. In this section the basic principles of ultrasonics will be discussed.

1.3.1 Background theory of ultrasonics

Ultrasonic waves are stress waves and, therefore the presence of a mass media is essential for its propagation. Ultrasound is a wave motion and obeys a general wave equation. Similar to light, the speed of ultrasound waves in a medium depends on the properties of that specific medium. It can be reflected from surfaces and refracted when going from one medium to another. When an ultrasound wave travels through a medium the amplitude of the wave decreases (attenuates). The attenuation could be caused by several factors such as, spreading of the wave front, conversion of the vibrations and mechanical energy to heat and scattering from irregular surfaces.
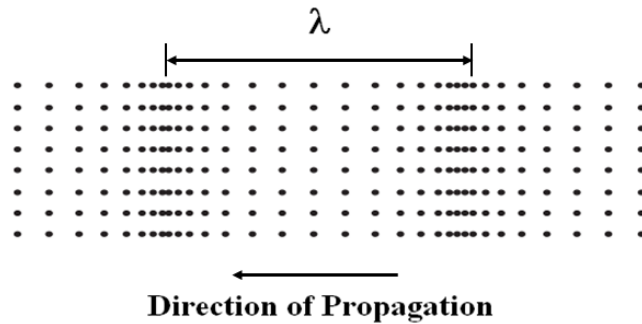
Figure 1-8: Longitudinal wave showing the wave length, λ, and the direction of the propagation.

When the ultrasound waves travel in a medium, the particles of the medium vibrate around their mean position. Ultrasound waves can be divided into three main categories which are longitudinal (compressive), shear and surface waves. Solids can transmit all the types, most liquids transmit only longitudinal waves and surface waves and gasses can only transmit longitudinal waves. Depending on the motion of the particles of the medium the longitudinal ultrasound waves (Figure 1-8) can be converted into shear waves as the energy passes from element to element by shear stress.

The velocity of ultrasound waves in polymer melt is a factor of medium's elastic properties and density. The velocity of the ultrasound waves, C_L, in polymer melts is [18]:

$$C_L = \sqrt{\frac{E}{\rho} \frac{1-\nu}{1+\nu} \frac{1}{1-2\nu}} \qquad \textbf{1-1}$$

Where ρ is the density, E is the modulus of elasticity and ν is the Poisson's ratio. When the polymer melt is subjected to the shearing stress, the macromolecular chains tend to align parallel to the direction of the shear flow. Therefore the modulus in the perpendicular direction to shear flow decreases due to orientation of the chains in the direction of flow. Reduction of modulus in normal direction to the direction of flow leads to lower ultrasound speeds in this direction according to Equation 1-1. The application of US vibrations is effected by customised US equipment. A description of this and the manner in which the US waves are exploited is given in the following section.

1.3.2 Components of an ultrasonic system

Ultrasonic waves are standing waves which are generated in the transducer and travel through the medium of booster and the sonotrode to be transferred into the melt or the liquid. Standing waves are generated by superposition of two set of same type of waves (transverse or longitudinal) having the same time period, amplitude, frequency and wave length travelling with the same speed along the same straight line but in opposite direction.

A type of standing waves which is being used in sonotrodes, is usually open at both ends. This is because the input end of the sonotrode which is in contact with the booster needs to be in maximum vibration amplitude to allow the wave to travel into the sonotrode efficiently. The output end is free vibrating end and acts as an open end, which constructed of two open end standing waves. A typical standing wave with both free ends is shown in Figure 1-9. As it is shown in Figure 1-9, the minimum length between two successive antinodes is $\lambda/2$.
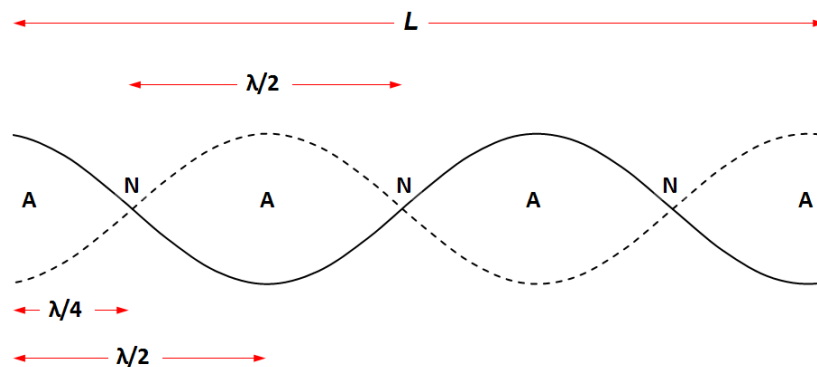
Figure 1-9: Typical standing wave with both free ends.

The possible standing waves with both free end pattern (first harmonic) for a known length of the medium (*L*) will be with wave length of:

First harmonic: $\lambda = 2L$

Second harmonic: $\lambda = L$

Third harmonic: $\lambda=2L/3$

n^{th} Harmonic: $\lambda=2L/n$

For a known wave length of λ the length of vibrating medium will be of integer multiplies of $\lambda/2$ which could be $\lambda/2$, $2\times\lambda/2$, $3\times\lambda/2$, $4\times\lambda/2$ ... $n\times\lambda/2$.

The ultrasonic equipment consisted of a power supply unit, transducer, booster and the horn. The ultrasonic power supply transfers the 50/60 Hz voltage to a high frequency (20 kHz) electrical energy (Figure 1-10).
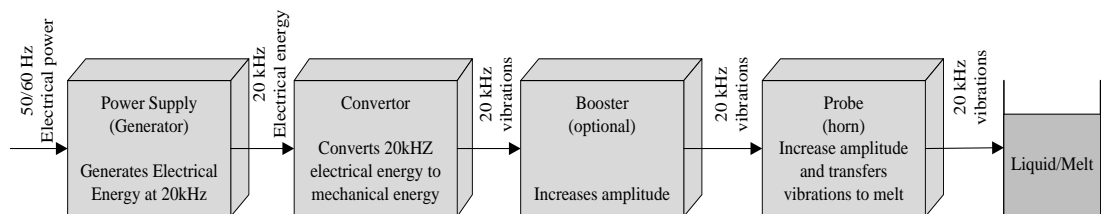
Figure 1-10: Ultrasonic system for generation of ultrasound waves.

High frequency voltage is then applied to the piezoelectric crystals within the converter, where it is changed to small mechanical vibrations with the same frequency as electrical energy (20 KHz). The vibrating motion generated by the converter (transducer) is normally too low, in terms of vibrations amplitude, for practical use and so it is necessary to magnify or amplify this motion. The converter's longitudinal vibrations then can be amplified by the booster and transmitted to the sonotrode. Usually sonotrodes are half a wavelength or multiple half wave length long depending on the application and the desired distance from the sample.

The transmitted longitudinal vibrations from the booster is then amplified by the horn and transmitted to the liquid as Ultrasonic waves consisting of alternate compressions and rarefactions.

1.3.2.1 Power Supply

The power supply (see Figure 1-10) is basically a transformer that converts electrical power to the required frequency and voltage. In order to achieve a steady ultrasound delivery it is necessary to monitor voltage, current and frequency of the current from the power supply regularly.

1.3.2.2 Transducer

The transducer converts the supplied electrical power to mechanical vibrations. Transducers used in modern power ultrasonic systems are based upon the pre-stressed piezoelectric design. In a transducer a number of piezoelectric elements are bolted together by a screw through the transducer clamps and the disks. The piezo elements would be of pre-polarized lead/titanate/zirconate composition which has high activity, low loss and ageing characteristics. By application of an alternating voltage to a length of polarized piezoelectric rod, the dimension of the rod will change in sympathy with the applied voltage. The frequency and amplitude of the transducer is defined by frequency of the applied electric current, the piezoelectric resonant length respectively. Transducer is a tuned system that resonates at the desired operating frequency.

1.3.2.3 Booster

A booster is connected between the transducer end and the sonotrode and amplifies the intensity of the vibrations. The booster is usually a tuned half wave piece so that it increases or decreases the amplitude passed from the transducer to the sonotrode. A booster has different masses on each end and the difference is defined in a way to have a certain gain ratio where gain ratio is the ratio between the amplitude at the sonotrode end of the booster and the amplitude at the transducer end of the booster.

1.3.2.4 Sonotrode

Sonotrode is an element of ultrasonic system that receives the vibrations generated by transducer through the booster and magnifies them to higher amplitude which is more suitable for practical use. Sonotrodes like other components of an ultrasonic system are

resonant at the operating frequency and can be made in any shape (Figure 1-11) depending on the application to it. Usually the sonotrodes are half a wavelength long and if longer distances from the sample are required, they can be designed in multiple half lengths long.
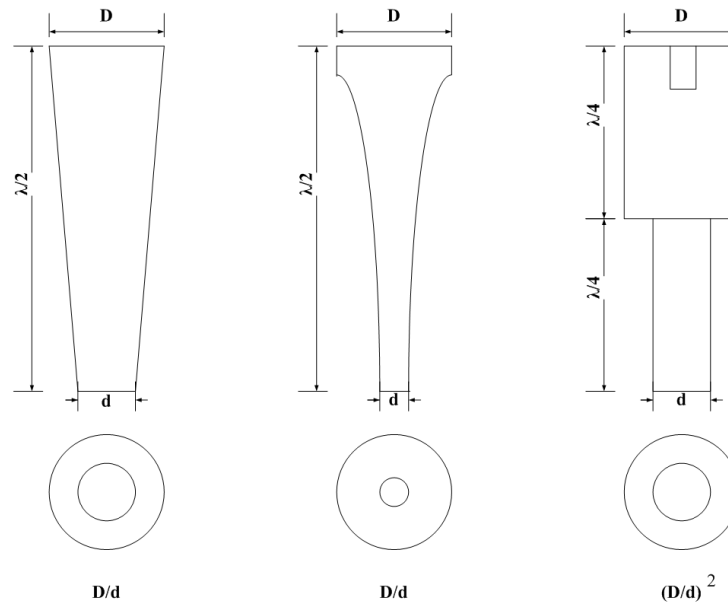
Figure 1-11: Typical designs of sonotrodes with different magnifications.

The material of the sonotrodes should be of high dynamic fatigue strength, low acoustic loss and resistant to erosion caused by cavitations. The materials favoured for many industrial applications are titanium alloys, stainless steel and aluminium alloys.

1.3.3 Effects of Ultrasound

Depending on the applications, ultrasonics can have different effects on a process. The main possible effects are as follows:

- Heat dissipation

Ultrasonic waves can be easily converted to thermal energy. This effect has been employed in plastic and metal welding to generate friction between the surfaces to be joined. The generated heat from friction melts the two surfaces and thus can be used to join them together in a very short cycle time.

- Cavitation

Ultrasound waves locally generate very high pressure pulses and when the pressure is removed due to the decompression part of the wave cycle, small bubbles of vapour are formed. This effect is called cavitation and can happen in liquids subjected to ultrasound. However, the viscosity of the liquid plays an important role in the creation of cavitation and for high viscosity liquids/melts cavitations do not occur. When formed, the vapour bubbles are extremely unstable and when they collapse they generate high energy shock waves in the liquid. The enormous number of the bubbles which have been formed and collapsed can affect the properties of the liquid by creating high temperatures and pressures when the bubbles collapse.

- Decrease of friction

Another effect of high frequency ultrasound waves is that the surface of the sonotrode and the medium tend to separate from each other. This can be obtained by the separation of the surfaces or reduction of the friction to zero. The very high frequency movement of sonotrode generates a low friction zone on the boundary layers of the surfaces which are in contact with the polymer melt.

1.3.4 Applications of Ultrasonics

Ultrasonics has been employed in a variety of industrial applications some of which are listed below.

- Sonochemistry, i.e. influencing chemical reaction rates

- Ultrasonic cleaning, i.e. ultrasonic cleaning baths

- Ultrasonic welding, i.e. plastic and metal welding

- Ultrasonic sieving, i.e. industrial ultrasonic sieves

- Ultrasonic machining, i.e. ultrasonic drills

- Non destructive ultrasonic testing, i.e. inspection of airplane parts

1.4 Thesis Outline

The effects of ultrasound have been studied on numerous occasions in the polymer processing industry. There are several applications of ultrasound in polymer processing such as ultrasonic welding, non destructive testing, online monitoring, etc.

The aim of this study was to develop an ultrasonic system which is a part of the extrusion system. An annular die was chosen for the development as it is used in several processes such as pipe, film and blow moulding. The extrusion of polyolefins was carried out with and without presence of ultrasonic vibrations on 3 extruders with different flow rates to investigate the effects of ultrasonic vibrations on the extrudate and processing parameters.

The objective of this thesis was to use the application of ultrasonic vibrations in extrusion. The material was confined to polyethylene because of the favourable processing conditions of PE and very aggressive form of the vibrations.

The objective was achieved in following developments and chapters:

Chapter 2

- The determination of the effective penetration depth of ultrasound waves in a polymer melt.

Chapter 3

- The design of a housing block for the sonotrode to be fitted to a lab scale extruder (25mm).

- To carry out lab scale extrusion trials of commercial pipe grade polyethylene with and without the presence of ultrasound.

Chapter 4

- The design of an ultrasonic horn which could be used as an annular die.

- The modifications of the initial design to optimize the performance of the sonotrode and to design a 2nd generation sonotrode and housing block to be fitted to a pilot scale extruder (50mm).

- To carry out pilot scale extrusion trials of different grades of polyethylene with and without ultrasound.

- To carry out pipe extrusion trials with commercial pipe grade polyethylenes and to investigate the effect of ultrasound on the processing conditions of the pipes.

- To carry out pipe extrusion trials with an unfilled polyethylene resin, the same polyethylene resin filled with 20%wt and 40%wt $CaCO_3$ with and without ultrasound to study the effect of ultrasonic vibrations in presence of fillers.

Chapter 5

- The design and manufacture of a 3rd generation ultrasonic horn and housing block.

- To carryout extrusion trials with PE80 and the third generation ultrasonic die using a 90mm extruder.

- To investigate the effects that USV's have on the properties and structure of extruded polymers.

1.5 References

1. Woodward, A. and J. Sauer, *The dynamic mechanical properties of high polymers at low temperatures Fortschritte Der Hochpolymeren-Forschung*. 1958, Springer Berlin / Heidelberg. p. 114-158.

2. Stockmayer, W.H., *Introduction to physical polymer science, by L. H. Sperling, Wiley-Interscience, New York, 1986, 439 pp. Price: $39.50.* Journal of Polymer Science Part C: Polymer Letters, 1989. **27**(4): p. 146-146.

3. Brydson, J., *Plastics Materials (7th Edition)*. 1999, Elsevier. p. 218.

4. Kennedy, M.A., A.J. Peacock, and L. Mandelkern, *Tensile Properties of Crystalline Polymers: Linear Polyethylene*. Macromolecules, 1994. **27**(19): p. 5297-5310.

5. Rodriguez, F., *Principles of polymer systems*. 1982: Hemisphere Pub. Corp.

6. Mitchell, B.S., *An introduction to materials engineering and science for chemical and materials engineers*. 2004: Wiley-Interscience.

7. Fox, T.G. and S. Loshaek, *Influence of molecular weight and degree of crosslinking on the specific volume and glass temperature of polymers*. Journal of Polymer Science, 1955. **15**(80): p. 371-390.

8. Stutz, H., K.H. Illers, and J. Mertes, *A generalized theory for the glass transition temperature of crosslinked and uncrosslinked polymers*. Journal of Polymer Science Part B: Polymer Physics, 1990. **28**(9): p. 1483-1498.

9. Vasile, C., *Handbook of polyolefins*. 2nd ed., rev. and expanded / edited by Cornelia Vasile. ed. 2000, New York: Marcel Dekker.

10. Eisenberg, A., *In: Physical Properties of Polymers*, in *ACS*. 1984: Washington, DC. p. 57-95.

11. Chee, K.K., *Dependence of glass transition temperature on chain flexibility and intermolecular interactions in polymers.* Journal of Applied Polymer Science, 1991. **43**(6): p. 1205-1208.

12. Ram, A., *Fundamentals of polymer engineering*. 1997, New York ; London: Plenum Press.

13. Sperling, L.H., *Introduction to physical polymer science*. 4th ed. ed. 2006, New York ; [Chichester]: Wiley. xxx, 845 p.

14. Clara, S., L. MariaLaura Di, and P. Emilia Di, *Crystallization of Polyolefins*, in *Handbook of Polyolefins*. 2000, CRC Press. p. 223-248.

15. Crawford, R.J., *Plastics engineering*. 3rd ed. 1998, Boston: Butterworth-Heinemann. xvi, 505 p.

16. *Extrusion Principles*.

17. Plastics Pipe, I., *The Plastics Pipe Institute handbook of polyethylene pipe*. 2008, Irving, TX: The Plastics Pipe Institute.

18. Li, J., et al., *An in-process ultrasonic approach to investigating the relaxation of orientation and disorientation of polymer melts.* Polymer Engineering & Science, 2008. **48**(5): p. 987-994.

Chapter 2

The Effect of Ultrasonic Vibrations on Stationary Polyolefin Melts

2.1 Introduction

When a liquid is subjected to an ultrasonic field a feature of this is the nucleation and growth of bubbles that subsequently suddenly collapse. This can result in shock waves imparting a high temperature and a high pressure [1] that can be sufficient to cause the scission of chemical bonds and the formation of macro-radicals. The transient, localized hot spots can have sufficient energy to activate high energy chemical reactions. It has been reported [2-4], these hot spots have temperatures of as high as 5000°C, pressures of about 1,000atm and heating/cooling rates above 10^{10} K/s.

According to the general mechanism of cavitation, when the viscosity of the liquid (solution) goes beyond 2.0 Pas, cavitations do not form [5]. The high viscosity of polyethylene including the pipe extrusion grade that was employed in this study prevented

the formation of cavities and thus the energy of the vibrations was transferred uniformly into the melt. Ultrasonic waves are mechanical waves that propagate at a higher frequency than sound in the human audible range. When an ultrasound wave travels through a medium, it suffers a loss in its energy due to various mechanisms, such as spreading, scattering and absorption [6-32].

In a homogeneous material, where energy losses due to scattering may be considered negligible, the absorption is attributable to thermal conductivity, viscous effects and other molecular processes. The absorbed energy results in a temperature rise in the medium that can be used to provide information about the acoustic field and penetration depth.

In order to design a polymer melt flow channel that would enable the most effective transfer of ultrasonic energy to the material, the penetration depth of the USV's within the melt had to be determined. The intensity of the waves or any other parameter which is the direct consequence of introducing ultrasonic vibrations into polymer medium can be measured at different distances from the ultrasonic horn to determine the effective penetration depth. Amongst all the measurable direct effects of the application of ultrasonic vibrations to a polymer, temperature is the easiest one to measure and record. An experimental arrangement to define the penetration depth was set up to enable the polymer melt temperatures to be measured from the surface of the ultrasonic horn through the polymer melt away from the surface of the horn.

2.2   Materials

A commercial pipe extrusion grade Polyethylene (PE80), melt flow rate of 0.33 g/10min under a load of 5Kg at 190°C, was used in this study. PE80 is a commercial pipe grade of HDPE manufactured by BOREALIS which contains carbon black to increase the material's UV resistance. Samples of the materials were supplied by Polypipe Terrain in a standard granular form.

2.3   Ultrasonic Horn Design

A 250W ultrasonic generator provided by Solbraze[1] was employed to carry out the experiments. The UM250 ultrasonic generator is capable of delivering 250W of ultrasonic waves with frequency of 20 KHz. The transducer needed to be protected in terms of temperature and the horn was therefore supplied with an air cooling collar requiring connection to a compressed air supply.
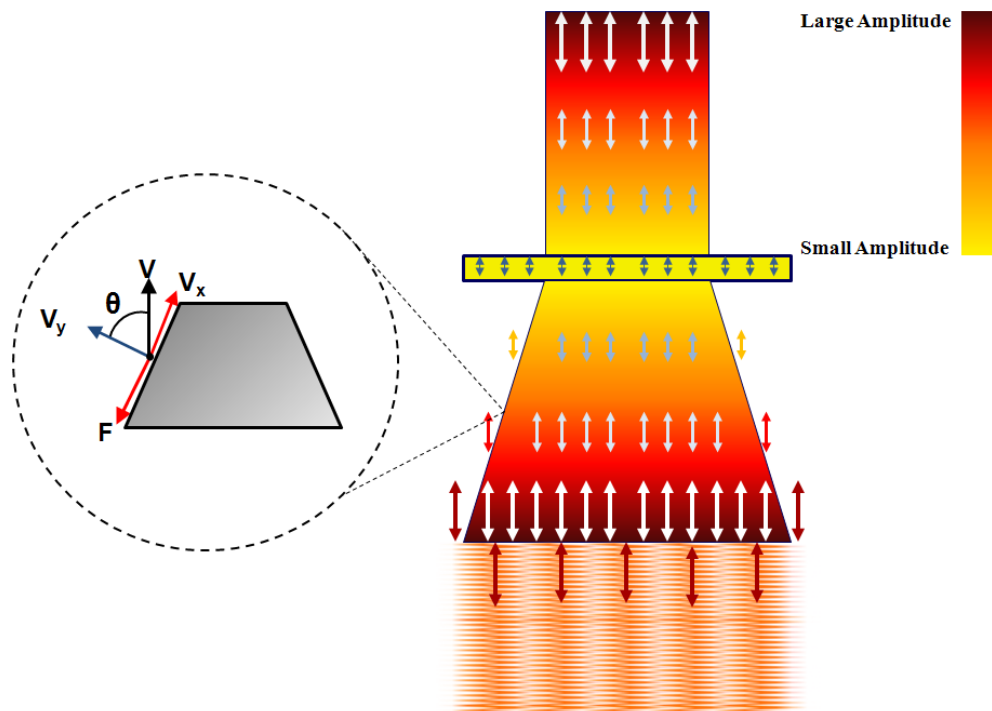
Figure 2-1: Schematic diagram of the G1 ultrasonic horn demonstrating the amplitude of ultrasound vibrations in the horn. V shows the direction of the vibration and V_x and V_y are components of the ultrasonic vibration parallel and perpendicular to the direction of the melt flow, respectively.

The horn was designed in a conical shape. The idea behind the conical design of the horn was to allow the molten polymer to flow over the horn from the top of the conical section to the bottom which has a larger cross sectional area (shown in Figure 2-1). Due to the slope of the horn in the conical section, the longitudinal vibrations would be resolved into components of compressive and shear vibrations at the surface of the horn. The

---

[1] Solbraze Ltd was part of Sonoflow consortium. The company's contribution to project was supplying the ultrasonic generator and advising the other collaborators in ultrasonic field.

compressive component is the one that will penetrate the melt whereas the longitudinal vibrations will only move parallel to the surface of the horn.

In order to maximize the effect of ultrasonic vibration the material passed over the bottom of the horn. This surface was at an anti-node and therefore vibrated at the maximum amplitude with the compressive wave action.

The first generation horn, G1, can be seen in Figure 2-2, this was screwed to the booster at the top. The flange in the middle of the horn was for clamping the horn in the ultrasonic die block. It is important to note that this was set at a nodal point so that none or very little US vibration energy was transferred to the die block. The power supply unit, converter and the booster were supplied and tuned by Solbraze to fit the custom built Aluminium horn.
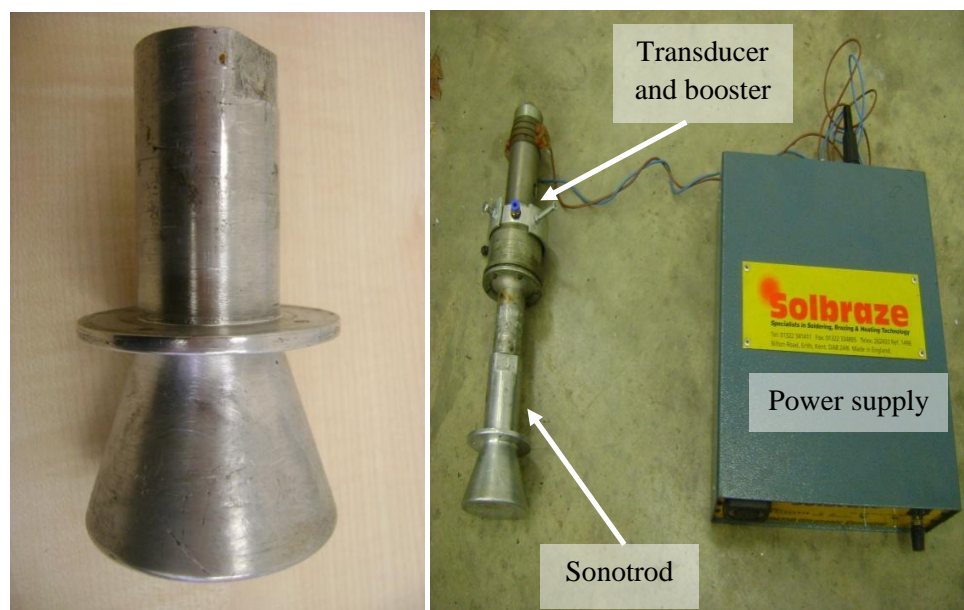
Figure 2-2: The G1 horn (Aluminium made) and the ultrasonic unit.

2.4   Batch Sonication Results

2.4.1 Initial Setup

A bench top scale apparatus was designed as shown in Figure 2-3. The mould was equipped with three thermocouples, one to control the temperature of heated melt chamber and the other two to measure the polymer melt temperature.
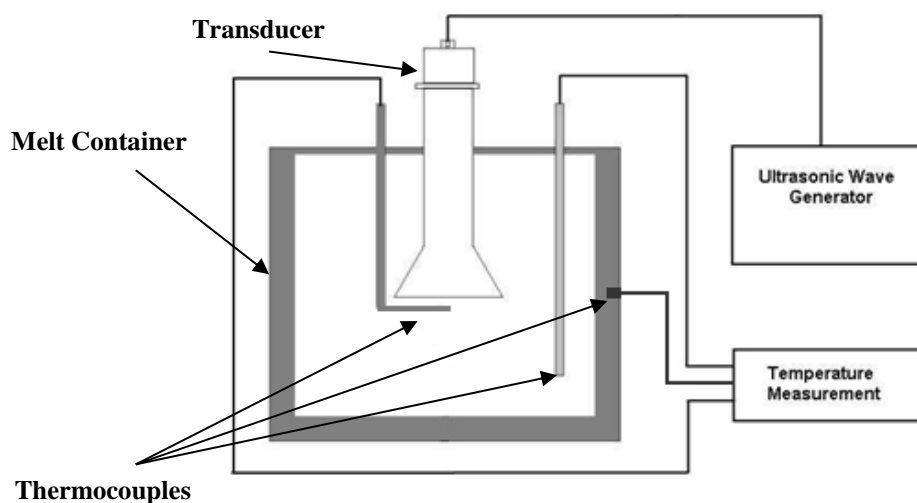
Figure 2-3: Schematic diagram of initial batch sonication setup.

The other two thermocouples were placed in the polymer melt, one of them with a known distance under the ultrasonic horn and the other far away from the horn in the polymer to measure the bulk polymer melt temperature during sonication. The thermocouple for the container and the heater band were both used to control the temperature of the container. Figure 2-4 shows the set up used for initial batch sonication experiments.
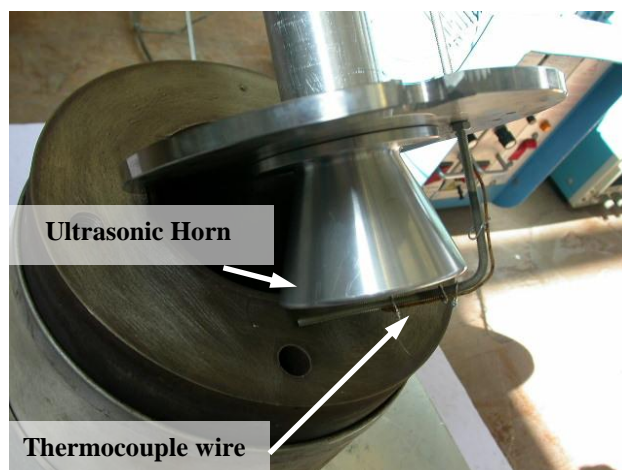
Figure 2-4: Initial batch sonication trials set up.

The ultrasonic horn was screwed and fixed on a steel plate that sat on the container which also acted as a lid. The steel plate was then bolted to the container to keep the horn at a known height from the bottom of the mould and from the walls of the container.

The polyethylene needed to be in its molten state when filling the container. This enabled the melt to reach the test temperature fast and more efficiently than if the polymer granules were heated in the container. PE80 granules were extruded using a BETOL J2525 extruder[2] and the melt was transferred directly into the container. The filled container was then given enough time for the temperature to stabilize.

The temperatures were recorded for the experiments with bench top setup and the results are presented in Figure 2-5, Figure 2-6 and Figure 2-7. Obtained results showed an inconsistency in the readings although the same procedure had been repeated for all the tests. As these results are not reproducible, it was decided to check the equipment to ensure that the thermocouple was placed at the same distance from the horn in different runs.
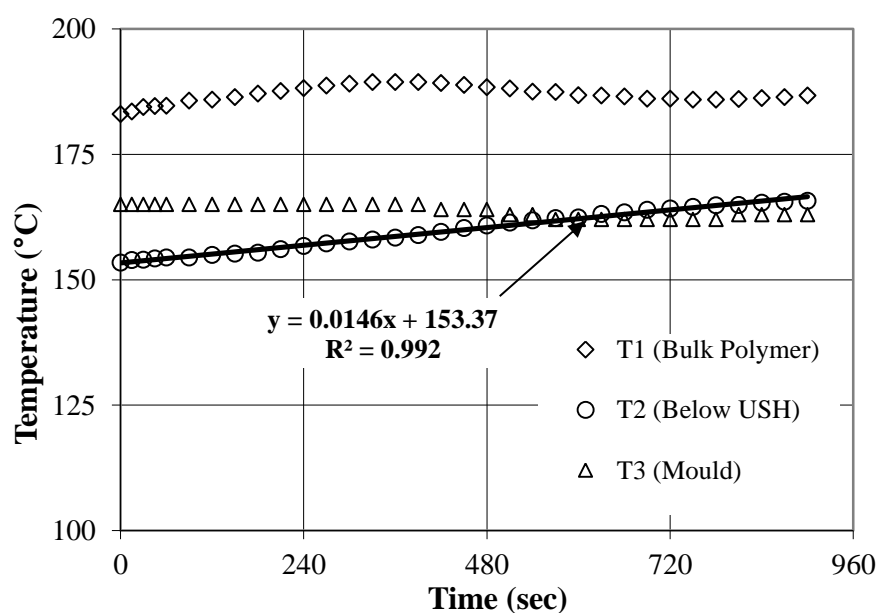
Figure 2-5: Temperature vs. Time for the first trial of initial batch sonication setup. Temperature readings were fitted to a linear equation as shown above, y is the temperature and x is the time in seconds.

---

[2] The technical details of the extruder will be discussed in Chapter 3.
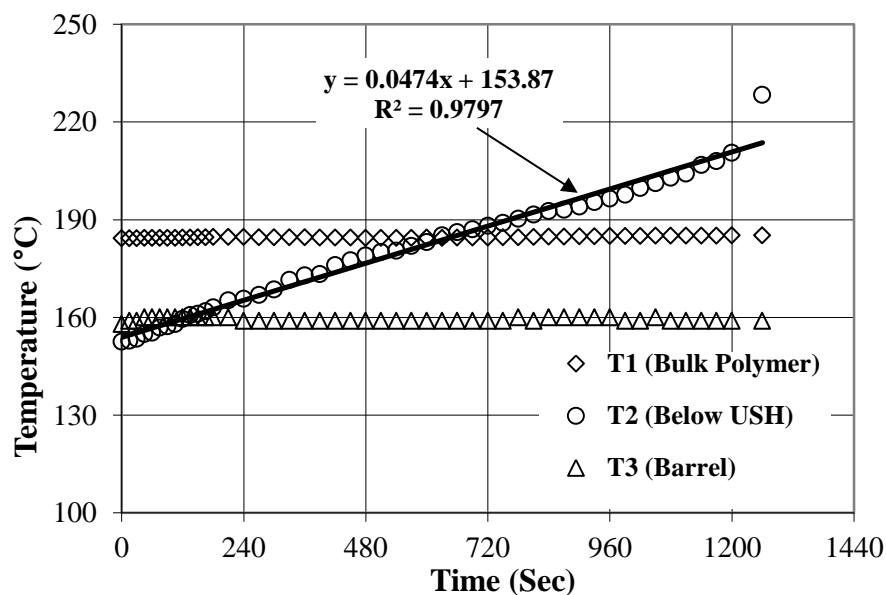
Figure 2-6: Temperature vs. Time for the second trial of initial batch sonication setup. Temperature readings were fitted to a linear equation as shown above, y is the temperature and x is the time in seconds.
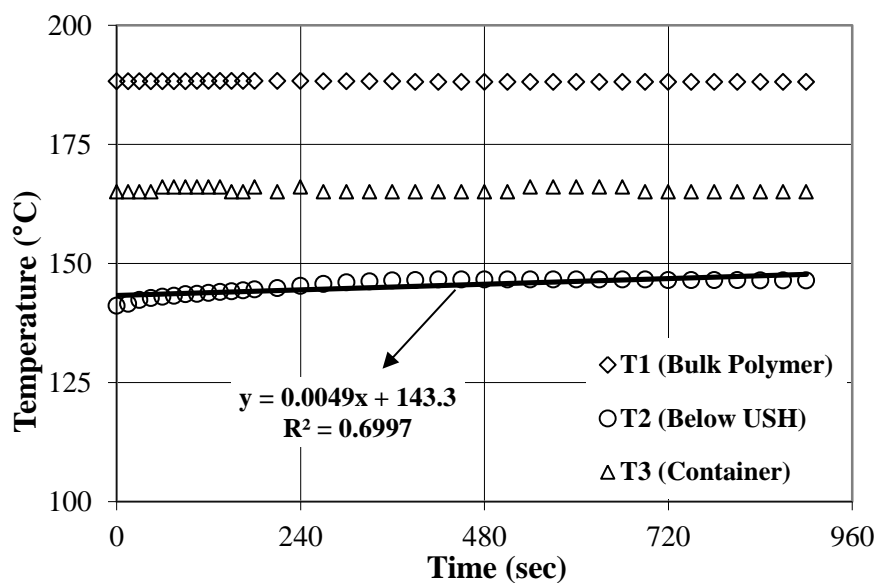
Figure 2-7: Temperature vs. time for the third trial of initial batch sonication setup. Temperature readings were fitted to a linear equation as shown above, y is the temperature and x is the time in seconds.

Several sonication trials using the initial setup proved that, this arrangement was not appropriate and reliable for data collection because the results were unrepeatable and inconsistent. In some results a sharp rise in temperature as a function of time was

experienced. The inconsistency of the temperature readings could possibly be due to contact between the thermocouple and the horn surface. The thermocouple and the horn surface could come into contact with each other because of close distance between the thermocouple and sonotrode surface and the flexibility of the part that was used to keep the thermocouple in place.

2.5   Modified Arrangement

In order to keep the thermocouple in a known distance (4mm) from the horn a new design was set up (Figure 2-8).
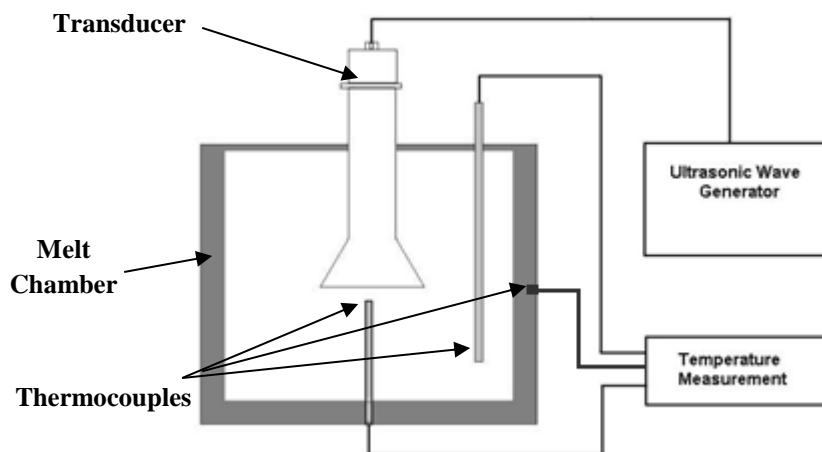
Figure 2-8: Modified design of the bench-top equipment.
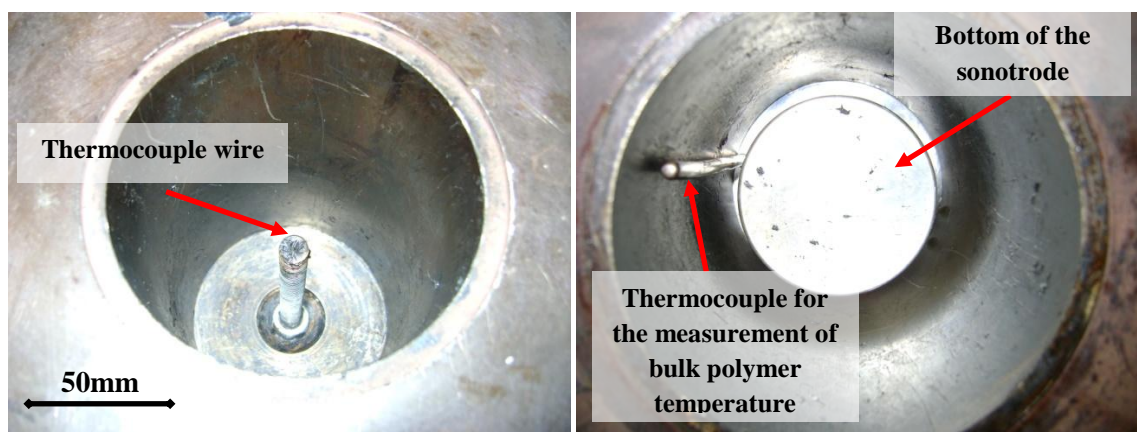
Figure 2-9: Bottom of the mould with the thermocouple tube placed (left), Top of the mould where the ultrasonic horn and other thermocouple attached on (right).

In the new design a metal tube with a central hole was screwed to the bottom of the container. A thermocouple wire was passed through the hole up to the end of the tube and positioned underneath the ultrasonic horn. The distance between the horn and the thermocouple could be adjusted by up to 2-3cm by unscrewing the tube containing the thermocouple wire. The schematic diagram of this setup can be seen in Figure 2-8. Photographs from the top and bottom of this setup are shown in Figure 2-9. As mentioned earlier the polyethylene melt at 185°C was produced by an extruder and transferred into the container. The complete assembly was then given an appropriate time (30-45 minutes) for the material to be stabilized at the required testing temperature.
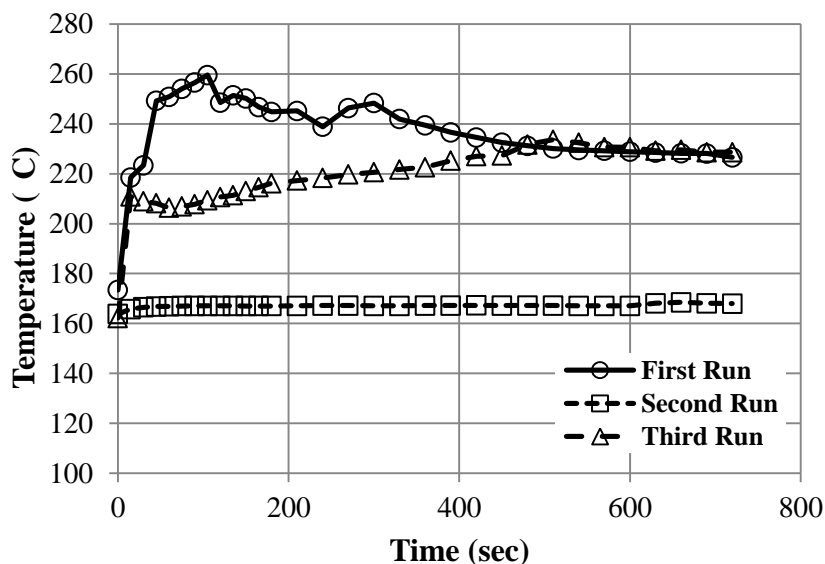
Figure 2-10: Temperature vs. Time plot for three runs using new setup.

The temperatures of the thermocouples under the horn and in the bulk polymer were checked regularly until the temperature fluctuations became insignificant. After the temperature had stabilized the ultrasonic vibrations were applied to the polyethylene melt and the temperatures were recorded during the sonication.

During the sonication process, as it can be seen in Figure 2-10, a rise in temperature was measured under the probe as expected, however the rate of increase of the temperature was not reproduced in the tests.

The only reason for variations in the effect of ultrasound could be as a result of inconsistent radiation of ultrasonic waves to the polymer melt. To investigate the

inconsistency in the effects of the ultrasound vibrations the demanded power of the ultrasonic generator can be monitored. The input current of the ultrasonic generator could be monitored as a representative to demanded power. The electric current of the power line to the generator was measured. Measurements of the current in the circuit of ultrasonic generator showed different current values for the three runs while the rest of the parameters were kept constant.

Table 2-1: Electrical current values measured for Sonication trials.

Experiment	Melt Temp $^{\circ}$C	Electric Current A
1	199	0.032
2	199	0.11
3	196	0.024

The readings (shown in Table 2-1) confirmed that the ultrasonic generator was not delivering constant power and the generated vibrations were not continuous and were fluctuating. These inconsistencies made the experiment unrepeatable and impractical to carry out more experiments. The generator was of the design to deliver power on demand which meant that if the vibration of the media required more power the generator would consume more power. Although an attempt has been made to keep all the parameters constant in the experiments, there were some possible reasons for the errors and inconsistencies. Some of these are: the presence of the trapped air in the molten polymer, degradation of the polymer in the temperature stabilization time, not fully immersion of horn in the polymer. All these parameters can affect power draw from the ultrasonic generator and thereby change the electrical current.

2.6   Conclusion

Although an attempt was made to create the same conditions for all of the tests, according to that mentioned above and the fact that wave speed through polymer melt is a function of viscosity and temperature, a conclusion must be that the static sonication was not a good representative for in-line equipment. The viscosity of polymers is dependent on shear rate and temperature so the viscosity will change in an in-line setup and therefore consequently it will change how the waves will penetrate the polymer melt. With the results for PE80

above, it has been decided to manufacture the inline equipment based on less than a 4mm effective penetrating depth of waves. The housing block for the first generation ultrasonic horn was manufactured with a clearance of 2mm between the horn and the housing block wall. This clearance could be increased if needed but for initial experiments of the ultrasonic assisted extrusion it was essential to identify the potential benefits from ultrasonic vibrations. This could then can be improved and optimised for better results.

2.7 References

1.   Flint, E.B. and K.S. Suslick, *The Temperature of Cavitation.* Science, 1991. **253**(5026): p. 1397-1399.

2.   Suslick, K.S., *Sonoluminescence and sonochemistry.* 1997 Ieee Ultrasonics Symposium Proceedings, Vols 1 & 2, 1997: p. 523-532.

3.   Suslick, K.S., et al., *Acoustic cavitation and its chemical consequences.* Philosophical Transactions of the Royal Society of London Series a-Mathematical Physical and Engineering Sciences, 1999. **357**(1751): p. 335-353.

4.   Suslick, K.S., W.B. McNamara, and Y. Didenko, *Hot spot conditions during multi-bubble cavitation.* Sonochemistry and Sonoluminescence, 1999. **524**: p. 191-204.

5.   Li, H.L., Y.C. Zhang, and J.Y. Chen, *Functionalization of high density polyethylene in melt state through ultrasonic initiation and its effect on mechanical properties of glass fiber reinforced composites.* Polymer Bulletin, 2007. **59**(3): p. 427-438.

6.   Abu-Zahra, N.H., *Real-time viscosity and density measurements of polymer melts using dielectric and ultrasound sensors fusion.* Mechatronics, 2004. **14**(7): p. 789-803.

7.   Afifi, H., et al., *Ultrasonic studies on polystyrene/styrene butadiene rubber polymer blends filled with glass fiber and talc.* Ultrasonics, 2006. **44**: p. E1439-E1445.

8.   Bae, J.R. and M.H. Yi, *Ultrasonic velocity and absorption measurements in binary solutions of poly(acrylic acid) and in water solutions.* Journal of the Korean Physical Society, 2002. **41**(1): p. 171-174.

9.   Biwa, S., S. Idekoba, and N. Ohno, *Wave attenuation in particulate polymer composites: independent scattering/absorption analysis and comparison to measurements.* Mechanics of Materials, 2002. **34**(10): p. 671-682.

10.   Castaings, M., et al., *Finite element predictions for the dynamic response of thermo-viscoelastic material structures.* Journal of the Acoustical Society of America, 2004. **115**(3): p. 1125-1133.

11.   Coates, P.D., et al., *In-process vibrational spectroscopy and ultrasound measurements in polymer melt extrusion.* Polymer, 2003. **44**(19): p. 5937-5949.

12.   Contamine, R.F., et al., *Power Measurement in Sonochemistry.* Ultrasonics Sonochemistry, 1995. **2**(1): p. S43-S47.

13.   Graham, I.S., L. Piche, and M. Grant, *Experimental-Evidence for Localization of Acoustic-Waves in 3 Dimensions.* Physical Review Letters, 1990. **64**(26): p. 3135-3138.

14.   Gronroos, A., et al., *Ultrasonic depolymerization of aqueous polyvinyl alcohol.* Ultrasonics Sonochemistry, 2001. **8**(3): p. 259-264.

15.   Hodnett, M. and B. Zeqiri, *A strategy for the development and standardisation of measurement methods for high power cavitating ultrasonic fields: review of high power field measurement techniques.* Ultrasonics Sonochemistry, 1997. **4**(4): p. 273-288.

16.   Hosten, B., C. Bacon, and C. Biateau, *Finite element modeling of the temperature rise due to the propagation of ultrasonic waves in viscoelastic materials and experimental validation.* Journal of the Acoustical Society of America, 2008. **124**(6): p. 3491-3496.

17.   Kanthale, P.M., et al., *Mapping of an ultrasonic horn: link primary and secondary effects of ultrasound.* Ultrasonics Sonochemistry, 2003. **10**(6): p. 331-335.

18.   Kanwal, F. and R.A. Pethrick, *Ultrasonic degradation studies of poly(ethylene oxide), poly(ethylene adipate) and poly(dimethylsiloxane).* Polymer Degradation and Stability, 2004. **84**(1): p. 1-6.

19.   Kim, H. and J.W. Lee, *Effect of ultrasonic wave on the degradation of polypropylene melt and morphology of its blend with polystyrene.* Polymer, 2002. **43**(8): p. 2585-2589.

20.   Klima, J., et al., *Optimisation of 20 kHz sonoreactor geometry on the basis of numerical simulation of local ultrasonic intensity and qualitative comparison with experimental results.* Ultrasonics Sonochemistry, 2007. **14**(1): p. 19-28.

21.   Li, H.L. and Y.Z. Chen, *Mechanism for effect of ultrasound on polymer melt in extrusion.* Journal of Polymer Science Part B-Polymer Physics, 2007. **45**(10): p. 1226-1233.

22.   Li, Y.T., et al., *Mechanochemical degradation kinetics of high-density polyethylene melt and its mechanism in the presence of ultrasonic irradiation.* Ultrasonics Sonochemistry, 2005. **12**(3): p. 183-189.

23.   Lin, S.Y. and F.C. Zhang, *Measurement of ultrasonic power and electro-acoustic efficiency of high power transducers.* Ultrasonics, 2000. **37**(8): p. 549-554.

24.   Liu, S.J. and Y.T. Dung, *Hot embossing precise structure onto plastic plates by ultrasonic vibration.* Polymer Engineering and Science, 2005. **45**(7): p. 915-925.

25.   Loning, J.M., C. Horst, and U. Hoffmann, *Investigations on the energy conversion in sonochemical processes.* Ultrasonics Sonochemistry, 2002. **9**(3): p. 169-179.

26.   Maffezzoli, A. and F. Lionetto, *Polymer Characterization by Ultrasonic Wave Propagation.* Advances in Polymer Technology, 2008. **27**(2): p. 63-73.

27.   Nosov, M.I., et al., *Measurement of the propagation rate and damping rate of ultrasound in kapron texturized yarns.* Fibre Chemistry, 1984. **15**(5): p. 366-368.

28.   Pinkerton, J.M.M., *The Absorption of Ultrasonic Waves in Liquids and its Relation to Molecular Constitution.* Proceedings of the Physical Society. Section B, 1949. **62**(2): p. 129.

29.   Romdhane, M., C. Gourdon, and G. Casamatta, *Development of a Thermoelectric Sensor for Ultrasonic Intensity Measurement.* Ultrasonics, 1995. **33**(2): p. 139-146.

30.   Shore, J.D., et al., *Model for melt fracture instabilities in the capillary flow of polymer melts.* Physical Review Letters, 1996. **77**(4): p. 655-658.

31.   Wilkens, V., *Thermoacoustic ultrasound power measurement using evaluation of transient temperature profiles.* 2002 Ieee Ultrasonics Symposium Proceedings, Vols 1 and 2, 2002: p. 1399-1402.

32.   Yan, Z.Y., et al., *The considerations and guides of the wattmeter method for measuring output acoustical power of Langevin-type transducers - I: theory.* Ultrasonics, 1997. **35**(7): p. 533-541.

Chapter 3

Lab Scale In-line Ultrasonic

Assisted Extrusion of Polyolefins

3.1   Introduction

One of the most important fields in the plastics industry is polymer materials processing; and extrusion is one of the most extensively used technique for this.

Typical products of extruders are pipe, window profiles, blown film, sheet, tubing, coated paper, plastic filaments for brush bristles, carpet fibres, vinyl siding window frames and as of many other linear products. Depending on the end product, there is different downstream processing equipment, the extrudate may be blown into a pipe/film, spun, folded, and rolled. Most common substances for extrusion are plastics but rubber, metals and food stuffs are also quite often processed via extrusion.

The extensive use of polymer materials in the economy requires not only the creation of novel technological processes but also the improvement of existing processing methods to optimize their efficiency. Sharkskin melt fracture is one of the significant problems in extrusion of polymers and especially in the film blowing process. The appearance of shark skin is a limiting factor for production rates in extrusion processing operations such as pipe extrusion, film blowing and blow moulding. Increasing or removing the critical shear stress or shear rate limitation would be beneficial to manufacturing by allowing increased rates of production.

The ultimate targets of the enhancement of extrusion processing are to increase productivity and improve the product quality. However in extrusion the transmissive capacity is limited and low as a result of presence of a great hydraulic resistance to the shaping heads/dies. The development of methods for lowering the resistance of the dies by reducing the viscosity of the polymer melts in the die section, is therefore very important for speeding up the extrusion processing [1-3].

The application of vibrations to the polymer melts to reduce the melt viscosity during processing and to improve the mechanical properties of the products has been widely studied previously [4-9]. The idea of modifying the flow regimes in a polymer processing apparatus by applying ultrasonic vibrations is not new. Attempts have been made in the past to study the effect of the micro-movement of an ultrasonic frequency at the melt flow channel's walls in polymer extrusion or injection moulding [10-17]. This technique was realized by introducing mechanical or tuned ultrasonic vibrations in the flow channel wall. Compared with the low intensity/frequency vibrations that affect the material by generating friction at the contact surfaces, the ultrasonic waves are widely employed to influence a medium through shatter, cavitations and mechanical action.

A recent development of melt vibration technology has been with more attention to improving the processing behaviour of the polymers [18-20]. In general, there are three objectives for the application:

- To homogenize the melt and increase the density of the moulded products by increasing the rate of crystallisation [21-24].

- To improve the processability of the polymer by reducing the pressure required to generate a known throughput rate and to control the morphological structure of the polymer.

- To generate heat locally by internal friction within the melt at the flow channel wall and to decrease the surface stress at the interface between the melt and the flow channel wall in the die to increase throughput.

Several effects of the application of ultrasound to polymers have been reported [25, 26]. The application of an ultrasound field to a polymer melt in the shaping zone seems to be an efficient way to do this. Most ultrasonic tests have used a 20 KHz frequency (quartz crystal natural resonating frequency) and 5-30 μm vibrational displacement. Several interesting effects were claimed, such as melt pressure reductions and increases in the output when ultrasonic vibrations, either longitudinal or transverse, were applied at the die wall [12, 27-29].

Previous research related to the application of ultrasonic vibrations during the flow of polymer melts showed two big features [5, 7, 9, 10, 17, 30-35]. One was focused on the macroscopic flow behaviour [4, 11, 14, 17, 30, 33, 34, 36], these studies showed that the flow rate increased for a given pressure drop, or that the pressure drop was reduced for a fixed flow rate; the flow rate at which melt fracture occurred was postponed; the appearance of the extrudates was improved, as well as reductions of the specific power consumption and extrudate swelling. Other feature was that the chemical structures of the original molecules could be changed by ultrasonic vibration. The mechanochemical degradation of polymer melts, devulcanization of rubber and the formation of free radicals under influence of ultrasonic waves have been investigated previously [6, 34, 37-41].

Ultrasound oscillations have been applied to different polymeric materials and employed in numerous processing methods. The reduction of the viscosity of the solution of natural polymers by ultrasound was investigated [24, 42]. When polymer solutions are subjected to high intensity ultrasonic vibrations, polymer chain scission was observed that consequently caused a decrease in the molecular weight and viscosity[42, 43].

The influence of mechanical vibrations on the poiseuille flow of a non-Newtonian fluid have been studied for longitudinal [27-29] and transverse [44, 45] vibrations.

Ultrasonic vibrations have been previously employed in injection moulding. The apparatus and method was used to control the crystallization mechanism of plastics in the [46].

The application of ultrasound on the extrusion of polymers is much wider than other areas of polymer processing because extrusion is a continuous process while the other processes are intermittent such as injection moulding, compression moulding etc. The effects of ultrasound were used for the devulcanization of recycled rubber and to improve some mechanical properties of the rubber [38, 47-49]. When the ultrasound vibrations of 20~100 KHz were applied opposite to the discharging direction of the rubber through the extruder, rubber sheets with the lower die swell and good dimension accuracy were obtained [50].

During extrusion, high-intensity ultrasound waves affected the die characteristics by reducing the die pressure, die swell ratio and melt fracture [14, 48, 51-54]. It was also applied to the process [55] for eliminating the unstable flow of a polybutene melt. The influence of different intensities of ultrasonic vibrations on polystyrene melt characteristics have also been studied previously [2, 13, 56-60]. Ultrasonic vibrations have also been employed to modify the crystalline structure of polyolefins in the film extrusion process [23] with the aim of improving the productivity as well as the quality of the product [16, 48, 53, 61].

Previous studies have also shown that the onset of melt fracture was accompanied by wall slip and the failure of adhesion or inconsistent adhesion at the polymer-metal interface in the die [62, 63]. There are several factors that can affect the onset of melt fracture and these are molecular properties (molecular weight distribution, cross linking) and the processing parameters (temperature, material of the die and extrudate)[56]. There are numerous well known methods for reducing the melt fracture (blending, chemical modification adding processing aids) but not all of them are cost effective[64, 65].

Superimposing oscillations upon a constant pressure gradient flow of a viscoelastic liquid produces very large increases in flow rate compared with the stationary flow [66, 67].

More recently the effect of both longitudinal and transverse vibrations were studied and a reduction in die pressure, the die swell rate and also an improvement of the mechanical properties were observed [12]. Mechanical oscillations also have an effect on the rheological and mechanical properties of some extrudates. It has been reported that the superposition of ultrasonic waves in extrusion could increase the flow rate of the extrudate without increasing the power consumption of the process for high output rates and it could also decrease the viscosity of polymer melts and improve production rates [48, 66].

Most of the reported studies on the application of ultrasonic vibrations during melt flows [14, 39, 48-50, 52, 54] are for polymer melts flowing through channels with vibrating walls, that is, the shaping channels themselves act as a vibration source. The use of vibrations applied to flow channels may alter the conventional wall-stick condition ($V_z=0$) during melt flow. It's reported that the flow of polymer melt along the channel subjected to ultrasound vibrations is accompanied by a phenomenon, which is equivalent to slippage, by means of a thin layer with a decreased viscosity next to the wall [31, 68]. Generally, a reduction in viscosity and/or an increase in temperature as well as an alteration of the channel wall boundary conditions are proposed as major causes for this behaviour.

A European patent application in 1988 related to the shear processing of thermoplastics in the presence of ultrasonic vibrations. The published results employed ultrasonic vibrations that were applied at an angle of less than 45° to the direction of the polymer melt flow. The extrusion pressure was said to be reduced by 10–23% with the extrudate swelling only slightly reduced and the onset of flow instability was delayed [4, 5, 7, 10, 11, 15, 17, 30, 69-77].

The effects of ultrasound on polymer melts is a complex phenomenon; this should include both physical and chemical factors according to the possible effects that ultrasound could have on the fluid mediums. However, more studies on the causes and effects of the application of ultrasonic vibrations are needed.

In previous studies ultrasonic waves were applied to the die walls or surfaces but a feature that distinguishes this work from previous studies is that, the ultrasonic horn was secured in the melt while the polymer melt flows over the ultrasonic horn. Also the conical shape

of the ultrasonic horn allows simultaneous delivery of shear and compressive waves into the polymer melt where as earlier studies focused either on shear or compressive waves, with the compressive waves known to be more effective.

In this chapter, an ultrasound assisted extrusion setup is described, that allows the application of ultrasound vibration to the polymer melt at the shaping head (the die). The characterization of the extrudate structure and processing parameters were combined to investigate the mechanism for the effect of ultrasound on the polymer melt flow.

3.2   Experimental

3.2.1   Materials

Two commercial pipe extrusion grades of polyethylene were used PE80 and PE100. PE80 and PE100 had melt flow rates of 0.33 g/10min and 0.24 g/10min respectively under a load of 5.0Kg at 190°C. PE80 and PE100 are both commercial pipe grades of HDPE containing carbon black. The materials were manufactured by BOREALIS[1] and were supplied by Polypipe Terrain[2] in the typical granular form.

3.2.2   Design of 1st generation ultrasonic horn (G1) and the housing block

The assembly that accommodated the ultrasonic horn as seen in the Figure 3-1 consisted of three sections that are the top block, mid block (feed block) and bottom block. The top block secured the ultrasonic horn by clamping the flange between the top and mid block. The melt flow channel in the ultrasonic die is shown in Figure 3-2.

---

[1] Borealis is a leading provider of chemical and innovative plastics solutions, the PE80 and PE100 were both manufactured by Borealis.

[2] Polypipe Terrain is one of the Sonoflow Consortium partners and is one of the largest plastic piping systems manufacturers.
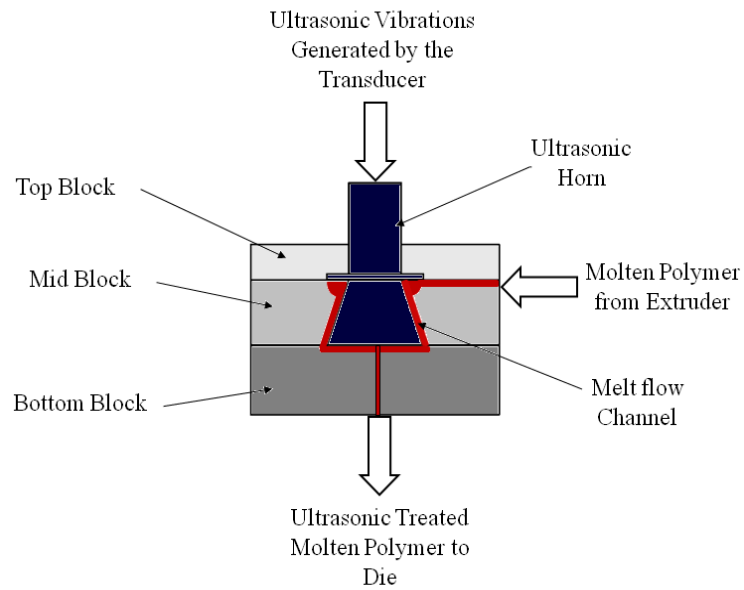
Figure 3-1: Schematic diagram of the ultrasonic horn and the housing block, melt flow channel is shown in red.

The G1 as described earlier in Chapter 2 was a cylinder that was attached to a truncated cone with a flange (see Figure 3-3). The horn was designed to have a node in the flange as shown in Figure 2-1 where the horn was clamped between the two die blocks. The conical shape of the horn allowed the melt to benefit from both compressive and shear ultrasonic waves.
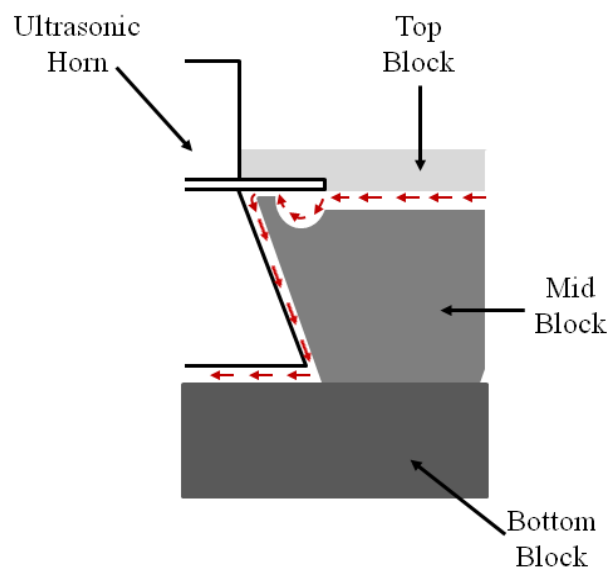
Figure 3-2: Schematic diagram of the ultrasonic die showing the melt flow channel (red arrows).
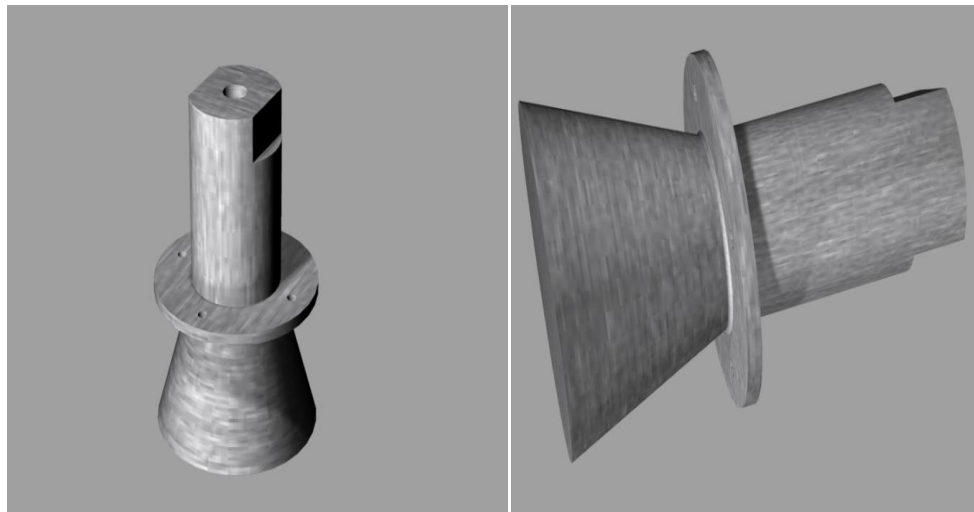
Figure 3-3: 3D Model of first generation ultrasonic horn.

The polymer melt that was produced by the extruder entered the housing block through a 4mm feed hole (shown in Figure 3-4).
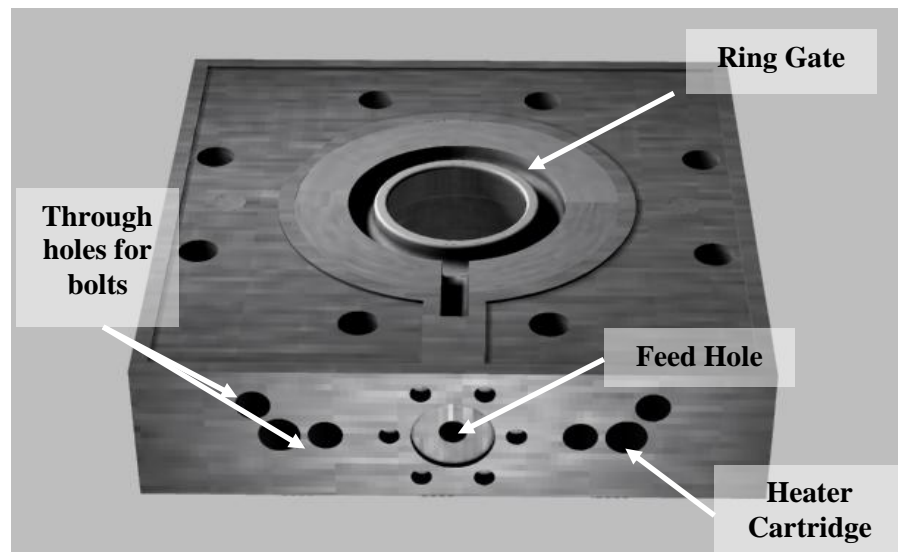
Figure 3-4: 3D Model of mid block and the ring gate.

The melt flowed through the feed hole to the gate section of the mid block, where it was fed around the horn equally from the annular feed channel on the ring gate. In order to distribute the molten polymer evenly around the neck of the horn the ring had a depth of 1mm. The horn was clamped between top block and mid block by the flange positioned at node point of the horn profile as shown in Figure 3-5.
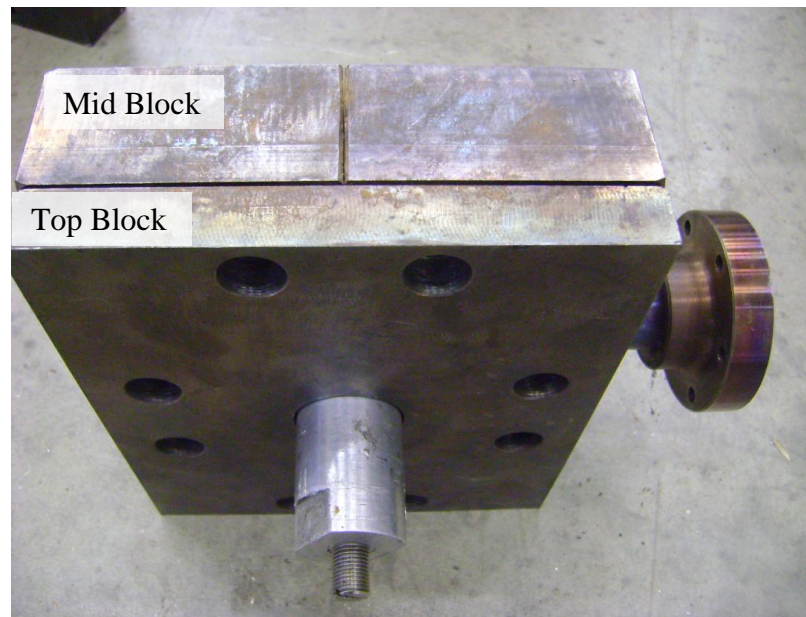
Figure 3-5: Ultrasonic horn clamped between top block and mid block.

With the feed arrangement, the polymer melt flowed uniformly over the conical section of the horn. The clearance between the horn and the outer walls of the flow channel was set to 2mm along the melt flow path. The decision for using this figure was based on the results obtained from the static sonication of the polymer melt. The polymer melt then flowed over the front of the horn (base of the cone) and out of the ultrasonic block through an 8mm diameter hole at the centre. A slit die was connected to the ultrasonic block. A pressure transducer was fitted to the bottom block (see Figure 3-6) to measure the melt pressure at the die exit. The whole block was divided into two heating zones, one on the mid block and one on the bottom block (Figure 3-7). The mid block had a central split line to allow it to be fitted over the conical horn. Two short heater cartridges were installed in each heater hole; one from the right half and the other from the left half of the mid block thus allowing the assembly to be separated without removing the cartridge heaters.
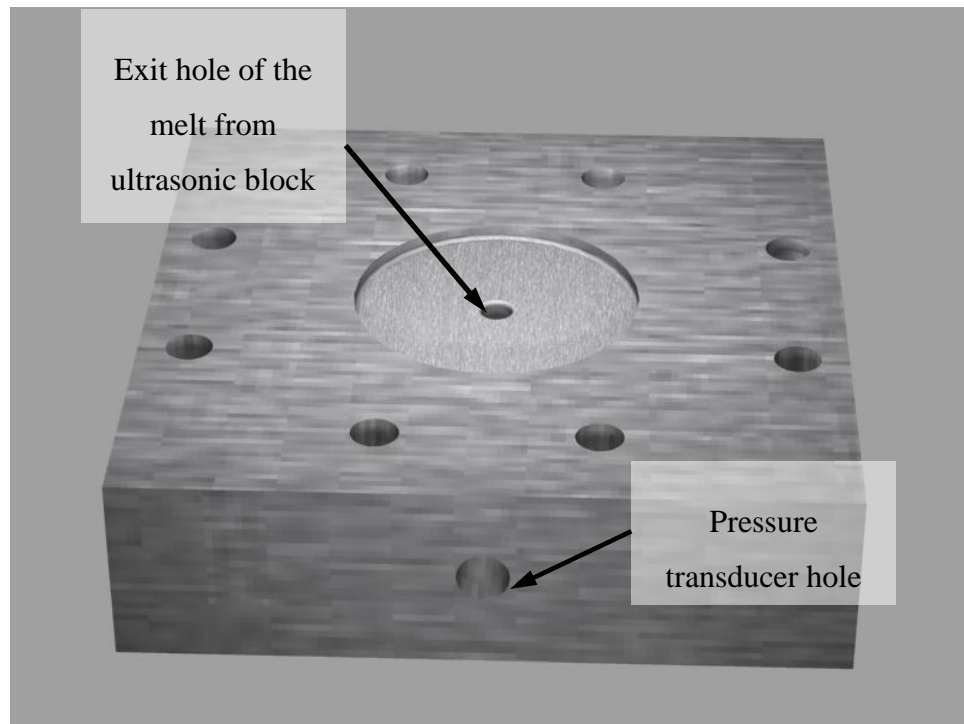
Figure 3-6: 3D Model of the bottom block of the ultrasonic housing block.
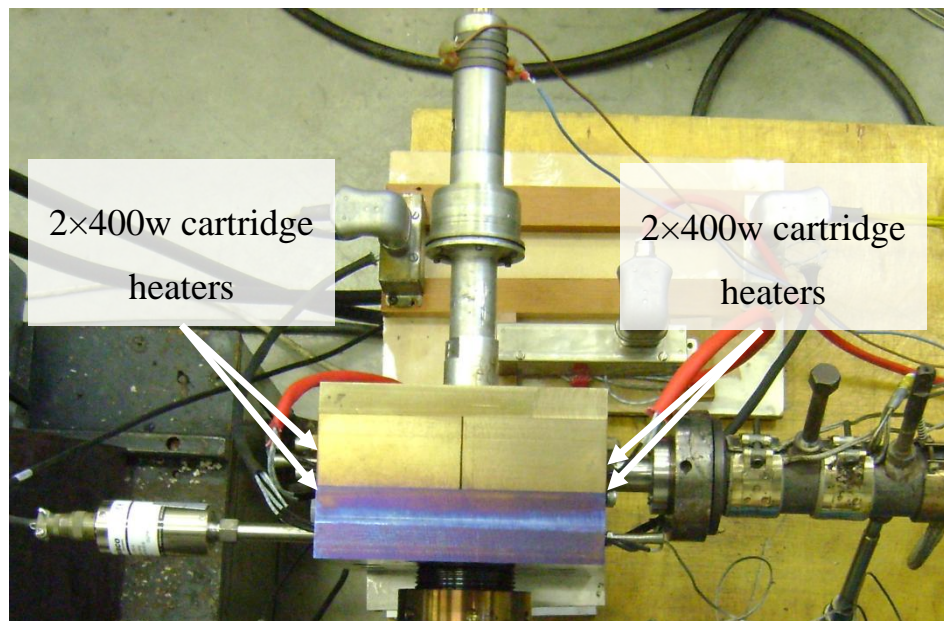
Figure 3-7: Heating arrangement for mid block of the ultrasonic housing block.

Other related pictures for the assembly of the ultrasonic housing block are all presented in Appendix A. The housing block and the G1 horn were designed at Brunel and manufactured by Bootham Engineers[3].

3.2.3 Extrusion of polyolefins by single screw extruder

The most common extruder in plastic processing is the single screw extruder. As described earlier in Chapter 1, an extruder consists of a screw housed in a heated barrel. Most of the barrels are also equipped with a cooling system (air/water). The solid resin is flood fed from the feed throat at one end of the extruder barrel and this can be fed under gravity from the hopper. At the other end of the barrel an adaptor and die are installed. The die forms the extrudate to the required shape which is cooled down to the ambient temperature using blown air and/or a water bath. The extrusion process consists of several parts. The nature of these parts is determined by the specific products. The extruder system that was used to carry out the extrusion processes for this work will be described in detail in the following section.

3.2.3.1 Barrel and feeding

A Betol 2525J 'Jockey' extruder was used for plasticizing the polymer. The screw was a typical 25mm polyolefin screw with L/D ratio of 20:1. The barrel featured a transducer port at the die end that was used to measure the melt pressure in the experiments. The feed throat was kept cold by circulating water through a cooling jacket to prevent the polymer granules from melting in the feed section of the barrel.

3.2.3.2 Heating system of the extruder

The heating system consisted of 5 heater bands, 3 of them 350w and the other 2 were 150w each. The heaters were positioned along the barrel to provide a controlled heating profile along the extruder barrel.

---

[3] Bootham Engineers is one of the Sonoflow consortium partners and has expertise in tool making and manufacturing of molding tools.

Figure 3-8: heating bands of the barrel (left) and power distribution box for heaters and thermocouples.

There was no cooling system fitted to this extruder and the temperatures were only controlled by the power input from the heater bands and heat conducted away to the surroundings.

3.2.3.3 Temperature controllers

The temperature of the 3 barrel zones was controlled by Omron E5CJ temperature controllers connected to the 3 barrel thermocouples. The controllers used the PID control loop feedback mechanism to control the temperature of the barrel and unlike basic PID temperature controllers these benefited from the self tuning feature. As mentioned earlier there was no cooling system installed on the extruder so the shear heating of the resin melt elevated the temperatures on the barrel to some extent above the set temperatures in the controllers.

3.2.3.4 Torque and screw speed indicators

The screw speed was set by a dial control which could be locked at a desired point if required. The screw speed was displayed on a digital scale on the control panel. The torque in terms of percentage of the total motor power (1.5kW) was displayed on an analogue scale.

3.2.3.5 Screw geometry

The screw was a standard polyolefin screw which had a uniformly tapered compression to the metering zone. This promoted a good melt seal whilst processing and ensured that no flow of the polymer melt was able to travel back towards hopper end of the barrel. The screw was 580mm long with processing length of 530mm and a flight diameter of 25.5mm.

3.2.4   In-situ rheometer die

The slit die that formed the extrudate used in this setup, was also used as an inline rheometer (Figure 3-9). The pressure drop of the polymer melt was measured at two/three points with a known distance between them. From these values the viscosity of the melt was calculated. The die channel width was 24mm and the depth of the channel was 2.5mm. The distance between the two transducers in the die was 80mm. This assembly was connected to the ultrasonic block via a collar with an internal thread and recessed lip. Over this lip a spigot was bolted onto the die with six M6 bolts. Through the centre of the spigot was an 8mm channel that leads to the land section of the die.

3.2.4.1 Heating of the slit die

The die was composed of top and bottom sections with a central split line. Each section was heated by a separate control unit and cartridge heaters with one heating zone on the top plate and another on the bottom plate.
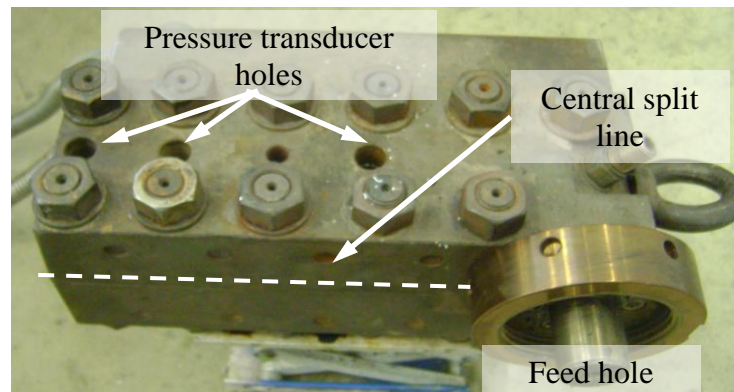
Figure 3-9: Slit die rheometer showing the feed hole and also the pressure transducer holes.

3.2.5   Characterization and Testing

3.2.5.1 Processing Parameters

There were several processing parameters that could be recorded and compared for the conventional and ultrasonic assisted processing. In order to discover the benefits of the introduction of the ultrasonic waves to the polymer extrusion it was necessary to measure as many parameters as possible for comparison. The parameters that were measured in the extrusion experiments were melt pressures, temperatures and power consumption. The details of the measurements are as follows.

- **Pressure**: a total of 5 Dynisco and Kistler pressure transducers were fitted to the barrel, the ultrasonic block and the slit die to monitor the pressure of the polymer melt at the metering zone of the barrel, the interface between the extruder and the ultrasonic die and at the exit of the ultrasonic die. The transducers were all wired to Dynisco 1390 digital monitors. The meters could be switched on/off and calibrated independently. The recorded values for the melt pressures in the slit die were used to calculate the viscosity of the melt.

- **Extruder Motor Current:** Extruder motor power draw was calculated from the motor size (kW) and the torque measurements. An analogue dial which was fitted on the extruder control panel was used to measure the motor torque. A Hall effect

standard multimeter was used to measure the motor current. The motor current values were used as an indication of the motor power consumption.

- **Temperature**: The temperatures of the extruder barrel, ultrasonic block, slit die and the extrudate were recorded. The barrel temperatures were read from the digital meters installed on the controller panel. The temperatures for the ultrasonic block and the slit die recorded were measured using the digital meters in the auxiliary temperature controller boxes.

- **Output rate**: The output rate of the extrudate was determined by taking the extrudate produced during a known period of time and weighing it. In order to increase the accuracy of the results 3 measurements were taken and the average value was reported.

3.2.5.2 Material Properties

The ultrasonic vibrations despite their effects on the processing parameters, were believed to make significant changes to the material's structure too. To study the level of changes in the properties of the product it was essential to carry out several tests and characterization techniques on the extrudates. Mechanical, thermal and rheological properties of the extrudates were the main targets of the characterization techniques used in this study. The details of the tests were as follows.

- **Mechanical Properties**

  Tensile Properties: Dumbbell Tensile Test samples were punched from the extruded strips using the CEAST punch cutter with the standard dimensions of Type 5A specimens as defined in BS EN ISO 527-2:1996. The tensile tests were carried out on the Instron machine equipped with Zwick/Roell Smart Pro software and drive motor. The tests were carried out with crosshead speed of 1mm/sec and 5mm/sec for modulus measurement and yield strength measurement of the samples, respectively. The modulus of the samples was calculated in the initial linear part of the stress strain curve in strain range of 0.05% to 0.25%.

Dynamic Mechanical Analysis: Dynamic Mechanical Analysis was used to investigate material's glass transition temperature and dynamic mechanical properties. The DMA tests were performed on a TA Instruments – Q800 in the temperature range of -140°C up to 50°C with heating rate of 3°C/min.

- **Thermal Properties**

Differential Scanning Calorimetry (DSC): Standard differential scanning calorimetry was carried out on samples prepared from the extrudate at different screw speeds as well as from the resin granules to determine the degree of crystallinity, melting point and enthalpy of melting. DSC tests were performed on a TA Instruments – DSC Q2000 using standard aluminium pans under nitrogen purge gas atmosphere from -80°C to 180°C with the heating rate of 10°C/min and cooling rate of 5°C/min.

- **Rheological Tests**

Melt Flow Rate: The melt flow rates of the polymers were determined using a HAAKE Melt Flow ST. The tests were carried out using a 5Kg load at 190°C for each material. 5 samples were taken and the average value reported.

Capillary Rheometry: The rheological properties of the granules were measured at different shear rates and temperatures. Capillary tests were performed on granules using the GOTTFERT Rheograph 6000 in a single bore mode for shear rates of 1.152s^{-1} to 2553.75s^{-1} and temperature range of 170°C to 190°C with increment of 5°C. In order to compare the rheological properties of the extruded samples with and without USVs, samples cut from extruded materials were also tested using the same test setting used for the granules.

3.3   Results and Discussion

3.3.1   Extrusion processing

Two sets of extrusion experiments were carried out, one with and one without the slit die. For each material, the processing was carried out at 5 different screw speeds. All the processing parameters were recorded for both the conventional and ultrasonic assisted extrusion processes. The slit die and Betol chill rolls were employed to produce polymer strips. The temperature setting of the extruder for the production of the strips is shown in Table 3-1. The polymer test strips were produced by cooling the extrudate from the slit die using chill rolls.

Table 3-1: Processing temperature of PE strips.

Screw Speed	Barrel Temperature			US Block		Die
(rpm)	zone 1	zone 2	zone 3	Temp.		Temp.
10 – 50	160	180	195	195	195	190

After the initial runs, it was noticed that the material was leaking from the die between the mid, top and bottom plates. The high pressure in the die pushed the material through the plates. This was corrected by reducing the contact area between the plates as shown in Figure 3-10.

Figure 3-10: The contact surfaces between top and mid block. The contact surfaces of top block (right) with mid block (left) is shown with light blue.

After the modification of the mid block, the melt leak was resolved and the rest of the trials were carried out.

3.3.2   Processing Parameters

The effect of USVs on the processing parameters of melt pressure (barrel, ultrasonic block and die), temperature, output rate and extruder power consumption was investigated. Two sets of experiments were carried out using the two commercial grades of polyethylene (PE80 and PE100). The initial extrusion trials were carried out without the presence of the slit die for both the conventional and ultrasonic assisted processes with only the processing parameters being investigated. The extrusion with the slit die was then carried out with the same two polyethylenes. In order to study the effect of different residence times in the ultrasonic block, the experiments were carried out for a range of output rates. The screw speed was taken as being representative of the output rate because it is directly proportional to the output rate. Amongst the processing parameters that were affected most notably were the barrel pressure, the melt temperature and the extruder motor current.
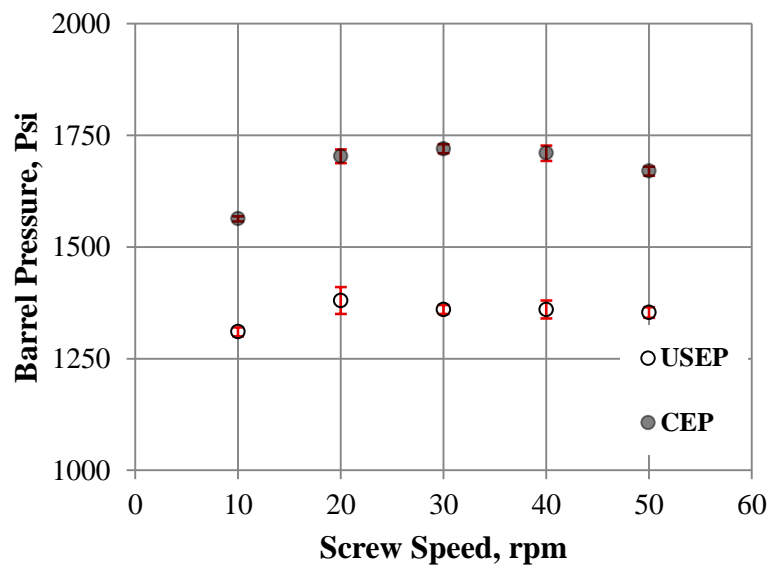
Figure 3-11: Barrel pressure vs. extruder screw speed for PE80 without slit die.

All the experiments were repeated three times and the values plotted were the averages of all three sets of measurements. The results are shown in Figure 3-11.

It can be seen from Figure 3-11 that by applying the ultrasonic vibrations during extrusion, the barrel pressure decreased and the pressure reduction (P_{CEP} - P_{USEP}) decreased slightly by increasing the screw speed. The higher screw speeds meant a lower residence time of the melt in the ultrasonic block and therefore, less exposure to the ultrasonic vibrations. The results presented in Figure 3-11 show this effect. A possible reason for the reduction of the melt pressure at the barrel by the application of the ultrasonic vibrations could be that a decrease in the friction between the horn and the polymer melt was created and caused the melt to effectively slide over the ultrasonic horn.
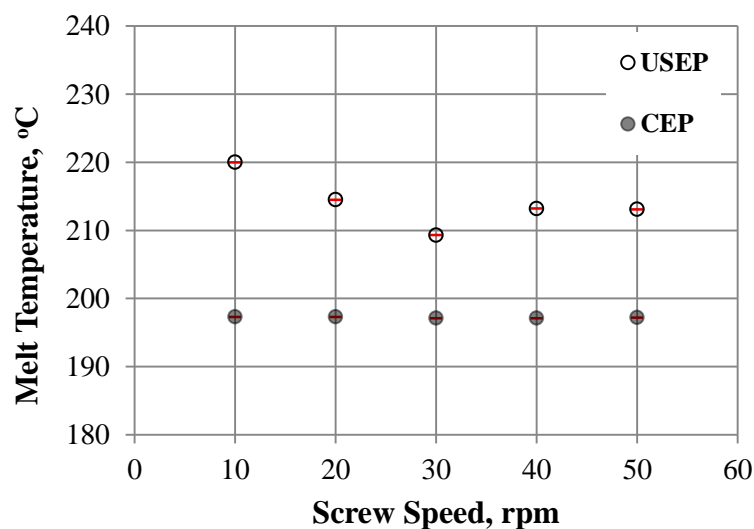
Figure 3-12: Melt temperature vs. extruder screw speed for PE80 without slit die.

A reduction in the barrel pressure will enhance the processing by affecting one of the following parameters.

A higher pressure at the barrel end will require more work to push the material forward and thus will demand more power from the extruder motor. By application of ultrasonic vibrations the head pressure and consequently the barrel pressure can be reduced which can reduce the required amount of work done by the extruder motor to push the polymer melt forward to the end of the barrel.

The melt temperature of the extrudate (not the melt temperature in the barrel) increased as a result of the presence of the ultrasonic waves. It can be seen in Figure 3-12 that the increase in temperature followed a similar pattern to that of the barrel pressure. The

increase in the temperature by the application of the ultrasonic waves was greater for the lower screw speeds than for the higher screw speeds.

This melt temperature increase will be of benefit for the processing of plastics for the following reasons:

- It will allow processing at higher throughput rates (shear rates) by reducing the occurrence of melt flow instabilities and melt flow distortion [9, 34].
- It will allow higher production rates, decrease production time and thus will lead to lower processing cost (labour, machinery etc) as more products can be produced in a certain amount of time.
- It will reduce the materials viscosity by increasing the temperature which will make the flow easier.
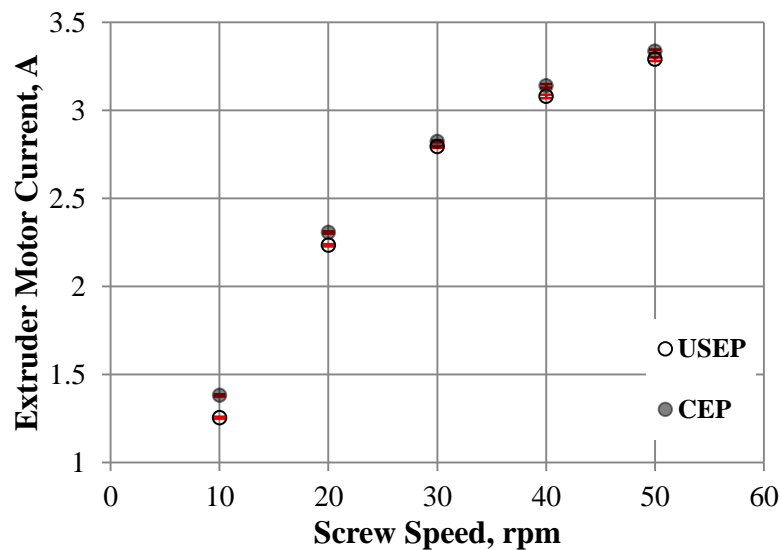
Figure 3-13: Extruder motor current vs. extruder screw speed for PE80 without slit die.

The most important effect of the application of ultrasonic vibrations on polymer processing could be the reduction of the power consumption due to its effects on melt pressure and temperature. The extruder power consumption is represented by the extruder motor current as shown in Figure 3-13. Its value decreased by the application of the ultrasonic vibrations around 10% for the lowest screw speed (10 rpm) and 1.5% for the highest screw speed (50

rpm). It is clear that the reduction of the power consumption will reduce the processing costs.

The same experiments were carried out with PE100 and similar results confirmed a consistency with the results obtained from PE80 experiments.
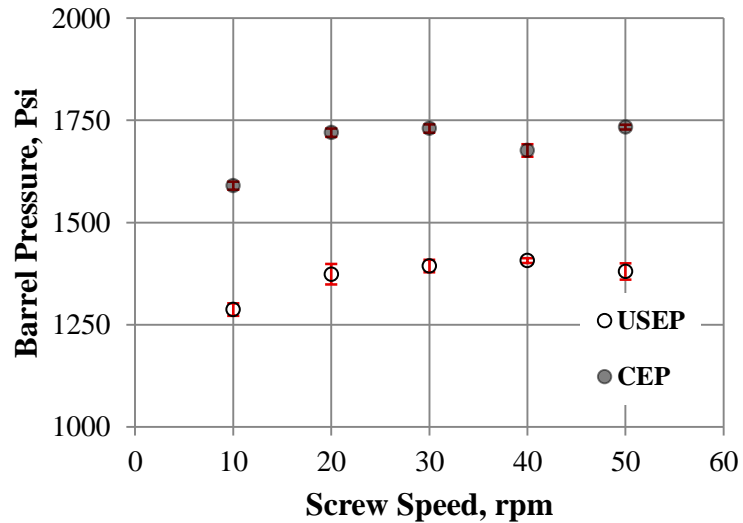
Figure 3-14: Barrel Pressure vs. extruder screw speed for PE100 without the slit die.
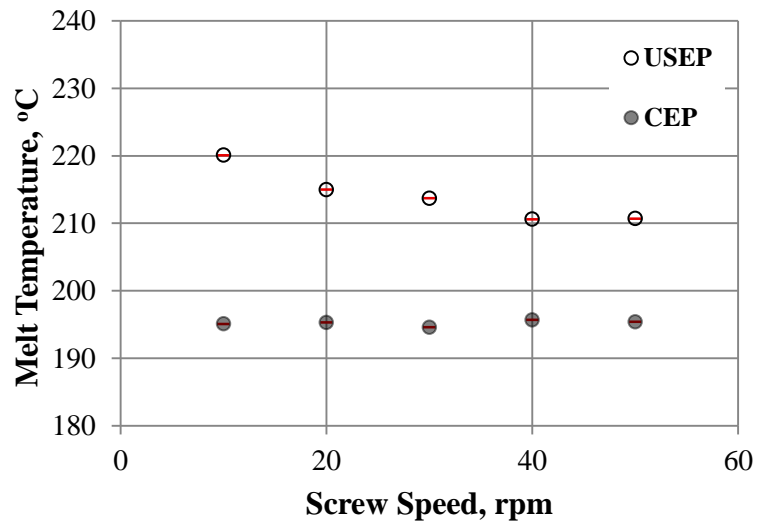
Figure 3-15: Melt temperature vs. Extruder screw speed for PE100 without the slit die.

The melt pressure in the barrel for the extrusion of PE100 with and without the presence of ultrasonic waves is shown in Figure 3-14. For both materials (PE80 and PE100), the application of the ultrasonic vibrations reduced the barrel pressure by an average of 19%.

Figure 3-15 shows the melt temperature of PE100 extruded conventionally and with application for ultrasonic waves at 5 different screw speeds.
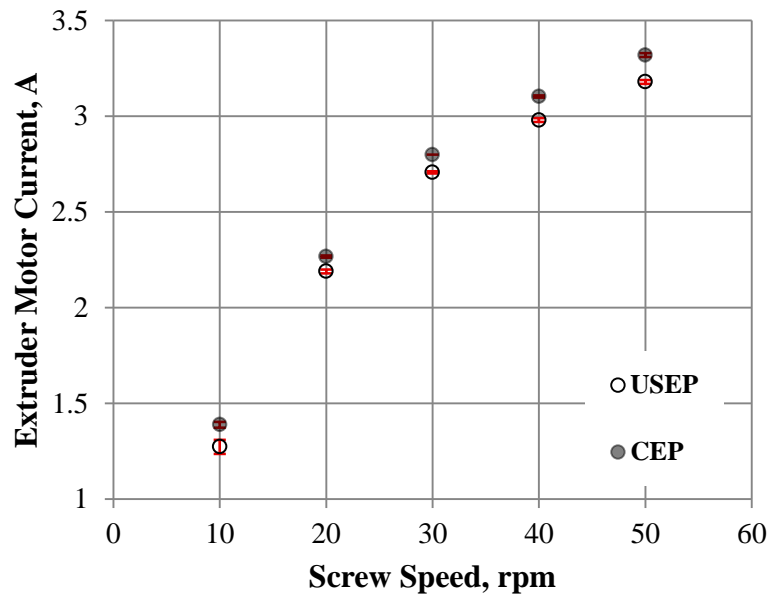
Figure 3-16: Extruder motor current vs. Extruder screw speed for PE100 without slit die.

Applying the ultrasonic vibrations while processing of the PE100 increased the melt temperature by 1% more than the PE80 and the extruder motor also demanded 1% less current. This could be as a result of the slightly higher viscosity of the PE100 than PE80 that allowed a greater dissipation of the ultrasonic waves as heat when travelling through the molten polymer. The extruder motor current results for processing of the PE100 shown in Figure 3-16.

A possible explanation for this could be that, a polymer with higher viscosity than the other (viscosity of PE100 greater than that of PE80) acts as a damping medium for the ultrasonic waves and decreases its penetration depth. At the same time, as a result of higher viscosity the heat generation by dissipation of the ultrasonic waves is greater for a polymer with higher viscosity. The higher the viscosity the more difficult it would have been to push the

melt through the ultrasonic block. Ultrasonic vibrations however, make the melt slip over the ultrasonic horn more easily and at the same time increase the temperature locally. This would promote an easier flow of the polymer melt and would require less power.

The extruder barrel pressure as seen in Figure 3-11 and Figure 3-14 for PE80 and PE100 processing increased by increasing the screw speed up to 30rpm and after that it remained constant. The presence of the die in an extrusion process creates resistance to the flow of the polymer melt through it and consequently leads to an increase in extruder barrel pressure. By plotting the characteristics of a circular die and the extruder operating at different screw speeds it can be concluded that by increase of the extruder screw speed the operating point reaches the plateau region of the die characteristic (see Figure 3-17). In this region by further increase of the extruder screw speed the pressure drop remains almost constant where as the throughput rate increases.
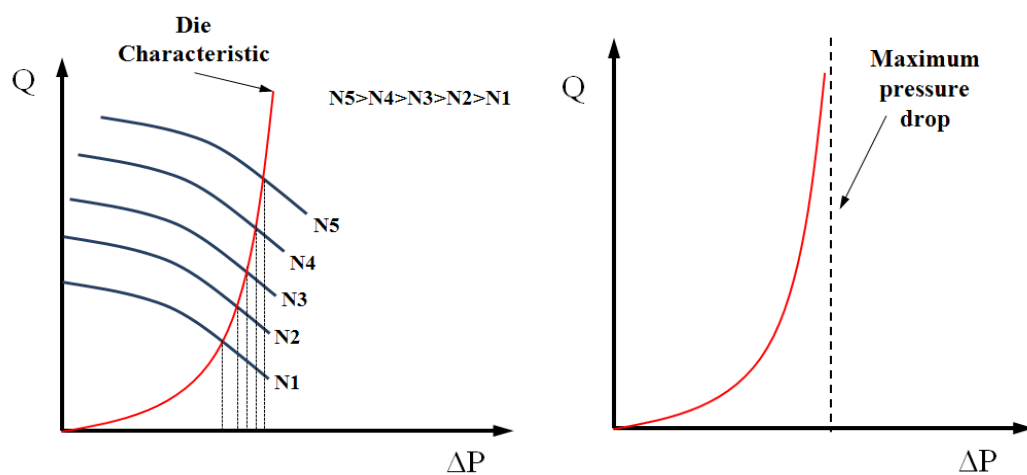
Figure 3-17: Extruder and die characteristic and operating points at different screw speeds adapted from [78] (left), maximum pressure drop for a die according to die characteristic (right) where Q is the output rate, N is the screw speed and ΔP is the pressure drop in the extruder barrel.

The melt temperature of both PE80 and PE100 increased by the application of ultrasonic vibrations. However, difference in the melt temperature reduces as the screw speed increases above 30rpm. Increase in the screw speed does not change the temperature difference. The possible explanation for this could be that for screw speeds above 30rpm the exposure time of the melt to the USVs is too small to make any measurable difference. The USEP extruded melt temperature, however, remained constant for all the screw

speeds. This could be explained by the fact that, increase of screw speed decreased the residence time where in the other hand contributed to heating of the melt through shearing of the melt. The processing parameters that were not affected significantly by the application of the ultrasonic vibration (temperature profile of the extruder barrel and output rate) were also recorded and plotted against the extruder screw speed for both the PE80 and PE100 extrusions. These results can be found in Appendix B.

Using the strip die with the pressure transducers, the rheological properties of polymer melt could be measured during the extrusion. The readings from the two pressure transducers were recorded for each screw speed. The distance between the transducers (80mm), the channel width and height (24mm×25mm), the material flow rate and its melt density (764 Kg/m^3) were all known. With this data the shear rate and shear stress could be calculated for each screw speed with following equations[79].

$$\tau_w = \frac{\Delta P H}{2L} \qquad\qquad \textbf{3-1}$$

τ_w is the wall shear stress, ΔP the pressure drop in the length of the channel, H the height of the channel and L the length of the channel.

$$\gamma_a = \frac{6Q}{WH^2} \qquad\qquad \textbf{3-2}$$

γ_a is the apparent shear rate, Q the volumetric output rate, W the width of the channel and H is the height of the rectangular channel.

It can be seen in Figure 3-18, that the barrel pressure was reduced around 100 Psi by the application of ultrasonic vibrations. Installing the slit die on the extruder generated a big flow resistance that lead to higher pressures in the ultrasonic block and extruder barrel. The ultrasonic vibrations had the same effect on the polymer melt flow but with presence of the slit die these effects were of smaller value (around 100 Psi for melt pressure) when compared to the ultrasonic assisted extrusion of the polymers without the slit die. On the other hand presence of slit die increased the pressure in the ultrasonic block that affected the performance of the ultrasonic system. The only contribution of the ultrasonic vibrations to reduce slit die flow resistance was to deliver polymer melt with higher temperatures and

thus slightly lowered the viscosities (around 20 to 400 Pa.s depending on the extrusion screw speed) compared to conventional extrusion.

Figure 3-19 shows the extruder barrel pressure measured for different output rates for the extrusion of the PE80 with and without presence of ultrasound and with and without the slit die. It can be seen that the effect of the ultrasonic vibrations on the barrel pressure was significantly higher when the slit die was not present.
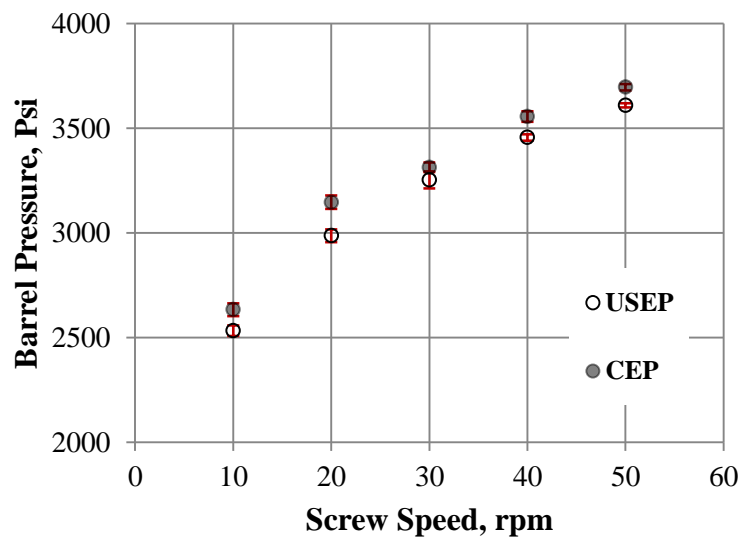
Figure 3-18: Barrel pressure vs. Extruder screw speed for PE80 with the slit die
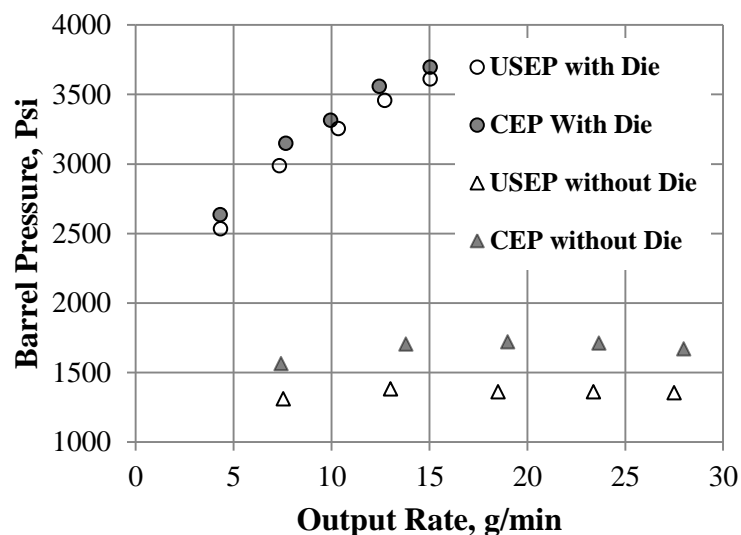
Figure 3-19: Barrel pressure vs. Extruder Output rate for PE80 processing with and without presence of slit die.

The effect of the USVs on the barrel pressure without the slit die was approximately twice the effect with the die. In the extrusion without slit die, application of USVs reduced the resistance of the ultrasonic block to the melt flow and consequently the barrel pressure was reduced. The resistance of the slit die to the melt flow is greater than the ultrasonic block as it can be seen from the pressure generated in the extruder barrel shown in Figure 3-11 and Figure 3-18. By addition of the slit die to the extrusion process, effect of the application of USVs on the barrel pressure became less significant. Then it is quite clear from Figure 3-19 that the barrel pressure was more flow dependant and had an almost linear relationship with output rate while processing with the slit die. The barrel pressure for processing without slit die however was less dependent on the output rate as it can be seen in Figure 3-19. The reason for this is that for processing without the slit die the only resistance was the ultrasonic block which was far less than the resistance of the slit die and the ultrasonic block. This changed the die characteristic and increased the slope, meaning that slope of the linear function between pressure drop and throughput rate was higher for processing with presence of slit die when compared with the slope of the linear function obtained for processing without the slit die (see Figure 3-17).
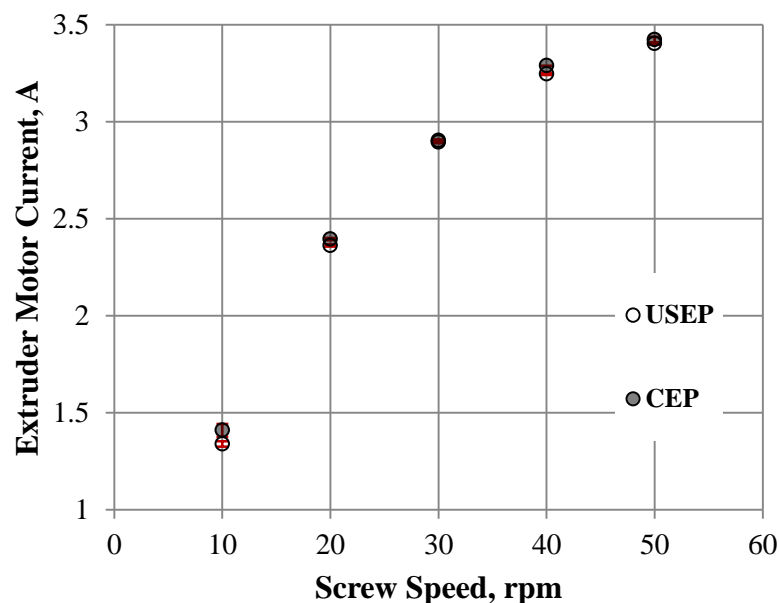
Figure 3-20: Extruder Motor Current vs. Extruder screw speed for PE80 with slit die.
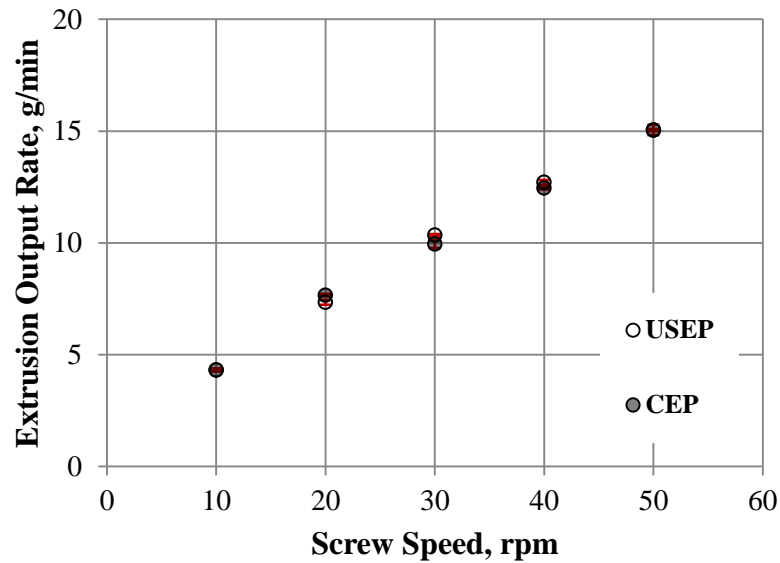
Figure 3-21: Extruder output rate plotted against screw speed for extrusion of PE80 with slit die.

However, the resistance of the die block (ultrasonic block and the slit die) as seen in Figure 3-18 decreased by introduction of ultrasonic vibration to the polymer melt. Figure 3-20 shows that the motor current required for processing PE80 with the slit die decreased but not significantly (around 0.02-0.07A over the range of screw speed) with the application of the ultrasonic vibrations. By comparing the effect of the USVs on the motor current for the extrusion with and without the slit die it can be seen that they had a more noticeable effect on the extruder motor current when processing without slit die.

The measurement of the output rates for the extrusion of PE80 indicated that the output rate through the slit die was not affected by the presence of the ultrasonic vibrations as shown in Figure 3-21.

Power law equation (see Equation 3-3) was fitted to the calculated rheological properties for this setting and the parameters can be seen in Figure 3-22.

$$\eta = k\gamma^{n-1} \qquad\qquad \text{3-3}$$

Where η is the apparent viscosity, k the consistency index, γ the apparent shear rate and n is the power law index.

$$\eta_{USEP} = 40697\gamma^{0.2507}$$
$$R^2 = 0.9993$$

$$\eta_{CEP} = 40423\gamma^{0.2528}$$
$$R^2 = 0.9997$$
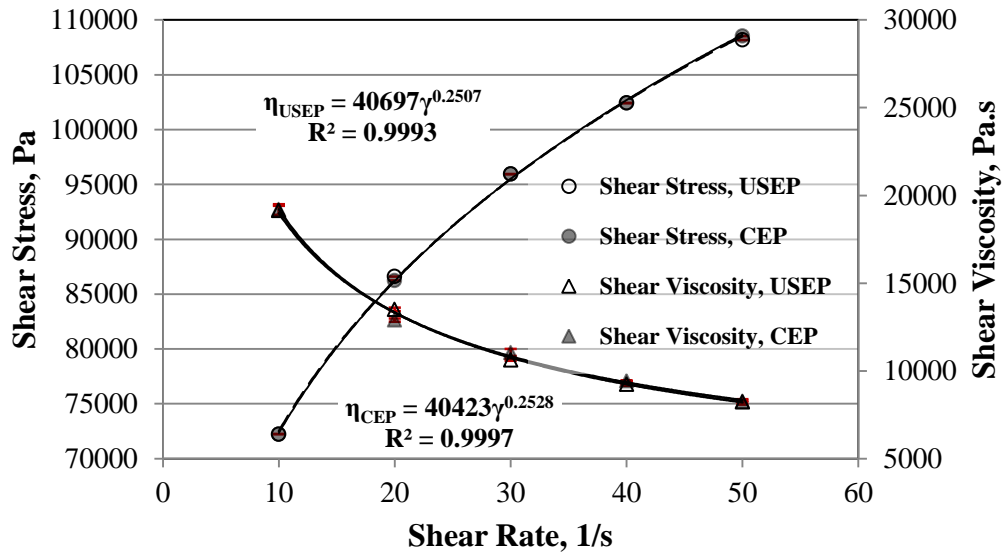
Figure 3-22: Shear stress & Shear viscosity vs. Shear rate for processing of PE80.

The difference between the polymer melt viscosities, measured during slit die trials, processed in the conventional and ultrasonic assisted extrusion can be seen by comparing the power law index (n) and melt consistency index (k) for each curve (Figure 3-22). The shear viscosity for the polymer melt processed with ultrasound was of a slightly lower value when compared with the viscosity of PE80 melt processed conventionally.

3.3.3   Mechanical Testing

3.3.3.1 Tensile Testing

Tensile tests were carried out on dumbbell-shaped test specimens with a gauge length (extensometer) of 25mm and speed of 1 mm/min for the modulus measurements and gauge length of 50mm and speed of 5 mm/min for the rest of the test. Samples were extended to well past yield point.

The test pieces were cut from polymer strips processed with and without ultrasonic vibrations. The tests were carried out on 10 samples from each screw speed and the averages of these results are presented in Figure 3-23. It can be seen from Figure 3-23 that young's modulus for the USV processed samples were greater (~4%) than the conventionally extruded samples for strips processed at 10rpm and 20rpm screw speeds

and this value was almost the same for strips processed at the other screw speeds. Bigger differences were expected between the modulus values for higher USV exposure times (lower screw speeds) and it can be seen from the graph in Figure 3-23 that this trend was applicable for screw speeds of 10rpm and 20rpm.
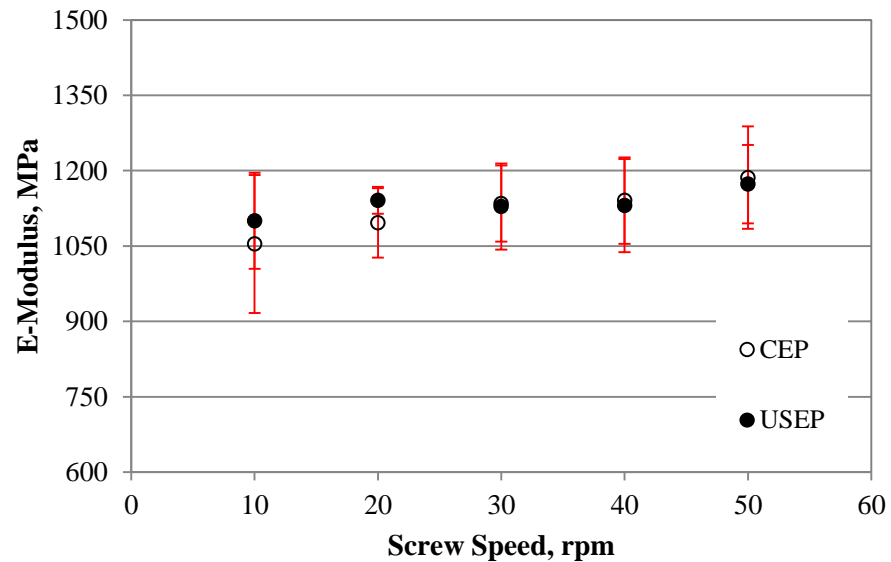
Figure 3-23: Young's Modulus vs. Screw Speed for PE80 dumbbell specimens.

In order to reduce the errors caused by the sample preparation the samples were cut from the same part of the strips. The difference mentioned between the modulus values could be partially due to the sample preparation errors and user errors as it can be seen from calculated standard deviation for the results.

The young's modulus of a material is based on its initial slope of the stress-strain curve or stiffness of material and this could be affected by several possible errors such as slip of the extensometer on the sample.
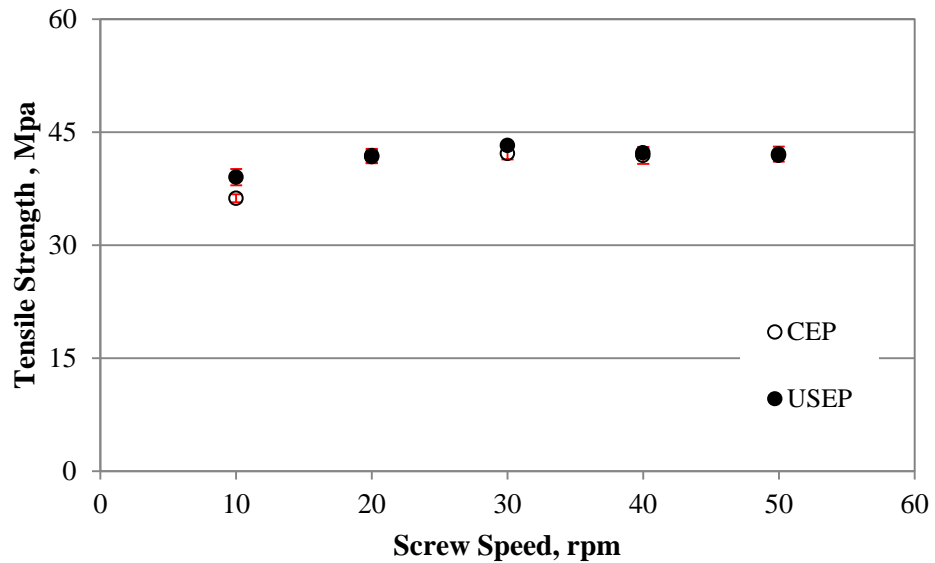
Figure 3-24: Tensile strength of PE80 strips vs. Screw Speed

The necking did not occur for the tested samples (see Figure 3-26) and the strain hardening process started after elongation up to possible yield. For this reason the yield point strength was not measurable for the tested samples. Because of the ductile nature of the polyethylene (ductility), tensile test up to break could have taken considerable time; therefore it was decided to carry out the tensile tests to 60% strain. The tensile strength of the samples in the given strain range was calculated and plotted against the screw speed and is shown in Figure 3-24. It can be seen that, except for the strips processed at 10rpm, the strength of the samples did not change with application of the ultrasonic vibrations. This could be a result of the higher exposure of the melt processed at 10rpm to the ultrasonic vibrations when compared to the strips produced at the other screw speeds.

The stress strain data taken for 10 tested samples was used to generate an average curve using Origin Pro software (mathematical software which can generate average curves from several set of data). The average curves of samples produced with and without the presence of ultrasonic vibrations plotted for each screw speed separately from these curves different stress strain behaviour of the tested samples could be observed. The stress strain curve for 10rpm is shown in Figure 3-25 where for both CEP and USEP processed samples no

necking point can be seen. The curves for the rest of the strips processed at the other screw speeds are provided in Appendix B.
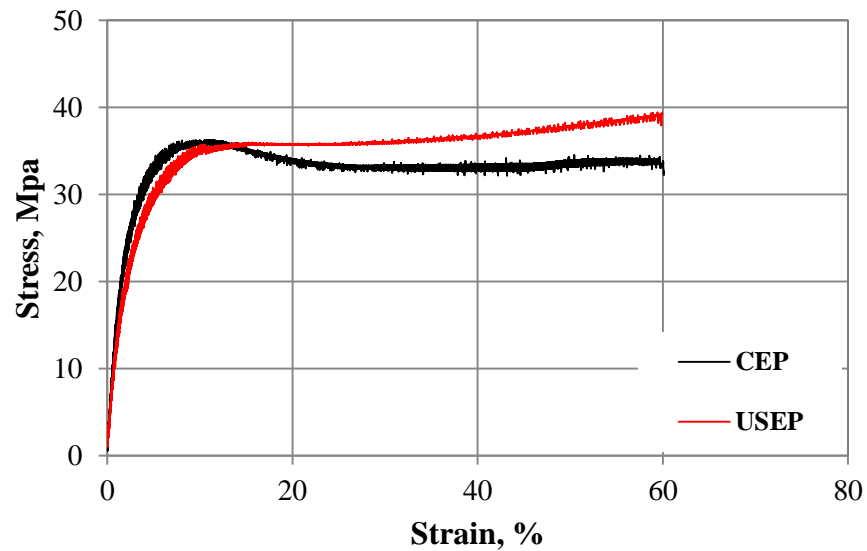
Figure 3-25: Stress vs. Strain for PE80 strips produced at 10rpm with and without presence of ultrasonic vibrations.

Figure 3-26: Tensile test samples of PE80 strips before (right) and after test (left).

It can be seen in Figure 3-25 that the young's moduli of the samples (initial slope of the curve) are similar while the strength of the samples processed with USV was higher compared to the CEP samples. This could be possibly explained by the entanglements of the chains as a result of application of the ultrasonic vibrations. Photographs of a tensile test sample taken before and after testing are shown in Figure 3-26. It can be seen from

Figure 3-26 that there is no visible evidence of neck formation on the tested samples; this is in agreement with the test results as the yield point was not observed on the stress strain curves of the tests.

3.3.3.2 Dynamic Mechanical Analysis

Dynamic Mechanical Analysis (DMA) was used to investigate the mechanical properties of the samples in a temperature range down to -140°C. Rectangular bars were cut from the strips for the DMA tests. The samples were 8mm wide and 1.5mm thick. The DMA tests were performed on a TA Instruments – Q800 in the temperature range of -140°C up to 50°C with the heating rate of 3°C/min.
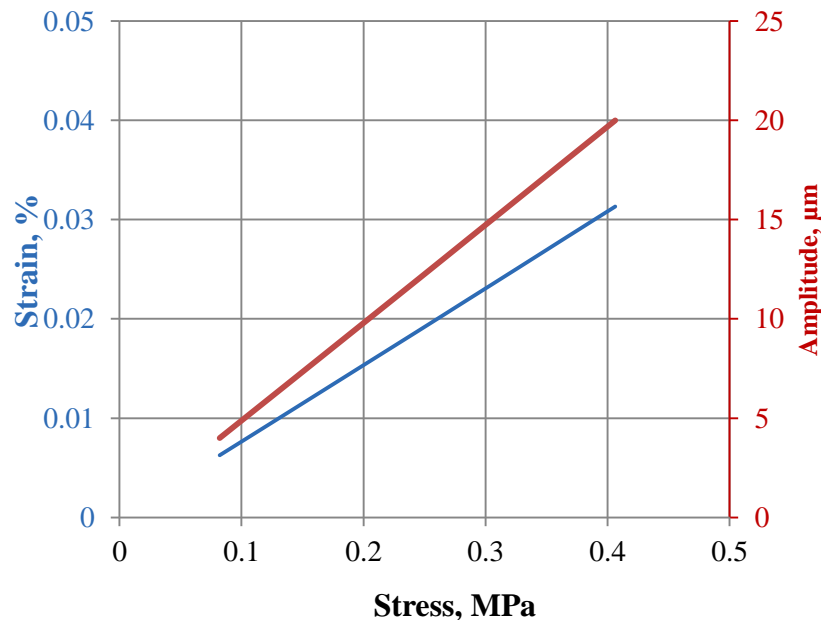
Figure 3-27: Strain vs. Stress curve (left axis) and the Amplitude vs. Stress curve (right axis) for bars of PE80 processed at 10rpm conventionally tested at 35°C.

The DMA tests were carried out on the samples in the single cantilever mode using two standard conditions, a strain sweep and a temperature/frequency sweep. Strain sweep is the test mode which applies sinusoidal waves with different amplitudes and frequencies and measures the force required to reach the defined amplitudes. The stress and the strain are then calculated and used to determine the linear viscoelastic region of the sample. The

amplitude which is within the linear viscoelastic region could be then used for the temperature/frequency sweep test. In the temperature/frequency test a sinusoidal wave with known amplitude and different frequency/ies is applied to the sample in a range of temperature and its response is measured.

Figure 3-27 shows the results obtained from the strain sweep test for PE80 bars processed at 10rpm with the conventional extrusion method carried out at 35°C and with frequency of 1Hz. The stress strain curve for the polyethylene bars at 35°C shows the linear behaviour of the material at the given range of strain. It was important to carry out the DMA tests in the linear viscoelastic region, and thus it was decided to carry out the temperature/frequency tests with amplitudes between 5µm to 20µm. From the determination of the linear viscoelastic region from the strain sweep test, it was decided to carry out the frequency sweep tests with the amplitude of 15µm.
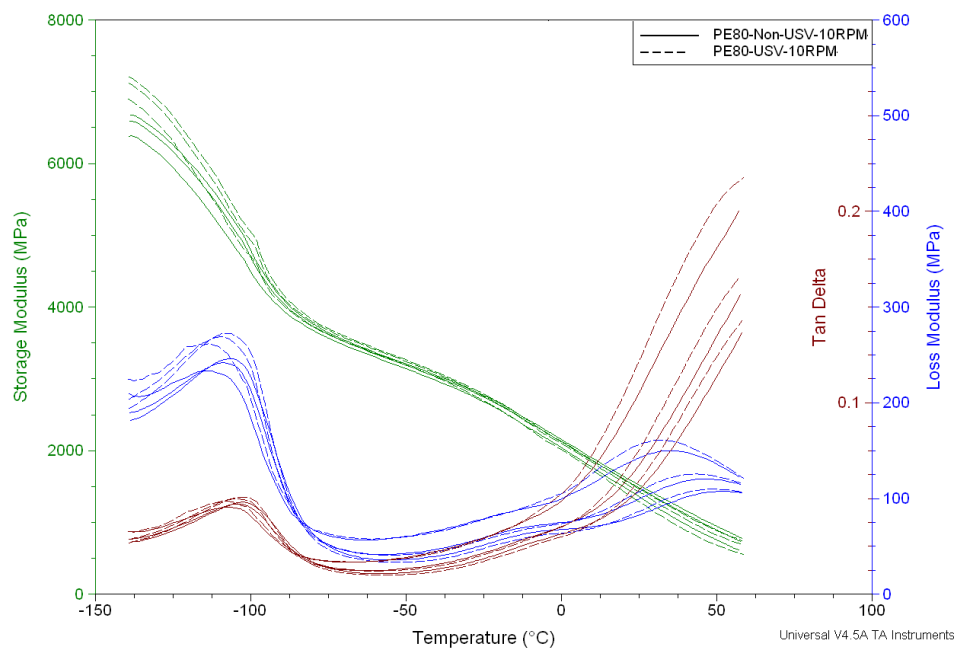
Figure 3-28: DMA Results of PE80 strips produced at 10rpm with and without USVs. The solid line represents the CEP samples data and the dashed line is for USEP samples while for each set of data the curves from top to bottom represent data acquired at 1Hz, 5Hz and 10Hz respectively.

The samples were tested in the temperature range of -140°C up to 50°C and with frequencies of 1, 5 and 10Hz. The results of the tests for samples produced at 10rpm are

shown in Figure 3-28. The Tanδ peak around -100°C represents a transition which is the material's glass transition temperature [80]. The same experiments were repeated for all the samples produced at the other screw speeds.

The results obtained for the 5 different processing speeds are shown in Appendix B. The results suggest that the application of ultrasonic vibrations did not affect the dynamic mechanical properties of the products. In Figure 3-28, it can be seen that the dynamic mechanical properties (storage and loss modulus) of PE80 bars extruded at 10rpm did not change by the application of ultrasonic vibrations. The Tanδ peak was used to determine the glass transition temperatures at frequencies of 1, 5 and 10 Hz and the results are shown in Table 3-2. A small increase (~1°C) in T_g values of the samples was observed by the application of the ultrasonic vibrations (see Table 3-2).

Table 3-2: T_g values obtained from Tanδ peak from DMA tests at frequencies of 1, 5 and 10 Hz for PE80 strips produced at different screw speeds with and without ultrasound.

Screw Speed	Frequency (Hz)	CEP	USEP
	1	-109.45	-108.12
10rpm	5	-104.89	-104.12
	10	-102.34	-101.81
	1	-109.69	-108.74
20rpm	5	-105.61	-105.23
	10	-102.81	-102.14
	1	-108.6	-108.15
30rpm	5	-103.83	-103.61
	10	-101.75	-101.57
	1	-109.27	-108.69
40rpm	5	-105.96	-105.13
	10	-103.21	-102.93
	1	-108.74	-108.31
50rpm	5	-103.71	-103.57
	10	-101.76	-101.29

The time-dependant polymer cooperative segmental mobility as function of temperature follows the Arrhenius equation that is used in many situations [81-87] to investigate the diverse molecular energy dynamics according to,

$$f = Ae^{-\frac{E_a}{RT_g}} \qquad\qquad\qquad \textbf{3-4}$$

$$In \; f \; = In \;\; Ae^{-\frac{E_a}{RT_g}} \qquad\qquad\qquad \textbf{3-5}$$

$$In(f) = \ln(A) - \frac{E_a}{RT_g} \qquad\qquad\qquad \textbf{3-6}$$

Where f is the frequency applied for a test run, A is the pre-exponential factor, E_a is the activation energy and R is the gas constant ($8.314 \; J.K^{-1}.mol^{-1}$). Plotting $ln(f)$ as function of $1/T_g$ gives a linear relationship (Figure 3-29) where:

$$Slope = -\frac{E_a}{R} \qquad\qquad\qquad \textbf{3-7}$$

The obtained glass transition temperatures were then used to calculate the activation energy of T_g.
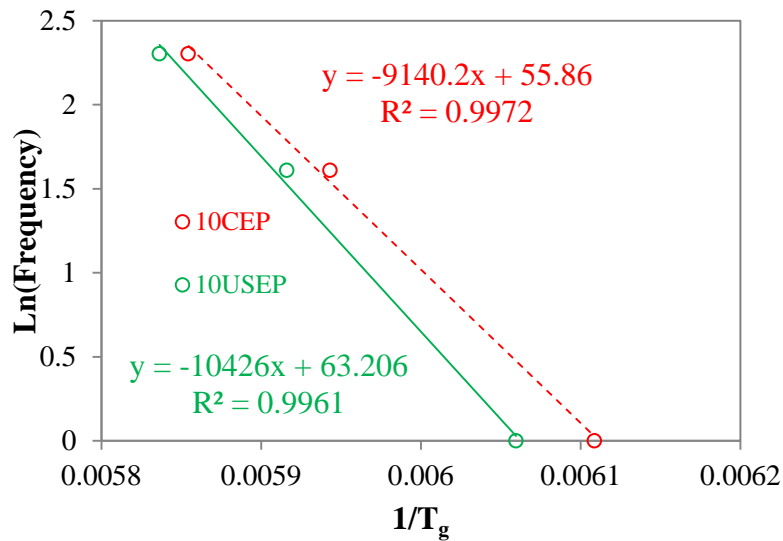
Figure 3-29: The Arrhenius plot for the Tg of the PE80 strips produced at 10rpm by CEP and USEP process measured at different frequencies.

The activation energy of the glass transition temperature was calculated for samples and shown in Table 3-3. Lower activation energy of glass transition temperature is an indication of the homogenous structure/composition of the polymer [88-90].

Table 3-3: T_g activation energies and the regression coefficient of the linear fit obtained from DMA tests for PE80 strips produced at different screw speeds with and without ultrasound (Ea values are in KJ.mol-1).

	10rpm		20rpm		30rpm		40rpm		50rpm	
	E_a	R^2	E_a	R^2	E_a	R^2	E_a	R^2	E_a	R^2
CEP	318.16	0.99	328.59	0.98	329.50	1.00	372.21	0.97	320.80	0.99
USEP	362.91	0.99	344.41	0.96	344.91	1.00	394.21	0.99	324.56	0.99

The calculated activation energies of the samples showed that with the application of ultrasound vibrations the activation energy increased where the maximum increase was observed for samples produced at 10rpm (14%). The difference for the calculated activation energy of the T_g between the CEP and USEP processed samples at higher screw speeds was however, significantly smaller than what observed for samples produced at 10rpm. This could be explained by the greater ultrasonic exposure time of the samples processed at 10rpm when compared with samples processed at higher screw speeds.

Changes in the molecular structure of the samples such as chain scission, disentanglement or branching of the chains could lead to an increase or decrease of the T_g. Some of the factors that could be affected by the ultrasonic vibrations are the chain lengths and chain entanglements. It has been reported previously that the application of ultrasonic vibrations to polyolefins could lead to chain scission and the formation of macro radicals that could cause cross linking [72, 91]. However, the appearance of this effect depends on several factors such as molecular weight, chain branching, chain stiffness, ultrasonic vibration intensity and the application time. Chain scission will lead to lower glass transition temperatures, where cross linking increases the glass transition temperature by reducing the mobility of the chains[92-96]. The increase in T_g, although it is not significant (~1°C), suggests that the molecular structure of the samples could have been affected by the application of USVs.

3.3.4   Thermal Analysis

3.3.4.1 Differential Scanning Calorimetry (DSC)

Differential Scanning Calorimetry (DSC) tests were carried out on the PE80 granules and the processed strips. Approximately 10mg were tested in standard aluminium pans with a heating rate of 10°C/min and cooling rate of 5°C/min. The melting temperature, crystallisation temperature, enthalpy of melting and the crystallisation enthalpy were determined from the tests (see Figure 3-30).
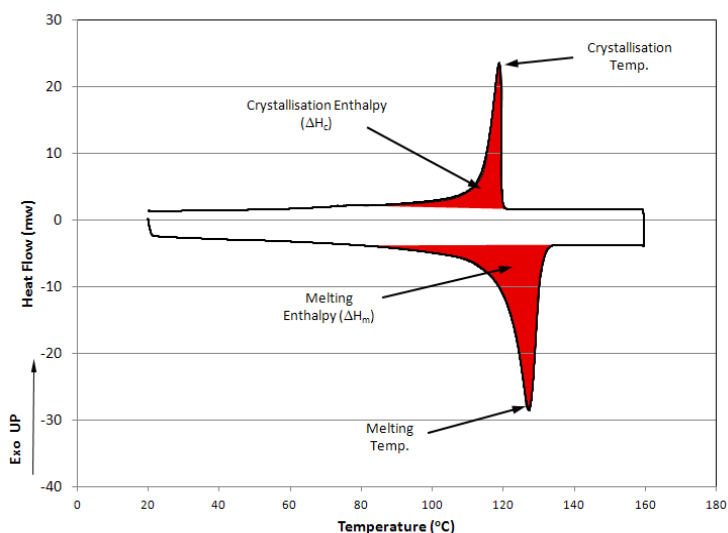
Figure 3-30: Typical PE heat/cool DSC cycle showing melting and crystallisation enthalpies also melting and crystallisation temperature.

The DSC tests were carried out on the PE80 granules in a heat/cool/heat cycle to omit the thermal history. A heat/cool/heat cycle examines the sample with its given thermal history, it uses the cool for additional data and to impose a known thermal history and uses the second heat to examine the sample with a known thermal history as imposed by the cool. However, for comparing the samples processed with and without presence of USVs with similar thermal history it will not be necessary to perform a heat/cool cycle.

Table 3-4 shows the results of DSC tests on the PE80 granules. The thermal properties from each heating cycle are labelled with the cycle name. Comparing the results for first

and second heating cycle it can be noticed that the melting temperature did not change much from first to second heating cycle.

Table 3-4: Thermal properties of PE80 granules obtained from a heat/cool/heat cycle showing melting temperature/crystallisation temperature and melting/crystallisation enthalpies.

$T_{m,1}$ (°C)	$T_{m,2}$ (°C)	T_c (°C)	$\Delta H_{m,1}$ (J/g)	$\Delta H_{m,2}$ (J/g)	ΔH_c (J/g)
128.46	130.95	117.75	116.2	119.3	137.3

All the samples produced with similar method and processing temperatures, which means all of them will have similar thermal history therefore it will not be necessary to carry out heat/cool/heat cycles and a heat/cool cycle will suffice. A heat/cool cycle was used to investigate the thermal properties of samples obtained from the produced strips. All the results were taken from the original DSC curves (provided in Appendix B) and were plotted versus the screw speed for both the conventional and ultrasonic assisted extrusion processes. The results for the melting temperatures of PE80 strips produced at different screw speeds are shown in Figure 3-31. Figure 3-32 shows the crystallisation temperature of the PE80 strips. From the results presented in Figure 3-31 and Figure 3-32 it could be concluded that neither the melting temperature nor the crystallisation temperature were changed by the application of the ultrasonic vibrations to the polymer melt.
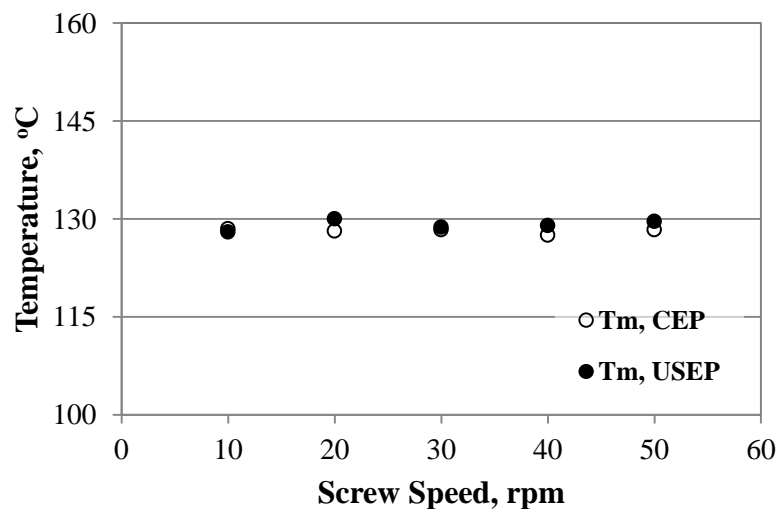
Figure 3-31: Melting temperature vs. screw speed for PE80 strips with and without presence of ultrasonic vibrations.
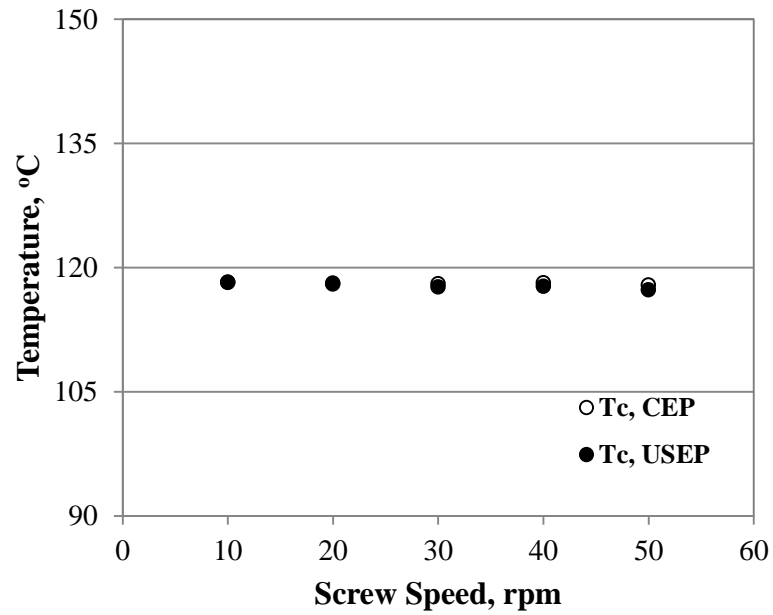
Figure 3-32: Crystallisation Temperature vs. screw speed for PE80 strips produced with and without presence of ultrasonic vibrations.
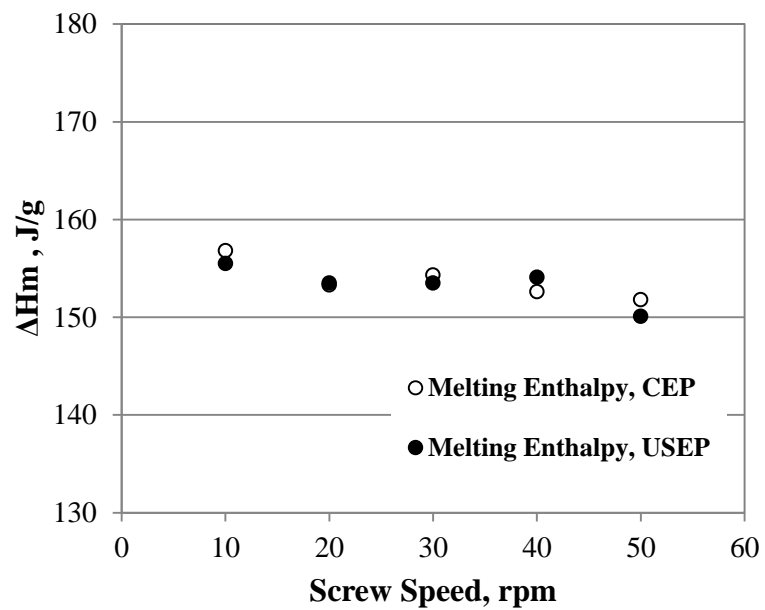
Figure 3-33: Melting enthalpy vs. screw speed for PE80 strips produced with and without presence of ultrasonic vibrations.
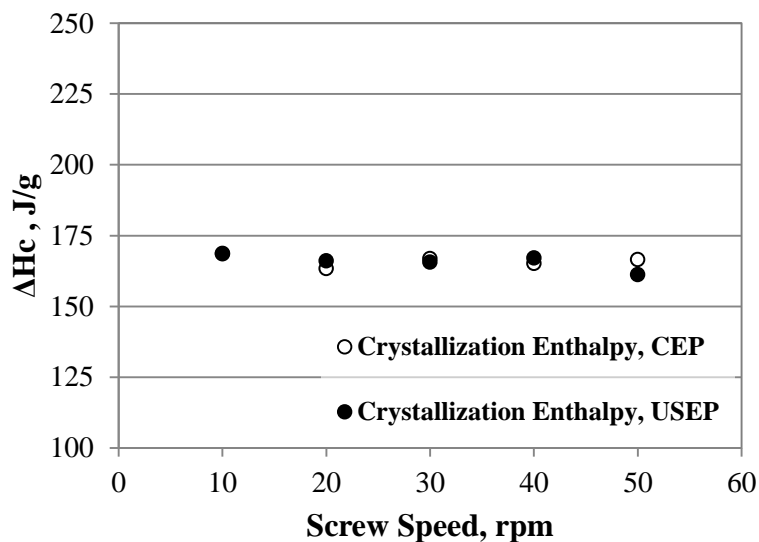
Figure 3-34: Crystallisation enthalpy vs. screw speed for PE80 strips produced with and without presence of ultrasonic vibrations.

The heat of fusion or melting enthalpy represents the degree of crystallinity of the material and therefore significant changes in melting enthalpy indicate considerable differences in the crystalline structure of the polymer. The heating enthalpy for each sample was calculated by measuring the area of the melting peak (see Figure 3-30) in their DSC curve and plotted against the processing screw speeds; the plot is shown in Figure 3-33. It can be seen that the ultrasonic vibrations did not appear to have an effect on the polymer's degree of crystallinity. In addition, the crystallisation enthalpy as measured by DSC remained unchanged for the materials processed with and without ultrasound as shown in Figure 3-34.

3.3.5   Rheological Tests

3.3.5.1 Melt Flow Rate

MFR standard tests were carried out on Polyethylene PE80 commercial grade and 5 samples were used to determine the average value that could be used for the material's MFR. The tests were carried out at $190^{o}C$ and with the loading weight of 5Kg. The MFR results for the PE80 and PE100 shown in Table 3-5 and are in agreement with manufacturers data.

Table 3-5: MFR results and test conditions for PE80 and PE100.

Material	PE80	PE100
Temperature	190°C	190°C
L/D	4	4
Load (Kg)	5	5
Avg. MFR	0.335	0.236

3.3.5.2 Capillary Rheometry

Capillary Rheology tests were carried out on both PE80 and PE100 granules at different temperatures to investigate the polymer melt rheological properties and its dependency on temperature which could be useful in setting the processing temperatures. The rheology tests were carried out in the temperature range of 170°C to 190°C and in a shear rate range of 1.152s^{-1} to 2553.75s^{-1}. In addition to this capillary rheometry tests were carried out in the same shear rate range and at 190°C on extruded PE80 strips processed with and without presence of USVs. The experiments were repeated 3 times for accuracy. A flow curve for each material and each temperature was generated for the apparent shear rate and the apparent shear stress. The results were then fitted to the power law equation. The acquired data fitted with the power law equation quite well for all the data sets as can be seen from the Figure 3-35.

$$\tau = 40507\gamma^{0.2865}$$
$$R^2 = 0.9827$$
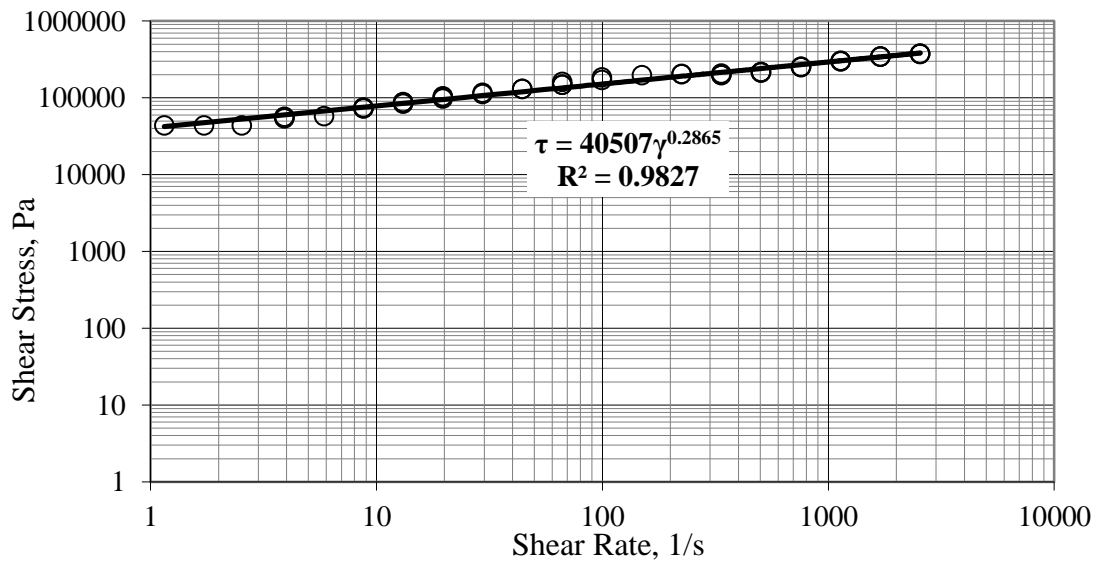
Figure 3-35: Shear Stress vs. Shear Rate for PE80 Granules at 190°C.

$$\eta = 40507\gamma^{0.714}$$
$$R^2 = 0.9972$$
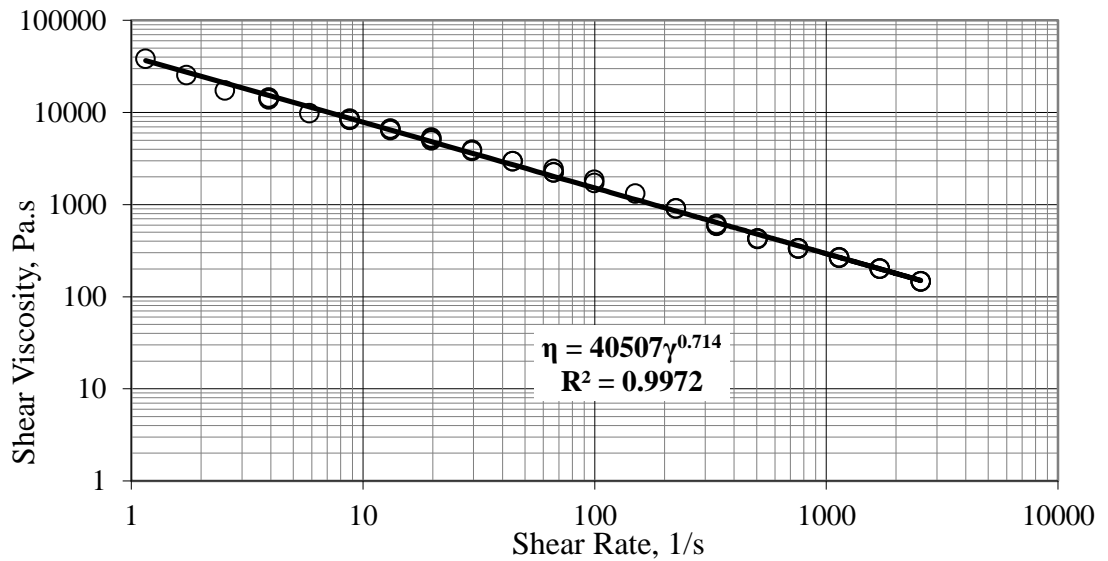
Figure 3-36: Shear Viscosity vs. Shear Rate for PE80 granules at 190°C.

Figure 3-35 and Figure 3-36 show the results of the capillary rheology tests that were carried out on the PE80 at 170°C. The fitting of the data to the power law was with a high regression coefficient. All the other results for the PE80 and PE100 were analysed and fitted with power law equation (see Equation 3-3) and are presented Appendix B. The fitted power law parameters; power law index (n) and consistency parameter (k); are summarised in Table 3-6.

Table 3-6: Power law parameters of equations fitted to capillary rheometry data of the PE80 tested at temperatures of 170, 175, 180, 185 and 190°C.

Temperature	Consistency Parameter	Power Law Index
170	44707	0.29
175	43821	0.2842
180	40140	0.2961
185	40097	0.2942
190	40507	0.2865

A plot of the melt consistency parameter (k) and the power law index (n) against temperature (Figure 3-37) shows that polyethylene's *k-value*, which can be used to represent the polymer's viscosity, decreased as expected. The *n-values* remained almost unaffected by an increase of the temperature and the slight changes which could be

accounted for by experimental errors; do not follow any sort of trend that can be explained by rheological equations and principles.

The apparent viscosity of the melt was calculated from shear stress and shear rate values and plotted against the shear rate for all the temperatures (shown in Figure 3-38).
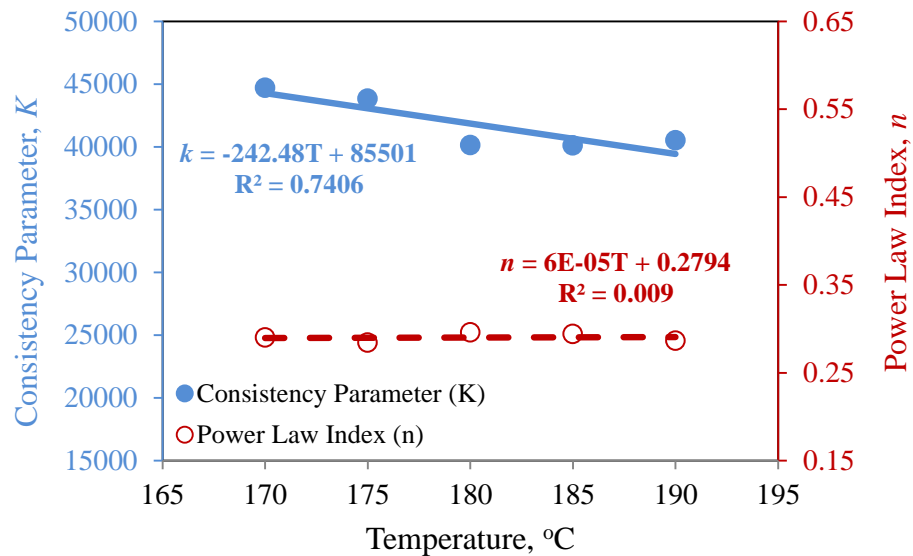
Figure 3-37: Power law parameters (k and n) of PE80 from fitted equations onto accuired data for temperatures from 170°C up to 190°C.
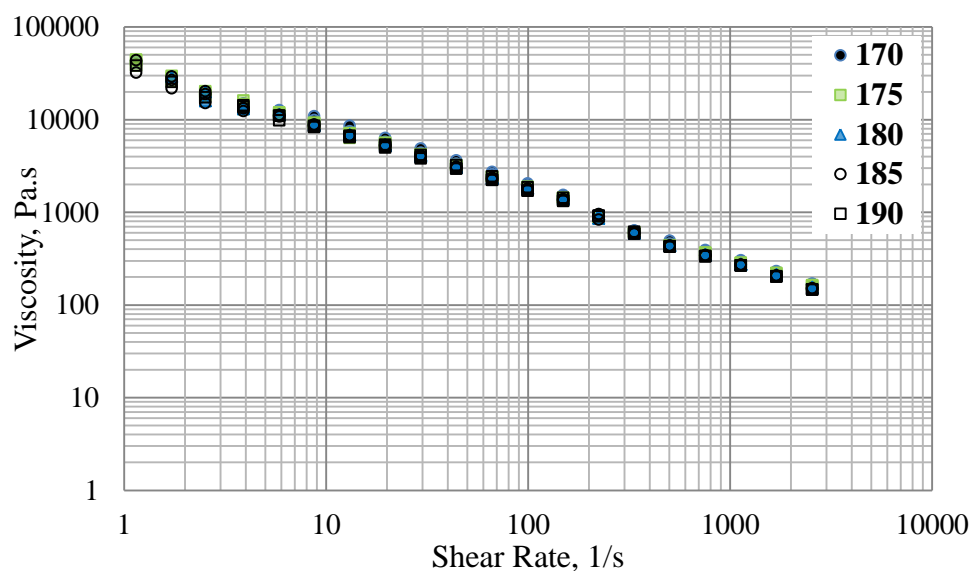
Figure 3-38: Viscosity of PE80 at different Temperatures vs. Shear Rate.

The same capillary rheometry tests were carried out on the PE100 and the shear stress-shear rate plot at 190°C is shown in Figure 3-39. The flow curve of the PE100 at 190°C can be seen in Figure 3-40.
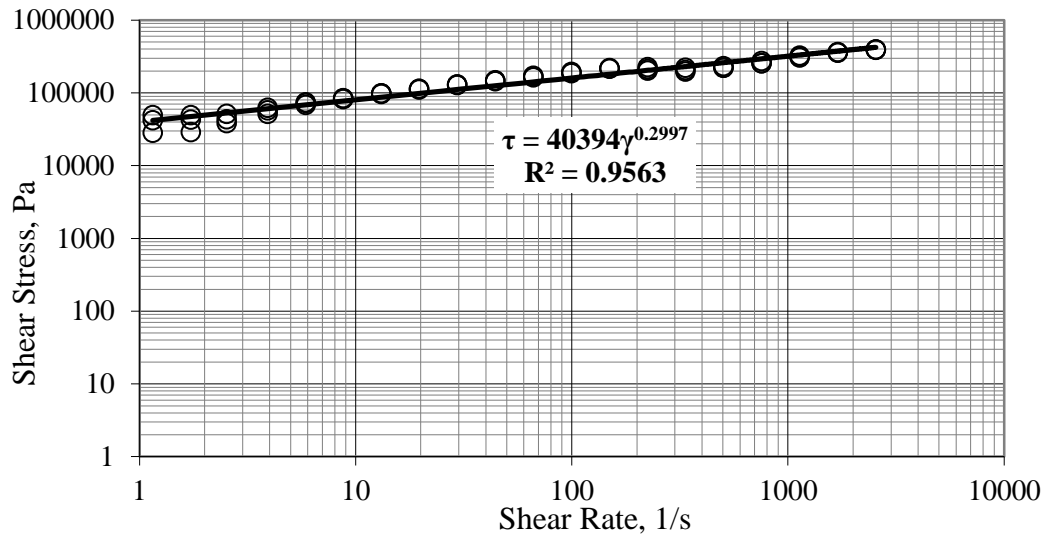
Figure 3-39: Shear Stress vs. Shear Rate for PE100 Granules at 190°C.
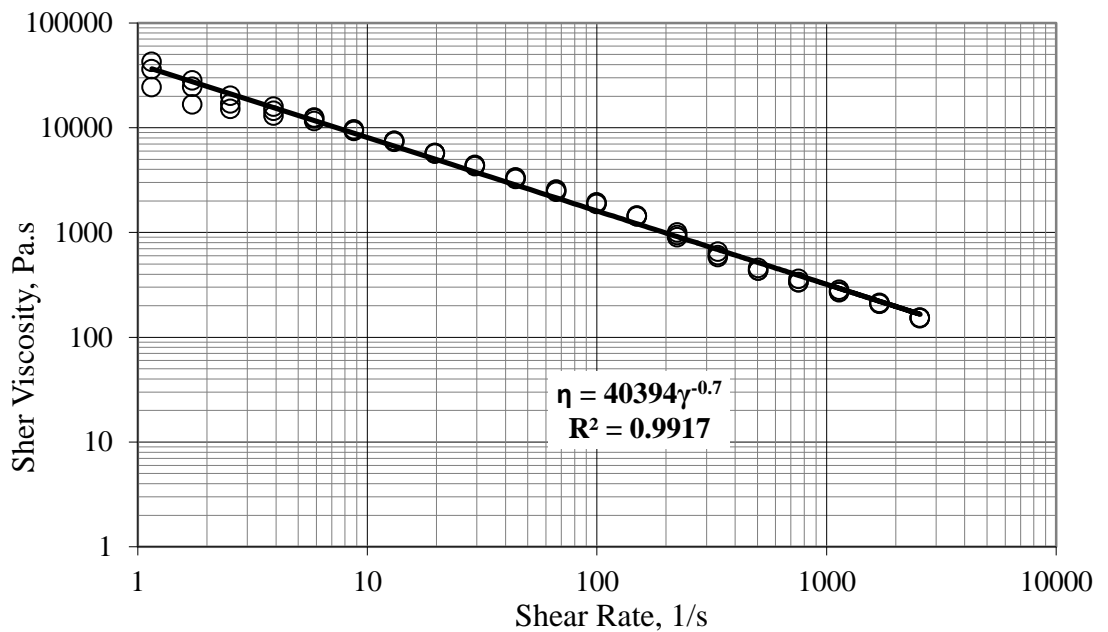
Figure 3-40: Shear Viscosity vs. Shear Rate for PE100 granules at 190°C.
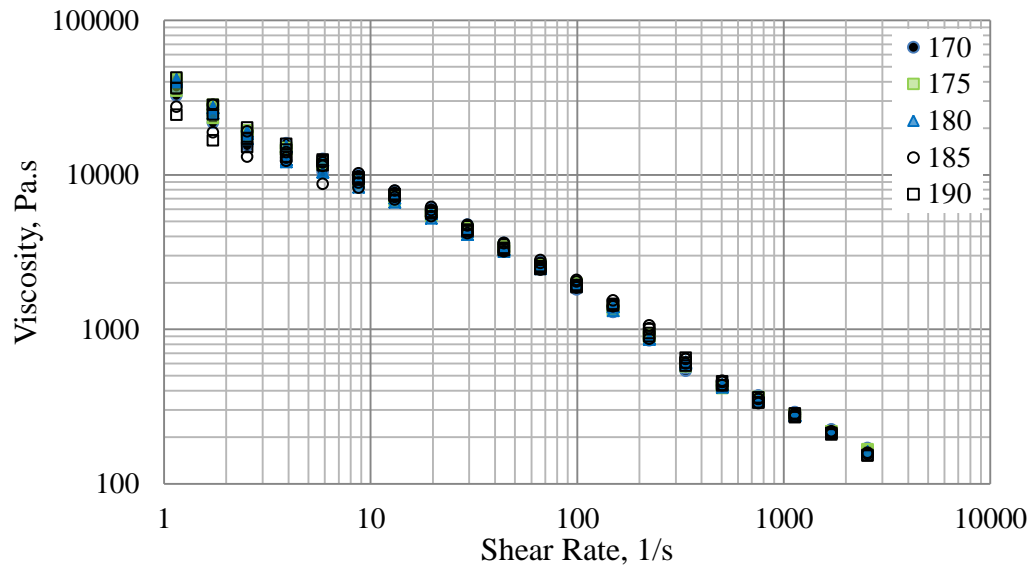
Figure 3-41: Viscosity of PE100 at different Temperatures vs. Shear Rate.

The calculated viscosities of the PE100 melt at different temperatures were plotted against shear rate and shown in Figure 3-41. The viscosity of the PE100 melt decreased by increasing temperature as expected. The decrease of the consistency parameter of the fitted power law (k) is shown in Figure 3-42.
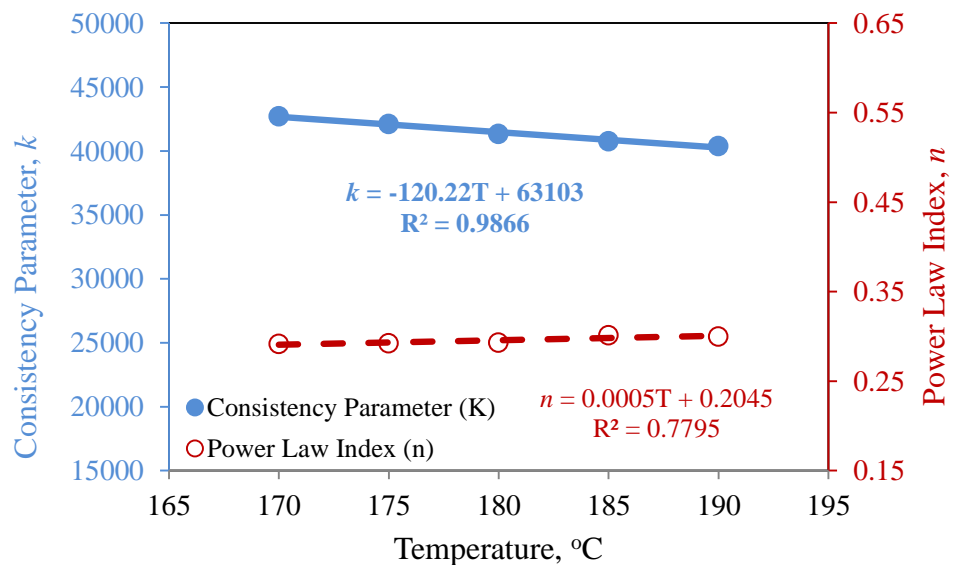
Figure 3-42: Power law parameters (k and n) of PE100 from fitted equations onto acquired data for temperatures from 170°C up to 190°C.

The dependency of the viscosity on temperature can be represented by k, comparing the slope of the linear fit on k values for the PE80 and PE100 suggests that PE80's viscosity is more temperature sensitive than PE100's viscosity.

The produced strips of PE80 with and without presence of USVs were cut and then used for capillary tests. The tests were carried out at 190°C and in the same shear range as granules. The obtained apparent shear stress and shear rate were used to generate a flow curve of the extruded strips at each screw speed. The calculated viscosity is plotted against the shear rate and is shown in Figure 3-43 for strips extruded at 10rpm with and without USVs.
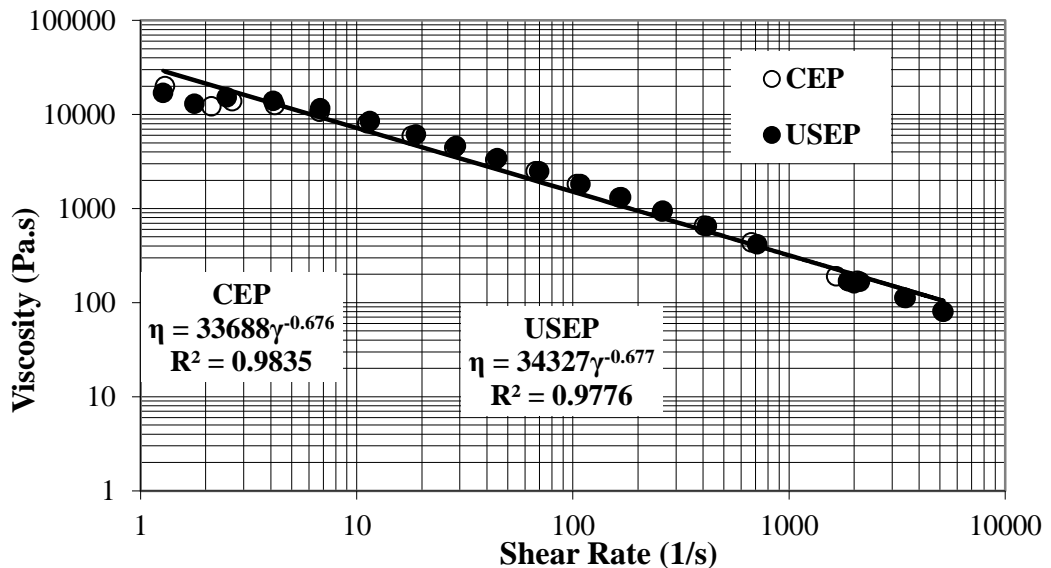
Figure 3-43: Shear Viscosity vs. Shear Rate for PE80 extruded strips with and without application of USVs.

As seen in Figure 3-43 the apparent shear viscosity measured for PE80 extruded strips did not change by application of ultrasonic vibrations. The viscosity of melt is dependant on the molecular weight and the chain length of the polymers especially for high molecular weight polymers such as polyethylene. Therefore these results suggest that ultrasonic vibrations did not affect the chain properties of the polymer melt and as a result of that, the viscosity of the melt remained intact by the application of ultrasonic vibrations. The results obtained from the capillary tests for the extruded strips produced at the rest of the screw

speeds are also in agreement with the results of the strips extruded at 10rpm. These results are presented in Appendix B.

3.4   Conclusion

It has been shown that the application of ultrasonic vibrations to the polymer melt resulted in some changes to the processing parameters and also to the material properties. The effect of the ultrasonic vibrations on the parameters that were affected are summarised below.

- The melt pressure at the metering zone of the extruder barrel decreased by approximately 25% when processing without the strip dies. This value was reduced to 2-3% when processing with the strip die.

- The power consumption of the extrusion process at different screw speeds decreased in the region of 1-9% when processing the PE80 without the strip die and 0.2-5% when processing with the die.

- The measured temperature of the extrudate leaving the ultrasonic die increased 16-23°C depending on the extruder screw speed.

- The tensile test results suggest that by the application of ultrasonic vibrations during the extrusion the young's modulus of the extrudate increased around 45 MPa for samples processed at 10 and 20 rpm but for samples processed at higher screw speeds the values of the young's modulus were similar for USV and conventionally extruded strips. The strength of the extrudate increased by around 2 Mpa for samples processed at 10 rpm by the application of the ultrasonic vibrations and there was no significant difference between conventional and USV extruded samples processed at higher screw speeds.

- The storage and loss moduli obtained from the DMA tests remained unaffected following the application of the ultrasonic vibrations. The glass transition of the samples increased around 1°C for the samples prepared with ultrasonic extrusion compared to the conventional process.

- The results of DSC tests suggested that the melting and crystallisation temperatures did not change by introducing ultrasonic vibrations to the polymer melt.

- The melting and crystallisation enthalpy values of the strips processed with and without the presence of the ultrasonic vibrations indicated that these properties were not affected by the application of the USVs.

- The PE80's viscosity was more temperature sensitive compared to PE100 and it can be concluded from the capillary rheometry test results. Comparison of the rheology results for the conventional and ultrasonic assisted extruded strips suggest that application of the ultrasonic vibrations did not change the rheological properties of the extruded products and melt structure.

The characterization of the extruded samples suggested that polyethylene extrusion and the formed product could benefit from the application of ultrasound to the polymer melt.

In the extrusion of PE80 it was shown that by the application of ultrasonic waves the pressure drop in the die decreased. The volumetric flow rate through a channel die can be derived from Equation 3-1 and Equation 3-2. It can be seen in Equation 3-8, that Q is directly related to the pressure drop and viscosity of the melt.

$$Q = \frac{\Delta P W H^3}{12 \mu L} \qquad\qquad \textbf{3-8}$$

Where Q is the volumetric flow, L the length of the die channel, H the height of the die channel, W the width of the die channel, μ the viscosity of the melt and ΔP is the pressure drop in the die.

The flow rates for processing of PE80 strips with and without presence of ultrasonic waves were similar as shown in Figure 3-21. By comparing Equation 3-8 for the same volumetric flow rates of ultrasonic assisted and conventional extrusion, it can be seen that the viscosity should be reduced to compensate for the reduction of pressure drop to keep the volumetric flow out of the die unchanged. However, the change of pressure drop measured at the slit die was not of significant value which suggests that the viscosity change was not considerable.

It was shown in Figure 3-11 that the reduction of the extruder barrel pressure from conventional processing to ultrasonic assisted was significant for extrusion without the slit die. By adding the slit die to the extrusion line; however, the reduction in the extruder barrel pressure was reduced when compared to processing without slit die. It can be concluded that with the addition of the slit die to the extrusion line; it presented an extra resistance to the flow of the polymer melt after the ultrasonic block and thus the process did not benefit from the reduction in the die resistance. Therefore the ultrasonic vibrations should be applied in the high resistance end of the die. Based on this conclusion the ultrasonic block was redesigned to operate as a die meaning that USV's was applied in the die itself and not in a feed section to the die. This gives the opportunity to benefit from the reduction of pressure in the barrel with similar throughput rates.

From the tensile results it can be concluded that an increase (4%) of the young's modulus values at 10rpm and 20rpm could be only related to the application of the ultrasonic vibrations to the melt as the other processing parameters were kept similar for both CEP and USEP extrusion. Young's modulus is related to small elastic movements in the material; therefore tensile results suggest that USVs affect the level of crystallinity that reflects the proportions of amorphous and crystalline phase in the sample. However, the DSC results proved that the degree of crystallinity remained unchanged by introducing USVs to the polymer melt. DMA results showed that the glass transition temperature of the CEP and USEP samples was almost similar. From these results it can be said that the crystalline phase of the polyethylene has not been affected by presence of the USVs. The standard error values calculated for the tensile results were high enough to match the difference between the Young's modulus values for the CEP and USEP results. The difference in the modulus could, therefore, be accounted for by experimental errors. Although a difference was observed between the yield strength values for the samples produced in the CEP and USEP mode at 10rpm but at higher screw speeds the exposure of the melt to the USVs was not enough to be measured.

Therefore it could be said that the ultrasonic vibrations affect the polymer structure but it could have been not sufficient to make significant measurable changes by tensile, DMA and DSC characterization techniques.

The tensile, DMA and DSC results confirmed that the structure of the polymer was not changed during extrusion with ultrasonic waves; however, the results from the extrusion trials showed that the processing parameters were affected by the presence of the ultrasonic waves.

By comparing the extrusion results from the sets of experiments carried out without the slit die and with the slit die, it can be said that the effects observed in the extrusion processing parameters were not the result of permanent changes to the polymer structure.

A possible explanation for this is that the dissipation of the ultrasonic waves increases the energy of the polymer chains, enabling them to move more easily. The free movement of the polymer chains would consequently result in a reduction of the pressure generated by the flow resistance.
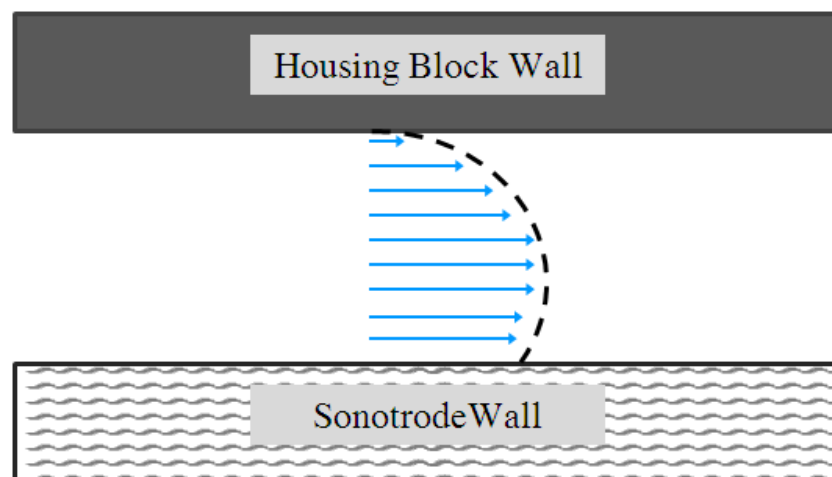
Figure 3-44: Velocity profile of the molten polymer flowing through the channel between ultrasonic die and the housing block.

Ultrasonic waves also change the boundary layer characteristics for the flow of the melt over the ultrasonic horn by reducing the adhesion of the melt to the sonotrode and generating a melt slipping effect. However, it should be considered that the melt will still have the similar flow pattern and boundary layer where it comes to contact with the housing block walls. Thus, the extrusion process here only benefits from reducing the flow resistance on one side of the melt where it is in contact with the sonotrode. The introduction of ultrasonic waves to the walls of the housing block would maximize the

effect of ultrasound on the processing parameters. Based on above mentioned theory the velocity profile for the melt between the ultrasonic horn and the housing block die should be similar to the flow of a viscous fluid between two parallel plates where there is reduced resistance to the flow close to one of the plates. As there was no permanent change measured in the polymer structure, then all the effects observed in the processing parameters should be as a result of either local temperature rise or the modification to the flow pattern. Considering the proposed theory on the flow of the polymer melt through the channel between the ultrasonic die and the housing block, the velocity profile could be similar to that illustrated in Figure 3-44.

The velocity profile shown in Figure 3-44 can be the possible explanation for the experimental results obtained from ultrasonic assisted extrusion, where a significant pressure drop was observed in the ultrasonic block for extrusion with and without slit die in presence of ultrasonic vibrations.

The tensile, DMA and DSC results showed that there was no permanent change in the polymer as a result of application of ultrasonic vibrations; therefore the changes in processing parameters could be the result of a reduction of the resistance to flow in the ultrasonic die.

It was concluded that by addition of conventional dies to the extrusion line, the presented resistance by conventional dies reduced the effect of ultrasonic vibrations on the processing parameters. Therefore to improve the effect of the ultrasonic vibrations they should be applied at the high resistance end of the die.

It was necessary to investigate the effect of USV's for higher melt flow rates to determine its potential for many of the industrial applications including pipe production. However, from the current results the effect of ultrasonic vibrations for higher flow rates is not significant and measurable with the abovementioned methods. In order to benefit from the effects of ultrasonic vibrations at high throughput rates either the exposure time or the ultrasonic vibration power should be increased.

3.5   References

1.   Agassant, J.F., *Polymer processing : principles and modeling*. 1991, Munich: Hanser. 475p.

2.   Cogswell, F.N., *Polymer melt rheology: a guide for industrial practice*. 1981: G. Godwin in association with Plastics and Rubber Institute.

3.   Harris, J., *Rheology and non-Newtonian flow*. 1977, London: Longman. xxxvii,338p.

4.   Wu, H., et al., *Improved Processing Behaviors and Mechanical Properties of Polyolefin Elastomer Blends Prepared by Ultrasound-Assisted Extrusion.* Journal of Applied Polymer Science, 2009. **112**(4): p. 2136-2142.

5.   Peng, B., W.Y. Guo, and Q.P. Ruan, *Ultrasonic Oscillations Effect on Extrusion Processing, Structure, and Properties of Blends of Propylene Based Plastomer and Ethylene/1-Octene Copolymer.* Journal of Reinforced Plastics and Composites, 2009. **28**(22): p. 2701-2715.

6.   Isayev, A.I., C.K. Hong, and K.J. Kim, *Continuous mixing and compounding of polymer/filler and polymer/polymer mixtures with the aid of ultrasound.* Rubber Chemistry and Technology, 2003. **76**(4): p. 923-947.

7.   Wu, H., et al., *Effects of ultrasonic oscillations on processing behavior and mechanical properties of metallocene-catalyzed linear low-density polyethylene/low-density polyethylene blends.* Journal of Applied Polymer Science, 2004. **94**(6): p. 2522-2527.

8.   Gao, X., et al., *Effect of vibration extrusion on high-density polyethylene.* Journal of Applied Polymer Science, 2007. **106**(1): p. 552-557.

9.   Peng, B., et al., *Effects of ultrasonic oscillations on rheological behavior and mechanical properties of novel propylene-based plastomers.* Journal of Applied Polymer Science, 2007. **106**(3): p. 1725-1732.

10.   Alexandru, I.T. and S.D. Voicu, *EXTRUSION PROCESS AND EXTRUSION HEAD WITH ULTRASONIC ACTIVATION*. 1997: Romania.

11.   Cao, Y. and H. Li, *Influence of ultrasound on the processing and structure of polypropylene during extrusion.* Polymer Engineering & Science, 2002. **42**(7): p. 1534-1540.

12.   Casulli, J., et al., *The oscillating die: A useful concept in polymer extrusion.* Polymer Engineering & Science, 1990. **30**(23): p. 1551-1556.

13. Chen, Y. and H. Li, *Effect of ultrasound on the viscoelasticity and rheology of polystyrene extruded through a slit die.* Journal of Applied Polymer Science, 2006. **100**(4): p. 2907-2911.

14. Isayev, A.I. *Effect of Sound and Ultrasound Waves on Polymer Extrusion.* in *23rd Israel Conference on Mechanical Engineering.* 1990. Technion, Haifa.

15. Lee, B.-l. and C. Cranston, *Shear processing thermoplastics in the presence of ultrasonic vibration.* 1988, The B. F. Goodrich Company (Akron, OH) USA.

16. Peshkovskii, S.L., M.B. Generalov, and I.N. Kaufman, *Effect of ultrasonic vibrations on the flow of a viscoelastic liquid.* Mechanics of Composite Materials, 1971. **7**(6): p. 979-981.

17. Piau, J.M. and M. Piau, *Easier flow of viscoplastic materials with ultrasonic longitudinal wall motion.* Journal of Non-Newtonian Fluid Mechanics, 2002. **104**(2-3): p. 185-226.

18. Kuttruff, H., *Ultrasonics : fundamentals and applications.* 1991, London: Elsevier Applied Science. 452p.

19. Rozenberg, L.D., *Physical principles of ultrasonic technology.* 1973, New York ; London: Plenum Press. 515p.

20. RYU, J.G., et al., *Power ultrasonic irradiation on the mechanical properties of polymer blends.* Vol. 2. 2004, Brookfield, CT, ETATS-UNIS: Society of Plastics Engineers. 5.

21. Allan, P.S. and M. Bevis, *U.S. Patent 4,925,161.* 1985.

22. Lemelson, J., *U.S. Patent 4,288,398*, U.S. Patent, Editor. 1981.

23. Pendleton, J.W., *Apparatus for applying ultrasonic vibration to thermoplastic polymers during forming*, in *U.S. Patent 3,298,065.* 1965.

24. Ibar, J.P., *Control of polymer properties by melt vibration technology: A review.* Polymer Engineering & Science, 1998. **38**(1): p. 1-20.

25. Bomal, Y. and P. Godard, *Melt viscosity of calcium-carbonate-filled low density polyethylene: Influence of matrix-filler and particle-particle interactions.* Polymer Engineering & Science, 1996. **36**(2): p. 237-243.

26. Suslick, K.S. and G.J. Price, *Applications of ultrasound to materials chemistry.* Annual Review of Materials Science, 1999. **29**(1): p. 295-326.

27. Manero, O. and B. Mena, *An interesting effect in non-newtonian flow in oscillating pipes.* Rheologica Acta, 1977. **16**(5): p. 573-576.

28.   Manero, O., B. Mena, and R. Valenzuela, *Further developments on non-Newtonian flow in oscillating pipes.* Rheologica Acta, 1978. **17**(6): p. 693-697.

29.   Mena, B., O. Manero, and D.M. Binding, *COMPLEX FLOW OF VISCOELASTIC FLUIDS THROUGH OSCILLATING PIPES - INTERESTING EFFECTS AND APPLICATIONS.* Journal of Non-Newtonian Fluid Mechanics, 1979. **5**(APR): p. 427-448.

30.   Li, H.L. and Y.Z. Chen, *Mechanism for effect of ultrasound on polymer melt in extrusion.* Journal of Polymer Science Part B-Polymer Physics, 2007. **45**(10): p. 1226-1233.

31.   Panov, A.K., et al., *STUDY OF THE PROCESS OF EXTRUSION OF POLYMER MELTS UNDER THE ACTION OF ULTRASONIC VIBRATIONS.* Doklady Akademii Nauk Sssr, 1992. **322**(3): p. 560-564.

32.   Kiselyova, O.F., et al., *Extrusion of polymers during ultrasonic action.* Journal of Applied Polymer Science, 2004. **91**(2): p. 693-696.

33.   Wei, L., et al., *Effect of ultrasound on the processability and mechanical properties of poly(butylene terephthalate)/talc composites.* Journal of Applied Polymer Science, 2011. **122**(4): p. 2708-2714.

34.   Guo, S., et al., *Ultrasonic improvement of rheological and processing behaviour of LLDPE during extrusion.* Polymer International, 2003. **52**(1): p. 68-73.

35.   Kim, K.Y., et al., *Rheological properties of polypropylene modified by high-intensity ultrasonic waves.* Journal of Applied Polymer Science, 2006. **99**(5): p. 2132-2137.

36.   Li, J., S. Guo, and M. Liang, *Effects of ultrasonic oscillation on processing behaviors of PS, EPDM, and PS/EPDM blend.* Journal of Applied Polymer Science, 2006. **100**(3): p. 1856-1863.

37.   Li, Y.T., et al., *Mechanochemical degradation kinetics of high-density polyethylene melt and its mechanism in the presence of ultrasonic irradiation.* Ultrasonics Sonochemistry, 2005. **12**(3): p. 183-189.

38.   Levin, V.Y., S.H. Kim, and A.I. Isayev, *Vulcanization of ultrasonically devulcanized SBR elastomers.* Rubber Chemistry and Technology, 1997. **70**(1): p. 120-128.

39.   Levin, V.Y., et al., *Ultrasound devulcanization of sulfur vulcanized SBR: Crosslink density and molecular mobility.* Rubber Chemistry and Technology, 1996. **69**(1): p. 104-114.

40.   Fujiwara, H., et al., *Mechanochemical block copolymerization in heterogeneous systems of the solid poly(vinyl chloride) with styrene by ultrasonic irradiation - II.*

Effect of several forms of suspension polymerized poly(vinyl chloride) particles. Polymer Bulletin, 1994. **33**(3): p. 317-323.

41.   Fujiwara, H., et al., *Mechanochemical block copolymerization in heterogeneous systems of the solid poly(vinyl chloride) with styrene by ultrasonic irradiation.* Polymer Bulletin, 1992. **28**(2): p. 189-196.

42.   Suslick, K.S., *Ultrasound: its chemical, physical, and biological effects.* 1988: VCH Publishers.

43.   Price, G.J. and P.F. Smith, *Ultrasonic degradation of polymer solutions. 1. Polystyrene revisited.* Polymer International, 1991. **24**(3): p. 159-164.

44.   Kazakia, J.Y. and R.S. Rivlin, *EFFECT OF LONGITUDINAL VIBRATION ON POISEUILLE FLOW IN A NON-CIRCULAR PIPE.* Journal of Non-Newtonian Fluid Mechanics, 1979. **6**(2): p. 145-154.

45.   Kazakia, J.Y. and R.S. Rivlin, *The influence of vibration on Poiseuille flow of a non-Newtonian fluid, I.* Rheologica Acta, 1978. **17**(3): p. 210-226.

46.   Lemelson, J. and H. Jerome, *Apparatus and method for controlling the internal structure of matter.* 1976.

47.   Isayev, A.I., J. Chen, and A. Tukachinsky, *NOVEL ULTRASONIC TECHNOLOGY FOR DEVULCANIZATION OF WASTE RUBBERS.* Rubber Chemistry and Technology, 1995. **68**(2): p. 267-280.

48.   Isayev, A.I., C.M. Wong, and X. Zeng, *Effect of oscillations during extrusion on rheology and mechanical properties of polymers.* Advances in Polymer Technology, 1990. **10**(1): p. 31-45.

49.   Isayev, A.I., S.P. Yushanov, and J. Chen, *Ultrasonic devulcanization of rubber vulcanizates. I. Process model.* Journal of Applied Polymer Science, 1996. **59**(5): p. 803-813.

50.   Keishiro, O., *Jpn Patent 91 253 323, 1991*, in *Chem Abstr 1992,116, 108130v.*

51.   Basedow, A.M. and K.H. Ebert, *ULTRASONIC DEGRADATION OF POLYMERS IN SOLUTION.* Advances in Polymer Science, 1977(22): p. 83-148.

52.   Isayev, A.I., C.M. Wong, and X. Zeng, *Flow of Thermoplastics in Dies with Oscillating Boundary.* SPE Technical Papers, 1987. **33**: p. 207-210.

53.   Isayev, A.I., C.M. Wong, and X. Zeng, *Flow of Thermoplastics in an Annular Die under Orthogonal Oscillations.* Journal of Non-Newtonian Fluid Mechanics, 1990. **34**(3): p. 375-397.

54.   Wong, C.M., C.H. Chen, and A.I. Isayev, *Flow of Thermoplastics in an Annular Die under Parallel Oscillations.* Polymer Engineering and Science, 1990. **30**(24): p. 1574-1584.

55.   Peshkovskii, S.L., et al., *Acoustic cavitation and its effect on flow in polymers and filled systems.* Polymer Composites, 1983. **4**(2): p. 126-134.

56.   Kazatchkov, I.B., et al., *Influence of molecular structure on the rheological and processing behavior of polyethylene resins.* Polymer Engineering & Science, 1999. **39**(4): p. 804-815.

57.   Sombatsompop, N. and R. Dangtungee, *Flow visualization and extrudate swell of natural rubber in a capillary rheometer: Effect of die/barrel system.* Journal of Applied Polymer Science, 2001. **82**(10): p. 2525-2533.

58.   Sukhadia, A.M., in *SPE ANTEC* 1997: USA.

59.   Wang, J. and R.S. Porter, *On the Viscosity-Temperature Behavior of Polymer Melts.* Rheologica Acta, 1995. **34**(5): p. 496-503.

60.   Wang, S.-Q. and P.A. Drda, *Superfluid-Like Stick−Slip Transition in Capillary Flow of Linear Polyethylene Melts. 1. General Features.* Macromolecules, 1996. **29**(7): p. 2627-2632.

61.   Fridman, M.L., S.L. Peshkovsky, and G.V. Vinogradov, *The rheology of thermoplastics under conditions of spiral flow and vibrations on extrusion.* Polymer Engineering & Science, 1981. **21**(12): p. 755-767.

62.   Ramamurthy, A.V., *Wall Slip in Viscous Fluids and Influence of Materials of Construction.* Journal of Rheology, 1986. **30**(2): p. 337-357.

63.   Kalika, D.S. and M.M. Denn, *Wall Slip and Extrudate Distortion in Linear Low-Density Polyethylene.* Journal of Rheology, 1987. **31**(8): p. 815-834.

64.   Kim, Y.C. and K.S. Yang, *Effect of Peroxide Modification on Melt Fracture of Linear Low Density Polyethylene during Extrusion.* Polymer Journal, 1999. **31**(7): p. 579-584.

65.   Kim, Y.C., K.S. Yang, and C.-H. Choi, *Study of the relationship between shear modification and melt fracture in extrusion of LDPE.* Journal of Applied Polymer Science, 1998. **70**(11): p. 2187-2195.

66.   Isayev, A.I. and C.M. Wong, *Parallel superposition of small- and large-amplitude oscillations upon steady shear flow of polymer fluids.* Journal of Polymer Science Part B: Polymer Physics, 1988. **26**(11): p. 2303-2327.

67. Wong, C.M. and A.I. Isayev, *Orthogonal superposition of small and large amplitude oscillations upon steady shear flow of polymer fluids.* Rheologica Acta, 1989. **28**(2): p. 176-189.

68. Panov, A.K., et al., *REGULARITIES OF THE MELTED POLYMER FLOWS UNDER CONDITIONS OF ULTRASONIC VIBRATION.* Doklady Akademii Nauk Sssr, 1988. **303**(1): p. 155-158.

69. Chen, G., S. Guo, and H. Li, *Ultrasonic improvement of rheological behavior of polystyrene.* Journal of Applied Polymer Science, 2002. **84**(13): p. 2451-2460.

70. Iclanzan, T., D. Stan, and M. Abadie, *A possible new ultrasonic thermo-pellicular effect and applications.* International Journal of Material Forming, 2008. **1**(0): p. 743-746.

71. Kim, H. and J.W. Lee, *Effect of ultrasonic wave on the degradation of polypropylene melt and morphology of its blend with polystyrene.* Polymer, 2002. **43**(8): p. 2585-2589.

72. Li, Y., et al., *Studies on Rheological Behavior and Structure Development of High-Density Polyethylene in the Presence of Ultrasonic Oscillations During Extrusion.* Journal of Macromolecular Science, Part B, 2006. **45**(1): p. 39-52.

73. Lin, H. and A.I. Isayev. *EFFECT OF HIGH INTENSITY ULTRASONIC WAVES ON POLYPROPYLENE, POLYAMIDE 6 AND THEIR BLENDS.* in *61st Annual Technical Conference, ANTEC.* 2003. USA.

74. Nam, G., et al. *Modification of PP by High Intensity Ultrasonic Wave and Its Characterization of Rheological Properties.* in *ANTEC -CONFERENCE PROCEEDINGS.* 2005. USA.

75. Van Prooyen, M., T. Bremner, and A. Rudin, *Mechanism of shear modification of low density polyethylene.* Polymer Engineering & Science, 1994. **34**(7): p. 570-579.

76. Venet, C. and B. Vergnes, *Experimental characterization of sharkskin in polyethylenes.* Journal of Rheology, 1997. **41**(4): p. 873-892.

77. Wang, S.Q., P.A. Drda, and Y.W. Inn, *Exploring molecular origins of sharkskin, partial slip, and slope change in flow curves of linear low density polyethylene.* Journal of Rheology, 1996. **40**(5): p. 875-898.

78. Birley, A.W., B. Haworth, and J. Batchelor, *Physics of plastics : processing, properties, and materials engineering.* 1992, Munich ; New York: Hanser Publishers ; New York : Oxford University Press [distributor].

79. Webb, D., *Design sheet of Inner Shell 2*, B. University, Editor. 2011, Polypipe Terrain.

80.   Zhang, J., et al., *The stress field induced by contact with asperities.* Journal of Materials Engineering, 1990. **12**(4): p. 271-278.

81.   Pedroso, A.G. and D.S. Rosa, *Mechanical, thermal and morphological characterization of recycled LDPE/corn starch blends.* Carbohydrate Polymers, 2005. **59**(1): p. 1-9.

82.   Li, G., P. Lee-Sullivan, and R. Thring, *Determination of Activation Energy for Glass Transition of an Epoxy Adhesive Using Dynamic Mechanical Analysis.* Journal of Thermal Analysis and Calorimetry, 2000. **60**(2): p. 377-390.

83.   Zhou, H. and G.L. Wilkes, *Orientation Anisotropy of the Mechanical α Relaxation of High-Density Polyethylene Films Having a Well-Defined Stacked Lamellar Morphology.* Macromolecules, 1997. **30**(8): p. 2412-2421.

84.   Hoffman, J.D., G. Williams, and E. Passaglia, *Analysis of the α, β, and γ relaxations in polychlorotrifluoroethylene and polyethylene: Dielectric and mechanical properties.* Journal of Polymer Science Part C: Polymer Symposia, 1966. **14**(1): p. 173-235.

85.   Leszczynska, A. and K. Pielichowski, *Application of thermal analysis methods for characterization of polymer/montmorillonite nanocomposites.* Journal of Thermal Analysis and Calorimetry, 2008. **93**(3): p. 677-687.

86.   Manzur, A. and F. Hernández-Sánchez, *Activation Energy for the Glass Transition of a Confined Elastomer in HDPE/PP Blends.* Journal of Macromolecular Science, Part B, 2006. **45**(1): p. 139-152.

87.   Komalan, C., et al., *Dynamic mechanical analysis of binary and ternary polymer blends based on nylon copolymer/EPDM rubber and EPM grafted maleic anhydride compatibilizer.* eXPRESS Polymer Letters, 2007. **1**(10): p. 641-653.

88.   Alves, N.M., J.L. Gómez Ribelles, and J.F. Mano, *Study of the Molecular Mobility in Polymers with the Thermally Stimulated Recovery Technique—A Review.* Journal of Macromolecular Science, Part C, 2005. **45**(2): p. 99-124.

89.   Alves, N.M., J.F. Mano, and J.L. Gómez Ribelles, *Molecular mobility in polymers studied with thermally stimulated recovery. II. Study of the glass transition of a semicrystalline PET and comparison with DSC and DMA results.* Polymer, 2002. **43**(13): p. 3627-3633.

90.   Sauer, B.B. and Y.H. Kim, *Structural Heterogeneity in Poly(methyl methacrylate) Glasses of Different Tacticity Studied by Thermally Stimulated Current Thermal Sampling Techniques.* Macromolecules, 1997. **30**(11): p. 3323-3328.

91.   Li, H.L., Y.C. Zhang, and J.Y. Chen, *Functionalization of high density polyethylene in melt state through ultrasonic initiation and its effect on mechanical*

properties of glass fiber reinforced composites. Polymer Bulletin, 2007. **59**(3): p. 427-438.

92. Vasile, C., *Handbook of polyolefins*. 2nd ed., rev. and expanded / edited by Cornelia Vasile. ed. 2000, New York: Marcel Dekker.

93. Eisenberg, A., *In: Physical Properties of Polymers*, in *ACS*. 1984: Washington, DC. p. 57-95.

94. Fox, T.G. and S. Loshaek, *Influence of molecular weight and degree of crosslinking on the specific volume and glass temperature of polymers.* Journal of Polymer Science, 1955. **15**(80): p. 371-390.

95. Stutz, H., K.H. Illers, and J. Mertes, *A generalized theory for the glass transition temperature of crosslinked and uncrosslinked polymers.* Journal of Polymer Science Part B: Polymer Physics, 1990. **28**(9): p. 1483-1498.

96. Chee, K.K., *Dependence of glass transition temperature on chain flexibility and intermolecular interactions in polymers.* Journal of Applied Polymer Science, 1991. **43**(6): p. 1205-1208.

Chapter 4

Pilot Scale In-line Ultrasonic Assisted Pipe Extrusion of Polyolefins

4.1   Introduction

High intensity ultrasonic waves were employed to develop an innovative extrusion process in recent years, in which the ultrasonic waves were applied into the polymer melt while processing [1-8].

It is well known that flow of the polymer melt through a die is a key stage of the polymer extrusion process. The high hydrodynamic resistance caused by the viscose flow of a polymer melt through the die and the distortions of the final products as a result of melt fracture are the main challenges when attempting to increase the throughput of the extrusion processes. There are other available solutions for this problem such as the addition of processing aid or plasticizers and the adjustment of the extrusion parameters (temperature setting, processing pressure and rotation speed of the screw); but the

introduction of high frequency vibrations at the wall/die surfaces has the potential resolve this problem without modification of the material or the processing parameters. However, in some cases these methods are found to be inadequate and even inappropriate or to be limited due to polymer's thermal stability and its narrow processing window (such as PVC). At the same time, these methods mostly rely on the operators' experience and improvement of the extruder, which means an extra cost for processing expenses [9, 10].

During periodical shearing of the polymer melt on the wall surfaces of the die as a result of application of high frequency vibrations, structural changes such as polymer chain breaking can occur. Consequently, the occurrence of structural changes in the polymer melt leads to a reduction of the viscosity of the melt and the elasticity of the material [11-16]. The reduction of the effective viscoelastic characteristics of the polymer melt is proportional to the vibration intensity, which is determined by the product of the vibration frequency and the amplitude of the shearing. The changes to the viscoelastic properties of the polymer melt under the influence of ultrasonic vibrations is utilized to increase the output of the extruder in certain processing pressures [11]. The application of ultrasonic waves onto the polymer melt offers some major potential advantages to polymer processing and the extrusion process in particular. The possible effects are; the reduction of the die head pressure, die lip build up, melt fracture and an improvement of the extrudate surface quality. The effects of ultrasonic treatment have been studied in a wide range of applications in polymer extrusion and it was reported that the introduction of ultrasonic waves into the polymer melt is capable of improving the processing behaviour [17-19], the compatibilization of immiscible polymer blends (polymer and rubber blends) [3, 5, 17, 20-22], the breakdown of the 3D network in vulcanized rubber and the exfoliation and intercalation of nanoclays in polymer matrix nanocomposites [23, 24].

In polymer science, ultrasonic waves were also employed for the modification of polymers (chemistry during processing) and for the improvement of other processing methods such as injection moulding. In polymer chemistry, high intensity ultrasonic waves have been widely employed to induce mechanochemical degradation of polymeric materials in solutions to control the molecular weight and the molecular weight distribution in polymers. High temperature and pressure, frictional force, and the shock-wave energy

induced by the acoustic cavitations could lead to degradation of the polymers (which is beneficial) as well as to synthesize novel polymers and copolymers [25-35]. High intensity ultrasonic waves are capable of splitting the long chain polymer molecules during the melt extrusion [5]. By the breaking of the C-C bonds by ultrasonic waves into long chain C-C radicals [36], these radicals could terminate on the main body of the polymers as branches or alternatively, in filled systems they could end up on the filler surfaces.

Ultrasonic oscillations have been widely used in the injection moulding of polymers and from the patents available in the public domain the application of the ultrasound can be divided into three main categories which are:

1. The first category is to homogenize and increase the density of the moulded material by using mechanical vibration or ultrasonic waves [37-41].

2. The second category of patents is employing the effect of the frequency and amplitude of the vibration on the viscosity of the material. The dependency of the viscosity on above mentioned factors can be employed to manipulate parameters such as the nucleation and growth of crystals, blending and orientation [42-60]. The modifications could result in changes in the thermal and mechanical characteristics of the polymer and could lead for example to an increased tensile, flexural and impact strength, stiffness and also an increase in weld line strength, increased dimensional stability, and a decrease in the number of the voids and sink marks.

3. For the third category the vibrations were effectively used for the generation of local heat by pressure pulsations that lead to local elevated temperatures. The generated heat can be large enough in injection moulding to avoid the premature freezing of the injection gate that can result in a major reduction of the product shrinkage [61, 62]. Vibrations have been used to decrease surface stresses at the wall boundary layer for polymer melts in the die and non-Newtonian fluids inside the pipes [17, 19, 63-68]. Experiments carried out on vibrating walls and dies showed a reduction of the required pressure and temperature for processing. It was also reported that the mechanism which is responsible for the melt instability in annular dies was distorted by the application of the USVs, allowing for an increase in the throughputs without occurrence of shark skin or melt fracture [17, 69-74].

The techniques used in this category reduced the processing temperature and pressure by vibrating the wall surfaces, also it has been reported that the output rate in annular dies can be increased by introduction of vibrations into the die wall surfaces [17, 69-74].

Oscillations can be introduced into polymer melts in two possible ways. They could be applied either parallel or perpendicular to the direction of shear flow [21, 75]. In the parallel superposition the oscillations will coincide with the flow while in perpendicular form they are at 90° to each other. The oscillations could be of sonic frequency [14, 74, 76-89] or of an ultrasound frequency [81, 87, 90, 91] and it has been shown in the literature that with both ways of the application of the oscillations, the viscosity of the polymeric fluids decreased [21, 75]. The choice of either a parallel or perpendicular mode of application of the oscillations depended on the feasibility for the practical application.

By the application of vibrations into wall surfaces the friction between the polymer melt and the die walls became negligible that lead to a sliding movement of the polymer melt on the wall surfaces during extrusion [78, 82, 86]. This could be the cause for the reduction of pressure drop in the die for the extrusion of polystyrene, polyethylene, and polypropylene [81, 87, 88].

Introduction of oscillations during extrusion through a circular die in both longitudinal and transverse mode have been studied for a low density polyethylene (LDPE), polystyrene, and a 50/50 blend of high density polyethylene (HDPE) and LDPE; the oscillations altered the extrudate which led to improvements of mechanical properties and reduction of die pressure [74].

Typically, the change of the viscoelastic properties of the polymer in the ultrasonic frequency range can be induced with vibration amplitude of only a few micrometers. It was learnt from previous studies that the superposition of the ultrasonic waves with amplitudes of 5-30μm on capillary flow reduced the apparent viscosity and the die swell ratio of the polymer melt and also the shape of the extrudate considerably [81, 87, 92] as it can be seen from Figure 4-1 .
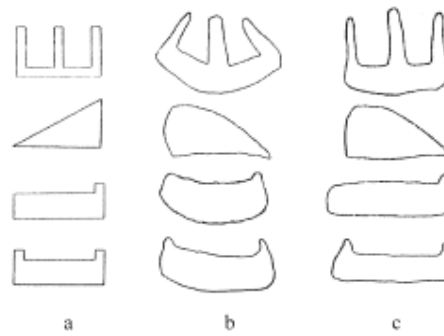
Figure 4-1: Characteristic contours of extruded poly vinyl chloride, polystyrene, and polythene: (a) sections of the designed shapes, (b) sections of conventionally extruded samples, and (c) section of the samples treated with ultrasonic waves [87].

Most of the recent studies on the application of ultrasonic vibrations were mainly focused on the following topics:

1. Effects of ultrasonic irradiation on the characteristics of the extrusion process including die temperature die pressure, flow rate of polymer melt, and rheological behaviour of polymer melt.[72, 93, 94]

2. Ultrasonic improvement of the compatibility and enhancement of the mechanical properties of polymer blends.[22, 95-98]

Inorganic fillers are being increasingly used to enhance mechanical properties of polymers [99-102]. The improvement of mechanical properties of the polymer melt is strongly dependant on the morphology and dispersion of the fillers in the polymer matrix. Poor dispersion of the fillers and week interaction of filler/matrix could drastically reduce the process ability and mechanical properties of the polymers. In order to achieve a homogenized dispersion of fillers and to improve the interactions of filler/matrix several methods usually employed:

- Surface treatment of fillers [101, 103, 104]
- Polar group functionalization of polymers [105, 106]
- Addition of a bifunctional component to interact with both filler and matrix [107]
- Mechanochemical modification of the fillers [108-110]

Polymer based nano composites are another field that have benefited from ultrasonic vibration. A number of studies have been carried out on filled systems focusing mainly on nanocomposite preparation [111-114] and in most of them better dispersion of filler and breakage of agglomerations were observed [111-113, 115-122].

Although a number of companies are benefitting from this technology, very little is known about the mechanism and its industrial scale setup in the open technical literature [123]. Most of the methods seen in the previous literature have used ultrasonic probes installed in a conventional die.

In this chapter the effects of ultrasonic waves will be investigated on extruded polyethylene pipes. High intensity ultrasonic oscillations were applied to the polymer melt during extrusion process and at the die zone for the production of a commercial grade of HDPE pipes. The extrusion grade of HDPE was also used with different concentrations of calcium carbonate in order to study the influence of the filler concentration on the effect of ultrasonic waves on the extrudate and processing parameters.

4.2   Experimental

4.2.1   Materials

Three different grades of polyethylene were used in this part of the study.

- A commercial pipe extrusion grade of polyethylene, pipe grade HDPE (PE80) which was supplied by Polypipe Terrain (manufactured by BOREALIS) with a melt flow rate of 0.33 g/10min under the load of 5.0Kg at 190°C, was used both for polymer strip and pipe processing.
- A high density polyethylene copolymer with narrow molecular weight distribution specially developed for injection/compression moulding and a general purpose extrusion grade HDPE. The low viscosity HDPE copolymer (Rigidex5130) which

was used for strip production was developed by INEOS[1] Polyolefins with an MFR of 2.4 g/10min under the load of 2.16 Kg at 190°C.

- The third grade of polyethylene (HYA600) was made by Exxon Mobil[2] and it was used for pipe extrusion, the MFR was 0.35 g/10min under the load of 2.16 at 190°C. All the materials were received in a granular form. A master batch with 80%wt calcium carbonate (supplied by DISTRUPOL[3]) and HYA600 were used for compounding of 20%wt (HYA600/20, φ_f=0.08) and 40%wt (HYA600/40, φ_f=0.19) filled composites.

4.2.2 Design of 2nd generation ultrasonic horn and the housing block

The second generation ultrasonic horn (G2) was designed to introduce the ultrasonic vibration into the melt in the die. The ultrasonic horn consisted of the conical section of the 1st generation horn (G1) that was followed by a cylindrical extension from the base of the cone.

The new design benefited from the previous design's conical section that produced components of compressive and shear oscillations. The extended cylindrical section increased the exposure of the polymer melt to the additional shear oscillations. The compressive oscillations (that were believed to be more effective) were applied when the molten polymer entered the ultrasonic die flowed over the conical section of the die while the shear oscillations were applied in the cylindrical section to make the flow of the melt through the die easier. The top block and the mid block both remained unchanged for the G2 ultrasonic horn. A new bottom block, however, was designed to fit the new horn design.

---

[1] A manufacturing, distribution, sales and marketing company of speciality and intermediate chemicals, including oxides, glycols, and esters.

[2] One of the largest petrochemical companies worldwide, providing the building blocks for a wide range of products, from packaging materials and plastic bottles to automobile bumpers, synthetic rubber, solvents and countless consumer goods.

[3] European leader in the sales, marketing, distribution and application development of an extensive range of thermoplastic polymers and elastomers.
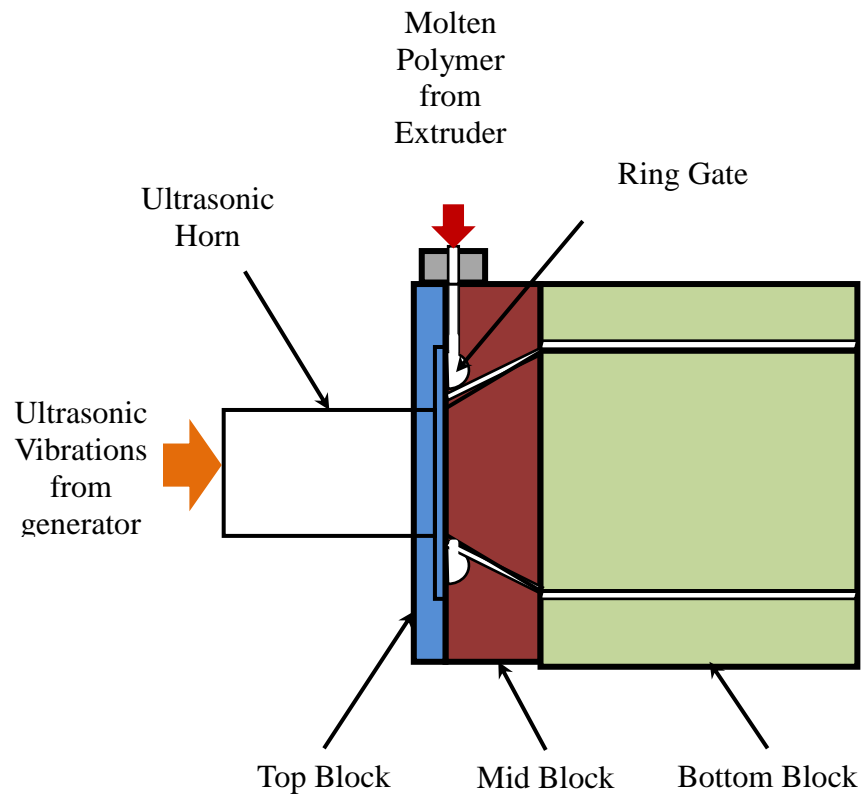
Figure 4-2: Schematic diagram of the G2 ultrasonic horn and the housing block.
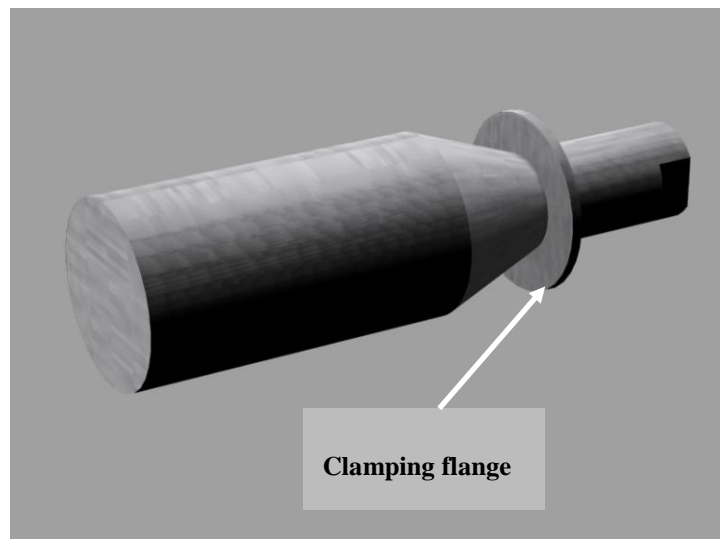

Figure 4-3: Side view of 3D model of the G2 ultrasonic horn showing the parallel section, conical section and the clamping flange of the horn.

As shown in Figure 4-2, the horn was clamped between the top block and the mid block by the flange section (shown in Figure 4-3) where the nodal point was located (where there is

no vibration or the vibration is minimum) according to FEA modelling of the horn. In order to minimize the damage to the horn by cavitations generated from the oscillations, the material of the horn was changed to grade 5 titanium. The proposed horn dimensions were modelled at Telsonic (the ultrasonic generator supplier) using FEA and with purpose built software package. The ultrasonic wave generator was supplied by Telsonic with nominal power value of 2.0Kw and with a fixed vibrating frequency of 20 KHz. The generator had an adjustable vibration amplitude switch that could be adjusted between 70% and 100% of the available power to the sonotrode.

The temperature on the bottom block was controlled by a DME Smart Series PID controller unit that controlled four 800W cartridge heaters. The temperature reading for the controller unit was provided by a thermocouple positioned 1-1.5cm from the surface on the centre of the bottom block. A pressure transducer hole was also placed on one side of the bottom block to enable melt pressure readings (shown in Figure 4-4).
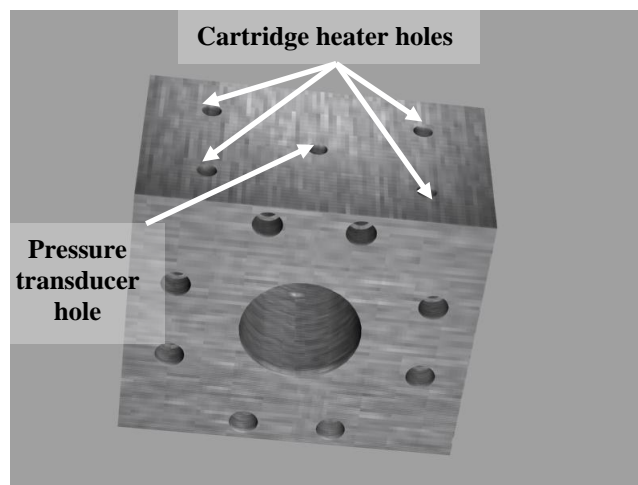
Figure 4-4: 3D model of bottom block showing the cartridge holes and the pressure transducer hole.
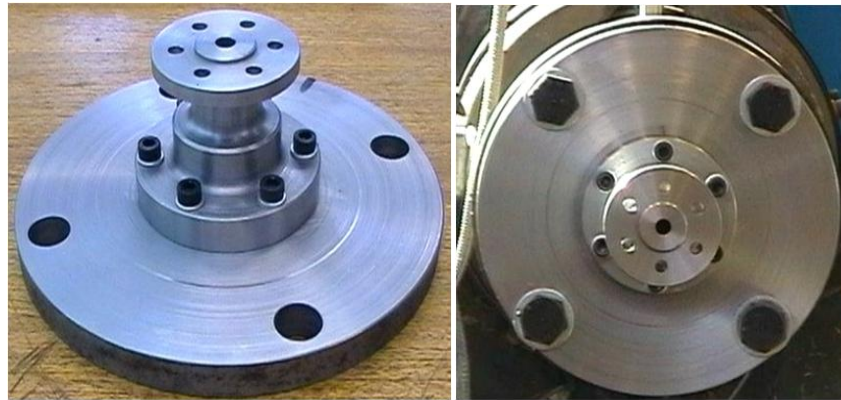
Figure 4-5: (Left) assembled adapter to deliver the polymer melt from extruder end to the ultrasonic block, (right) the adapter installed on the extruder showing the feed hole to the ultrasonic die in the front face.

To install the housing block on the 50mm extruder an adapter was manufactured to suit. The adapter consisted of a circular plate 15mm thick which took the feed from the extruder end (24mm) down to 16mm, which was the diameter of the feed entrance to the ultrasonic die (Figure 4-5). The adapter was not equipped with any heating source because of its short length; it was therefore given adequate time to be heated by the heater band on the extruder end through conduction. The design sketches, installation pictures for the housing block and the adapter are provided in Appendix C.

4.2.3 Extrusion of polyolefins by single screw extruder

Single screw extrusion is widely employed in the PE pipe manufacturing industry because of its low maintenance cost and ease of use. The effects of ultrasonic waves on the polymer melt were studied when processing in a 25mm single screw extruder. To be able to investigate the effects of ultrasonic waves for higher melt flow rates it was essential to move onto a larger extruder. With the 50mm screw extruder the effect of USV could be investigated at higher throughputs rates compared to those carried out on the 25mm extruder. The details of the extrusion process are described in this section.

4.2.3.1 Barrel and feeding

A Betol BK50 extruder was used to plasticize the polymer. The barrel featured a pressure transducer port that was fitted with a pressure transducer to measure the melt pressure in the barrel. The feed throat of the barrel was equipped with a water cooled jacket.

4.2.3.2 Heating system of the extruder

The heating system on the extruder consisted of 4 heaters that divided the barrel into 4 heating zones. The heaters were all wired to the control unit as shown in Figure 4-6. The extruder was air cooled and the barrel was covered in order to optimize the cooling.
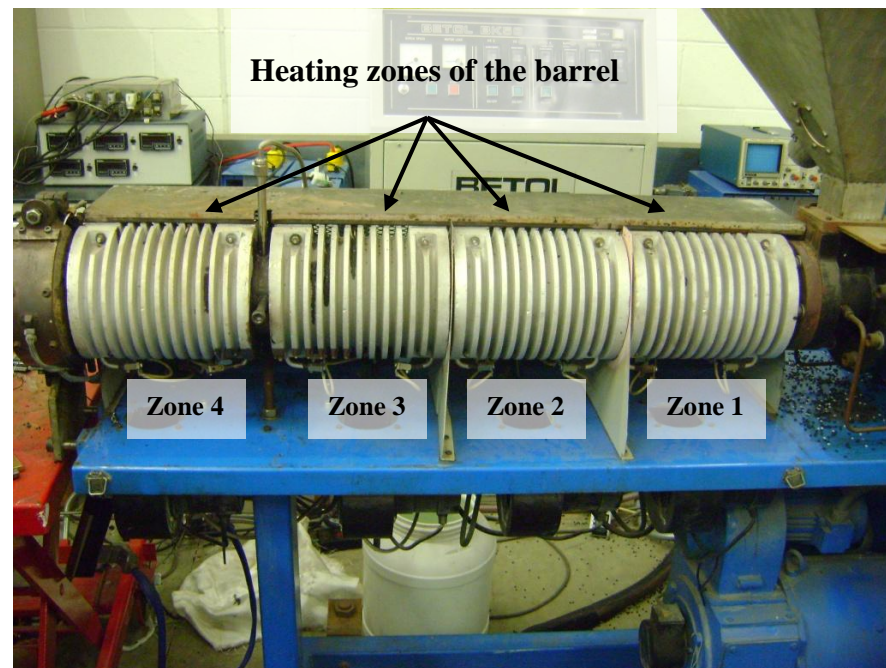
Figure 4-6: Extruder barrel and the 4 heating zones of the extruder barrel (the heater bands and the blower fan holes beneath each zone are also shown too).

4.2.3.3 Temperature controllers

Analogue Eurotherm temperature controllers were used to maintain the temperature on the set temperature. The controllers handled power input into the heaters and the start/stop of the blower fans for cooling of the barrel.

4.2.3.4 Motor Load and screw speed indicators

The motor load was displayed on an analogue scale that showed the current drawn by the extruder motor in amperes. The screw speed could be set by a dial that could be locked at a desired point if required. The screw speed was displayed on an analogue scale on the control unit.

4.2.3.5 Screw geometry

The screw was 1.4m long with the processing length of 1.25m. It was the gradual compression polyolefin screw with a diameter of 50mm and L/D ratio of 25:1.

4.2.4 Calendering System

A Betol calendaring system with 3 steel cooling rolls and 2 rubber pull rolls was used to make the polymer strips. The chill rolls were kept cool by circulating water at room temperature through them.

4.2.5 Sizing and calibration system

A Hettinga Reeve water/vacuum bath was employed for the forming and cooling of the extrudate in the pipe extrusion process. The water bath featured a sealed controllable vacuum section followed by the cooling section that used water sprays to cool down the product. A 63mm diameter sizing sleeve was fitted to the vacuum section. The bath also featured a water tank for circulation of the cooling water and a heat exchanger to control the water temperature.

4.2.6 Chiller

In order to maintain the water temperature a Tricool Engineering portable chiller was used. The chiller featured an independent coolant circuit (connected to the water bath's heat exchanger) and a temperature controller for temperatures ranges from 7°C to 27°C.

4.2.7 Ultrasound Generator

A TELSONIC SG-22 power supply was used to convert the mains electrical power to the required voltage, current and a frequency of 20 KHz. The power supply was connected to a TELSONIC SE2012 transducer with an air cooled aluminium collar to maintain the temperature of the transducer at room temperature. The transducer converted the electrical power into mechanical vibrations with amplitude of 20µm. The transducer was connected to the titanium booster which intensified the amplitude by the ratio of 1.5 which resulted in amplitude of 30µm at the end of the booster. The last piece of ultrasonic system was the ultrasonic horn or sonotrode. The sonotrode as mentioned earlier was made of titanium and it converted the waves by the ratio of 0.6 to vibrations with maximum amplitude of 18µm (at antinodes). Figure 4-7 shows the transducer, booster and the sonotrode before installing on the ultrasonic die.
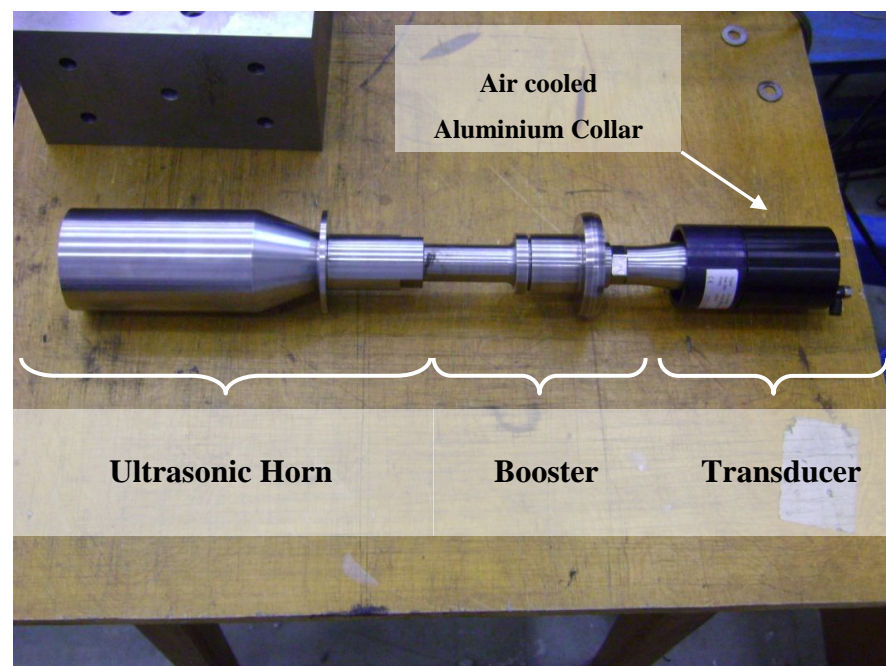
Figure 4-7: Ultrasonic transducer, booster and the G2 ultrasonic horn.

4.2.8 Characterization and Testing

4.2.8.1 Processing Parameters

Several processing parameters were recorded in Chapter 3 and compared for conventional and ultrasonic assisted extrusion processes. Same processing parameters were used to allow comparison between two different modes of extrusion and investigate the effects of ultrasonic vibrations on the processing parameters.

- **Pressure**: Three pressure transducers were fitted on the metering zone of the extruder barrel; ultrasonic block entrance and exit to record melt pressure while processing with and without ultrasound.

- **Extruder & Heaters power consumption:** The power consumption was one of the processing parameters those were believed to be affected by the application of ultrasonic waves. In order to measure the overall power consumption it was necessary to measure the power consumed by the extruder and the ultrasonic die heaters. The extruder was fitted with the power meter that allowed power measurements for a known processing time. Plug in power meters were used to measure the power consumed by the cartridge heaters in the ultrasonic housing block.

- **Temperature**: The temperatures for the 3 zones of the extruder barrel were not recorded as the temperature controllers installed on the control unit were analogue dials that only allowed the setting of the temperature.

  The temperatures of the two heating zones of the ultrasonic block and the melt temperature were recorded for the different processing methods at the different screw speeds used.

- **Output rate**: The output rates were measured by manually cutting and weighing the extrudate produced during the known time period. The measurements were repeated 3 times for accuracy of the results; the average of the measurements was then reported.

4.2.8.2 Material Properties

- **Mechanical Properties**

  Tensile Properties: Dumbbell Tensile Testing samples were punch cut from the strips using a CEAST punch cutter to produce samples with the standard dimensions of Type **5A** specimens described in **BS EN ISO 527-2:1996**. The same method was used to prepare samples from the extruded pipes. For consistency, all of the samples were cut from the same axial position to the feed gate in the ultrasonic die in the pipes. The tensile tests were carried out on an Instron machine equipped with Zwick/Roell Smart Pro software and drive motor. The tests were carried out up to 80% strain to measure Young's modulus and yield strength of the materials.

  Dynamic Mechanical Analysis: Samples were cut from the strips and pipes using the tool provided by TA instruments (parallel blades width of 5mm). For consistency of the results the samples were cut from the same areas related to the feed gate in the die. Dynamic Mechanical Analysis tests were performed on the polymer bars using a TA Instruments Q800 in temperature range of -140°C up to 80°C with a heating rate 3°C/min and the test frequencies of 1, 5 and 10 Hz.

- **Thermal Properties**

  Differential Scanning Calorimetry (DSC): Standard differential scanning calorimetry was carried out on samples that had been prepared from product at the different screw speeds to determine the degree of crystallinity, melting point, enthalpy of melting and enthalpy of crystallisation. The tests were performed on a TA Instruments DSC Q2000 using standard aluminium pans in a nitrogen purge gas atmosphere within the temperature range of -80°C to 180°C, with a heating rate of 10°C/min and the cooling rate of 5°C/min.

- **Rheological properties**

Parallel plate rheometry

The rheology of a polymer melt is very sensitive to small changes of the polymer structure. The important structural parameters defining the rheology of a polymer melt are molecular weight, molecular weight distribution and chain branching, and such information can be obtained with the Rotational Rheometer. As with the DMA, the Rotational Rheometer is a mechanical spectrometer capable of subjecting a sample to a dynamic (sinusoidal) or steady (linear) shear strain (deformation), and the resultant torque expended by the sample in response to the shear rate is measured. The Rotational Rheometer is mainly used to perform viscosity measurements and the material properties obtained can be:

- Dynamic shear flow behaviour (G', G'', tan delta or tanδ and the dynamic viscosity, η_d) as a function of frequency (time) and temperature.
- Steady shear flow behaviour (shear viscosity and shear stress) as a function of the shear rate.

The storage shear modulus G', loss shear modulus G'' and tanδ are obtained according to the following relationships:

$$\eta_d = \frac{G_d}{\omega} \qquad\qquad \textbf{4-1}$$

Where G_d is the dynamic shear modulus, ω is the angular frequency and η_d is the dynamic viscosity.

$$G'' = G_d \cdot \cos \delta \qquad\qquad \textbf{4-2}$$

$$G' = G_d \cdot \sin \delta \qquad\qquad \textbf{4-3}$$

$$Tan\ \delta = \frac{G''}{G'} \qquad\qquad \textbf{4-4}$$

An ARES (Advanced Rheometrics Expansion System) instrument from TA Instruments was used to measure G' and G'', as a function of frequency (time) for

the samples. Standard parallel plates with diameter of 25mm were employed to carry out frequency sweep tests at 190°C with the strain of 0.1% in the frequency range of 0.1 to 512 rad/sec.

4.3   Results and Discussion

4.3.1 Extrusion processing

4.3.1.1 Extrusion of the polyethylene Strips

Strips were produced from PE80 and Rigidex5130 at five different screw speeds of 8, 12, 16, 20 and 24 rpm with and without the presence of ultrasonic waves. The temperature setting of the extruder is summarised in Table 4-1.

Table 4-1: Temperature setting for processing of Rigidex5130 and PE80 strips.

Material	Barrel Heating Zones				Extruder Die Zones		Ultrasound Die Zones	
	T1	T2	T3	T4	T5	T6	T7	T8
Rigidex5130	160	165	170	170	175	175	175	175
PE80	175	180	185	190	190	190	190	190

In order to maintain the drawing ratio and hence the speed for the set screw speeds the conventional extrusion process was followed immediately by the ultrasonic assisted extrusion for each extrusion screw speed. The same processing procedure was repeated for all the above mentioned screw speeds. The extrusion of Rigidex5130/PE80 was started when the temperatures of the extruder and the die zones reached the set value. Prior to sample collection some material was extruded until the temperatures of the barrel and the die stabilized. The melt was then fed into the chill rolls where it solidified as a polymer strip.
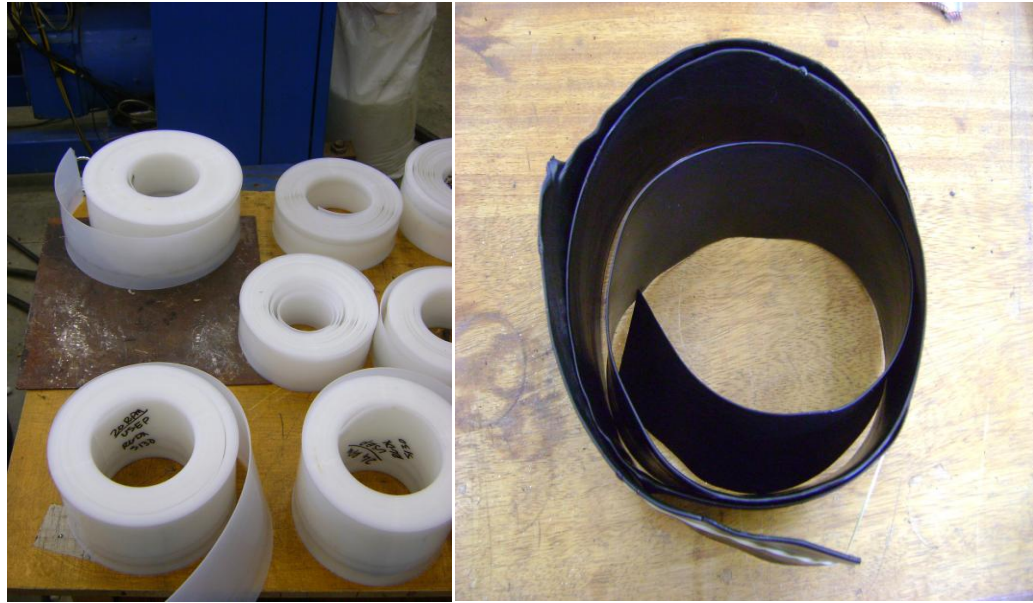
Figure 4-8: Rigidex5130 strips (Left) and PE80 strips (Right) produced at different screw speeds and in both CEP and USEP modes which were used for characterization tests.

Figure 4-8 shows the strips produced at different screw speeds using CEP and USEP extrusion process and processing parameters tabulated in Table 4-1, these strips then used for sample preparation of the characterization tests.

In the extrusion of the strips the barrel pressure, ultrasound die entrance pressure and ultrasonic die exit pressure were recorded. The time to consume 0.06/0.07 KWh was recorded using the digital watt meter fitted to the extruder. The measurements were then used for the power consumption calculation of the extruder. The same method was used to determine the power consumption of the ultrasound die and the ultrasonic generator when it was in use. The amount of KWh consumed within the measured time was then recorded and used for the calculation of the power consumption for the extruder, ultrasonic die heaters and the ultrasonic generator. The summation of the power consumed by the processing components was then recorded as the total processing power consumption.

$$Power\ Consumption, P\ KWh\ = Energy\ \ KW\ \times time\ to\ consume\ P(sec) \qquad \textbf{4-5}$$

$$Energy\ Consumed\ (KW) = P\ (KWh)/time\ to\ consume\ P(sec) \qquad \textbf{4-6}$$

$$Total\ Power\ Consumption = P_{Extruder} + P_{Die\ Heaters} + P_{Ultrasonic\ Generator} \qquad \textbf{4-7}$$

The extruder barrel pressure for the processing of Rigidex5130 is shown in Figure 4-9. It can be seen that the barrel pressure drops by the application of ultrasound which induces a reduction in the resistance of the die to the flow of the polymer melt.
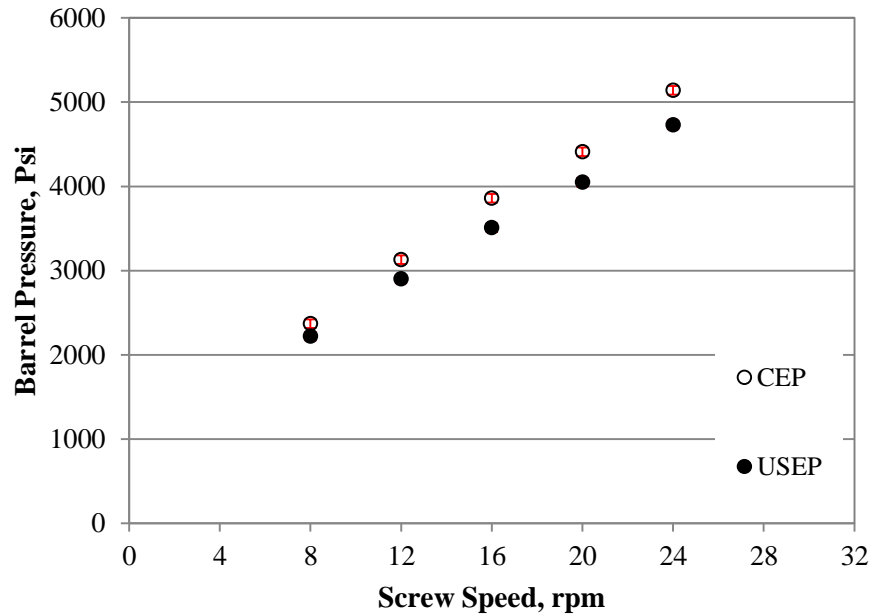
Figure 4-9: Extruder barrel pressure for CEP and USEP processing of Rigidex5130 strips.
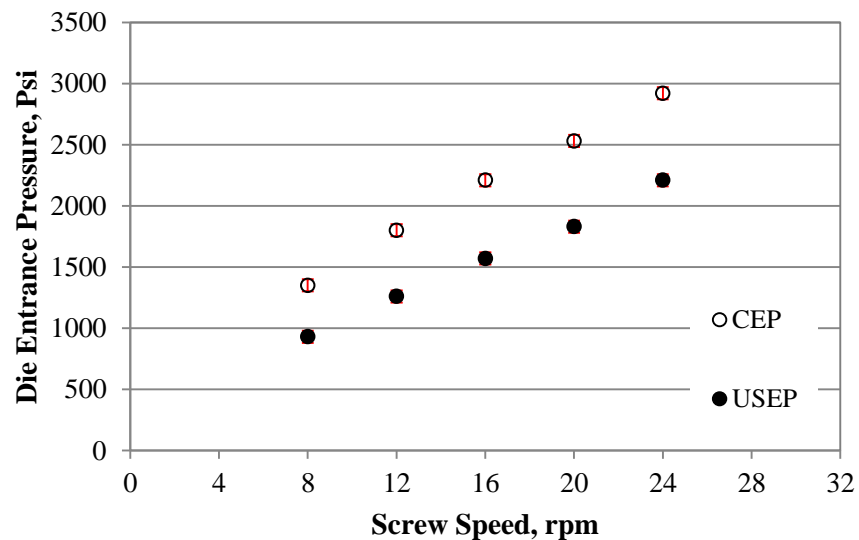
Figure 4-10: The ultrasonic die entrance pressure for CEP and USEP extrusion of Rigidex5130 strips.

112

The measured melt pressure at the entrance of the ultrasonic die (see Figure 4-10) showed a 24-31% reduction from CEP to USEP. The reduction of the melt pressure and increase of the melt temperature have been reported previously for the application of sound frequency waves into polymer melt at the die region [66, 88].

The ultrasound vibrations were applied in compressive (in the conical section of the die) and in shear mode (in conical and cylindrical section of the die) to the polymer melt flow in the G2 arrangement. The application of the ultrasound in the perpendicular direction to the melt flow generated more heat from the dissipation of the wave energy as the USVs try to vibrate the flowing melt in a compression-decompression mode. The compressive vibrations penetrated deeper into the polymer melt and their energy dissipation generated the heat that lead to a temperature rise. The vibrations applied in the shearing mode made the melt move more easily over the body of the ultrasonic horn.

Increasing the melt flow rate decreased the exposure time of the melt and consequently reduced the temperature rise as a result of the reduced contact time with the US horn. Higher flow rates of the melt, on the other hand accelerated the shearing of the melt over the parallel section of the horn that reduced the resistance of the die to the flow.
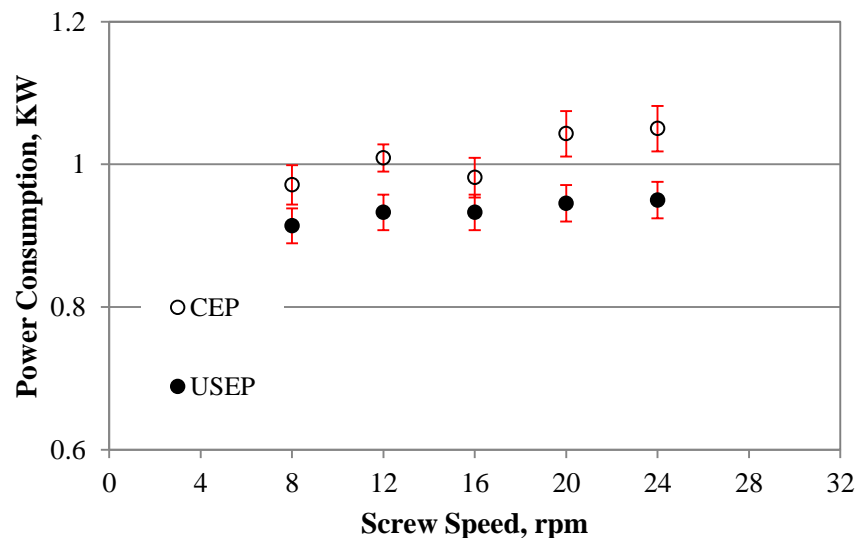
Figure 4-11: Total power consumption for CEP and USEP extrusion of Rigidex5130 strips.

The total power consumption for both the CEP and USEP extrusion of Rigidex5130 is shown in Figure 4-11 and, as expected, increased linearly with the increase of the screw speed. The results are in agreement to the results obtained from the 25mm extruder that are presented in section 3.3.2. The total power consumed for the extrusion of Rigidex5130 was reduced by the application of ultrasound during the extrusion by 5.8-9.5%.
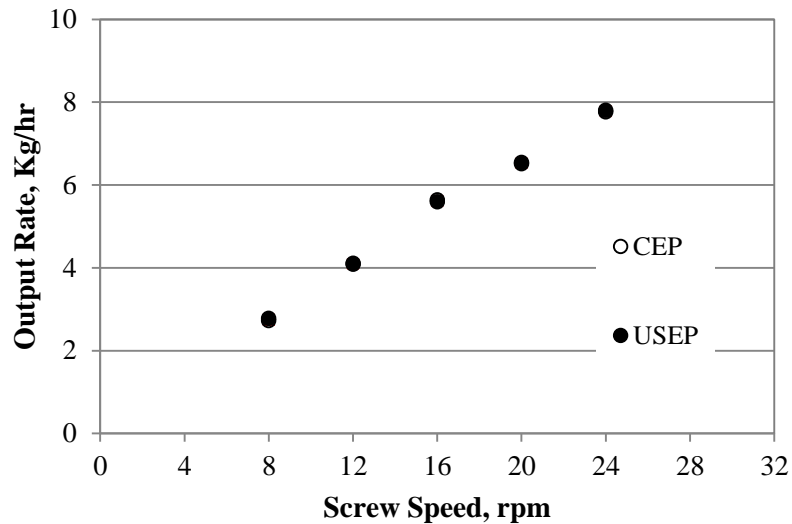
Figure 4-12: Output rates of polymer melt for different screw speeds measured for both CEP and USEP extrusion of Rigidex5130 strips.
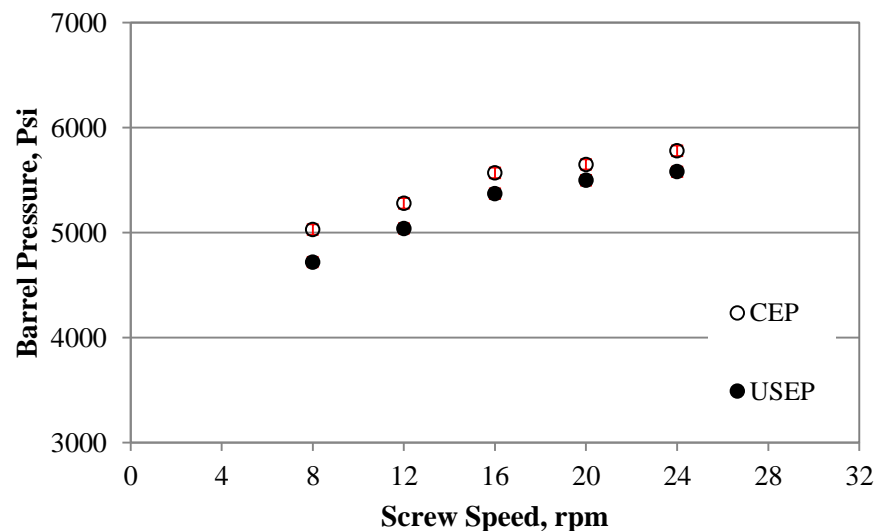
Figure 4-13: Extruder barrel pressure for CEP and USEP of PE80 strips.

The output rates were also measured for both processes and they are shown in Figure 4-12. No significant change was observed by the application of USVs. As expected the output rate from both the conventional and USEP extrusion increased linearly by increasing the screw speed. The power consumption measurements and output rate results of Rigidex5130 suggested that for processing of the similar amount of material, USEP extrusion will consume less power than CEP.
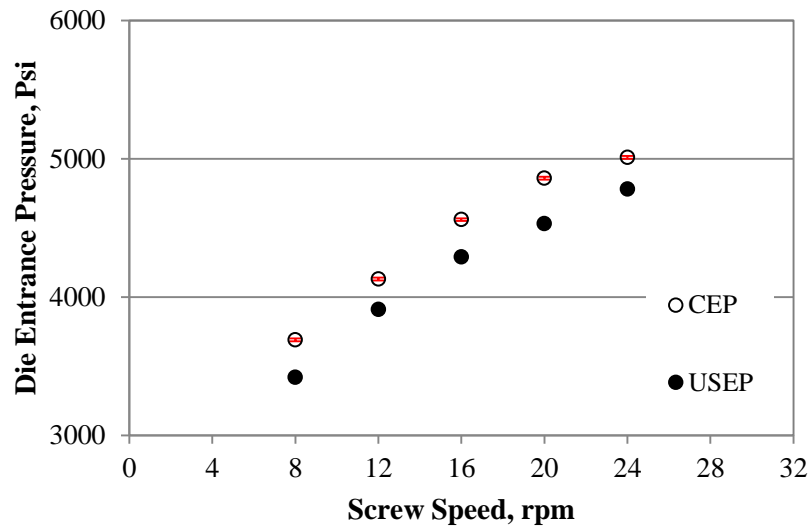
Figure 4-14: Ultrasonic die entrance pressure for CEP and USEP of PE80 strips.

Similar extrusion processing to Rigidex5130 was carried out on PE80 and strips were produced with both the CEP and USEP. The barrel pressure was recorded and is shown in Figure 4-13. It can be seen from the results that a drop in pressure was observed for the extruder barrel and the amount of the reduction (2.6-6.1% over the range of screw speed) of pressure was lower than the value observed for Rigidex5130 processing (6.3-9% over the range of screw speed). This means that the effect of ultrasonic vibrations on the extruder barrel pressure for the processing of PE80 was less than Rigidex5130. A possible explanation for this could be the higher viscosity of the PE80 compared to the Rigidex5130. The heat dissipation of the ultrasonic vibrations in the polymer melt is greater for the PE80 compared to the Rigidex5130 as a result of the viscosity difference.

As discussed earlier in Section 1.3.3 of Chapter 1, ultrasonic waves could generate heat and decrease friction. Polymer extrusion benefits from local generation of heat and

decrease of friction. The generated heat from the dissipation of the ultrasonic waves lead to a local rise in temperatures and thus the viscosity of the polymer melt was locally reduced. The lower local viscosities lead to an easier flow of the polymer melt and thus lowered the back pressure (barrel pressure) and die entrance pressure.

The decrease of the friction as a result of the high frequency shear vibration reduced the resistance of the die to the melt flow and consequently reduced the back pressure generated by the die. Figure 4-15 shows the total power consumption of the extrusion process for the production of the PE80 strips. The power consumption was measured for the 5 different screw speeds and it can be seen that the power consumed to produce strips at 8rpm by application of ultrasound was 4.2% lower than the amount of energy used to produce the strips at the same screw speed with conventional extrusion. The difference between power consumption of these two processes was reduced by increasing the screw speed. The difference between the power consumptions of USEP and CEP became almost zero at 24rpm which meant that although the application of the ultrasound does affect the die characteristics of the process as shown in Figure 4-14, the residence time of the melt in the ultrasonic die was not enough to affect the power consumption of the extrusion process. At higher melt flow rates, the ultrasonic generator will need more energy to maintain the operating frequency and amplitude, especially in the cylindrical section of the horn. The reason for this is the nature of the ultrasonic generators as they operate on the basis of power on demand. This means that if the vibration of the horn needs more energy the generator will consume more power to maintain the operating frequency and amplitude. Shear vibrations for the higher flow rates of the melt consume more power as a result of higher shear force on the horn that the horn has to overcome in order to vibrate while this force is lower for the lower screw speeds. Although there was no power readings for the ultrasonic generator alone but the power indicator, which was a LED display, showed higher power consumptions for higher screw speeds.
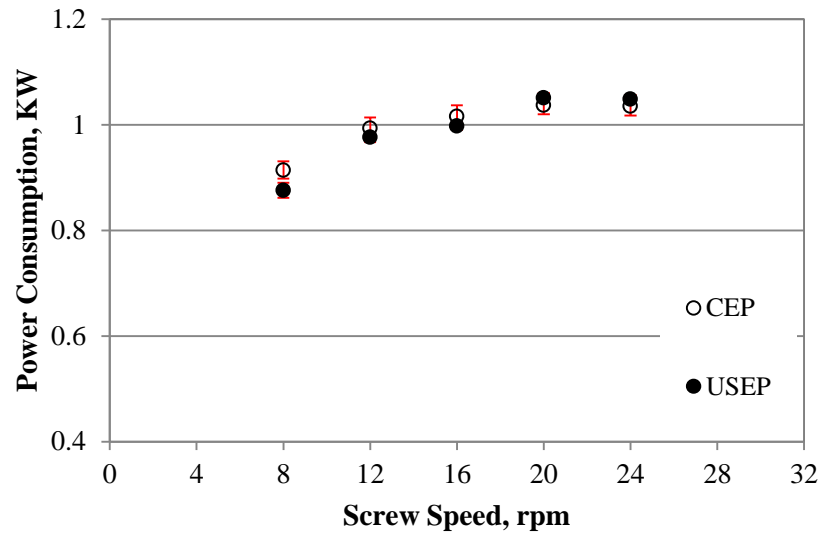
Figure 4-15: Total power consumption for CEP and USEP extrusion of PE80 strips.
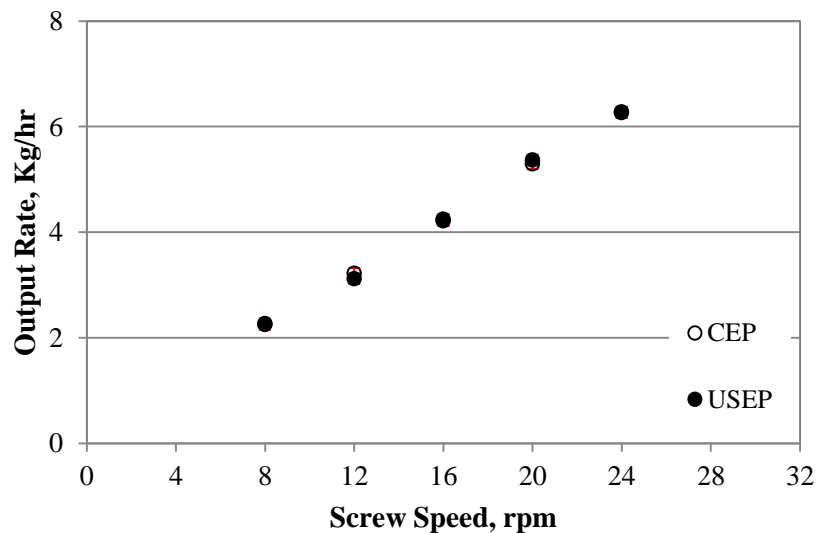
Figure 4-16: Output rates of polymer melt for different screw speeds measured for both CEP and USEP of PE80 strips.

The output rates for both USEP and CEP processes were measured at the different screw speeds and no difference between them was observed as it can be seen in Figure 4-16. Similar to Rigidex5130, the energy consumption measurements and the output rate results from the PE80 suggested that for processing a similar amount of material the USEP process consumed less energy when compared with the CEP only at lower screw speeds.

4.3.1.2 Extrusion of the polyethylene pipes

Pipes were produced from PE80, HYA600, HYA600/20 and HYA600/40 compounds at five different screw speeds of 12, 14, 16, 18 and 20 rpm with and without presence of the ultrasonic waves. The extrusion process was carried out for each screw speed until the processing parameters were stable before collecting any data or testing sample. The temperature setting of the extruder is summarised in Table 4-2. Because the processing temperatures for the HYA600 resin and the composites of HYA600 were similar they are both represented in Table 4-2 as HYA600.

Table 4-2: Temperature setting for processing of PE80 and HYA600 pipes.

Material	Barrel Heating Zones				Extruder Die Zones		Ultrasound Die Zones	
	T1	T2	T3	T4	T5	T6	T7	T8
PE80	200	200	200	200	200	200	205	205
HYA600	180	180	190	190	190	190	200	200

To start the production of the pipes the following procedure was carried out.

- A setup pipe with a length of three meters was positioned in the haul off and the water bath to enable the pulling of the extrudate through the water bath using the haul off.
- A sufficient length of the polymer was extruded to be tied onto the pipe and then the extruder was stopped.
- The extruded polymer was then tied onto the pipe using nylon cable ties to prevent water entering the inside of the pipe.
- The extrusion was started at the same time as the haul off.
- The water bath was brought forward close to the exit of the die.

Then using the haul off which was set on appropriate speed the extrudate pulled into the vacuum sizing sleeve of the water bath to get into the pipe form and solidify. The Pipe then entered the cooling section where water was sprayed onto the pipe to cool it down to the

ambient temperature before it reaches the haul off. For each screw speed about 3 to 4 meters of pipe was produced and the processing parameters recorded.

Figure 4-17 shows samples of the pipes produced with the PE80, HYA600 and HYA600 composites at different screw speeds using both CEP and USEP extrusion modes. The pipes then used for preparation of samples of the characterization tests.

Figure 4-17: Samples of the pipes which have been produced with PE80, HYA600, HYA600/20 and HYA600/40 from top to bottom.
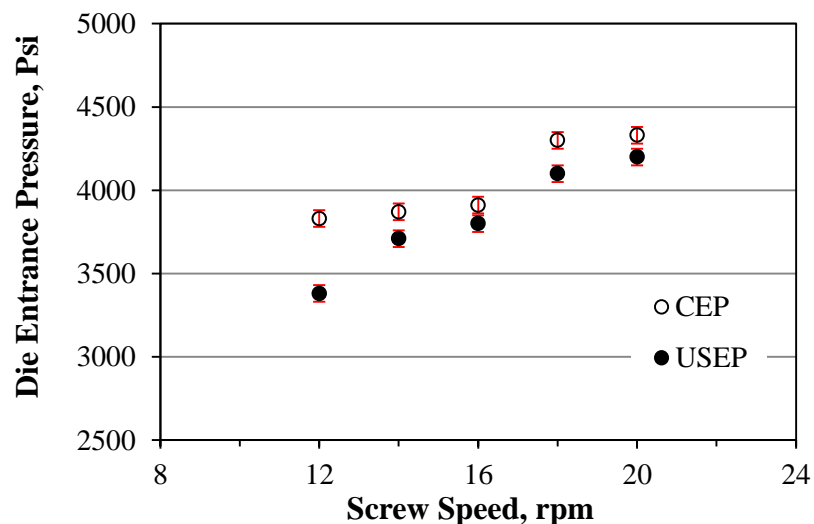
Figure 4-18: Ultrasonic die entrance pressure for CEP and USEP processing of PE80 pipes.

The die entrance pressures for the CE and USE processes are shown in Figure 4-18 for the PE80 pipes. It can be seen that the value of this pressure for the CE was higher than that

for the USE of the pipes at the same screw speed. The extruder barrel pressure also showed a similar behaviour to the die entrance pressure being lower for the USEP when compared to the CEP; the results were plotted against screw speed and are presented in Appendix C.

The power consumed by the die heaters, the ultrasonic generator (for USEP) and the extruder was measured and used to calculate the total power consumption. The calculation of the total power consumed was similar to the calculation that was carried out for the strip extrusion. The calculated power consumption for the processing of the PE80 pipes is shown in Figure 4-19. It can be seen that the power consumed to produce pipes at 12rpm USEP extrusion is 12.2% lower than 12rpm CEP. The difference in power consumption by increasing of the screw speed reduced until 20rpm where the difference between two values of the power consumption was negligible. As expected the power consumption increased almost linearly up to the screw speed of 18rpm for both CEP and USEP, but the consumed power increased slightly with an increase of the screw speed from 18rpm to 20 rpm. The reason for this could have been the increase of shear heating. The same behaviour has been observed for processing of PE80 strips at 20rpm and 24rpm as shown previously in Figure 4-15.
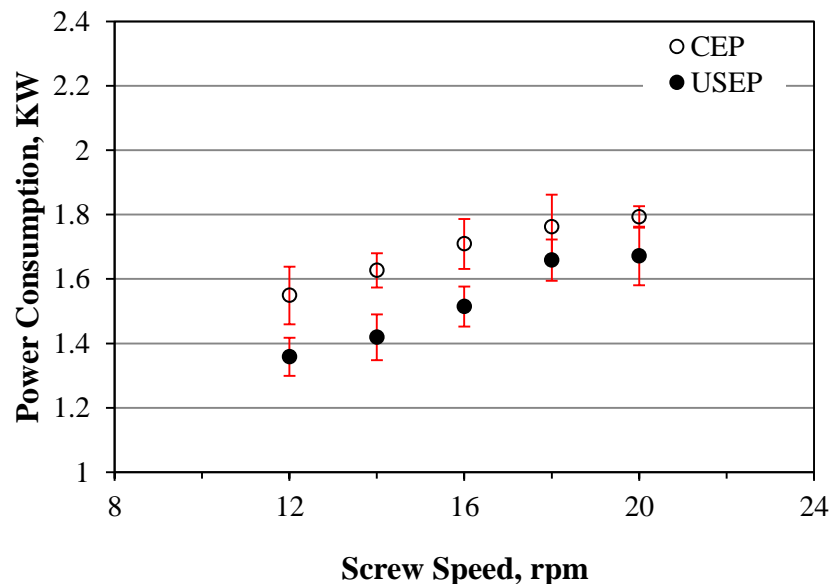
Figure 4-19: Total power consumption for CEP and USEP extrusion of PE80 pipes.

The line speeds of the pipe production were determined by measuring the length of pipe produced in a known amount of time for each screw speed. The calculated line speed along with the weight of 0.5m of the pipes produced at each screw speed; was then used for the determination of the output rates of the pipe extrusion process using Equation 4-8.

$$Output\ Rate\ \left(\frac{Kg}{hr}\right) = 120 \times Line\ Speed\ \left(\frac{m}{min}\right) \times weight\ of\ 0.5m\ pipe\ (Kg)$$

4-8

The output rates remained unchanged by the application of ultrasound to the extrusion of pipes and as shown in Figure 4-20. This was similar to the previous results on the production of the strips and, as it was expected theoretically, the output rates of the extrudate increase linearly with the extrusion screw speed.
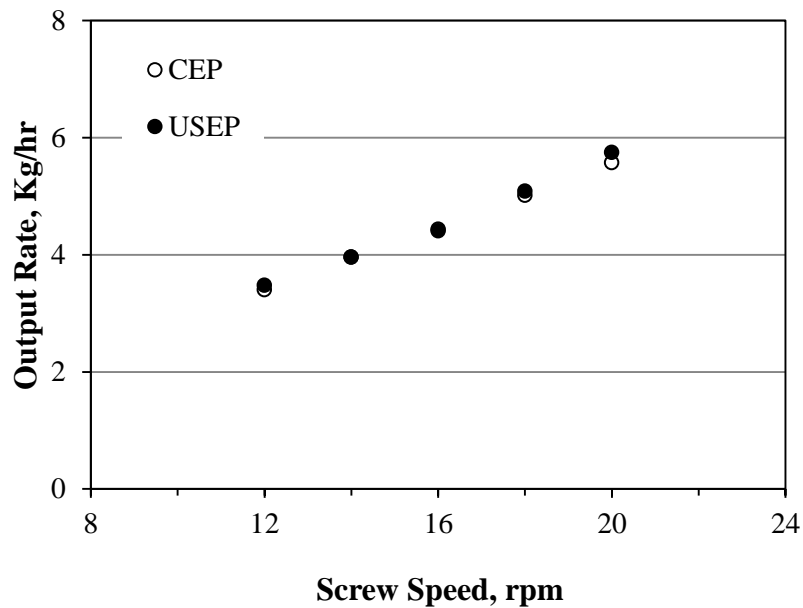
Figure 4-20: Output rates for different screw speeds measured for both CEP and USEP extrusion of PE80 pipes.

121
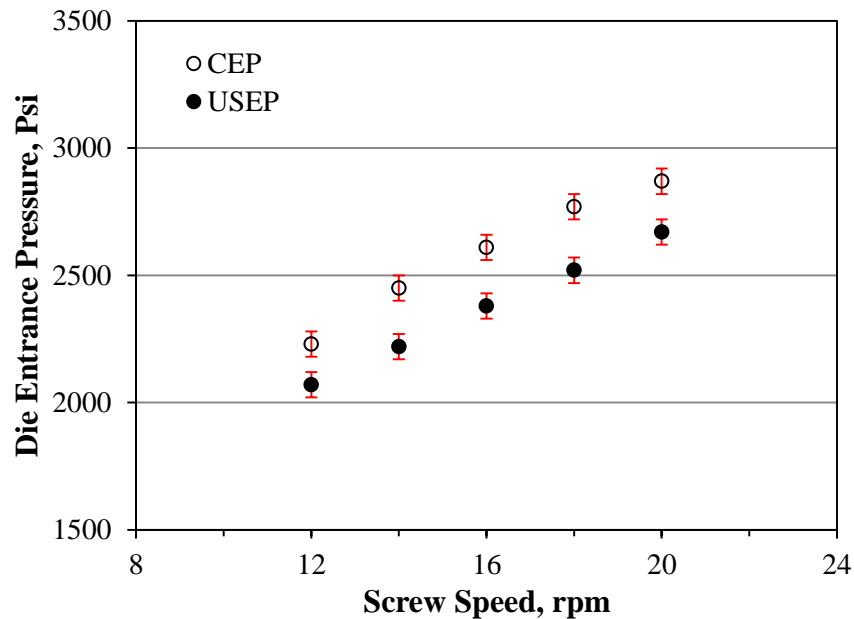
Figure 4-21: Ultrasonic die entrance pressure for CEP and USEP of HYA600 pipes.

HYA600/20 and HYA600/40 were used for production of the pipes to investigate the effect of the ultrasound waves with and without presence of the fillers. The compounds were prepared by weighing and mixing the appropriate amounts of the master batch and the base resin. The prepared compounds were then used for pipe extrusion with the conditions shown in Table 4-2. The processing parameters were recorded during the extrusion of the pipes.

For the HYA600 pipes both the extruder barrel pressure (presented in Appendix C) and the die entrance pressure (shown in Figure 4-21) dropped in presence of the ultrasound waves by 3.4-3.9% and 6.9-9.3% respectively. This was a similar result to the extrusion of the PE80 pipes.

The total power consumed by the HYA600 pipe extrusion was measured and plotted against the screw speed and this is shown in Figure 4-22. The power consumed was reduced in the region of 12.4-22% from the CEP to USEP.
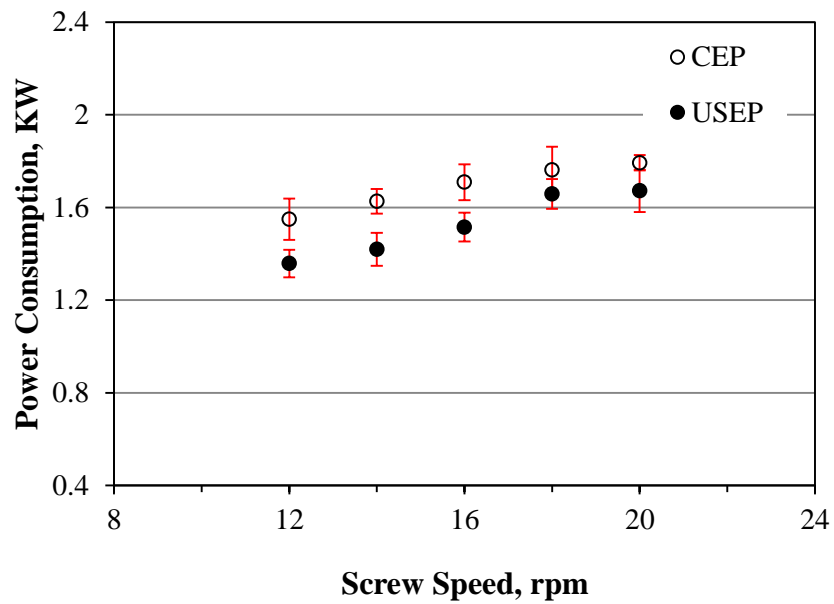
Figure 4-22: Total power consumption for CEP and USEP extrusion of HYA600 pipes.
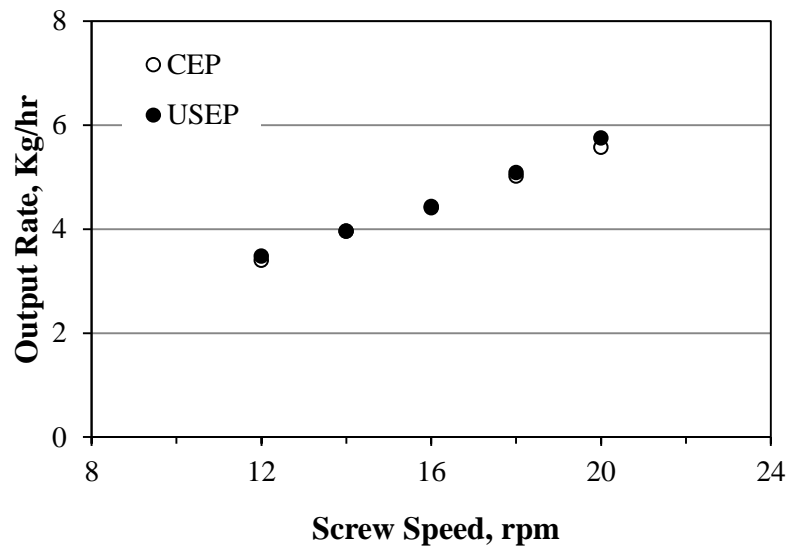
Figure 4-23: Output rates for different screw speeds measured for both CEP and USEP extrusion of HYA600 pipes.

While the barrel pressure, die entrance pressure and energy consumption of the process were affected by application of ultrasound waves, the output rates remained unchanged from the CEP to the USEP as it can be seen in Figure 4-23.
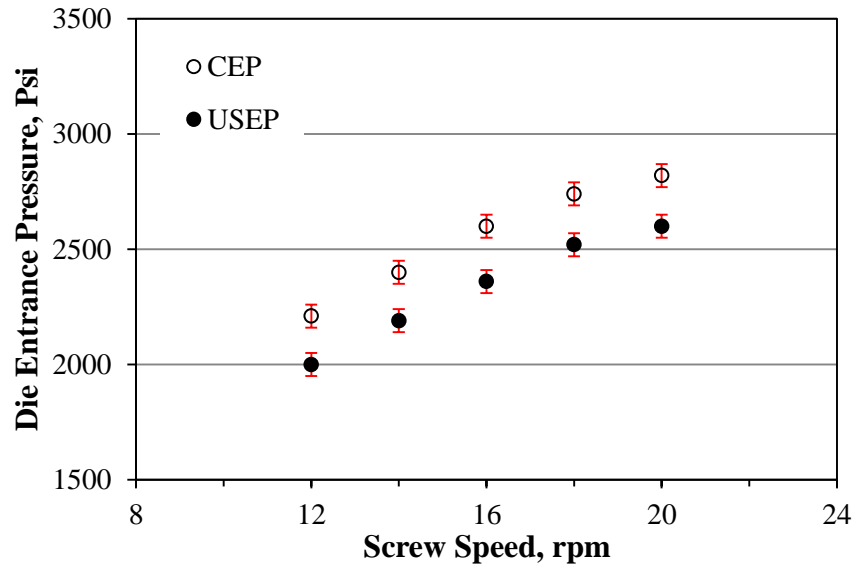
Figure 4-24: Ultrasonic die entrance pressure for CEP and USEP of HYA600/20 pipes.

The same temperature setting for the HYA600 extrusion was used for the pipe extrusion of HYA600/20. The line speeds that were used to produce HYA600 pipes were maintained for the processing of the HYA600/20 pipes. The polymer melt pressure was measured at the metering zone of the extruder barrel (presented in Appendix C) and at the entrance of the ultrasonic die for the HYA600/20. The die entrance pressure for the CEP and USEP processing of the HYA600/20 is presented in Figure 4-24.

For the HYA600/20 compound the die entrance pressure dropped between 7.5-9.5% (for processing at screw speeds of 20rpm to 12rpm, respectively) with the introduction of the ultrasonic waves which is higher than the pressure drop observed in the HYA600 pipe extrusion that varied in the range of 6.9-9.3% (for processing at screw speeds of 20rpm to 12rpm, respectively).

The total power consumption for the extrusion of HYA600/20 pipes was lower for the USE, than the CE as shown in Figure 4-25. At all the screw speeds the difference in power consumption is approximately 21% lower for the USE than CE. This reduction of power consumption was maintained over the range of the screw speeds from 12 to 20rpm.
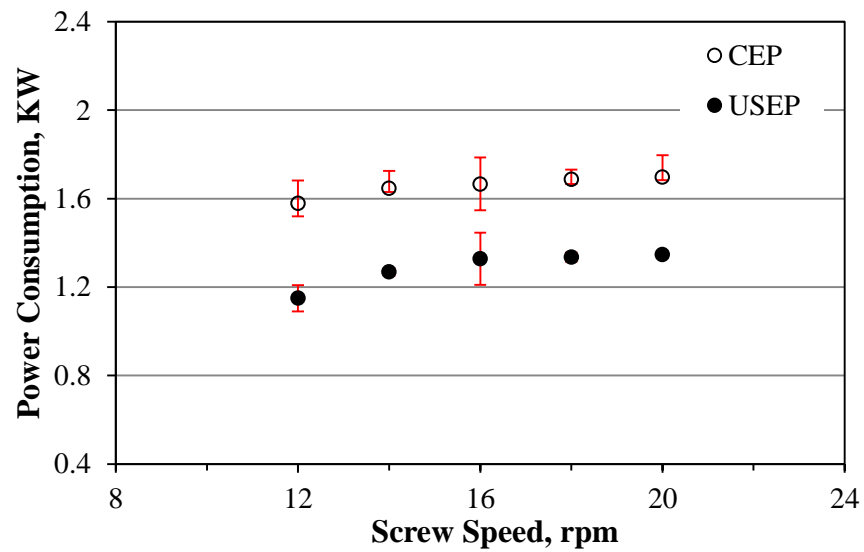
Figure 4-25: Total power consumption for CEP and USEP of HYA600/20 pipes.

Figure 4-26 shows the output rate for the HYA600/20 pipes that was measured for screw speeds of 12 to 20rpm, as expected from previous experiments the presence of ultrasonic vibrations did not affect the output rate.
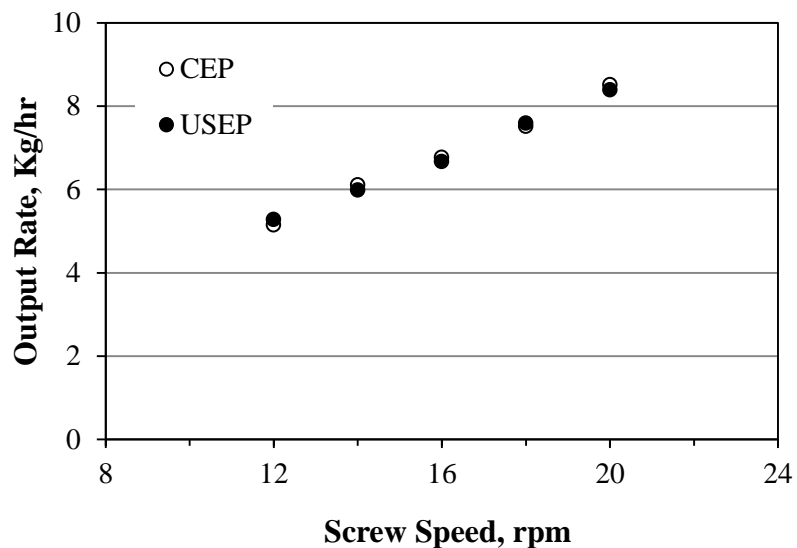
Figure 4-26: Output rates for different screw speeds measured for both CEP and USEP of HYA600/20 pipes.
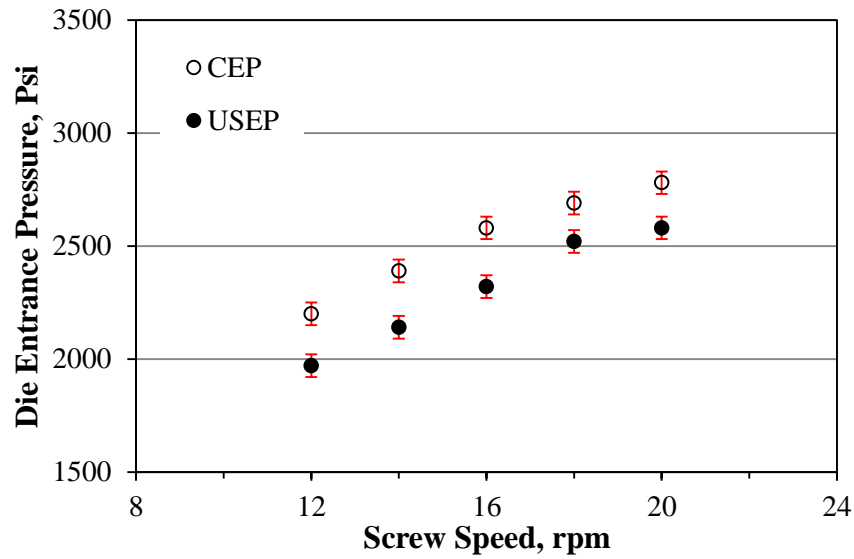
Figure 4-27: Ultrasonic die entrance pressure for CEP and USEP of HYA600/40 pipes.

The extrusion of HYA600/40 was carried under similar conditions to extrusion of the HYA600. The line speeds for the different screw speeds were also kept the same as for the HYA600 and HYA600/20. The extruder barrel pressure (presented in Appendix C) and the die entrance pressure which is shown in Figure 4-27 decreased with the application of ultrasound in the regions of 4.6-7% and 6.3-10.4% respectively.
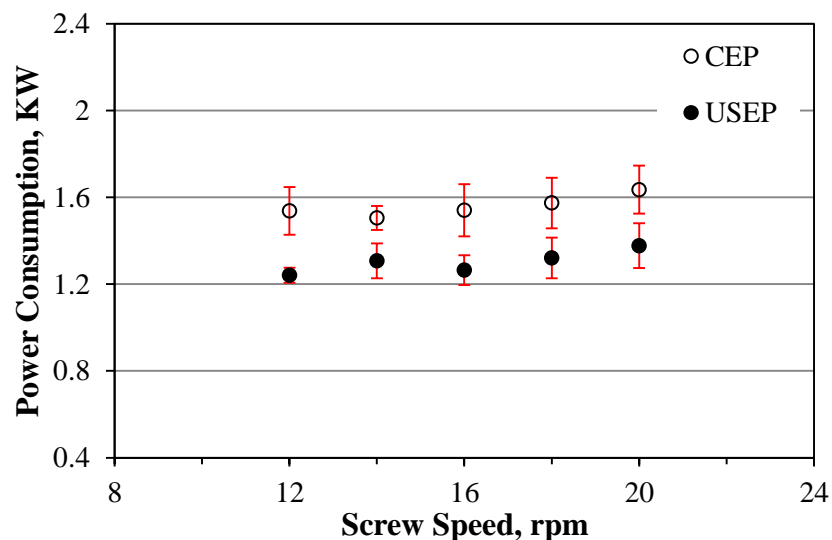
Figure 4-28: Total power consumption for CEP and USEP of HYA600/40 pipes.

Figure 4-28 shows the total power consumption for the processing of the HYA600/40 pipes at different screw speeds. The total energy consumed by the extruder, die heaters and the ultrasonic generator reduced by 13.1-19.2% for USE compared to CE. Figure 4-22 shows that the total power increased linearly with an increase in the screw speed. However, by considering the power consumption measurements for the composites (Figure 4-25 and Figure 4-28), it can be seen that the slope of the linear fit to the results is lower for the composites when compared with the resin. Therefore it can be said that the total power consumption for the extrusion of the HYA600 composites is less sensitive to changes in the screw speed in the range of screw rotation speeds investigated. This can be explained by increase in the contribution of the shear heating to the process heating as a result of viscosity increase.

The output rates for processing the HYA600/40 pipes were also measured in the same way as the HYA600 and HYA600/20 pipes. The measured output rates are plotted against the screw speed and are shown in Figure 4-29. It can be seen that the output rate remained unchanged from CEP to USEP.
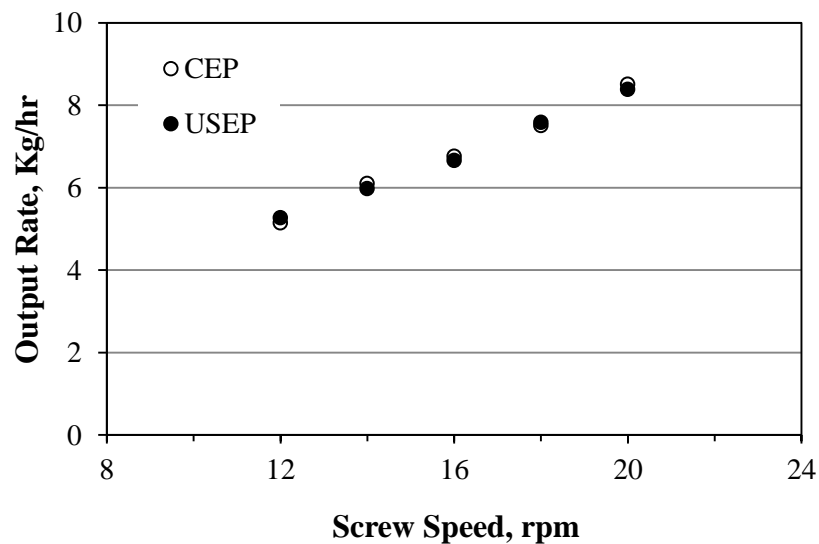
Figure 4-29: Output rates for different screw speeds measured for both CEP and USEP of HYA600/40 pipes.

The specific heat capacity of CaCo3 is 0.9 KJ/(Kg.K) whereas polyethylene's specific heat capacity range from 1.8 up to 2.4 KJ/(Kg.K) [124]. Addition of $CaCO_3$ to the polyethylene decreased the heat capacity of the composite compared to the resin and at the same time increased the heat conductivity of the composite as the fillers are more conductive to heat than the polyethylene melt. The reduction in the heat capacity leads to a lower total power consumption for extrusion of HYA600/40 when compared to HYA600/20 and the resin. However, presence of $CaCO_3$ increased the viscosity of the composite when compared with the resin [125] and as a result of that the generated heat from shear heating and ultrasonic vibrations increases.

The increase in the viscosity of the compound compared to the resin would demand extra power from the extruder motor. On the other hand the heat capacity of the compound is lower than the resin therefore energy needed to melt the resin is lower and compensates for higher extruder motor power consumption. The specific heat capacity of particle filled polymer matrix composites can be predicted with rule of mixtures for the composites.

$$C_c = C_p \phi_p + C_m \phi_m \qquad\qquad \textbf{4-9}$$

Where C is the specific heat capacity, Φ is the filler volume fraction and subscripts c, p and m denote composite, particle and matrix, respectively. The specific heat capacity of the composites were then calculated and shown in Table 4-3 based on specific heat capacities of 0.9 KJ/(Kg.K) and 2.4 KJ/(Kg.K) for calcium carbonate particles and polyethylene resin, respectively. By using calculated specific heat capacities the amount of energy required to heat 1 Kg of the resin/composites from the room temperature (21°C) up to the melting temperature (130°C) was calculated and presented in Table 4-3.

Table 4-3: The amount of heat required to bring 1Kg of the material from room temperature to the melting temperature.

Filler volume fraction	Heat Capacity (KJ/KgK)	Required heat to melt 1Kg of the material (KJ)
0	2.4	256.8
0.08	2.28	243.96
0.19	2.115	226.305

The calculated values in Table 4-3 indicate that melting of the same amount of the composites require less energy when compared with the resin. The presence of the filler in the HYA600 composites lead to lower total power consumption compared to the total power consumption of the resin and it is in agreement with the presented results in this section.

4.3.2 Mechanical Testing

As it was discussed earlier in Chapter 3 the introduction of ultrasound into polymer melts during extrusion not only affected the processing parameters but also could modify the product's mechanical properties as it also reported in the previous literature [3, 111, 121, 126-128]. The mechanical properties of the samples produced by the extrusion process were investigated by tensile testing and dynamic mechanical analysis.

4.3.2.1 Tensile Testing

The tensile tests were carried out with a gauge length (extensometer) of 25mm and at a speed of 1 mm/min for the modulus measurements and a gauge length (cross head grip separation) of 50mm and the test speed of 5 mm/min for the rest of the test. The samples were extended well past their yield point.

4.3.2.1.1 Tensile properties of the strips

The extruded strips were left under room conditions for at least two weeks prior to the tensile testing. The samples were then left at the testing environment temperature for 24 hours prior to testing in order to allow them to reach the environment temperature.

Standard dumbbell shape tensile samples (as described in Section 4.2.8.2) were punch cut from the strips. For each screw speed from 5 to 9 samples were tested and the test was continued up to post yield elongation (80% strain). The Young's modulus values were calculated and the average values of the results are plotted as a function of screw speed in Figure 4-30.
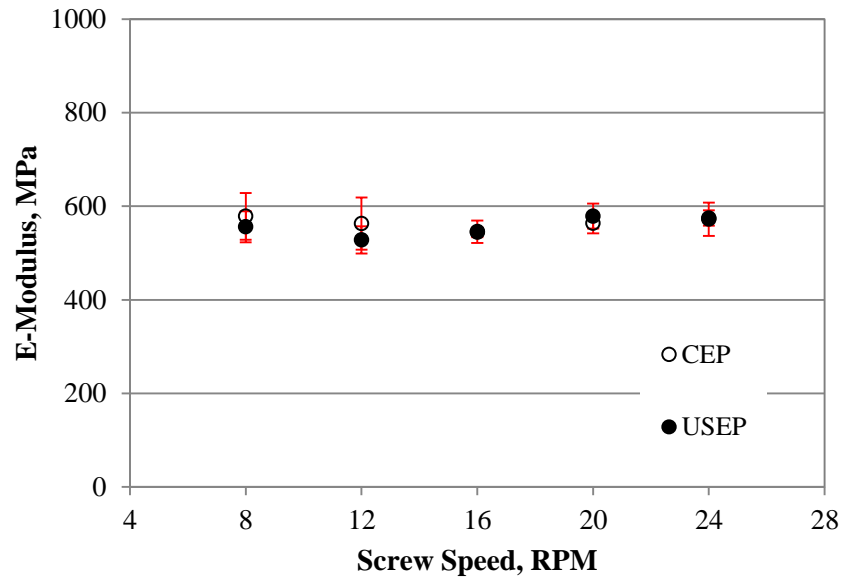
Figure 4-30: Young's Modulus values of Rigidex5130 strips produced by CEP/USEP extrusion at different Screw Speeds.

It can be seen from the results that the modulus shows a slight increase for USEP strips compared to CEP strips only for 8rpm and 12rpm. The modulus values for the rest of the screw speeds were similar for both CEP and USEP strips.

Yield strength values were obtained from the stress strain curves of the samples. The average yield strength values for the samples processed at each individual screw speed were calculated and plotted against the screw speed as shown in Figure 4-31. In common with the E-modulus values, the yield stress measured for CEP and USEP samples were not significantly different as can be seen in Figure 4-31.
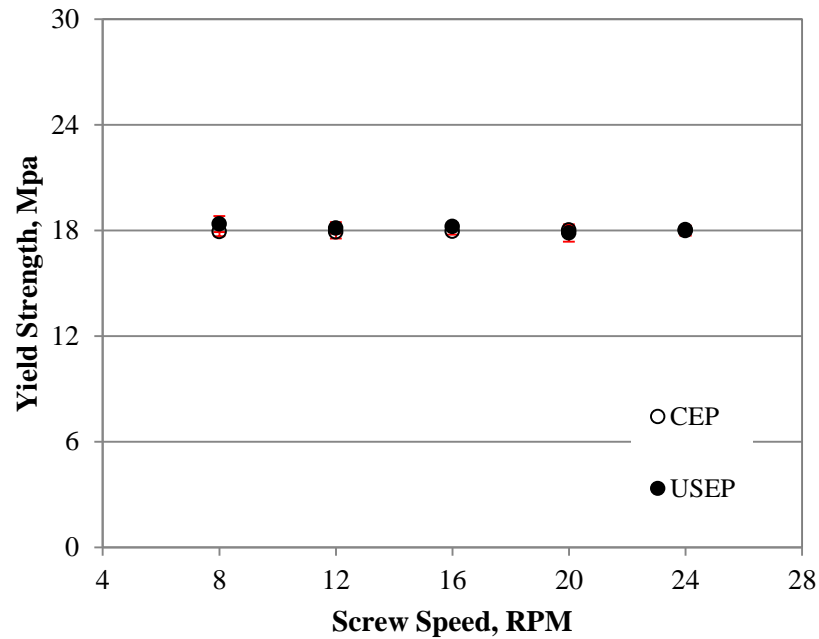
Figure 4-31: Yield strength at different Screw Speed for Rigidex5130 strips produced by CEP/USEP.

The Young's modulus from the tensile tests showed that the mechanical behaviour of the CEP and USEP samples at small strains are similar. Young's modulus is a representation of the bonding forces between the polymer molecules and also the morphology of the polymer. From the values of Young's modulus for the CEP and USEP samples, it can be concluded that the presence of ultrasonic vibrations has not affected the bonding forces between the molecules and chains.

As illustrated in Figure 4-31, the application of ultrasonic vibrations did not change the material's yield strength. It can be said therefore, that the measured mechanical properties of Young's modulus and yield strength, did not change by the application of the ultrasonic vibrations.
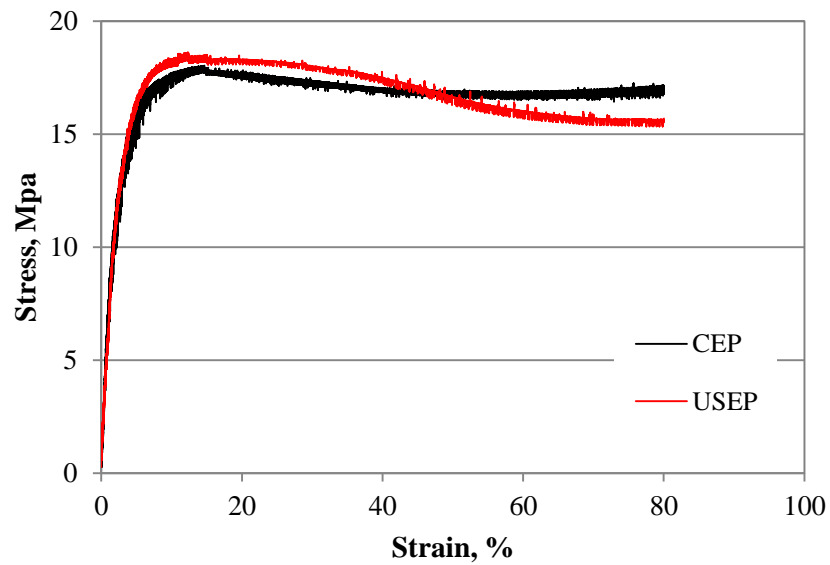
Figure 4-32: Stress vs. Strain for Rigidex5130 strips produced at 8rpm by CEP and USEP.
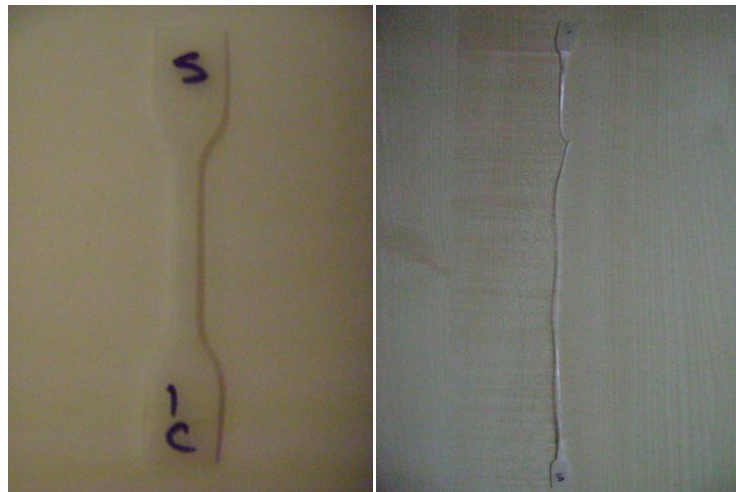
Figure 4-33: Tensile samples of Rigidex5130 before (left) and after (right) test.

The stress/strain data of the tensile tests were extracted and were used to generate an average curve for the tested samples using Origin Pro software. The average values were then fitted with a moving average trend line with the period of 5 to smooth the generated results. An average curve was generated for each screw speed individually for samples produced with and without presence of ultrasound. The stress strain curve for 8rpm is

shown in Figure 4-32 where it can be seen that the CEP and USEP samples showed quite similar behaviour to the applied stress. A small neck forms within the rectangular section of the test specimen at the yield point. After formation of the neck, the polymer chains get oriented and aligned parallel to the direction of the elongation. The orientation of the polymer chains leads to localized strengthening. The neck is an indication of the resistance to the deformation in this section and thus the elongation proceeds by the extension of the neck along the gauge length of the specimen. The failure of the specimen may only take place after the neck has fully extended along the gauge length. Similar curves were generated for the samples produced at other screw speeds and they are presented in Appendix C. Tensile test samples of Rigidex5130 before and after test are shown in Figure 4-33.

The same tensile test procedure to Rigidex5130 samples was carried out on PE80 strips. The tensile properties were determined for strips produced at the different screw speeds.
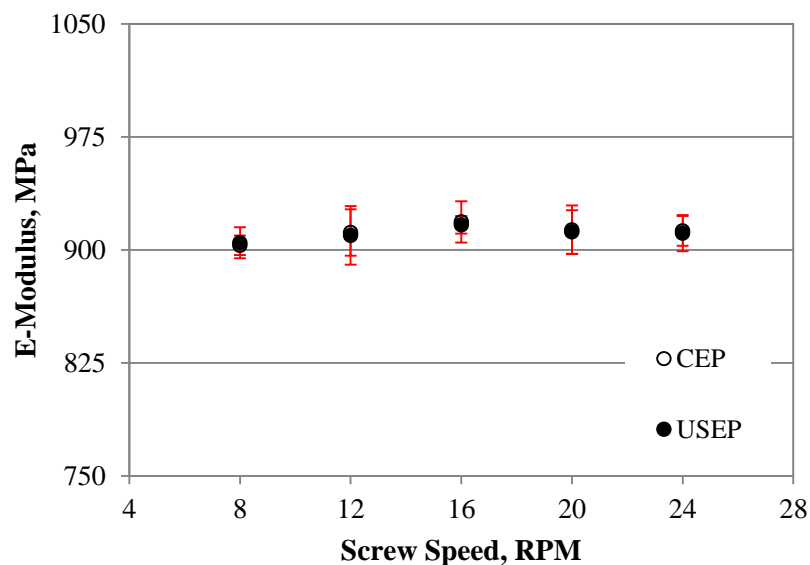
Figure 4-34: Young's Modulus values of PE80 strips produced by CEP/USEP at different Screw Speeds.

Figure 4-34 shows the Young's modulus of strips produced by CEP and USEP at the different screw speeds. These results suggest that the elastic properties and the microstructure of the amorphous and the crystalline regions have not been affected by the

application of the ultrasonic vibrations or the effect was not measurable by the conducted tests.
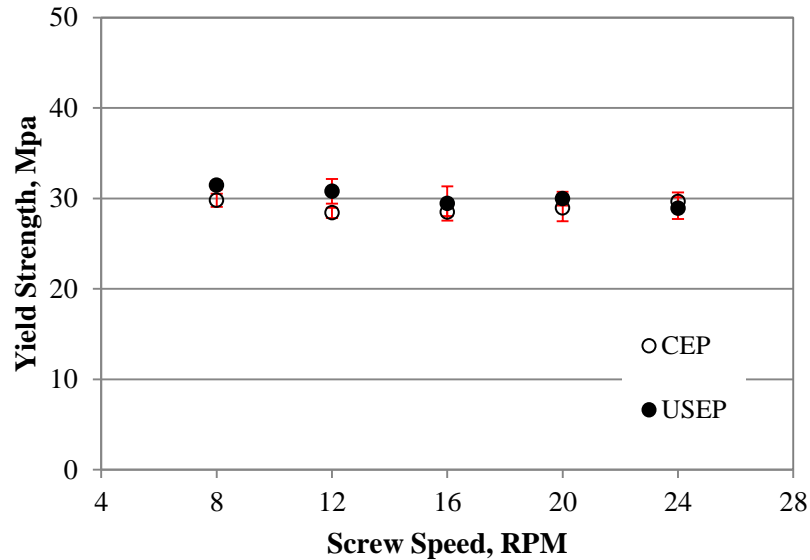
Figure 4-35: Yield strength at different Screw Speed for PE80 strips produced by CEP/USEP.

The material's response to an applied stress at large elongations can be investigated by the determination of the yield strength from the stress/strain curves. The yield strength values were obtained from the tensile results and plotted for the samples produced at the different screw speeds for the CEP and USEP. The yield strengths of the samples are shown in Figure 4-35. It can be seen that the samples produced by USEP are of a slightly higher strength compared to the samples produced by CEP. The difference in the yield strength values of the samples reduced by increasing the screw speed as a result of the lower residence time in the ultrasonic die. As it was discussed earlier for the production of the strips in Chapter 3, the effects caused by the ultrasonic waves are directly related to the residence time in the ultrasonic die. An increase of the throughput rate led to a decrease in the residence time in the ultrasonic die. A reduction in the residence time, therefore, reduced the effects of the ultrasonic vibrations. The residence time in the ultrasonic die varied in the range of ~30 seconds at the highest screw speeds up to ~97 seconds at the lowest screw speed.
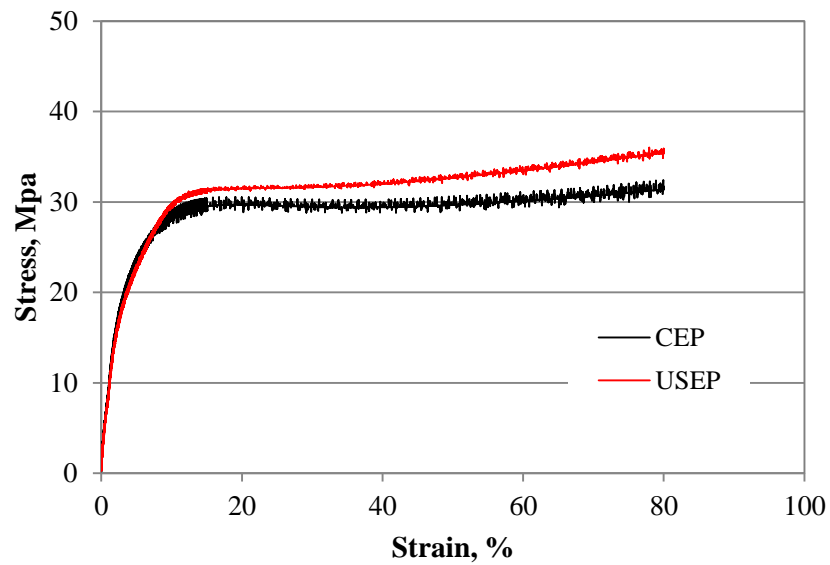
Figure 4-36: Average stress vs. Strain for PE80 strips produced at 8rpm produced by the CEP and USEP.

Figure 4-37: PE80 tensile samples before (left) and after (right) test.

The stress strain values of several samples processed at each screw speed were used to generate an average curve for samples processed by CEP and USEP. The average stress strain curve for the PE80 samples produced at 8rpm by CEP USEP is shown in Figure 4-36. The average stress strain curves for the samples produced at the other screw speeds were generated and presented in Appendix C. The tensile samples before and after the test are shown in Figure 4-37.

4.3.2.1.2 Tensile properties of the pipes

The pipes were given at least 2 weeks before tensile testing. Standard dumbbell shape tensile samples (as described in 4.2.8.2) were punch cut from the pipes. The prepared samples were then left at the testing environment 24hr prior to the test to allow the samples to reach the environment temperature. In order to ensure the consistency of the samples all of them were cut from same section of the pipes (relative to the position of the feed channel in the sonic die block). For each screw speed 3 to 7 samples were tested and the test continued up to the post yield elongation up to 80% strain.
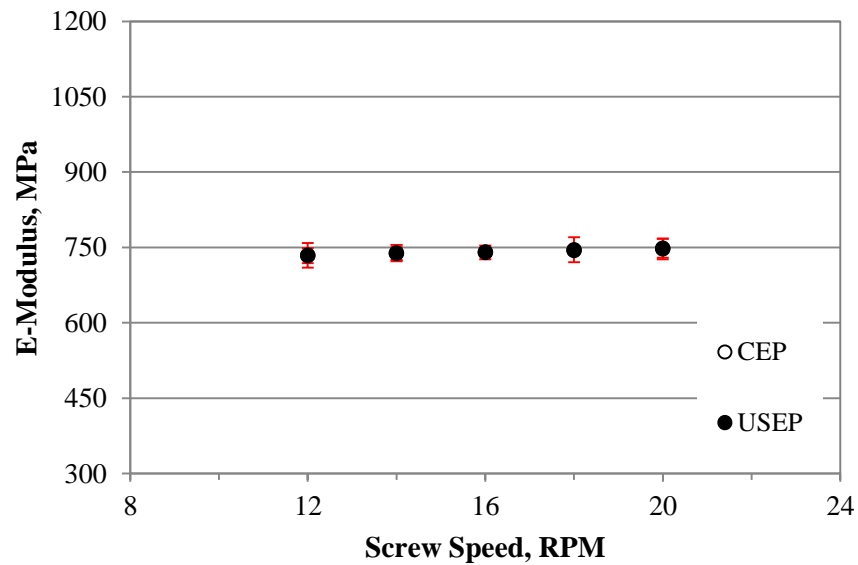
Figure 4-38: Young's Modulus values of PE80 pipes produced by CEP/USEP at different Screw Speeds.

The Young's modulus values for CEP and USEP samples of the PE80 pipes were obtained from the stress strain curves of the samples produced at different screw speeds. The calculated modulus values for CEP and USEP samples were then plotted against screw speed as shown in Figure 4-38. The modulus of the samples was around 750 MPa and it can be seen the presence of ultrasonic vibrations did not affect the tensile modulus of the pipes produced at the different screw speeds. Similar results were obtained from the PE80 strips and this indicates that by application of the ultrasonic vibrations, the elastic properties of the amorphous and crystalline regions and their microstructure which play an

important role in small strains and consequently on modulus values of the samples remained unchanged.

Figure 4-39 shows the yield strength of the CEP and USEP pipes. By considering the standard deviation of the measured values and a comparison of the yield strength of CEP and USEP pipes at different screw speeds, it can be said that the yield strength remains unchanged by application of ultrasonic vibrations. This suggests that application of ultrasonic vibrations during extrusion process did not have adverse effect on the mechanical properties of the products.

Small changes to factors affecting tensile strength such as changes to molecular weight, chain conformation, degree of crystallinity could be the reason for the differences observed between CEP and USEP yield strengths as shown in Figure 4-39 these results needs to be confirmed by other characterization techniques such as DSC, DMA and rheological analysis.
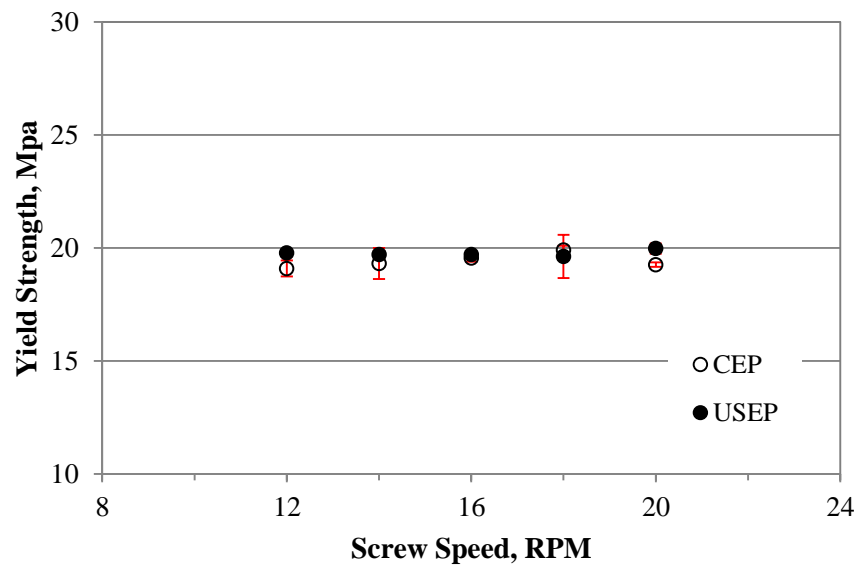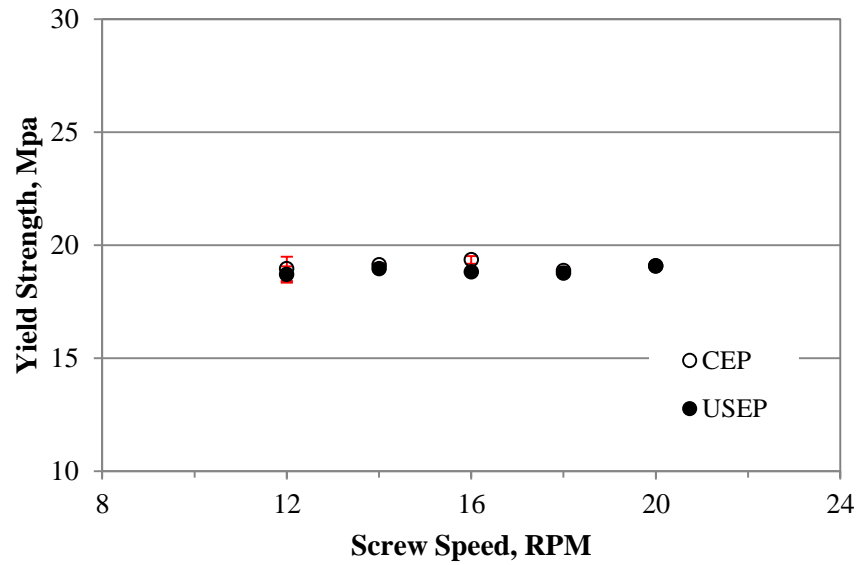

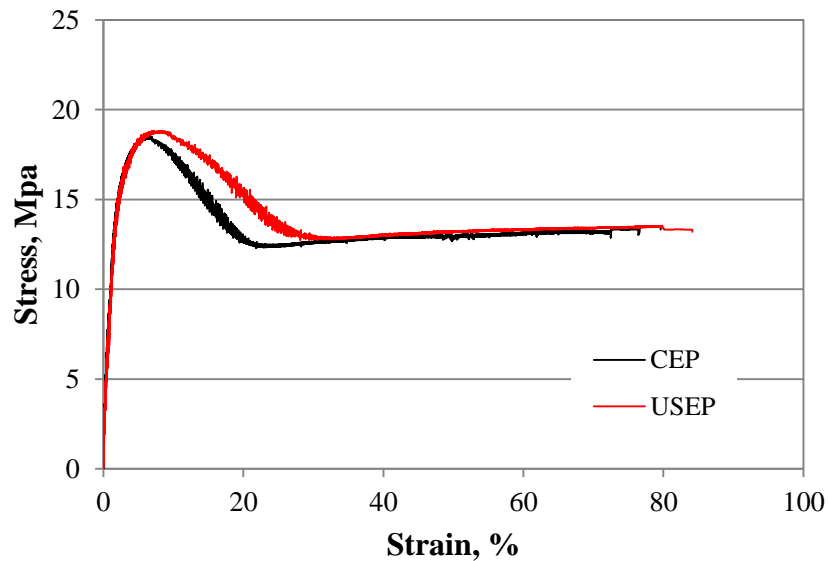**Figure 4-39: Yield strength at different Screw Speed for PE80 pipes produced by CEP/USEP**
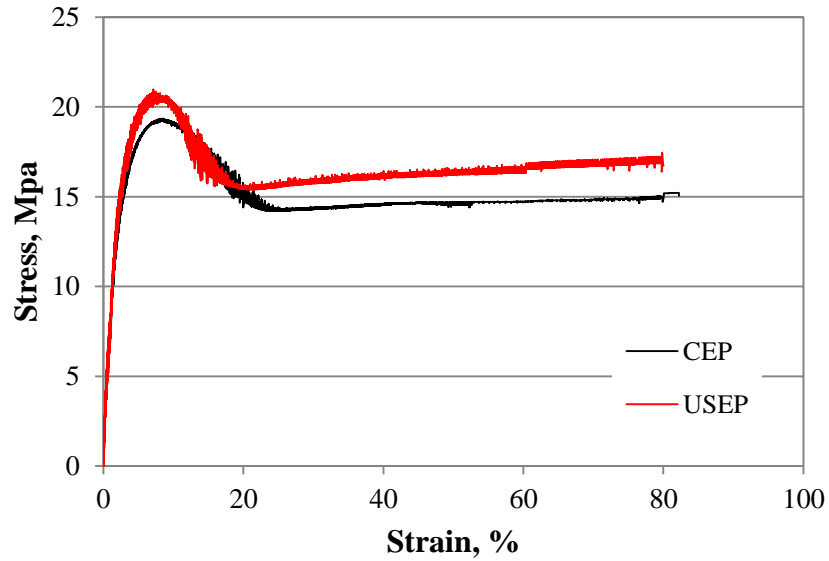
Figure 4-40: Average stress vs. Strain for PE80 pipes produced at 12rpm produced by CEP and USEP.

The average stress strain curve for the PE80 pipes were generated for pipes processed with and without presence of USVs at different screw speeds with the same method described in 4.3.2.1.1. The average curve for pipe samples produced at 12rpm is shown in Figure 4-40 and the rest of the average stress strain curves for pipes produced at the rest of the screw speeds are presented in Appendix C.
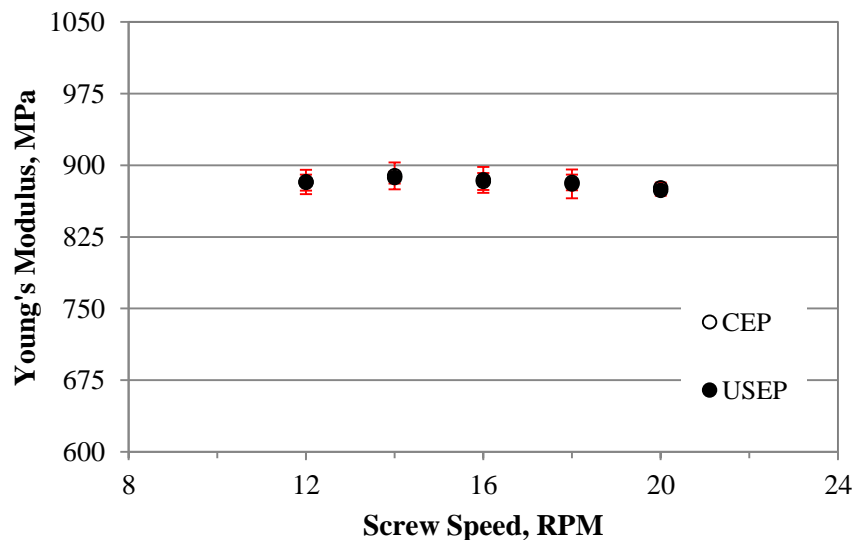
Figure 4-41: Young's Modulus values of unfilled HYA600 pipes produced by CEP/USEP at different Screw Speeds.

The values of Young's modulus for the HYA600 pipes produced at the different screw speeds from 12 rpm to 20rpm for both the CEP and USEP extruded samples are shown in Figure 4-41. It can be seen from the modulus values plotted in Figure 4-41 that the modulus of the samples was the same for the CEP and the USEP. The HYA600 and the PE80 were commercial resin grades of HDPE and although they were possibly different in molecular weight (according to MFR values) both had a similar structure and composition. Therefore, in the light of the PE80 results, no significant difference with the application of ultrasonic vibrations was expected, and was observed, in the tensile properties.
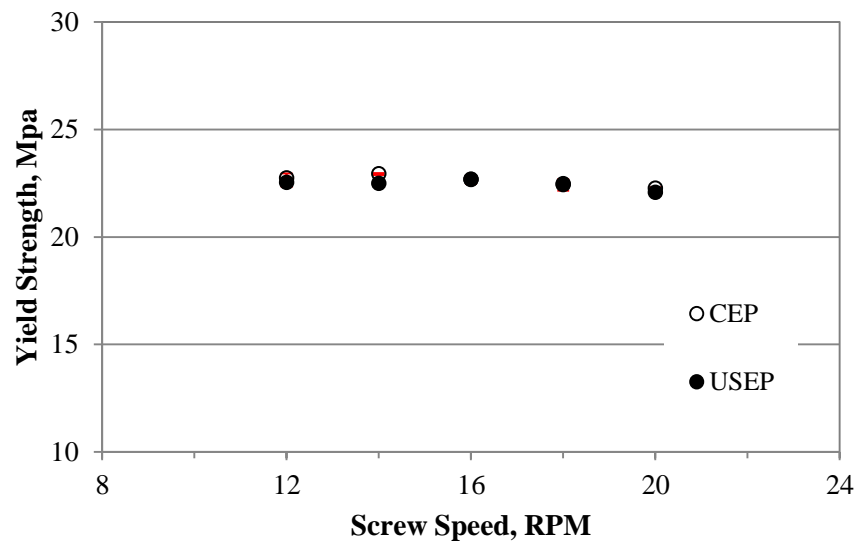
Figure 4-42: Yield strength at different Screw Speed for unfilled HYA600 pipes produced by CEP/USEP extrusion.

The yield strengths of the HYA600 pipes were obtained from the stress strain curves and are shown in Figure 4-42 for CEP and USEP samples produced at the different screw speeds. The yield strength of the pipes remained unchanged by the application of the ultrasonic vibrations except for the pipes produced at 12rpm and 14rpm that showed a small difference between the CEP and USEP samples' yield strength. The pipes produced at 16, 18 and 20rpm conventionally had a similar yield strength to that of pipes produced with the presence of ultrasonic vibrations.

The small difference between yield strengths for the pipes produced at 12 and 14rpm can be accounted for by means of experimental errors. The observed difference could also be

related to changes to the conformation of the chains, crystalline structure or molecular weight of the polymer as a result of application of the ultrasonic vibration but as it can be seen the difference is not significant and measurable. However, changes to abovementioned parameters could affect the tensile modulus of the pipes but as shown in Figure 4-41 the modulus of the conventionally processed pipes were similar to the pipes produced by ultrasonic vibrations. Therefore, it can be said that the change occurred by application of the ultrasonic vibrations are not visible in small strains (tensile modulus results) but they do have more influence on the mechanical behaviour of the pipes in larger strains (yield strength).
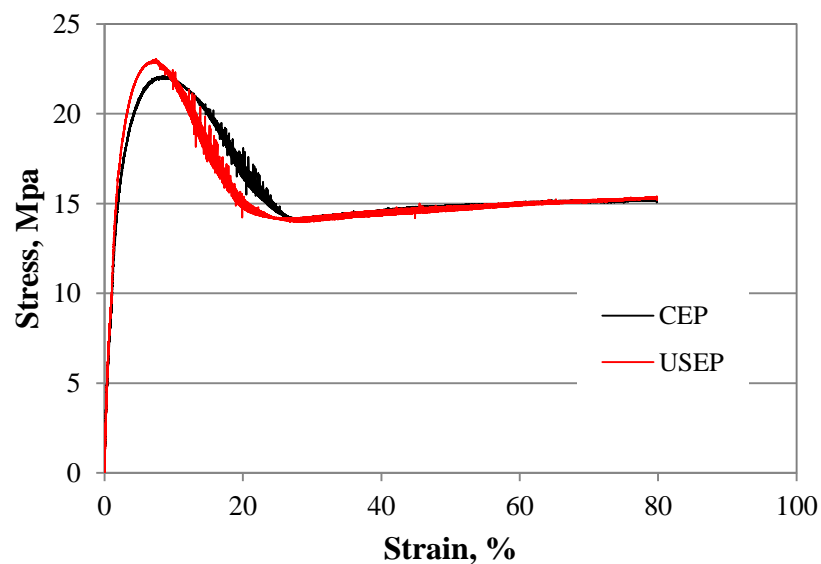
Figure 4-43: Average stress vs. Strain for unfilled HYA600 pipes produced at 12rpm produced by CEP and USEP.

The average stress strain curve of the pipes produced at 12rpm is shown in Figure 4-43. It can be seen that the tensile response of the CEP pipes are quite similar to that of USEP pipes. At small strains, where the Young's modulus was calculated, the stress/strain curves for the CEP and USEP pipes coincide. However, a small difference was observed in the yield point for the pipes produced at 12 rpm and this difference was even smaller for pipes produced at 14 rpm. The tensile curves of the pipes produced at the rest of the screw speeds were similar to each other and essentially no difference was observed between the

CEP and the USEP samples. The stress/strain curves for the pipes produced at the other screw speeds are presented in Appendix C.
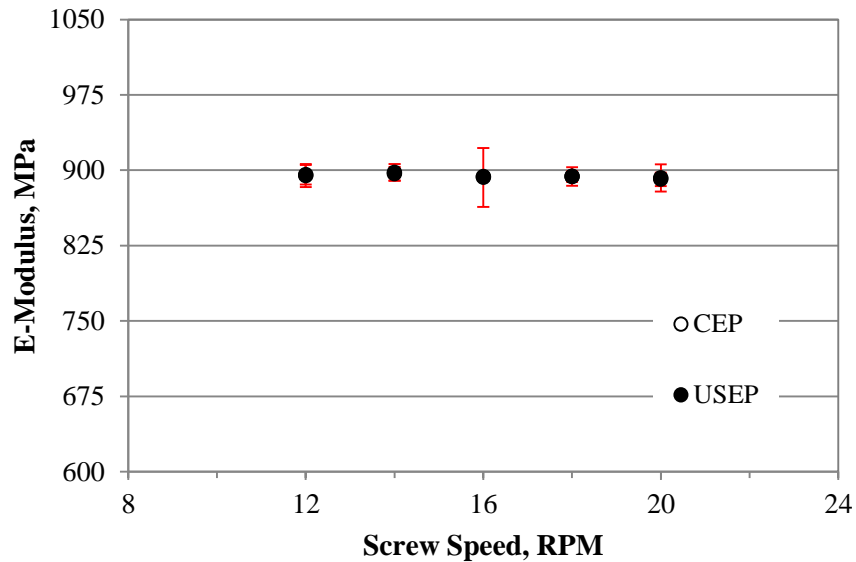
Figure 4-44: Young's Modulus values of HYA600/20 pipes produced by CEP/USEP at different Screw Speeds.

The tensile modulus of the HYA600/20 pipes were obtained from initial part of the stress/strain curves and are shown in Figure 4-44 for the pipes produced at screw speeds of 12rpm to 20rpm. The measured modulus values for the HYA600/20 pipes as seen in Figure 4-44 showed no difference between the USEP and CEP produced pipes. By comparing the tensile results for HYA600 and HYA600/20 pipes, it was shown that for both materials the presence of the ultrasonic vibrations did not have an effect on the modulus of the pipes. As expected, the addition of the filler to HYA600 increased the young's modulus of the pipes when compared with HYA600.

The comparison of the yield strength of the CEP and USEP pipes (shown in Figure 4-45) suggests that the application of the ultrasonic vibrations didn't have an effect on the yield strength of HYA600/20 pipes. The yield strength of the pipes decreased by the addition of the calcium carbonate filler but the yield strength values remained unaffected by application of the ultrasonic vibrations.

141

Figure 4-45: Yield strength at different Screw Speed for HYA600/20 pipes produced by CEP/USEP.

Figure 4-46: Average stress vs. Strain for HYA600/20 pipes produced at 12rpm produced by CEP and USEP.

The average stress strain curves for the HYA600/20 pipes produced at 12rpm are shown in Figure 4-46. The addition of calcium carbonate to HYA600 did not seem to make a significant change to the effects of the ultrasound on the mechanical properties as they remained almost unchanged for both the HYA600 pipes and HYA600/20 pipes.

The modulus of elasticity for the HYA600/40 pipes produced by CEP and USEP extrusion was calculated from the initial part of the tensile curves and plotted for different screw speeds as shown in Figure 4-47. It can be seen from Figure 4-47, the tensile modulus of the pipes remained unchanged by application of the ultrasonic vibrations. This result is similar to that of the HYA600 and HYA600/20 pipes. A comparison of the modulus of the HYA600/40 with HYA600 and HYA600/20 pipes shows that the tensile modulus increased with an increase in the filler content. However, as it was mentioned earlier for HYA600/20 pipes, the presence of the filler did not have an influence on the effect of the ultrasonic vibrations on the young's modulus of the pipes.
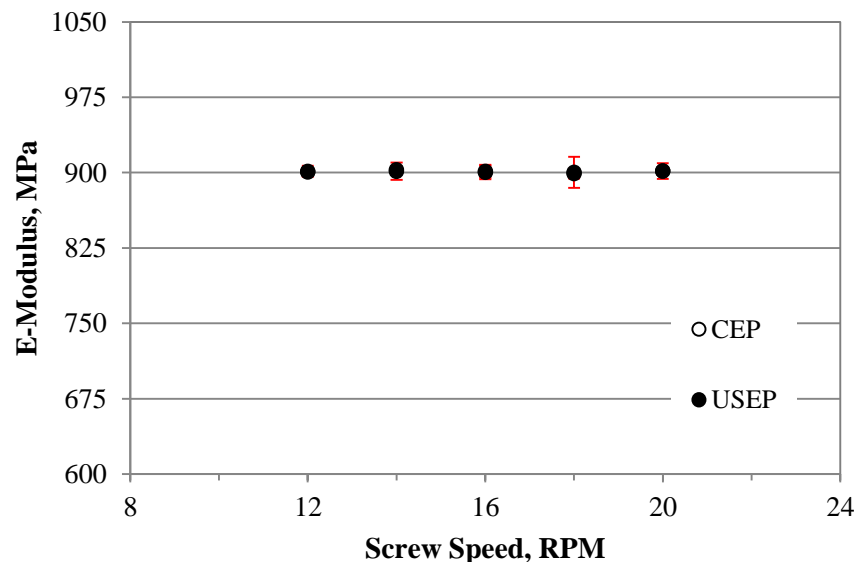
Figure 4-47: Young's Modulus values of HYA600/40 pipes produced by CEP/USEP at different Screw Speeds.

Figure 4-48 shows the yield strength of both CEP and USEP HYA600/40 pipes produced at different screw speeds. As shown in Figure 4-48, the yield strength of the pipes has not been affected by the application of ultrasonic vibrations during extrusion. However, the yield strength of the pipes decreased with an increase of the filler content when compared to the HYA600 and HYA600/20 pipes.
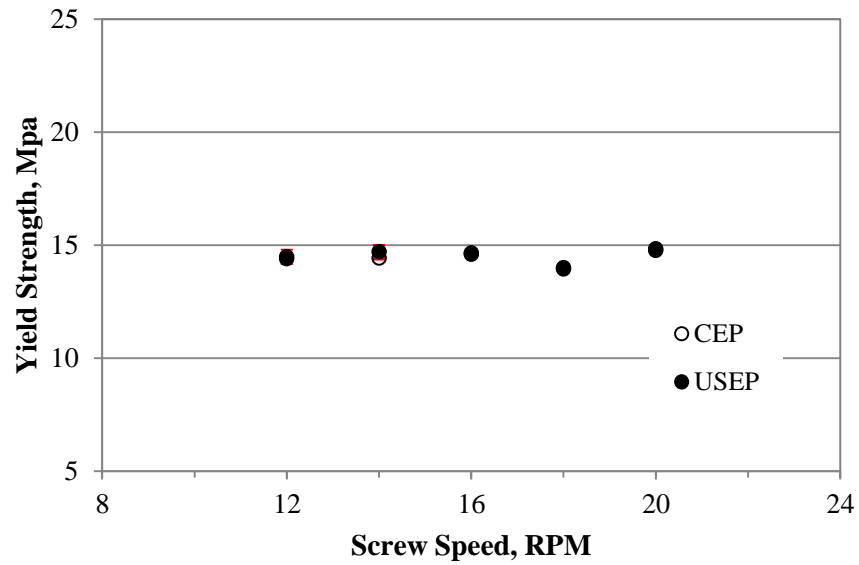
Figure 4-48: Yield strength at different Screw Speeds for HYA600/40 pipes produced by CEP/USEP.
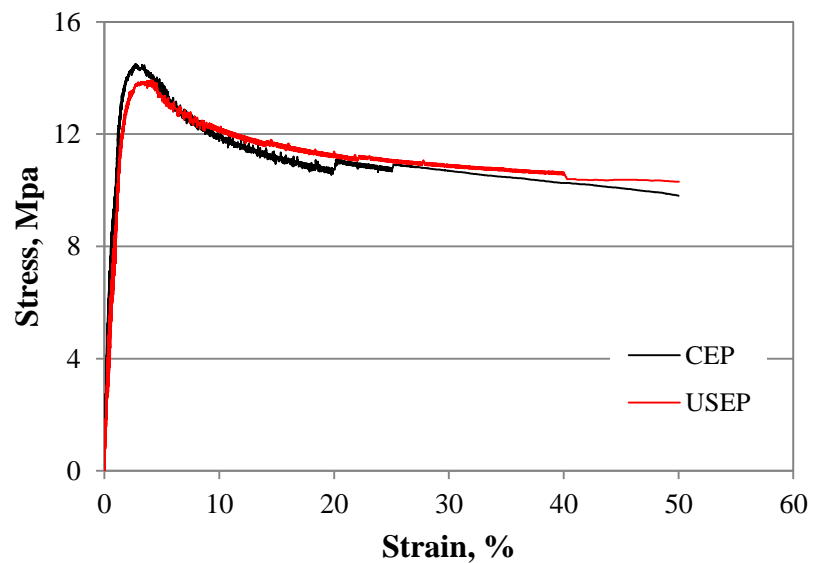
Figure 4-49: Average stress vs. Strain for HYA600/40 pipes produced at 12rpm produced by CEP and USEP.

The average stress strain curves for the CEP and USEP HYA600/40 pipes are shown in Figure 4-49. The stress strain curves for the pipes produced at other screw speeds are presented in Appendix C. From the tensile curve of the pipes produced at 12rpm it can be

seen that pipes produced by both extrusion processes have an almost similar tensile behaviour.

Tested samples from the pipes are shown in Figure 4-50. It can be seen that the PE80, HYA600 and HYA600/20 samples didn't break in the testing strain range (up to 80%) whereas the HYA600/40 samples did break. As seen in Figure 4-50 the PE80 samples were in the drawing part of the stress strain curve. The HYA600 and HYA600/20 deformed past the yield point to form a neck that progressed unbroken to the end of the test (80% strain) The HYA600/40 samples, however, formed a neck after the yield point but failed before the 80% strain limit of the test
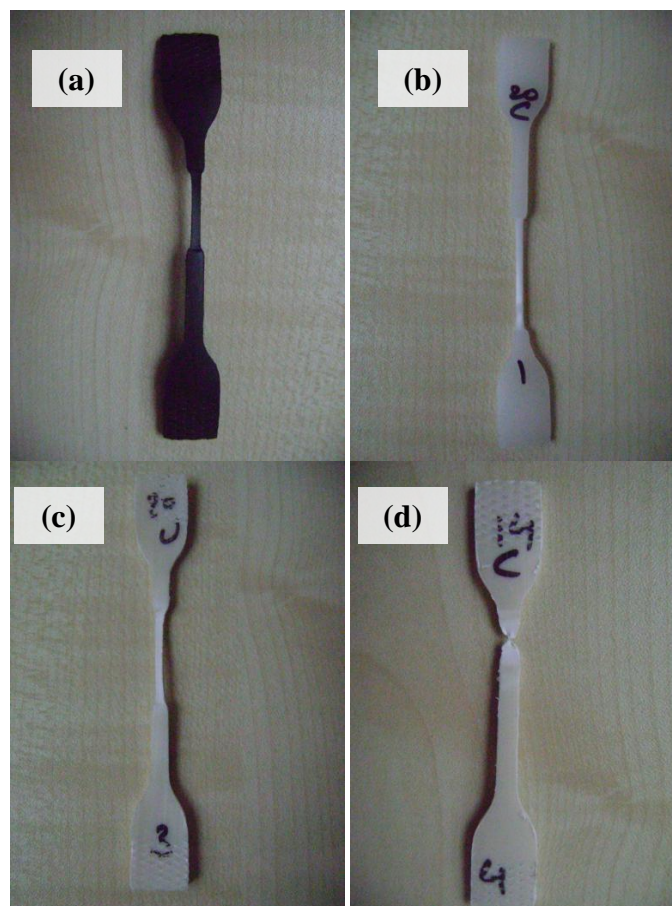
Figure 4-50: Tested samples of PE80 (a), HYA600 (b), HYA600/20 (c) and HYA600/40 (d).

4.3.2.1.3 The effect of the filler on the mechanical properties

In order to investigate the effect of ultrasonic vibrations in presence of fillers for HYA600 and its composites, it was necessary to determine the effect of filler content on the tensile properties of the HYA600 extruded conventionally and compare it with tensile properties of them in presence of ultrasonic vibrations.

The volume fraction of the calcium carbonate particles in the composites was determined using Equation 4-9.

$$\phi_p = \left[1 + \frac{\rho_p}{\rho_m} \left(\frac{1}{w_p} - 1 \right) \right]^{-1} \qquad \qquad \textbf{4-10}$$

Where *p* and *m* denote particle and matrix respectively while Φ is the volume fraction, *w* is the weight fraction and ρ represents the density.

Taking the density of the matrix (ρ_m) as 954 Kgm^{-3} and density of the calcium carbonate particles (ρ_p) as 2700 Kgm^{-3} gave the filler volume fractions of 0.08 and 0.19 for 20%wt and 40%wt filled HYA600 composites, respectively.

The incorporation of particles into the polymers increases the Young's modulus of the polymer. The composite modulus is controlled: particle size and particle size distribution, particle/matrix adhesion and particle loading.

The particle size effect on the modulus of the composite systems is more significant when the particle size is smaller than a critical value. For bigger particles the size effect on the modulus becomes insignificant. The critical particle size depends on particle and matrix and also particle/matrix adhesion [129]. The strength of the composite increases with an increase of the surface area of the particles. This is the result of a better stress transfer between the matrix and the particles. For known filler content, smaller particles have the larger surface area and therefore the effect of particles is more significant compared to that of bigger particles.

Young's modulus is measured in small strains therefore particle matrix adhesion doesn't have a significant effect on the modulus of the composites. However, adhesion between the

matrix and the particles play a critical role on the effect of the particles on the strength of the composites. The adhesion strength at the interface between the matrix and the particle controls the load transfer mechanism between them and subsequently affects the strength of the composite.

An increase of the filler content increased the young's modulus of the composite systems consistently. The effect of the particle loading on the strength of the composites is complicated as the particle size, shape and particle/matrix adhesion also have a critical role here. Because of the stress concentration on the filler surface, the strength of the composite is generally lower than that of the matrix and the yield strength decreases with increase in the particle loading [129, 130].

By the application of ultrasonic vibrations while processing it is a possibility that the high intensity ultrasonic vibrations lead to the breaking of the calcium carbonate particles and therefore modify the size of the particle and consequently tensile properties of the composites. It is important therefore, to compare the composites with a known amount of the filler processed at different screw speeds for both CEP and USEP methods which can help to understand the effect of ultrasonic vibrations on the tensile properties by modification of the fillers.

The young's modulus of a particulate filled polymer matrix composite is generally determined by the elastic properties of the particle and matrix components, the volume fraction of the particles and their aspect ratio. For spherical particles where the aspect ratio equals unity, the modulus of the composite will depend on the filler loading and size. The modulus of the fillers are usually higher than that of the polymers, therefore the modulus of a composite could be enhanced by the addition of the particles to the matrix.

The mechanical properties, such as elastic modulus and tensile strength of the particulate filled composites are achievable by the number of empirical and semi-empirical equations. The modulus of particle filled polymer matrix composites can be predicted by the following equations. These equations are originally developed for fibre reinforced composites, where it assumed the simplest arrangement of the fibres either in series

(Reuss) or in parallel (Voigt). Assuming iso-strain and iso-stress conditions for these two cases the upper and lower bound can be predicted by following equations respectively,

$$E_c = E_p \phi_p + E_m \phi_m \qquad \textbf{4-11}$$

$$E_c = \frac{E_p E_m}{E_p \phi_m + E_m \phi_p} \qquad \textbf{4-12}$$

Where E is the elastic modulus, Φ is the particle volume fraction and subsequent *c, m,* and *p* represent composite, matrix and particle phases, respectively.

These models are applicable to most particulate filled composites. In general, the modulus of the composites should fall between the lower and upper bound modulus values calculated by Equation 4-10 and 4-11 respectively, although it is possible for a composite system to disobey Voigt-Reuss bounds [131, 132].
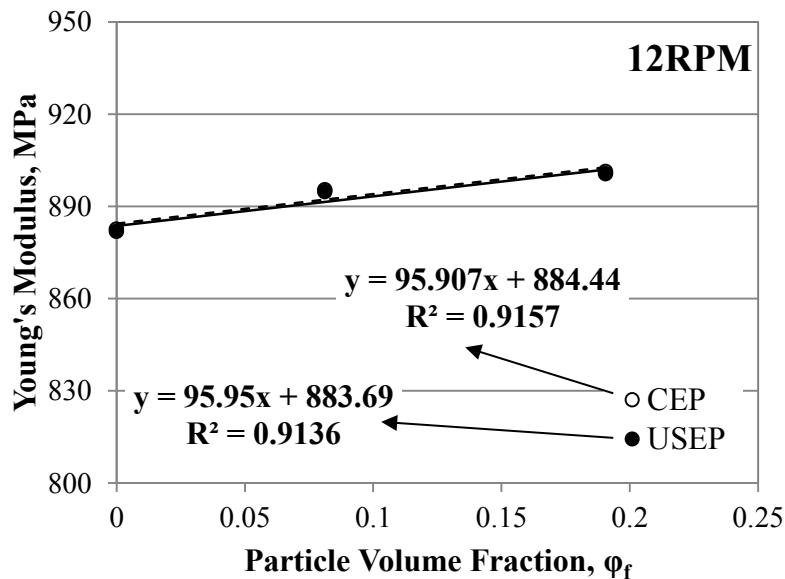
Figure 4-51: Elastic Modulus of HYA600 composites vs. particle volume fraction for pipes produced at 12 rpm with and without presence of ultrasonic vibrations.

Figure 4-51 shows the young's modulus values determined for HYA600 and the HYA600 composites against the particle volume fraction for both the CEP and USEP pipes produced at 12rpm. As it was expected the addition of calcium carbonate particles increased the modulus of the composites linearly with the filler volume fraction. The

tensile modulus of the composites produced at the other screw speeds were also plotted versus the particle volume fraction and these are presented in Appendix C.

Taking the elastic modulus of the calcium carbonate particles (E_f) as 26GPa and by using Equation 4-10 and Equation 4-11 the lower and upper bounds of the modulus for the composites could be calculated. The calculated theoretical modulus (Reuss model) and the experimental results for both CEP and USEP pipes are shown in Figure 4-52. The experimental results of the elastic modulus obtained from the HYA600 composites violated the Voigt-Reuss bounds and it can be seen that for both CEP and USEP pipes they are smaller than predicted values by the Reuss model, which is the lower bound of the predicted values. The reason for the experimental data to fall outside of the theoretical prediction range could be as a result of the presence of particle agglomerations and thus a poor dispersion of the primary particles. It can be said therefore, that the tensile response of the HYA600 composites was not according to Voigt-Reuss models and was not predicted by them. The results of the composites produced at other screw speeds were similar to that of composites produced at 12rpm and presented in Appendix C.
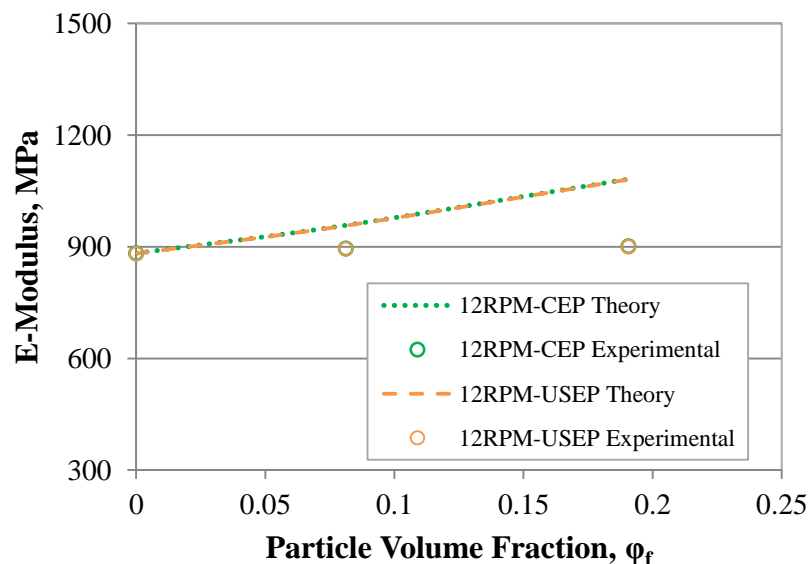
Figure 4-52: Experimental and theoretical Young's modulus of the HYA600 composites produced at 12rpm with and without presence of ultrasonic vibrations vs. particle volume fraction.

In order to be able to determine the efficiency of the particles in the composite systems it was necessary to fit the experimental data to a theoretical/semi-empirical model. The modulus of the particulate filled composites could also be predicted by an approximate method, the modified rule of mixtures[133]:

$$E_c = \chi_p E_p \phi_p + E_m \left(1 - \phi_p\right) \qquad \text{4-13}$$

Where $0 < \chi_p < 1$ is the particle strengthening factor. Rearranging the Equation 4-12 gives the composite modulus as a function of fibre volume concentration (Equation 4-13) with a slope of $(\chi_p E_p - E_m)$.

$$E_c = \left(\chi_p E_p - E_m\right) \phi_p + E_m \qquad \text{4-14}$$

Using the slope of the E_c vs. Φ_p and having the E_p and E_m, the particle strengthening factor (χ_p) could be calculated for the pipes produced at each screw speed. The calculated strengthening factors are plotted against extrusion screw speeds and are shown in Figure 4-53. By comparing the strengthening factors at different screw speeds for CEP pipes with USEP it is evident that ultrasonic vibrations did not have significant effect on the strengthening potential of the particles. For the composites produced by CEP and USEP the strengthening factor is around 0.04.
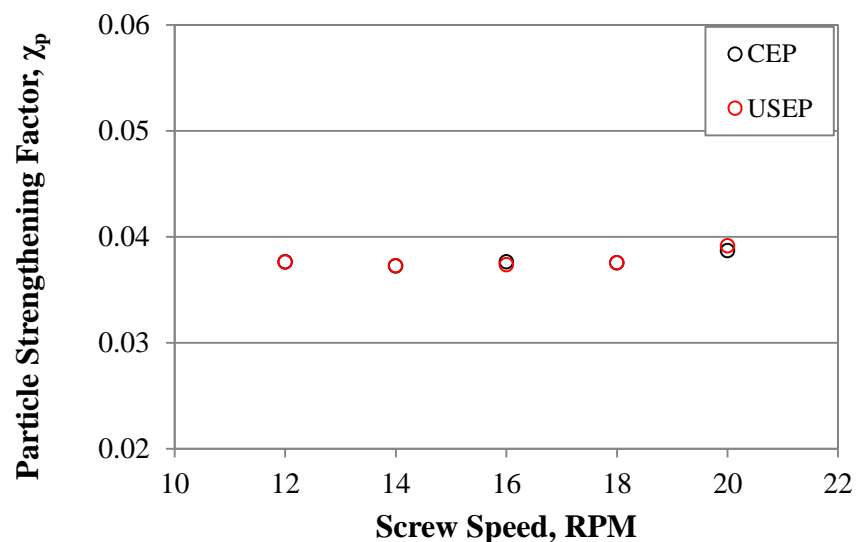
Figure 4-53: Particle strengthening factor vs. screw speed for CEP and USEP HYA600 Composites.

The yield strength of the particle filled composites plotted against particle loading and shown in Figure 4-54 for pipes produced at 12rpm with and without the ultrasonic vibrations. The plots of yield strength against particle volume fraction for HYA600 composites extruded at 14, 16, 18 and 20rpm are presented in Appendix C.

It can be seen that yield strength of the composites decreased in a linear manner with an increasing particle volume fraction. The experimental data could be fitted into a simple theoretical model that indicates a linear decrease of the composite with an increase in the particle loading.
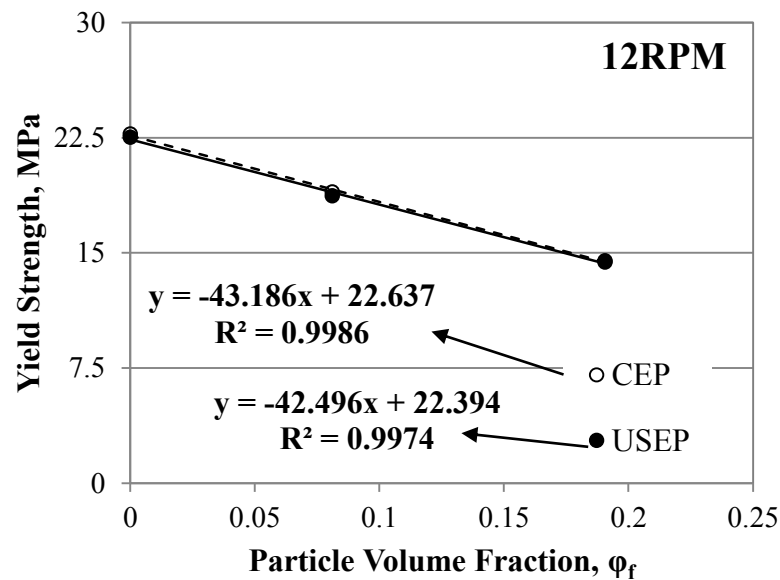
Figure 4-54: Yield Strength of the HYA600 composites vs. particle volume fraction for the pipes produced at 12 rpm with and without presence of ultrasonic vibrations.

A very simple linear expression that can be used here is [134, 135]:

$$\sigma_c = \sigma_m\ (1 - \phi_p) \qquad\qquad \textbf{4-15}$$

Where σ_c and σ_m are yield strengths of composite and matrix respectively, Φ_p is the particle volume fraction. By rearranging this equation into the following form, it can be seen that the slope of the linear fitted trend line should be equal to the yield strength of the matrix.

$$\sigma_c = \sigma_m - \sigma_m\phi_p \qquad\qquad \textbf{4-16}$$

151

However, as shown in Figure 4-54 the slope of the best linear equation fitted to the CEP data points have a slope of -43.186 which should have been -22.74 according to Equation 4-15. This indicated that the rate of the strength reduction with an increase of the particle loading is bigger than the value predicted by Equation 4-14.

As noted above, although yield strength of the composites showed a linear decrease by increasing particle loading but the slope of this linear decrease was bigger. For this reason a factor could be added to Equation 4-14 known as strength reduction factor (S_r). For an ideal match with equation 4-14 the strength reduction factor (S_r) will be equal to unity and for HYA600 composites it will be greater than 1.

$$\sigma_c = \sigma_m \left(1 - S_r \phi_p \right) \qquad\qquad \textbf{4-17}$$

According to Equation 4-15 the slope of the linear fit to the experimental data will be equal to $S_r\Phi_p$, therefore the particle strengthening factor could be determined for the composites produced at different screw speeds and then compared for the CEP and USEP modes.
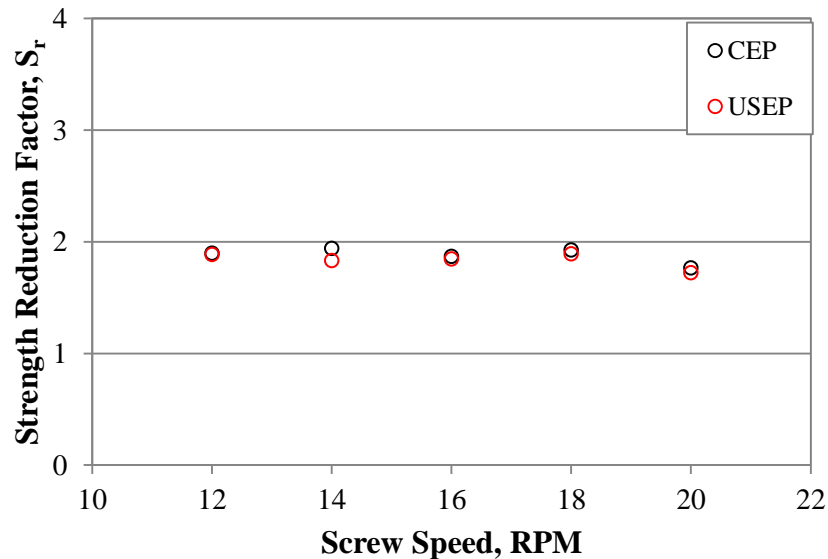
Figure 4-55: Strength reduction factor vs. screw speed for CEP and USEP HYA600 Composites.

The strength reduction factors for HYA60 composites were calculated and shown in Figure 4-55. The strength reduction factors for the composites were around 2 for the range of

extrusion screw speeds and there was no significant difference observed between the CEP and USEP pipes.

4.3.2.2 Dynamic Mechanical Analysis

Small rectangular bars were cut from the extruded strips to carry out DMA on them. The DMA tests were performed on a TA Instruments Q800 in the temperature range of -140°C to 80°C with a heating rate of 3°C/min. The DMA tests were carried out on the specimens in the single cantilever mode. Strain sweep tests were done on each sample prior to the multi frequency sweep to ensure that the tests were being carried out in the linear visco elastic region of the samples.

The strain sweep test was carried out for amplitudes between 5µm to 20µm at 35°C on samples prepared from the strips produced at 8rpm using the conventional extrusion process. The resultant stress strain curve is shown in Figure 4-56.
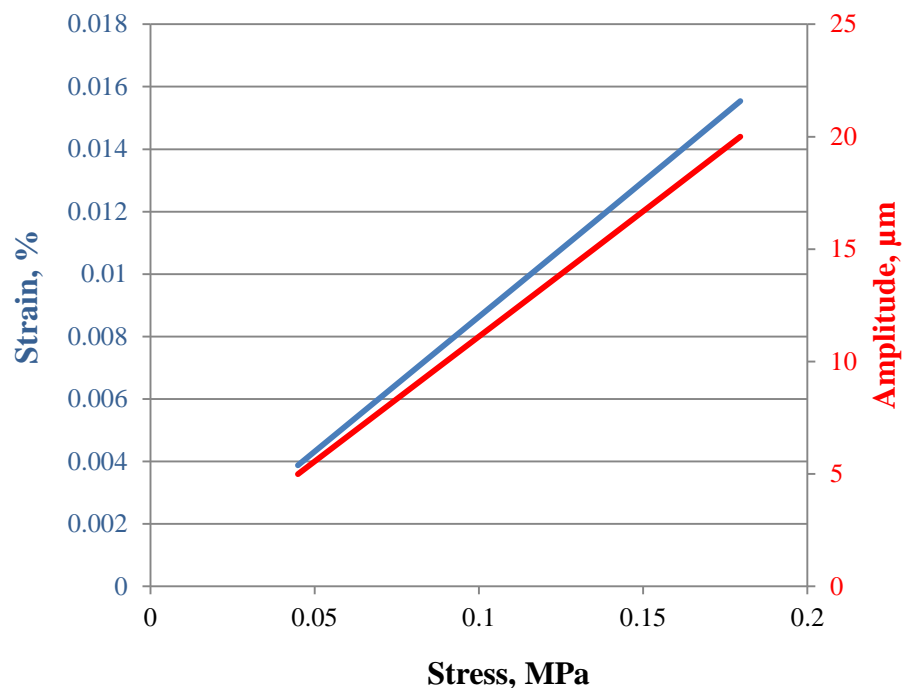
Figure 4-56: Strain vs. Stress (left axis) and the Amplitude vs. Stress curve (right axis) at 35°C for Rigidex5130 samples produced by CEP at 8rpm.

The strain sweep results confirmed that the tests were in the linear visco elastic region if they were carried out with amplitudes between 5µm to 20µm. It was decided to carry out the multi frequency tests with the amplitude of 15µm at three different frequencies of 1, 5 and 10 HZ.

4.3.2.2.1 DMA results of the strips

The results from the multi frequency tests were used for the determination of the T_gs of the samples and the 3 values obtained from the 3 different frequencies were then fitted to the Arrhenius equation to calculate the activation energy of the T_g for each sample. The DMA results for the samples produced at 8rpm are shown in Figure 4-57. These data were then used to determine the T_g of the samples (Tanδ peak used for T_g determination).
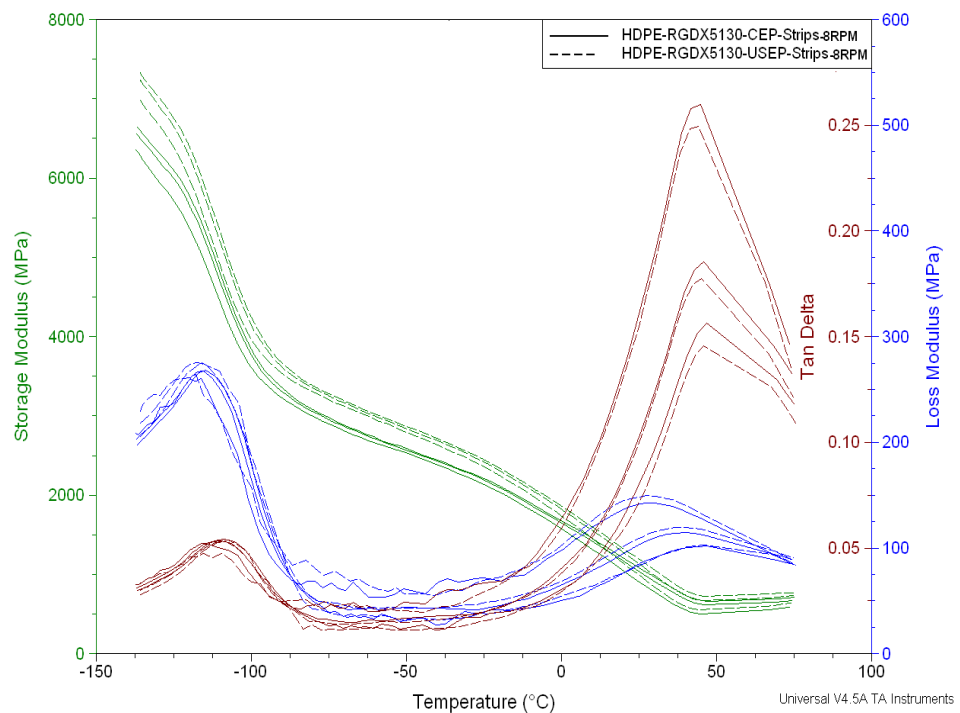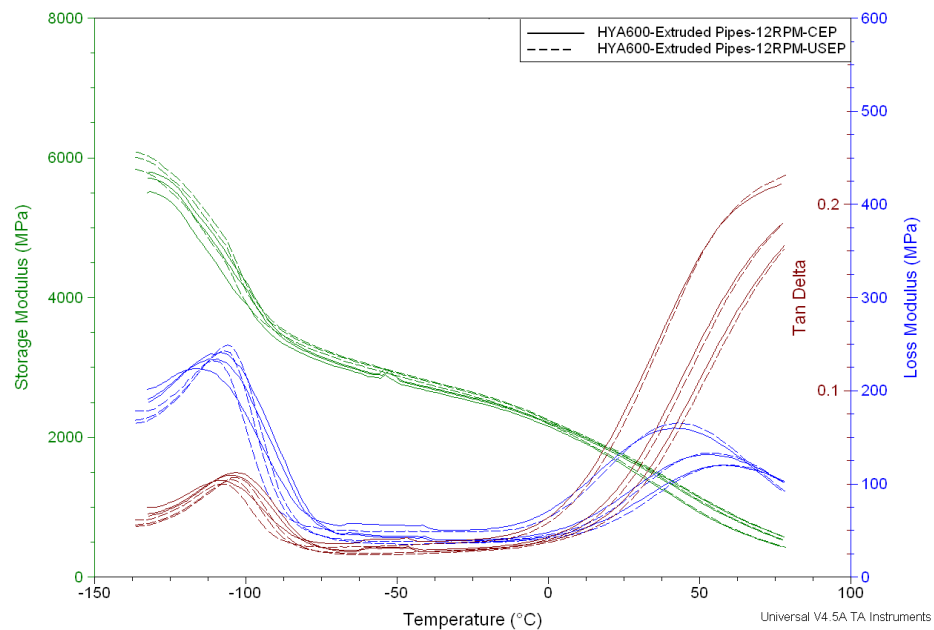

Figure 4-57: DMA Results of Rigidex5130 strips produced at 8rpm by both USEP and CEP. The solid line represents the CEP data and the dashed line is for the USEP samples. For each set of data the curves from top to bottom represent data acquired at 1Hz, 5Hz and 10Hz respectively.

It can be seen from the storage modulus curves in Figure 4-57 that the difference between the CEP and USEP samples is noticeable at low temperatures but not at room temperature for all the tested frequencies. The DMA results for the rest of the screw speeds are presented in Appendix C. The obtained Tg values from the Tanδ peaks (Table 4-4) were then used to calculate E_a (activation energy of T_g) of the samples by constructing an Arrhenius plot for each sample and to use the slope of the linear fit for the determination of the activation energy for the molecular rearrangement that gave rise to the T_gs of the samples.

Table 4-4: T$_g$ values obtained from Tanδ peak from DMA tests at frequencies of 1, 5 and 10 Hz for Rigidex5130 strips produced at the different screw speeds.

Screw Speed	Frequency (Hz)	CEP	USEP
	1	-117.91	-116.32
8rpm	5	-112.76	-111.65
	10	-111.77	-110.47
	1	-115.02	-114.15
12rpm	5	-111.08	-110.23
	10	-110.13	-109.3
	1	-115.99	-114.16
16rpm	5	-111.84	-110.45
	10	-110.8	-109.27
	1	-115.49	-114.32
20rpm	5	-111.53	-110.26
	10	-109.89	-108.56
	1	-115.36	-114.15
24rpm	5	-111.81	-110.03
	10	-110.29	-109.45
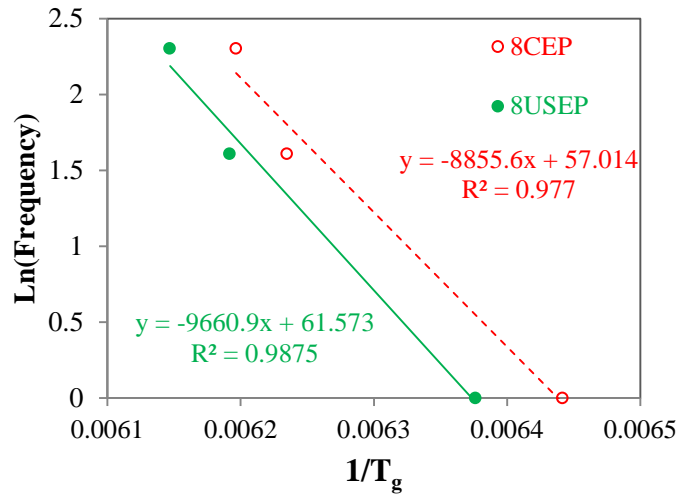
Figure 4-58: The Arrhenius plot for the T_g of the Rigidex5130 strips produced at 8rpm by CEP and USEP measured at different frequencies.

Plotting *ln(f)* as a function of *1/T_g* gives a linear relationship (Figure 4-58) where the slope is *–Ea/R*.

The obtained slopes from Figure 4-58 were the used to calculate E_a for each screw speed and processing method (CEP / USEP). The activation energies of Rigidex5130 with the regression coefficient for the linear fit are summarised in Table 4-5.

Table 4-5: T_g activation energies and the regression coefficient of the linear fit obtained from the DMA tests for Rigidex5130 strips produced at the different screw speeds (E_a values are in KJ.mol^{-1}).

	8rpm		12rpm		16rpm		20rpm		24rpm	
	E_a	R^2	E_a	R^2	E_a	R^2	E_a	R^2	E_a	R^2
CEP	308.25	0.97	405.24	0.98	378.96	0.98	366.88	0.99	405.42	0.99
USEP	336.28	0.98	412.45	0.98	418.09	0.99	362.46	0.99	409.8	0.96

From the T_gs of the Rigidex5130 samples shown in Table 4-4, it can be seen that with the application of ultrasound the glass transition temperature of the product shows a slight increase (~1°C). The application of ultrasonic vibrations during extrusion not only increased the T_g but it can also be seen that the activation energy of the USEP samples was also increased except at 20rpm where it was slightly lower than for the CEP. The possible cause for the changes in the T_g and the activation energies could be a modification to the

polymer chain and its molecular structure induced by the application of ultrasonic vibrations. The chain stiffness, chain interactions and chain length have a significant effect on the glass transition temperature. In previous literature [126], chain scission of HDPE and the formation of macroradicals as a result of application of USV's have been reported. Scission of the polymer chains will increase the mobility and therefore decrease the T_g. On the other hand the macroradicals could end up on the main chain and cause cross linking between chains that could possibly cause an increase in the T_g.
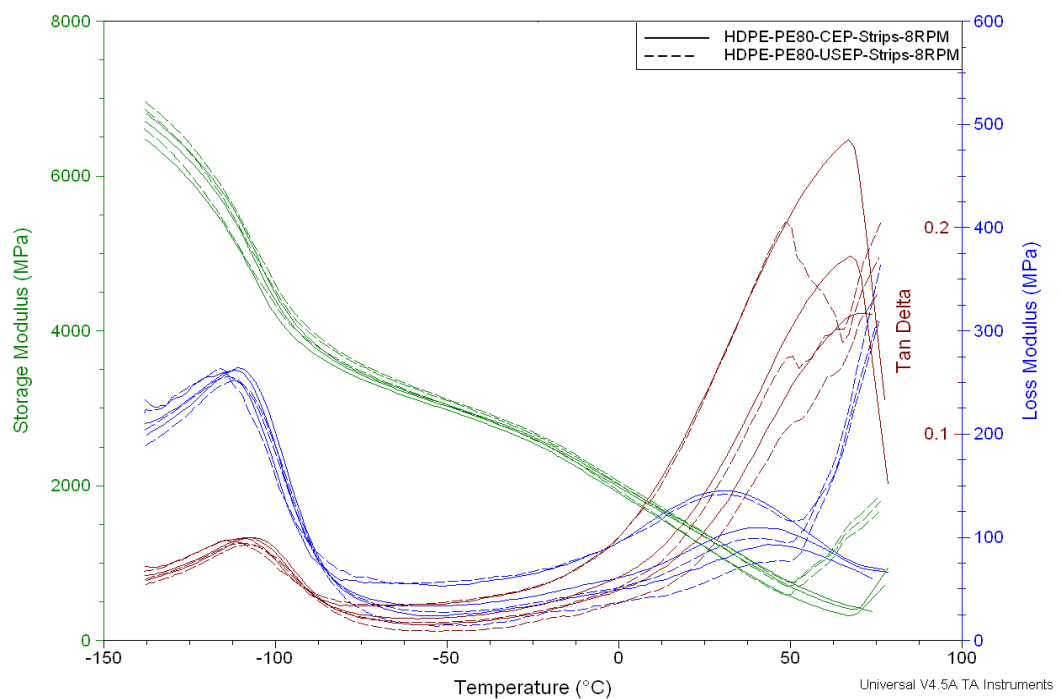
Figure 4-59: DMA Results of PE80 strips produced at 8rpm by both USEP and CEP. The solid line represents the CEP sample data and the dashed line is for USEP samples while for each set of data the curves from top to bottom represent data acquired at 1Hz, 5Hz and 10Hz respectively.

The DMA multi frequency tests on the PE80 strips were carried out with the same conditions as for the Rigidex5130. The multi frequency result for the PE80 strips produced at 8 rpm (the curves for other screw speeds presented in Appendix C) is shown in Figure 4-59.

Table 4-6: T_g values obtained from Tan δ peak from DMA tests at frequencies of 1, 5 and 10 Hz for PE80 strips produced at the different screw speeds.

	Frequency (Hz)	CEP	USEP
8rpm	1	-112.03	-111.03
	5	-109.36	-108.36
	10	-107.64	-106.99
12rpm	1	-113.68	-112.64
	5	-110.69	-109.67
	10	-109.72	-108.64
16rpm	1	-112.99	-111.86
	5	-109.34	-108.4
	10	-108.73	-107.73
20rpm	1	-111.26	-110.34
	5	-106.76	-106.16
	10	-104.74	-103.66
24rpm	1	-112.1	-111.98
	5	-107.33	-107.31
	10	-104.46	-104.72

Table 4-7: T_g activation energies and the regression coefficient of the linear fit obtained from DMA tests for PE80 strips produced at the different screw speeds (Ea values are in KJ.mol^{-1}).

	8rpm		12rpm		16rpm		20rpm		24rpm	
	E_a	R^2	E_a	R^2	E_a	R^2	E_a	R^2	E_a	R^2
CEP	493.03	0.99	517.36	0.99	462.82	0.97	335.19	1	288.21	0.99
USEP	538.14	0.99	521.33	0.99	488.78	0.97	334.81	0.99	302.40	0.99

The glass transition temperatures extracted from the Tan δ curves for the strips processed at 12, 16, 20 and 24rpm are summarised in Table 4-6. It can be seen that, similar to Rigidex5130, the glass transition temperatures increased slight by the application of ultrasonic vibrations. The T_gs at the different frequencies were used to calculate activation energy for the glass transition. The calculated values of E_a for the PE80 strips are tabulated and shown in Table 4-7. The activation energy of the T_g increased by the presence of ultrasound during processing and was possibly due to the proposed theory of chain scission and cross linking that was discussed earlier in Chapter 3.

4.3.2.2.2 DMA results of the pipes

The multi frequency DMA tests were carried out in the temperature range of -140°C to 80°C with a heating rate of 3°C/min for both the CEP and USEP pipes. The results for the PE80 pipes produced at 12rpm with and without presence of ultrasound are shown in Figure 4-60 (the curves for other screw speeds are presented in Appendix C).
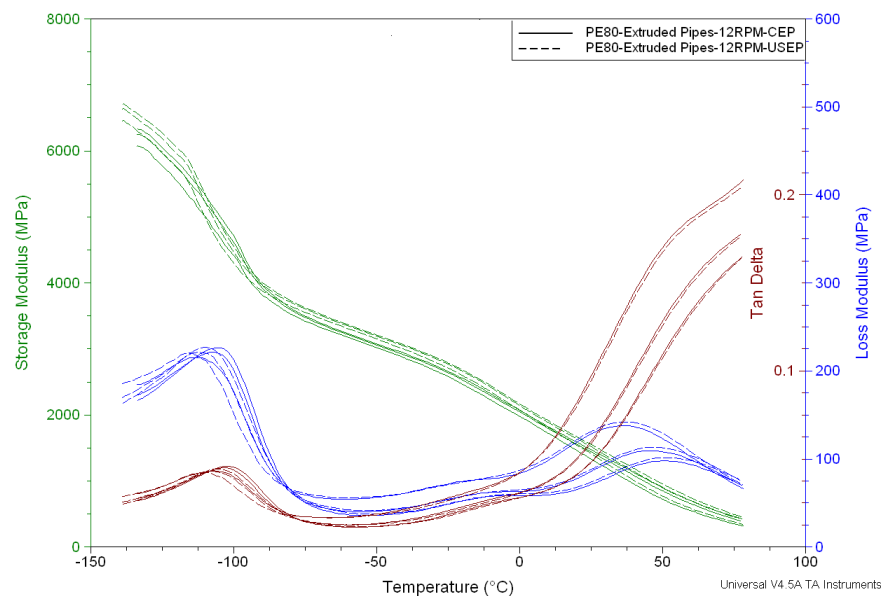
Figure 4-60: DMA Results of PE80 pipes produced at 8rpm by both USEP and CEP. The solid lines represent the CEP data and the dashed lines are the USEP data. For each set of data the curves from top to bottom represent data acquired at 1Hz, 5Hz and 10Hz.

It can be seen in Figure 4-60 that the USEP pipes had a slightly higher storage modulus compared to the CEP pipes at very low temperatures. However, the difference between CEP and USEP dynamic mechanical properties became negligible at room temperature. The Tan δ curves were used to extract the T_gs for the samples shown in Table 4-8. The T_gs were then used to construct the Arrhenius plot for each screw speed individually and to calculate the activation energy of the glass transition temperature.

Table 4-8: Tg values obtained from the Tan δ peak of the DMA tests at frequencies of 1, 5 and 10 Hz for the PE80 pipes.

	Frequency (Hz)	**CEP**	**USEP**
12rpm	1	-107.24	-106.82
	5	-105.43	-104.76
	10	-101.92	-101.42
14rpm	1	-107.59	-107.23
	5	-105.82	-104.37
	10	-101.89	-101.39
16rpm	1	-107.92	-107.58
	5	-104.23	-103.85
	10	-101.26	-101.03
18rpm	1	-107.97	-107.41
	5	-104.64	-104.41
	10	-101.35	-101.12
20rpm	1	-107.89	-107.56
	5	-105.48	-105.44
	10	-101.45	-101.32

The glass transition temperatures showed a slight increase by the application of ultrasound while processing. The increase of the T_gs are about 1°C or less with the maximum increase for the pipes produced at 12rpm which is the lowest screw speed and has the highest residence time in the ultrasonic die.

Table 4-9: T_g activation energies and the regression coefficient of the linear fit obtained from DMA tests for PE80 pipes produced at the different screw speeds (Ea values are in KJ.mol^{-1}).

	12rpm		14rpm		16rpm		18rpm		20rpm	
	E_a	R^2	E_a	R^2	E_a	R^2	E_a	R^2	E_a	R^2
CEP	398.28	0.84	363.33	0.82	345.71	0.97	344.67	0.95	336.09	0.87
USEP	404.82	0.88	390.94	0.94	353.10	0.98	361.91	0.94	340.27	0.84

An increase in the activation energies was observed by the application of ultrasonic vibrations during extrusion (Table 4-9) which alongside with the increase in the glass transition temperature suggested the occurrence of chain scission and cross linking by the application of ultrasound. However, the observed changes are not significant and they might not have an effect on the mechanical and structural properties of the pipes.

DMA multi frequency tests under the same conditions were carried out on HYA600 (Figure 4-61), 20% filled HYA600 and 40% filled HYA600 pipes and they are presented in Appendix C. The T_gs were determined (Table 4-10) for all the pipes that were produced with and without the presence of ultrasound at the screw speeds of 12rpm to 20rpm. It can be seen from the glass transition temperatures in Table 4-10 for the HYA600 pipes and the filled pipes, the glass transition temperature increased by around 1°C. The values at the different screw speeds cannot be compared with each other because of the different cooling rates and drawing rates in the die.

Figure 4-61: DMA Results of HYA600 pipes produced at 8rpm by both USEP and CEP. The solid line represents the CEP data and the dashed line the USEP samples while for each set of data the curves from top to bottom represent data acquired at 1Hz, 5Hz and 10Hz.

Table 4-10: Tg values obtained from the Tanδ peak from DMA tests at frequencies of 1, 5 and 10 Hz for HYA600 pipes produced at the different screw speeds.

	Frequency (Hz)	HYA600		HYA600+20%wt CaCo3		HYA600+40%wt CaCo3	
		CEP	USEP	CEP	USEP	CEP	USEP
12rpm	1	-108.23	-107.63	-108.23	-107.21	-108.84	-108.41
	5	-103.6	-102.92	-104.32	-104.1	-105.41	-105.1
	10	-101.26	-100.92	-102.71	-101.73	-103.13	-102.94
14rpm	1	-107.41	-107.33	-108.17	-107.84	-108.35	-107.84
	5	-103.47	-103.05	-105.71	-104.67	-104.34	-104.19
	10	-101.29	-101.54	-101.45	-101.08	-103.77	-103.05
16rpm	1	-107.04	-106.58	-107.72	-107.43	-108.34	-107.94
	5	-103.49	-103.35	-104.85	-104.69	-104.21	-103.65
	10	-101.43	-101.03	-102.93	-102.73	-101.83	-101.59
18rpm	1	-107.33	-107.1	-107.49	-107.4	-108.36	-107.88
	5	-103.39	-103.08	-104.95	-104.65	-103.86	-103.23
	10	-101.06	-100.96	-102.75	-102.65	-101.34	-101.29
20rpm	1	-107.1	-106.89	-107.43	-106.05	-108.39	-107.59
	5	-103.95	-103.54	-104.5	-104.19	-104.14	-104.1
	10	-100.46	-100.23	-101.4	-100.46	-102.04	-101.56

The T_g values have been used to calculate the activation energy for each pipe grade and screw speed. The E_a values for the HYA600 pipes are shown in Table 4-11. It can be seen that the activation energies increased slightly from the CEP to the USEP samples at the same screw speeds.

The DMA results for the strips and pipes showed that by the application of ultrasound during extrusion, the glass transition temperatures increased by almost 1°C which is not significant and the activation energy of the T_g rose by ~12-19 Kj.mol^{-1} over the range of

screw speed as a result of sonication. According to previous studies, lower values of activation energy are an indication of homogenous polymer chains in terms of their structural regularity and/or composition [136-138].

Table 4-11: Tg activation energies and the regression coefficient of the linear fit obtained from DMA tests for HYA600 pipes produced at the different screw speeds (Ea values are in KJ.mol^{-1}).

		12rpm		14rpm		16rpm		18rpm		20rpm	
		E_a	R^2	E_a	R^2	E_a	R^2	E_a	R^2	E_a	R^2
HYA600	CEP	327.83	0.99	376.49	0.99	413.63	0.99	368.80	0.99	338.90	0.94
	USEP	339.51	0.99	388.33	0.99	419.37	0.98	376.07	0.99	347.09	0.95
HYA600 /20	CEP	406.36	0.99	320.06	0.87	477.30	0.98	481.58	0.95	377.78	0.94
	USEP	421.19	0.98	335.17	0.93	487.84	0.98	482.97	0.98	383.14	0.84
HYA600 /40	CEP	397.17	0.98	451.33	0.96	351.22	0.99	326.30	0.99	357.55	0.99
	USEP	416.10	0.99	460.07	0.99	359.02	0.99	344.09	0.99	382.48	0.98

4.3.3 Thermal Analysis

4.3.3.1 Differential Scanning Calorimetry (DSC)

Differential Scanning Calorimetry tests in a heat/cool cycle were done on samples taken from the PE strips and pipes. Samples sizes of ~10mg and standard aluminium pans and heating rate of 10°C/min and cooling rate of 5°C/min were used for the tests.

4.3.3.1.1 DSC results of the strips

The DSC heat flow/temperature curves (presented in Appendix C) were used for the determination of the melting temperature, crystallisation temperature, melting enthalpy and crystallisation enthalpy. The results are shown in Table 4-12.

Table 4-12: Thermal properties of the strips produced from Rigidex5130 and PE80.

	Screw Speed (rpm)	T_m (°C)		T_c (°C)		ΔH_m (J/g)		ΔHc (J/g)	
		CEP	USEP	CEP	USEP	CEP	USEP	CEP	USEP
Rigidex5130	8	130.23	130.07	120.27	120.18	169.7	170.4	202.2	205.8
	12	130.34	129.90	120.26	120.30	170.0	170.4	207.2	205.3
	16	130.00	129.60	120.26	120.39	171.6	171.9	210.2	208.9
	20	130.02	129.69	120.28	120.25	169.0	174.6	203.2	206.1
	24	130.17	129.75	120.12	120.25	171.2	173.8	201.8	207.0
PE80	8	128.95	128.64	117.86	118.01	168.1	168.9	177.4	178.8
	12	128.37	128.72	117.86	117.76	161.9	166.2	177.4	177.0
	16	128.75	128.25	117.73	118.14	164.0	166.9	175.9	181.0
	20	128.89	128.53	117.65	117.86	162.4	161.5	173.6	174.5
	24	128.62	128.43	117.74	117.91	163.0	159.7	173.5	174.5

For the Rigidex5130 strips it can be seen from Table 4-12 that the melting temperatures and crystallisation temperatures remained unaffected by the presence of the ultrasound except for screw speeds of 20 and 24rpm where a noticeable difference in melting and crystallisation enthalpy can be seen. The melting enthalpy of the Rigidex5130 strips processed with USEP is higher than the CEP strips by 5.6 J/g and 2.6 J/g for 20 and 24 rpm respectively. This difference based on 293 J/g for 100% crystalline polyethylene [127] makes around 1.91% and 0.88% increase in degree of crystallinity which is not a significant change in degree of crystallinity and this change is possibly small enough to affect mechanical properties and for that reason have not been detected in tensile tests.

The thermal properties obtained from the DSC tests for PE80 were similar to that of Rigidex5130 and did not show any significant changes by the application of the ultrasonic vibrations during extrusion. Equal melting enthalpies for the CEP and USEP strips suggested that the degree of crystallinity of the products remained unaffected by the presence of the ultrasonic vibrations. There are differences between the melting enthalpy of the PE80 strips processed with USEP and CEP for the screw speeds of 8, 12 and 16rpm and the heat of fusion for USEP samples was higher than for the CEP samples. For the rest of the screw speeds the USEP samples had lower melting enthalpy when compared to the CEP strips. The maximum difference between the USEP and CEP enthalpies of melting was 4.3 J/g for the strips produced at 12 rpm which was not significant when compared to

the heat of melting for 100% crystallinity. A considerable change in crystallinity of the strips was not therefore observed by the application of the ultrasound.

4.3.3.1.2 DSC results of the pipes

The DSC tests were carried out on samples prepared from pipes with the same condition used for the strips. The heat flow/temperatures curves obtained from the tests (provided in Appendix C) were used for the determination of the melting and crystallisation temperature as well as the melting and crystallisation enthalpy of the pipe samples. The determined thermal properties of the pipes are summarised in Table 4-13.

Table 4-13: Thermal properties of pipes produced from PE80, HYA600, HYA600/20 and HYA600/40.

	Screw Speed (rpm)	T_m (°C)		T_c (°C)		ΔH_m (J/g)		ΔH_c (J/g)	
		CEP	USEP	CEP	USEP	CEP	USEP	CEP	USEP
PE80	12	128.57	128.43	117.23	117.36	147.8	156.4	158.0	166.6
	14	128.68	127.96	116.84	117.52	158.3	164.9	167.7	174.1
	16	128.99	128.74	117.32	117.34	158.5	162.5	166.1	175.2
	18	128.64	127.94	117.16	117.35	162.4	163.6	170.4	173.1
	20	128.96	129.28	117.30	117.09	159.6	158.7	167.0	165.6
HYA600	12	131.34	131.95	118.94	118.09	184.5	193.7	204.6	208.1
	14	131.48	131.44	118.59	118.66	185.1	191.7	201.1	200.8
	16	131.68	131.47	118.86	118.89	181.7	187.6	203.2	207.8
	18	132.07	131.85	118.72	118.84	181.3	184.2	201.5	205.3
	20	131.69	131.80	118.09	118.74	179.9	185.1	193.6	200.7
HYA600/20	12	129.28	130.53	120.06	119.58	139.2	141.4	156.2	156.5
	14	130.29	131.05	119.72	119.12	141.7	142.5	155.5	158.1
	16	130.57	130.60	119.68	119.70	143.8	145.4	158.2	161.7
	18	130.49	130.89	119.69	119.52	144.8	144.5	163.1	158.3
	20	129.70	129.92	120.15	119.96	143.4	143.1	162.8	162.4
HYA600/40	12	128.79	130.77	119.91	119.97	107.6	112.3	114.3	111.0
	14	128.61	128.51	119.96	120.01	108.8	112.1	120.5	118.0
	16	129.16	128.88	119.78	119.84	105.3	107.7	112.6	112.2
	18	128.20	128.30	120.01	119.92	104.4	103.6	114.0	108.6
	20	128.81	128.92	119.90	119.84	102.0	103.2	111.1	108.6

While the melting and crystallisation temperatures of the PE80 pipes remain unaffected (Table 4-13) with the application of ultrasound, the melting and crystallisation enthalpy of

them both increased which suggests the application of ultrasound waves increased the degree of crystallinity. The most significant change to the melting and crystallisation enthalpy (5% increase) was observed for samples produced at 12rpm screw speed. This could be explained by the fact that the exposure time for them was higher than samples processed at 20 rpm which showed 0.5% decrease in melting enthalpy by the application of ultrasonic vibrations.

The similar behaviour of thermal properties can be seen for the HYA600 samples and its filled compound pipes. The melting and crystallisation temperature for all the USEP pipe samples were similar (~0.6°C variation) compared to their respective CEP pipes while the melting enthalpies were higher by 9.2 J/g for the pipes produced at 12 rpm. The degree of crystallinity was therefore, slightly higher for USEP pipes.

From the results obtained from the pipes it can be said that the ultrasonic waves did not affect the crystallinity of the polymer pipes significantly and the observed variations in the crystallinity from CEP to USEP could possibly cause by a variation in the cooling water temperature and the cooling rate of the pipes.

4.3.4 Rheology

Rotational rheology tests were carried out on test specimens obtained from strips and pipes. The disk shaped test specimen was placed on the lower plate of the rheometer and the test chamber temperature was set to 190°C. The samples were given adequate time to reach the test temperature. The gap between the plates then set to 1mm and any excess material was removed.

4.3.4.1 Rheology results of the strips

Dynamic storage modulus, loss modulus and complex viscosity of the samples were plotted against frequency for conventionally extruded strips and then compared with the ultrasonic assisted samples.

The rheology results for the Rigidex5130 strips produced at 8rpm are shown in Figure 4-62.
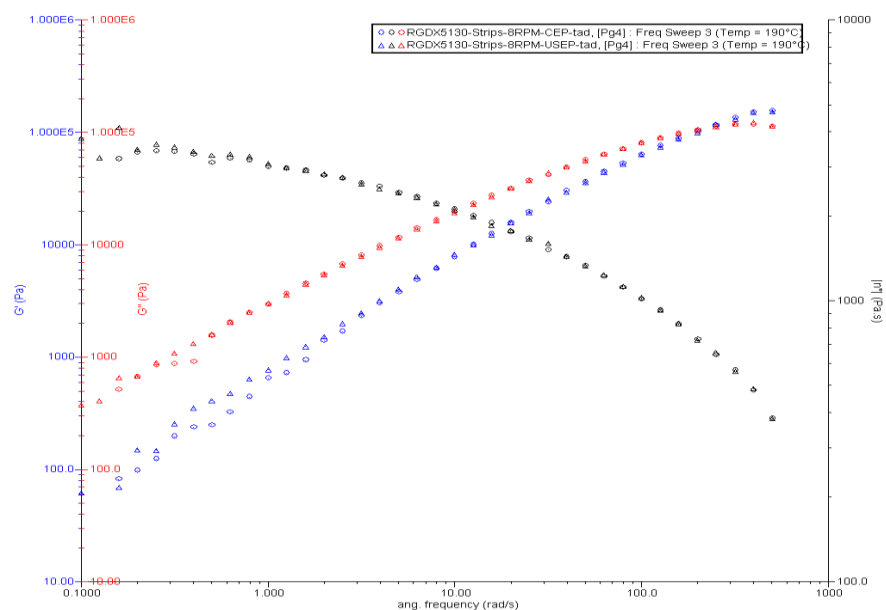
Figure 4-62: Dynamic shear storage modulus (G$^{'}$), loss modulus (G$^{''}$) and complex viscosity (η^{*}) plotted against angular frequency for Rigidex5130 strips produced at 8 rpm.

It can be seen from the rheology results shown in Figure 4-62, that the storage and loss moduli have not been affected by the presence of ultrasonic waves during the extrusion. The complex viscosity of the samples also showed no difference. A difference between CEP and USEP was observed for the storage/loss modulus at the angular frequencies lower than 1 rad/sec. This could be accounted for by possible instrumental errors. The difference between the storage/loss shear modulus of the CEP and USEP samples reduced to zero at higher angular frequencies.

The rheology results from the samples produced at 12, 14, 16, 20 and 24rpm did not show any changes to the viscosity of the strips by the application of ultrasonic waves.

Rheology tests were also carried out on samples obtained from PE80 strips. The shear storage modulus, loss modulus and complex viscosity were measured and plotted against the angular frequency as shown in Figure 4-63.

Comparing the storage and loss modulus showed that the mechanical characteristics of the melt were not affected by the application of ultrasonic waves. The complex viscosity values for both samples produced at 8rpm did not show significant changes.
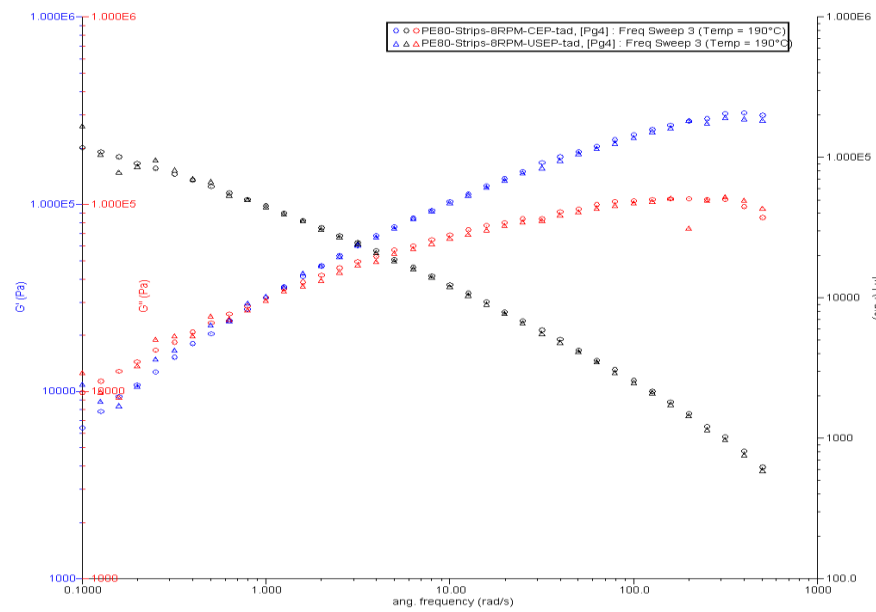
Figure 4-63: Dynamic shear storage modulus (G'), loss modulus (G") and complex viscosity (η*) plotted against angular frequency for PE80 strips produced at 8 rpm.

From comparing rheology results for both PE80 and Rigidex5130 it was found that presence of ultrasonic waves during extrusion did not affect the rheological properties of the extrudate.

The rheology results of the Rigidex5130 and PE80 strips produced at 12, 16, 20 and 24 rpm are presented in Appendix C.

4.3.4.2 Rheology results of pipes

Comparing the rheological properties obtained from the parallel plate rheology tests of PE80 pipes produced by conventional and ultrasonic assisted extrusion showed that application of ultrasonic waves on the polymer melt during extrusion did not affected the rheological properties of the melt such as $G^{'}$,$G^{"}$ and η^{*}. Figure 4-64 shows the acquired rheological properties of the pipes produced at 12 rpm with and without ultrasonic waves.
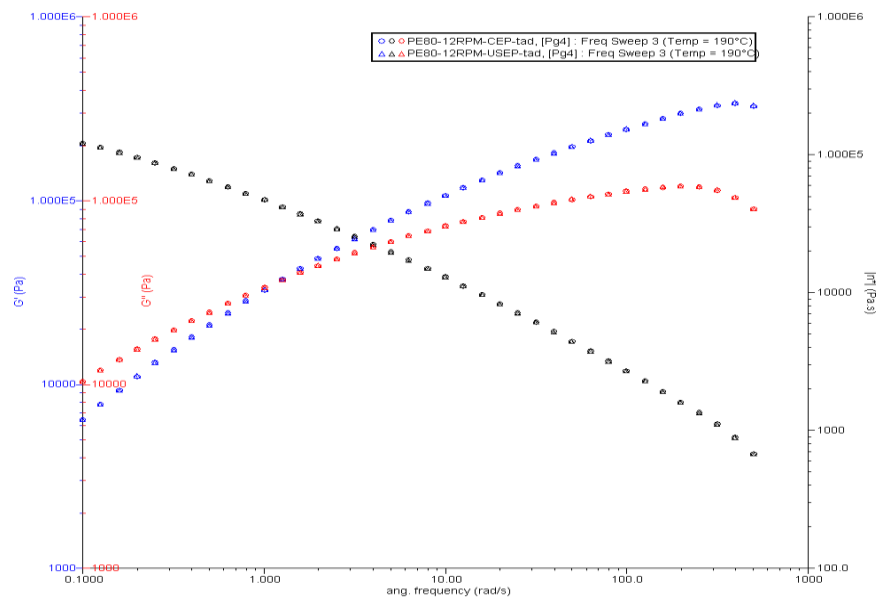
Figure 4-64: Dynamic shear storage modulus (G'), loss modulus (G") and complex viscosity (η*) plotted against angular frequency for PE80 pipes produced at 12 rpm with and without ultrasound.

The viscosity and storage modulus of the melt are very sensitive to structural changes in the polymer. For the rheological properties obtained from the pipes, only a small difference was observed between the samples produced with and without application of ultrasonic waves.
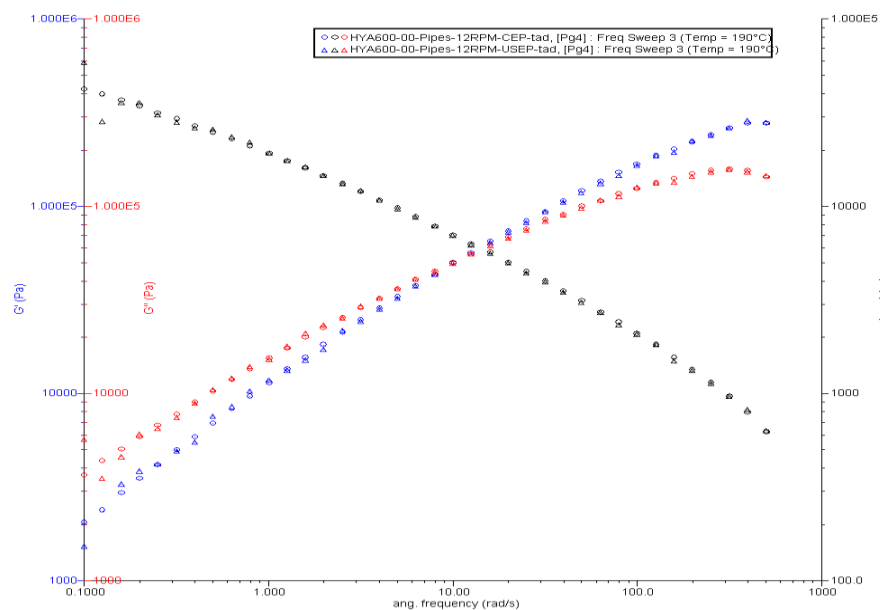
Figure 4-65: Dynamic shear storage modulus (G'), loss modulus (G") and complex viscosity (η*) plotted against angular frequency for HYA600 pipes produced at 12 rpm with and without ultrasound.

169

The test conditions for the rheology tests conducted on samples obtained from HYA600 pipes were similar to the experiments carried out on the PE80 pipes. Storage and loss modulus along with the complex viscosity were plotted against angular frequency. The results from the HYA600 pipes are shown in Figure 4-65.

The results obtained from the rheology tests carried out on samples from HYA600/20 and HYA600/40 pipes were similar to the PE80 and HYA600 results and did not show any changes to rheological properties of the samples with the application of ultrasonic waves during extrusion.
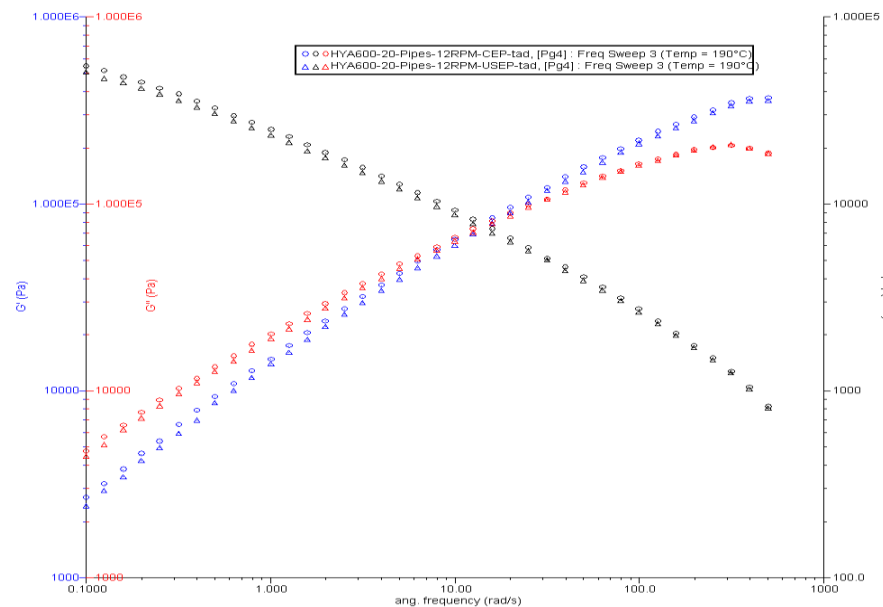
Figure 4-66: Dynamic shear storage modulus (G'), loss modulus (G") and complex viscosity (η*) plotted against angular frequency for HYA600/20 pipes produced at 12 rpm with and without ultrasound.

The rheology test results were used to investigate the effects of ultrasonic waves on the molecular chain structure of the polymer melt. The possible chain scission of the polymer melt could result in a lower viscosity. However, a comparable complex viscosity of the CEP and USEP extruded pipe samples suggested that the chain structure was not affected by the application of the ultrasonic vibrations. Figure 4-66 and Figure 4-67 show the

complex viscosity (η^*), shear storage modulus (G') and shear loss modulus (G") plotted against the angular frequency of the test.

The complex viscosity change by the application of ultrasonic waves on the extruded pipes of the base resin was negligible as shown in Figure 4-65. However, the viscosity results of the extruded HYA600 composites showed a small measurable decrease of the complex viscosity of the USEP pipes compared to the CEP pipes.
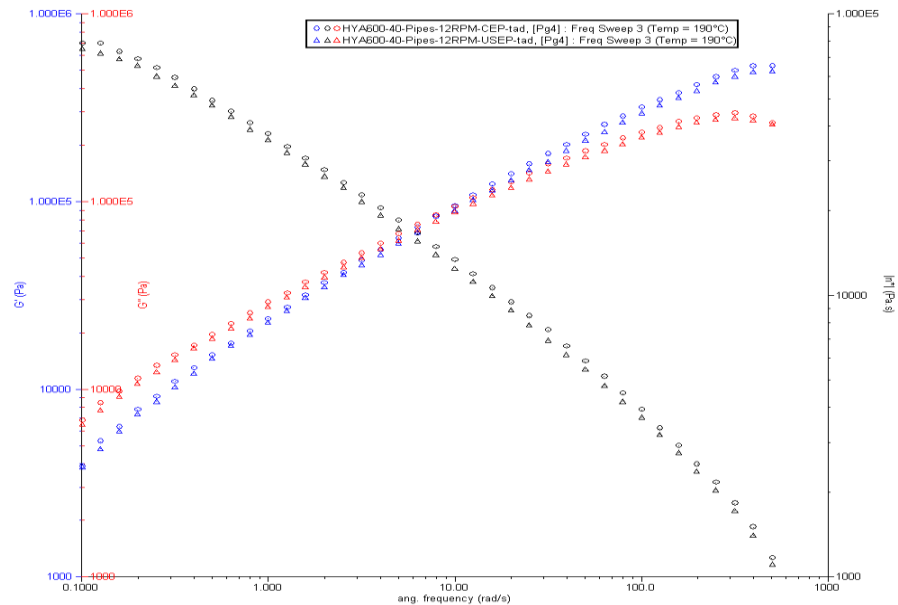
Figure 4-67: Dynamic shear storage modulus (G'), loss modulus (G") and complex viscosity (η*) plotted against angular frequency for HYA600/40 pipes produced at 12 rpm with and without ultrasound.

The reduction of the complex viscosity of the CEP processed HYA600/20 and HYA600/40 compared to the USEP pipes could be possibly as a result of a disentanglement of the polymer chains. A disentanglement of the chains could have been present in the HYA600 samples, but any effect was too small to be measurable. In the composites, however, as the calcium carbonate content increased the resin amount decrease. The fraction of the disentangled chains to the total chains in the composite increased when compared to the resin. The increased fraction of the disentangled chains leads to a more noticeable effect.

This could be also explained by the fact that presence of the filer increased the effect of ultrasonic vibrations by decreasing the chain relaxibility. Therefore ultrasonic vibrations

could have had more aggressive effect on the HYA600 composites when compared to their effect on the base resin.

4.4   Conclusion

By the introduction of ultrasound waves into the polymer melt during extrusion in an annular die, the processing behaviour and the materials' properties have been affected. The effects of the application of ultrasound reported in this chapter are summarised below.

4.4.1 Extrusion of the strips

- The extruder barrel pressure for the processing of the strips and pipes decreased with the application of ultrasound. For the processing of strips the reduction in the barrel melt pressure for Rigidex5130 was the lowest, 6.3%, at 12rpm and the greatest, 9%, at 16 rpm. The lowest and highest reductions for the barrel melt pressure by application of the ultrasound for the processing of the PE80 were 2.6% at 18 rpm and 6.1% at 8rpm.

- The reduction in the total power consumed for extrusion of the Rigidex5130 strips was between 4.9% (16rpm) and 9.5% (24rpm) as presented in Figure 4-11. The power consumption of the PE80 extrusion with the application of ultrasound reduced by 4.2% at 8rpm while for strips produced at 24rpm the power consumed increased by 1.4% from CEP to USEP.

- The extrudate output rate remained unaffected by application of ultrasound for the processing of the strips.

- The tensile properties (young's modulus and yield strength) of the Rigidex5130 and PE80 strips were not affected by the application of ultrasonic vibrations during extrusion.

- The DMA results showed that by the introduction of ultrasonic vibrations into the polymer melts in an annular die the storage and loss modulus did not change

significantly at room temperature while a small difference was observed near the glass transition temperature. However, the T_g increased by approximately 1°C and the T_g activation energy calculated for the strips increased for both the Rigidex5130 and the PE80 strips when ultrasonic vibrations were present during extrusion.

- The DSC tests showed that the melting and crystallisation temperature of the processed strips with and without ultrasound were equal and they were not affected by the application of ultrasonic vibrations except for Rigidex5130 strips processed at 20 and 24rpm where a small difference was observed. The heat of fusion and crystallisation enthalpy were similar for CEP and USEP strips and therefore the degree of crystallinity was unaffected by the application of the ultrasonic waves.

- Rheology results showed that the shear storage modulus, shear loss modulus and the complex viscosity of the strips was not affected by the application of ultrasonic vibrations during extrusion process.

4.4.2 Extrusion of the pipes

- For the processing of pipes the extruder barrel pressure and the die entrance pressure both reduced when processing with ultrasound. The reduction in the barrel melt pressure for the PE80 pipes was between 2.0% and 7.9%. The melt pressure for the unfilled HYA600 pipes decreased between 3.0% and 3.9% with the ultrasound. For the $CaCO_3$ filled compounds of HYA 600, the effect of the ultrasound on the processing pressure increased with the increase in the weight percentage of the filler. For 20%wt filled HYA600, the pressure decreased by 4.3% and 4.9% for screw speeds of 18 rpm and 8 rpm respectively while this value was between 4.6% (at 18 rpm) and 7% (at 20 rpm) for the 40%wt filled compound.

- The power consumption for the processing of the PE80 pipes reduced by 5.9% (at 18 rpm) to 12.8% (at 14 rpm). The power reduction in the processing of the HYA600 pipes was however considerably higher. For the processing of the unfilled HYA600 pipes the power consumption reduced by 12.4% (at 20 rpm) to 22% (at 18rpm) while the reduction percentage for the filled HYA600 compounds was between 20% (at

16rpm) and 27% (at 16rpm) for the 20%wt CaCO$_3$ filled HYA600 and between 13% (at 14 rpm) and 19% (at 12 rpm) for the 40%wt filled HYA600.

- The output rate of the extruder did not change by the application of the ultrasonic waves during the processing of the polyethylene pipes.

- The Young's modulus and the yield strength of the PE80, HYA600 and the composites pipes were not affected by the presence of the ultrasound.

- The storage modulus of the ultrasound treated pipes showed a slight increase compared to the CEP pipes at temperatures near the glass transition. The glass transition temperature of the pipes increased by ~1°C for the USEP pipes compared to CEP pipes. The activation energy of the T$_g$ for all the pipes increased with application of ultrasound when compared to CEP pipes.

- The melting and crystallisation temperature of the pipes did not change by the application of the ultrasonic waves but the heat of fusion increased slightly (~5J/g) for all the USEP pipes compared to the CEP pipes at the same screw speed.

- A comparison of the rheological properties ($G^{'}$, $G^{''}$ and η^{*}) of the pipes produced with and without presence of ultrasonic vibrations indicated that the application of the USVs did not have any effect on the viscosity of the melt.

A comparison of the processing parameters for the CEP and USEP extruded strips indicated that by the application of ultrasonic vibrations during extrusion the barrel pressure and total power consumption was reduced. As discussed earlier in Section 4.3.1.1 , a possible explanation for the reduction of the barrel pressure and the power consumption of the extrusion process was that the vibration of the ultrasonic horn in the parallel section, generated high frequency vibrations on the surface of the horn. These vibrations would be either transferred into the melt at the surface or reduce the friction between the melt and the ultrasonic horn. For the first assumption the temperature of the melt will increase locally and therefore lead to lower viscosities of the polymer melt in the boundary layer between the horn and the melt flow. If the second assumption was true, by assuming an equal wall resistance of the die walls in both sides of the die, sliding of the melt over the

surface of the horn theoretically reduces the resistance of the one side of the die wall and should reduce the back pressure caused by die wall resistance. There is a difference in the performance of the ultrasonic horn in the conical and parallel section. The positions of nodes and anti-nodes should be considered when comparing the conical and parallel section of the horn. The intensity of the ultrasonic vibrations was defined by the position of nodes/anti-nodes in the sonotrode.

The conical section of the horn applies compressive/shear high frequency vibrations into the polymer melt and could possibly cause chain breaking and the formation of the macro radicals.

The tensile properties of the strips and pipes were unaffected by the application of ultrasonic vibrations suggesting that the crystalline and amorphous structure of the polymer remained unaltered. The DMA results also supported the fact that mechanical properties of the strips and pipes were not affected by the ultrasonic vibrations.

The results obtained from the HYA600 composites and comparing them with the matrix resin indicated that the addition of the filler into the polymer matrix did not change the effect of ultrasonic vibrations on the processing parameters. The presence of the fillers could enhance the transfer of the USVs and therefore influence of them on the properties and the processing parameters of the composites.

There was a possibility of some chain breakage, the formation of macro radicals and consequently cross linking of the polymer chains by the application of ultrasonic vibrations. This was believed to be as result of the stress build up in polymer which was generated by high frequency vibrations that had a smaller period than relaxation time of the polyethylene. However, the mechanical and rheological results along with thermal properties obtained from DSC tests dismissed the occurrence of any modification to the polymer structure and indicated that the structure of the polymers remained intact by application of USVs.

From the results reported in this chapter, it can be concluded that the processing parameters were affected in a similar way to that shown in Chapter 3 with G1 ultrasonic

horn for lower output rates. It was concluded that the extrusion process benefited from the presence of ultrasound by the reduction in the total power consumption without negatively affecting the product properties. Although the current arrangement was successful in proving the potential for the application of ultrasonics in the plastic industry, the efficiency of the horn could be improved to further maximize the effect and benefits of ultrasound. This was achieved by redesigning of the ultrasonic horn (G3 horn) to increase the polymer melt exposure to the compressive waves which proved to be more penetrative and effective on the polymer melt.

4.5 References

1.   Byon, S.K. and J.R. Youn, *Ultrasonic processing of thermoplastic foam.* Polymer Engineering & Science, 1990. **30**(3): p. 147-152.

2.   Isayev, A.I. and J. Chen, *Apparatus for the Continuous Ultrasonic Devulcanization of Vulcanized Elastomers, US Patent*. 1994.

3.   Isayev, A.I., J. Chen, and A. Tukachinsky, *NOVEL ULTRASONIC TECHNOLOGY FOR DEVULCANIZATION OF WASTE RUBBERS.* Rubber Chemistry and Technology, 1995. **68**(2): p. 267-280.

4.   Isayev, A.I. and S. Mandelbaum, *Effect of ultrasonic waves on foam extrusion.* Polymer Engineering & Science, 1991. **31**(14): p. 1051-1056.

5.   Isayev, A.I., C.M. Wong, and X. Zeng, *Effect of oscillations during extrusion on rheology and mechanical properties of polymers.* Advances in Polymer Technology, 1990. **10**(1): p. 31-45.

6.   Isayev, A.I., S.P. Yushanov, and J. Chen, *Ultrasonic devulcanization of rubber vulcanizates. I. Process model.* Journal of Applied Polymer Science, 1996. **59**(5): p. 803-813.

7.   Peshkovskii, S.L., et al., *Acoustic cavitation and its effect on flow in polymers and filled systems.* Polymer Composites, 1983. **4**(2): p. 126-134.

8.   Tukachinsky, A., D. Schworm, and A.I. Isayev, *Devulcanization of Waste Tire Rubber by Powerful Ultrasound.* Rubber Chemistry and Technology, 1996. **69**(1): p. 92-103.

9.   Li, J., S. Guo, and M. Liang, *Effects of ultrasonic oscillation on processing behaviors of PS, EPDM, and PS/EPDM blend.* Journal of Applied Polymer Science, 2006. **100**(3): p. 1856-1863.

10.   Vigotsky, V., Plast Eng, 1996. **52**: p. 22.

11.   Basov, N.I., et al., *Increasing the output of plastics processing equipment by vibrating action on the melt.* Chemical and Petroleum Engineering, 1973. **9**(6): p. 495-498.

12.   Faitel'son, L.A. and M.G. Tsiprin, *Relation between the viscoelastic properties of polymer melts and the degree of filling, the frequency and the gradient of the vibration velocity.* Mekhanika Polimerov, 1968. **3**: p. 515-521.

13.   Faitel'son, L.A. and M.G. Tsiprin, *Thixotropic melts of filled polyethylene during periodic shear deformation.* Mekhanika Polimerov, 1968. **5**: p. 927-933.

14. Faitel'son, L.A., M.G. Tsiprin, and D.B. Prieditis, *Periodic deformation of a polyethylene melt in a tube extruder head.* Plasticheskie Massy, 1970. **9**: p. 36-38.

15. Leonov, A.I., M.G. Tsiprin, and L.A. Faitel'son, *Periodic deformation and viscous flow of solutions and melts of polymers.* Mekhanika Polimerov, 1969. **3**: p. 519-528.

16. Vinogradov, G.V., et al., *Action of vibration on the viscoelastic behavior of monodisperse polybutadienes.* Inzhenerno-Fizicheskii Zhurnal, 1971. **20**(3): p. 389-397

17. Casulli, J., et al., *The oscillating die: A useful concept in polymer extrusion.* Polymer Engineering & Science, 1990. **30**(23): p. 1551-1556.

18. Kazakia, J.Y. and R.S. Rivlin, *The influence of vibration on Poiseuille flow of a non-Newtonian fluid, I.* Rheologica Acta, 1978. **17**(3): p. 210-226.

19. Manero, O., B. Mena, and R. Valenzuela, *Further developments on non-Newtonian flow in oscillating pipes.* Rheologica Acta, 1978. **17**(6): p. 693-697.

20. Behrend, O., K. Ax, and H. Schubert, *Influence of continuous phase viscosity on emulsification by ultrasound.* Ultrasonics Sonochemistry, 2000. **7**(2): p. 77-85.

21. Isayev, A.I. and C.M. Wong, *Parallel superposition of small- and large-amplitude oscillations upon steady shear flow of polymer fluids.* Journal of Polymer Science Part B: Polymer Physics, 1988. **26**(11): p. 2303-2327.

22. Kim, H. and J.W. Lee, *Effect of ultrasonic wave on the degradation of polypropylene melt and morphology of its blend with polystyrene.* Polymer, 2002. **43**(8): p. 2585-2589.

23. Feng, W. and A.I. Isayev, *In situ compatibilization of PP/EPDM blends during ultrasound aided extrusion.* Polymer, 2004. **45**(4): p. 1207-1216.

24. Lapshin, S. and A.I. Isayev, *Continuous process for melt intercalation of PP–clay nanocomposites with aid of power ultrasound.* Journal of Vinyl and Additive Technology, 2006. **12**(2): p. 78-82.

25. Madras, G. and S. Chattopadhyay, *Effect of benzoyl peroxide on the ultrasonic degradation of poly(vinyl acetate).* Polymer Degradation and Stability, 2001. **73**(1): p. 33-38.

26. Chou, H.C.J. and J.O. Stoffer, *Ultrasonically initiated free radical-catalyzed emulsion polymerization of methyl methacrylate (II): Radical generation process studies and kinetic data interpretation.* Journal of Applied Polymer Science, 1999. **72**(6): p. 827-834.

27. Yildiz, G., H. Çatalgil-Giz, and A. Giz, *Effect of ultrasound on electrochemically initiated acrylamide polymerization.* Journal of Applied Polymer Science, 2002. **84**(1): p. 83-89.

28. Price, G.J., D.J. Norris, and P.J. West, *Polymerization of methyl methacrylate initiated by ultrasound.* Macromolecules, 1992. **25**(24): p. 6447-6454.

29. Matyjaszewski, K., et al., *Sonochemical Synthesis of Polysilylenes by Reductive Coupling of Disubstituted Dichlorosilanes with Alkali Metals.* Macromolecules, 1995. **28**(1): p. 59-72.

30. Fujiwara, H., et al., *Mechanochemical block copolymerization in heterogeneous systems of the solid poly(vinyl chloride) with styrene by ultrasonic irradiation - II. Effect of several forms of suspension polymerized poly(vinyl chloride) particles.* Polymer Bulletin, 1994. **33**(3): p. 317-323.

31. Fujiwara, H., et al., *Mechanochemical block copolymerization in heterogeneous systems of the solid poly(vinyl chloride) with styrene by ultrasonic irradiation.* Polymer Bulletin, 1992. **28**(2): p. 189-196.

32. Chen, K., S. Chen, and X. Xu, *Ultrasonic Degradation and Block Copolymerization of Polybutadiene with Acrylic Acid.* Journal of Macromolecular Science, Part A, 1992. **29**(1): p. 55-64.

33. Price, G.J., E.J. Lenz, and C.W.G. Ansell, *The effect of high-intensity ultrasound on the ring-opening polymerisation of cyclic lactones.* European Polymer Journal, 2002. **38**(9): p. 1753-1760.

34. Zhang, J., et al., *The stress field induced by contact with asperities.* Journal of Materials Engineering, 1990. **12**(4): p. 271-278.

35. Shen, Y., et al., *Ultrasonic Degradation and Copolymerization of Poly (Vinyl Alcohol) with Acrylonitrile.* Journal of Macromolecular Science: Part A - Chemistry, 1986. **23**(12): p. 1415-1431.

36. Basedow, A.M. and K.H. Ebert, *ULTRASONIC DEGRADATION OF POLYMERS IN SOLUTION.* Advances in Polymer Science, 1977(22): p. 83-148.

37. Pendleton, J.W., *Apparatus for applying ultrasonic vibration to thermoplastic polymers during forming*, in *U.S. Patent 3,298,065*. 1965.

38. Lemelson, J., *U.S. Patent 4,288,398*, U.S. Patent, Editor. 1981.

39. Allan, P.S. and M. Bevis, *U.S. Patent 4,925,161*. 1985.

40. Malloy, R.A., in *Plastic Part Design for Injection Molding*. 1993, Hanser/Gardner Publications. p. 59-60.

41. Allan, P.S., et al., *Shear controlled orientation technology for the management of reinforcing fibres in moulded and extruded composite materials.* Journal of Materials Processing Technology, 1996. **56**(1-4): p. 272-281.

42. Ibar, J.P., *FR Patent No. 79 06532*. 1979.

43. Ibar, J.P., *FR Patent No. 8004252*. 1980.

44. Ibar, J.P., *Vibro-molding: a new process to mold polymeric materials.* . Polymer Preprints (American Chemical Society, Division of Polymer Chemistry), 1980. **21**(1): p. 215-217.

45. Ibar, J.P., *Rheomolding: A New Process to Mold Polymeric Materials.* Polymer-Plastics Technology and Engineering, 1981. **17**(1): p. 11-44.

46. Ibar, J.P., *Method and Apparatus For Transforming The Physical Characteristics of Material By Controlling The Influence of Rheological Parameters.* 1986.

47. Ibar, J.P., *EP Patent 87402864.0*. 1987.

48. Ibar, J.P., *GB Patent No. 2046167*. 1990.

49. Ibar, J.P., *U.S. Patent No. 07.882,754*. 1990.

50. Ibar, J.P., *U.S. Patent No. 08/124,147*. 1993.

51. Ibar, J.P., *CA Patent No. 1,313,840*. 1993.

52. Ibar, J.P., *Instability in the rubbery state revealed by DSC of Rheomolded polystyrene samples.* Polymer Communications, 1983. **24**(11): p. 331-335.

53. Ibar, J.P., Modern Plastics, 1995. **25**(1): p. 85.

54. Ibar, J.P., Polyblends '95 Preprints, SPE RETEC on Polymer Alloys and Blends, 1995. **208**.

55. Ibar, J.P. *Injection Molding, H4-New Technologies and Developments, Part I.* in *Annual Technical Conference - Society of Plastics Engineers.* 1996.

56. Ibar, J.P. *Marketing and Management Division, H10-Economic and General Issues, "Potential Markets for Vibration Assist Molding".* in *Annual Technical Conference - Society of Plastics Engineers.* 1996.

57. Ibar, J.P. *Injection Molding Division, "Melt Viscosity Reduction of Plastics by Vibration During Filling in Injection Molding".* in *Annual Technical Conference - Society of Plastics Engineers.* 1997. Toronto.

58. Kikuchi, A. and R.F. Callahan. *Injection Molding, H4-New Technologies and Developments, Part I "Quality Improvements Resulting from Rheomolding".* in *Annual Technical Conference - Society of Plastics Engineers.*

59. Slonimskii, G.L. and e. al., Vysokomol. Soyed, 1974. **A16**(1): p. 579.

60. Nurmukhametov, S.N. and e. al., Mekhanika Polimerov, 1976. **4**: p. 579.

61. Hengesbach, H.A., et al., *Ausrustung von Spritzgiessmaschinen" (Equipping of Injection Molding Machines),* in *Report II–1 from IKV, at the Rhineland-Westphalian Technical University (RWTH) in Aachen.* 1976.

62. Schramm, K.W., *Injection Molding of Structural Parts Consisting of Plastic Molding Materials Utilizing Forced Oscillating Flow Processes.* 1976, Rhenish-Westphalian College of Technology.

63. Manero, O. and B. Mena, *An interesting effect in non-newtonian flow in oscillating pipes.* Rheologica Acta, 1977. **16**(5): p. 573-576.

64. Mena, B., O. Manero, and D.M. Binding, *COMPLEX FLOW OF VISCOELASTIC FLUIDS THROUGH OSCILLATING PIPES - INTERESTING EFFECTS AND APPLICATIONS.* Journal of Non-Newtonian Fluid Mechanics, 1979. **5**(APR): p. 427-448.

65. Shmidt, L.R. and J.L. Maxam, *Injection Molding Polycarbonate Optical Disks Using an Oscillatory Boundary Condition.* SPE ANTEC Technical Papers, 1992. **38**: p. 447.

66. Wong, C.M., C.H. Chen, and A.I. Isayev, *Flow of Thermoplastics in an Annular Die under Parallel Oscillations.* Polymer Engineering and Science, 1990. **30**(24): p. 1574-1584.

67. Zachariades, A.E. and B. Chung, *New polymer processing technologies for engineering the physical and mechanical properties of polymer products.* Advances in Polymer Technology, 1987. **7**(4): p. 397-409.

68. Shmidt, L.R. and J.L. Maxam, *Injection Molding Polycarbonate Compact Disks: Relationship between Process Conditions, Birefringence and Block Error Rate.* SPE ANTEC Technical Papers, 1998. **34**: p. 334.

69. Wu, H., et al., *Effects of ultrasonic oscillations on processing behavior and mechanical properties of metallocene-catalyzed linear low-density polyethylene/low-density polyethylene blends.* Journal of Applied Polymer Science, 2004. **94**(6): p. 2522-2527.

70. Peng, B., et al., *Effects of ultrasonic oscillations on rheological behavior and mechanical properties of novel propylene-based plastomers.* Journal of Applied Polymer Science, 2007. **106**(3): p. 1725-1732.

71. Wei, L., et al., *Effect of ultrasound on the processability and mechanical properties of poly(butylene terephthalate)/talc composites.* Journal of Applied Polymer Science, 2011. **122**(4): p. 2708-2714.

72. Guo, S., et al., *Ultrasonic improvement of rheological and processing behaviour of LLDPE during extrusion.* Polymer International, 2003. **52**(1): p. 68-73.

73. Kaiyuan, C., et al., *Effect of vibration extrusion on the structure and properties of high-density polyethylene pipes.* Polymer International, 2009. **58**(2): p. 117-123.

74. Casulli, J., J.R. Clermont, and B. Mena. *The oscillating die: A useful concept in polymer extrusion.* in *Xth International Congress on Rheology.* 1988: Australian Soc. of Rheol.

75. Wong, C.M. and A.I. Isayev, *Orthogonal superposition of small and large amplitude oscillations upon steady shear flow of polymer fluids.* Rheologica Acta, 1989. **28**(2): p. 176-189.

76. *USSR Pat. No. 394, 104.* 1973.

77. *USSR Pat. No. 413,937.* 1974.

78. *USSR Pat. No. 489,397.* 1974.

79. Fairbanks, T.H., *U.S. Pat. 3,663,668.* 1972.

80. Fridman, M.L., A.I. Isayev, and E.S. Smyslova. in *All-Union Conf. on High-Molecular Mass Compounds.* 1973. Kazan, USSR.

81. Fridman, M.L., S.L. Peshkovsky, and G.V. Vinogradov, *The rheology of thermoplastics under conditions of spiral flow and vibrations on extrusion.* Polymer Engineering & Science, 1981. **21**(12): p. 755-767.

82. Geneder, M.M., et al., Vysokomol. Soedin. Ser. B USSR, 1978. **20**: p. 364.

83. Geneder, M.M., et al., Plast. Massy USSR, 1978. **12**: p. 34.

84. Geneder, M.M., et al., Plast. Massy. USSR, 1982. **3**: p. 58.

85. Geneder, M.M., et al., Plastmass Sint. Smol. USSR, 1981. **3**: p. 26.

86. Isayev, A.I. and E.V. Katsytsevich. in *Machines and Technology of Rubber Processing.* 1977. Yaroslav, USSR.

87. Isayev, A.I., C.M. Wong, and X. Zeng, *Flow of Thermoplastics in Dies with Oscillating Boundary.* SPE Technical Papers, 1987. **33**: p. 207-210.

88.   Isayev, A.I., C.M. Wong, and X. Zeng, *Flow of Thermoplastics in an Annular Die under Orthogonal Oscillations.* Journal of Non-Newtonian Fluid Mechanics, 1990. **34**(3): p. 375-397.

89.   Lubartovich, S.A., et al., Kauch. Rezina, 1978. **1**: p. 18.

90.   Peshkovskii, S.L., M.B. Generalov, and I.N. Kaufman, *Effect of ultrasonic vibrations on the flow of a viscoelastic liquid.* Mechanics of Composite Materials, 1971. **7**(6): p. 979-981.

91.   Akastelov, A.I., et al., Kauch. Rezina USSR,, 1972. **31**: p. 17.

92.   Kiselyova, O.F., et al., *Extrusion of polymers during ultrasonic action.* Journal of Applied Polymer Science, 2004. **91**(2): p. 693-696.

93.   Chen, G., S. Guo, and H. Li, *Ultrasonic improvement of rheological behavior of polystyrene.* Journal of Applied Polymer Science, 2002. **84**(13): p. 2451-2460.

94.   Wu, H., et al., *Ultrasonic oscillations effect on rheological and processing properties of metallocene-catalyzed linear low density polyethylene.* Journal of Applied Polymer Science, 2003. **90**(7): p. 1873-1878.

95.   Chen, G., S. Guo, and H. Li, *Ultrasonic improvement of the compatibility and rheological behavior of high-density polyethylene/polystyrene blends.* Journal of Applied Polymer Science, 2002. **86**(1): p. 23-32.

96.   Feng, W. and A.I. Isayev. in *61st Annual Technical Conference, ANTEC*. 2003.

97.   Kim, H., et al. in *61st Annual Technical Conference, ANTEC*. 2003.

98.   Lin, H. and A.I. Isayev. *EFFECT OF HIGH INTENSITY ULTRASONIC WAVES ON POLYPROPYLENE, POLYAMIDE 6 AND THEIR BLENDS*. in *61st Annual Technical Conference, ANTEC*. 2003. USA.

99.   Badran, B.M., A. Gałęski, and M. Kryszewski, *High-density polyethylene filled with modified chalk.* Journal of Applied Polymer Science, 1982. **27**(10): p. 3669-3681.

100.   Bartczak, Z., et al., *Toughness mechanism in semi-crystalline polymer blends: II. High-density polyethylene toughened with calcium carbonate filler particles.* Polymer, 1999. **40**(9): p. 2347-2365.

101.   Fu, Q. and G. Wang, *Polyethylene toughened by rigid inorganic particles.* Polymer Engineering & Science, 1992. **32**(2): p. 94-97.

102.   Wang, Y., J. Lu, and G. Wang, *Toughening and reinforcement of HDPE/CaCO3 blends by interfacial modification—interfacial interaction.* Journal of Applied Polymer Science, 1997. **64**(7): p. 1275-1281.

103.	Fu, Q., G. Wang, and J. Shen, *Polyethylene toughened by CaCO3 particle: Brittle-ductile transition of CaCO3-toughened HDPE.* Journal of Applied Polymer Science, 1993. **49**(4): p. 673-677.

104.	Jancar, J., A. Dianselmo, and A.T. Dibenedetto, *The yield strength of particulate reinforced thermoplastic composites.* Polymer Engineering & Science, 1992. **32**(18): p. 1394-1399.

105.	Lei, J. and R. Zhou, *Mechanical properties and interfacial interaction of CaCO3 filled HDPE compatibilized with HDPE functionalized by ultraviolet irradiation.* Polymer Engineering & Science, 2000. **40**(7): p. 1529-1533.

106.	Xu, W., et al., *Effect of electron beam irradiation on mechanical properties of high density polyethylene and its blends with sericite-tridymite-cristobalite.* Journal of Applied Polymer Science, 2000. **78**(2): p. 243-249.

107.	Guo, S., et al., *A STUDY ON REACTIVE ENHANCEMENT OF FILLER-FILLED HIGH-DENSITY POLYETHYLENE.* Polymer-Plastics Technology and Engineering, 2000. **39**(2): p. 305-315.

108.	Hasegawa, M., Y. Akiho, and Y. Kanda, *Mechanochemical polymerization of methyl methacrylate initiated by the grinding of inorganic compounds.* Journal of Applied Polymer Science, 1995. **55**(2): p. 297-304.

109.	Oprea, C.V. and M. Popa, *Mechanochemically Synthesized Polymers with Special Properties.* Polymer-Plastics Technology and Engineering, 1989. **28**(9): p. 1025-1058.

110.	Pi, H., S. Guo, and Y. Ning, *Mechanochemical improvement of the flame-retardant and mechanical properties of zinc borate and zinc borate–aluminum trihydrate-filled poly(vinyl chloride).* Journal of Applied Polymer Science, 2003. **89**(3): p. 753-762.

111.	Isayev, A.I., C.K. Hong, and K.J. Kim, *Continuous mixing and compounding of polymer/filler and polymer/polymer mixtures with the aid of ultrasound.* Rubber Chemistry and Technology, 2003. **76**(4): p. 923-947.

112.	Kumar, R.V., et al., *Preparation and characterization of nickel–polystyrene nanocomposite by ultrasound irradiation.* Journal of Applied Polymer Science, 2002. **86**(1): p. 160-165.

113.	Xia, H. and Q. Wang, *Preparation of conductive polyaniline/nanosilica particle composites through ultrasonic irradiation.* Journal of Applied Polymer Science, 2003. **87**(11): p. 1811-1817.

114.	Li, Y., et al., *Effect of ultrasonic oscillations on the rheological behavior and morphology of Illite-filled high-density polyethylene composites.* Journal of Applied Polymer Science, 2005. **96**(2): p. 379-384.

115. Lapshin, S. and A.I. Isayev. *Continuous process for melt intercalation of PP-clay nanocomposites with aid of power ultrasound.* in *63rd Annual Technical Conference - Society of Plastics Engineers.* 2005.

116. Lee, E.C., D.F. Mielewski, and R.J. Baird, *Exfoliation and dispersion enhancement in polypropylene nanocomposites by in-situ melt phase ultrasonication.* Polymer Engineering & Science, 2004. **44**(9): p. 1773-1782.

117. Oh, J.S., A.I. Isayev, and M.A. Rogunova, *Continuous ultrasonic process for in situ compatibilization of polypropylene/natural rubber blends.* Polymer, 2003. **44**(8): p. 2337-2349.

118. Ryu, J., H. Kim, and J. Lee. in *Annual Technical Conference - Society of Plastics Engineers.* 2002.

119. Ryu, J., et al. in *Annual Technical Conference - Society of Plastics Engineers.* 2001.

120. Ryu, J., et al., *Power ultrasound effects for in situ compatibilization of polymer-clay nanocomposites.* Materials Science & Engineering, C: Biomimetic and Supramolecular Systems, 2004. **C 24**: p. 285.

121. Ryu, J.G., J.W. Lee, and H. Kim, *Development of poly(methyl methacrylate)-clay nanocomposites by using power ultrasonic wave.* Macromolecular Research, 2002. **10**(4): p. 187-193.

122. Tapale, M. and A.I. Isayev, *Continuous ultrasonic devulcanization of unfilled NR vulcanizates.* Journal of Applied Polymer Science, 1998. **70**(10): p. 2007-2019.

123. Rauwendaal, C. *Innovation in extrusion.* in *ANTEC FUNDAMENTALS FORUM/SPECIAL SESSIONS.* 2002. San Francisco, USA.

124. Roussel, M.D., et al. (2005) *The Use of Calcium Carbonate in Polyolefins Offers Significant Improvement in Productivity.*

125. Osman, M.A., et al., *Particle--particle and particle-matrix interactions in calcite filled high-density polyethylene---steady shear.* Journal of Rheology, 2004. **48**(5): p. 1167-1184.

126. Li, H.L., Y.C. Zhang, and J.Y. Chen, *Functionalization of high density polyethylene in melt state through ultrasonic initiation and its effect on mechanical properties of glass fiber reinforced composites.* Polymer Bulletin, 2007. **59**(3): p. 427-438.

127. Peng, B., W.Y. Guo, and Q.P. Ruan, *Ultrasonic Oscillations Effect on Extrusion Processing, Structure, and Properties of Blends of Propylene Based Plastomer and Ethylene/1-Octene Copolymer.* Journal of Reinforced Plastics and Composites, 2009. **28**(22): p. 2701-2715.

128. Wu, H., et al., *Improved Processing Behaviors and Mechanical Properties of Polyolefin Elastomer Blends Prepared by Ultrasound-Assisted Extrusion.* Journal of Applied Polymer Science, 2009. **112**(4): p. 2136-2142.

129. Fu, S.-Y., et al., *Effects of particle size, particle/matrix interface adhesion and particle loading on mechanical properties of particulate–polymer composites.* Composites Part B: Engineering, 2008. **39**(6): p. 933-961.

130. Pukanszky, B. and G. VÖRÖS, *Mechanism of interfacial interactions in particulate filled composites.* Composite Interfaces, 1993. **1**(5): p. 411-427.

131. Fu, S.-Y., X. Hu, and C.-Y. Yue, *A New Model for the Transverse Modulus of Unidirectional Fiber Composites.* Journal of Materials Science, 1998. **33**(20): p. 4953-4960.

132. Ma, L., et al., *Elastic and plastic analyses of functionally graded elements.* Matter Sci Forum, 2003. **731**(6): p. 423-425.

133. Fu, S.-Y., G. Xu, and Y.-W. Mai, *On the elastic modulus of hybrid particle/short-fiber/polymer composites.* Composites Part B: Engineering, 2002. **33**(4): p. 291-299.

134. Danusso, F. and G. Tieghi, *Strength versus composition of rigid matrix particulate composites.* Polymer, 1986. **27**(9): p. 1385-1390.

135. Levita, G., A. Marchetti, and A. Lazzeri, *Fracture of ultrafine calcium carbonate/polypropylene composites.* Polymer Composites, 1989. **10**(1): p. 39-43.

136. Alves, N.M., J.L. Gómez Ribelles, and J.F. Mano, *Study of the Molecular Mobility in Polymers with the Thermally Stimulated Recovery Technique—A Review.* Journal of Macromolecular Science, Part C, 2005. **45**(2): p. 99-124.

137. Alves, N.M., J.F. Mano, and J.L. Gómez Ribelles, *Molecular mobility in polymers studied with thermally stimulated recovery. II. Study of the glass transition of a semicrystalline PET and comparison with DSC and DMA results.* Polymer, 2002. **43**(13): p. 3627-3633.

138. Sauer, B.B. and Y.H. Kim, *Structural Heterogeneity in Poly(methyl methacrylate) Glasses of Different Tacticity Studied by Thermally Stimulated Current Thermal Sampling Techniques.* Macromolecules, 1997. **30**(11): p. 3323-3328.

Chapter 5

Industrial Scale In-line Ultrasonic Assisted Pipe Extrusion of Polyolefins

5.1 Introduction

The effects of ultrasonic vibrations on polyethylene melts during lab scale (25mm) and pilot scale (50mm) extrusion was investigated. It was found that the application of the ultrasonic vibrations reduced the extruder barrel pressure and the total power consumption without affecting the mechanical, thermal and rheological properties of the final products (strips and pipes). In order to determine the benefits from the ultrasonic vibrations in the extrusion of polyolefins in the plastic industry it was essential to study the effect of ultrasonics for higher melt throughputs.

By increasing the throughput rates of the polymer melt the residence time in the ultrasonic die will decrease and therefore, to achieve similar results to smaller extruders with an industrial scale extruder it was necessary to modify the design of the ultrasonic horn. The

new design and the third generation ultrasonic horn, G3 horn, used in this project was designed to be able to deliver longer exposure times for the melt to the US energy than the previous designs and thus would be better able to accomplish similar effects with the higher melt throughput rates than the previous horn designs.

This part of the study focuses on design of the G3 ultrasonic horn and the ultrasonic die, the installation and troubleshooting of the ultrasonic die, the design of the adapter for connecting a 90mm extruder to the ultrasonic die and the extrusion trials with and without presence of ultrasonic waves.

5.2   Experimental

5.2.1 Materials

A commercial pipe extrusion grade of polyethylene (PE80) that was supplied by Polypipe Terrain (manufactured by BOREALIS) with the melt flow rate of 0.33 g/10min under a load of 5.0Kg at 190°C was used both for all of the extrusion trials.

5.2.2 Design of 3rd generation ultrasonic horn and housing block

The G3 horn was designed as an upgrade of the second generation ultrasonic horn (G2 horn) by using a similar shape but extending the horn length. This was done in order to increase the residence time of the polymer melt in the ultrasonic die and also to introduce the corrugation to the surface of the cylindrical section of the horn to benefit from the effects of compressive ultrasonic waves.

The main changes to the ultrasonic horn were the extension of the cylindrical section and the introduction of a corrugation to the surface. As a result of these changes, the dimensions of other sections of the horn had to be modified to allow the horn to resonate at the natural frequency of the US system.
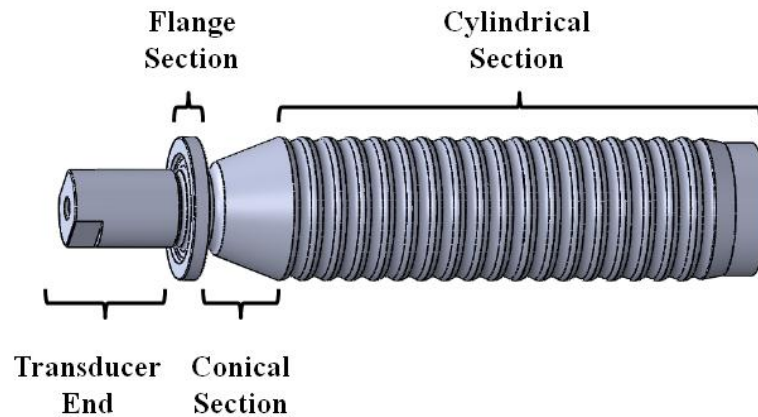
Figure 5-1: Different sections of third generation ultrasonic horn [1].

The FEA analysis on the proposed design of the ultrasonic horn was carried out by Telsonic. The length of the end section which was a cylindrical section with diameter of 65mm, adjusted to 15mm according to the FEA.

The flange of the ultrasonic horn which was the only contact point of the ultrasonic horn with the die body was 4mm thick in the previous design. By extending the cylindrical section of the horn, the applied shear force by the polymer melt on the horn increased. The flange section was the only part of the horn that held the horn in place and had to be able to endure the load applied to it. Thus it was recommended by the Polypipe engineering team to increase the thickness of the flange section to 8mm to strengthen this part to make it more robust than the previous design.

The dimensions of the conical section of the ultrasonic horn remained unchanged from the G2 horn to the G3 horn.

The total length of the cylindrical section was increased to 221mm and consisted of a corrugated section with a straight cylindrical section at the end of the horn (shown in Figure 5-1). The straight cylindrical section was 15mm long and was added to the end of the horn to allow the melt flow to get into a laminar flow form and to loose any turbulent flow effects created by the corrugated section of the horn.

The idea behind the introduction of the corrugated surface to the horn was to increase the exposure of the polymer melt to a compressive component of the ultrasonic vibrations.
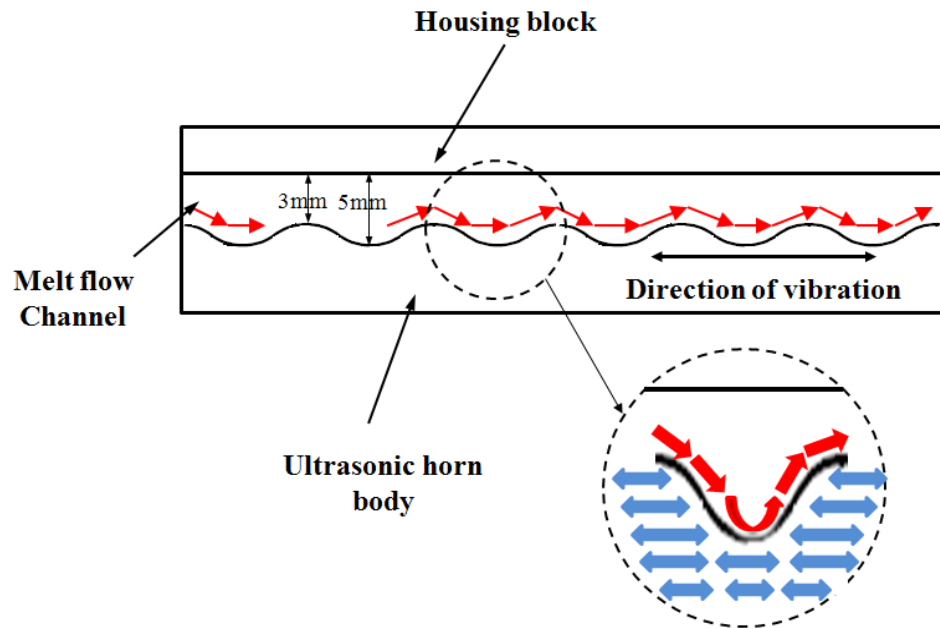
Figure 5-2: Schematic diagram of the corrugated section of the ultrasonic horn showing the expected flow pattern of the polymer melt.

Figure 5-2 illustrates the expected flow pattern of the polymer melt through the corrugated section of the horn. As the melt flowed over the peaks it was exposed to shear waves parallel to the flow direction when it flowed into the valleys the melt encountered a compressive component of the ultrasonic vibrations perpendicular to the flow direction. Thus the effect of this design was to intermittently expose the polymer melt to compressive waves along the length of the horn, in particular at the antinode sections. This arrangement was intended to gain the benefits from the compressive waves while the melt was progressing along the length of the ultrasonic horn. The FEA was used to dimension the horn and this was carried out by Telsonic on the horn design and the result is shown in Figure 5-3.
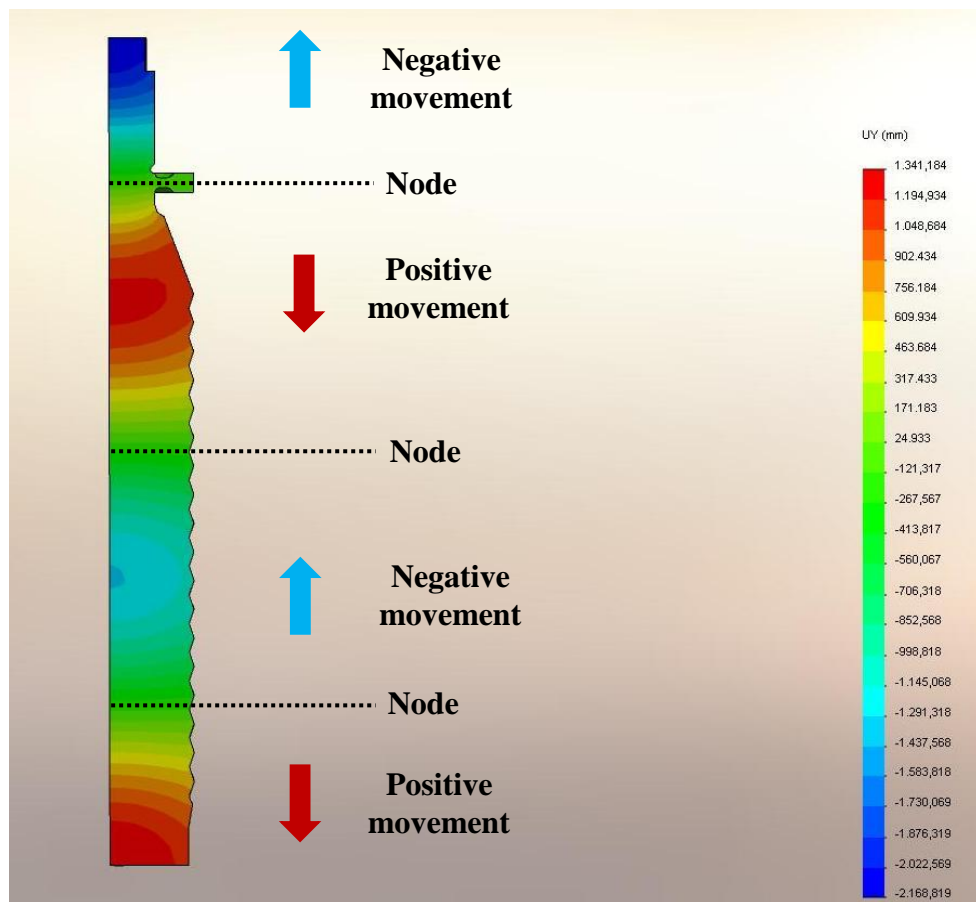
Figure 5-3: FEA modelling results of the ultrasonic horn showing displacement profile at different parts of the horn.

Figure 5-3 shows the displacement profile across the G3 horn. By assuming an axis along the ultrasonic horn with its positive direction toward the bottom of the horn, at the top of the ultrasonic horn the displacements are in the negative direction (shown with dark blue). The absolute value of the displacement decreases as it moves toward the node at the flange section and becomes almost zero at the node. Then it increases to reach the maximum positive displacement. The same pattern was repeated between the two nodes on the corrugated section of the horn. The FEA result presented in Figure 5-3 shows that the G3 horn had maximum vibration amplitude in negative direction at the top of the horn where it joined the booster. The length of the horn was adjusted to allow a maximum vibration amplitude at the end of the horn which is in agreement with the design basis of ultrasonic horns in that the length should be a multiple of half the wave length long.

The housing block for the 3rd generation ultrasonic horn consisted of 6 individual parts that were bolted together to hold the horn in place and allow the flow of the polymer melt over the horn. The ultrasonic housing block consisted of a top block, mid block with the ring gate, bottom block, the inner sleeve and the steering plate.

The Top block together with the midblock, were used to clamp the ultrasonic horn in the ultrasonic housing block. The ring gate design was based on the same principles used for designing the ring gate of the second generation ultrasonic housing block. The feed hole and clearance between the gate and the ultrasonic horn both were larger than the previous design to allow for greater throughputs.
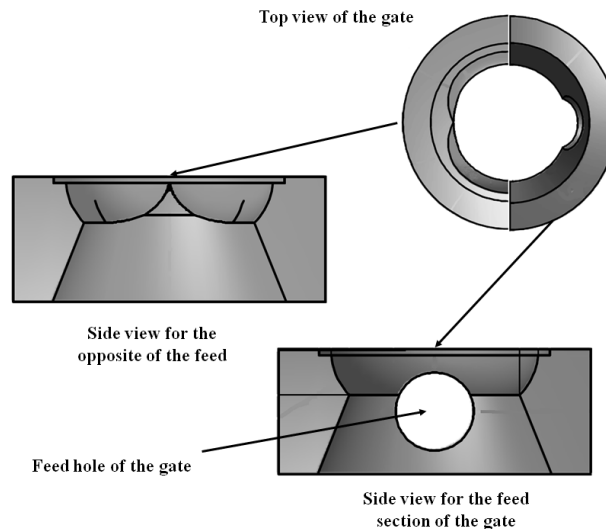
Figure 5-4: Ring gate design of the third generation ultrasonic housing block [2, 3] with a split line in the middle to allow installation of the horn.

The pressure at the opposite side of the feed hole in the ring gate was much lower than the feed side, therefore the polymer melt flows faster in the feed hole side when compared to opposite side. The clearance at the opposite side of the feed hole was restricted in the current design (shown in Figure 5-4) in order to avoid a dead spot in the melt flow and direct the melt to the conical section of the die and to consequently generate a uniform flow of the melt over the ultrasonic horn.

The other feature of the current design that differed from the previous design was the assembly of the bottom block. The bottom block consisted of three individual parts and

those were; the main body, the inner sleeve and the steering plate. The inner sleeve was designed in order to allow further modifications to the melt flow channel thickness in the corrugated section of the ultrasonic die. The clearance between the sleeve and the ultrasonic horn was 3mm for this setup and it could be reduced or increased for later trials by simply changing the sleeve. The inner sleeve was secured in the main body of the bottom block by 6 bolts. The inner sleeve and the main body featured a pressure transducer hole to enable a measurement of the melt pressure before the die exit.
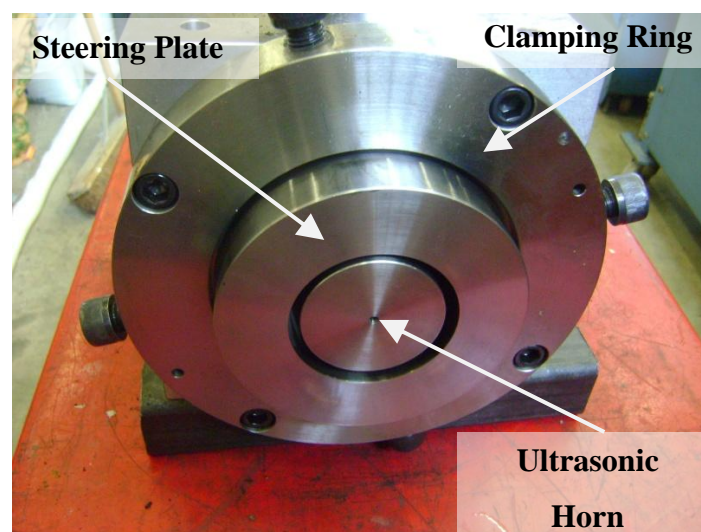
Figure 5-5: Steering plate installed on the 3rd generation ultrasonic setup showing the steering plate, clamping ring and the ultrasonic horn. The exit wall thickness of the pipe can be adjusted by 4 bolts placed on the steering plate.

One of the challenges in pipe manufacturing using the second generation ultrasonic die was to achieve a uniform thickness of the pipe wall. Although ultrasonic horn was used as a mandrel similar to conventional pipe dies, centring of the mandrel by using spider legs was not possible because of high frequency vibration of the ultrasonic horn. To overcome this problem a steering plate was designed and added to the end of the ultrasonic die. The steering plate could be moved by four bolts which were placed in an angle of 90° to each other. The installed steering plate on the ultrasonic die is illustrated in Figure 5-5.

An adapter was also designed to allow the fitting of the G3 die to the 50mm extruder to carry out initial proving trials prior to running it on a pipe extrusion line at Polypipe using a 90mm extruder.
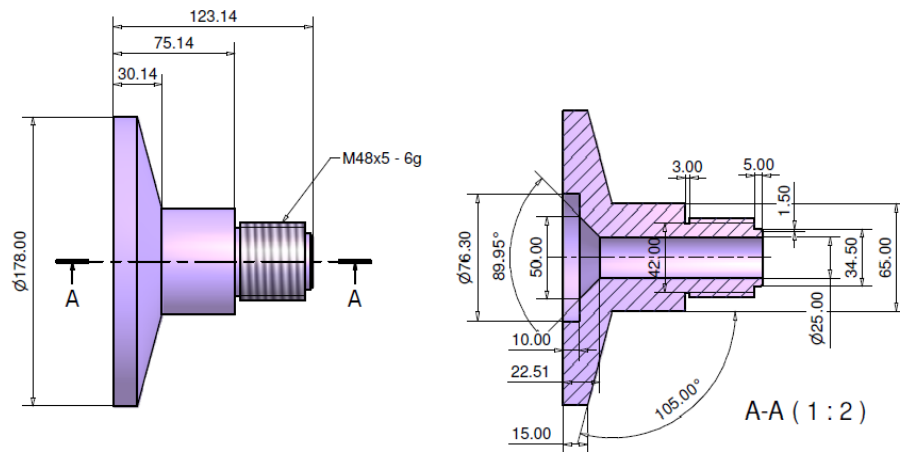
Figure 5-6: The details of the adapter connecting the 50mm extruder to the G3 die.
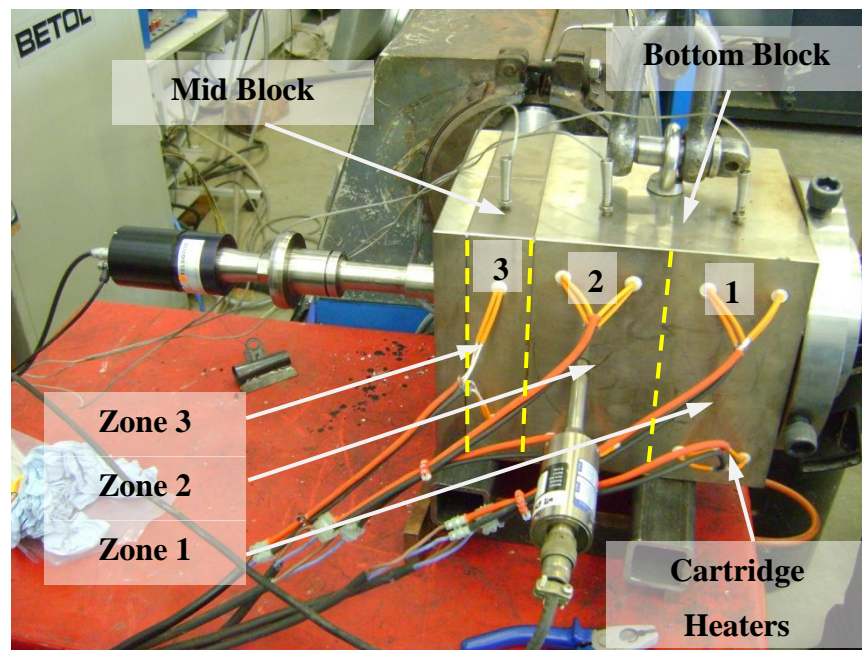
Figure 5-7: Ultrasonic Die with cartridge heaters installed on the mid block and bottom block, the three heating zones are showed in the picture.

The ultrasonic die was divided into three heating zones. The position of the two heating zones in the 1st half and the 2nd half of the bottom block are shown in Figure 5-7. The drawings and the installation pictures of the G3 ultrasonic horn and the housing block are presented in Appendix D.

5.2.3 Pipe extrusion of polyethylene by single screw extruder

The single screw extruder described in Section 4.2.3 was used for initial extrusion trials with the third generation ultrasonic die.

The industrial scale pipe extrusion was carried out using a 90mm Battenfeld Extrusionstechnik single screw extruder.

Unlike conventional pipe extrusion lines, the ultrasonic die had a cross head configuration. This did not allow the extruder, die and the vacuum/sizing bath to be aligned in a straight line. To solve this issue an adapter was required to take the polymer melt from the extruder to feed the ultrasonic die from the side. The adapter also needed to be kept at the processing temperature to avoid solidification of the melt inside the adapter.

The bypass/adapter consisted of "L" shaped halves, with the split line along the melt flow channel. The melt flow channel was a circular channel with diameter of 50mm that was reduced to 25mm diameter when entering the ultrasonic die. The gradual decrease of the melt flow channel diameter from 90mm at extruder to 50mm at the bypass entrance and 25mm at the ultrasonic die entrance ensured that there was no large single decrease in the flow channel cross sectional area. The pictures of the bypass are illustrated in Figure 5-8 where the construction of the different parts of the bypass can be seen.
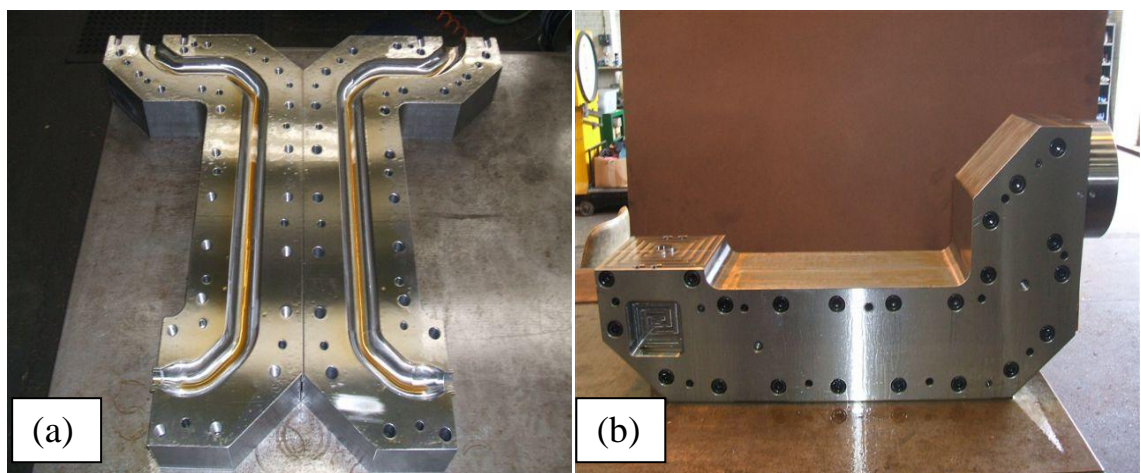
Figure 5-8: Bypass made to connect the 90mm extruder to the G3 ultrasonic die, showing the halves of the bypass (a) and the "L" shape of the by pass (b).

The pipe extrudate was pulled from the die to a vacuum sizing die and cooling bath for calibration and forming of the pipe section. The vacuum/sizing bath consisted of two sections each ~1.5m long. After leaving the vacuum bath the pipe entered a cooling bath where water was sprayed onto the pipe to cool it to room temperature.

At the end of the manufacturing line a padded haul off was used to pull the extrudate through the vacuum and cooling bath. The produced pipe was then cut into 3m long pipes.

5.2.4 Ultrasonic generator

A TELSONIC SG-22 power supply was employed for ultrasonic assisted pipe extrusion process. The generator is described in more detail in section 4.2.7.

5.3   Results and discussion

5.3.1 Extrusion Processing

The initial pipe extrusion of PE80 with the G3 die was carried out using 50mm Betol Extruder. The processing temperatures for the pipe extrusion of PE80 with the 50mm extruder in the laboratory and the 90mm extruder at Polypipe are summarised in Table 5-1.

Table 5-1: Processing temperatures for pipe extrusion trials of PE80 with 50mm and 90mm extruder.

Material	Barrel Zones						Die Zones				
	T1	T2	T3	T4	T5	T6	T7	T8	T9	T10	T11
PE80-50mm Extruder	180	180	190	195	200	200	205	205	N/A	N/A	N/A
PE80-90mm Extruder	200	200	200	200	200	200	200	200	200	200	200

The pipe extrusion process of PE80 with the 50mm Betol extruder was carried out as mentioned earlier in Section 4.3.1.2. Conventional pipe extrusion was carried out prior to the ultrasonic assisted extrusion process.

The ultrasonic assisted extrusion of PE80 using G3 horn was not successful and the ultrasonic generator was indicating that the horn was not vibrating at 20 KHz with the system showing an overload. The generator was thus not able to overcome the external forces (clamping and polymer melt) trying to prevent it from vibrating at the required frequency and amplitude.

The die was dismantled and the horn sent back to Telsonic for retuning and checking for any possible defects. The FEA modelling of the horn showed that the horn was functioning properly at room temperature.

The horn was then clamped in the ultrasonic die and tested at room temperature. The horn was functioning properly and continuously with no imperfection. The ultrasonic die was then heated to the processing temperature ~200°C and the horn tested again without the presence of material in the die.

The experiments with the ultrasonic horn at 200°C showed that the frequency indicator[1] on the ultrasonic generator moved downward by increasing of the temperature. The movement of the frequency indicator is related to the deviation from the set/designed frequency of the horn.

The horn was designed from a material with known Young's modulus and density at room temperature. It was tuned to be able to deliver a standing wave with amplitude of 18μm at the anti-node and frequency of 20 KHz. The increase in temperature, however, appeared to have a significant effect on US properties of the titanium [4, 5] and consequently on the performance of the horn. The effects from the temperature rise were significant enough to cause overloading of the generator resulting in the power being shut off.

---

[1] Frequency indicator was an LED display which shows the deviation from the set frequency and the limits are -0.5 to 0.5 where the midpoint (Ref=0) shows that the horn vibrates at required frequency.
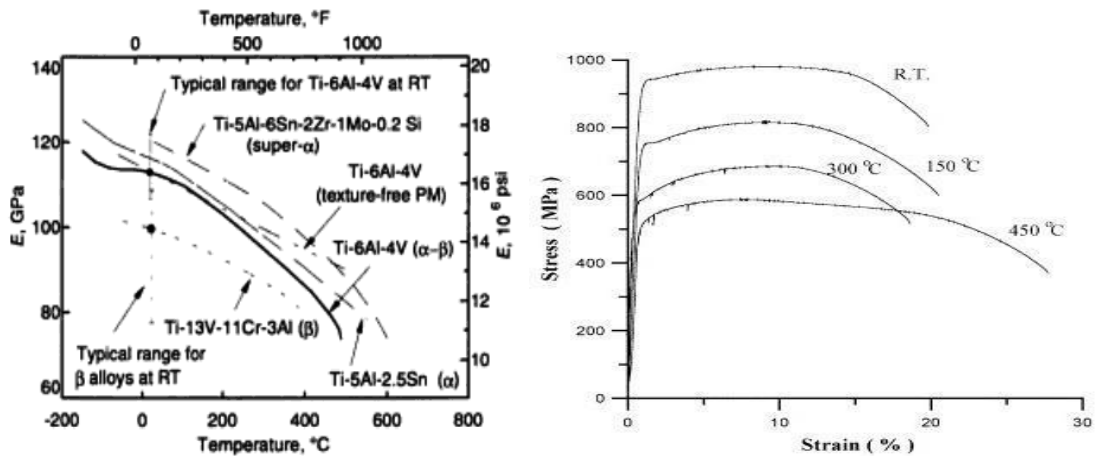
Figure 5-9: Temperature dependency of Young's modulus of titanium alloy [5] (left), change of the stress strain behaviour of the TI6AL4V alloy used for the sonotrode [4] (right).
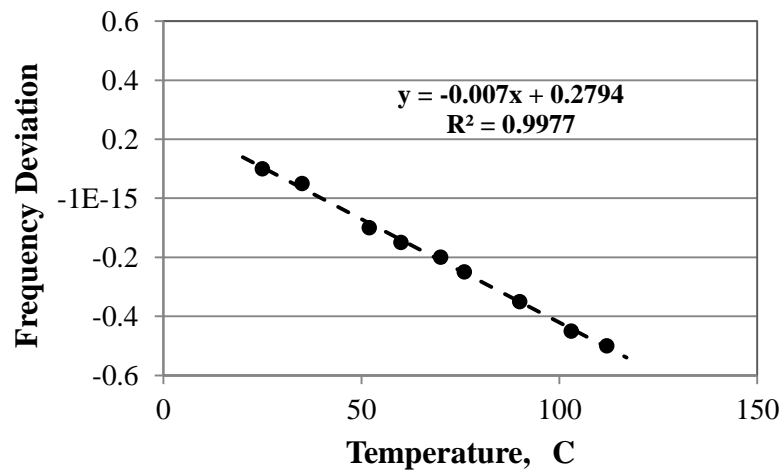
Figure 5-10: Frequency deviation from set value against temperature.

An explanation of this effect must have originated from the change of the physical properties of the titanium from room temperature to the die processing temperature. It can be seen from Figure 5-9 that the tensile modulus of the TI6AL4V alloy drops significantly by increasing of the temperature from room temperature to 150°C and these changes will affect the wave pattern and performance of the sonotrode consequently.

In order to determine the effect of temperature on the performance of the ultrasonic horn, it was heated and the performance (using the frequency indicator) was measured.
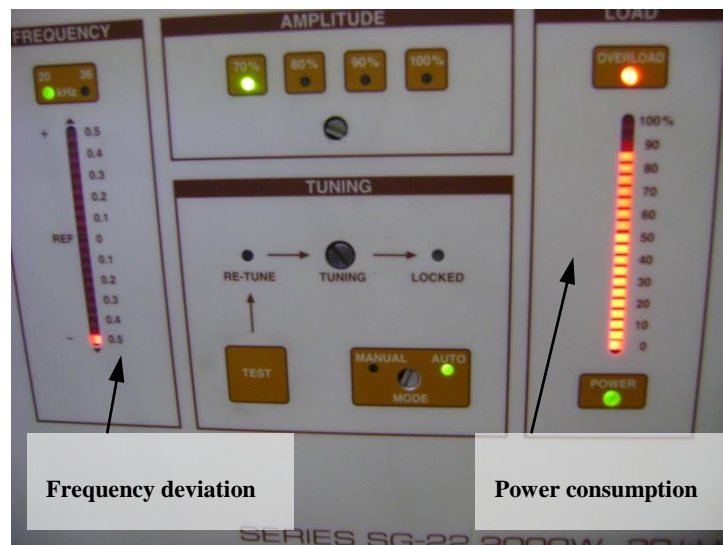
Figure 5-11: Ultrasonic generator when the sonotrode operates at 200°C.

The temperature of the horn was monitored by the attachment of the small plate thermocouple at the end of the ultrasonic horn. The Ultrasonic horn was then tested at different temperatures and the deviation from the reference frequency was measured and plotted against temperature. The obtained results from these experiments proved that ultrasonic horn's performance was in fact very temperature sensitive. It can be seen from the data presented in Figure 5-10 that the frequency of the sonotrode shifted away from the reference frequency in negative direction by increasing of the temperature. The maximum allowance for this deviation was -0.5. Greater deviations will cause the generator to overload and initiate a safety cut out. Figure 5-11 shows the ultrasonic generator control panel, where it can be seen that the sonotrode is operating with deviation of -0.5 from the reference frequency and the generator is overloaded.

The deviations were actually caused by a change in the natural frequency of the horn and, therefore, a movement of the nodal points. Nodal points had major role in the designing of the ultrasonic horn as one of the nodal points was used for clamping of the sonotrode. Movement of the nodal point that was used for clamping led to the vibration of the clamping flange. This consequently resulted in the vibration of the ultrasonic die itself and thus drew a great amount of power from the generator tat lead to the overloading of the generator.

The present ultrasonic horn reached the operating limit of -0.5 at 112°C which was well below the required processing temperature. This indicated that the reason for overloading of the ultrasonic system was a temperature shift of the natural frequency of the ultrasonic horn. It was also observed that by dispersing fine sand granules on the ultrasonic die block they vibrated when the ultrasonic horn was operating, this indicated that the ultrasonic horn was using power to vibrate the ultrasonic block in addition to delivering ultrasonic waves to the polymer melt.

In order to resolve the problem it was necessary to compensate for this negative deviation in the natural frequency of the horn. An FEA of the horn was carried out using the Ti alloy properties at 200°C. Based on these results Telsonic advised that reducing the mass of the ultrasonic horn will positively shift the frequency so it will be able to compensate for the negative deviations of the temperature rise. The transducer end of the ultrasonic horn had to be kept at the designed dimensions therefore it was recommended to grind the other end of the sonotrode and test the horn at room temperature until it shows reasonably positive deviation from the reference frequency at room temperature so by temperature rise the deviation drops down to the reference point.

Machining of the sonotrode in the scale of millimetres (the final dimensional change was about 15-20 mm) shifted the deviation 0.4 divisions from the reference when operating at room temperature and this was achieved by several trials. The sonotrode was then heated to the processing temperature and tested with continuous sonication. After the abovementioned modifications to the ultrasonic horn it functioned continuously close to the reference frequency and continuously. It was then decided to install the ultrasonic die on the 90mm extruder for pipe extrusion trials.
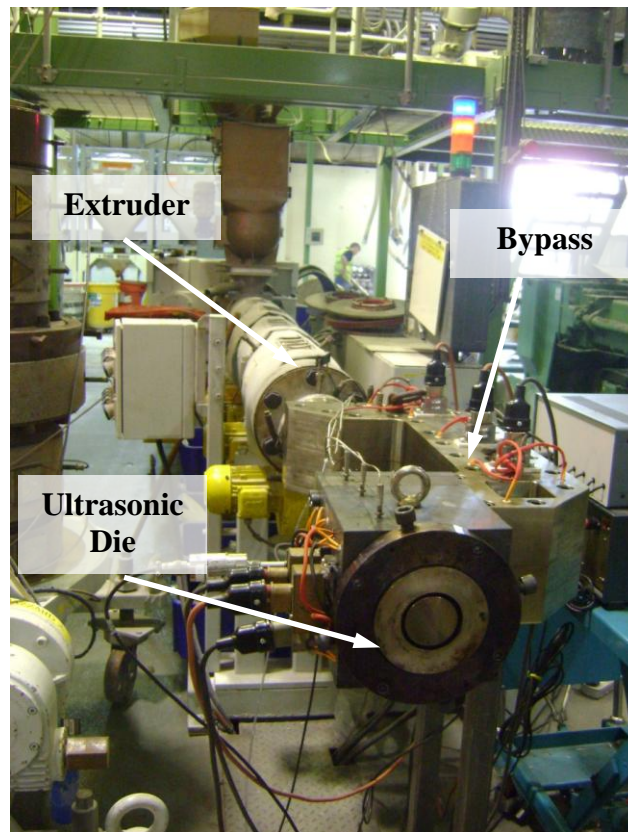
Figure 5-12: Ultrasonic die installed on 90mm extruder using the bypass.

The manufactured bypass with the ultrasonic die installed on the 90mm extruder is shown in Figure 5-12.

During continuous extrusion at 10rpm screw speed, it was observed that polymer melt was leaking from the join between the top and bottom halves of the bypass manifold (shown in Figure 5-13). The reason for this was the high pressure in the bypass section (~2000 Psi) that was generated by the resistance caused by the ultrasonic die. It was decided to carry on with the extrusion trials with current setting as dismantling of the bypass and solving the leakage problem was not feasible at the time and the leakage did not have any effect on investigating the ultrasonic wave effects during the pipe extrusion process.
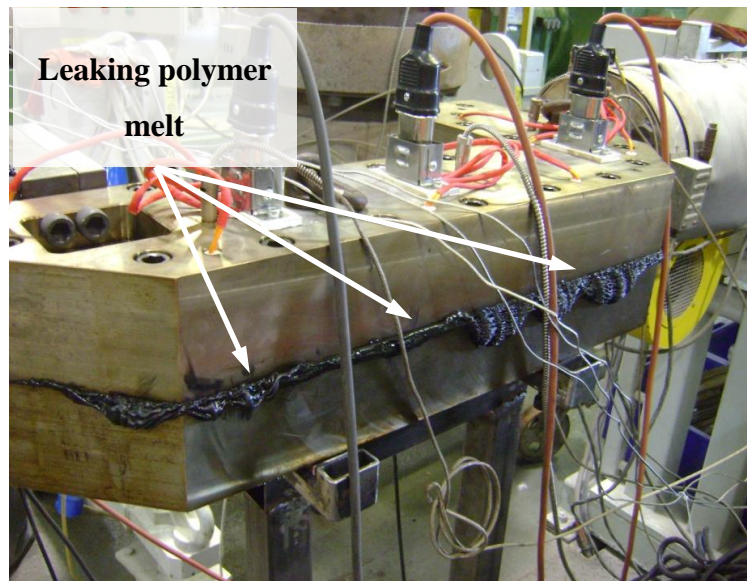
Figure 5-13: Leaking of the polymer melt from the bypass manifold.

The melt flow rate of the extruder was measured for three different screw speeds and the results are shown in Figure 5-14. The obtained results for the output rate of the extruder at three different screw speeds showed that the output rate is a linear function of screw speed as it was expected.
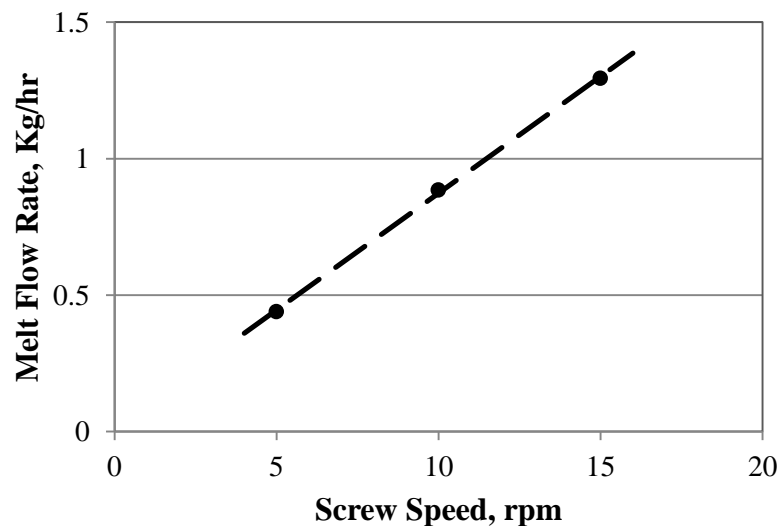
Figure 5-14: Melt flow rate vs. screw speed for extrusion of PE80 using 90mm extruder.

Pipe extrusion of PE80 with the ultrasonic die when the ultrasonic generator was not operating revealed that the melt flow was not uniform around the circumference of the die.

202

It was observed that the melt was flowing faster in the feed side of the ultrasonic die compared to the opposite side of the die.

The pipe pulling speed was uniform all around the circumference of the die but one side of the extrudate was flowing faster (melt exiting from the feed side of the die) than the other. As a result of this non uniform melt flow, the wall thickness of the pipe around its circumference was not uniform. In order to show that the melt flow and consequently the draw down ratio were not equal around the circumference of the pipe a straight line was drawn on the extrudate when leaving the die. For an equal pulling speed and draw down ratio the line should have remained straight on the pipe, however as it can be seen in Figure 5-15 the flow was faster in some areas compared to the others and this changed the straight line drawn on the extrudate to a "V" shape on the pipe (shown in Figure 5-15).
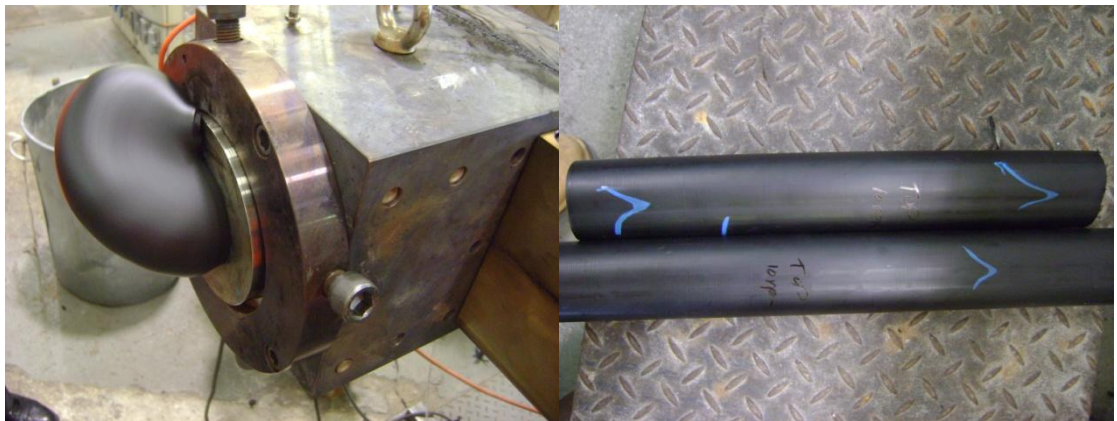
Figure 5-15: Non uniform flow of the molten polymer from the die (left) and uneven draw down of the polymer melt as a result of unequal flow of the melt.

The ultrasonic assisted extrusion was not successful as the ultrasonic horn was functioning at maximum power and then overloaded. This caused the ultrasonic generator to stop functioning continuously and start pulsing with overload light on. Although the sonotrode was functioning properly at Brunel when installed on the 50mm extruder, it was not able to operate normally using 90mm extruder. A possible explanation for this could have been the increasing of power drawn from the ultrasonic generator as a result of greater flow rates from the 90mm extruder than were generated by the 50mm extruder at Brunel. The rest of the processing parameters were similar to that of the trails carried out at Brunel.

5.4 Conclusion

From the experiments carried out in this section of the work it was learnt that the performance of the ultrasonic could be affected significantly by temperature rise. The problem could have been present at the previous generation of the sonotrode but, because of the smaller sizes of them, the effect was not as obvious as it was for the G3 sonotrode.

The modelling and simulation of the ultrasonic horn was carried out at elevated temperatures (200°C) in order to allow the effective operation of the ultrasonic horn with the current setup. For most current applications of an ultrasonic horn they are not required to operate at elevated temperatures and thus the effects of temperature on the functioning of a horn had not been previously encountered by Telsonic.

Suggested future work to solve the current problems and for the improvement of the performance of the sonotrode are as follows:

- Modelling of the ultrasonic horn at processing temperature.

- Find an alternative method for securing the ultrasonic horn in the die instead of clamping. Reduction of the of the contact area between the horn and die body helps to avoid transferring of the vibrations from the horn to the die body. The new design should be able to secure the horn in the die body with minimum contact area and sufficient applied force on the shut off surfaces to avoid leakage. This can be achieved with the use of metal O-rings to hold the ultrasonic die in place with minimum contact area.

- Redesign of the feed ring to enable better distribution of the melt around the ultrasonic horn. A bigger cross sectional area for the feed ring and a gradual increase in the clearance between the horn and the die body around the circumference of the feed ring. The gap could be smallest in the feed side of the feed ring where the pressure is the highest and the widest opposite the feed side where the melt pressure is the lowest compared to the other areas of the feed ring. The feed ring also can be redesigned in a way to have a split entering from the opposing sides of the die. The split feed could

enhance the melt distribution in the feed ring and allows a more uniform melt flow when compared to present design.

5.5 References

1. Hall, S., *Design Sheet for Special sonotrode 20kHz* B. University, Editor. 2011, Telsonic.

2. Webb, D., *Design sheet of Inner Shell 2*, B. University, Editor. 2011, Polypipe Terrain.

3. Webb, D., *Design sheet of Inner Shell 1*, B. University, Editor. 2011, Polypipe Terrain.

4. Wang, S.H., M.D. Wei, and L.W. Tsay, *Tensile properties of LBW welds in Ti–6Al–4V alloy at evaluated temperatures below 450 °C.* Materials Letters, 2003. **57**(12): p. 1815-1823.

5. Welsch, G., R.F. Boyer, and E.W. Collings, *Materials Properties Handbook: Titanium Alloys*. 1994: Asm International.

Chapter 6

Conclusion and future work

6.1 Ultrasonic effects on extrusion

The application of ultrasonic vibrations to the polymer melts was studied in three stages, as follows:

I. The ultrasonic waves were applied to a static polymer melt and the temperature change of the melt was measured beneath the ultrasonic horn. The results indicated that the effective penetration depth of the US waves in the polymer melt was less than 4 mm. Consequently therefore 2 mm thick flow channel around the horn was incorporated into the design of the first and second generation ultrasonic dies.

II. The effects of the ultrasonic vibrations were investigated for extrusion of two different grades of polyethylene in a relatively small extruder (25mm). With the application of the ultrasound waves the following effects were recorded.

  • The melt temperature increased at the die exit.

  • The die pressure and the barrel pressure decreased.

- The power consumption of the extrusion process reduced.

The tensile properties of the extruded samples were measured and they were similar for the CEP and the USEP samples. This was confirmed by comparable storage modulus values from DMA tests of the samples. The DMA results showed that by the application of the ultrasound the glass transition temperature of the polymer and the T_g activation energy of the samples increased from CEP to USEP (Section 3.3.3). The thermal properties such as T_m, T_c, ΔH_m and ΔH_c remained unchanged by introduction of ultrasound into the polymer melt during extrusion.

III. The effects of ultrasonic waves were studied for a greater flow rates than that used in the initial study. Two commercial grades of polyethylene were used for extrusion of the strips extrusion and four materials were used for the pipe while the number of the materials used for pipe extrusion was four. The results showed that for extrusion of the strips and pipes the application of ultrasonic waves to the polymer melt had the following effects:

- The barrel pressure and die entrance pressure reduced.
- The power consumption for the extrusion process reduced.

The effects of ultrasonic vibrations was variable with the material used and the processing screw speed, the values of effects for the strips and pipes are summarised in Section 4.4.1 and 4.4.2 respectively.

The tensile test results and the DMA results showed that these properties remained unchanged by application of ultrasound. The T_g measured by DMA tests increased ~1°C with the application of ultrasonic waves. Thermal and rheological properties of the extruded strips/pipes were not affected by the application of ultrasonic vibrations or the effects were too small to be measurable.

IV. Ultrasonic vibrations were applied onto the polyethylene melt in an industrial scale extruder (90mm). Commercial pipe grade polyethylene was used to carry out extrusion trials. The extrusion trials in presence of the ultrasonic vibrations were not successful. It was concluded that the ultrasonic vibrations propagation and

characteristics at elevated temperatures changed and consequently the ultrasonic generator and the ultrasonic horn was not functioning properly. In order to resolve this problem, the FEA analysis of the G3 horn was carried out using the mechanical properties of the horn material at 200°C and used to modify the ultrasonic horn which did not solve the problem. It came to conclusion that to improve the performance of the ultrasonic horn/die the sonotrode should be designed according to its operating temperature. The feed section of the ultrasonic die also needs to be redesigned to allow a better and uniform flow of the melt around the ultrasonic horn.

Generally it can be said that by the application of ultrasonic vibrations into the polymer melt at the die zone; the processing pressures, power consumption could be lowered without negative effect on the products mechanical or thermal properties. The effects are variable from one material to the other and at a screw speed to the other screw speed.

6.2   Contribution to science

Although ultrasonic vibrations have been introduced to polymer extrusion by previous workers, this work created a new approach to the application of ultrasonic energy to extrusion processing. The contributions of this study to related science are as follows:

- New designs and shapes of ultrasonic horn.

- Application of compressive and shear ultrasonic vibrations simultaneously.

- Integration of the ultrasonic horn into the pipe die and utilize it for pipe extrusion.

- Determination of ultrasonic vibrations effect on the polyolefin melt processing parameters and products characteristics.

- Identification of the operation temperature as a key factor in design of the ultrasonic horns used at elevated temperature.

6.3   Future work

The effects of ultrasonic vibrations were not significant enough to be applicable in plastic industry yet. To improve the efficiency and performance of the ultrasonic die, the current work could be continued with the following suggestion.

- Study the performance and efficiency of ultrasonic horn at elevated temperatures.

- Design of a flow path that can give a better and more uniform distribution of the polymer melt around the horn.

- Seek an alternative for clamping of the ultrasonic die to avoid loss of ultrasonic energy at the clamping flange.

- Study the efficiency of the ultrasonic horn in operational mode with simulation software.

- New designs of ultrasonic horn based on compressive waves and application of them in a controlled way. The compressive waves are more effectual than shear waves and could result in better efficiency of the ultrasonic horn.

- Studying the molecular structure of the treated and untreated samples and investigation of the ultrasonic vibrations effects on the orientation of the crystals and final product.

Appendix A

I. The Ultrasonic Block Assembly

Figure A-1: Side view of ultrasonic horn, mid block and the bottom block of the housing.
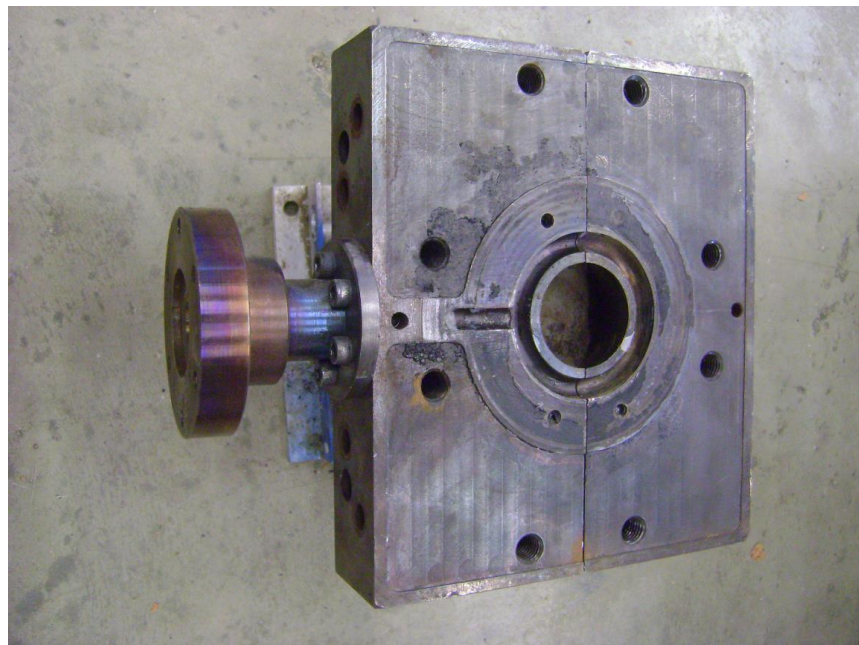
Figure A-2: Mid block and the adaptor to deliver the feed to ultrasonic block.

211
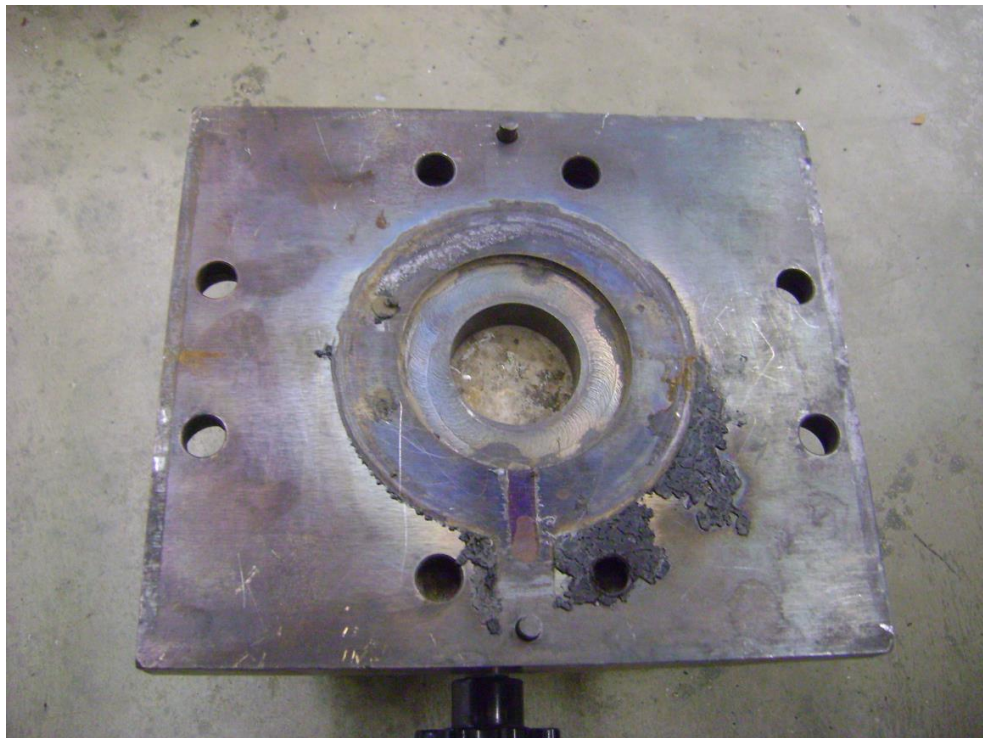
Figure A-3: Top block of the ultrasonic block.
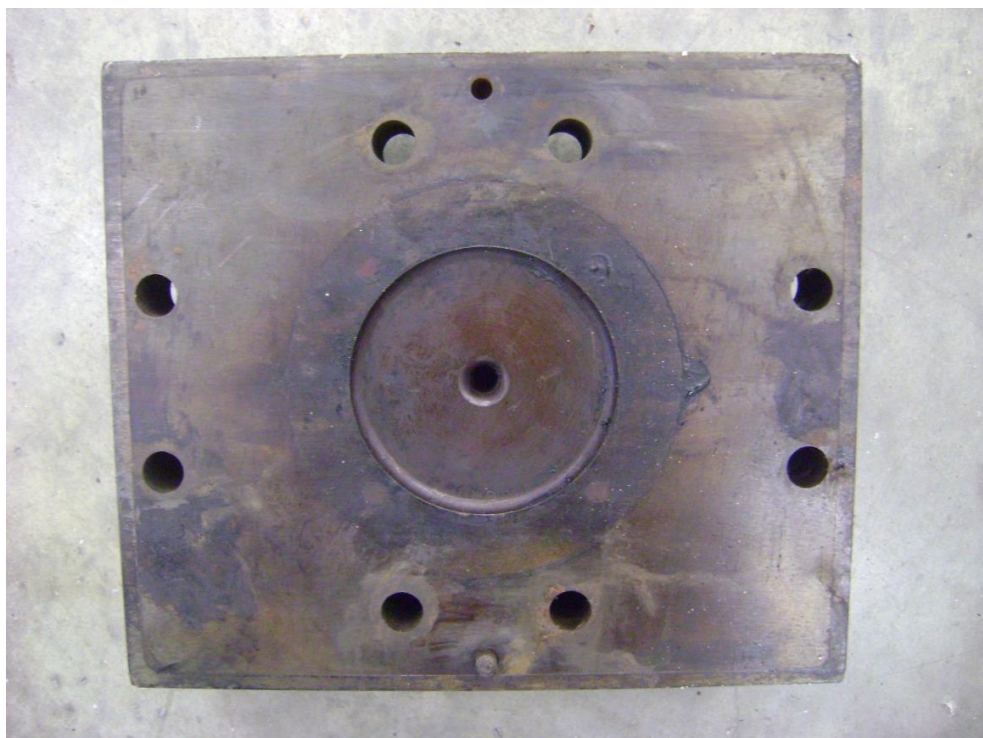
Figure A-4: Top view of the bottom block of the ultrasonic block.
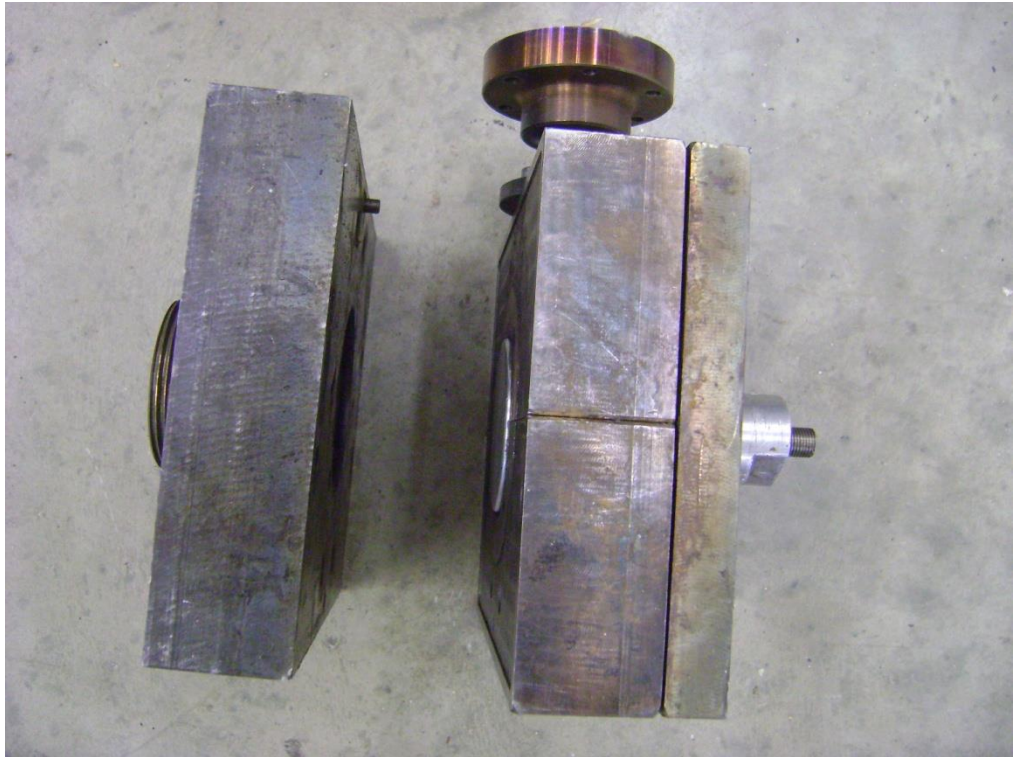
Figure A-5: Ultrasonic horn, the top block, the mid block and the bottom block.
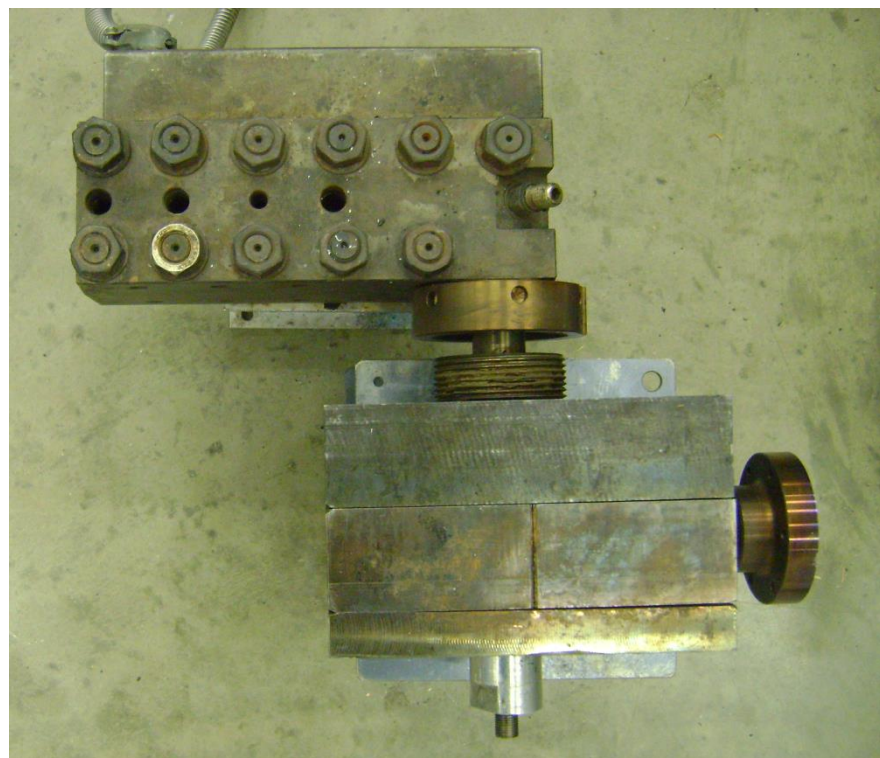
Figure A-6: Ultrasound housing block and the slit die.

Figure A-7: Ultrasonic horn, the transducer and the generator.

Appendix B

I.   Extrusion Results
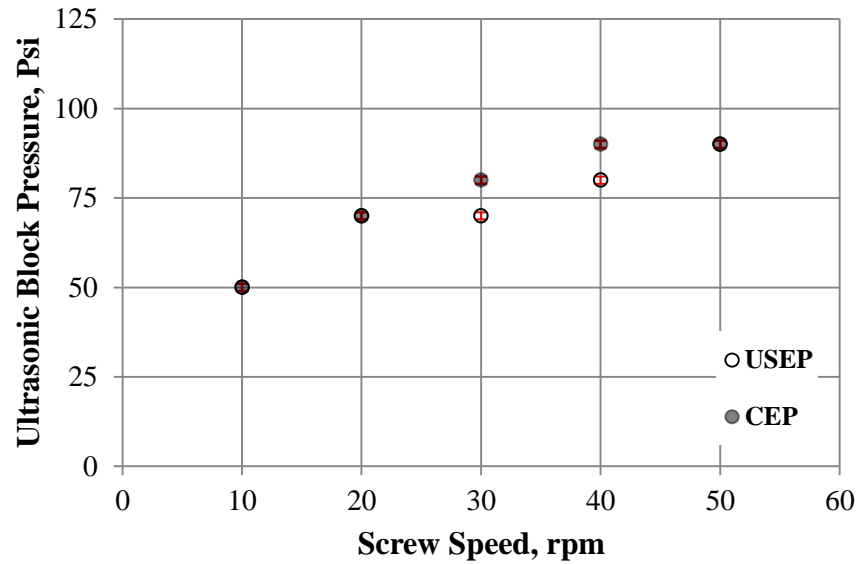
Figure B-1: Ultrasonic block pressure vs. Extruder screw speed for PE80 with out slit die.
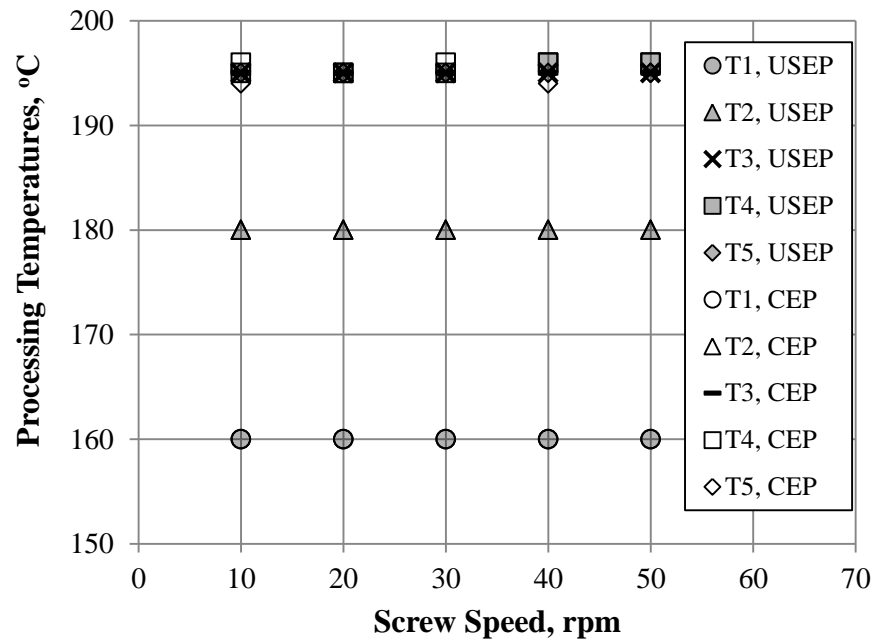
Figure B-2: Processing temperatures vs. Extruder screw speed for PE80 without slit die where T1-T3 are barrel temperatures and T4&T5 are ultrasonic block temperatures.
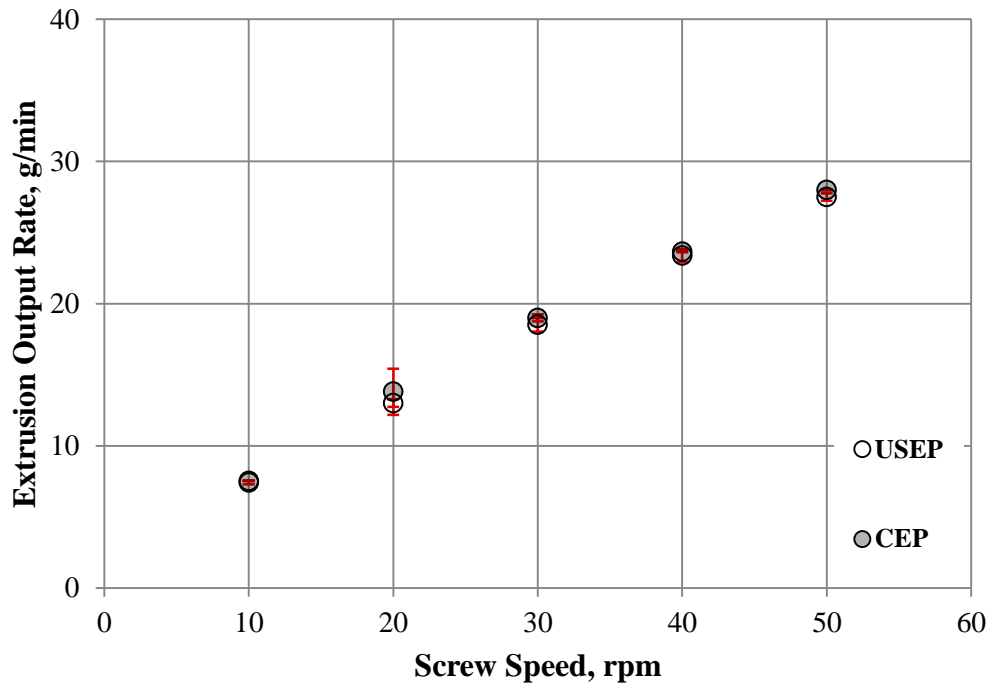
Figure B-3: Extrusion output rate vs. Extruder screw speed for PE80 without slit die.
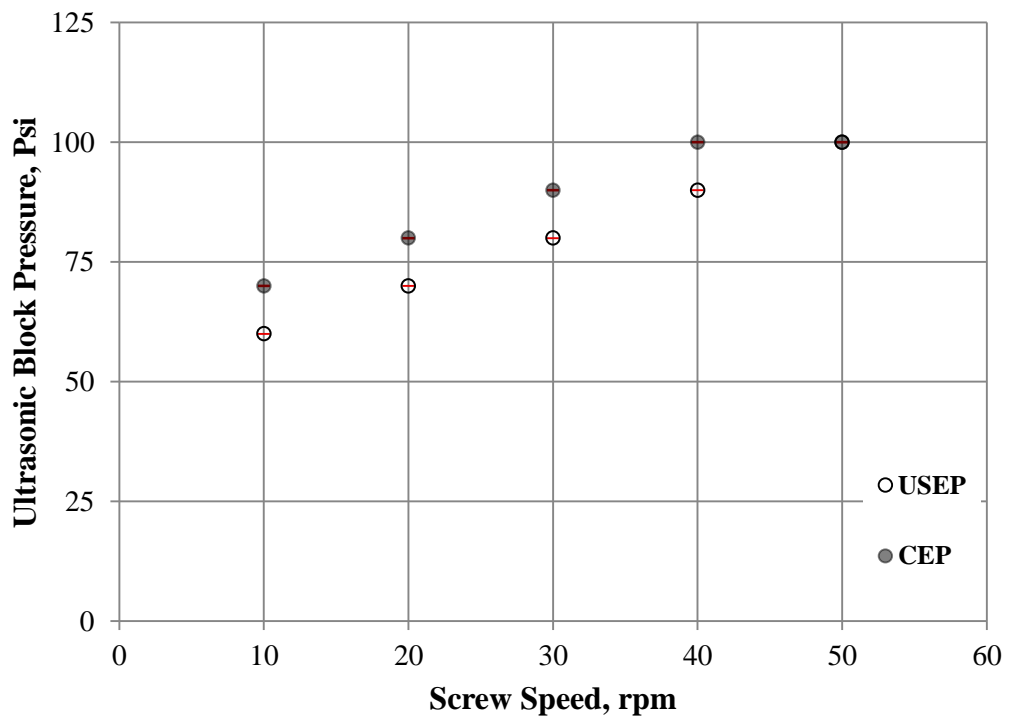
Figure B-4: Ultrasonic block pressure vs. Extruder screw speed for PE100 without slit die.
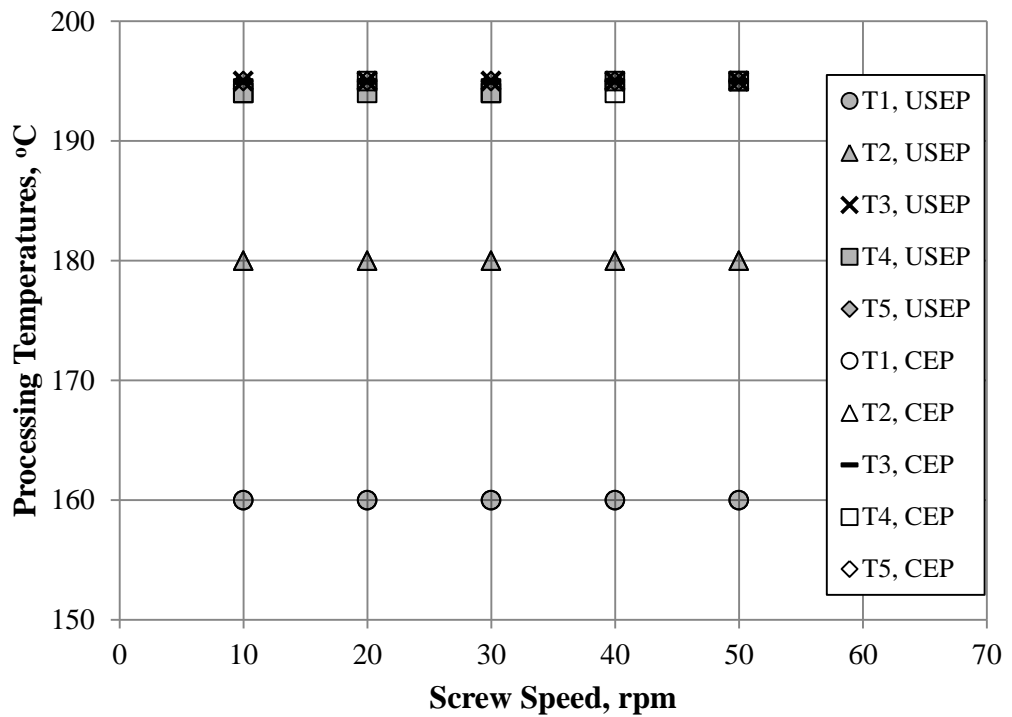
Figure B-5: Processing temperatures vs. Extruder screw speed for PE100 without slit die where T1-T3 are barrel temperatures and T4&T5 are ultrasonic block temperatures.
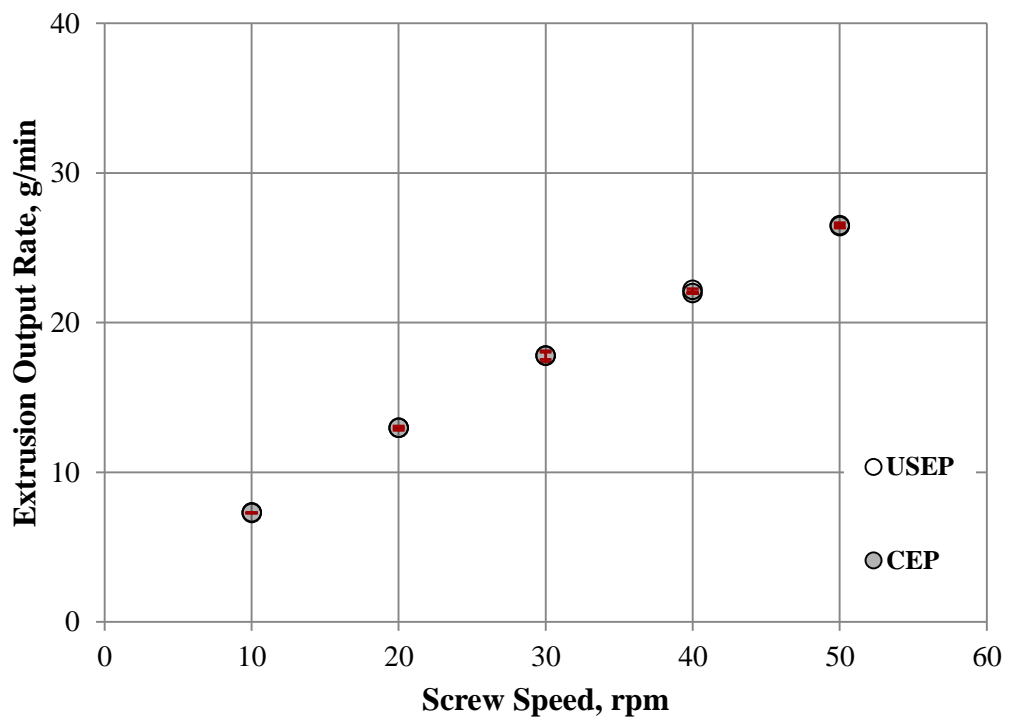
Figure B-6: Extrusion output rate vs. Extruder screw speed for PE100 without slit die.

II.   Tensile Results
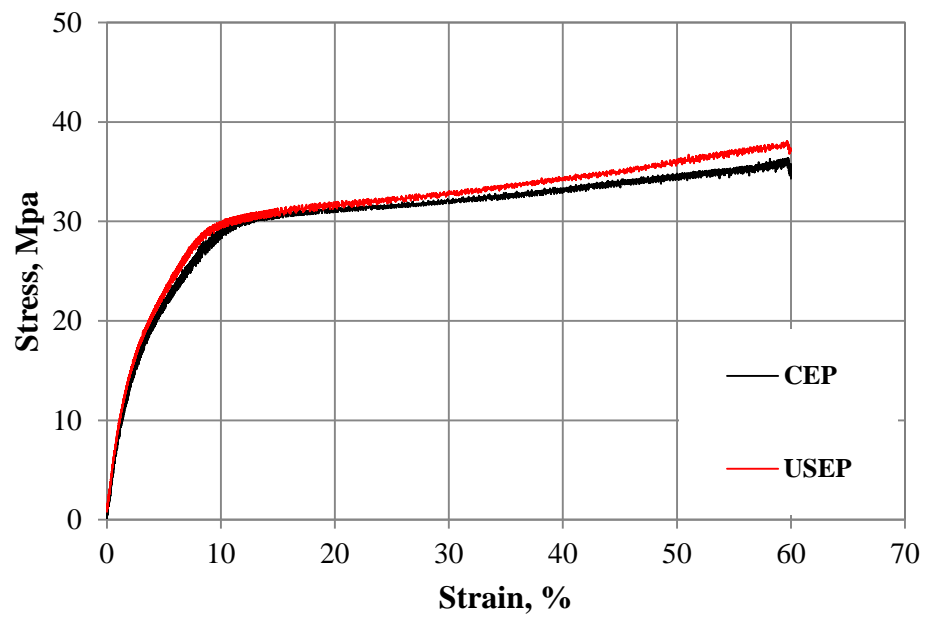
Figure B-7: Stress vs. Strain for PE80 strips produced at 20rpm with and without presence of ultrasonic vibrations.
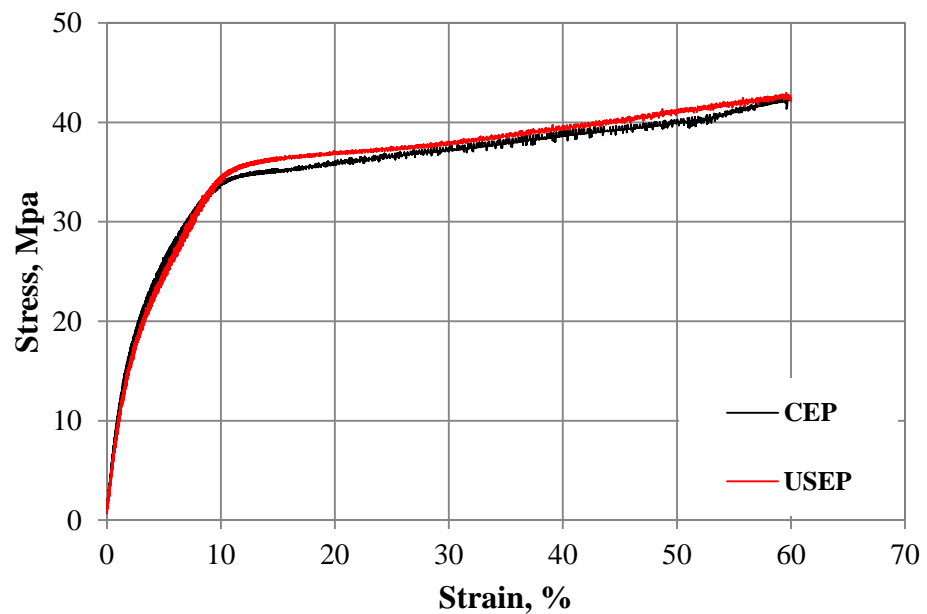
Figure B-8: Stress vs. Strain for PE80 strips produced at 30rpm with and without presence of ultrasonic vibrations.

218
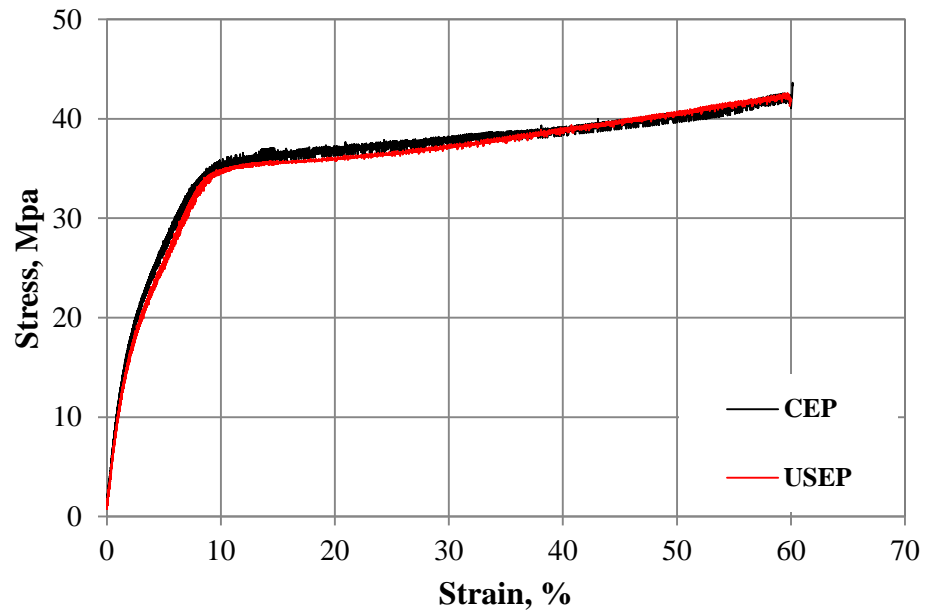
Figure B-9: Stress vs. Strain for PE80 strips produced at 40rpm with and without presence of ultrasonic vibrations.
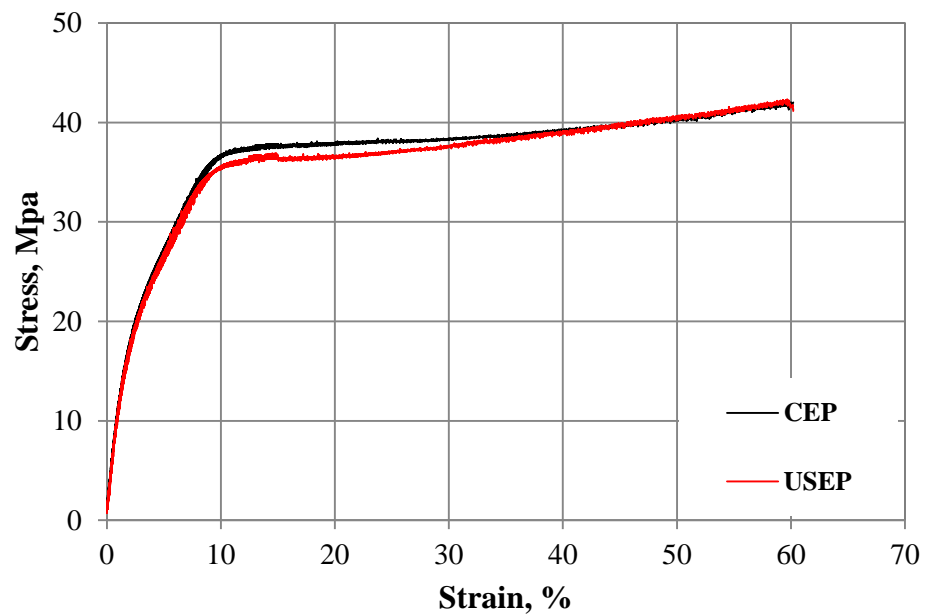
Figure B-10: Stress vs. Strain for PE80 strips produced at 50rpm with and without presence of ultrasonic vibrations.
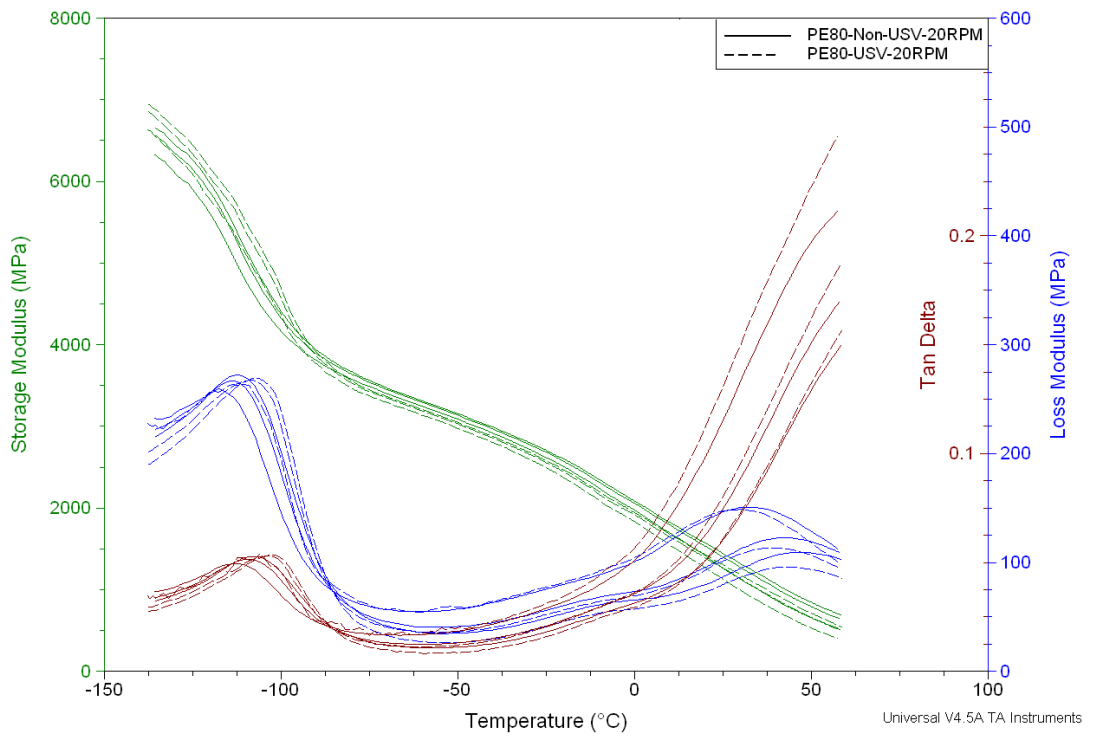
III.   DMA Results

Figure B-11: DMA Results of PE bars produced at 20rpm by both USEP and CEP methods.
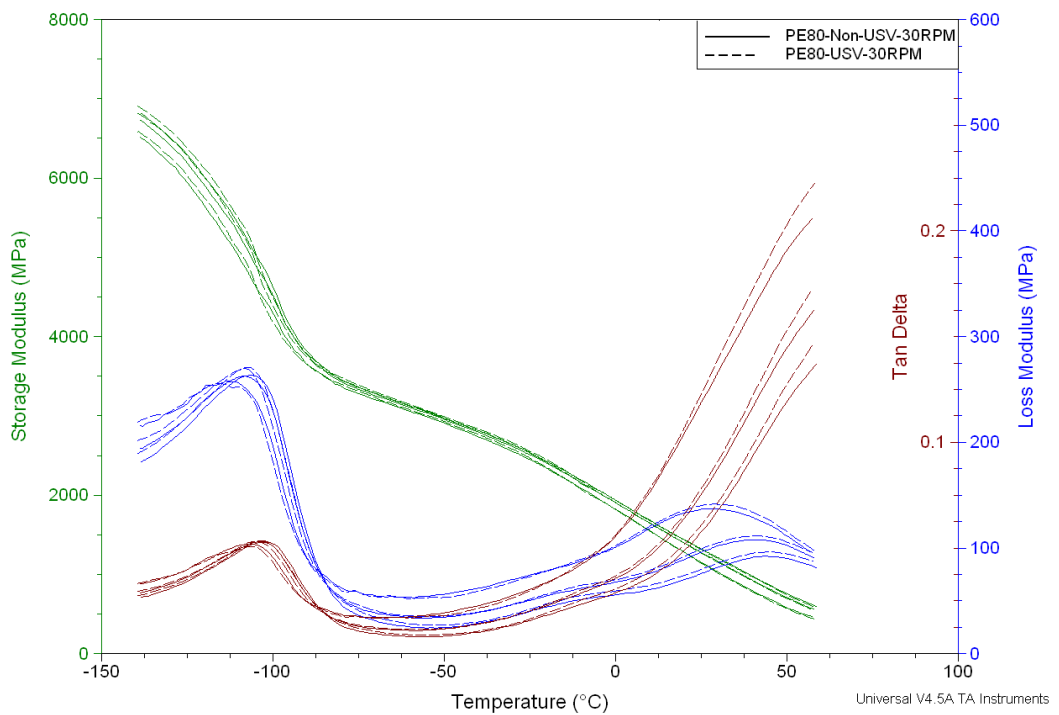
Figure B-12: DMA Results of PE bars produced at 30rpm by both USEP and CEP methods.
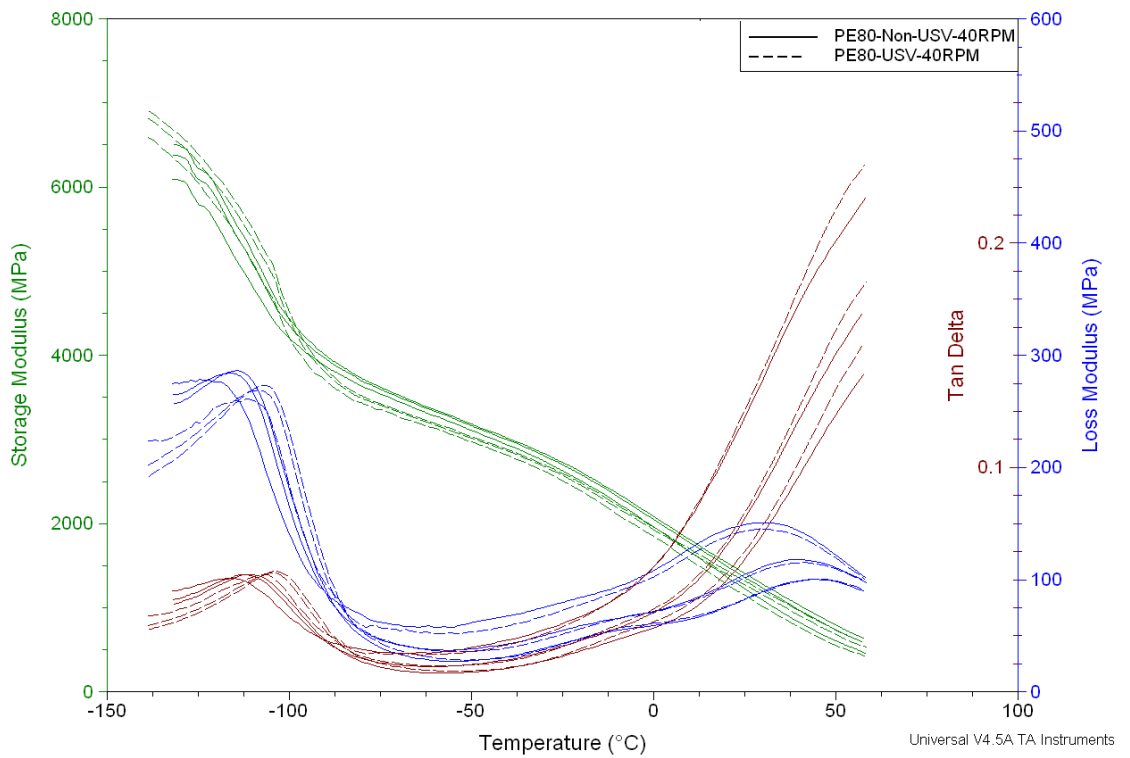
Figure B-13: DMA Results of PE bars produced at 40rpm by both USEP and CEP methods.
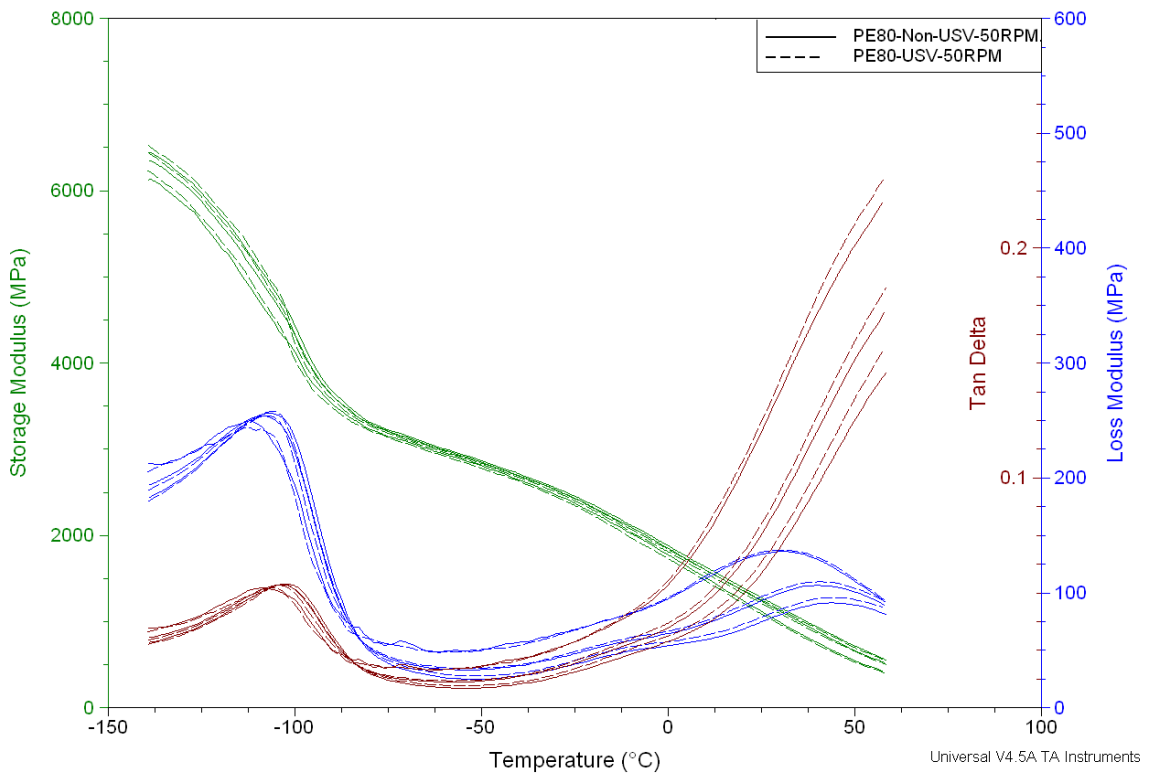
Figure B-14: DMA Results of PE bars produced at 50rpm by both USEP and CEP methods.

IV.   DSC Results
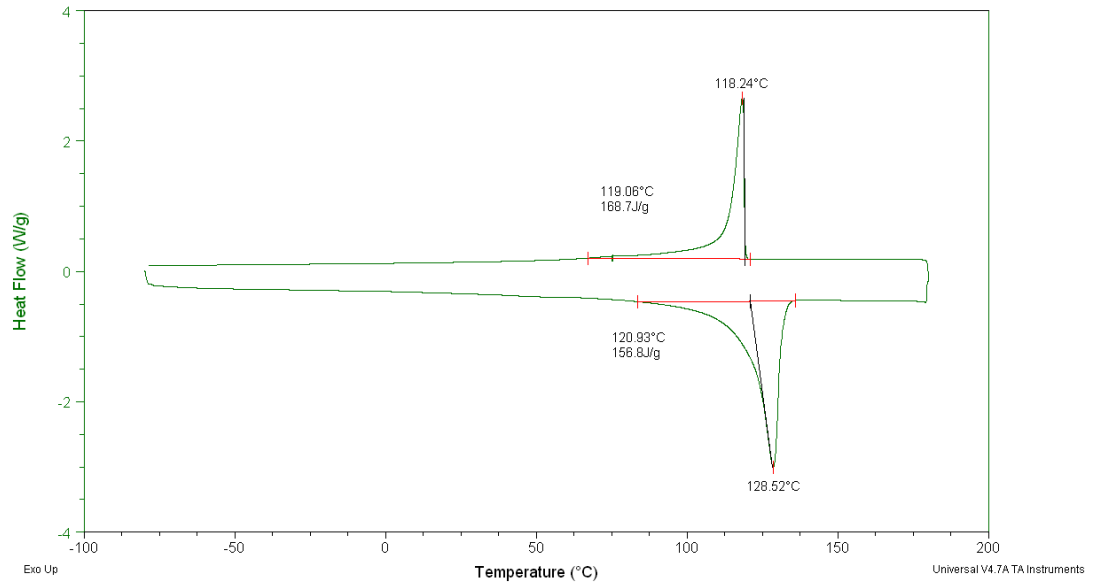
Figure B-15: DSC curve of PE80 strips produced at 10rpm with out presence of ultrasound.
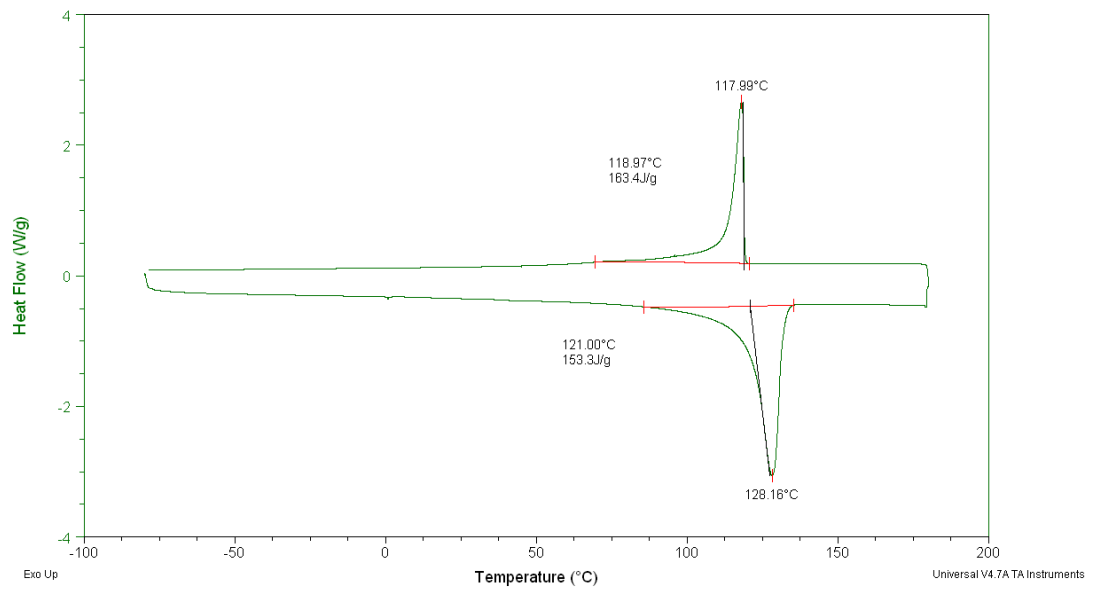
Figure B-16: DSC curve of PE80 strips produced at 20rpm with out presence of ultrasound.
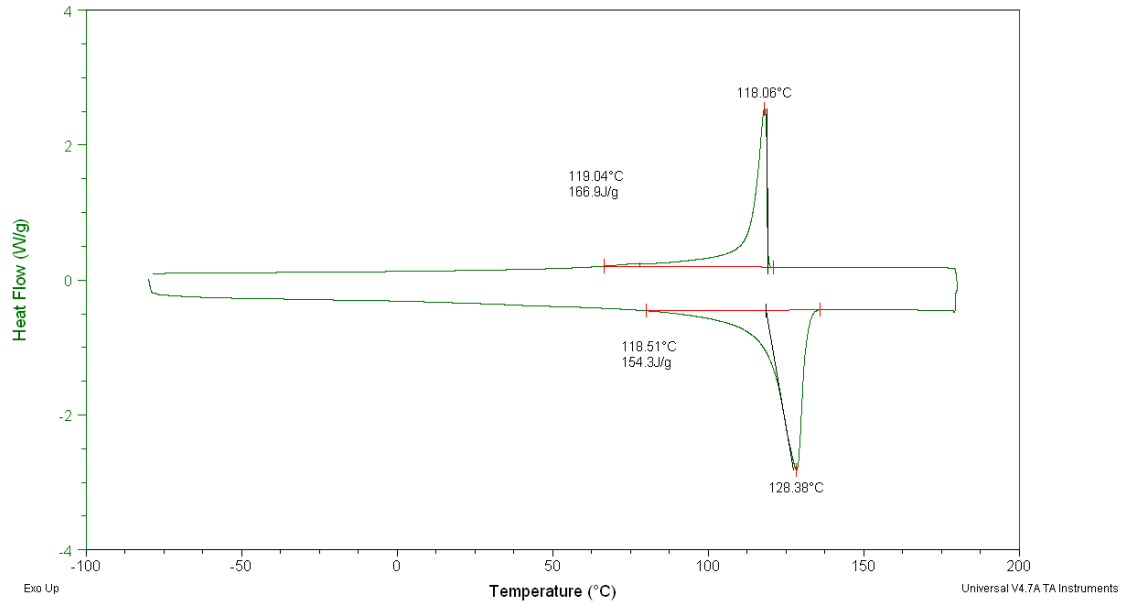
Figure B-17: DSC curve of PE80 strips produced at 30rpm with out presence of ultrasound.
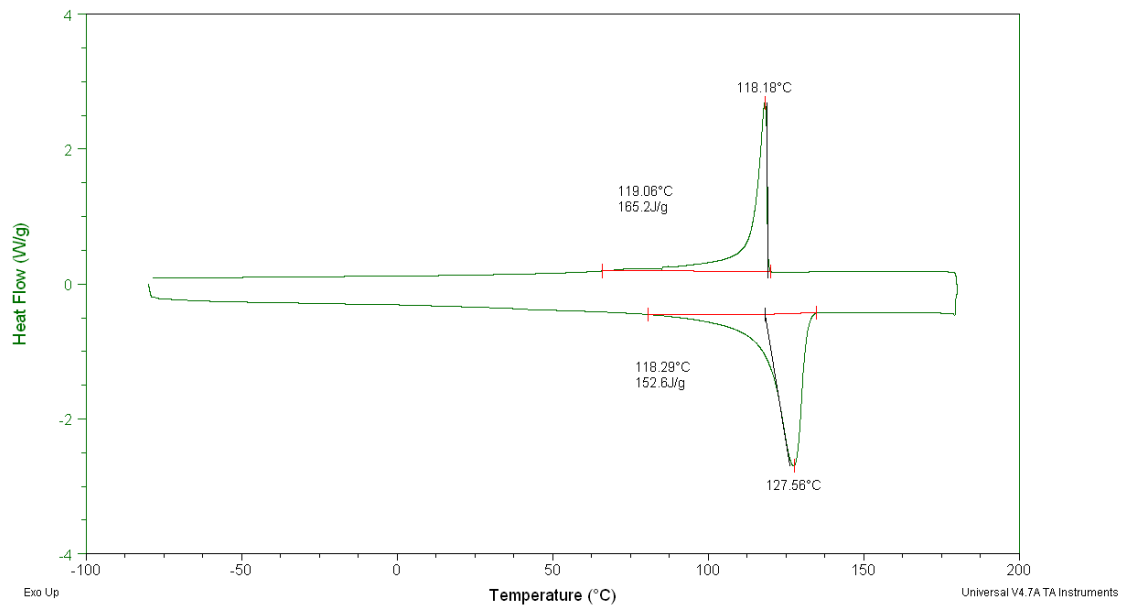
Figure B-18: DSC curve of PE80 strips produced at 40rpm with out presence of ultrasound.
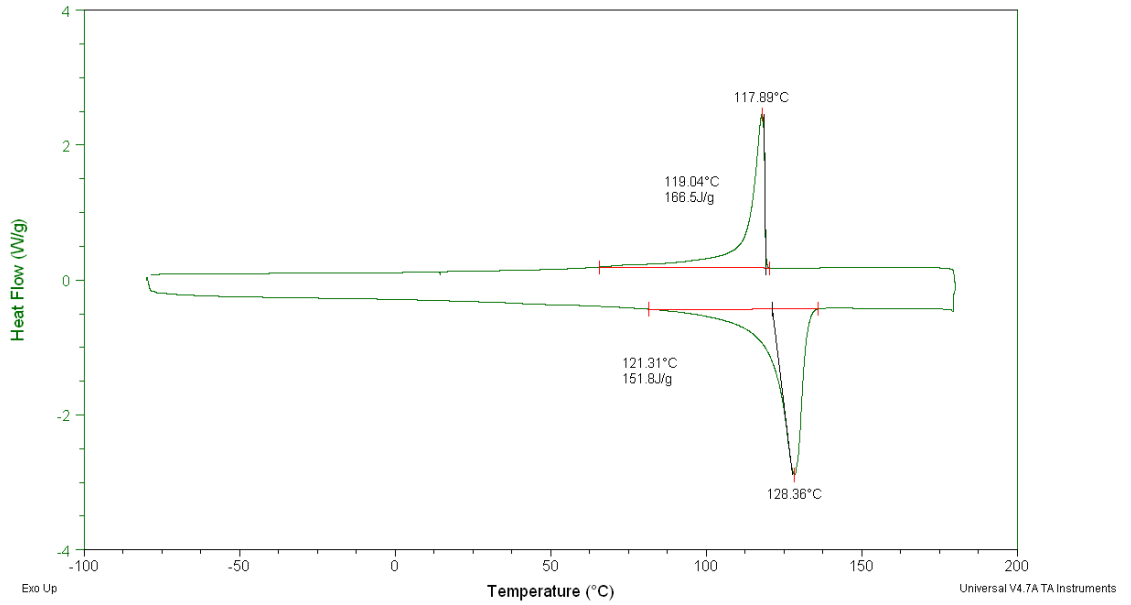
Figure B-19: DSC curve of PE80 strips produced at 50rpm with out presence of ultrasound.
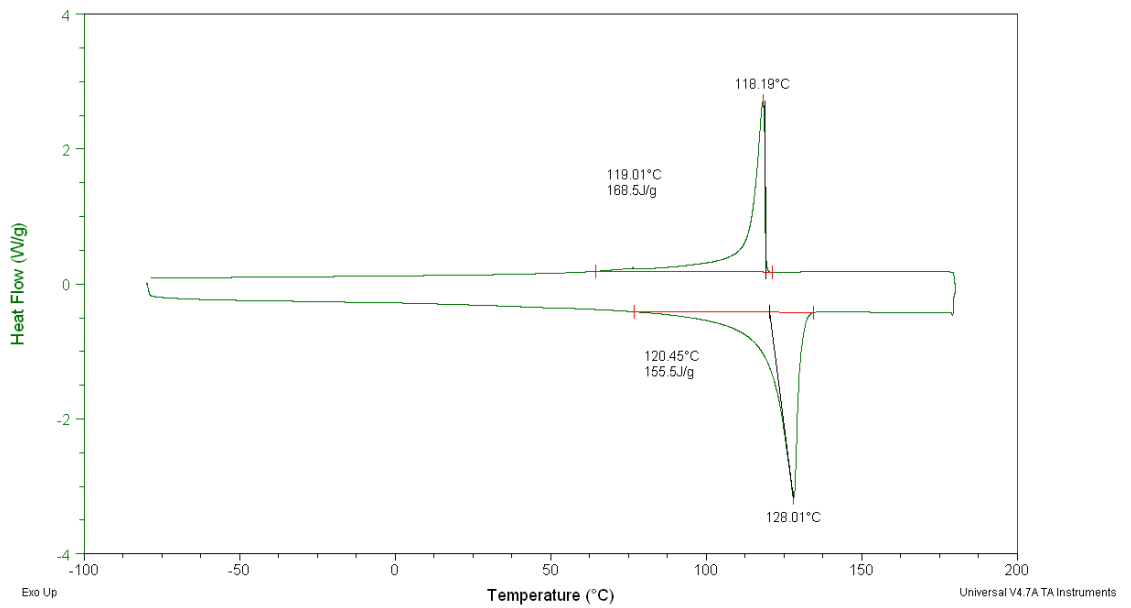
Figure B-20: DSC curve of PE80 strips produced at 10rpm with presence of ultrasound.
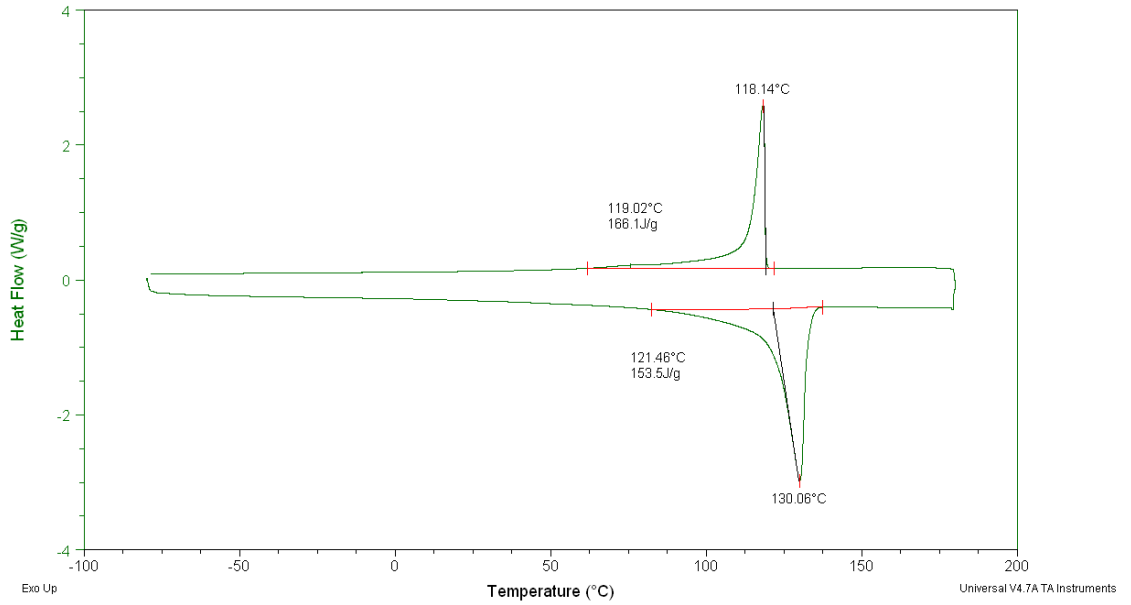
Figure B-21: DSC curve of PE80 strips produced at 20rpm with presence of ultrasound.
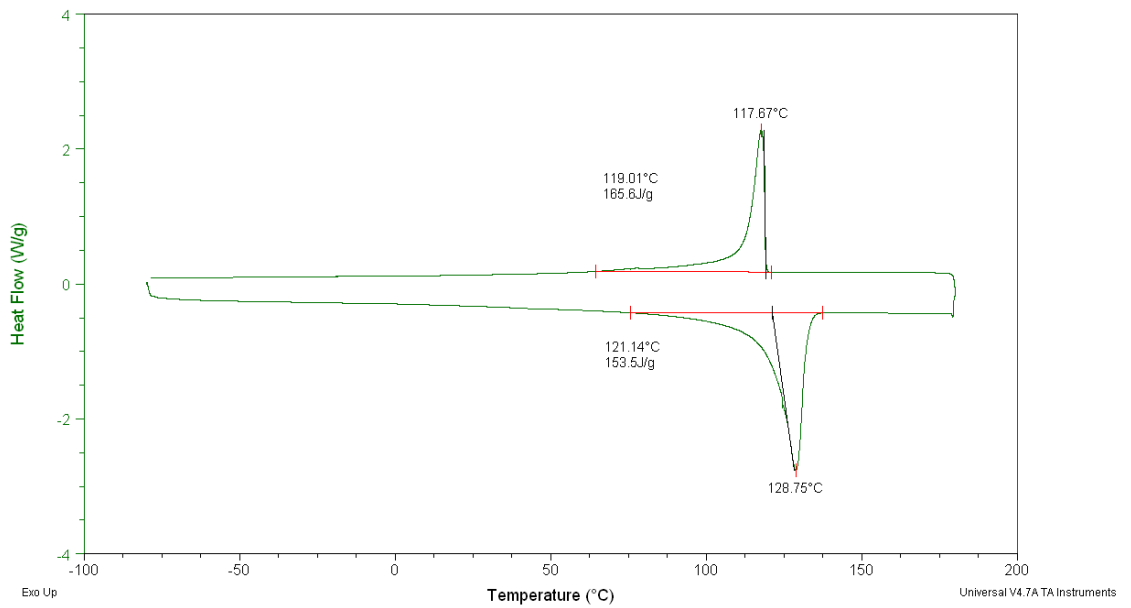
Figure B-22: DSC curve of PE80 strips produced at 30rpm with presence of ultrasound.
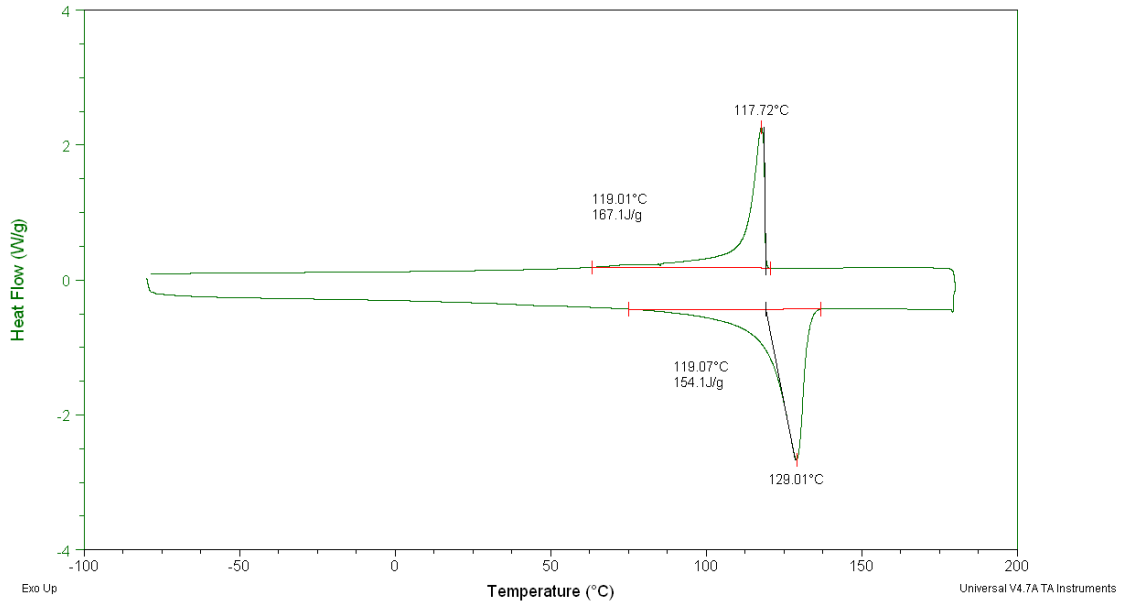
Figure B-23: DSC curve of PE80 strips produced at 40rpm with presence of ultrasound.
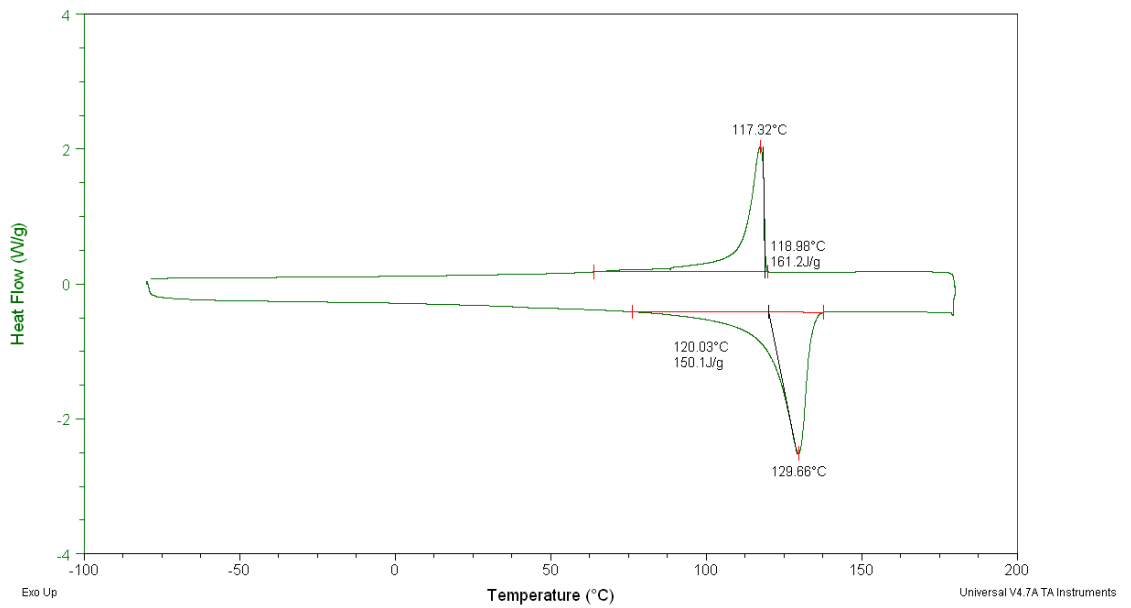
Figure B-24: DSC curve of PE80 strips produced at 50rpm with presence of ultrasound.

V. Capillary Rheology Results
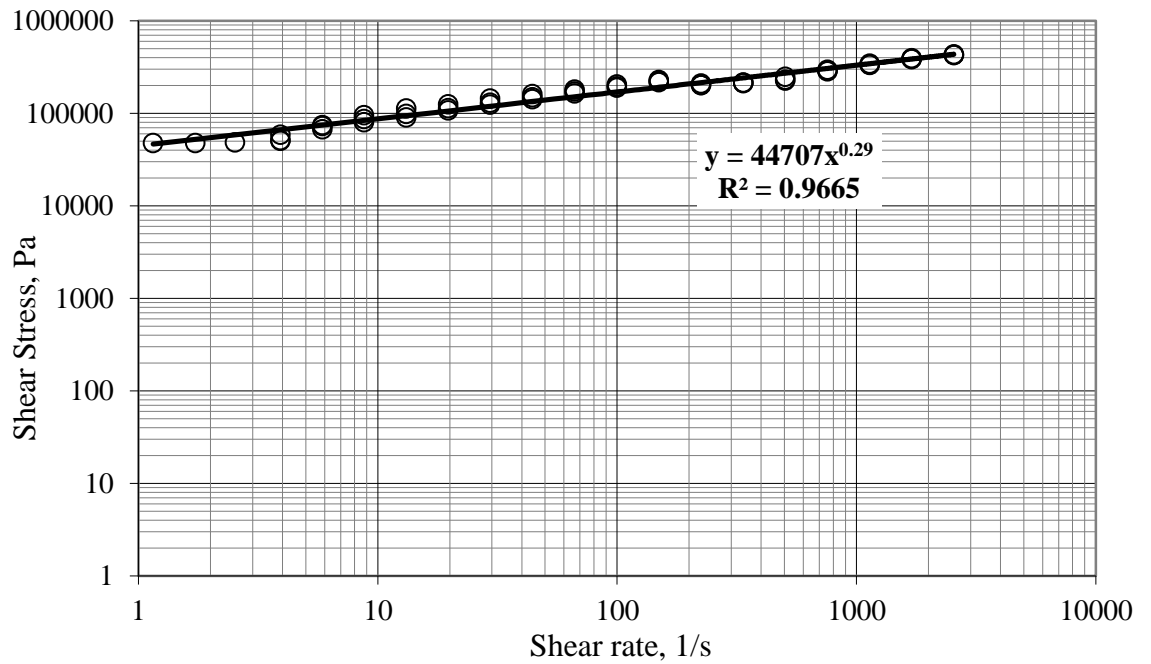
Figure B-25: Shear Stress vs. Shear Rate for PE80 Granules at 170°C.
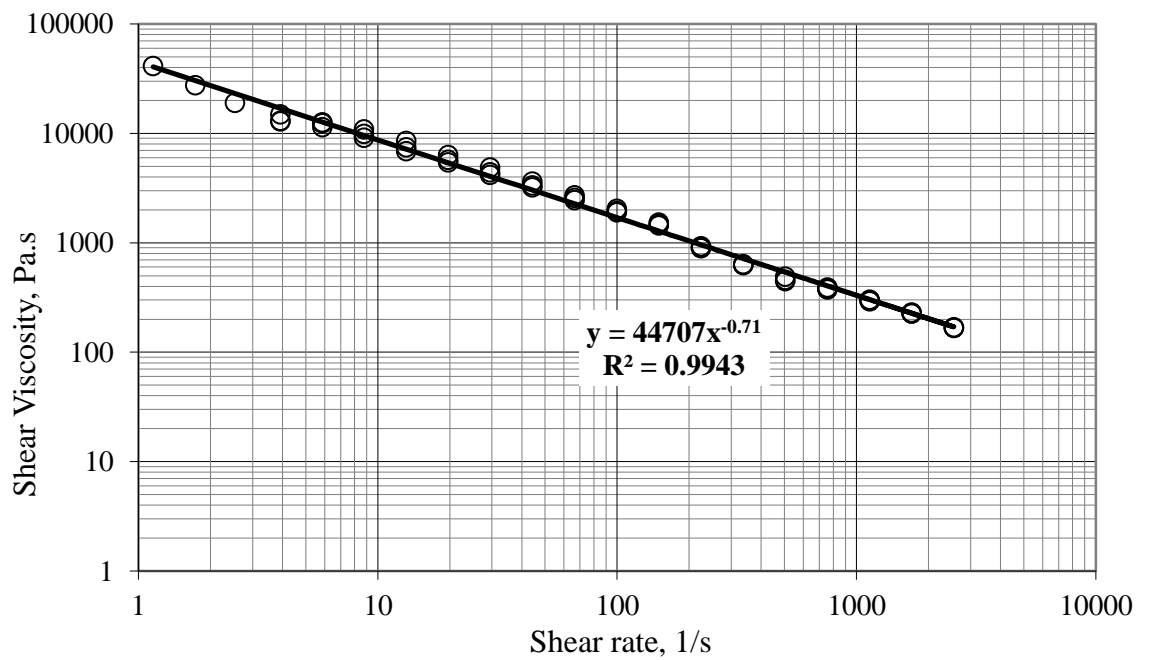
Figure B-26: Shear Viscosity vs. Shear Rate for PE80 granules at 170°C.
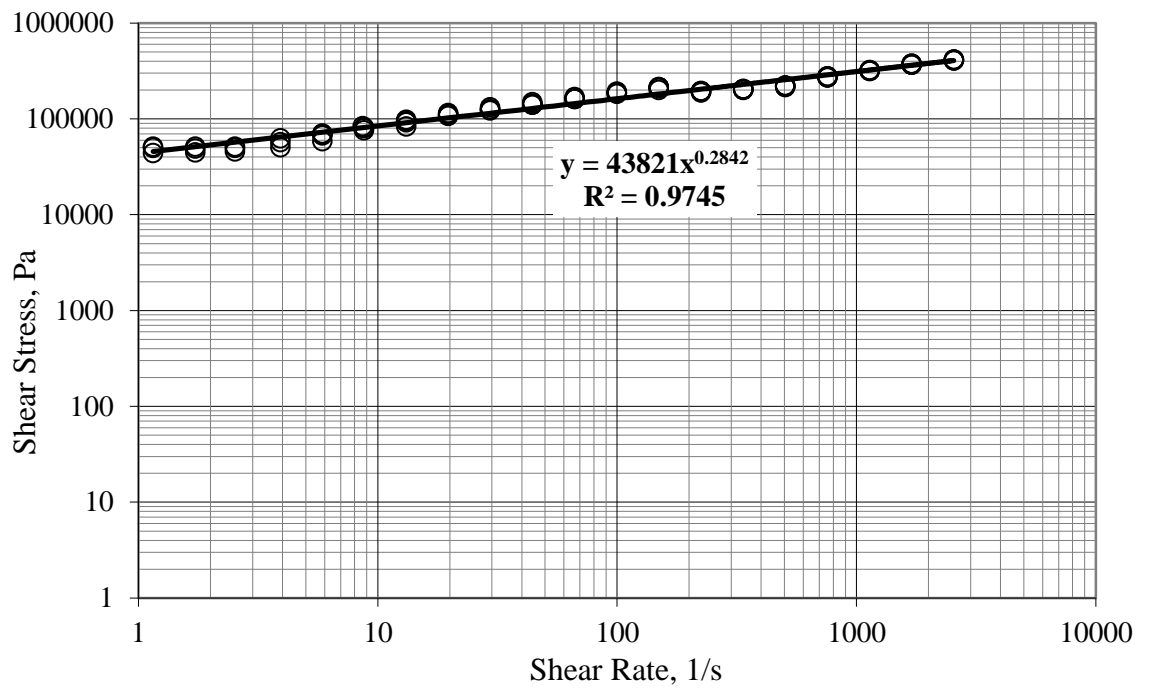
Figure B-27: Shear Stress vs. Shear Rate for PE80 Granules at 175°C.
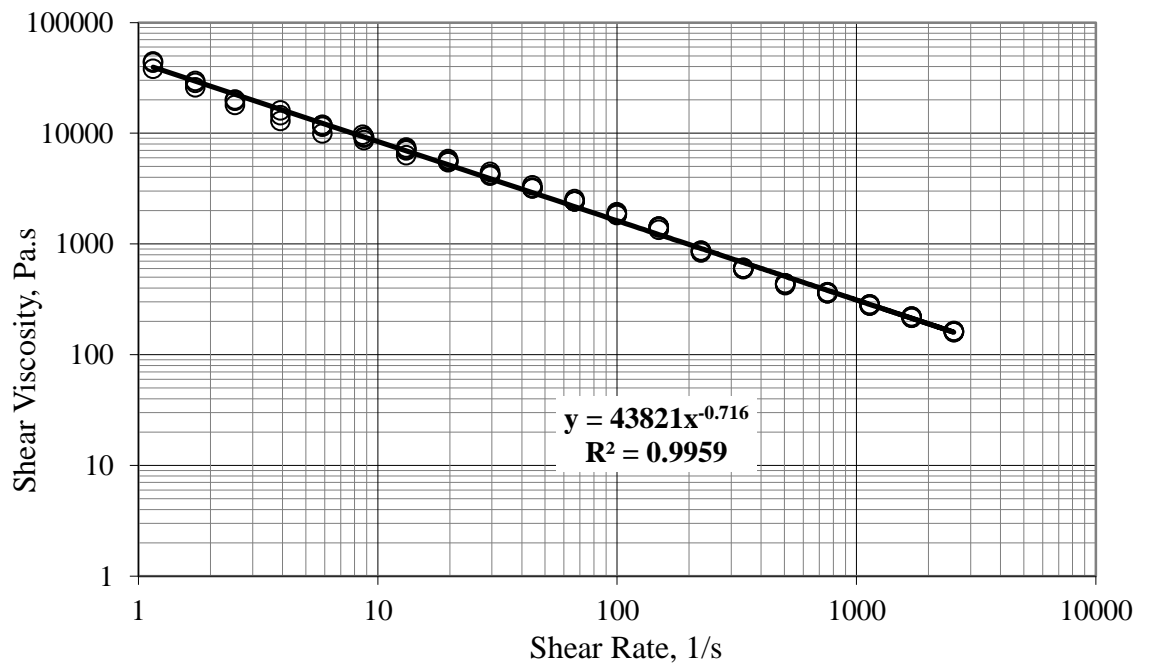
Figure B-28: Shear Viscosity vs. Shear Rate for PE80 granules at 175°C.
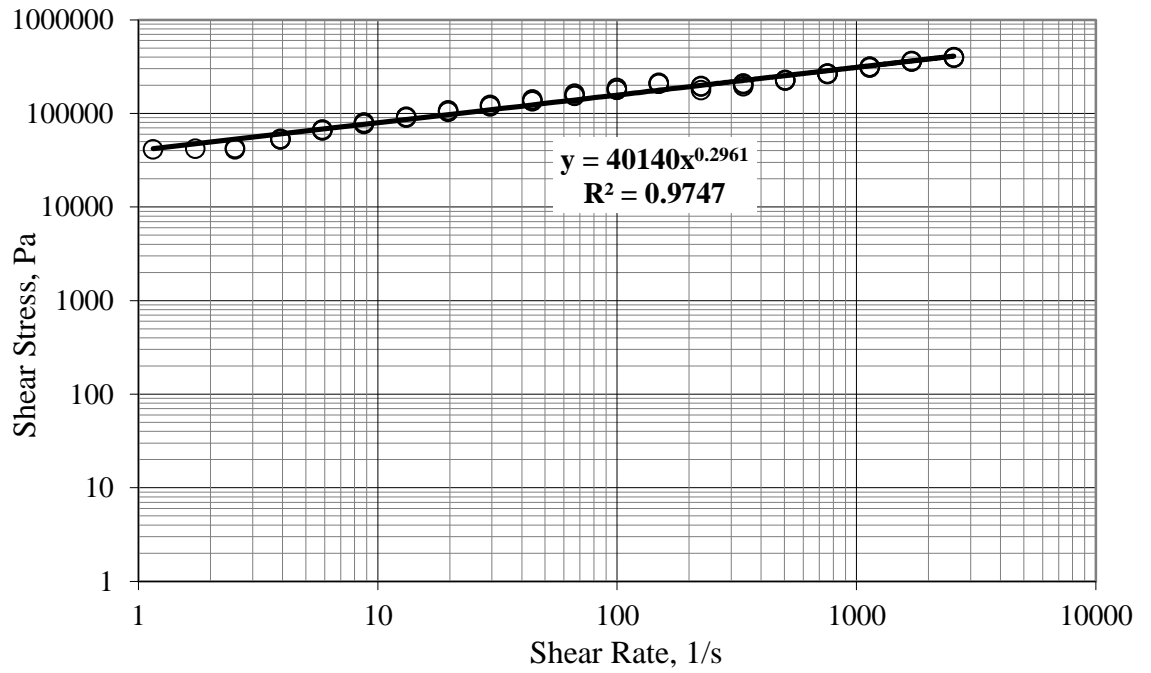
Figure B-29: Shear Stress vs. Shear Rate for PE80 Granules at 180°C.

$$y = 40140x^{0.2961}$$
$$R^2 = 0.9747$$
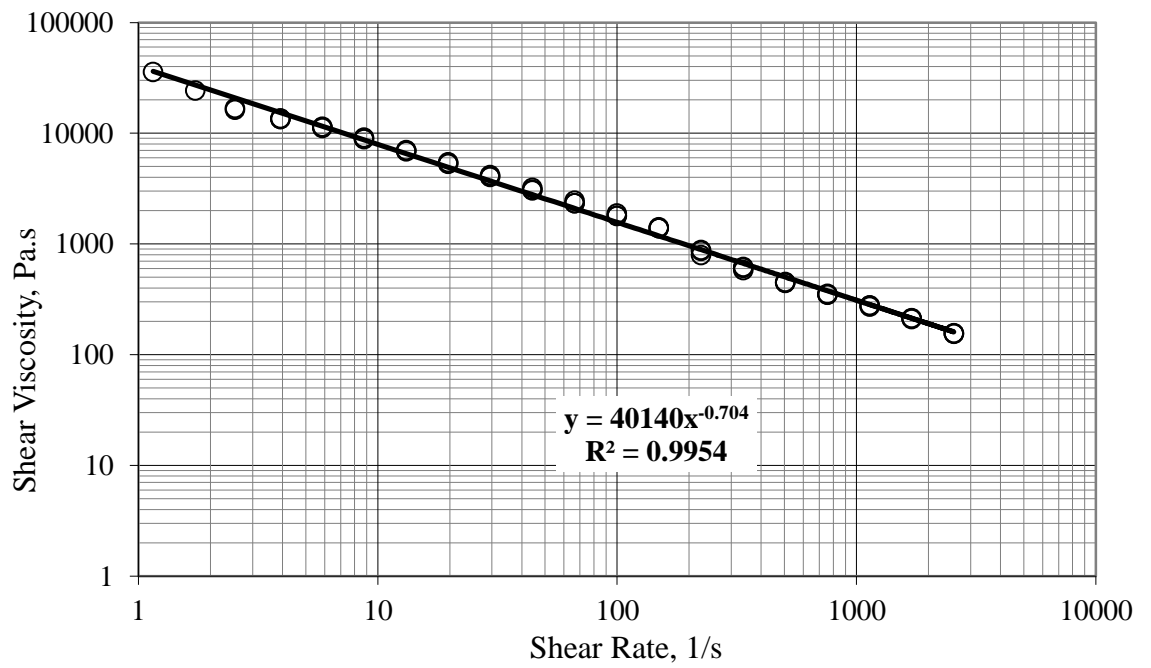
Figure B-30: Shear Viscosity vs. Shear Rate for PE80 granules at 180°C.

$$y = 40140x^{-0.704}$$
$$R^2 = 0.9954$$
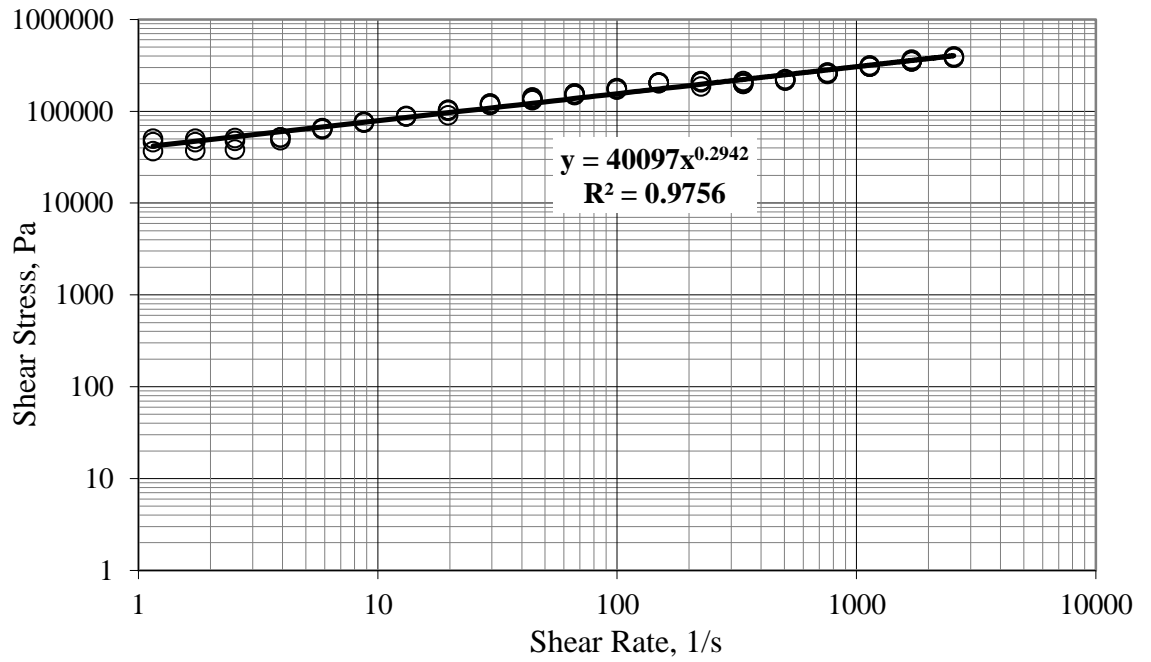
Figure B-31: Shear Stress vs. Shear Rate for PE80 Granules at 185°C.
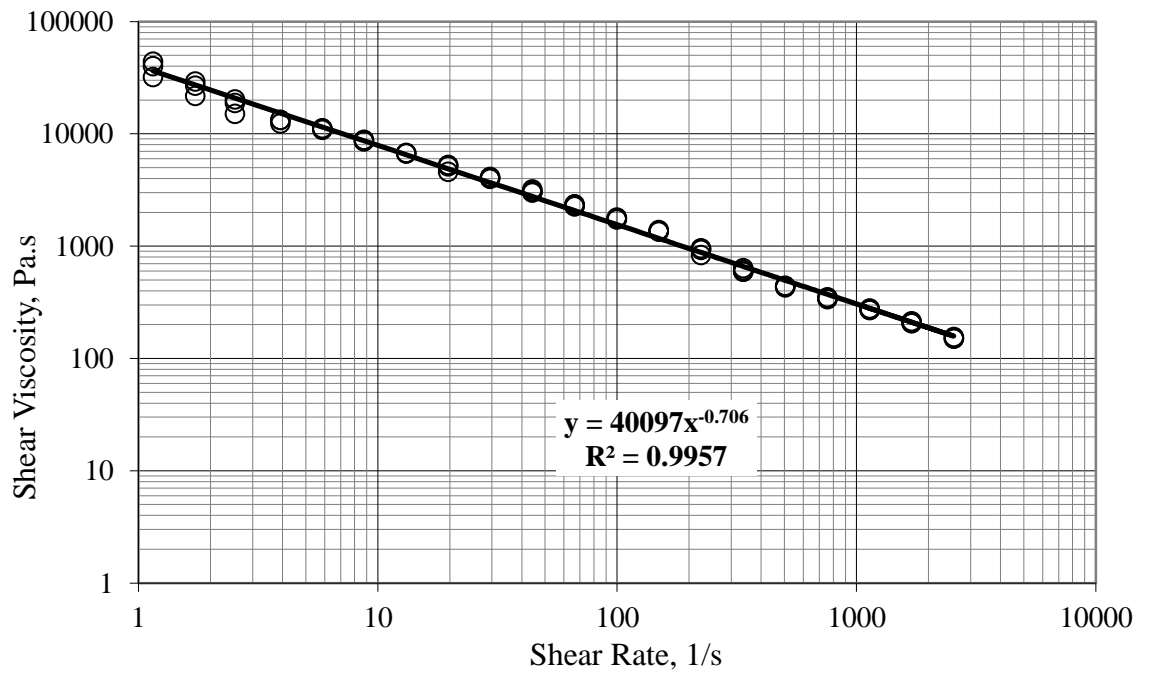
Figure B-32: Shear Viscosity vs. Shear Rate for PE80 granules at 185°C.
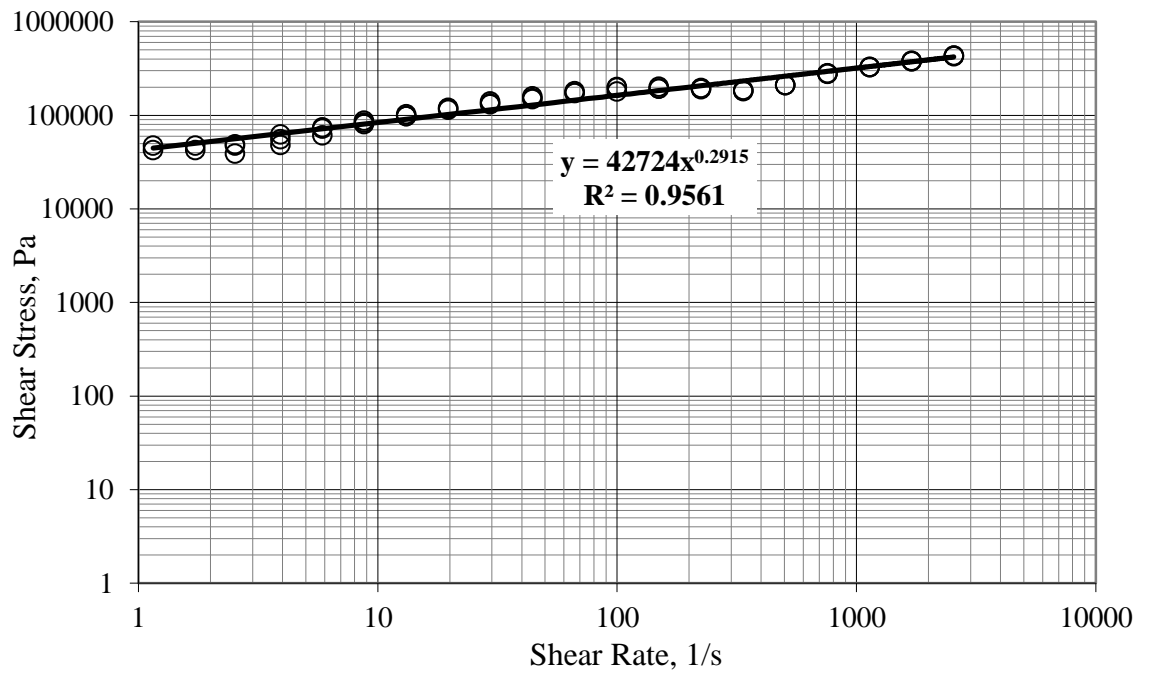
Figure B-33: Shear Stress vs. Shear Rate for PE100 Granules at 170°C.
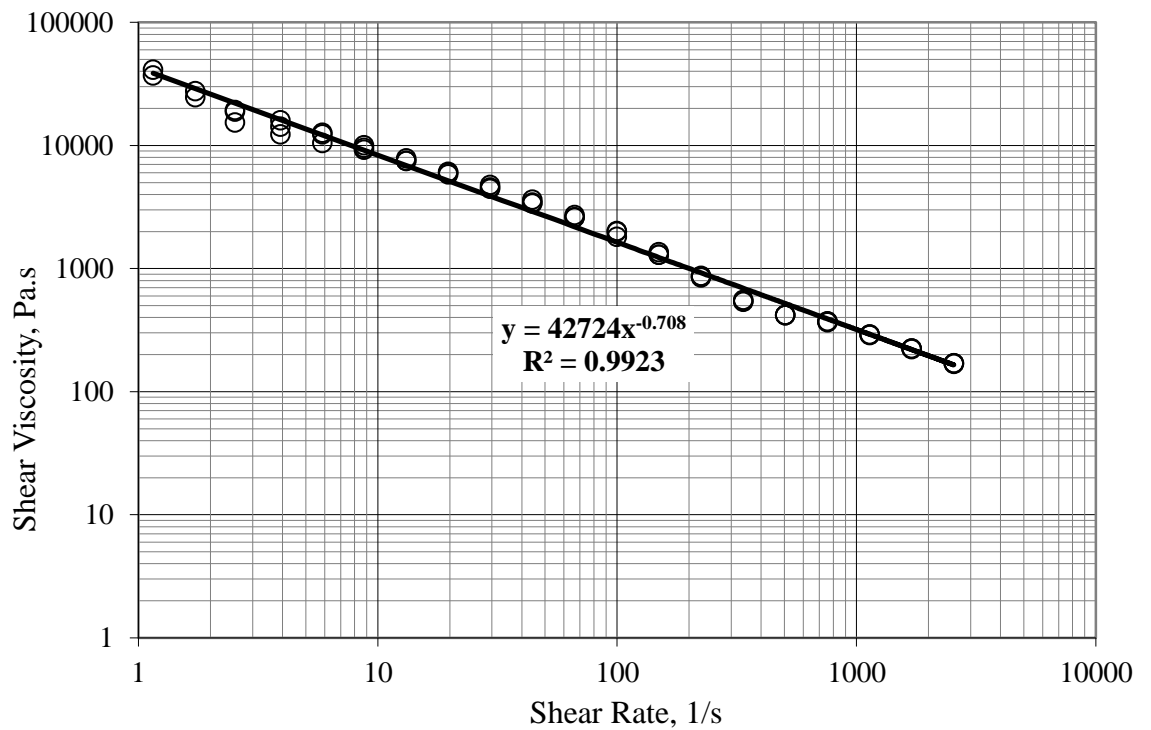
Figure B-34: Shear Viscosity vs. Shear Rate for PE100 granules at 170°C.
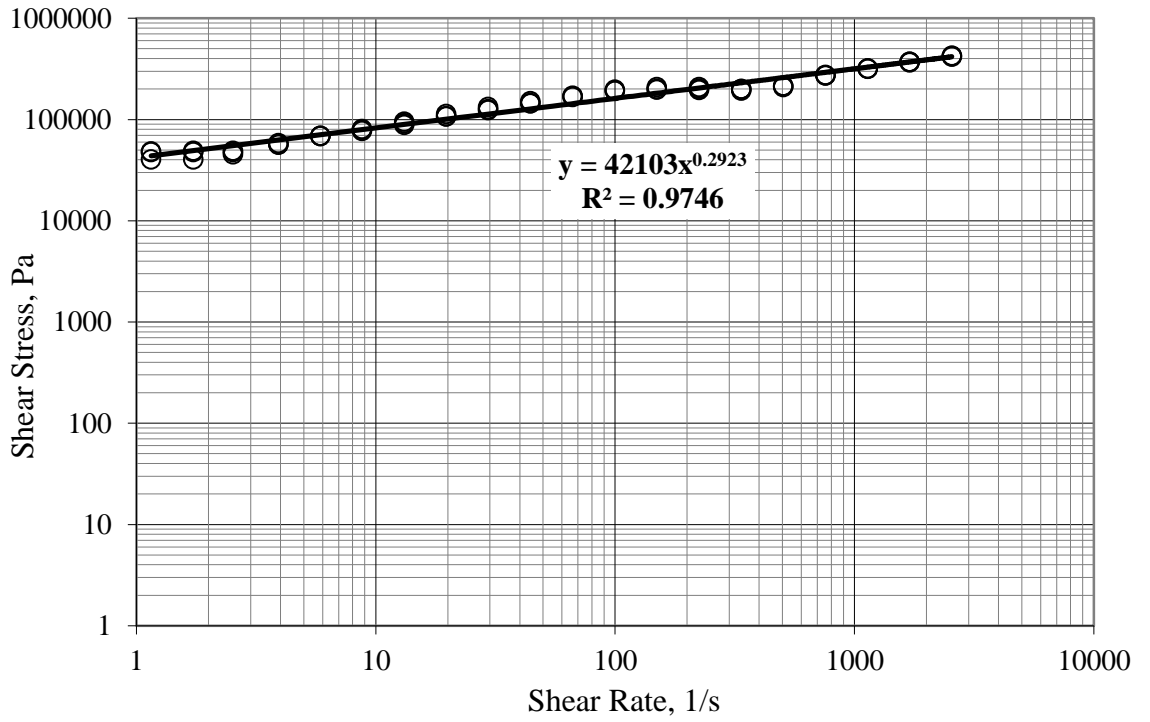
Figure B-35: Shear Stress vs. Shear Rate for PE100 Granules at 175°C.
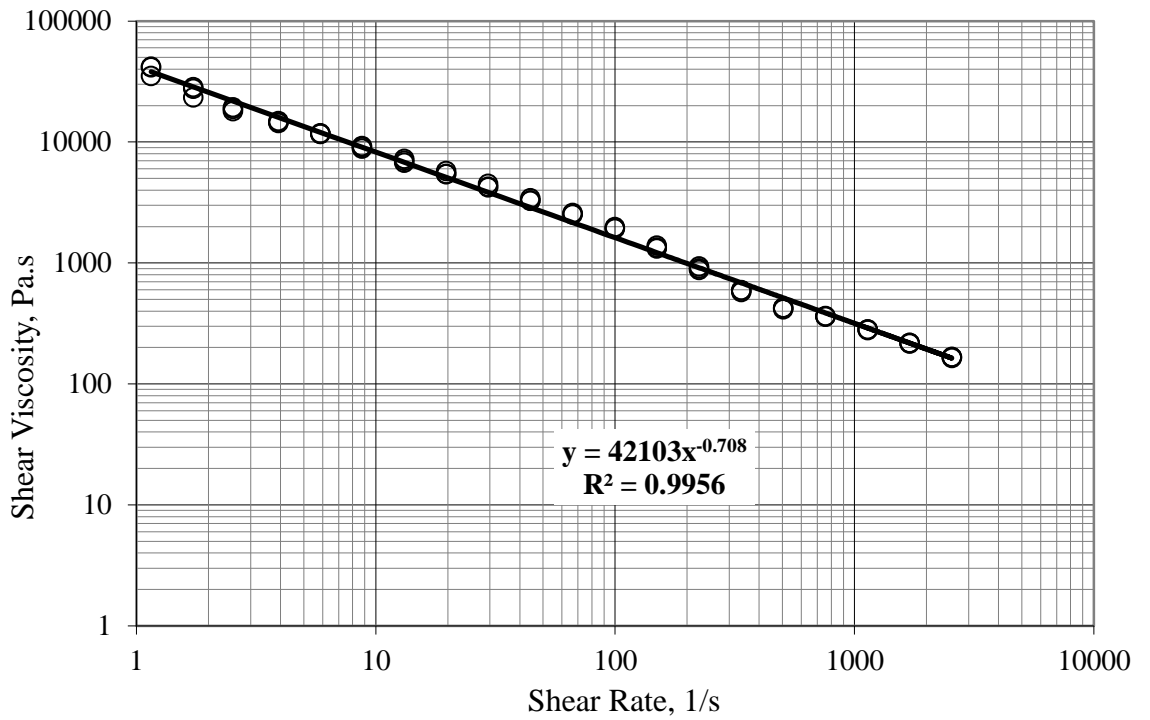
Figure B-36: Shear Viscosity vs. Shear Rate for PE100 granules at 175°C.
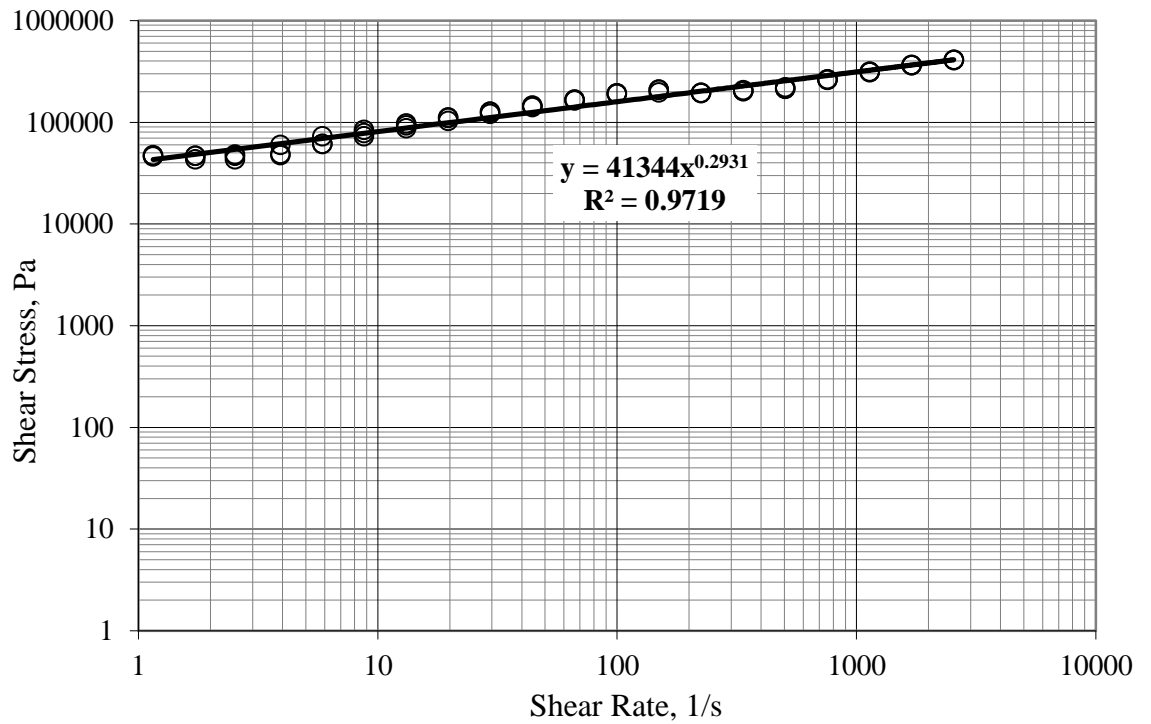
Figure B-37: Shear Stress vs. Shear Rate for PE100 Granules at 180°C.
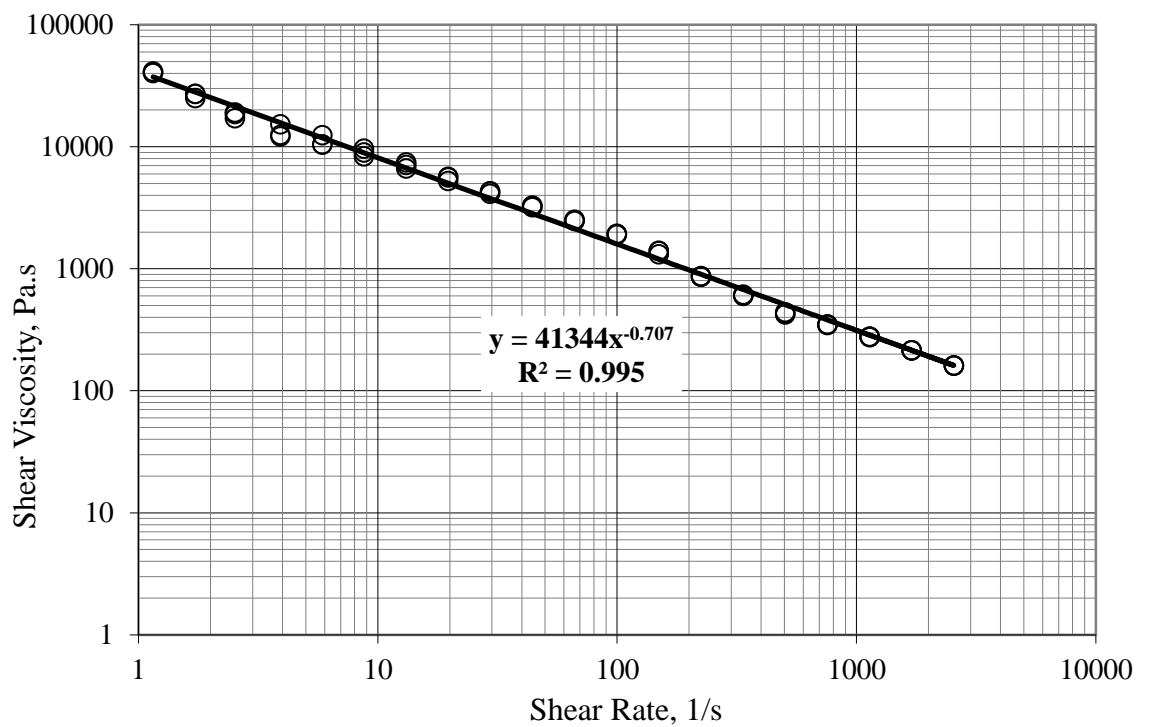
Figure B-38: Shear Viscosity vs. Shear Rate for PE100 granules at 180°C.

$$y = 40752x^{0.3012}$$
$$R^2 = 0.9394$$
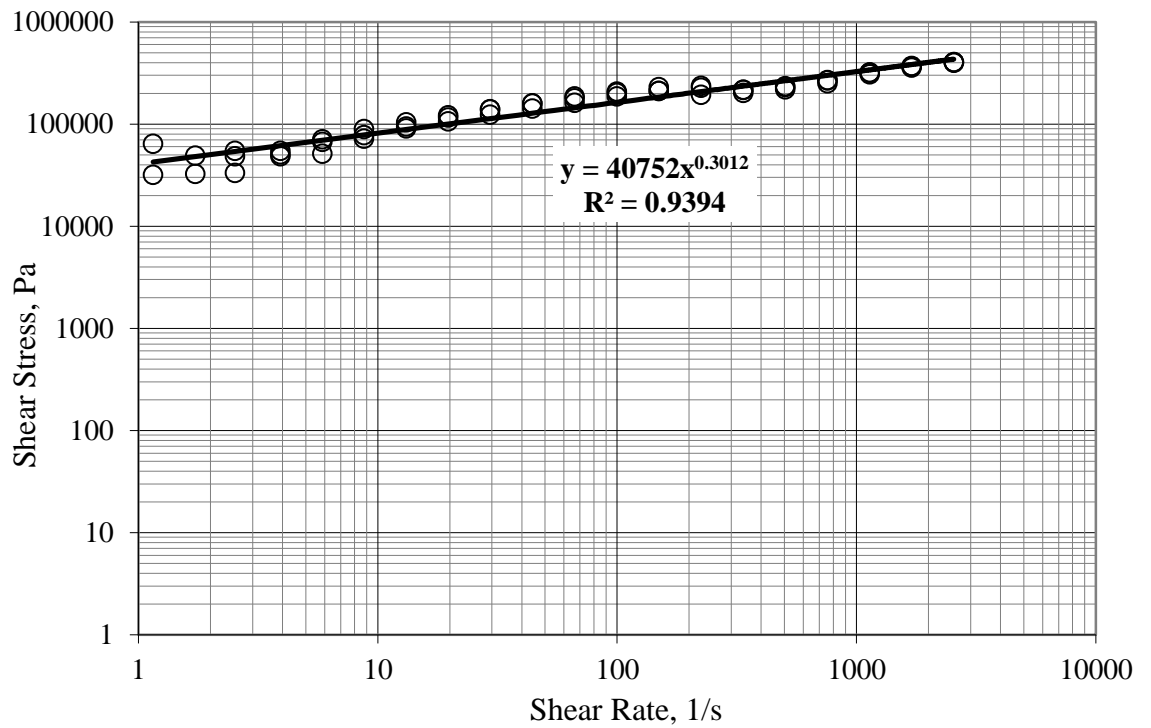
Figure B-39: Shear Stress vs. Shear Rate for PE100 Granules at 185°C.

$$y = 40752x^{-0.699}$$
$$R^2 = 0.9882$$
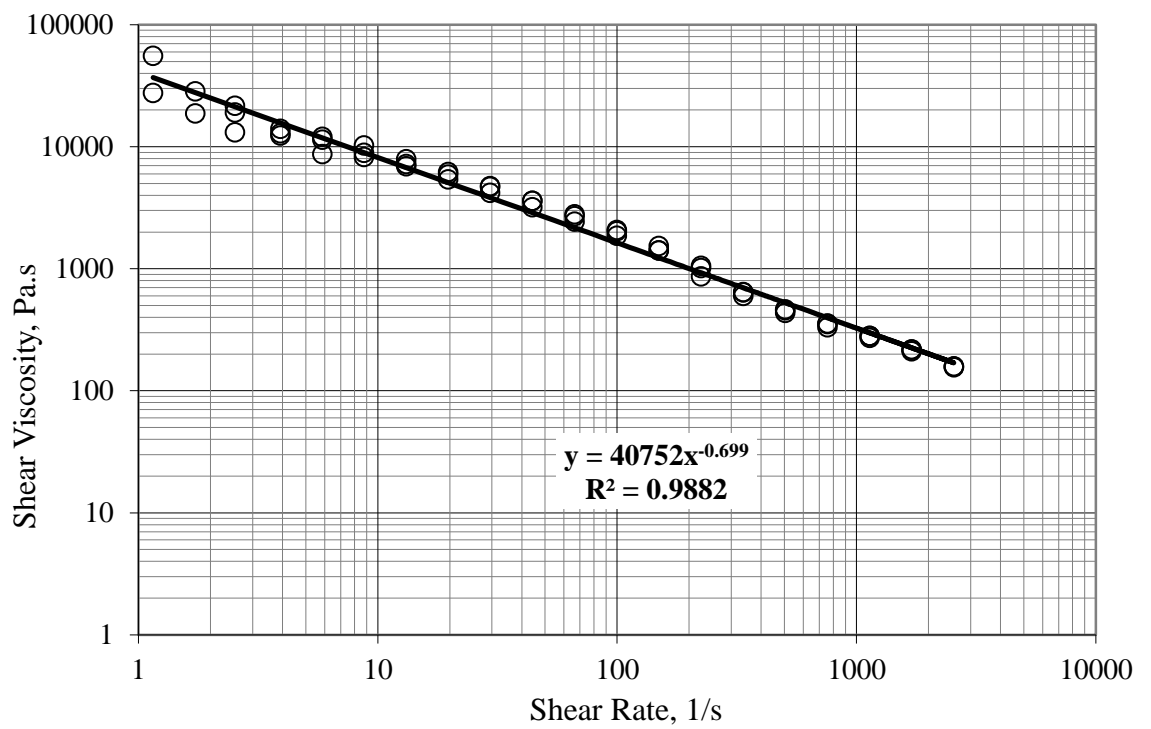
Figure B-40: Shear Viscosity vs. Shear Rate for PE100 granules at 185°C.

234
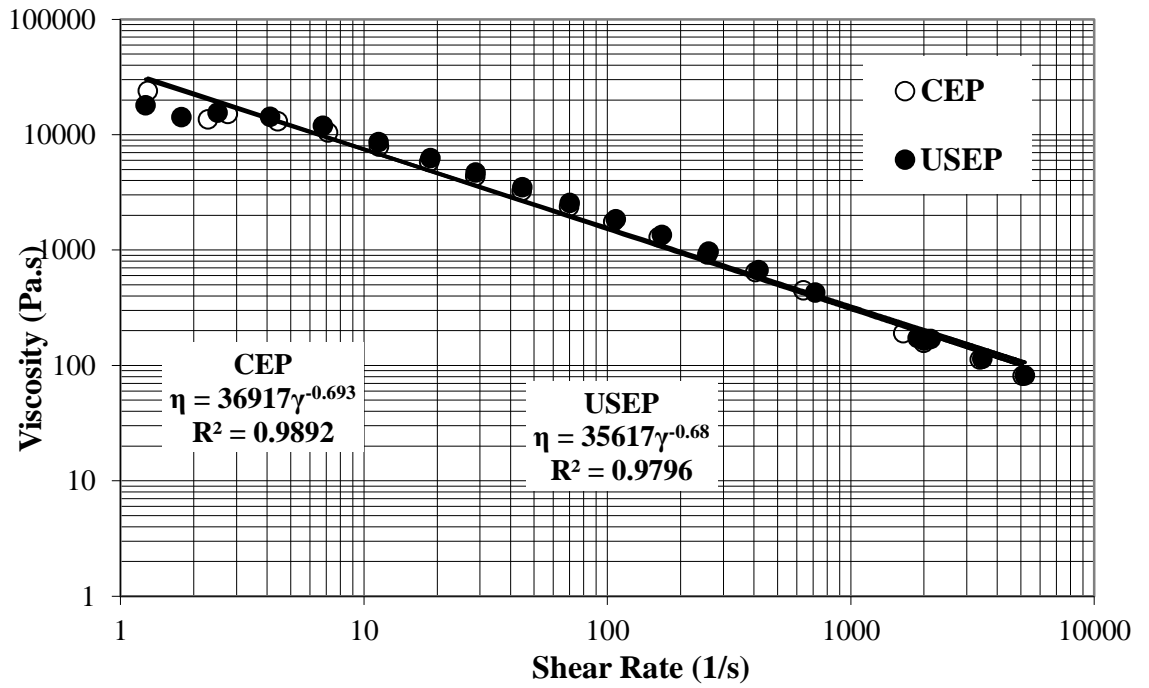
Figure B-41: Shear viscosity vs. shear rate for PE80 strips produced at 20 rpm with and without presence of ultrasonic vibrations.
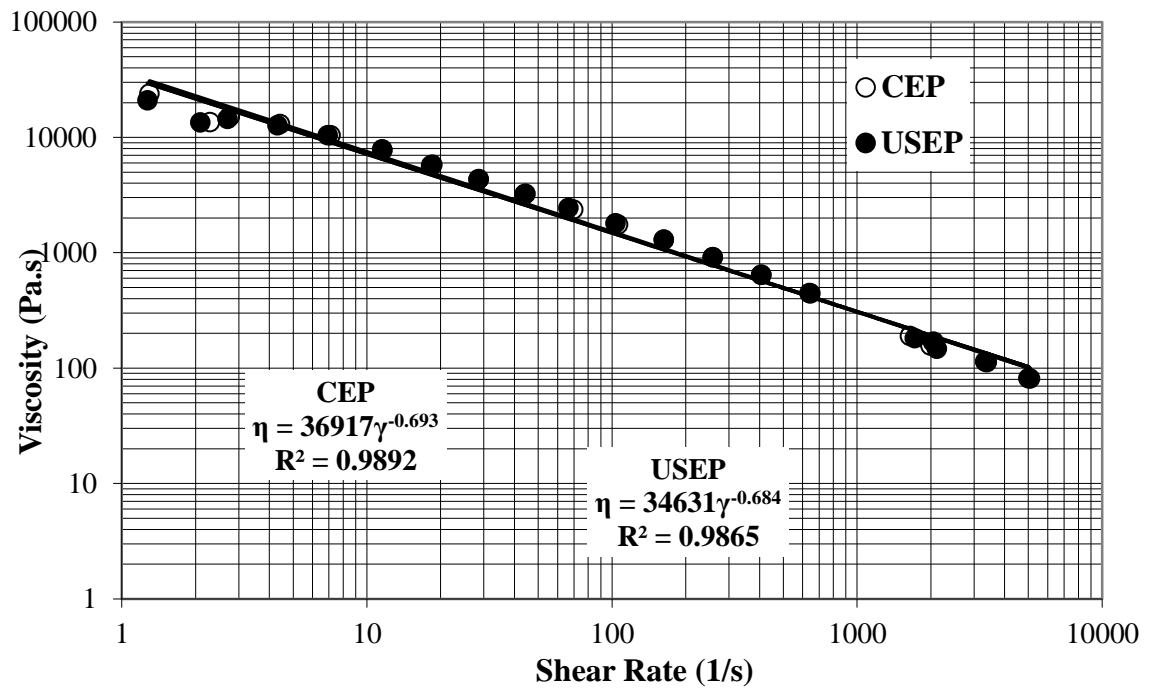
Figure B-42: Shear viscosity vs. shear rate for PE80 strips produced at 30 rpm with and without presence of ultrasonic vibrations.

235
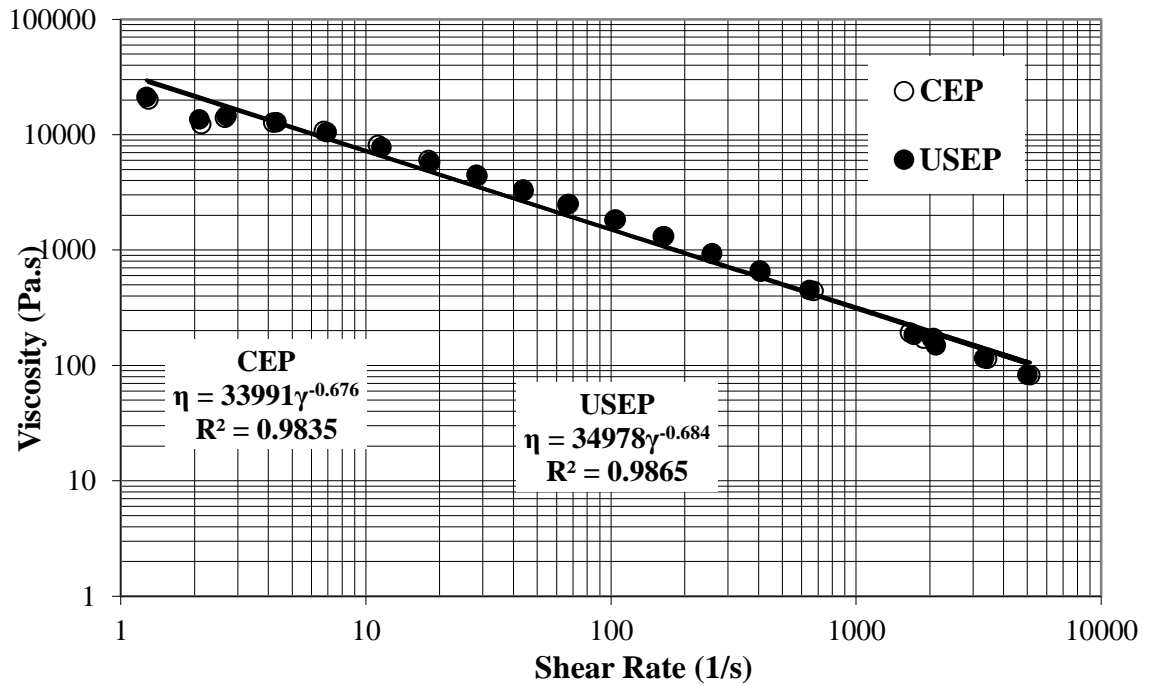
Figure B-43: Shear viscosity vs. shear rate for PE80 strips produced at 40 rpm with and without presence of ultrasonic vibrations.
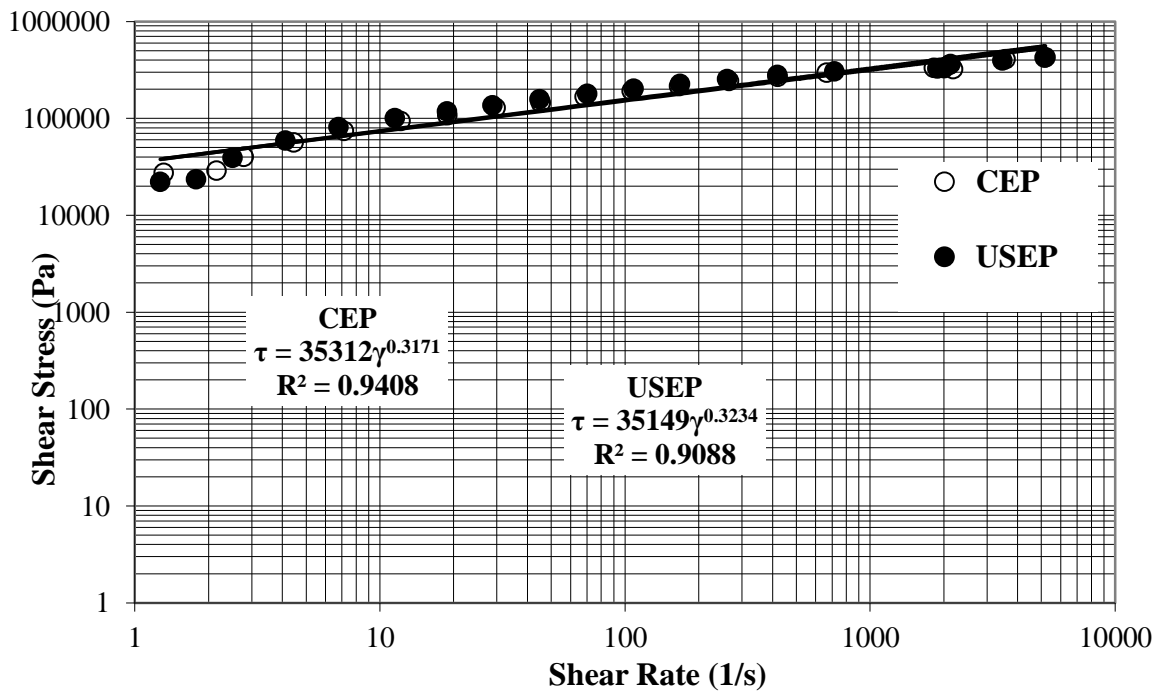
Figure B-44: Shear viscosity vs. shear rate for PE80 strips produced at 50 rpm with and without presence of ultrasonic vibrations.

Appendix C

I.   Assembly of the ultrasonic Die
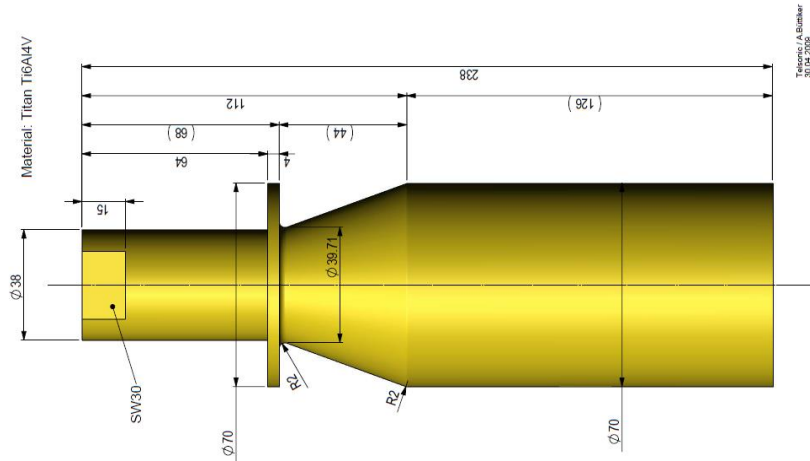
Figure C-1: Recommended dimensions of second generation ultrasonic horn by Telsonic.
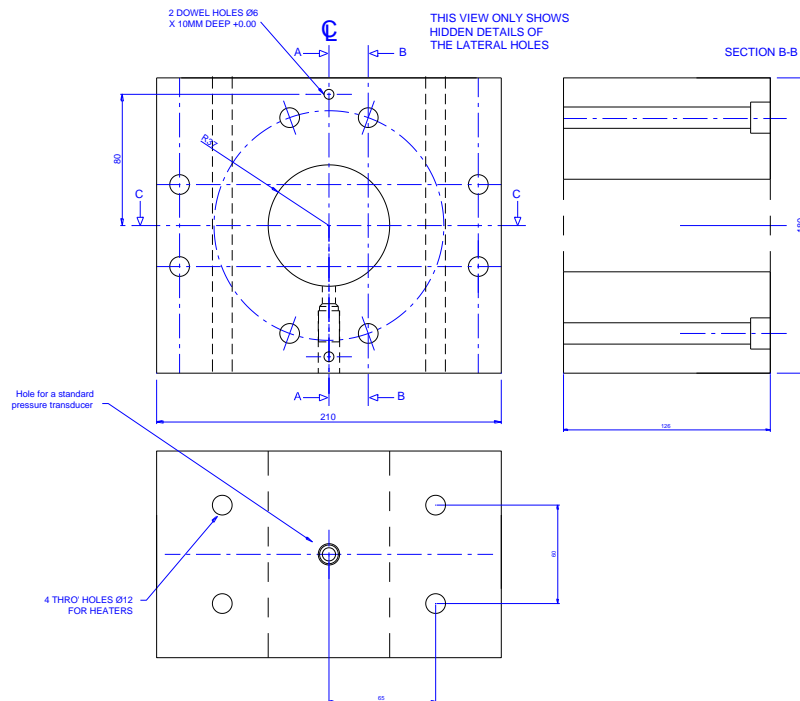
Figure C-2: Drawings of the end block for 2nd generation ultrasonic die.
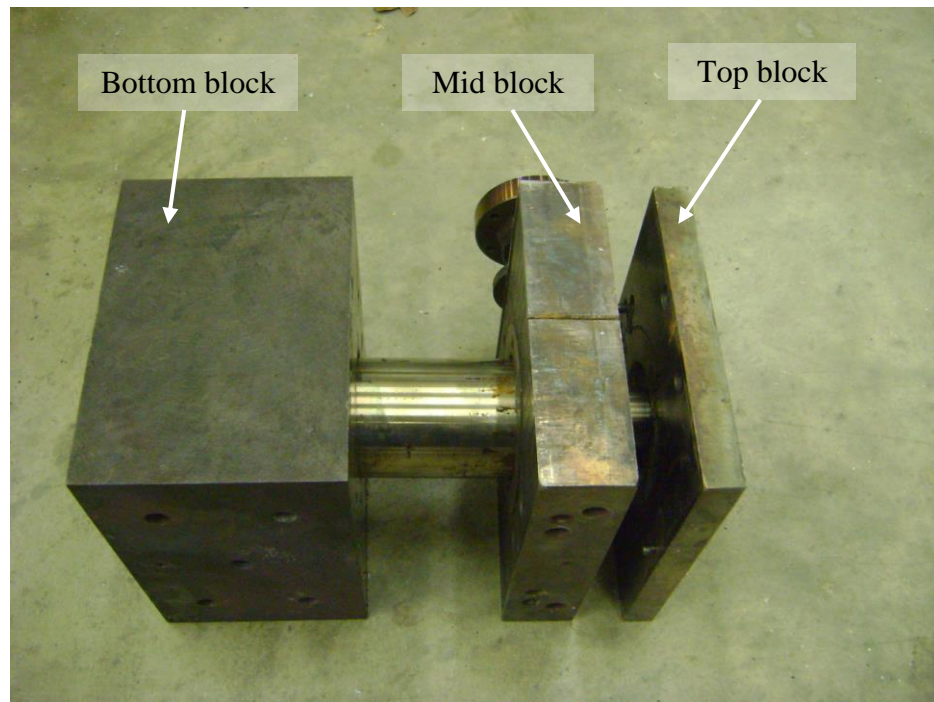
Figure C-3: Unassembled ultrasonic die housing block components from left to right the bottom block, mid block and the top block.
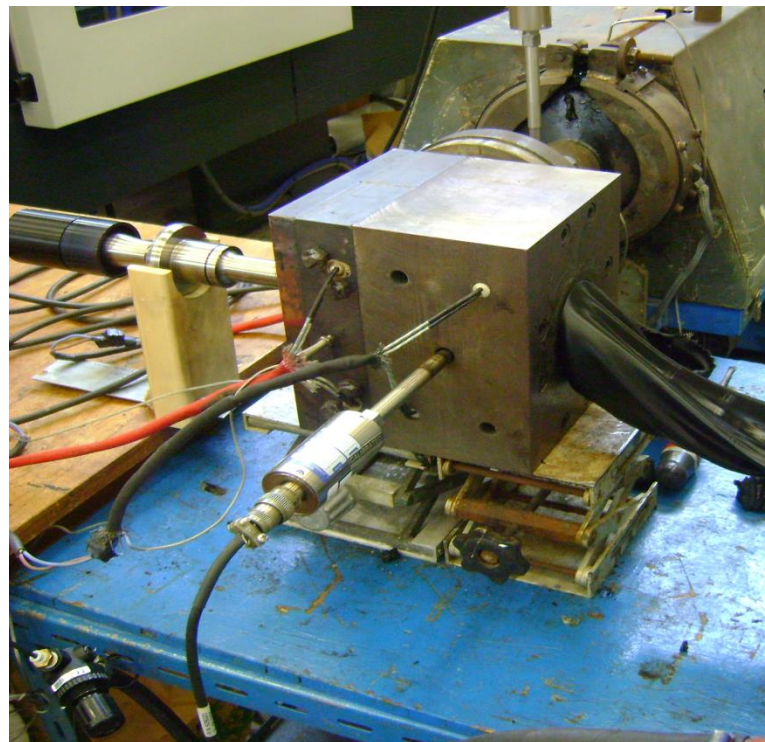
Figure C-4: Ultrasonic die installed on the extruder showing the ultrasonic transducer attached to the sonotrode.
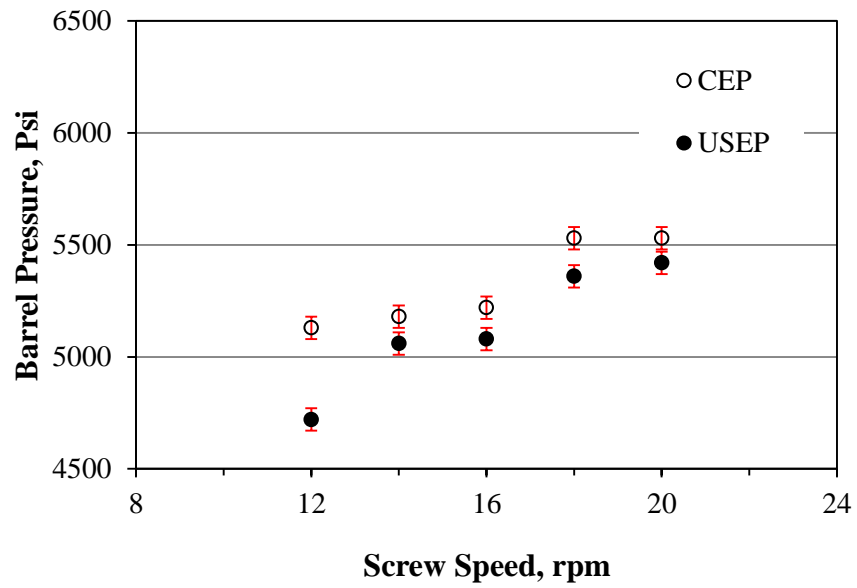
Figure C-5: Extruder barrel pressure for CEP and USEP processing of PE80 pipes.
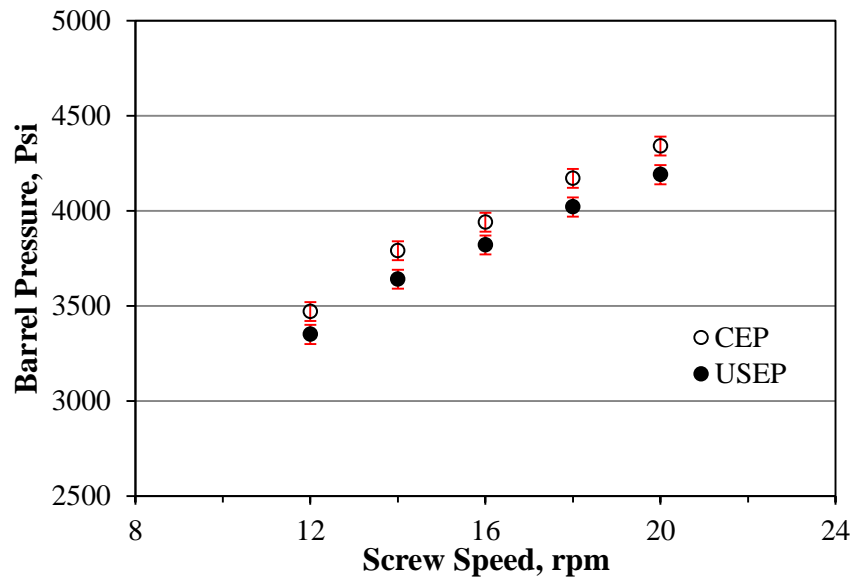
Figure C-6: Extruder barrel pressure for CEP and USEP processing of HYA600 pipes.
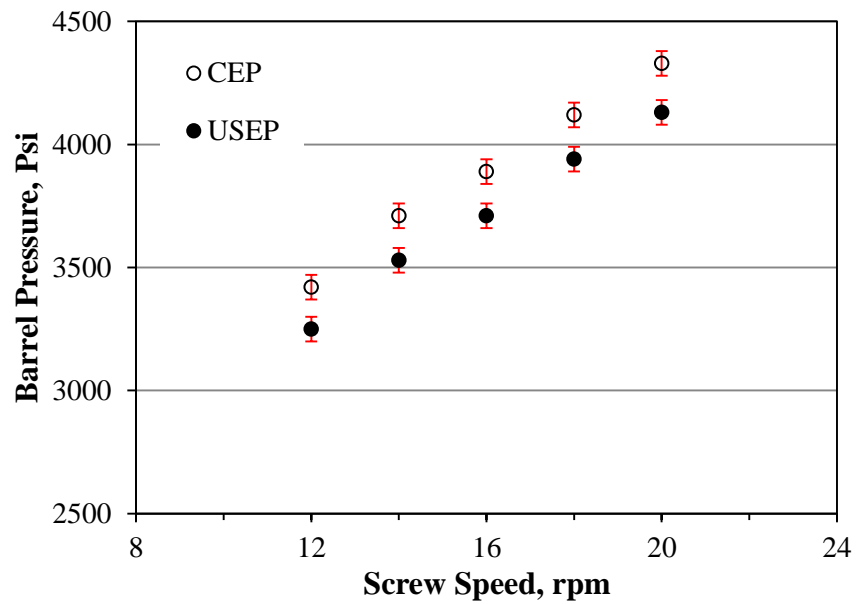
Figure C-7: Extruder barrel pressure for CEP and USEP processing of 20% filled HYA600 pipes.
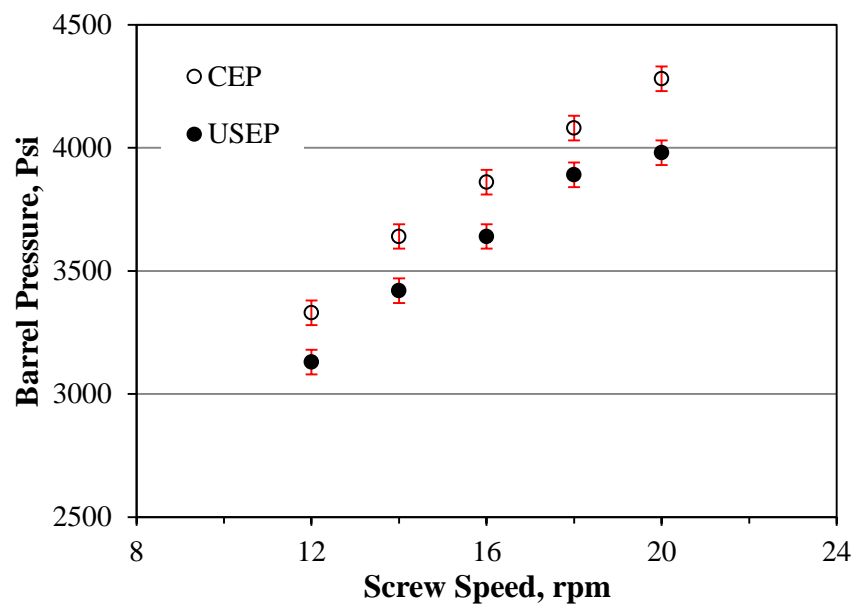
Figure C-8: Extruder barrel pressure for CEP and USEP processing of 40% filled HYA600 pipes.

II.　　Tensile Results
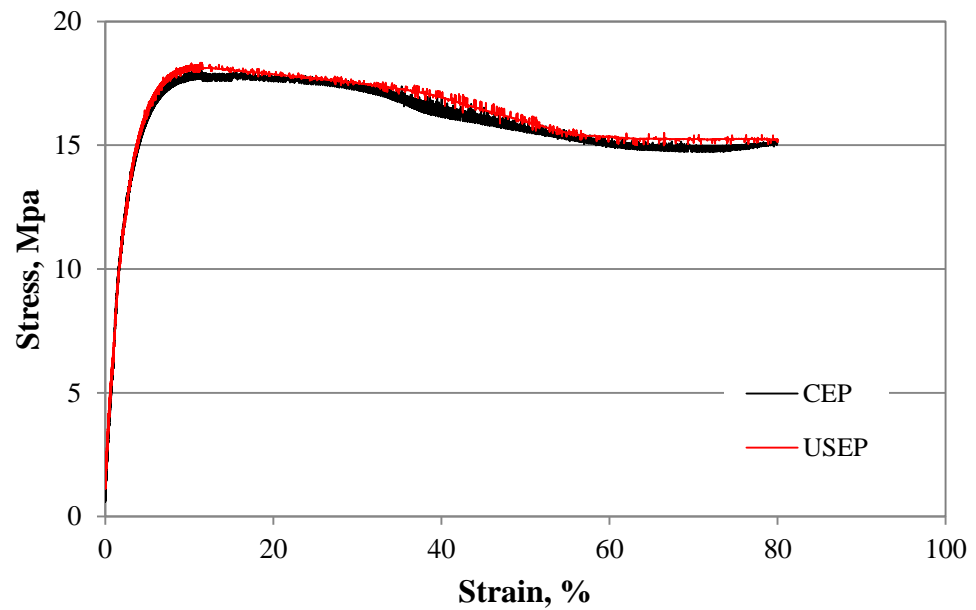
Figure C-9: Average stress vs. Strain for Rigidex5130strips produced at 12rpm produced by CEP and USEP process.
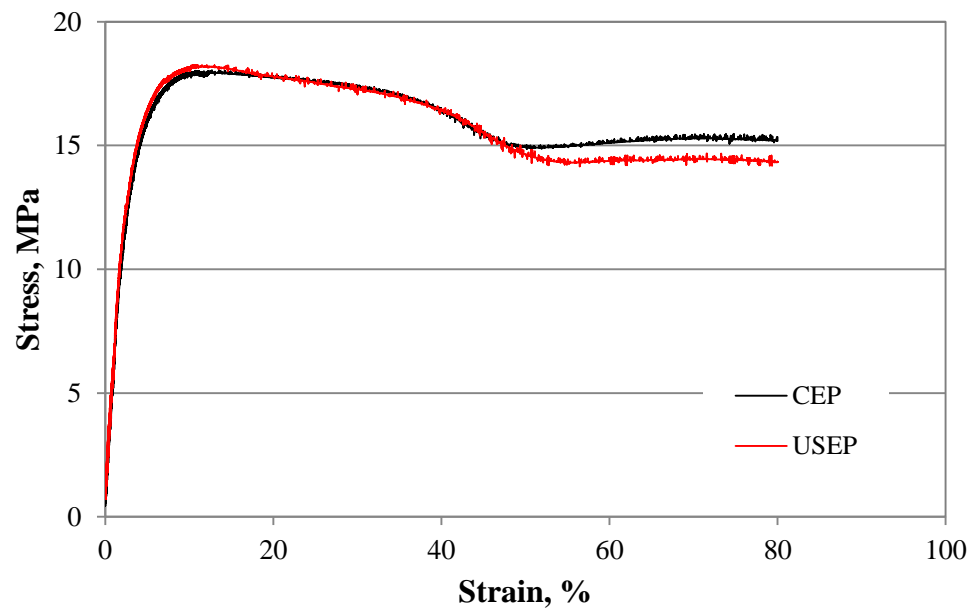
Figure C-10: Average stress vs. Strain for Rigidex5130 strips produced at 16rpm produced by CEP and USEP process.
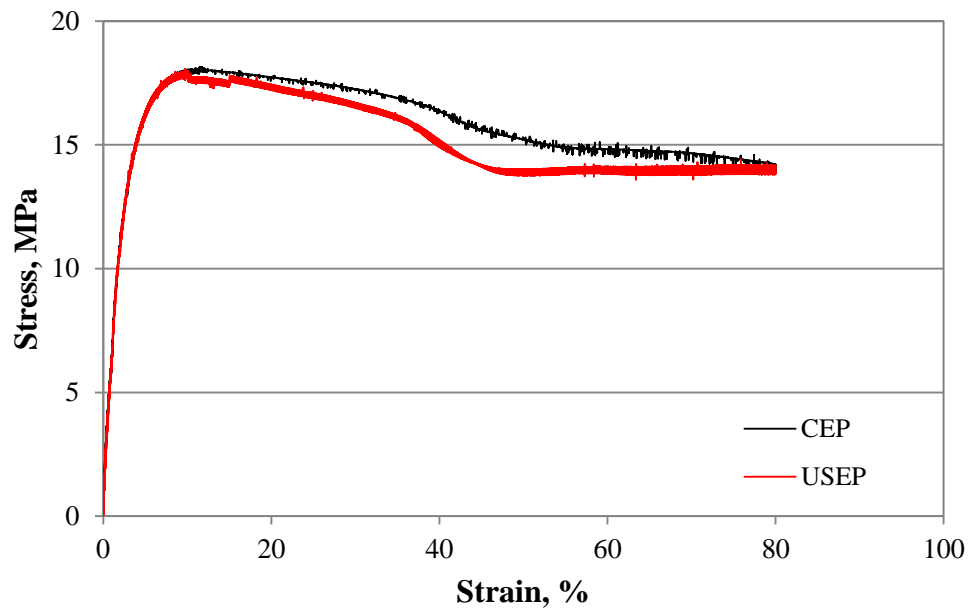
Figure C-11: Average stress vs. Strain for Rigidex5130 strips produced at 20rpm produced by CEP and USEP process.
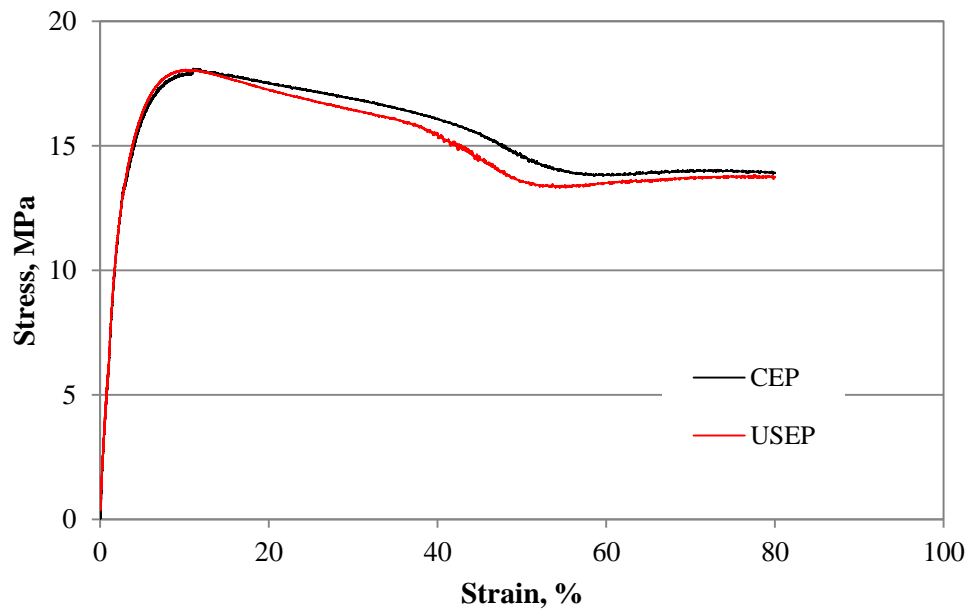
Figure C-12: Average stress vs. Strain for Rigidex5130 strips produced at 24rpm produced by CEP and USEP process.
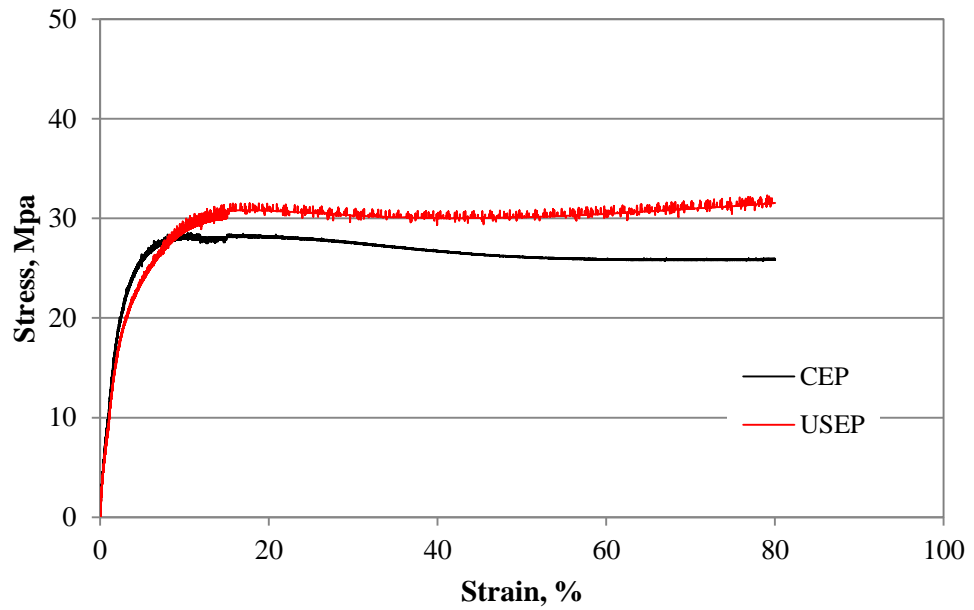
Figure C-13: Average stress vs. Strain for PE80 strips produced at 12rpm produced by CEP and USEP process.
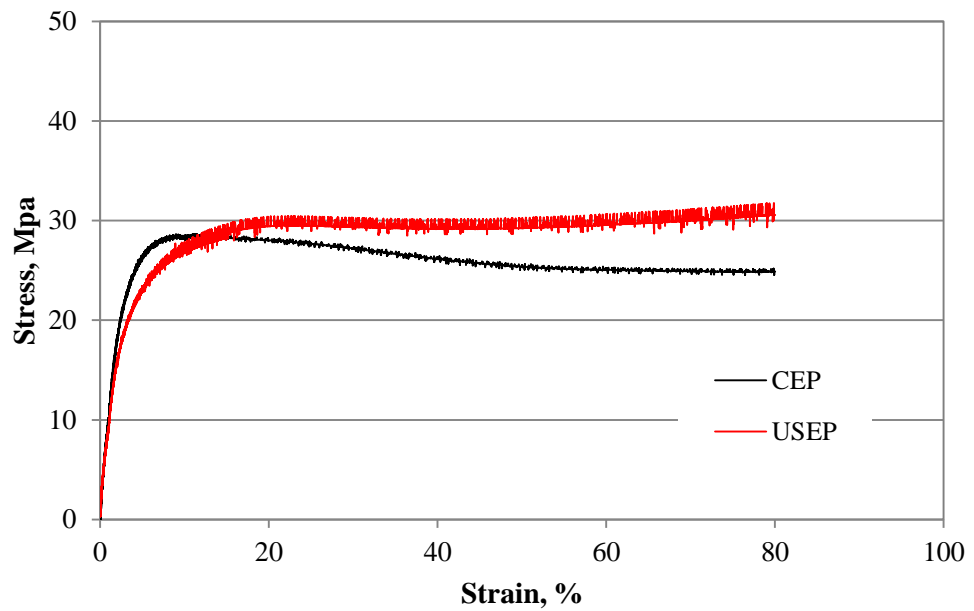
Figure C-14: Average stress vs. Strain for PE80 strips produced at 16rpm produced by CEP and USEP process.
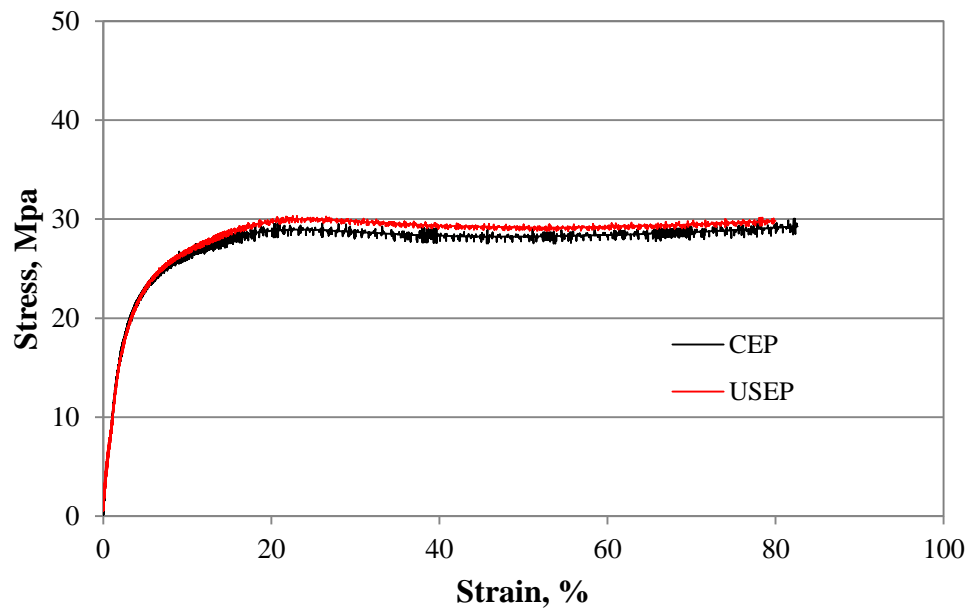
Figure C-15: Average stress vs. Strain for PE80 strips produced at 20rpm produced by CEP and USEP process.
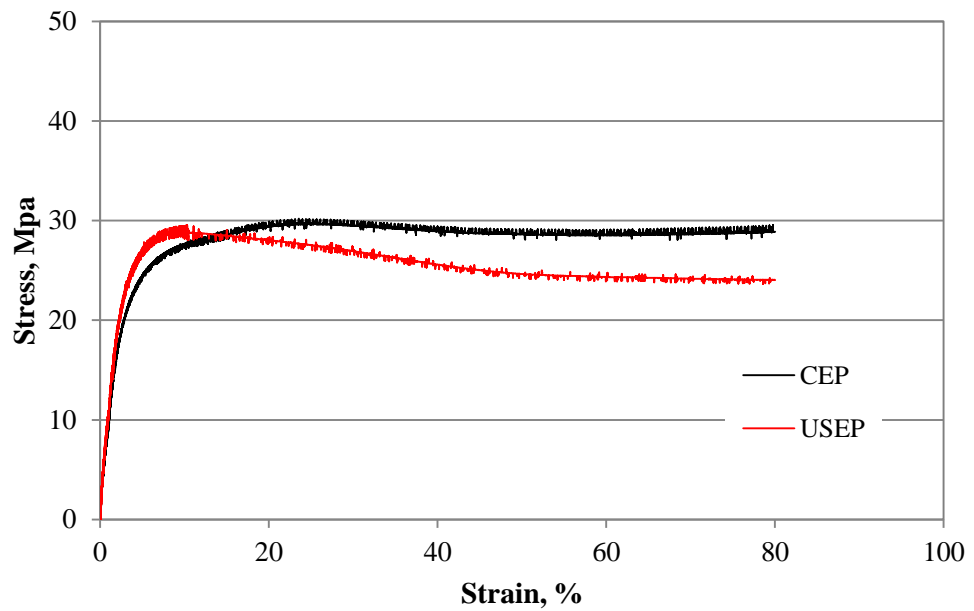
Figure C-16: Average stress vs. Strain for PE80 strips produced at 24rpm produced by CEP and USEP process.
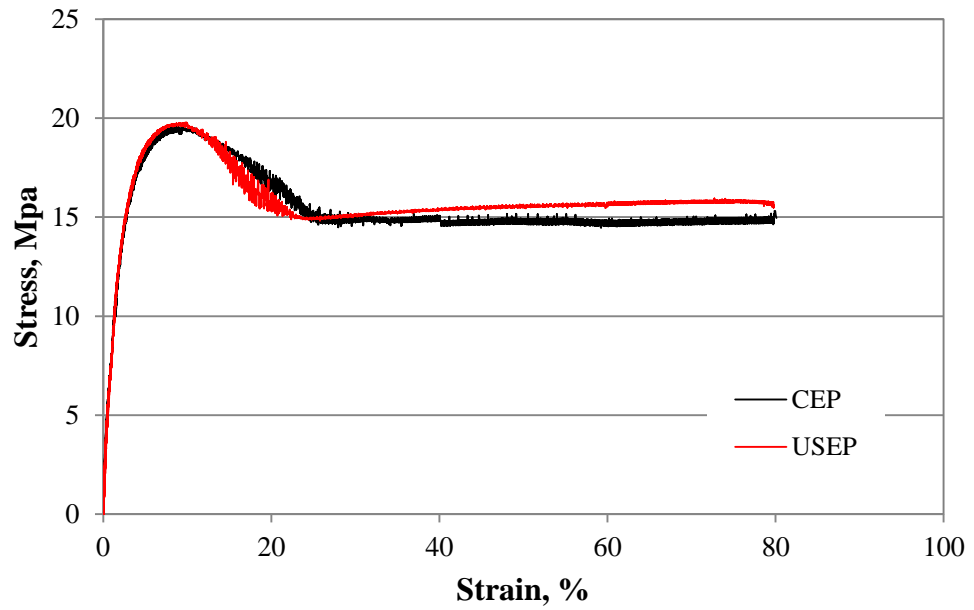
Figure C-17: Average stress vs. Strain for PE80 pipes produced at 14rpm produced by CEP and USEP process.
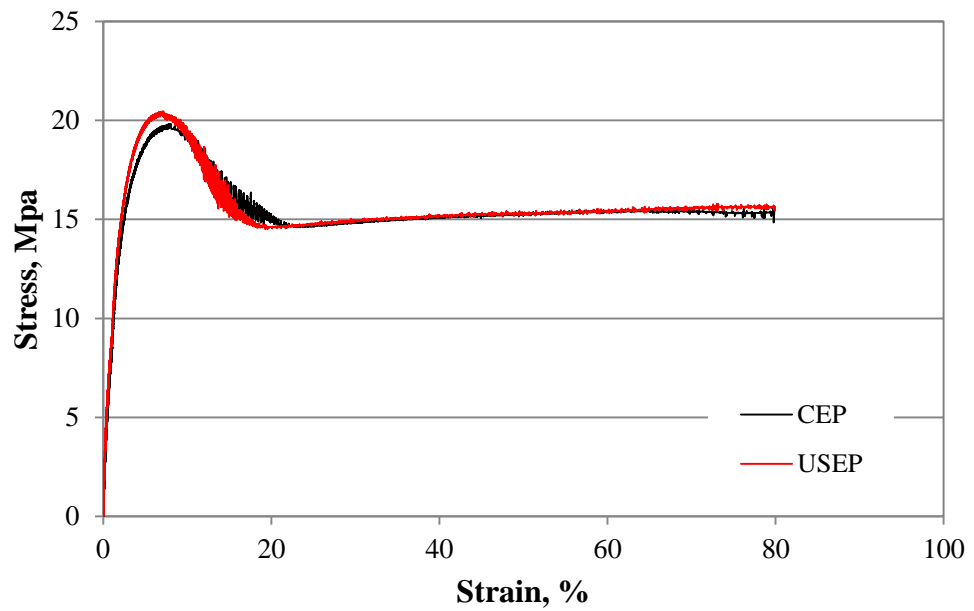
Figure C-18: Average stress vs. Strain for PE80 pipes produced at 16rpm produced by CEP and USEP process.
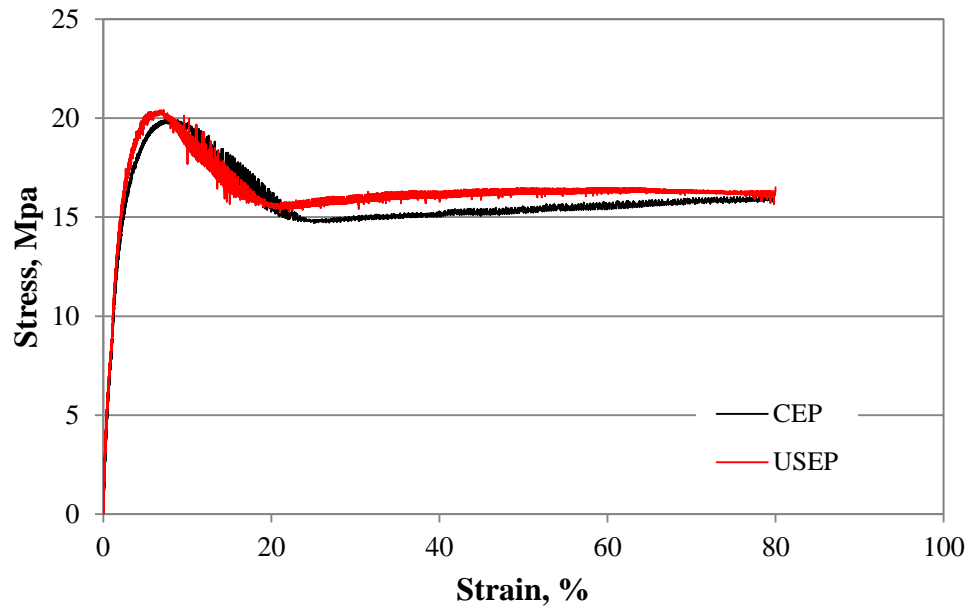
Figure C-19: Average stress vs. Strain for PE80 pipes produced at 18rpm produced by CEP and USEP process.
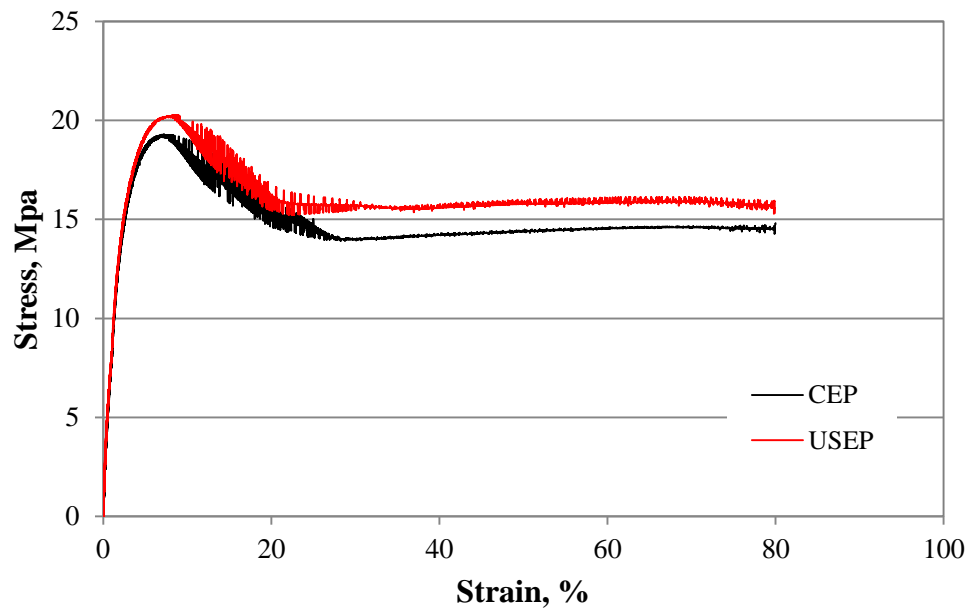
Figure C-20: Average stress vs. Strain for PE80 pipes produced at 20rpm produced by CEP and USEP process.
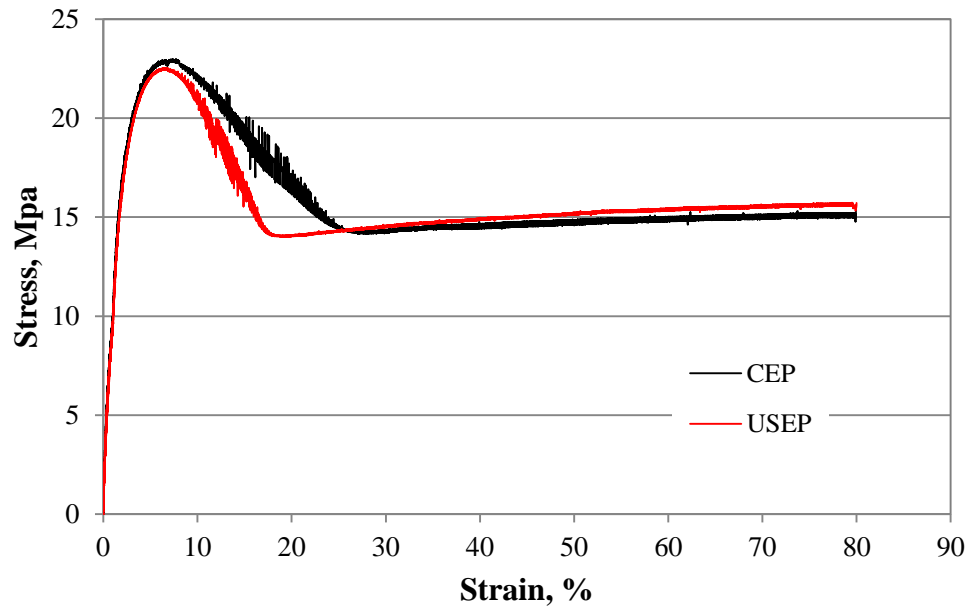
Figure C-21: Average stress vs. Strain for unfilled HYA600 pipes produced at 14rpm produced by CEP and USEP process.
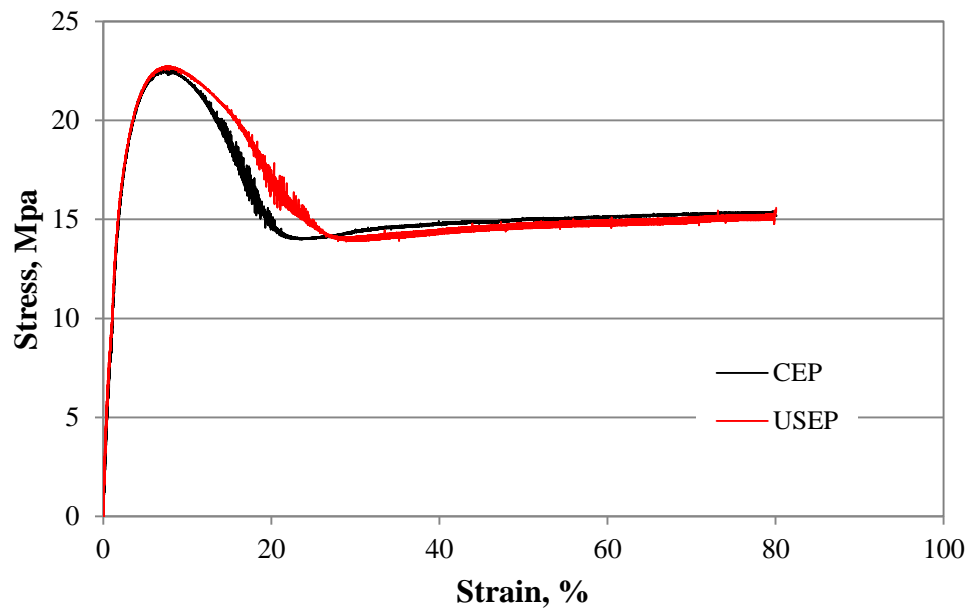
Figure C-22: Average stress vs. Strain for unfilled HYA600 pipes produced at 16rpm produced by CEP and USEP process.
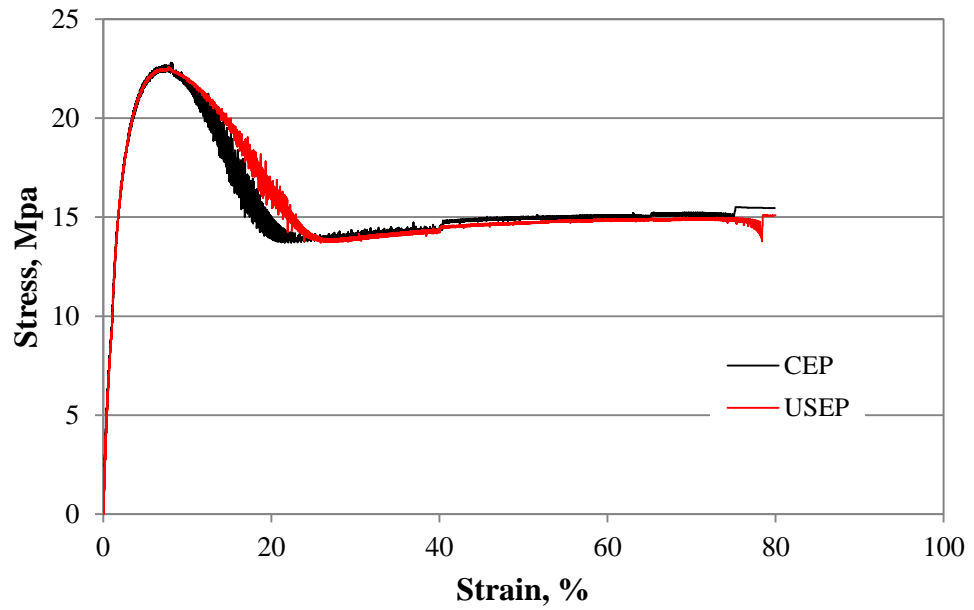
Figure C-23: Average stress vs. Strain for unfilled HYA600 pipes produced at 18rpm produced by CEP and USEP process.
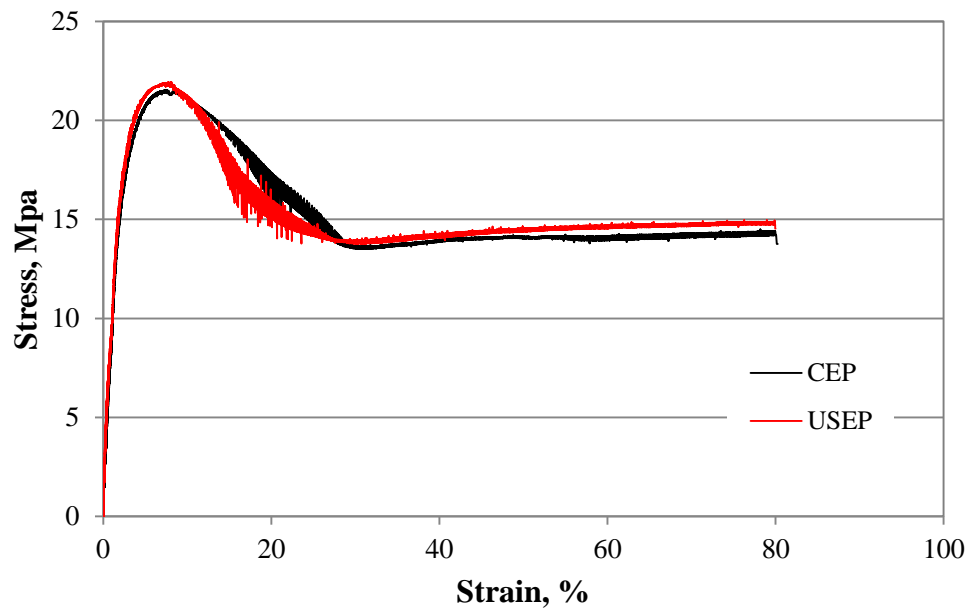
Figure C-24: Average stress vs. Strain for unfilled HYA600 pipes produced at 20rpm produced by CEP and USEP process.
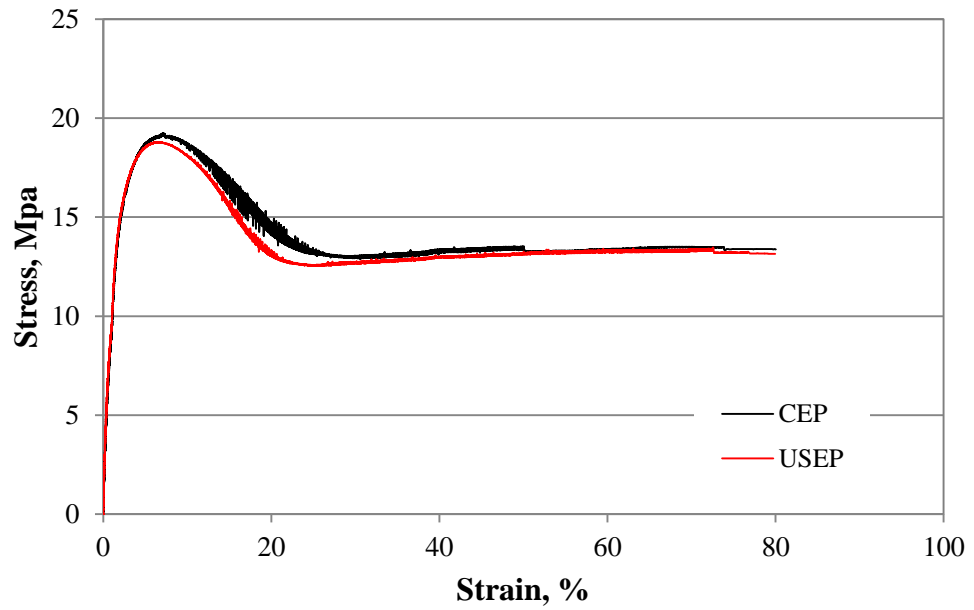
Figure C-25: Average stress vs. Strain for 20% filled HYA600 pipes produced at 14rpm produced by CEP and USEP process.
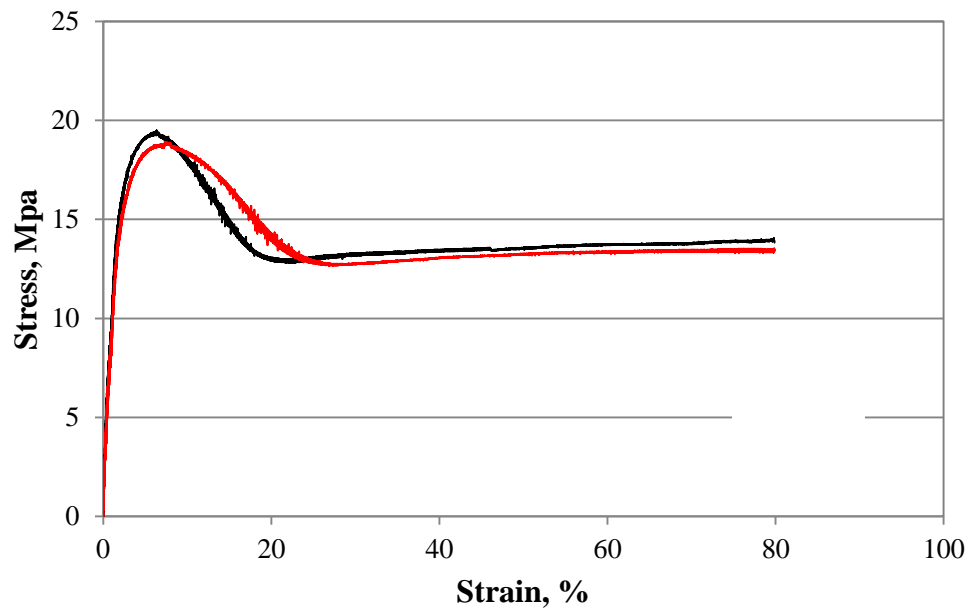
Figure C-26: Average stress vs. Strain for 20% filled HYA600 pipes produced at 16rpm produced by CEP and USEP process.
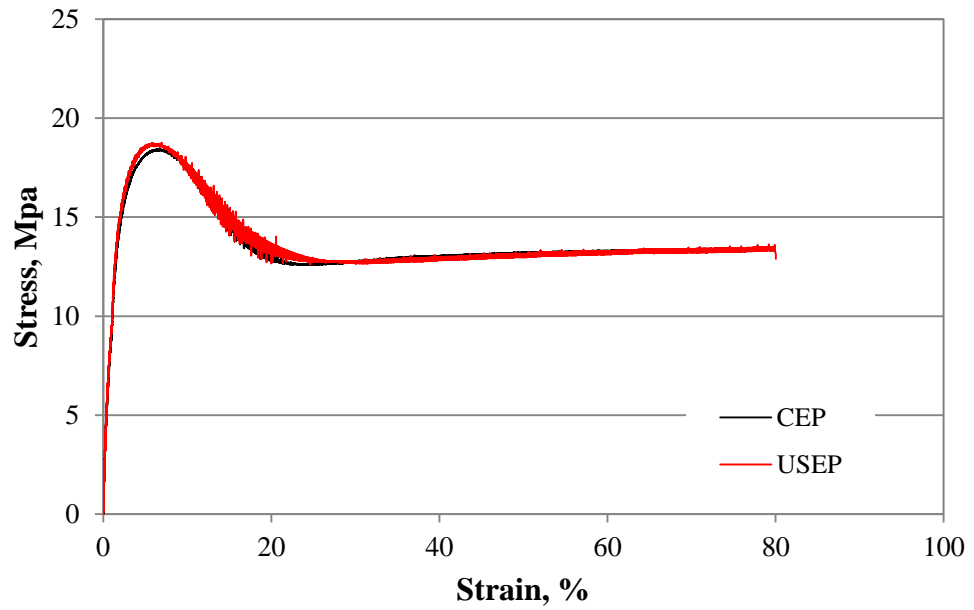
Figure C-27: Average stress vs. Strain for 20% filled HYA600 pipes produced at 18rpm produced by CEP and USEP process.
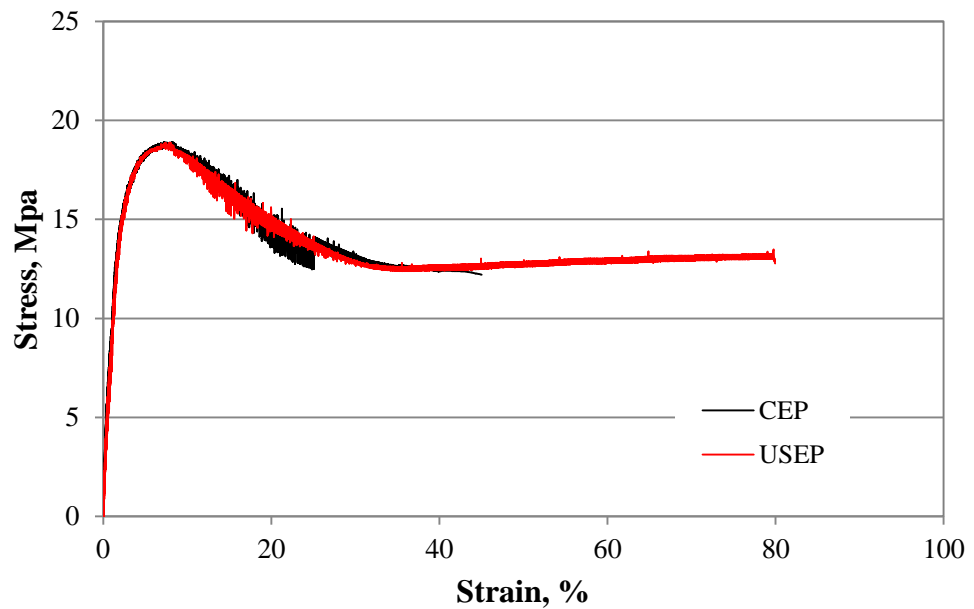
Figure C-28: Average stress vs. Strain for 20% filled HYA600 pipes produced at 20rpm produced by CEP and USEP process.
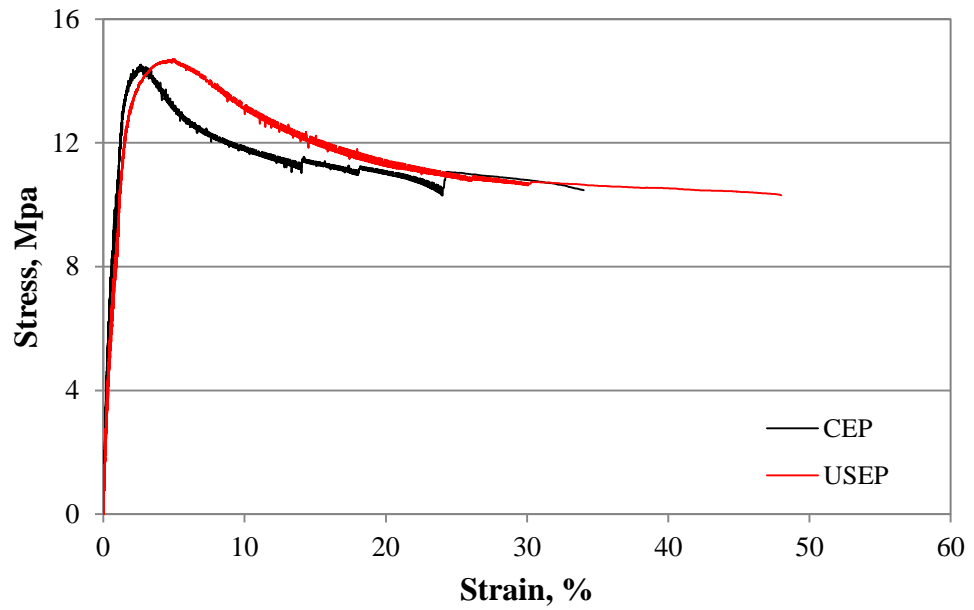
Figure C-29: Average stress vs. Strain for 40% filled HYA600 pipes produced at 14rpm produced by CEP and USEP process.
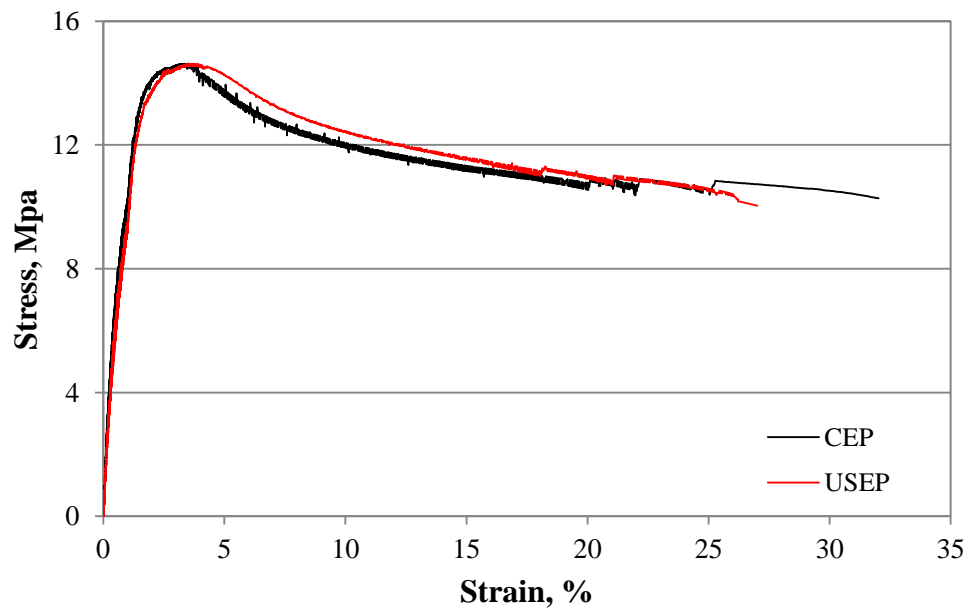
Figure C-30: Average stress vs. Strain for 40% filled HYA600 pipes produced at 16rpm produced by CEP and USEP process.

252
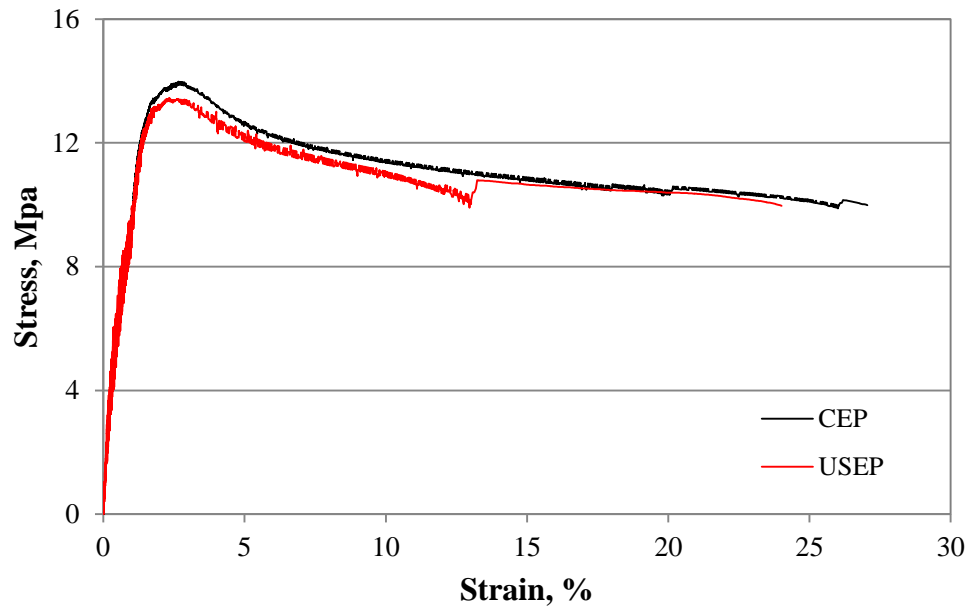
Figure C-31: Average stress vs. Strain for 40% filled HYA600 pipes produced at 18rpm produced by CEP and USEP process.
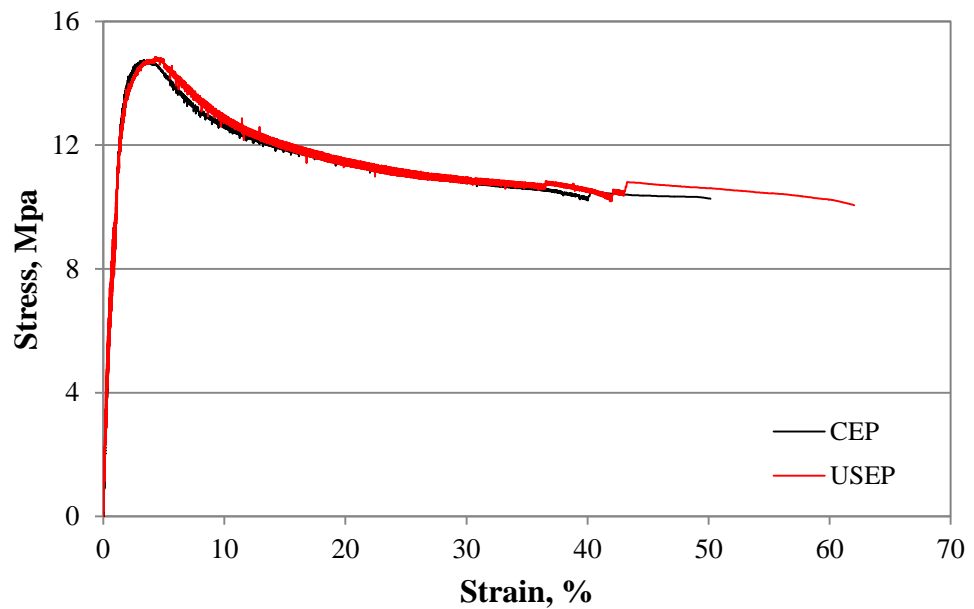
Figure C-32: Average stress vs. Strain for 40% filled HYA600 pipes produced at 20rpm produced by CEP and USEP process.
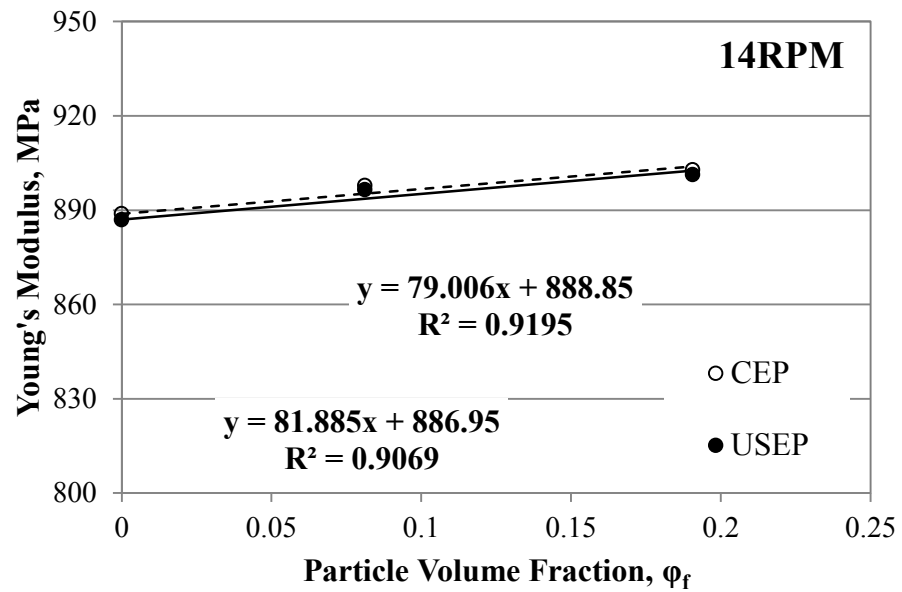
Figure C-33: Elastic Modulus of HYA600 composites vs. particle volume fraction for pipes produced at 14rpm with and without presence of ultrasonic vibrations.
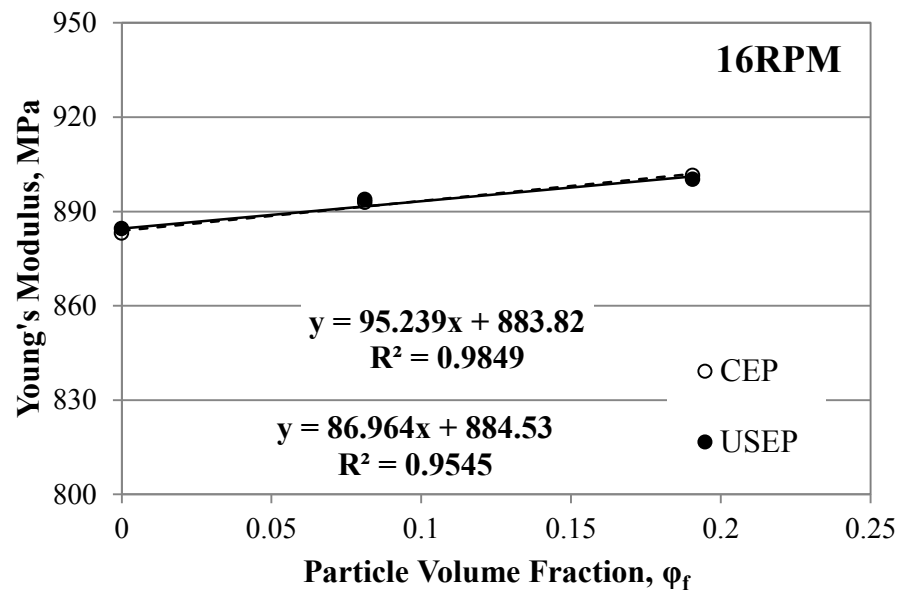
Figure C-34: Elastic Modulus of HYA600 composites vs. particle volume fraction for pipes produced at 16rpm with and without presence of ultrasonic vibrations.
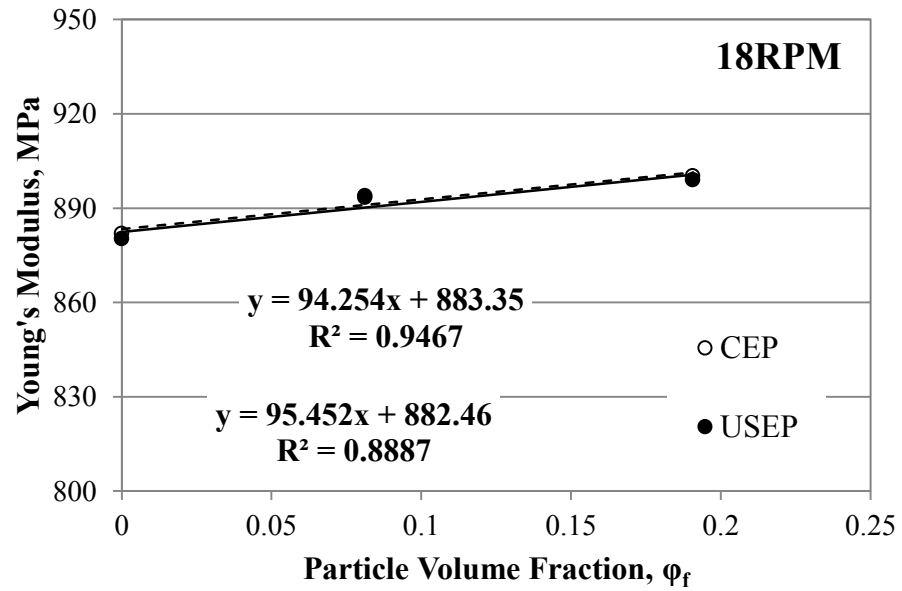
Figure C-35: Elastic Modulus of HYA600 composites vs. particle volume fraction for pipes produced at 18rpm with and without presence of ultrasonic vibrations.
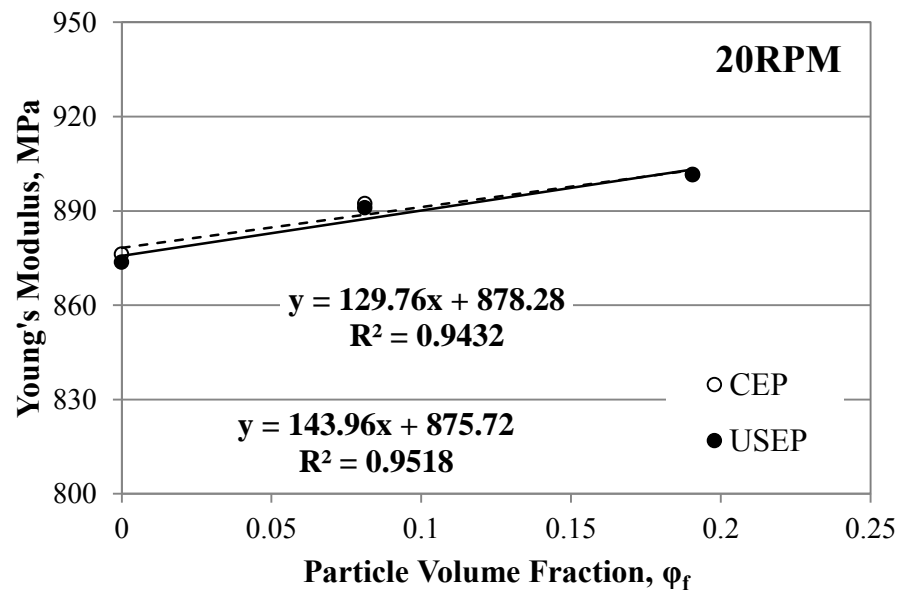
Figure C-36: Elastic Modulus of HYA600 composites vs. particle volume fraction for pipes produced at 20rpm with and without presence of ultrasonic vibrations.
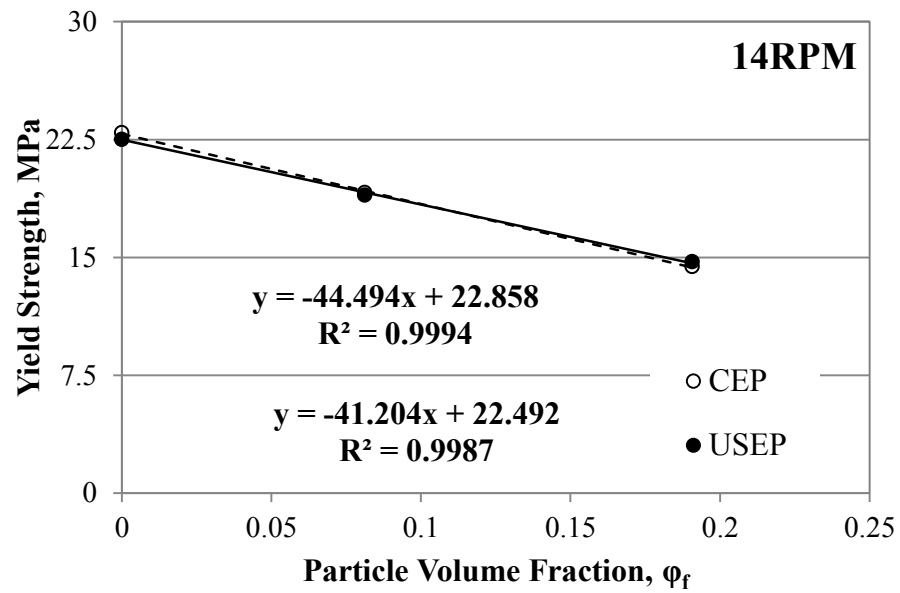
Figure C-37: Yield strength of HYA600 composites vs. particle volume fraction for pipes produced at 14rpm with and without presence of ultrasonic vibrations.
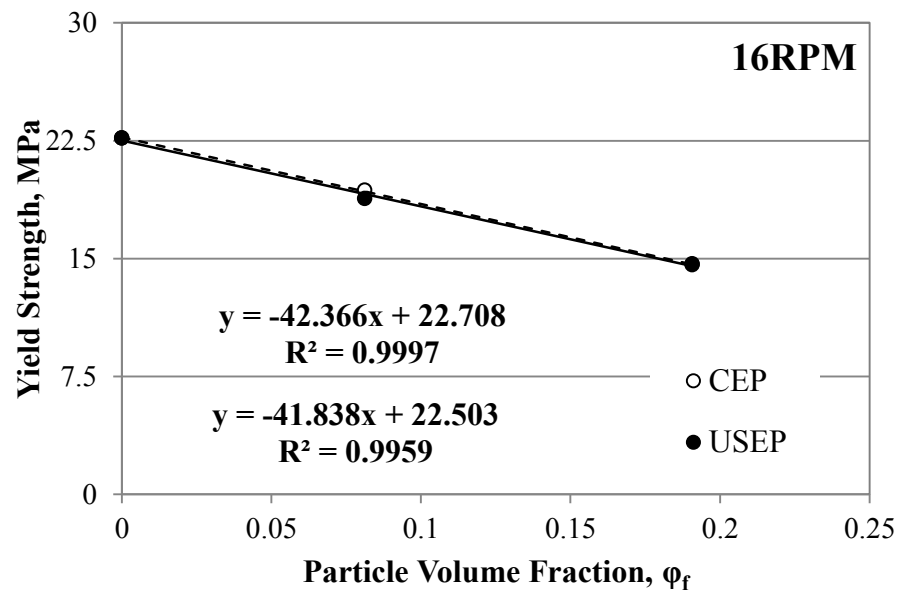
Figure C-38: Yield strength of HYA600 composites vs. particle volume fraction for pipes produced at 16rpm with and without presence of ultrasonic vibrations.

256
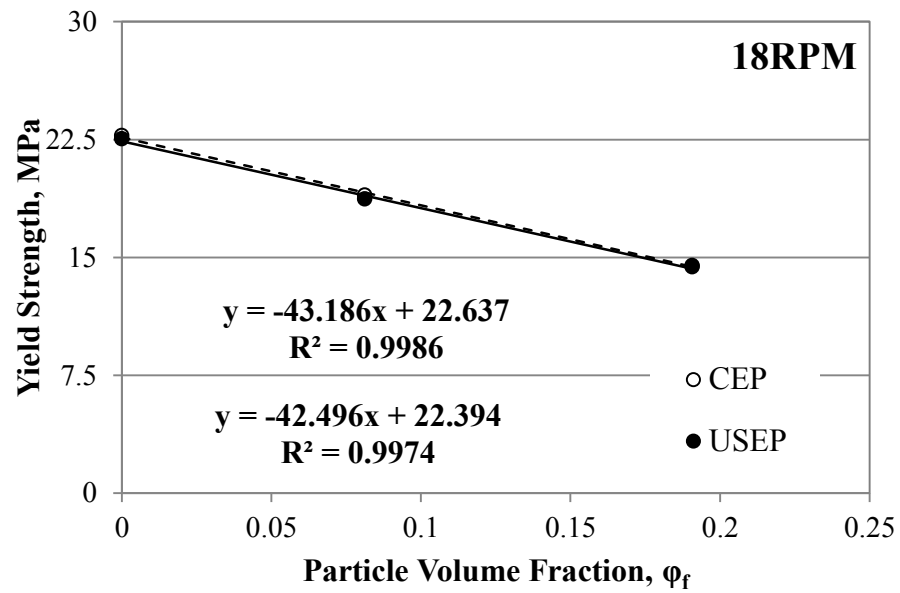
Figure C-39: Yield strength of HYA600 composites vs. particle volume fraction for pipes produced at 18rpm with and without presence of ultrasonic vibrations.
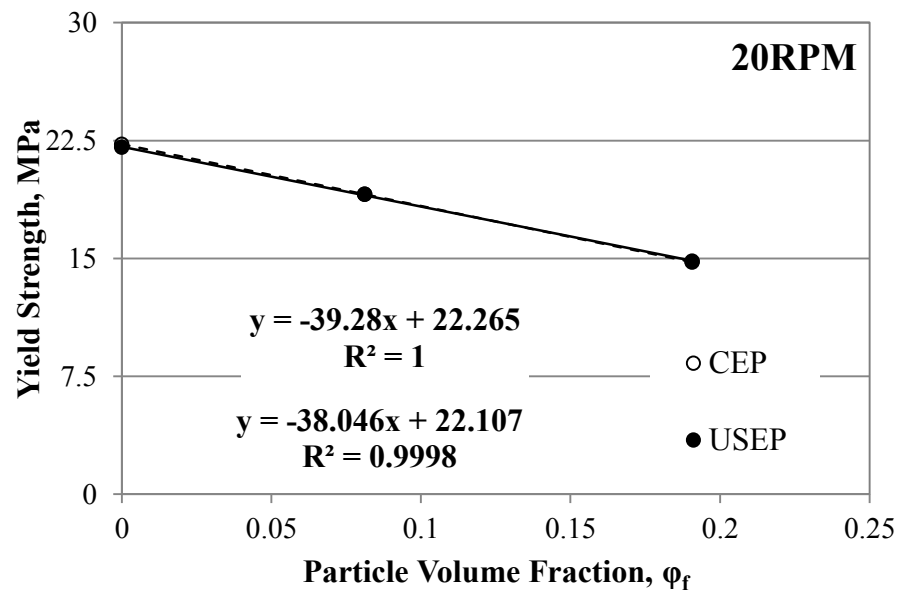
Figure C-40: Yield strength of HYA600 composites vs. particle volume fraction for pipes produced at 20rpm with and without presence of ultrasonic vibrations.
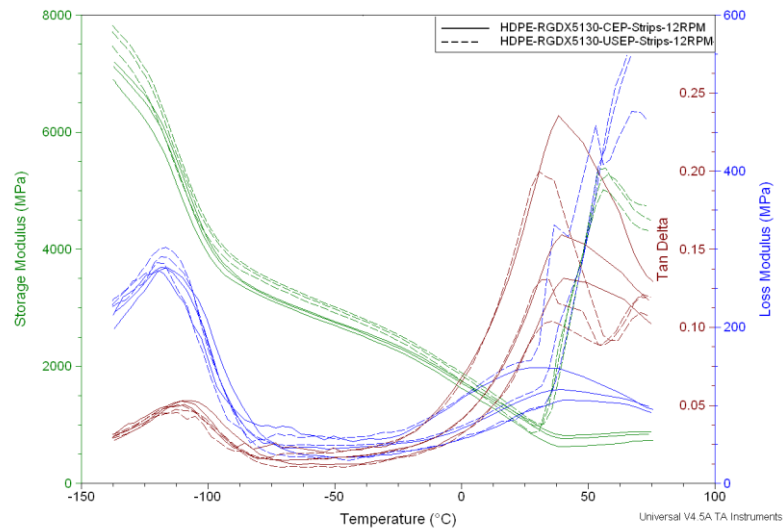
III. DMA Results

Figure C-41: DMA Results of Rigidex5130 strips produced at 12rpm by both USEP and CEP methods the solid line represents CEP samples data and the dashed line is for USEP samples while for each set of data the curves from top to bottom represent data acquired at 1Hz, 5Hz and 10Hz respectively.
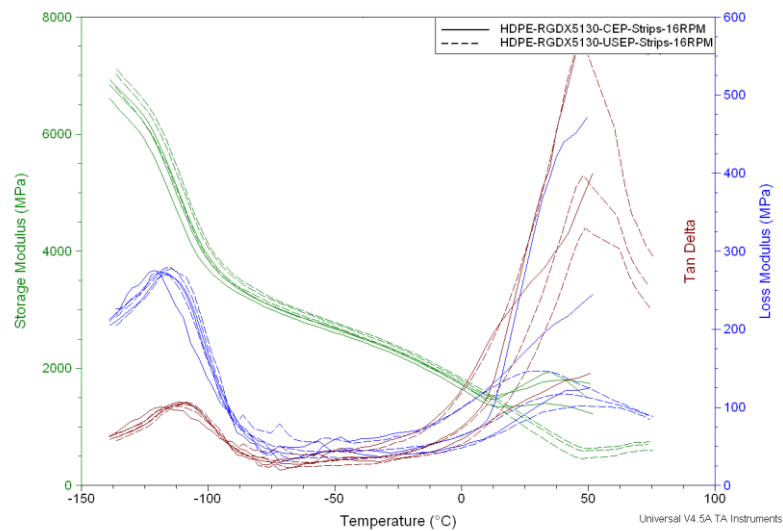
Figure C-42: DMA Results of Rigidex5130 strips produced at 16rpm by both USEP and CEP methods the solid line represents CEP samples data and the dashed line is for USEP samples while for each set of data the curves from top to bottom represent data acquired at 1Hz, 5Hz and 10Hz respectively.

258
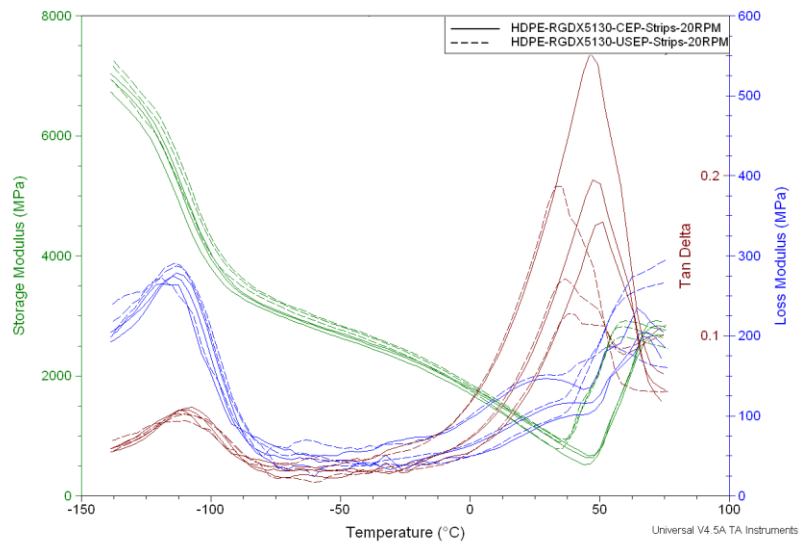
Figure C-43: DMA Results of Rigidex5130 strips produced at 20rpm by both USEP and CEP methods the solid line represents CEP samples data and the dashed line is for USEP samples while for each set of data the curves from top to bottom represent data acquired at 1Hz, 5Hz and 10Hz respectively.
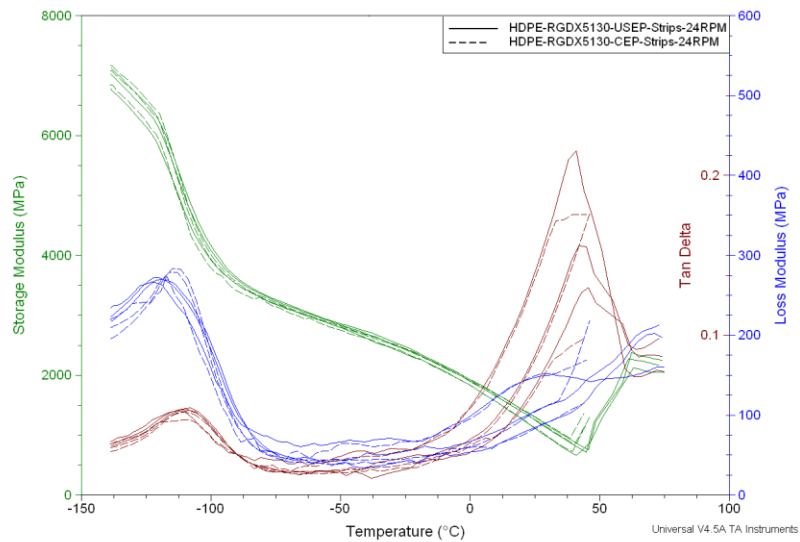
Figure C-44: DMA Results of Rigidex5130 strips produced at 24rpm by both USEP and CEP methods the solid line represents CEP samples data and the dashed line is for USEP samples while for each set of data the curves from top to bottom represent data acquired at 1Hz, 5Hz and 10Hz respectively.
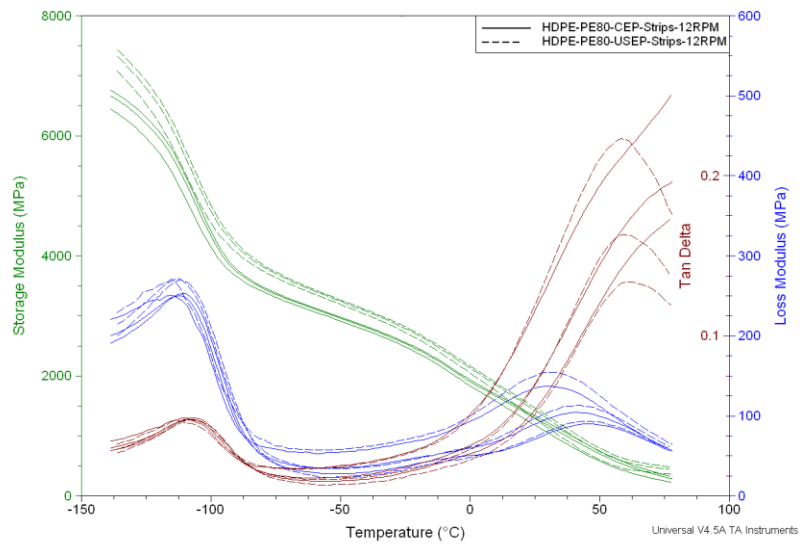
Figure C-45: DMA Results of PE80 strips produced at 12rpm by both USEP and CEP methods the solid line represents CEP samples data and the dashed line is for USEP samples while for each set of data the curves from top to bottom represent data acquired at 1Hz, 5Hz and 10Hz respectively.
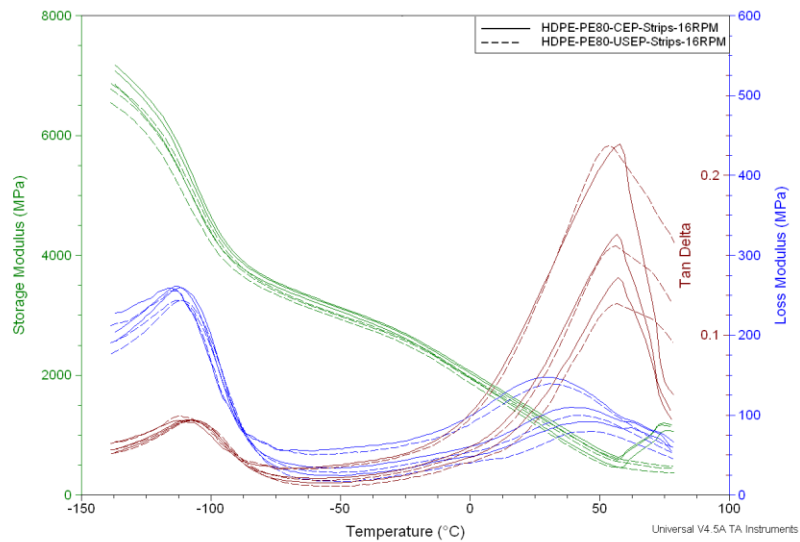
Figure C-46: DMA Results of PE80 strips produced at 16rpm by both USEP and CEP methods the solid line represents CEP samples data and the dashed line is for USEP samples while for each set of data the curves from top to bottom represent data acquired at 1Hz, 5Hz and 10Hz respectively.
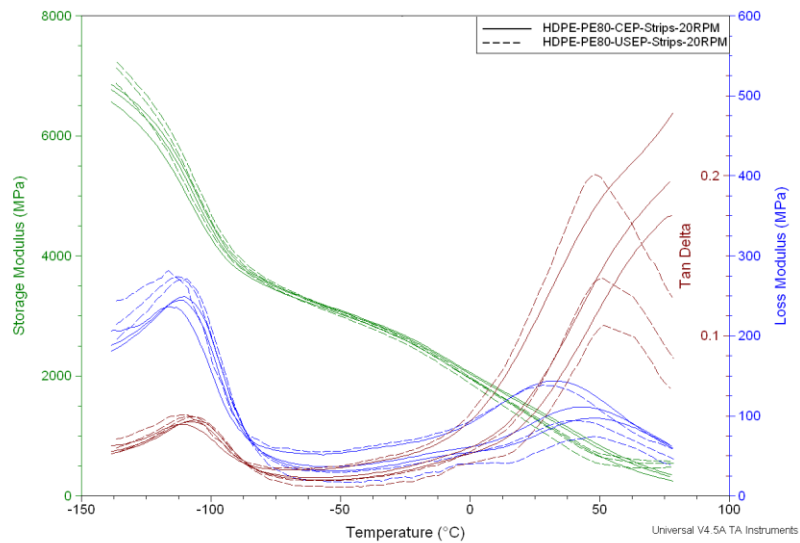
Figure C-47: DMA Results of PE80 strips produced at 20rpm by both USEP and CEP methods the solid line represents CEP samples data and the dashed line is for USEP samples while for each set of data the curves from top to bottom represent data acquired at 1Hz, 5Hz and 10Hz respectively.
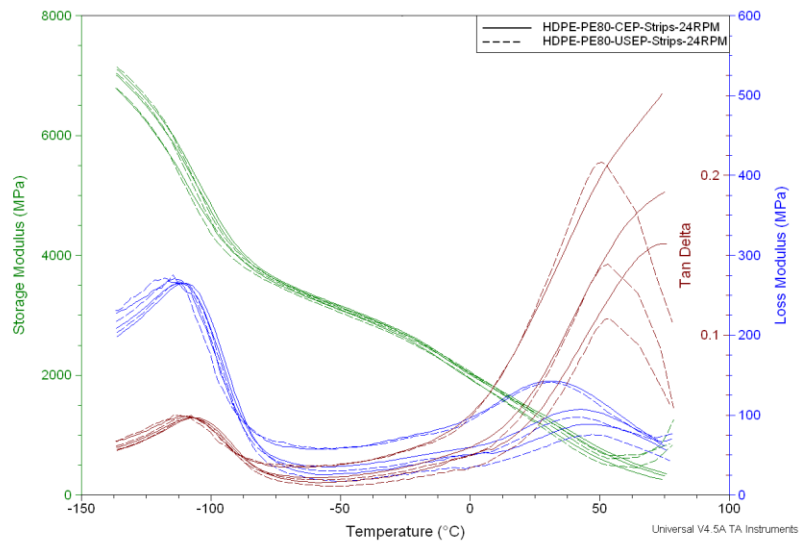
Figure C-48: DMA Results of PE80 strips produced at 24rpm by both USEP and CEP methods the solid line represents CEP samples data and the dashed line is for USEP samples while for each set of data the curves from top to bottom represent data acquired at 1Hz, 5Hz and 10Hz respectively.
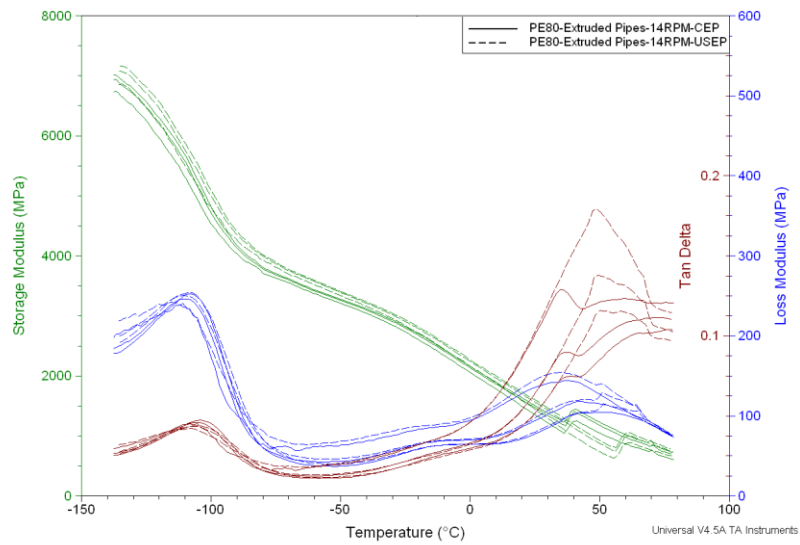
Figure C-49: DMA Results of PE80 pipes produced at 14rpm by both USEP and CEP methods the solid line represents CEP samples data and the dashed line is for USEP samples while for each set of data the curves from top to bottom represent data acquired at 1Hz, 5Hz and 10Hz respectively.
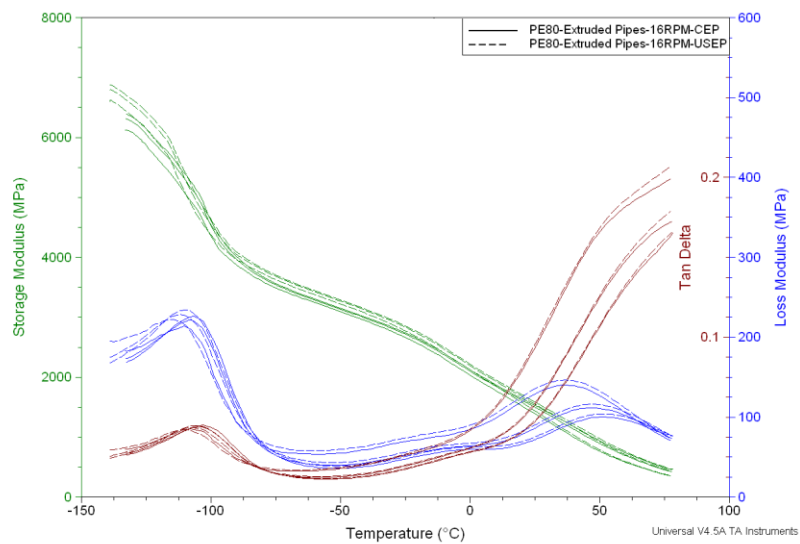
Figure C-50: DMA Results of PE80 pipes produced at 16rpm by both USEP and CEP methods the solid line represents CEP samples data and the dashed line is for USEP samples while for each set of data the curves from top to bottom represent data acquired at 1Hz, 5Hz and 10Hz respectively.
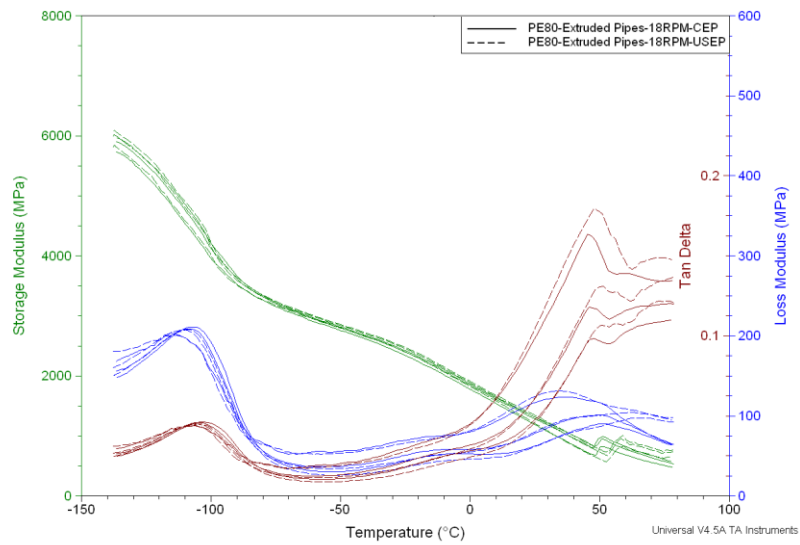
Figure C-51: DMA Results of PE80 pipes produced at 18rpm by both USEP and CEP methods the solid line represents CEP samples data and the dashed line is for USEP samples while for each set of data the curves from top to bottom represent data acquired at 1Hz, 5Hz and 10Hz respectively.
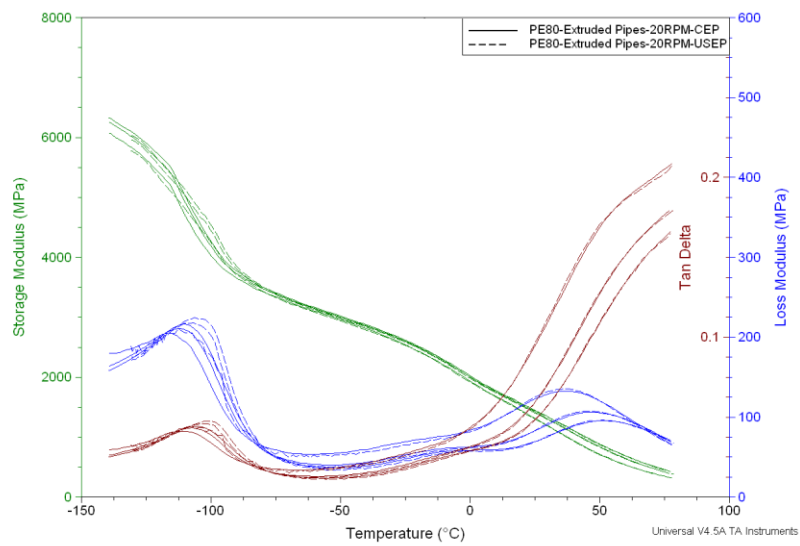
Figure C-52: DMA Results of PE80 pipes produced at 20rpm by both USEP and CEP methods the solid line represents CEP samples data and the dashed line is for USEP samples while for each set of data the curves from top to bottom represent data acquired at 1Hz, 5Hz and 10Hz respectively.
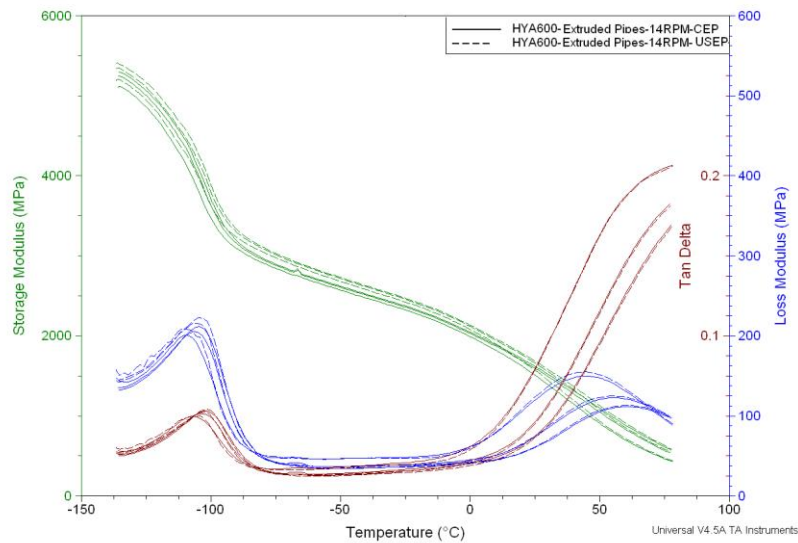
Figure C-53: DMA Results of unfilled HYA600 pipes produced at 14rpm by both USEP and CEP methods the solid line represents CEP samples data and the dashed line is for USEP samples while for each set of data the curves from top to bottom represent data acquired at 1Hz, 5Hz and 10Hz respectively.
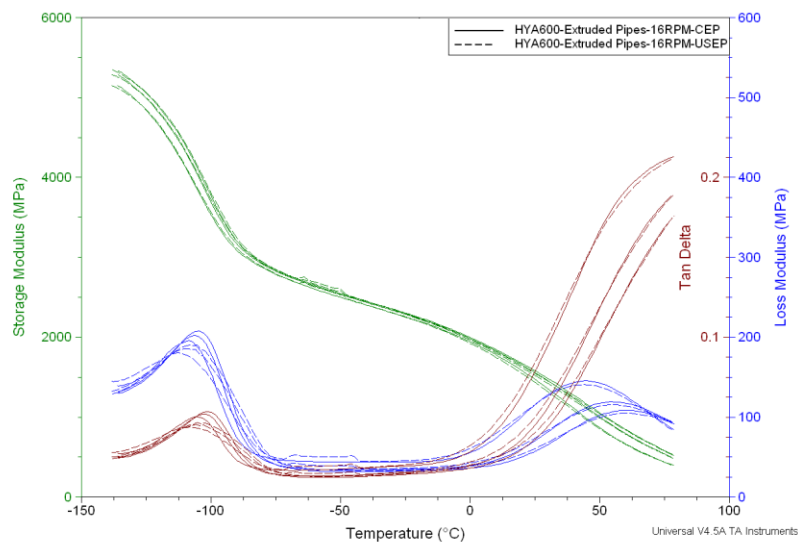
Figure C-54: DMA Results of unfilled HYA600 pipes produced at 16rpm by both USEP and CEP methods the solid line represents CEP samples data and the dashed line is for USEP samples while for each set of data the curves from top to bottom represent data acquired at 1Hz, 5Hz and 10Hz respectively.
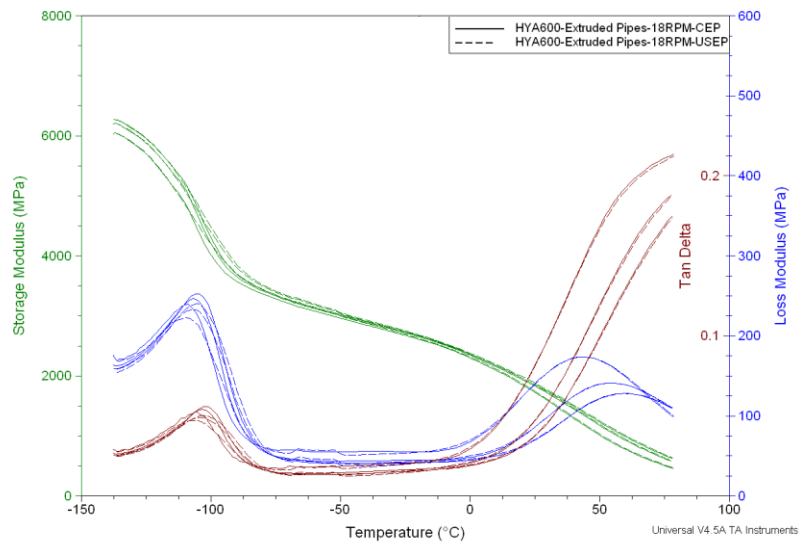
Figure C-55: DMA Results of unfilled HYA600 pipes produced at 18rpm by both USEP and CEP methods the solid line represents CEP samples data and the dashed line is for USEP samples while for each set of data the curves from top to bottom represent data acquired at 1Hz, 5Hz and 10Hz respectively.
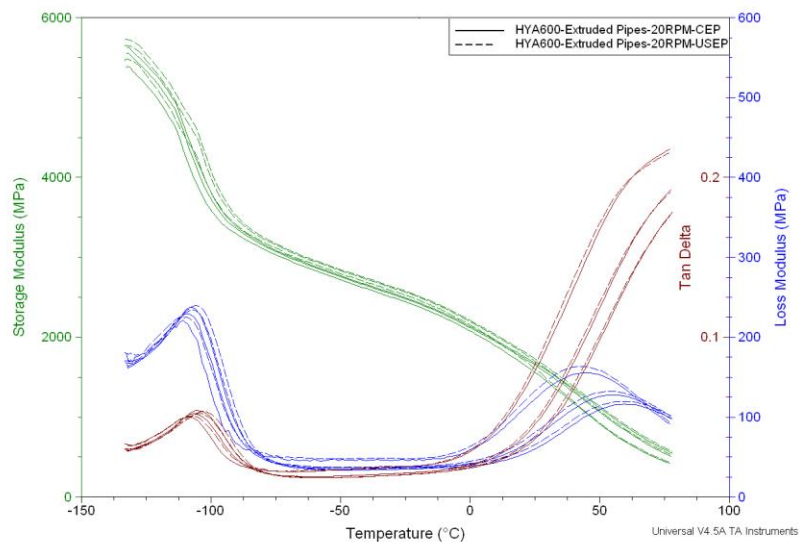
Figure C-56: DMA Results of unfilled HYA600 pipes produced at 20rpm by both USEP and CEP methods the solid line represents CEP samples data and the dashed line is for USEP samples while for each set of data the curves from top to bottom represent data acquired at 1Hz, 5Hz and 10Hz respectively.
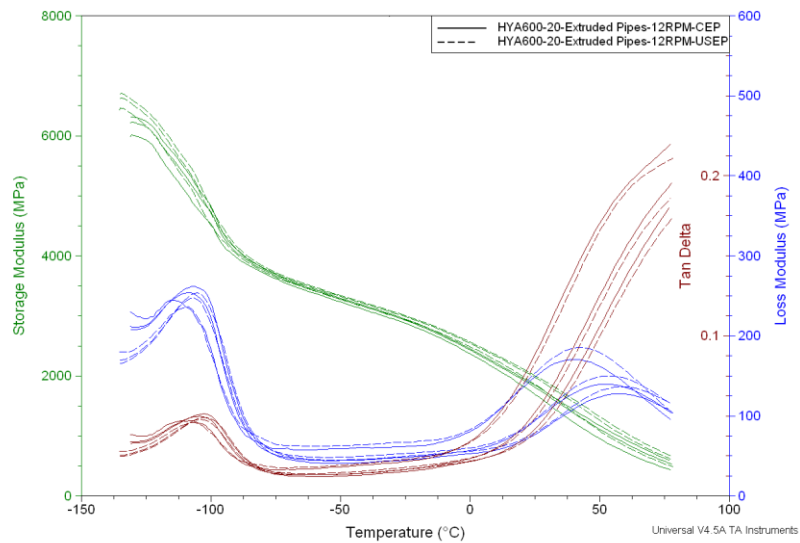
Figure C-57: DMA Results of 20%wt filled HYA600 pipes produced at 12rpm by both USEP and CEP methods the solid line represents CEP samples data and the dashed line is for USEP samples while for each set of data the curves from top to bottom represent data acquired at 1Hz, 5Hz and 10Hz respectively.
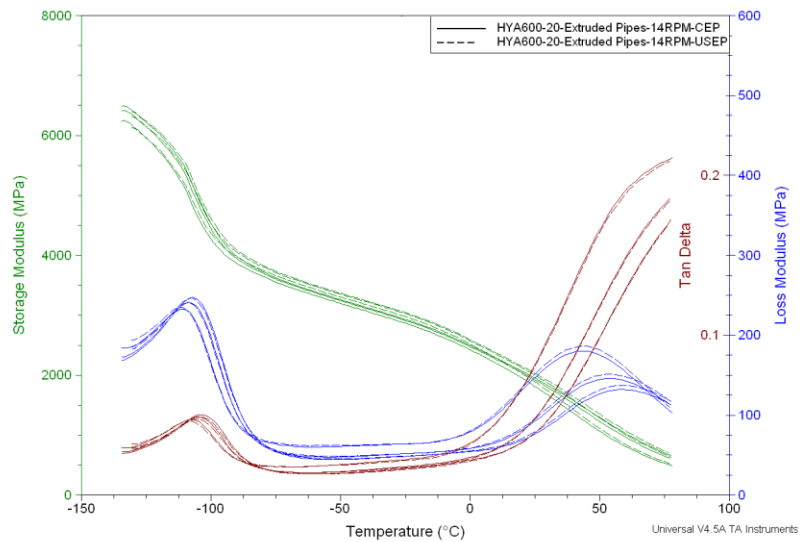
Figure C-58: DMA Results of 20%wt filled HYA600 pipes produced at 14rpm by both USEP and CEP methods the solid line represents CEP samples data and the dashed line is for USEP samples while for each set of data the curves from top to bottom represent data acquired at 1Hz, 5Hz and 10Hz respectively.
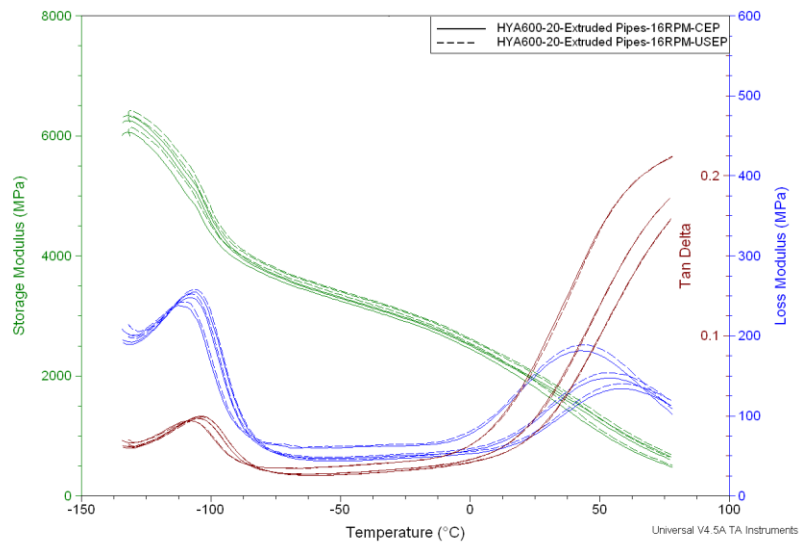
Figure C-59: DMA Results of 20%wt filled HYA600 pipes produced at 16rpm by both USEP and CEP methods the solid line represents CEP samples data and the dashed line is for USEP samples while for each set of data the curves from top to bottom represent data acquired at 1Hz, 5Hz and 10Hz respectively.
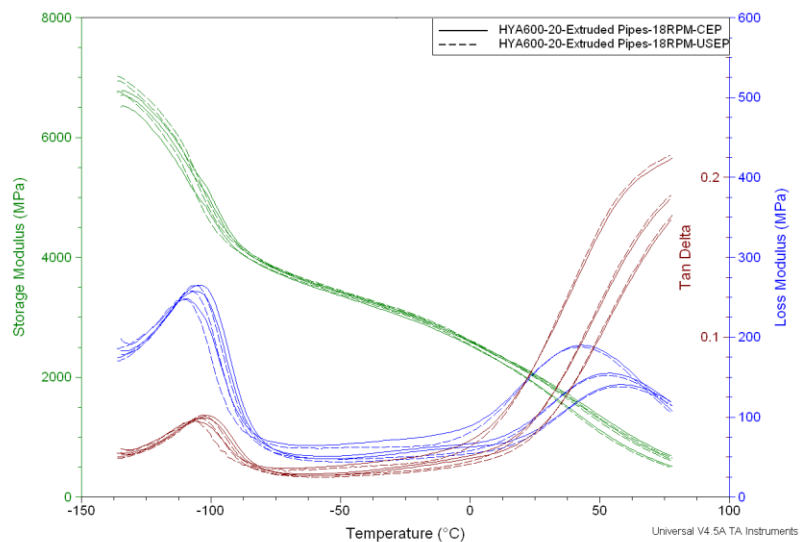
Figure C-60: DMA Results of 20%wt filled HYA600 pipes produced at 18rpm by both USEP and CEP methods the solid line represents CEP samples data and the dashed line is for USEP samples while for each set of data the curves from top to bottom represent data acquired at 1Hz, 5Hz and 10Hz respectively.
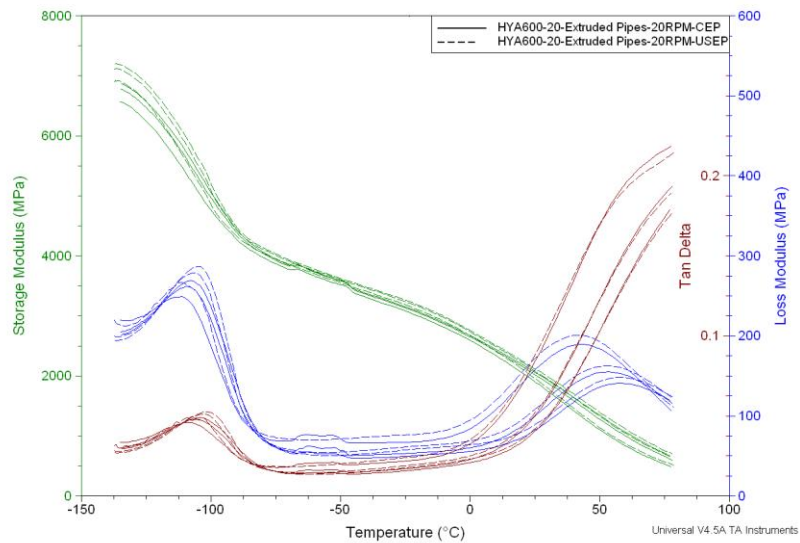
Figure C-61: DMA Results of 20%wt filled HYA600 pipes produced at 20rpm by both USEP and CEP methods the solid line represents CEP samples data and the dashed line is for USEP samples while for each set of data the curves from top to bottom represent data acquired at 1Hz, 5Hz and 10Hz respectively.
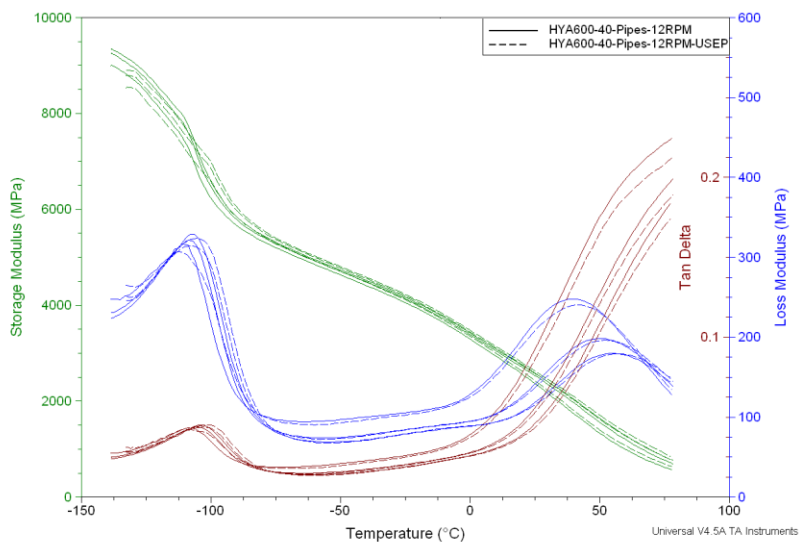
Figure C-62: DMA Results of 40%wt filled HYA600 pipes produced at 12rpm by both USEP and CEP methods the solid line represents CEP samples data and the dashed line is for USEP samples while for each set of data the curves from top to bottom represent data acquired at 1Hz, 5Hz and 10Hz respectively.
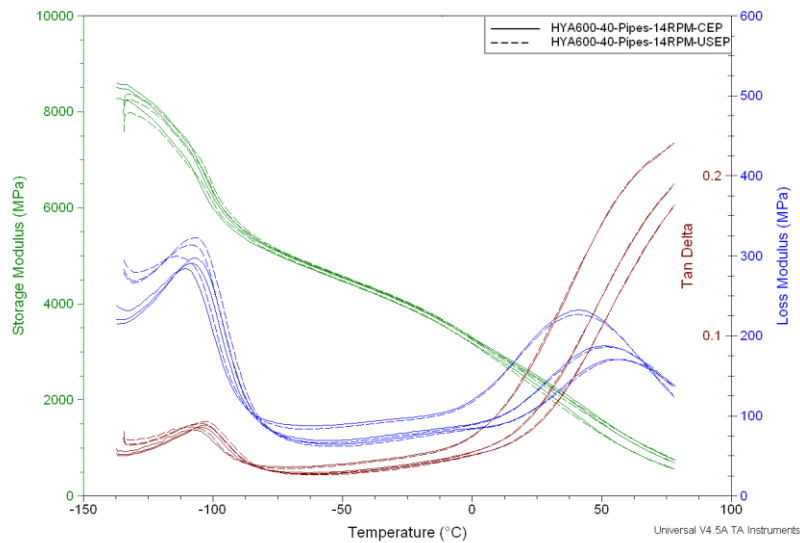
Figure C-63: DMA Results of 40%wt filled HYA600 pipes produced at 14rpm by both USEP and CEP methods the solid line represents CEP samples data and the dashed line is for USEP samples while for each set of data the curves from top to bottom represent data acquired at 1Hz, 5Hz and 10Hz respectively.
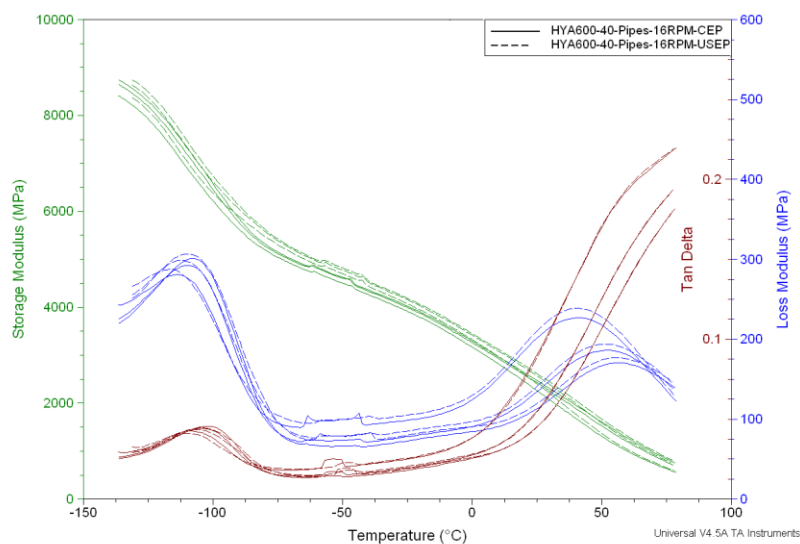
Figure C-64: DMA Results of 40%wt filled HYA600 pipes produced at 16rpm by both USEP and CEP methods the solid line represents CEP samples data and the dashed line is for USEP samples while for each set of data the curves from top to bottom represent data acquired at 1Hz, 5Hz and 10Hz respectively.
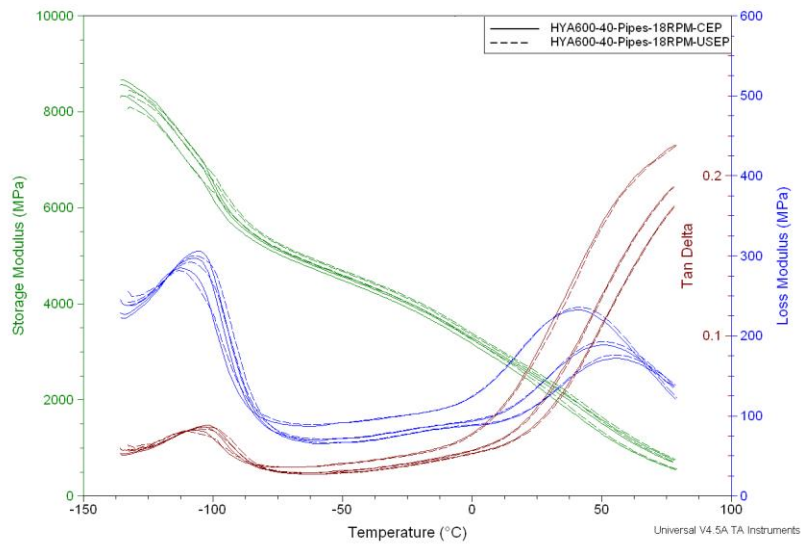
Figure C-65: DMA Results of 40%wt filled HYA600 pipes produced at 18rpm by both USEP and CEP methods the solid line represents CEP samples data and the dashed line is for USEP samples while for each set of data the curves from top to bottom represent data acquired at 1Hz, 5Hz and 10Hz respectively.
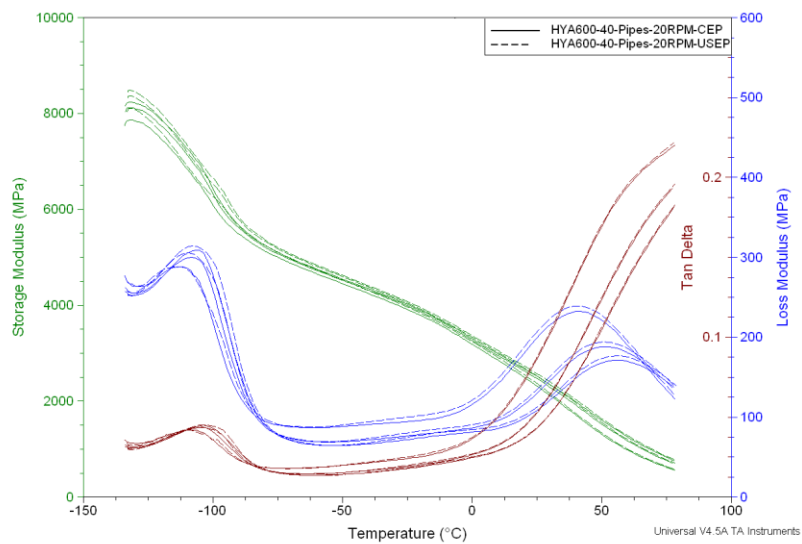
Figure C-66: DMA Results of 40%wt filled HYA600 pipes produced at 20rpm by both USEP and CEP methods the solid line represents CEP samples data and the dashed line is for USEP samples while for each set of data the curves from top to bottom represent data acquired at 1Hz, 5Hz and 10Hz respectively.

IV. DSC Results
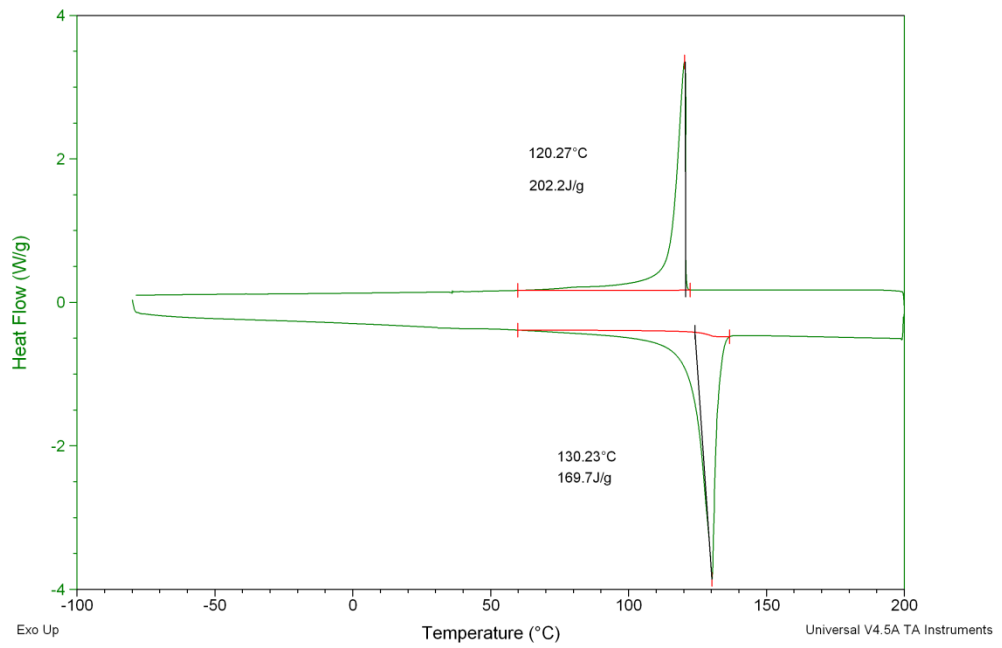
Figure C-67: DSC heat flow vs. temperature curve for Rigidex5130 strips produced at 8rpm without presence of ultrasound.
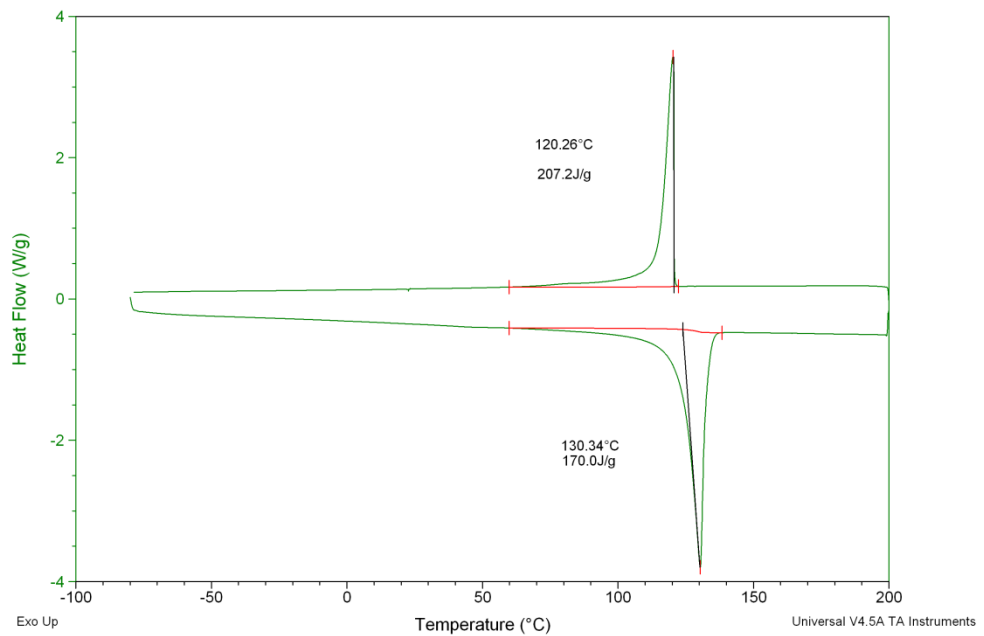
Figure C-68: DSC heat flow vs. temperature curve for Rigidex5130 strips produced at 12rpm without presence of ultrasound.
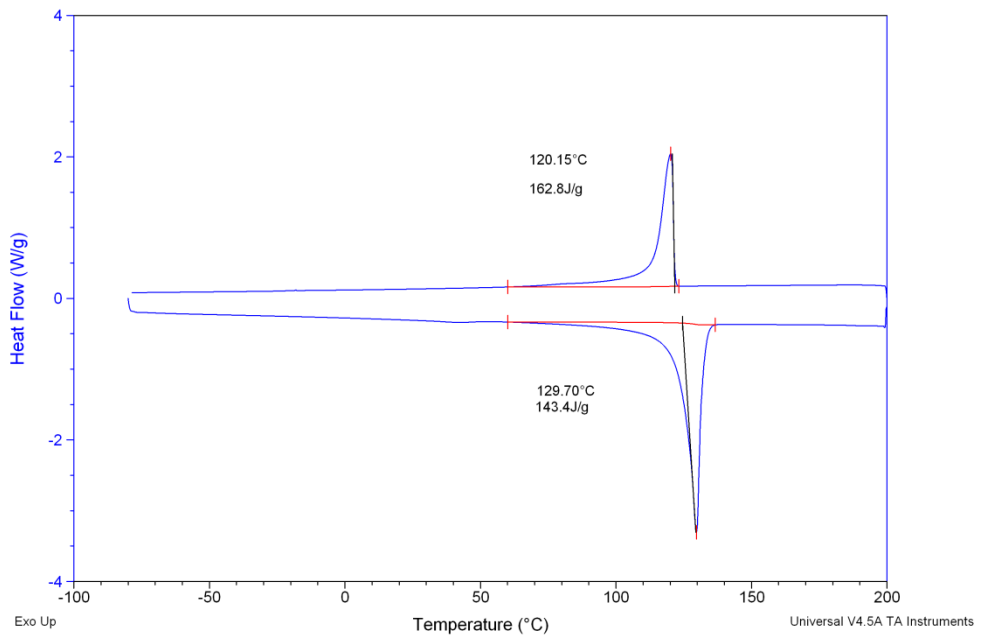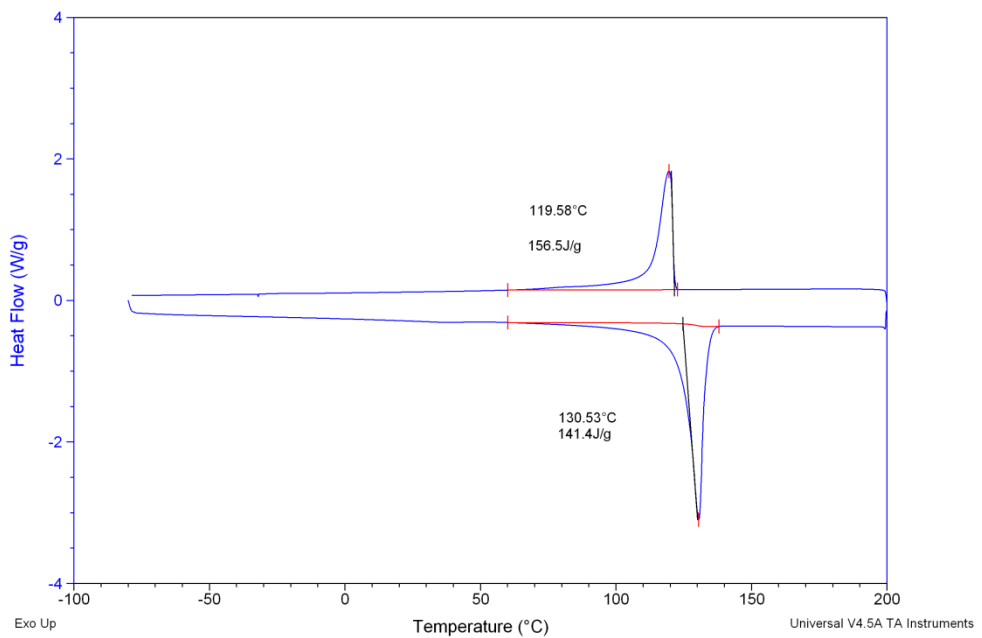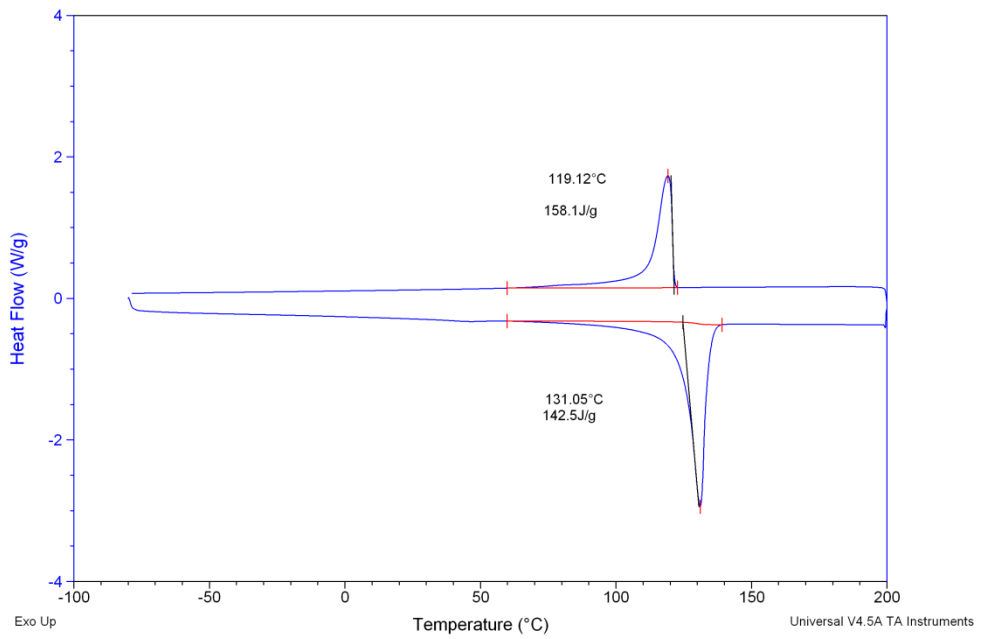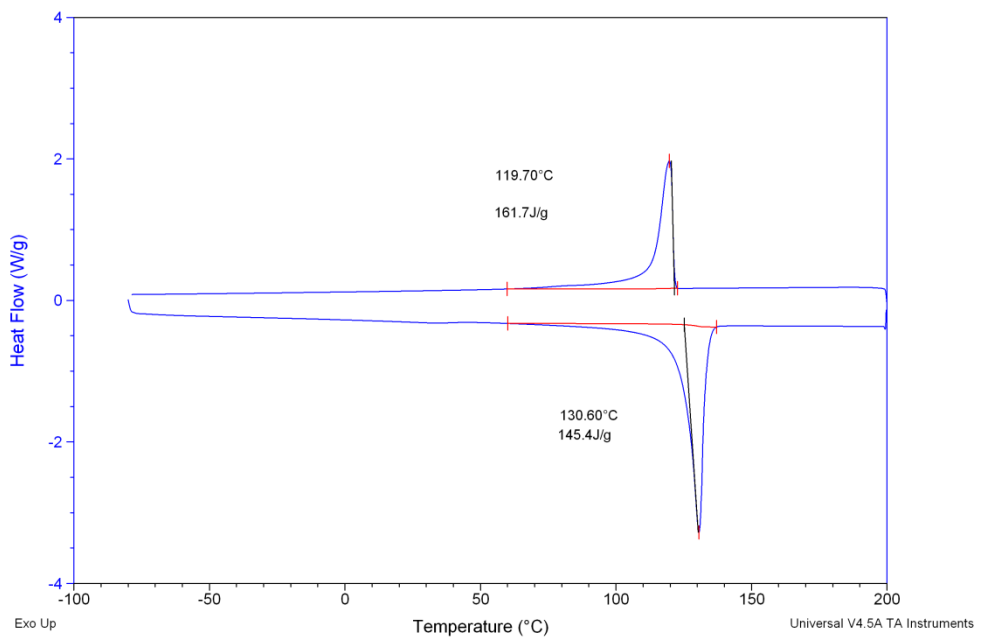
271
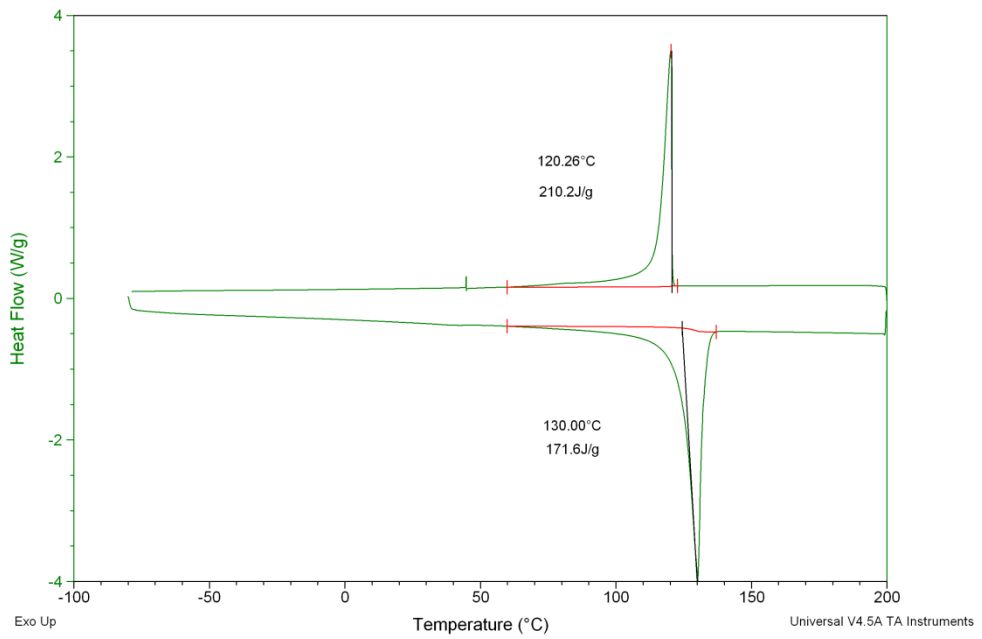
Figure C-69: DSC heat flow vs. temperature curve for Rigidex5130 strips produced at 16rpm without presence of ultrasound.
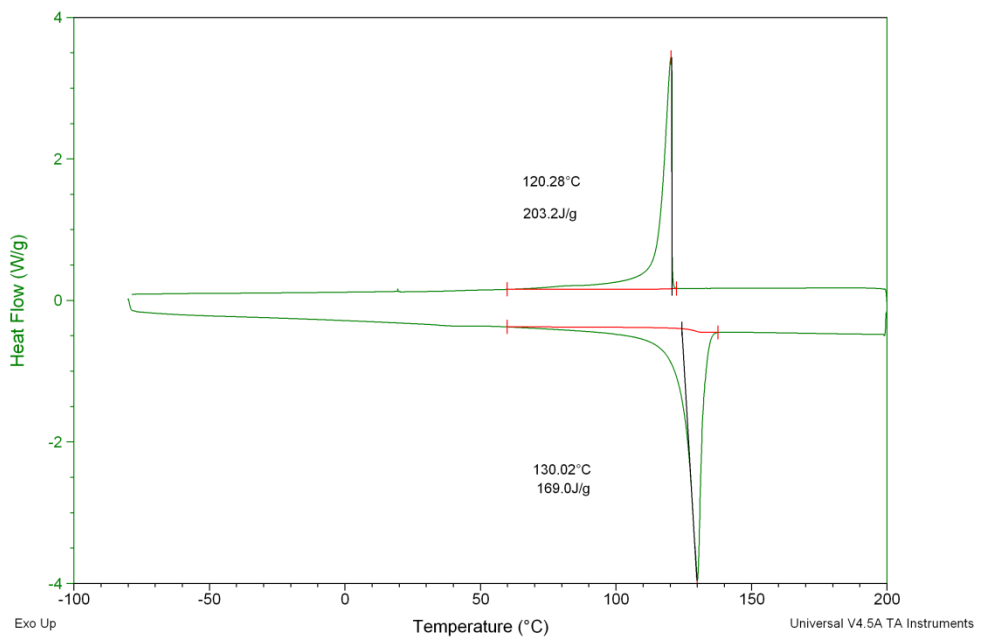
Figure C-70: DSC heat flow vs. temperature curve for Rigidex5130 strips produced at 20rpm without presence of ultrasound.
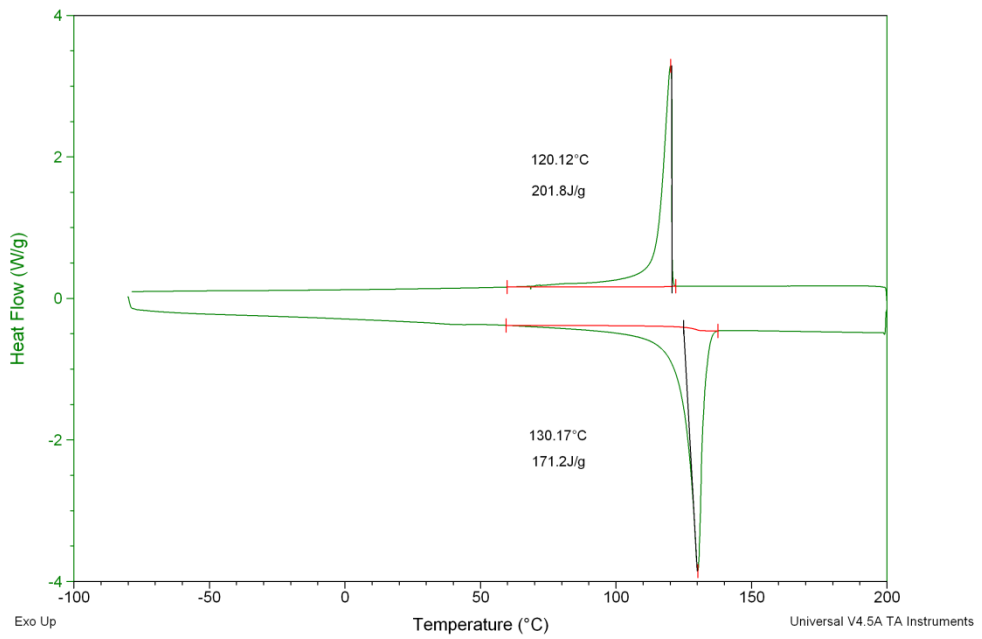
Figure C-71: DSC heat flow vs. temperature curve for Rigidex5130 strips produced at 24rpm without presence of ultrasound.
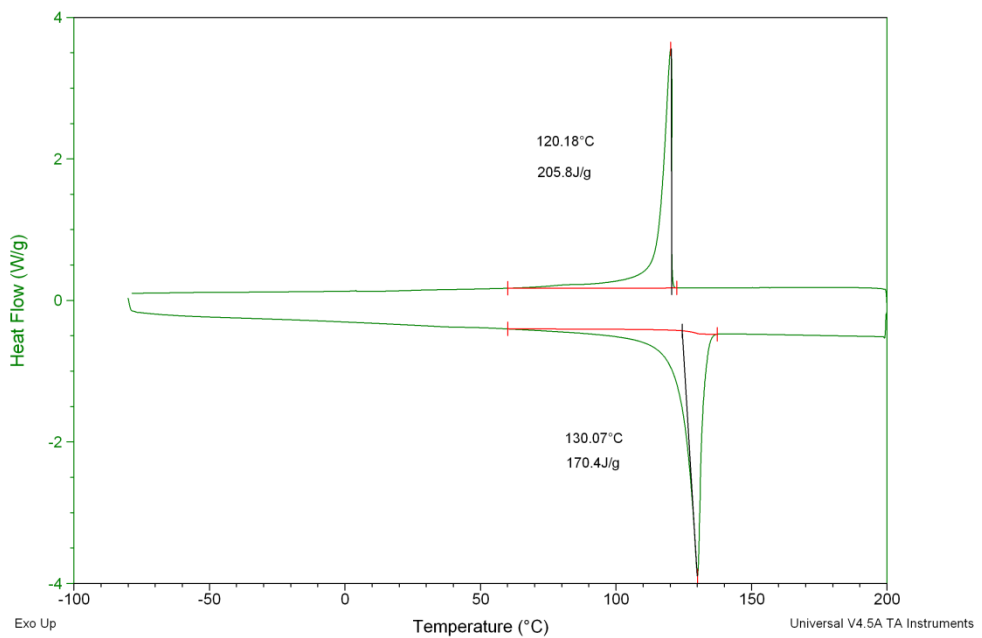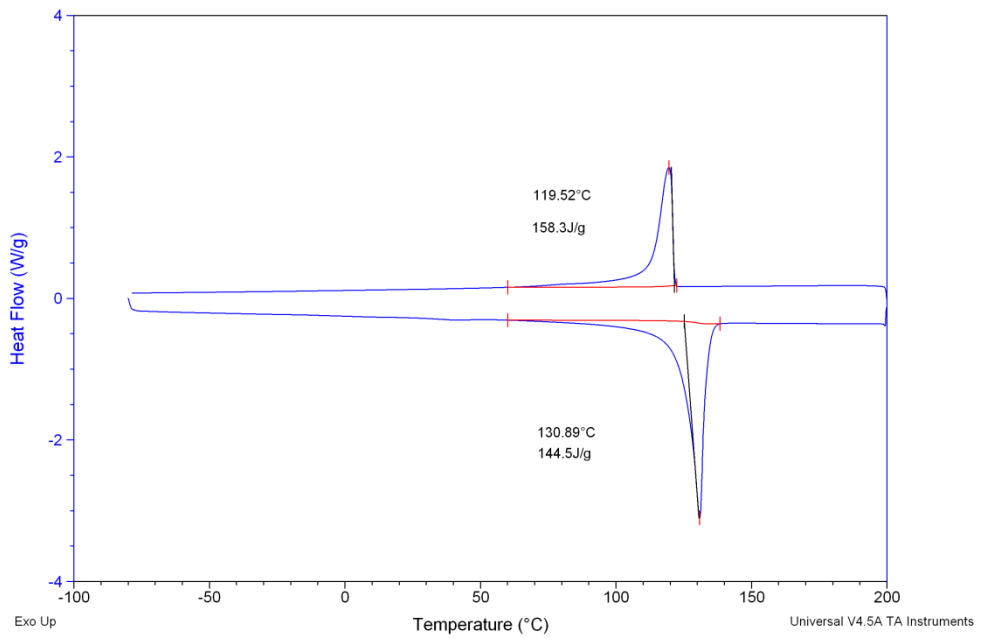

Figure C-72: DSC heat flow vs. temperature curve for Rigidex5130 strips produced at 8rpm with presence of ultrasound.
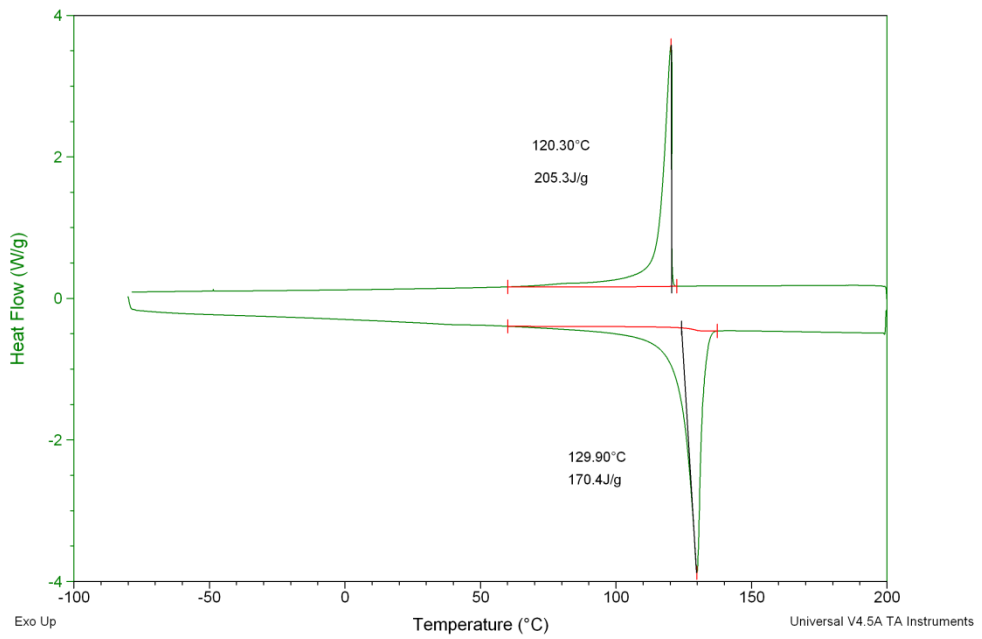
Figure C-73: DSC heat flow vs. temperature curve for Rigidex5130 strips produced at 12rpm with presence of ultrasound.
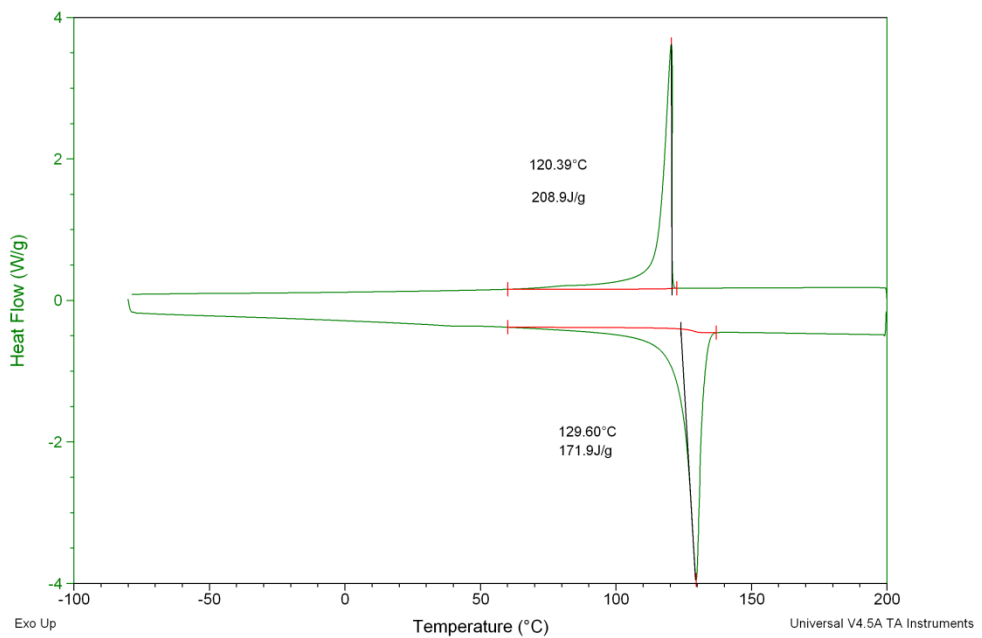
Figure C-74: DSC heat flow vs. temperature curve for Rigidex5130 strips produced at 16rpm with presence of ultrasound.
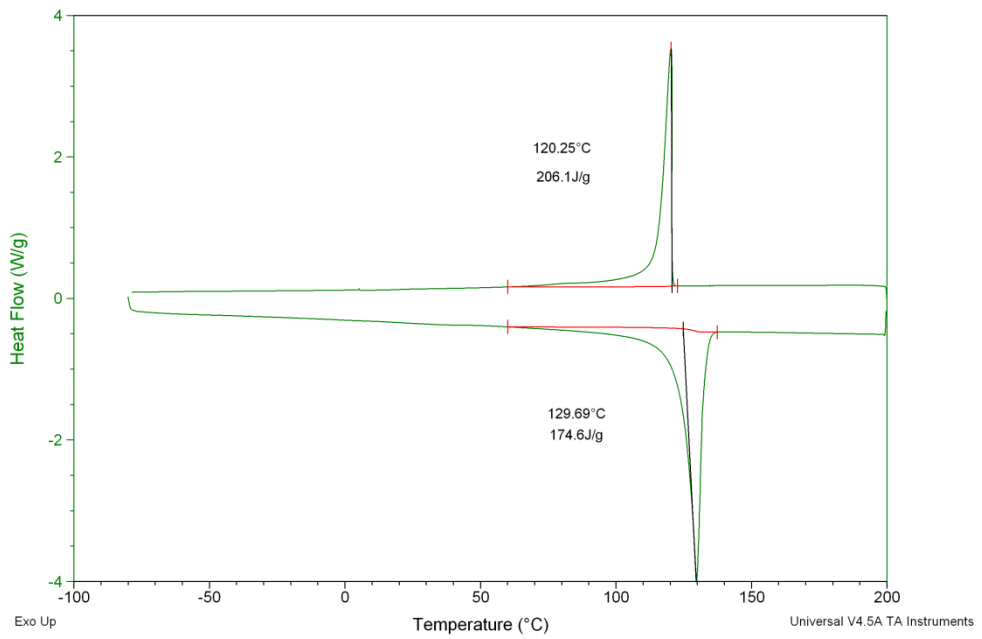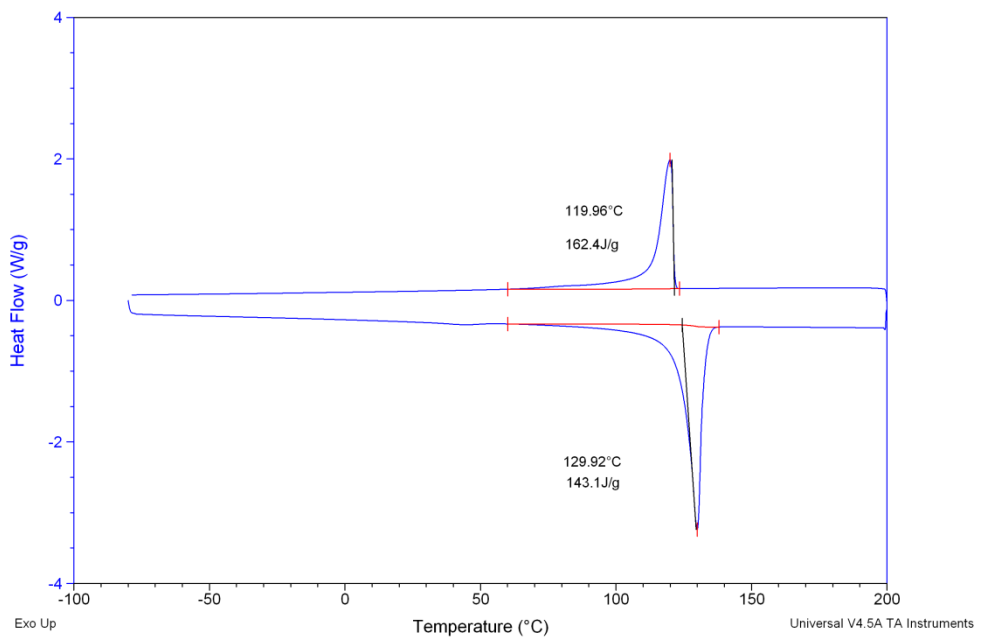
Figure C-75: DSC heat flow vs. temperature curve for Rigidex5130 strips produced at 20rpm with presence of ultrasound.
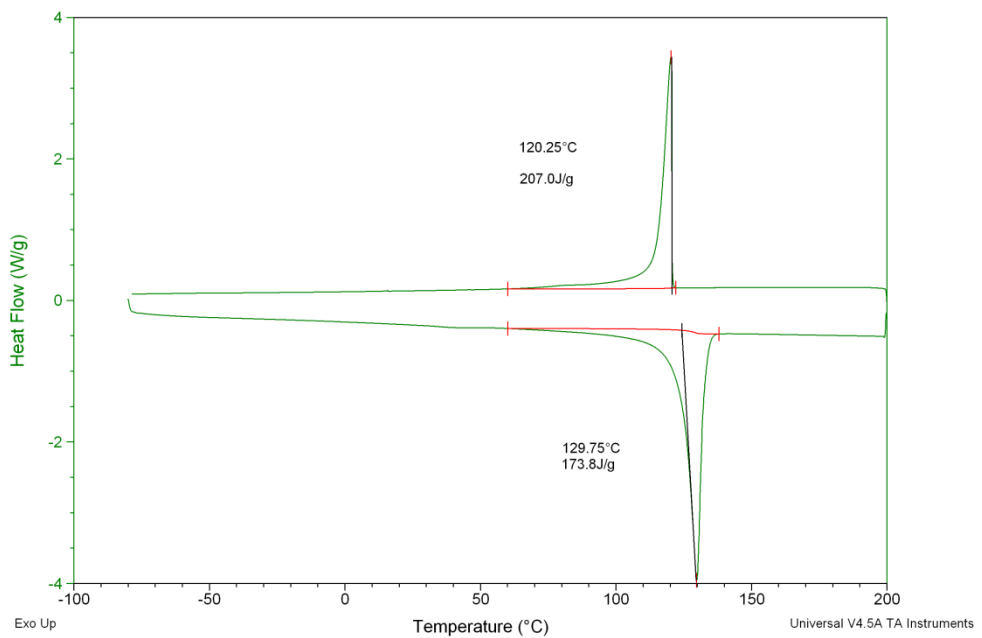
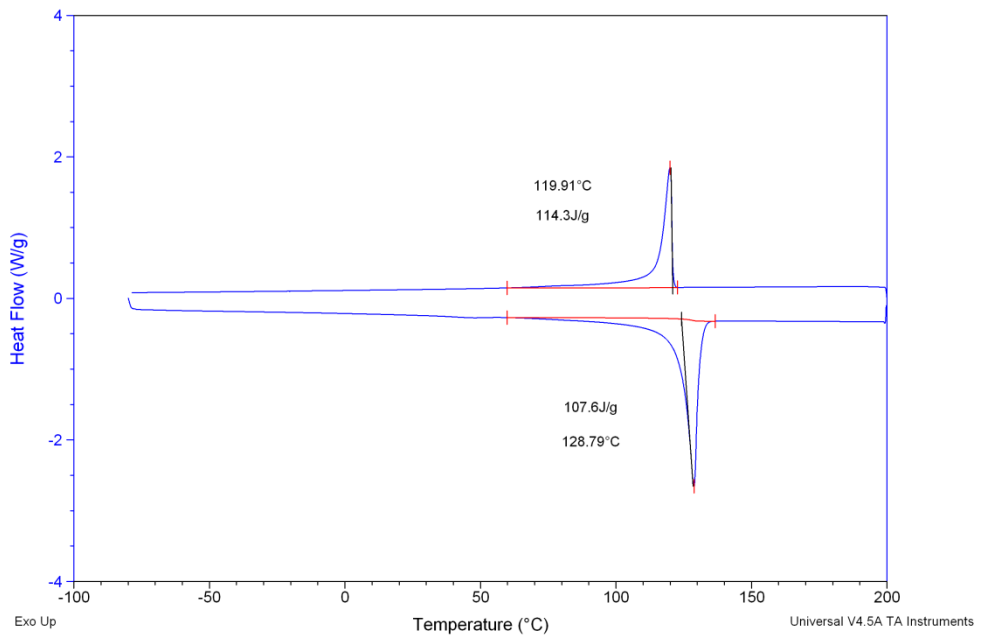**Figure C-76: DSC heat flow vs. temperature curve for Rigidex5130 strips produced at 24rpm with presence of ultrasound.**
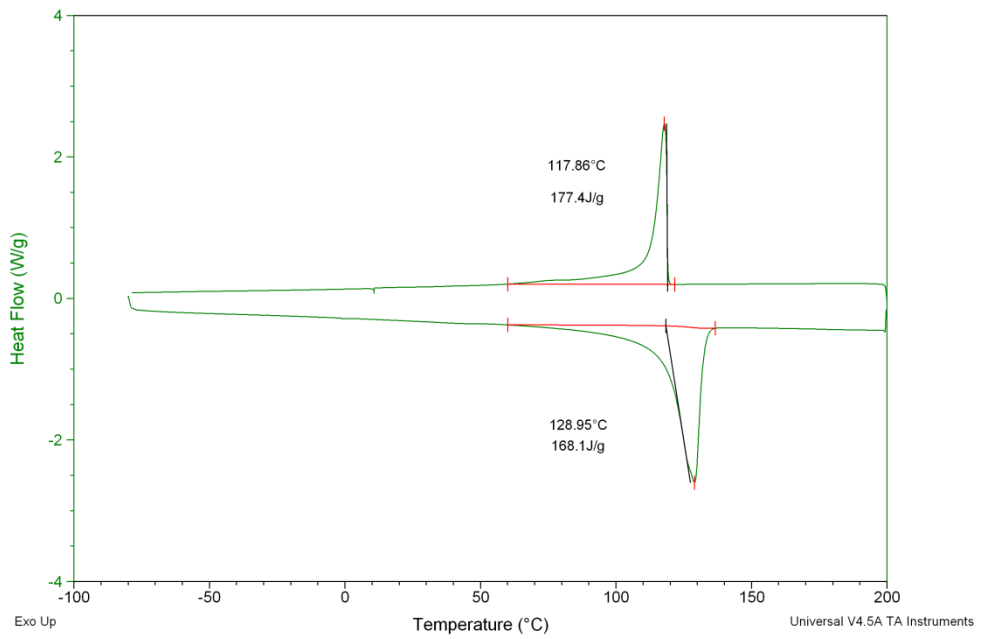
Figure C-77: DSC heat flow vs. temperature curve for PE80 strips produced at 8rpm without presence of ultrasound.
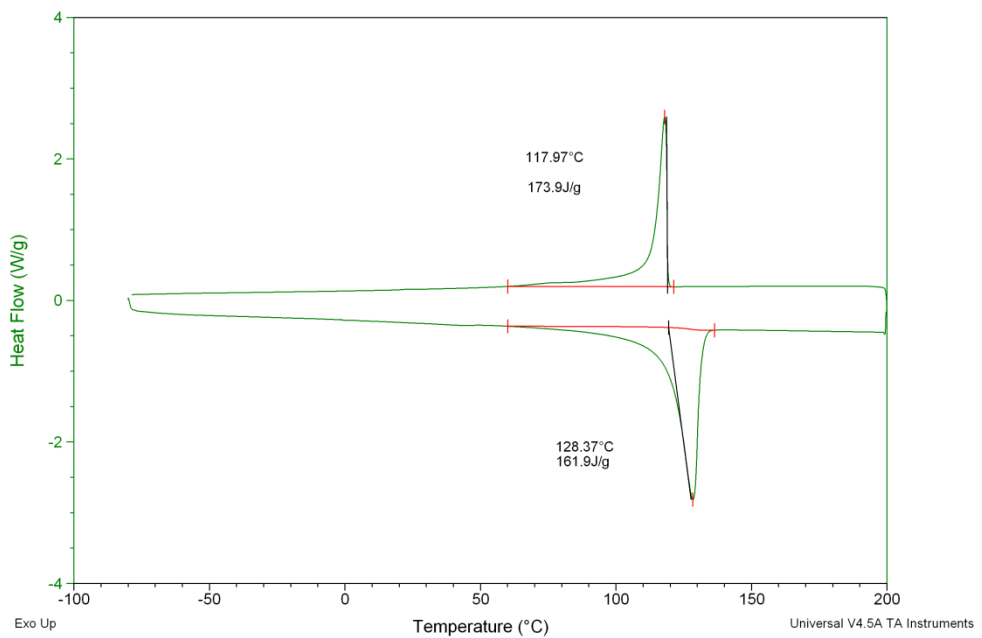
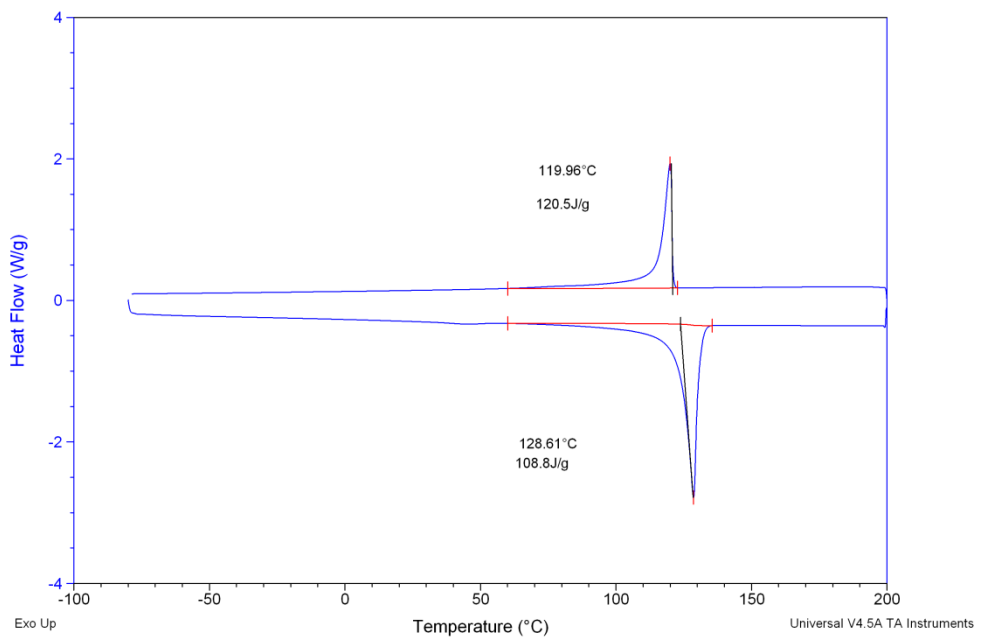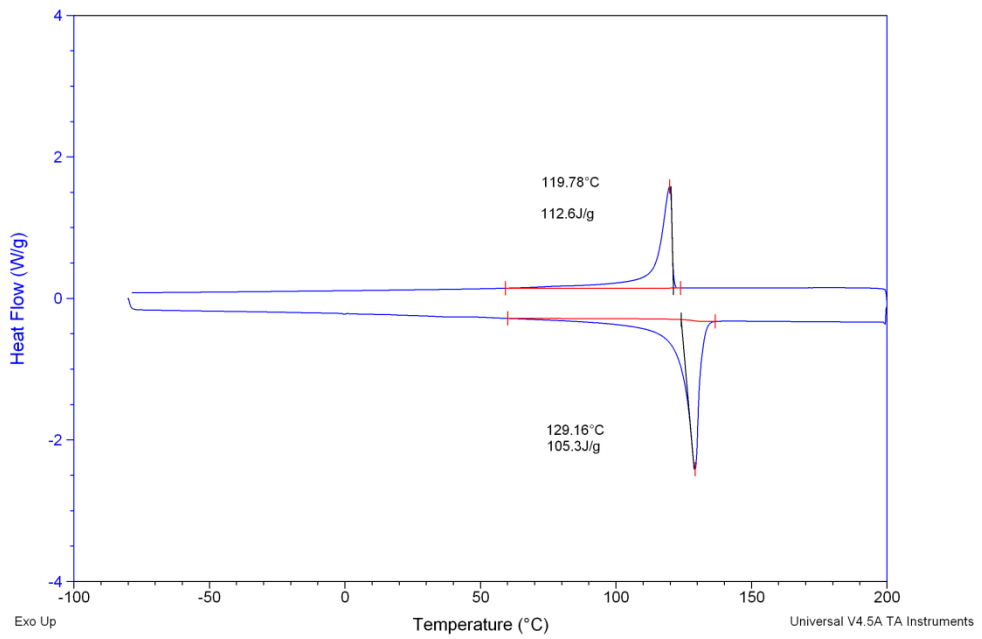**Figure C-78: DSC heat flow vs. temperature curve for PE80 strips produced at 12rpm without presence of ultrasound.**
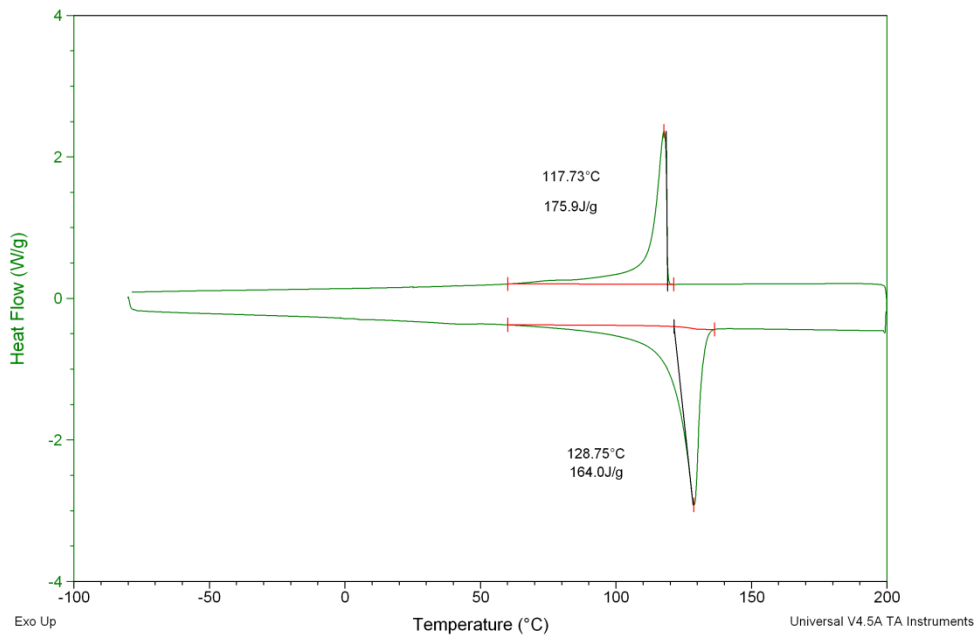
Figure C-79: DSC heat flow vs. temperature curve for PE80 strips produced at 16rpm without presence of ultrasound.
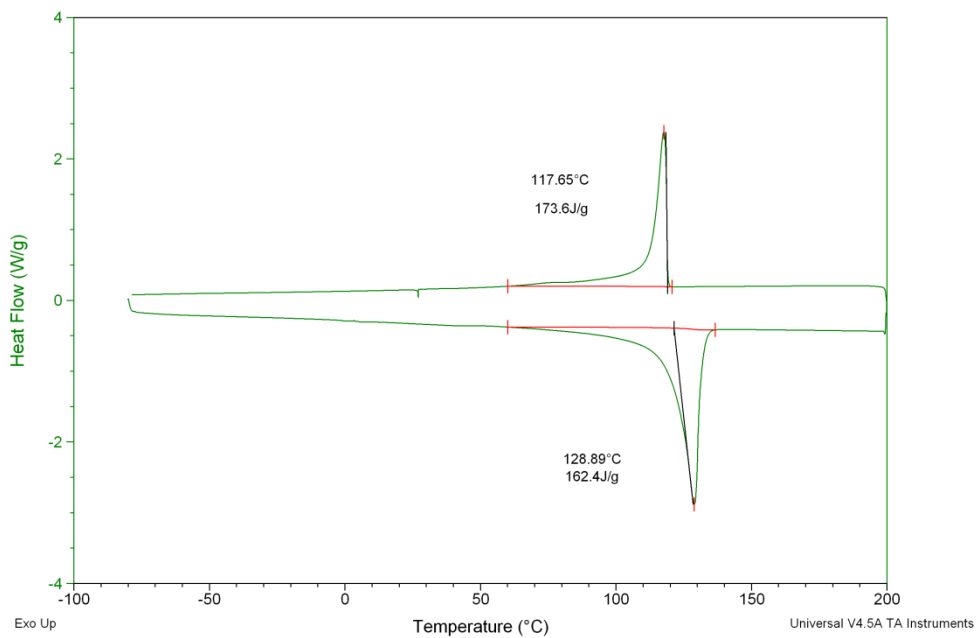
Figure C-80: DSC heat flow vs. temperature curve for PE80 strips produced at 20rpm without presence of ultrasound.
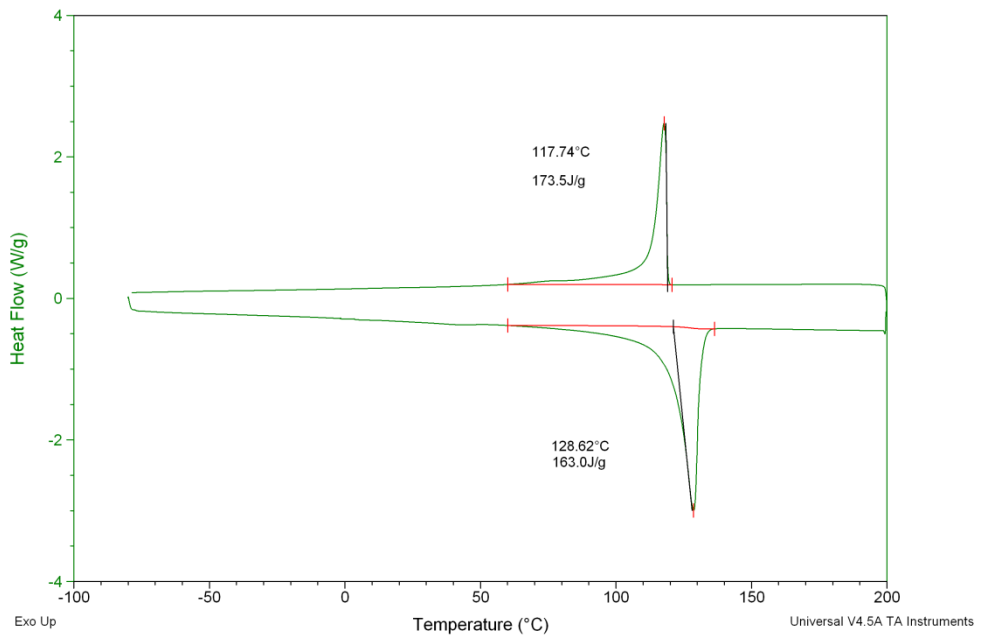
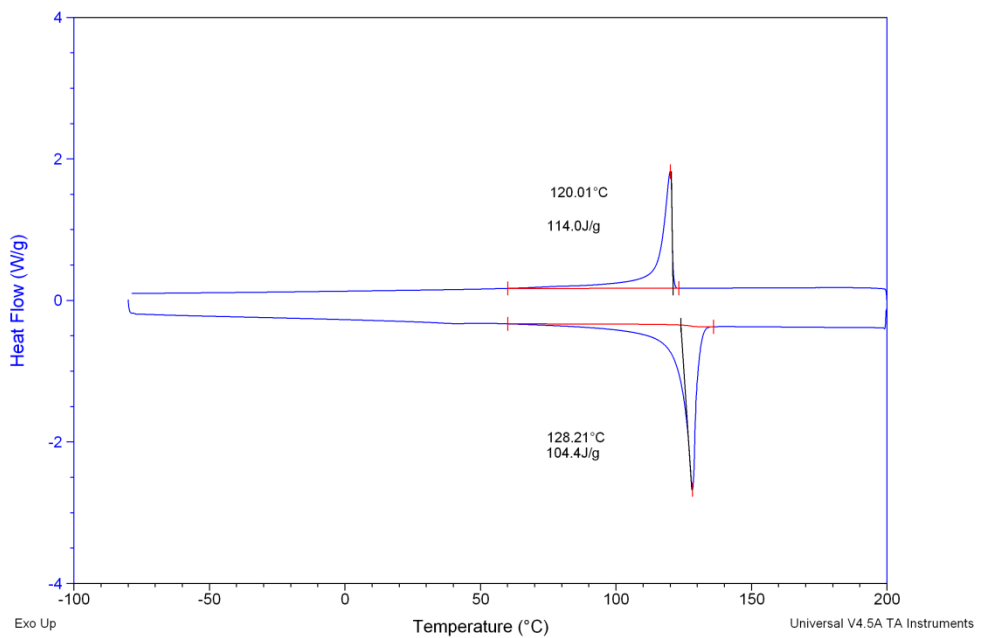**Figure C-81: DSC heat flow vs. temperature curve for PE80 strips produced at 24rpm without presence of ultrasound.**
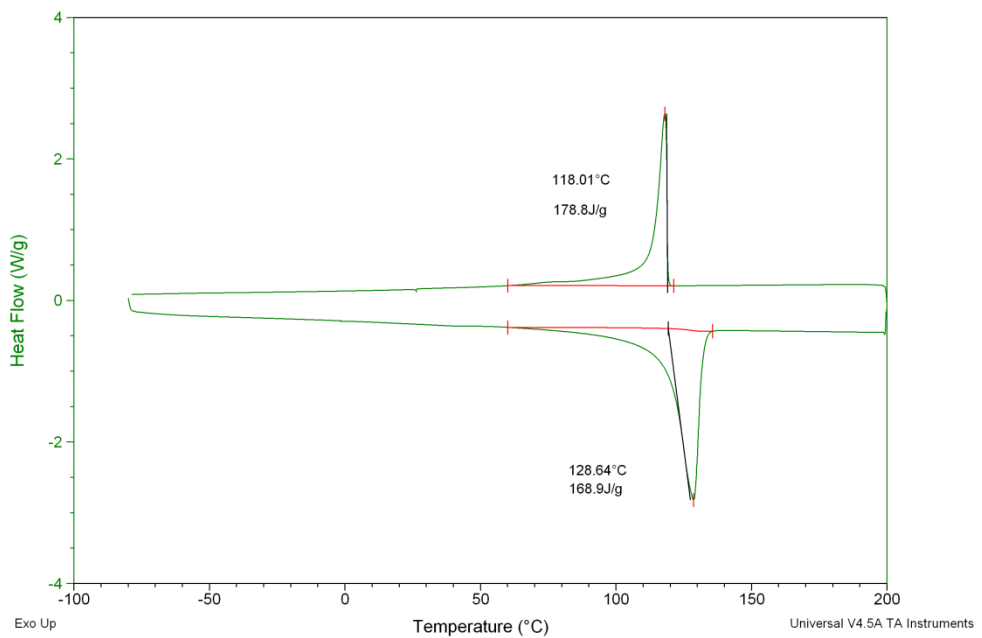
Figure C-82: DSC heat flow vs. temperature curve for PE80 strips produced at 8rpm with presence of ultrasound.
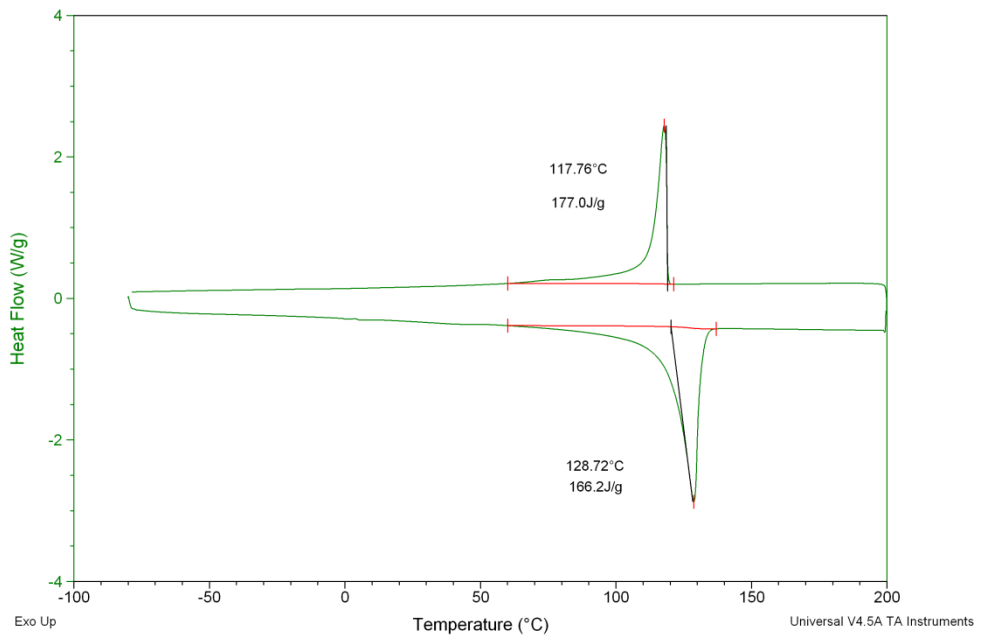
Figure C-83: DSC heat flow vs. temperature curve for PE80 strips produced at 12rpm with presence of ultrasound.
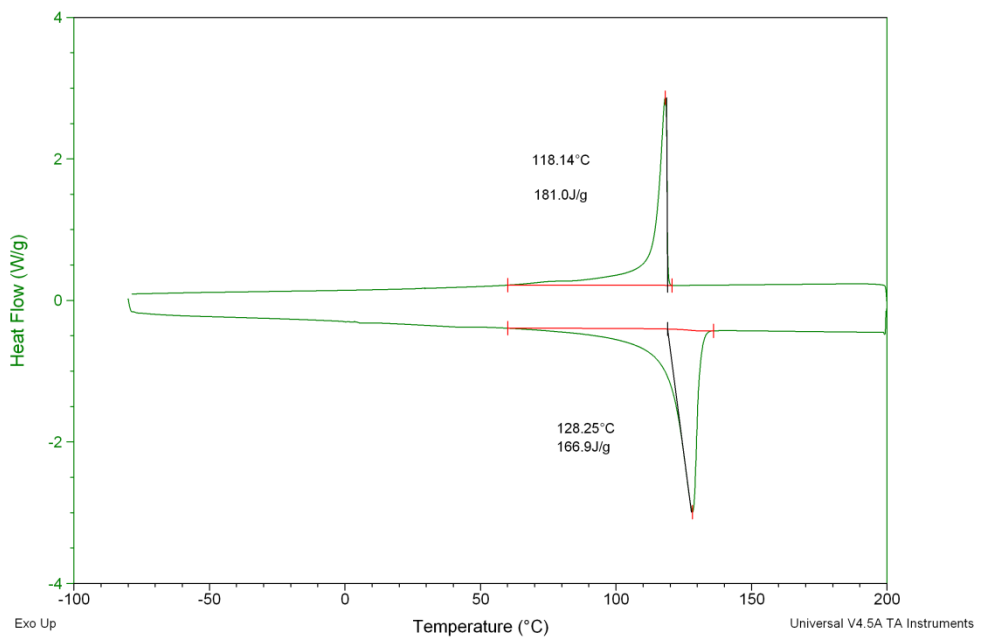
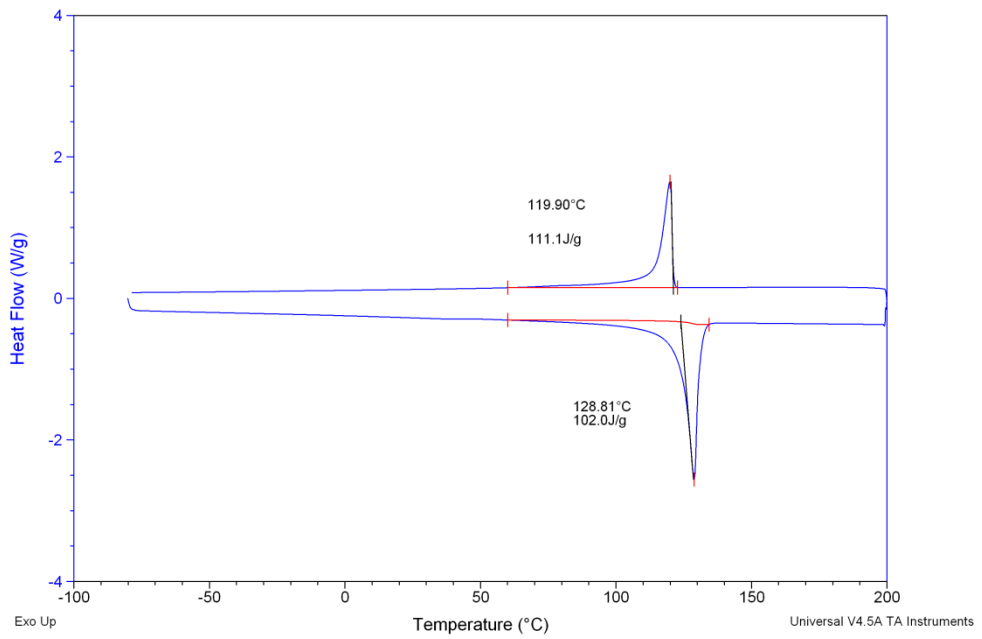**Figure C-84: DSC heat flow vs. temperature curve for PE80 strips produced at 16rpm with presence of ultrasound.**
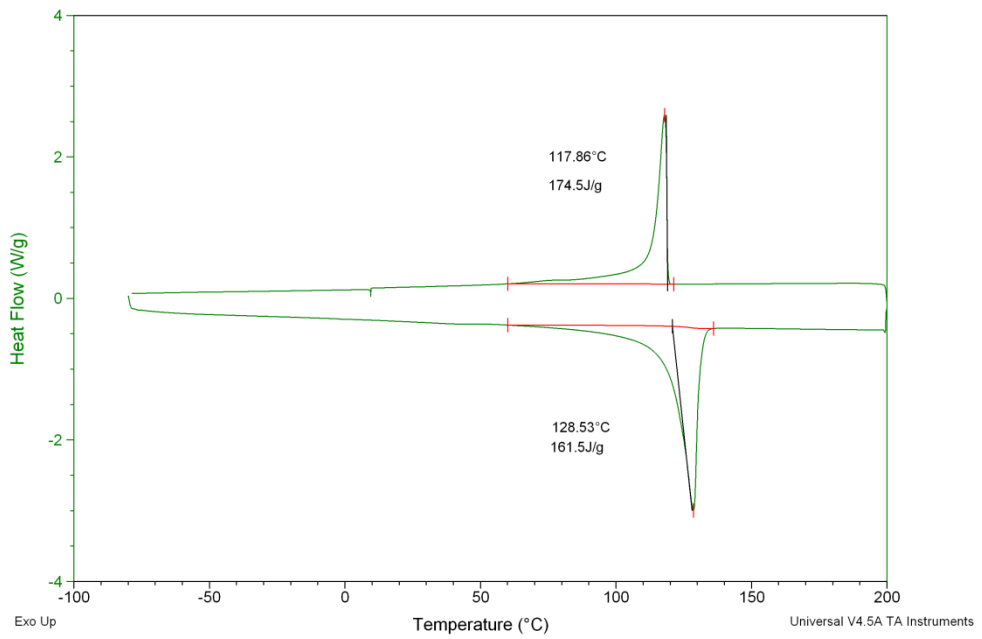
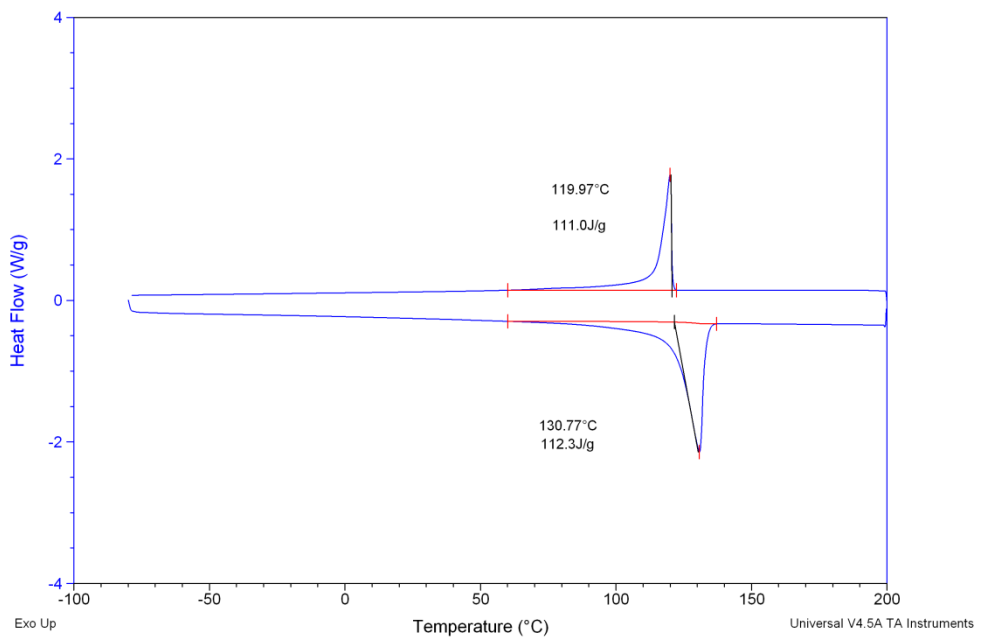**Figure C-85: DSC heat flow vs. temperature curve for PE80 strips produced at 20rpm with presence of ultrasound.**
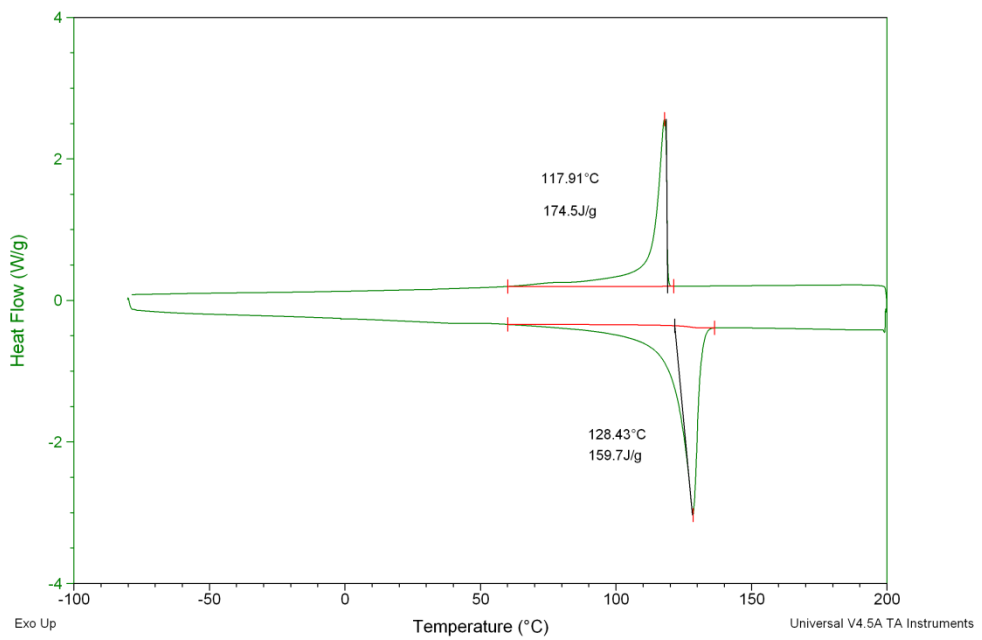
Figure C-86: DSC heat flow vs. temperature curve for PE80 strips produced at 24rpm with presence of ultrasound.
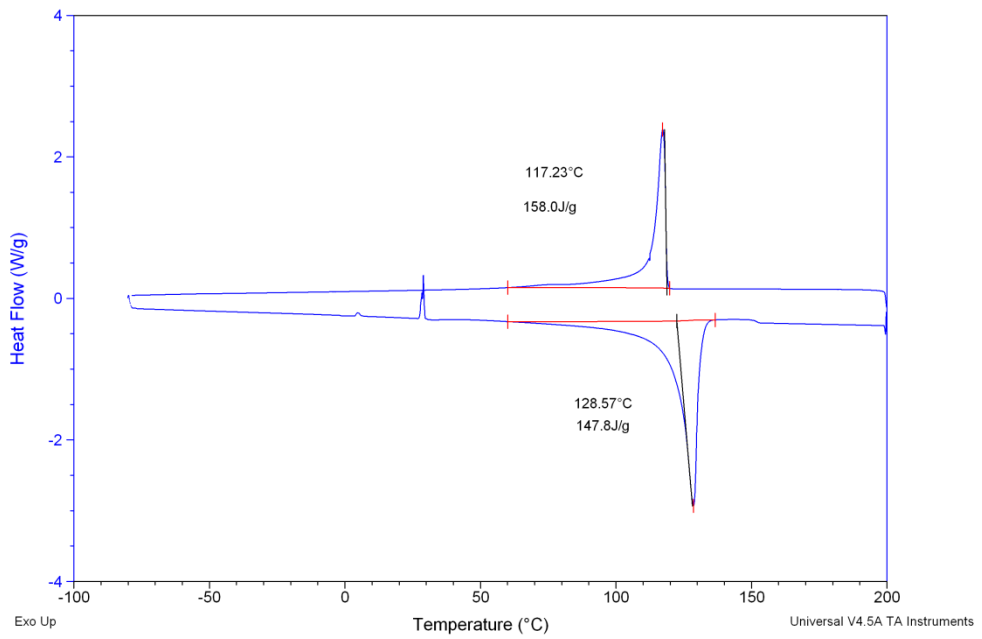
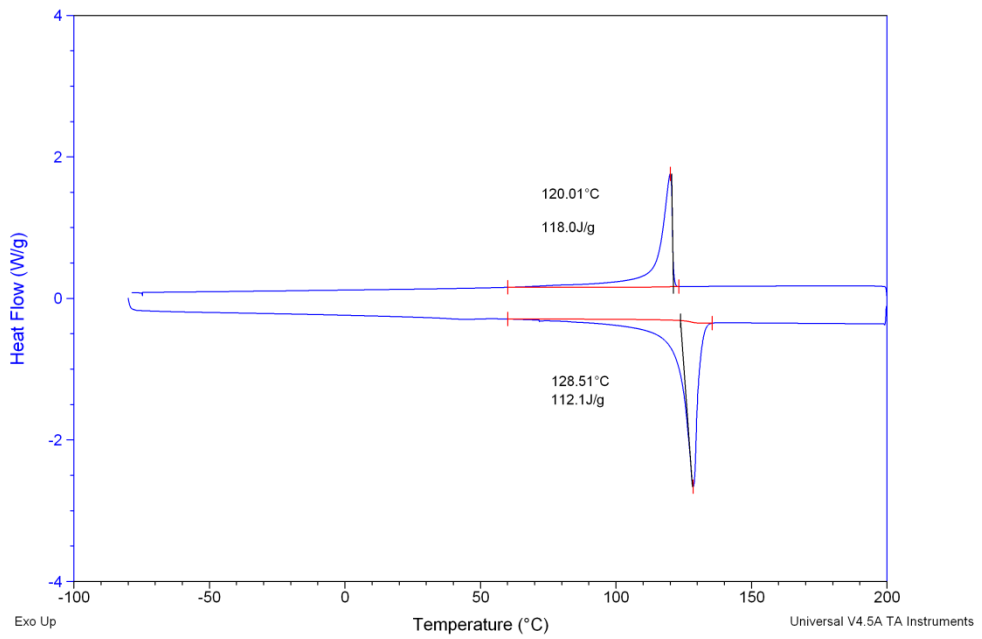**Figure C-87: DSC heat flow vs. temperature curve for PE80 pipes produced at 12rpm without presence of ultrasound.**
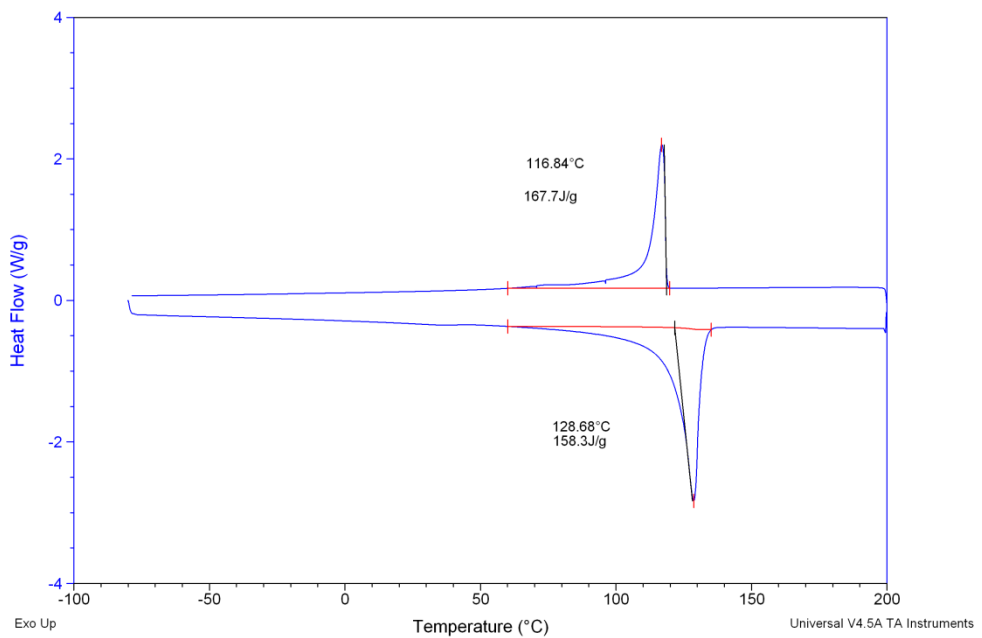
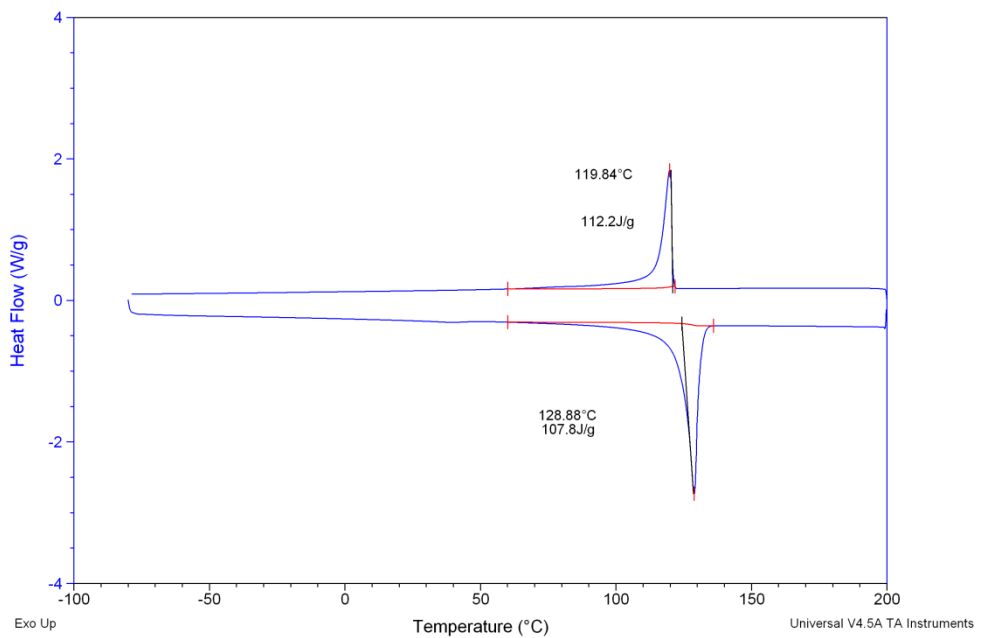**Figure C-88: DSC heat flow vs. temperature curve for PE80 pipes produced at 14rpm without presence of ultrasound.**
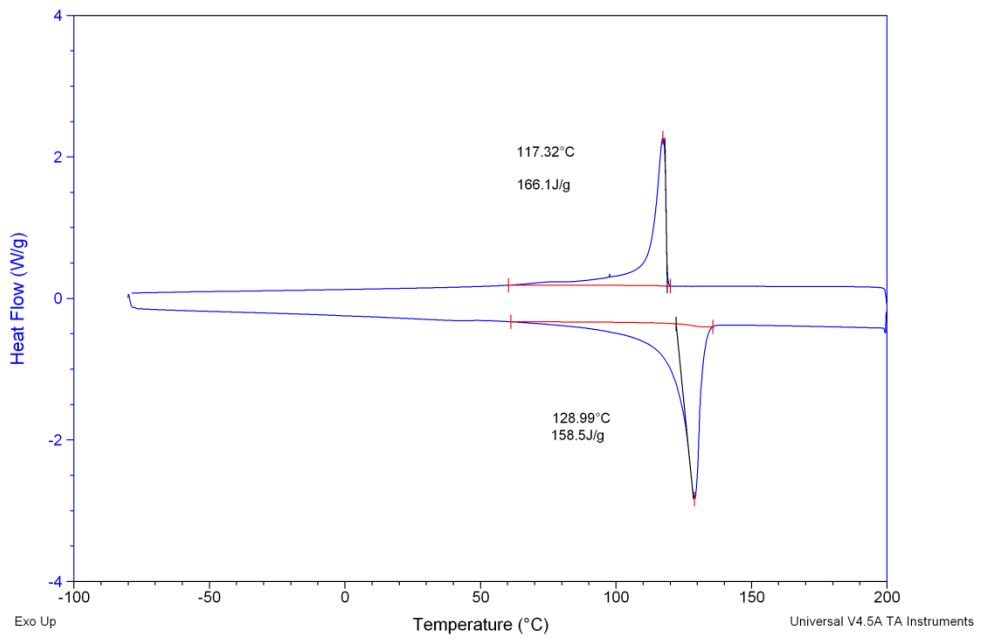
Figure C-89: DSC heat flow vs. temperature curve for PE80 pipes produced at 16rpm without presence of ultrasound.
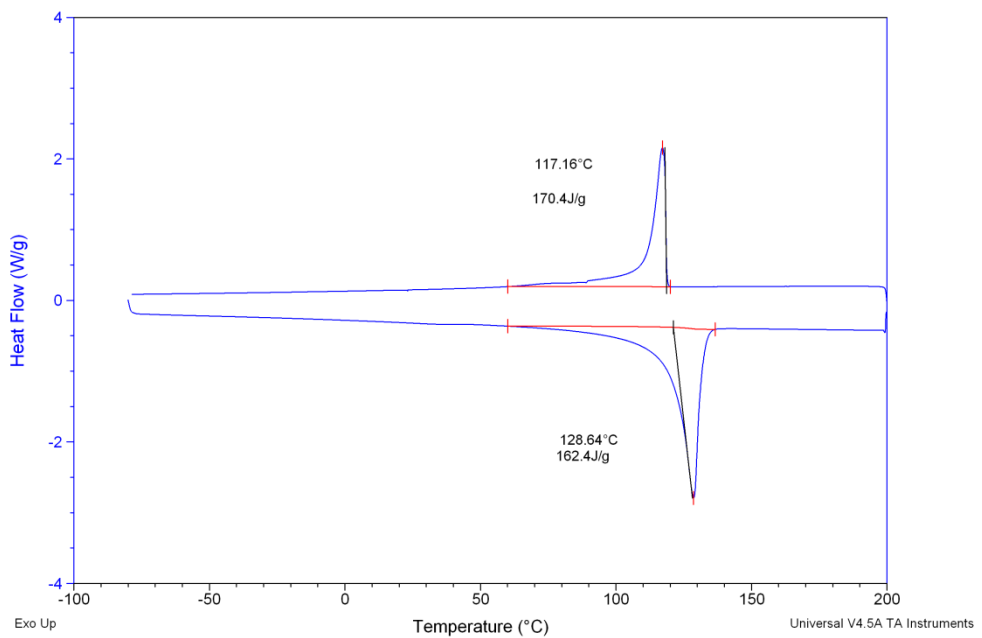
Figure C-90: DSC heat flow vs. temperature curve for PE80 pipes produced at 18rpm without presence of ultrasound.
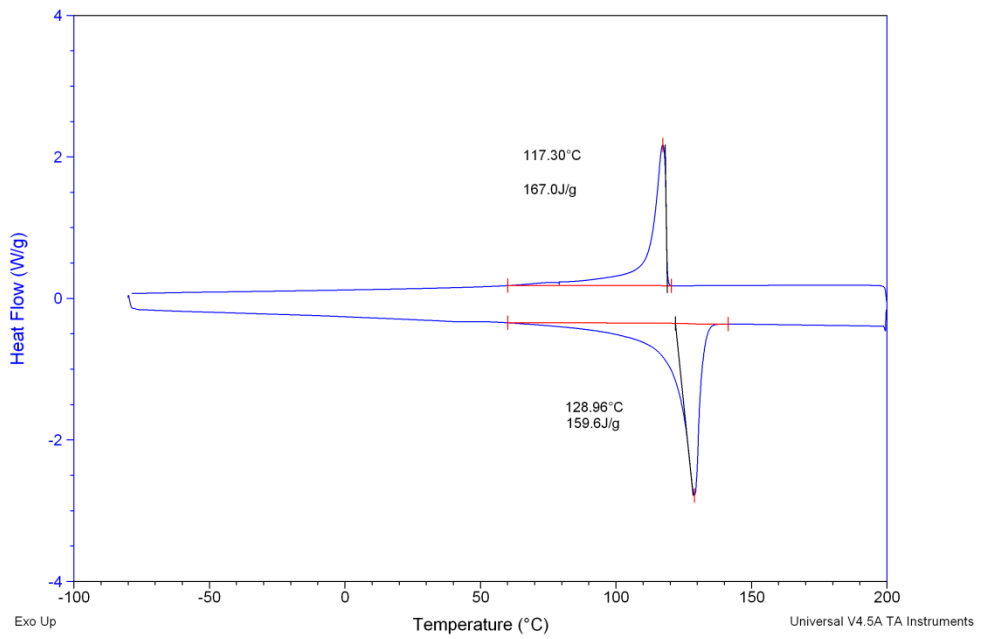
Figure C-91: DSC heat flow vs. temperature curve for PE80 pipes produced at 20rpm without presence of ultrasound.
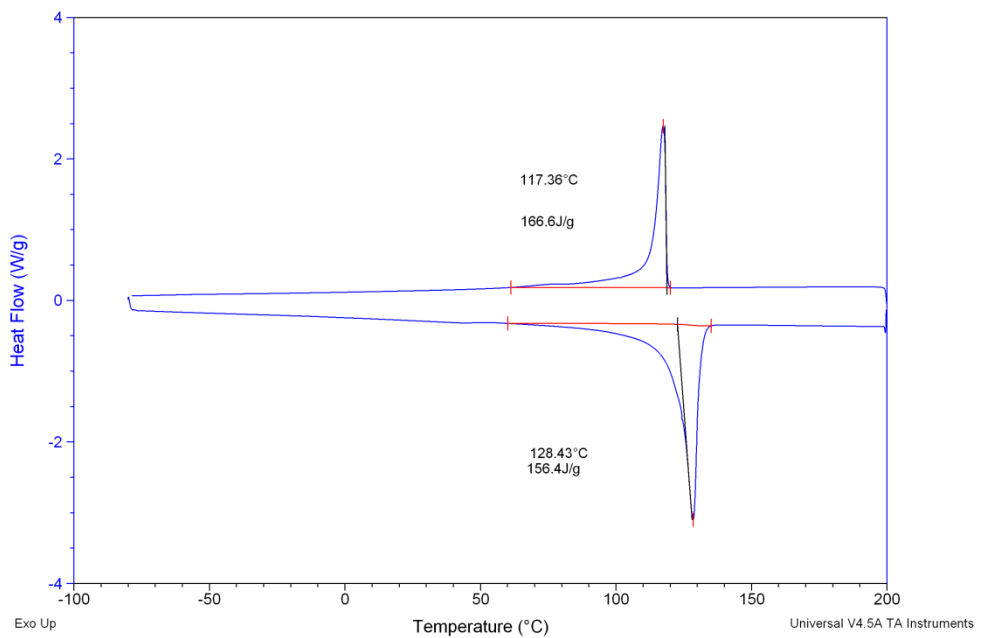
Figure C-92: DSC heat flow vs. temperature curve for PE80 pipes produced at 12rpm with presence of ultrasound.
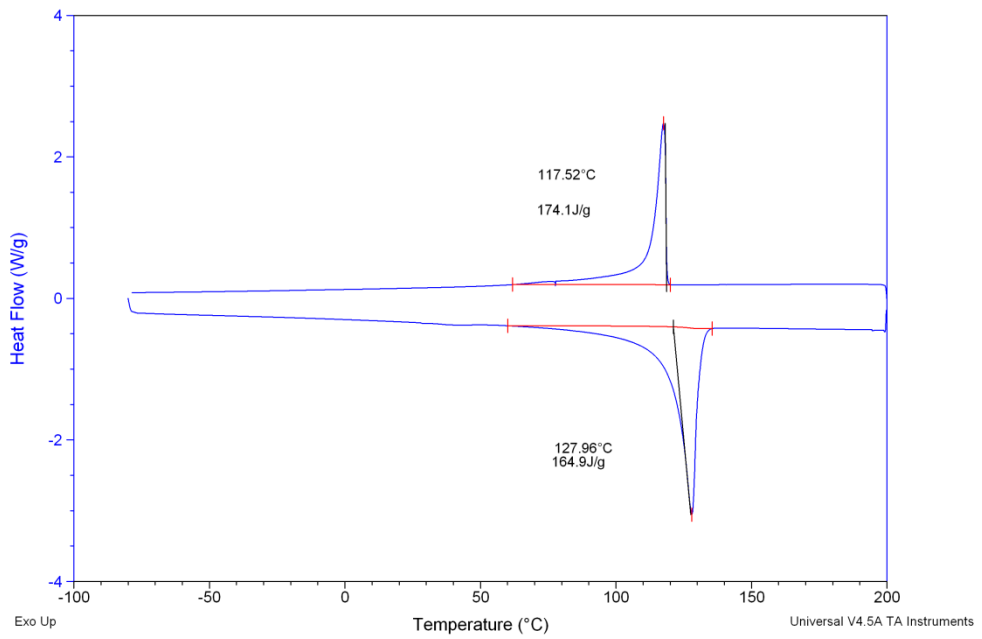
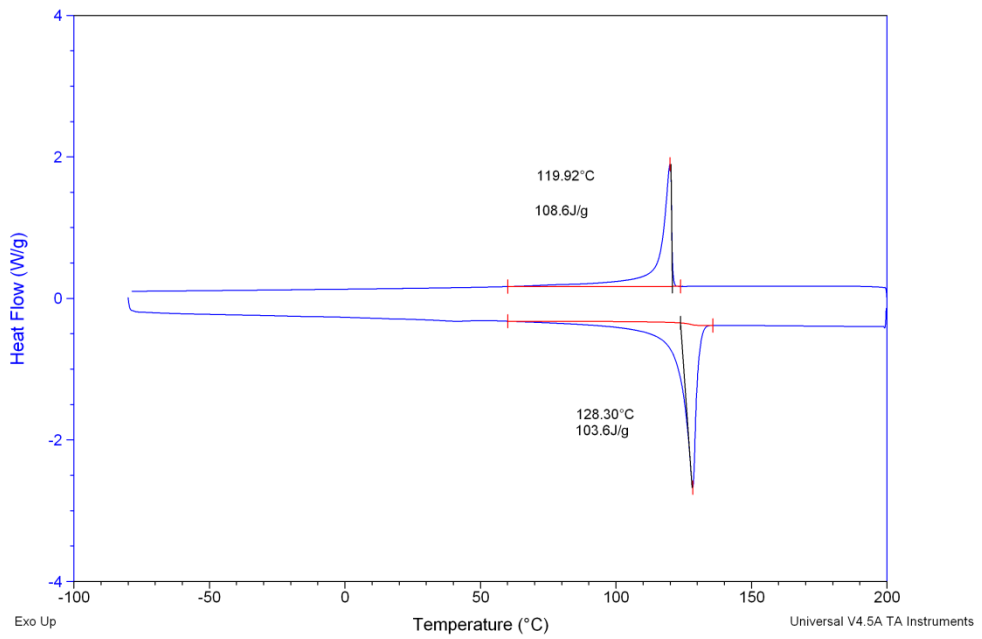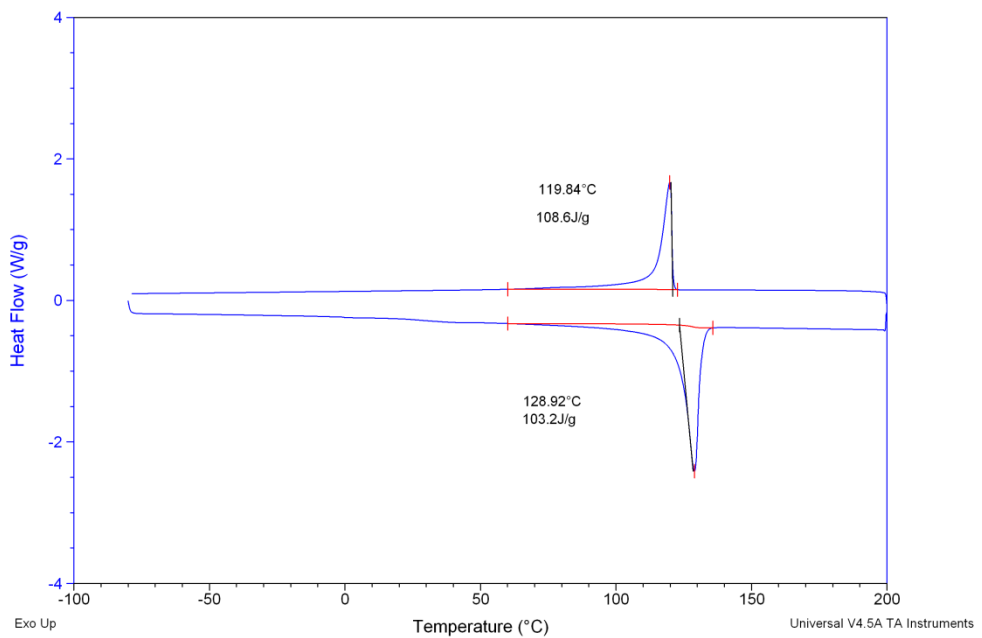**Figure C-93: DSC heat flow vs. temperature curve for PE80 pipes produced at 14rpm with presence of ultrasound.**
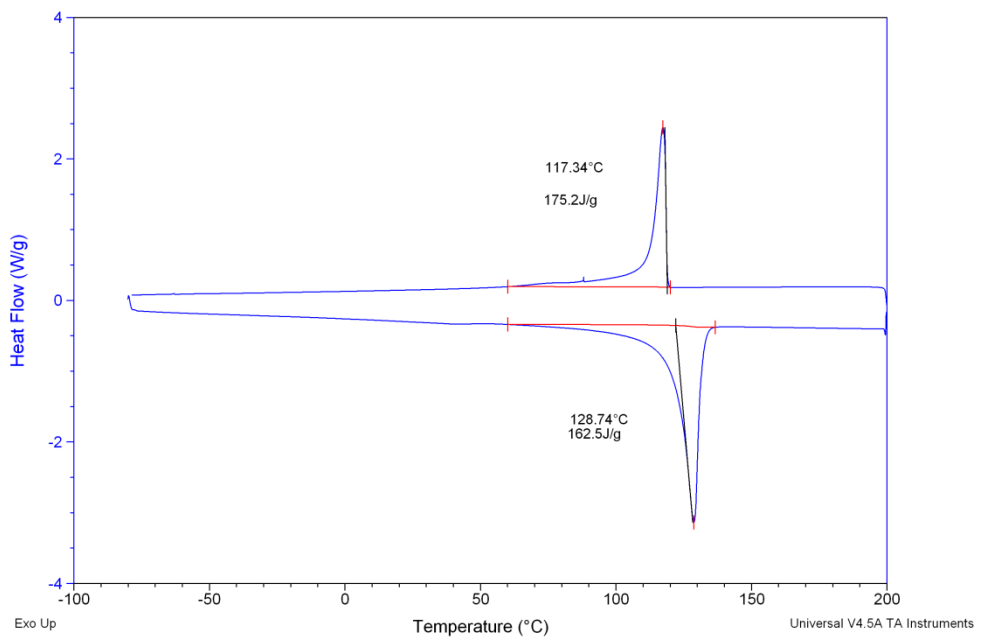
Figure C-94: DSC heat flow vs. temperature curve for PE80 pipes produced at 16rpm with presence of ultrasound.
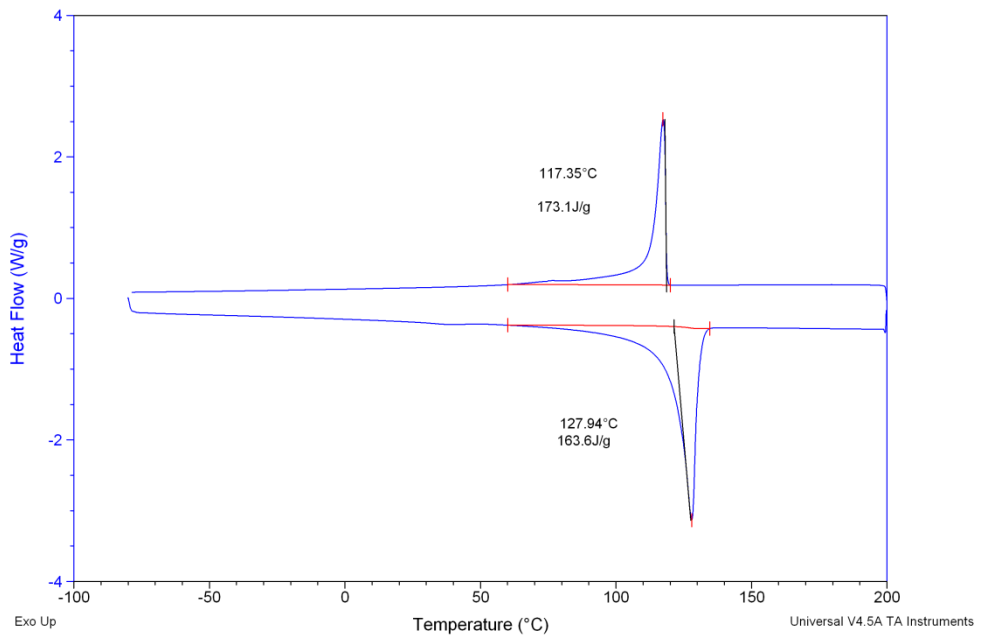
Figure C-95: DSC heat flow vs. temperature curve for PE80 pipes produced at 18rpm with presence of ultrasound.
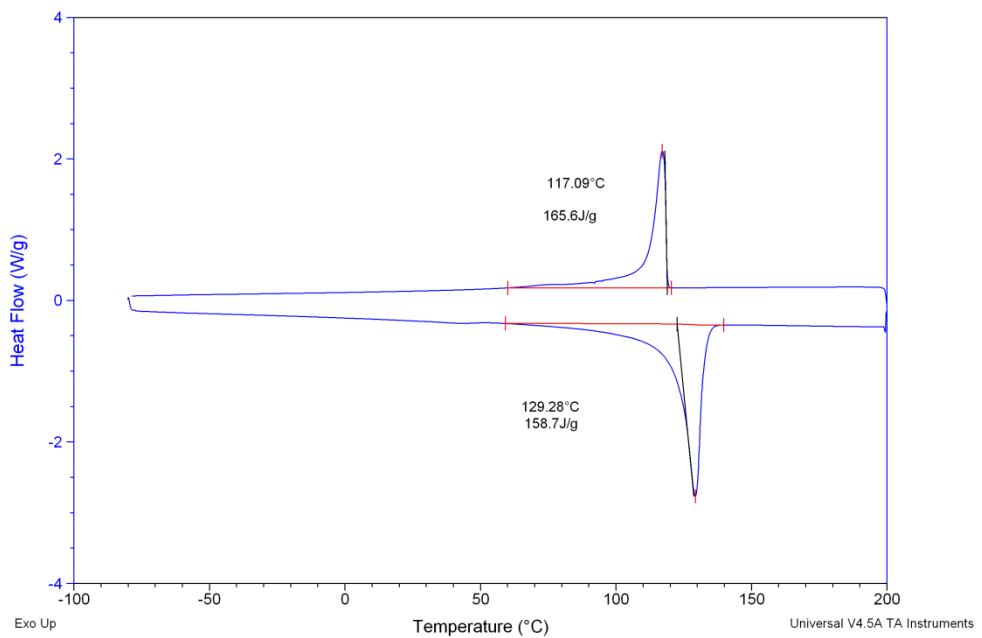
Figure C-96: DSC heat flow vs. temperature curve for PE80 pipes produced at 20rpm with presence of ultrasound.

285
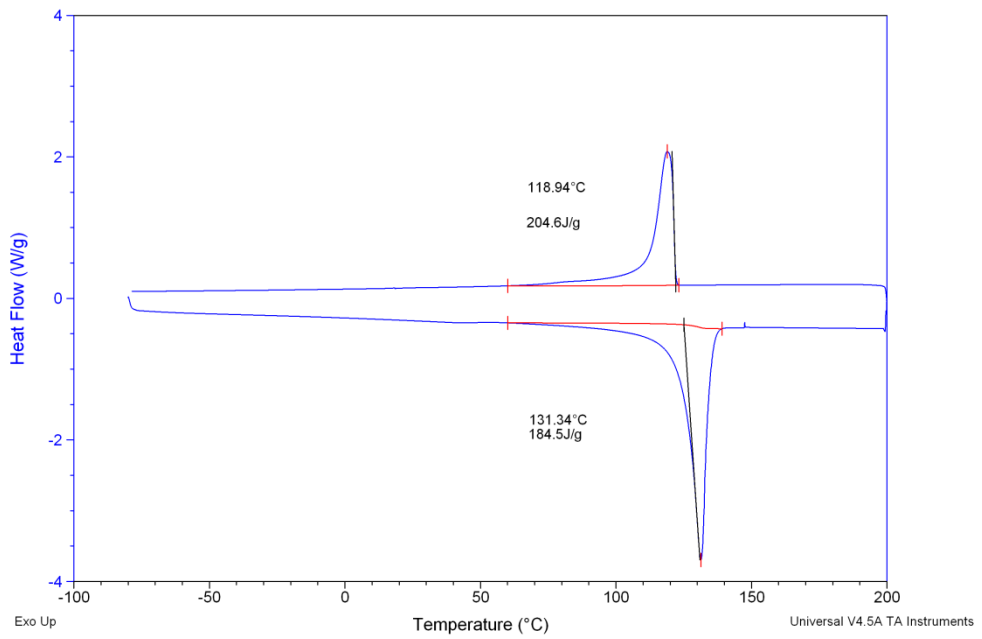
Figure C-97: DSC heat flow vs. temperature curve for unfilled HYA600 pipes produced at 12rpm without presence of ultrasound.
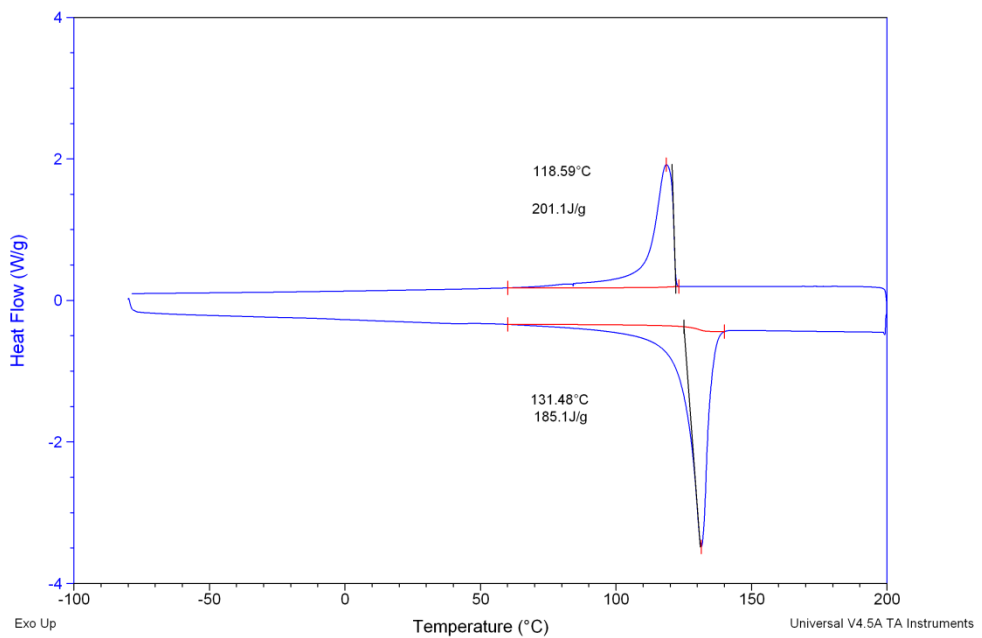
Figure C-98: DSC heat flow vs. temperature curve for unfilled HYA600 pipes produced at 14rpm without presence of ultrasound.
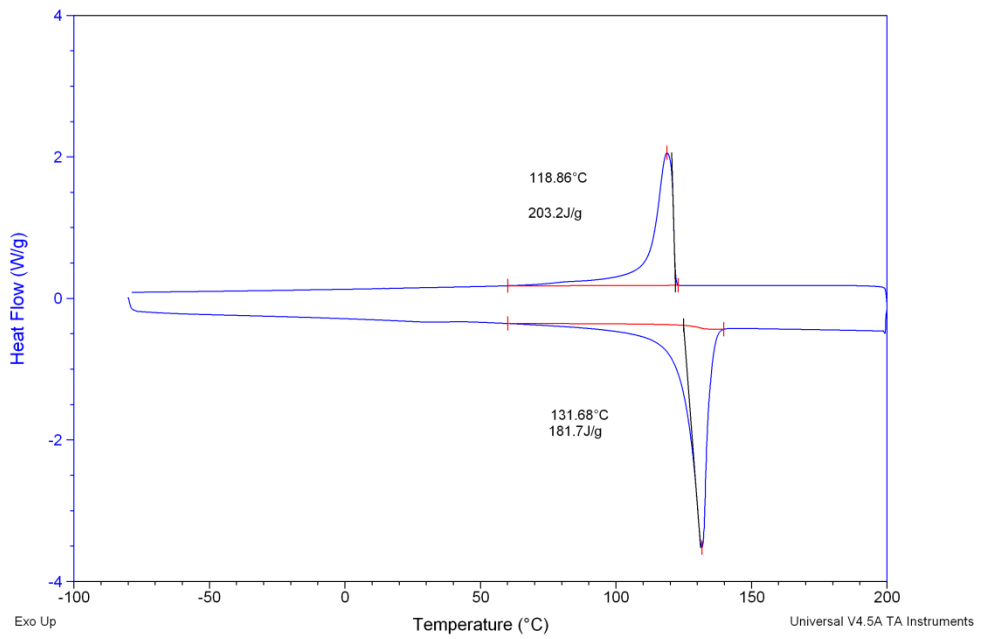
Figure C-99: DSC heat flow vs. temperature curve for unfilled HYA600 pipes produced at 16rpm without presence of ultrasound.
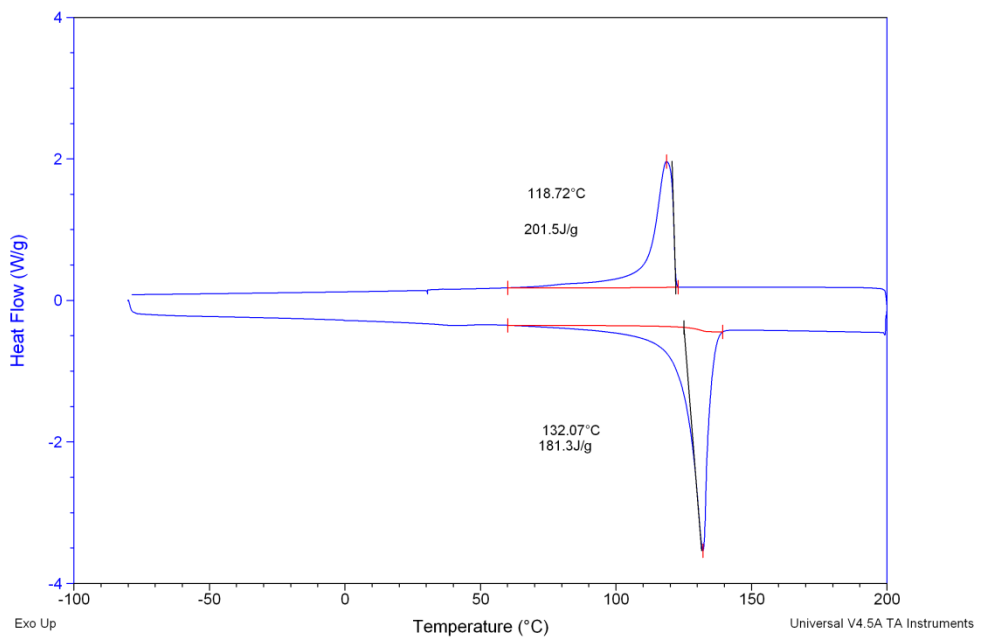
Figure C-100: DSC heat flow vs. temperature curve for unfilled HYA600 pipes produced at 18rpm without presence of ultrasound.
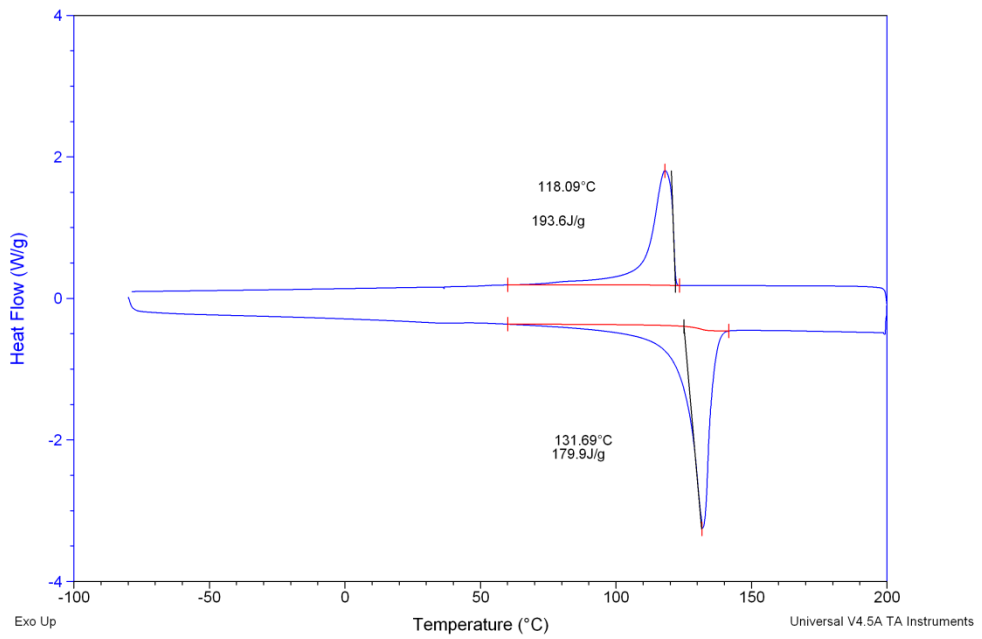
Figure C-101: DSC heat flow vs. temperature curve for unfilled HYA600 pipes produced at 20rpm without presence of ultrasound.
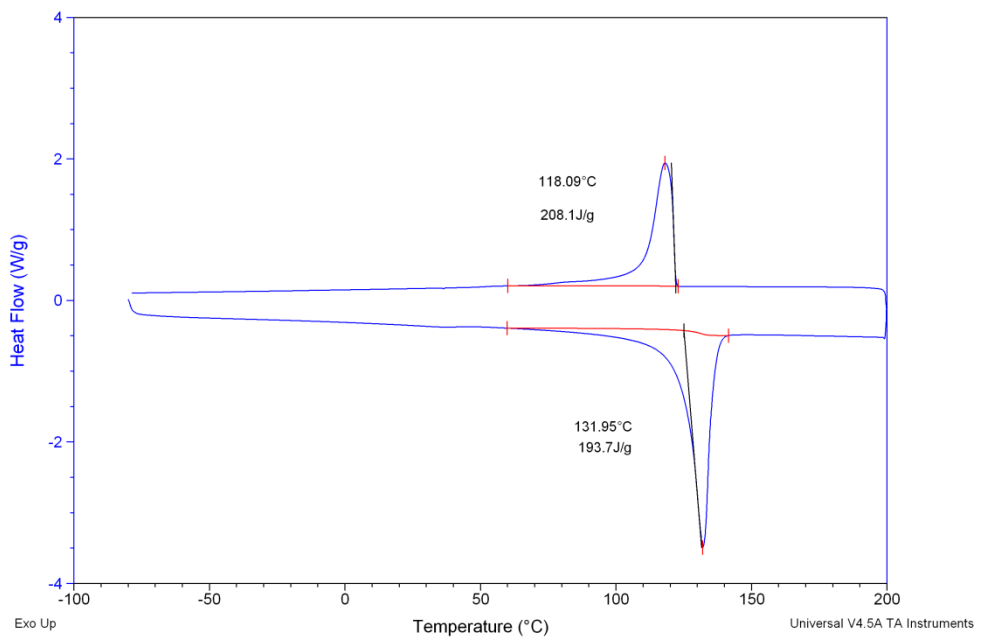
Figure C-102: DSC heat flow vs. temperature curve for unfilled HYA600 pipes produced at 12rpm with presence of ultrasound.
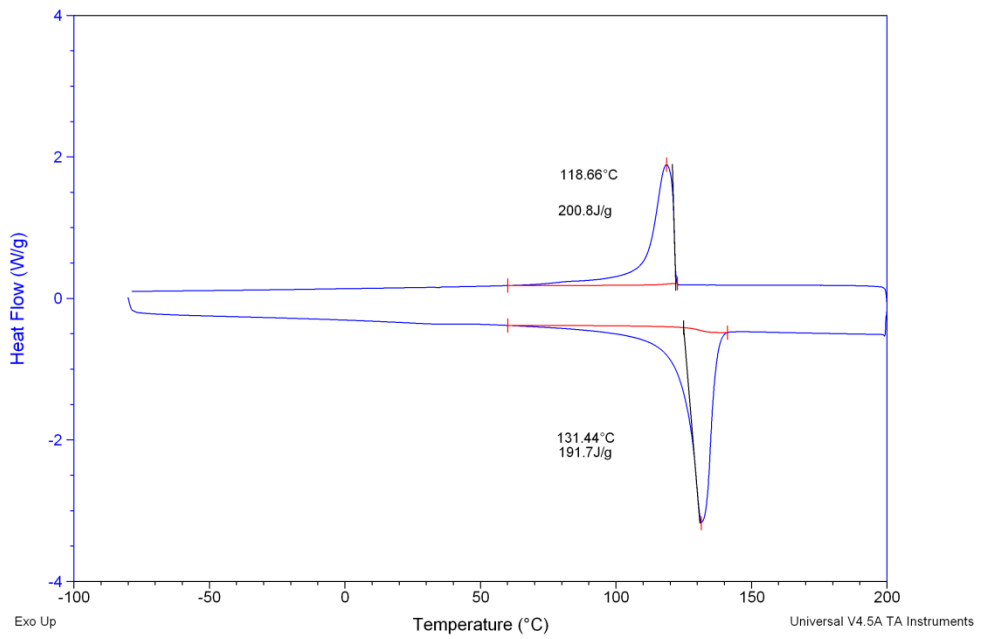
Figure C-103: DSC heat flow vs. temperature curve for unfilled HYA600 pipes produced at 14rpm with presence of ultrasound.
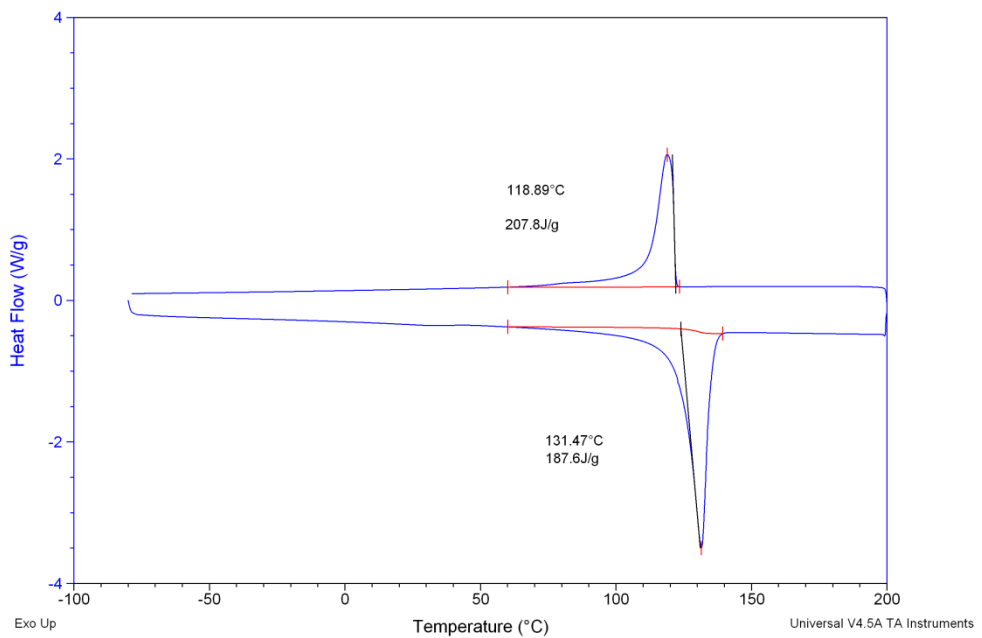
Figure C-104: DSC heat flow vs. temperature curve for unfilled HYA600 pipes produced at 16rpm with presence of ultrasound.
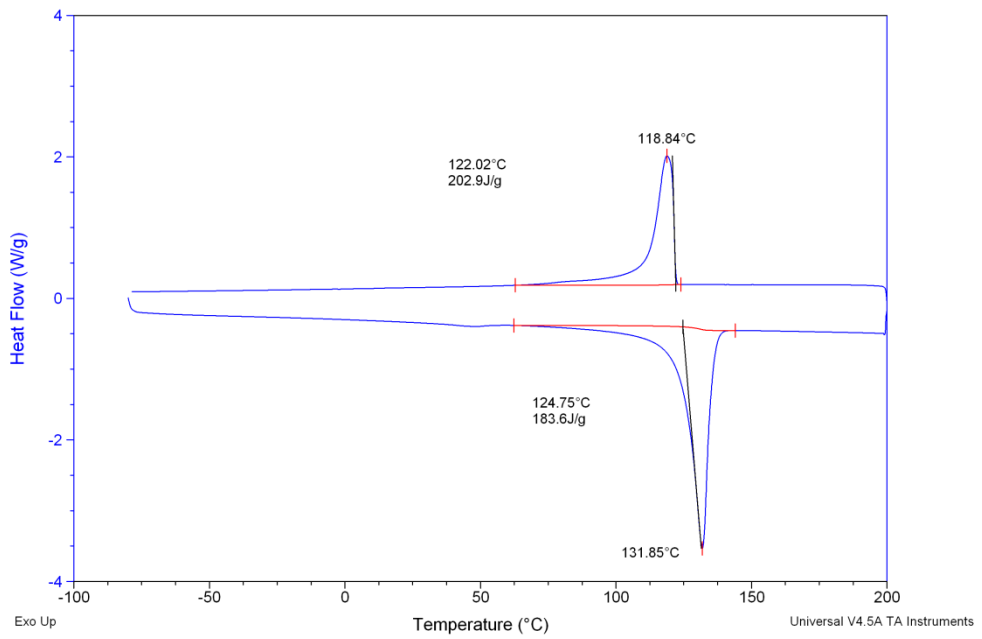
Figure C-105: DSC heat flow vs. temperature curve for unfilled HYA600 pipes produced at 18rpm with presence of ultrasound.
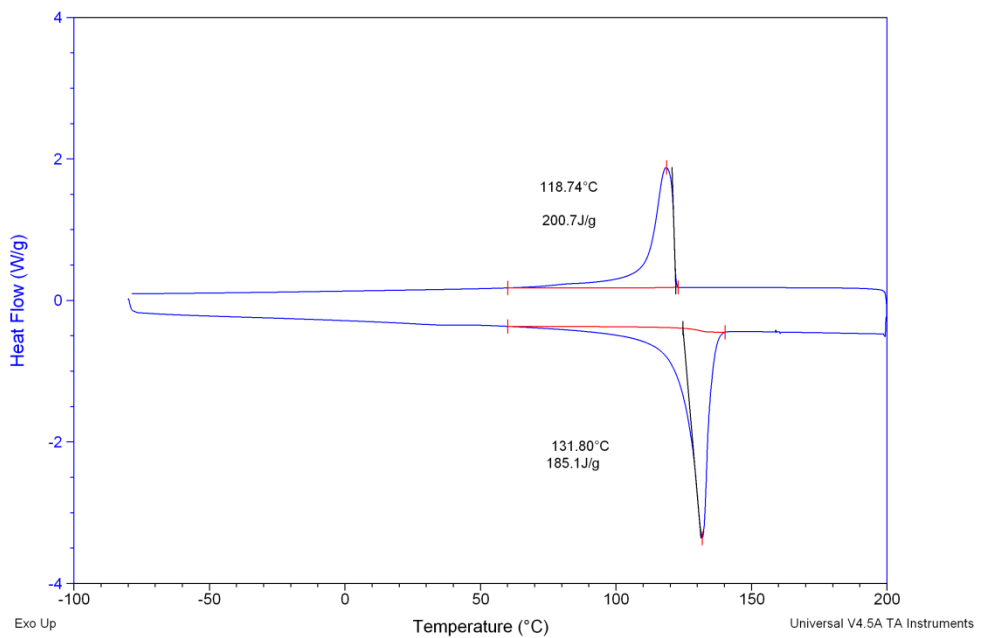
Figure C-106: DSC heat flow vs. temperature curve for unfilled HYA600 pipes produced at 20rpm with presence of ultrasound.
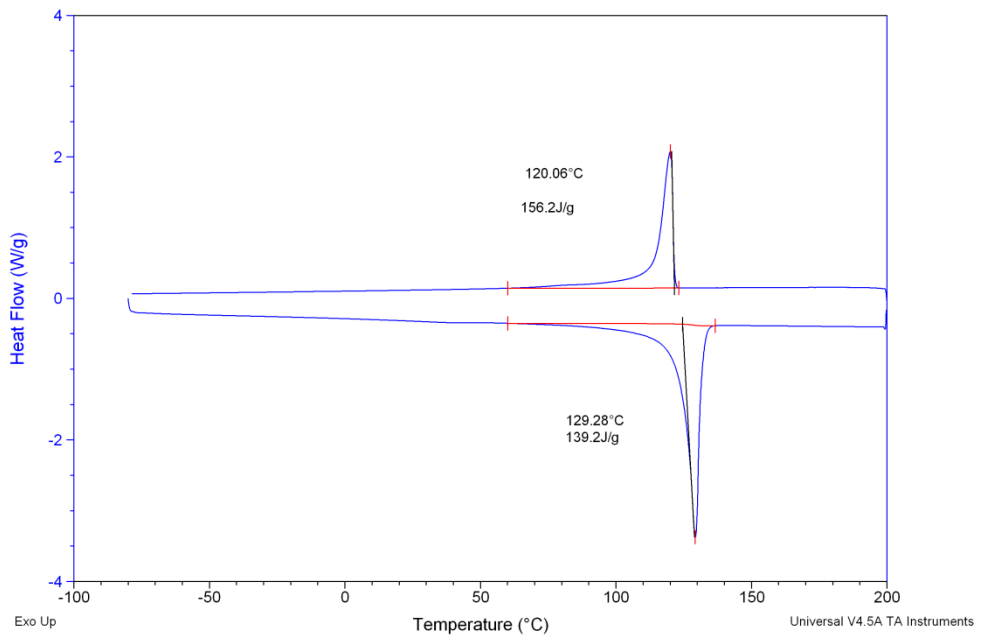
Figure C-107: DSC heat flow vs. temperature curve for 20%wt filled HYA600 pipes produced at 12rpm without presence of ultrasound.
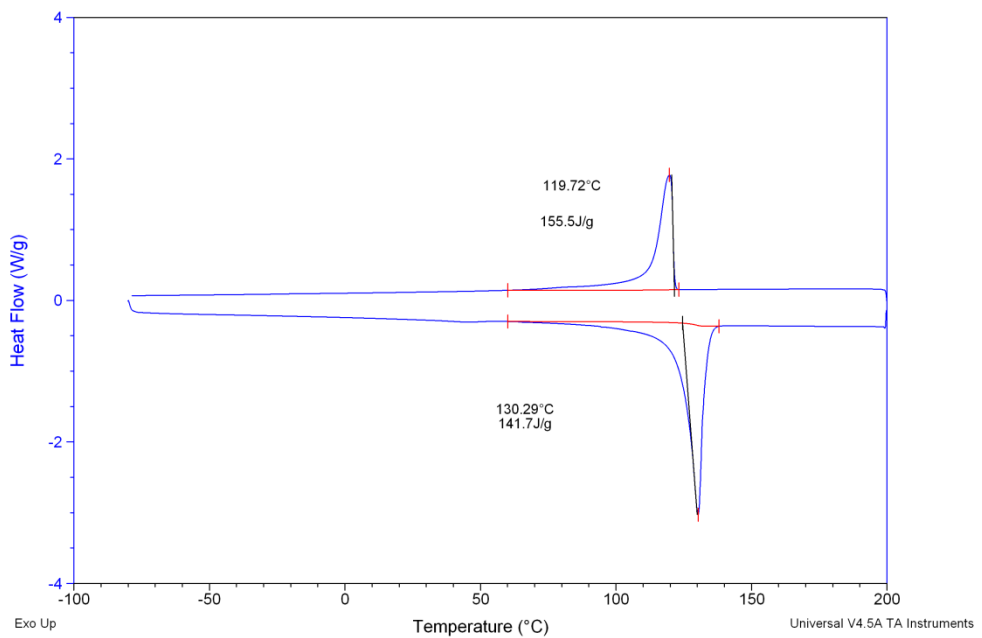
Figure C-108: DSC heat flow vs. temperature curve for 20%wt filled HYA600 pipes produced at 14rpm without presence of ultrasound.
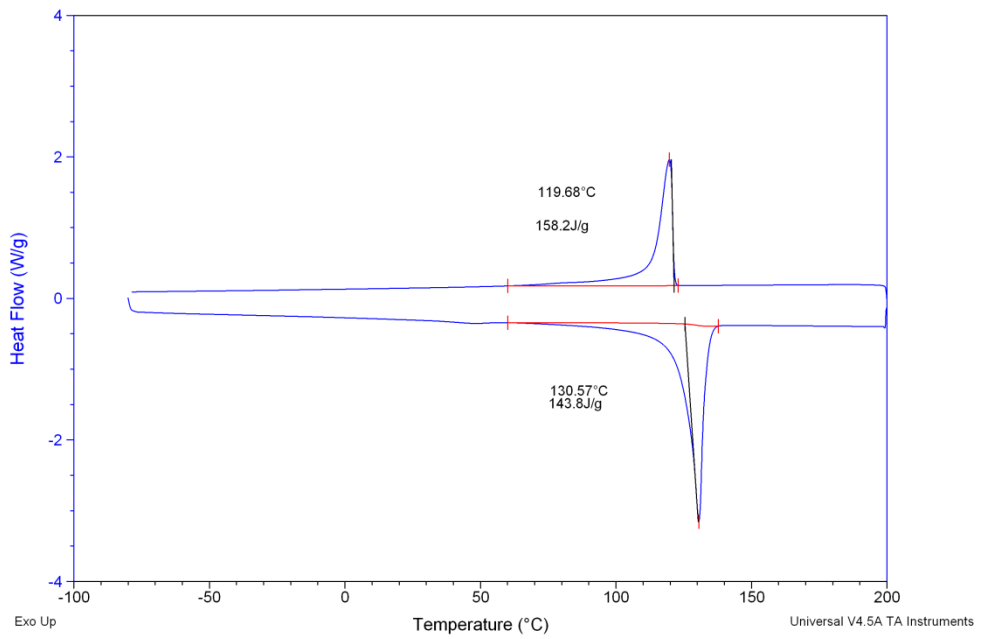
Figure C-109: DSC heat flow vs. temperature curve for 20%wt filled HYA600 pipes produced at 16rpm without presence of ultrasound.
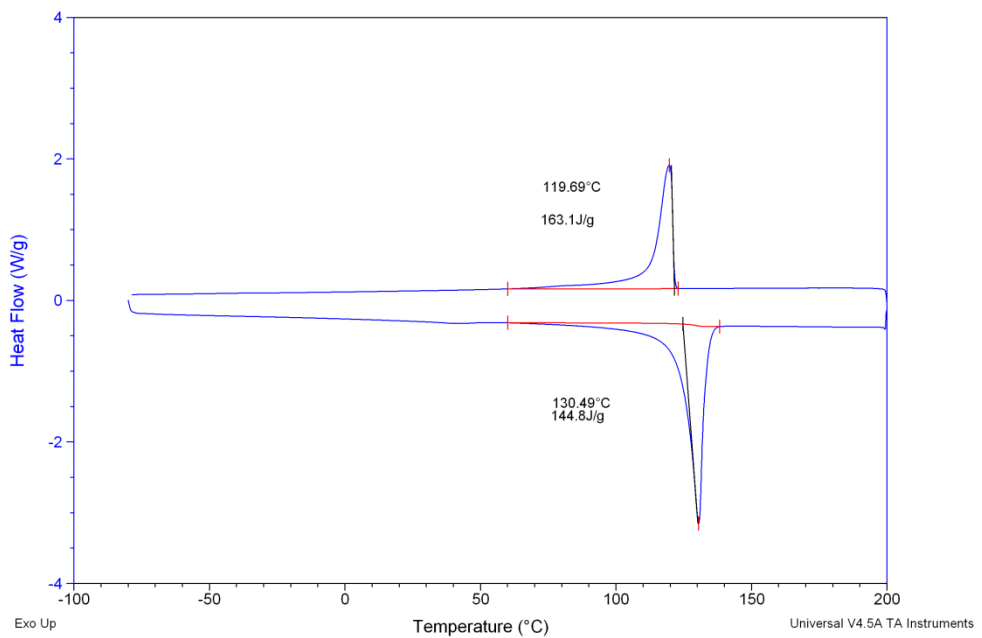
Figure C-110: DSC heat flow vs. temperature curve for 20%wt filled HYA600 pipes produced at 18rpm without presence of ultrasound.

Figure C-111: DSC heat flow vs. temperature curve for 20%wt filled HYA600 pipes produced at 20rpm without presence of ultrasound.

Figure C-112: DSC heat flow vs. temperature curve for 20%wt filled HYA600 pipes produced at 12rpm with presence of ultrasound.

293

Figure C-113: DSC heat flow vs. temperature curve for 20%wt filled HYA600 pipes produced at 14rpm with presence of ultrasound.

Figure C-114: DSC heat flow vs. temperature curve for 20%wt filled HYA600 pipes produced at 16rpm with presence of ultrasound.

Figure C-115: DSC heat flow vs. temperature curve for 20%wt filled HYA600 pipes produced at 18rpm with presence of ultrasound.

Figure C-116: DSC heat flow vs. temperature curve for 20%wt filled HYA600 pipes produced at 20rpm with presence of ultrasound.

Figure C-117: DSC heat flow vs. temperature curve for 40%wt filled HYA600 pipes produced at 12rpm without presence of ultrasound.

Figure C-118: DSC heat flow vs. temperature curve for 40%wt filled HYA600 pipes produced at 14rpm without presence of ultrasound.

Figure C-119: DSC heat flow vs. temperature curve for 40%wt filled HYA600 pipes produced at 16rpm without presence of ultrasound.

Figure C-120: DSC heat flow vs. temperature curve for 40%wt filled HYA600 pipes produced at 18rpm without presence of ultrasound.

Figure C-121: DSC heat flow vs. temperature curve for 40%wt filled HYA600 pipes produced at 20rpm without presence of ultrasound.

Figure C-122: DSC heat flow vs. temperature curve for 40%wt filled HYA600 pipes produced at 12rpm with presence of ultrasound.

Figure C-123: DSC heat flow vs. temperature curve for 40%wt filled HYA600 pipes produced at 14rpm with presence of ultrasound.

Figure C-124: DSC heat flow vs. temperature curve for 40%wt filled HYA600 pipes produced at 16rpm with presence of ultrasound.

Figure C-125: DSC heat flow vs. temperature curve for 40%wt filled HYA600 pipes produced at 18rpm with presence of ultrasound.

Figure C-126: DSC heat flow vs. temperature curve for 40%wt filled HYA600 pipes produced at 20rpm with presence of ultrasound.
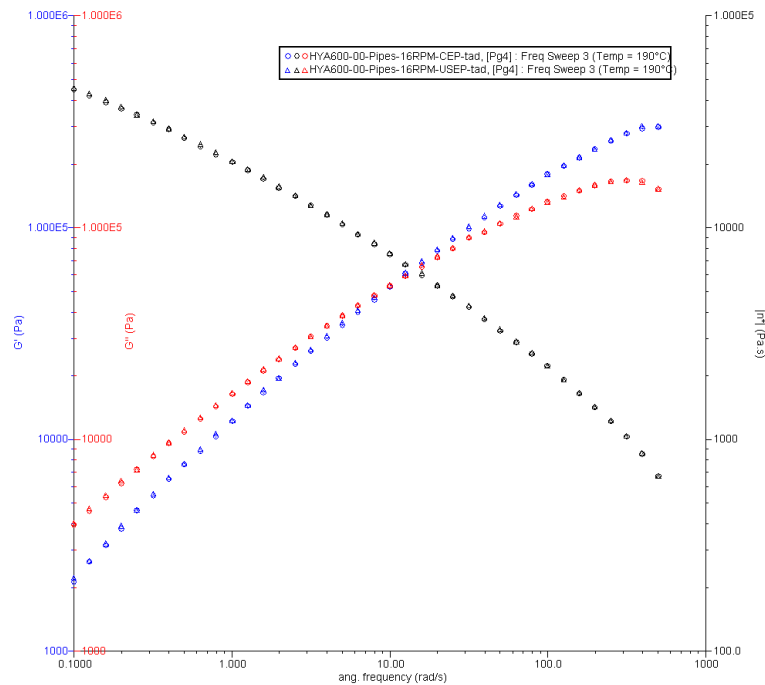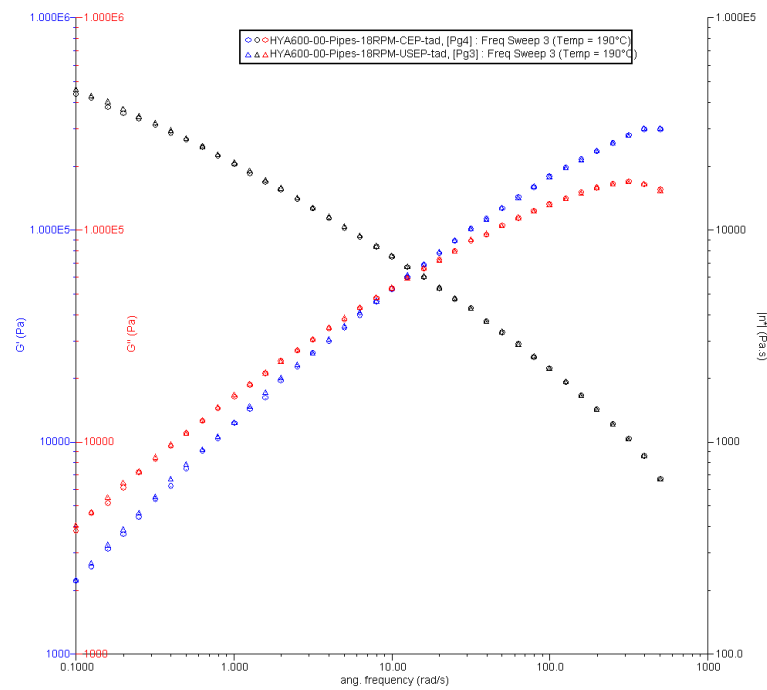
300

V. Rheology Results
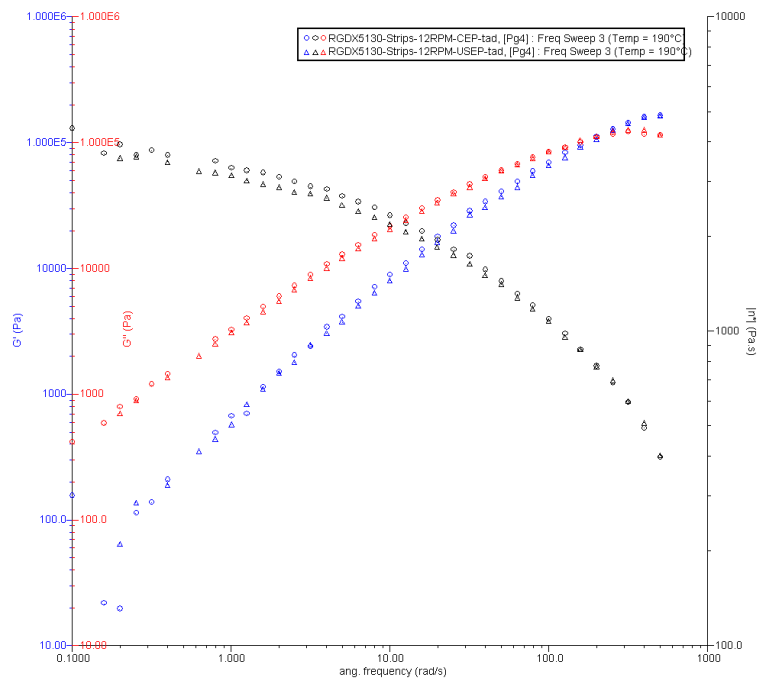
Figure C-127: Dynamic shear storage modulus (G'), loss modulus (G") and complex viscosity (η*) plotted against angular frequency for Rigidex5130 strips produced at 12 rpm with and without ultrasound.
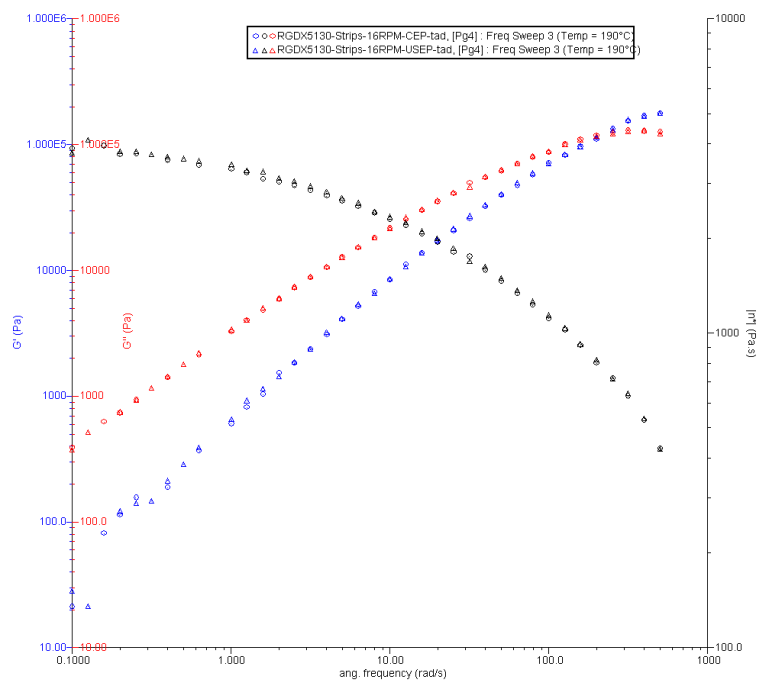
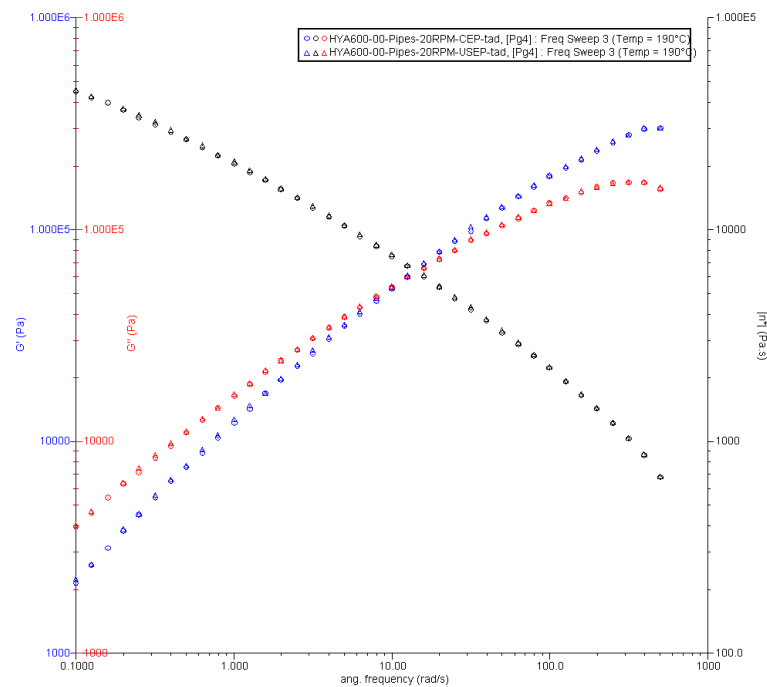**Figure C-128: Dynamic shear storage modulus (G'), loss modulus (G") and complex viscosity (η*) plotted against angular frequency for Rigidex5130 strips produced at 16 rpm with and without ultrasound.**
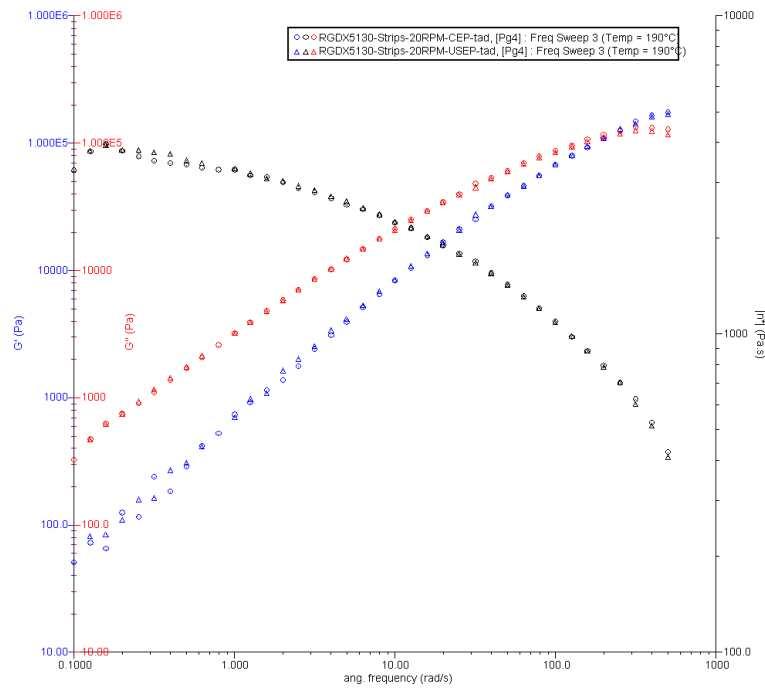
Figure C-129: Dynamic shear storage modulus (G'), loss modulus (G") and complex viscosity (η*) plotted against angular frequency for Rigidex5130 strips produced at 20 rpm with and without ultrasound.
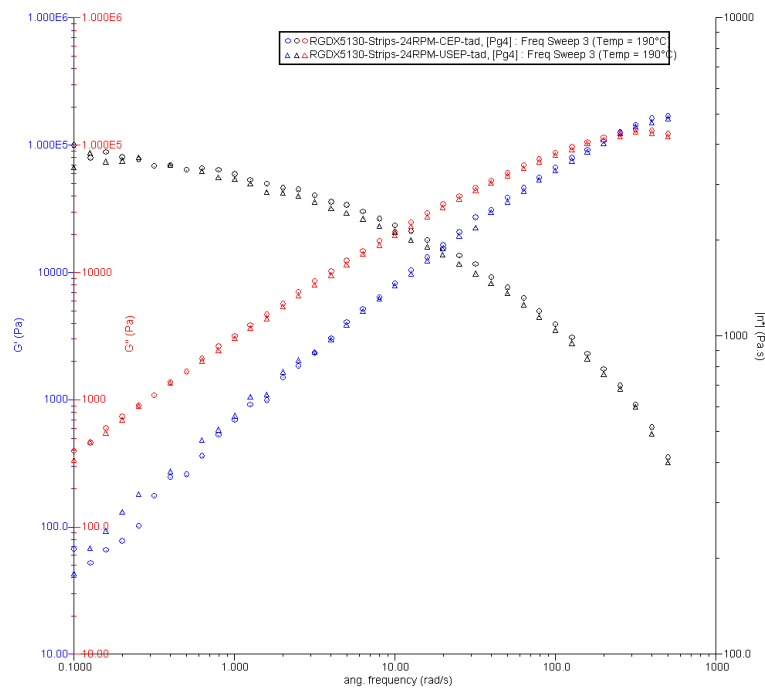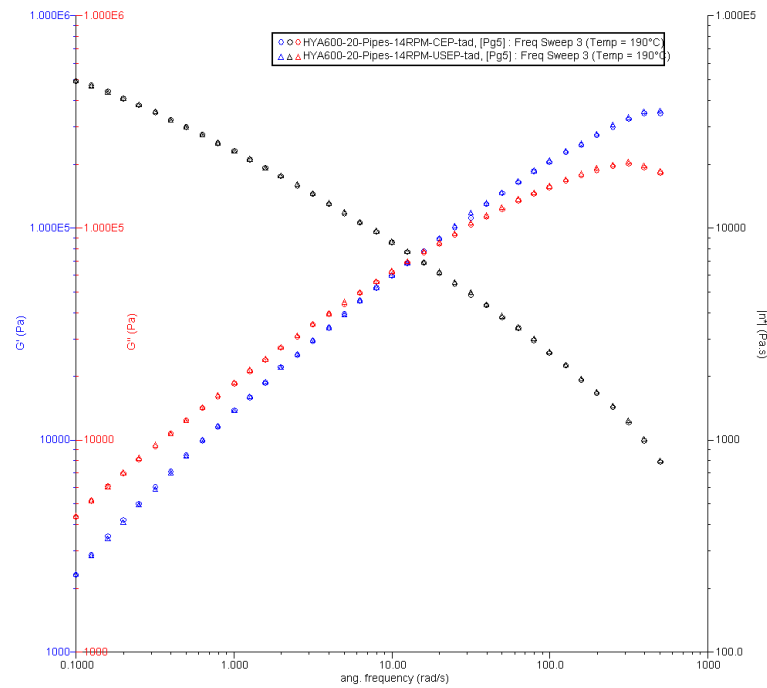

Figure C-130: Dynamic shear storage modulus (G'), loss modulus (G") and complex viscosity (η*) plotted against angular frequency for Rigidex5130 strips produced at 24 rpm with and without ultrasound.
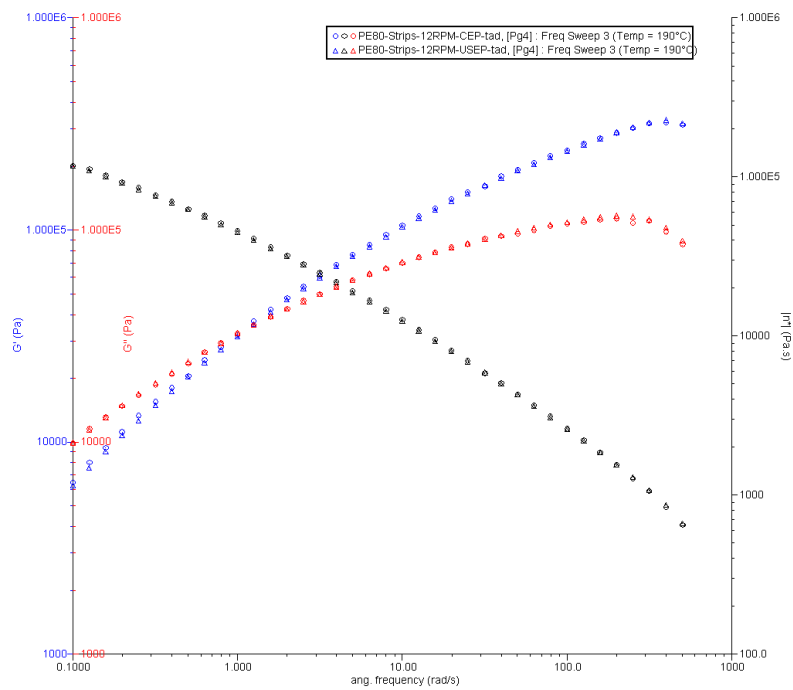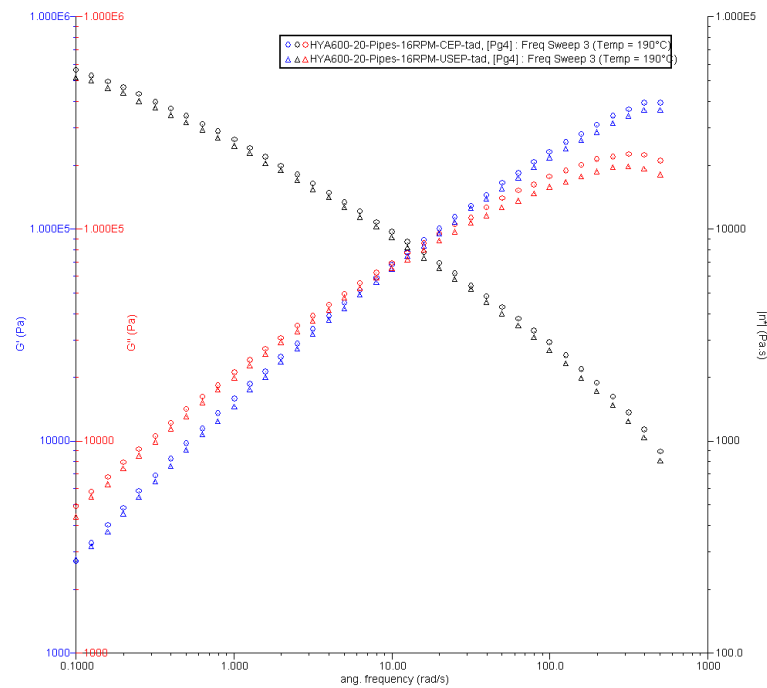
Figure C-131: Dynamic shear storage modulus (G'), loss modulus (G") and complex viscosity (η*) plotted against angular frequency for PE80 strips produced at 12 rpm with and without ultrasound.
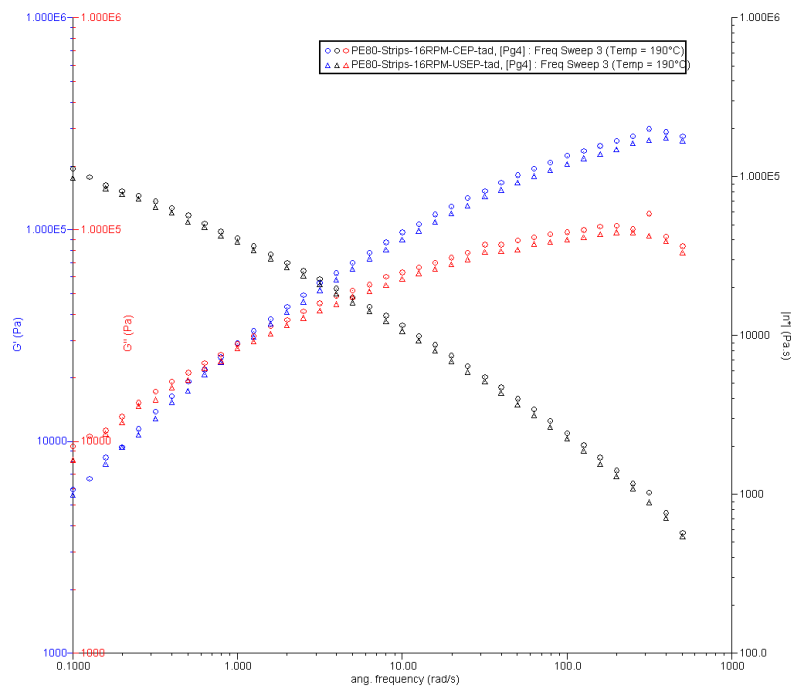
Figure C-132: Dynamic shear storage modulus (G'), loss modulus (G") and complex viscosity (η*) plotted against angular frequency for PE80 strips produced at 16 rpm with and without ultrasound.
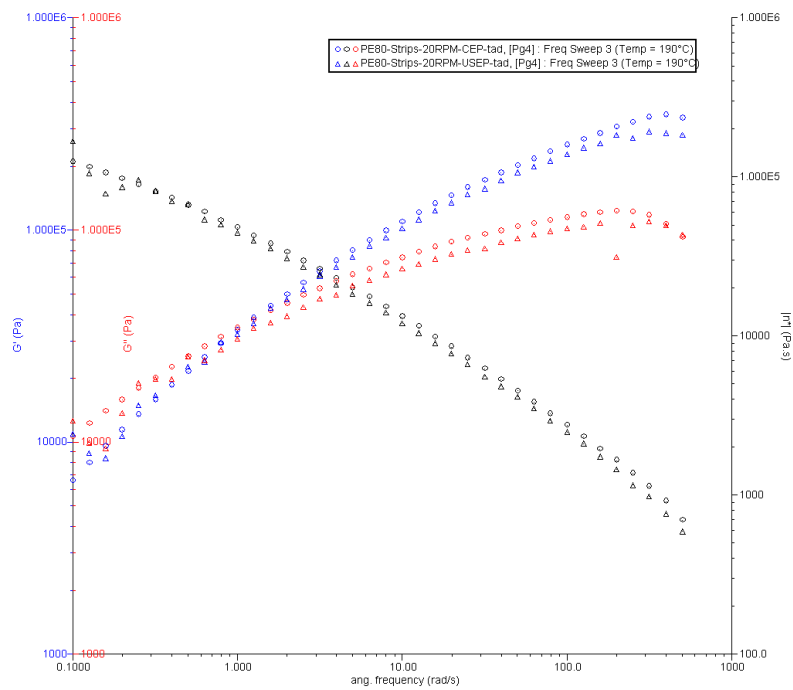
Figure C-133: Dynamic shear storage modulus (G'), loss modulus (G") and complex viscosity (η*) plotted against angular frequency for PE80 strips produced at 20 rpm with and without ultrasound.
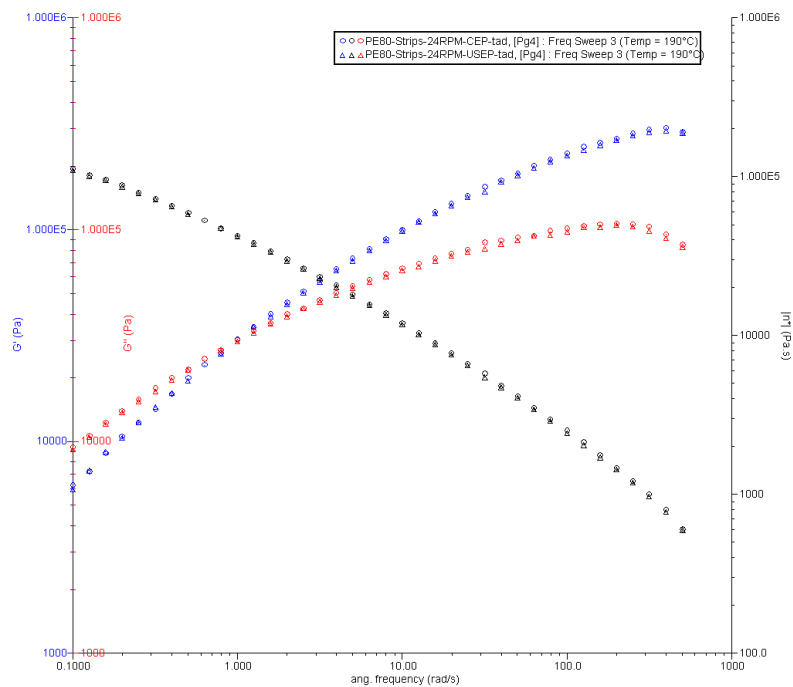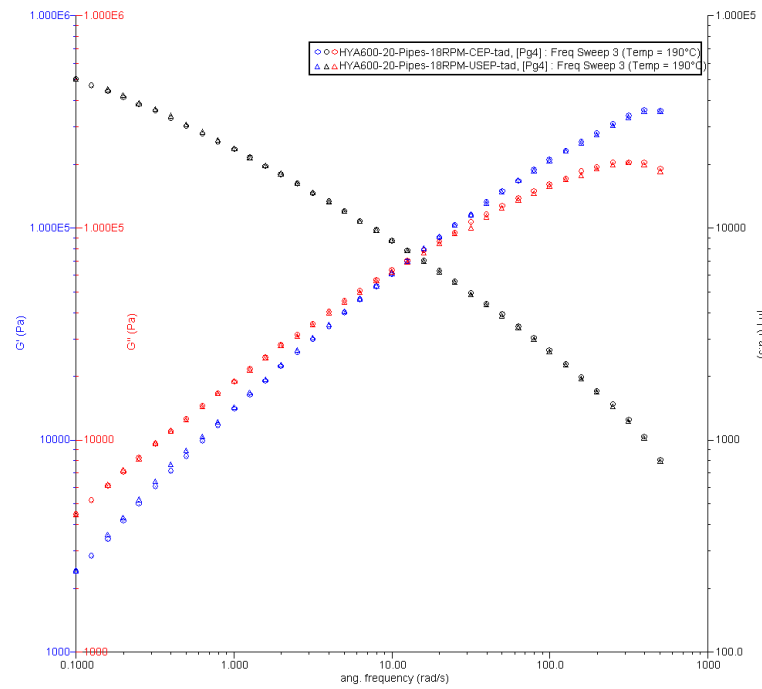

Figure C-134: Dynamic shear storage modulus (G'), loss modulus (G") and complex viscosity (η*) plotted against angular frequency for PE80 strips produced at 24 rpm with and without ultrasound.
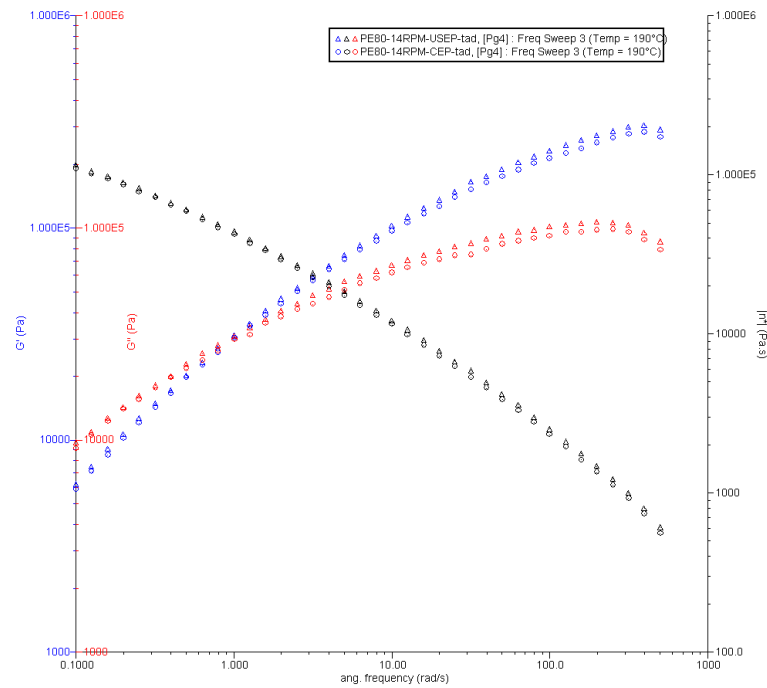
Figure C-135: Dynamic shear storage modulus (G'), loss modulus (G") and complex viscosity (η*) plotted against angular frequency for PE80 pipes produced at 14 rpm with and without ultrasound.
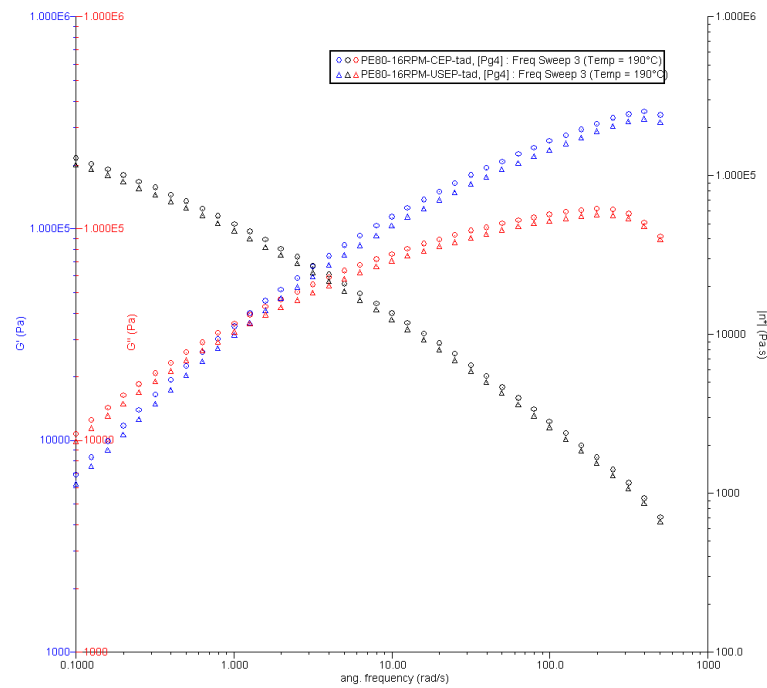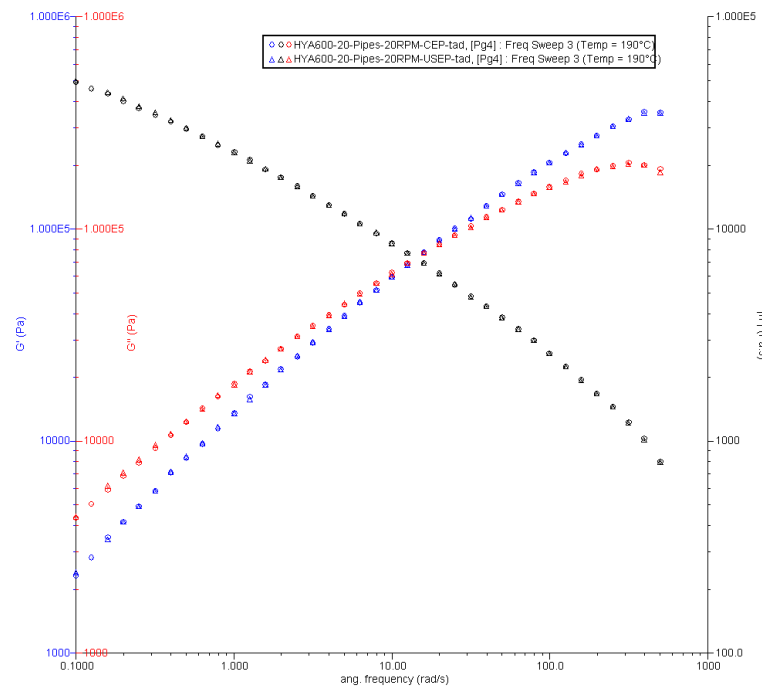

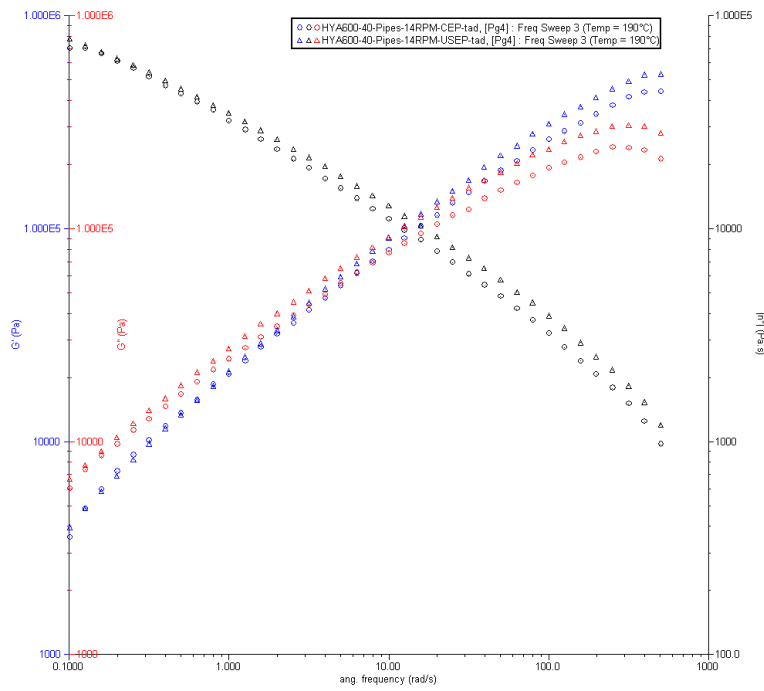**Figure C-136: Dynamic shear storage modulus (G'), loss modulus (G") and complex viscosity (η*) plotted against angular frequency for PE80 pipes produced at 16 rpm with and without ultrasound.**
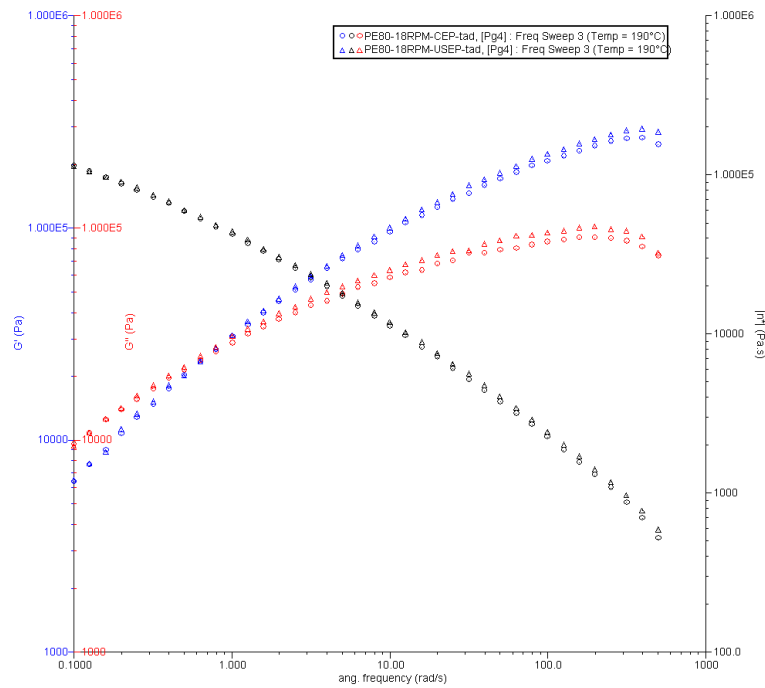
Figure C-137: Dynamic shear storage modulus (G'), loss modulus (G") and complex viscosity (η*) plotted against angular frequency for PE80 pipes produced at 18 rpm with and without ultrasound.
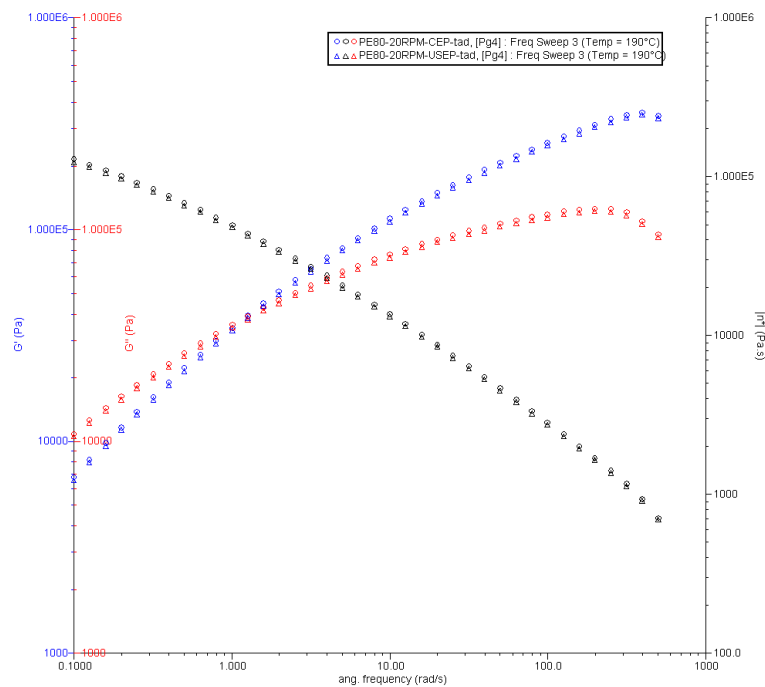
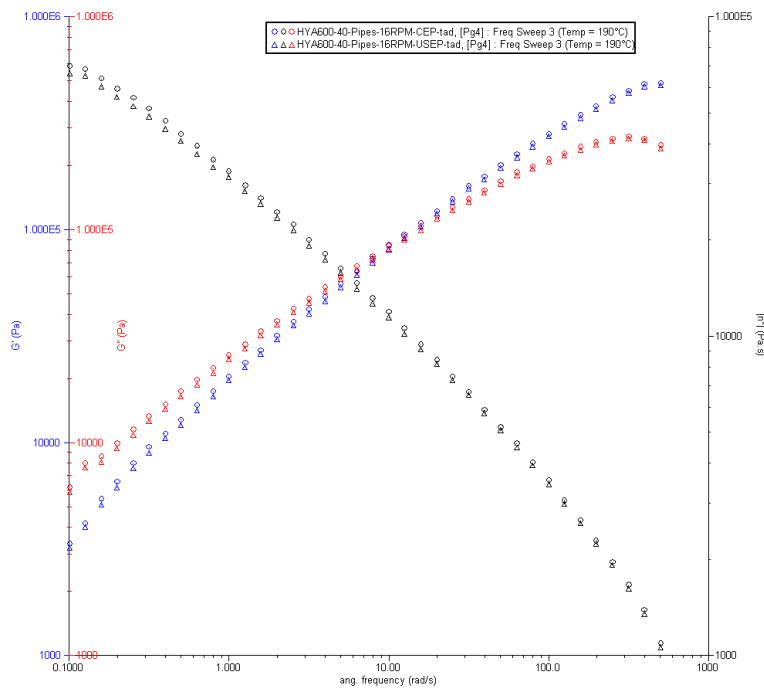**Figure C-138: Dynamic shear storage modulus (G'), loss modulus (G") and complex viscosity (η*) plotted against angular frequency for PE80 pipes produced at 20 rpm with and without ultrasound.**

306
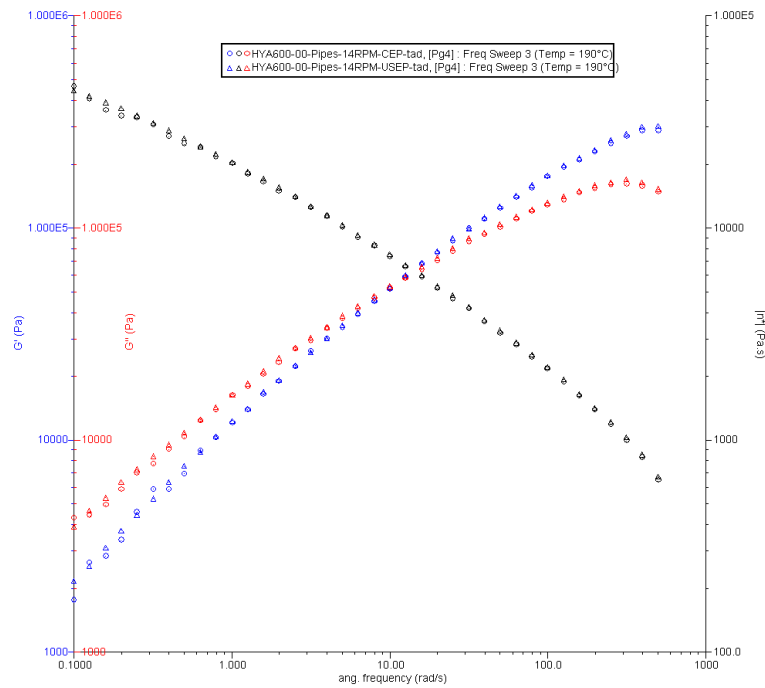
Figure C-139: Dynamic shear storage modulus (G'), loss modulus (G") and complex viscosity (η*) plotted against angular frequency for HYA600 pipes produced at 14 rpm with and without ultrasound.

Figure C-140: Dynamic shear storage modulus (G'), loss modulus (G") and complex viscosity (η*) plotted against angular frequency for HYA600 pipes produced at 16 rpm with and without ultrasound.
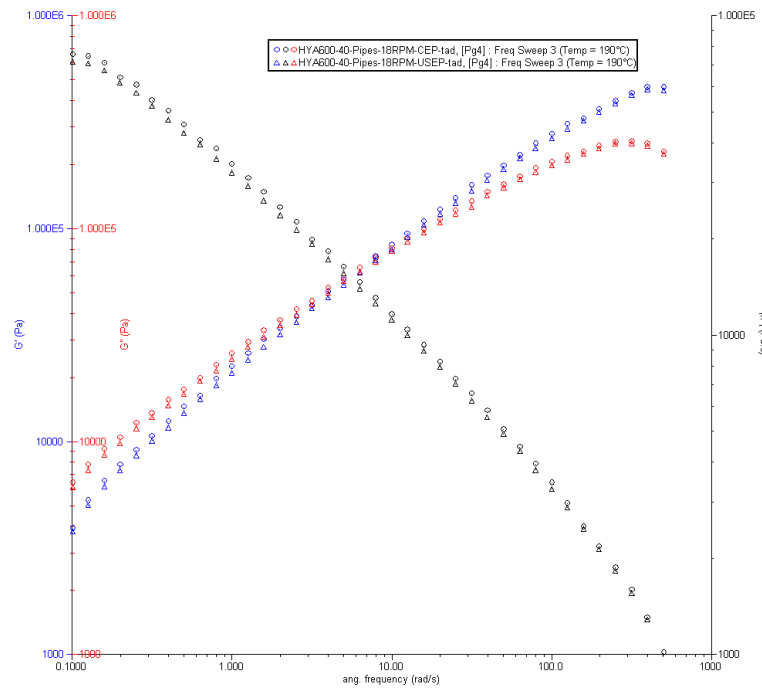
307

Figure C-141: Dynamic shear storage modulus (G'), loss modulus (G") and complex viscosity (η*) plotted against angular frequency for HYA600 pipes produced at 18 rpm with and without ultrasound.
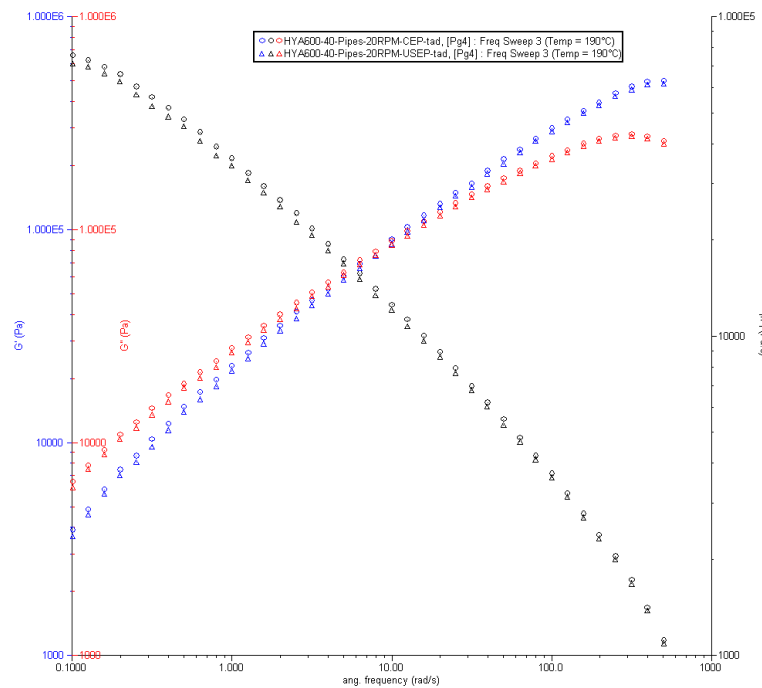

Figure C-142: Dynamic shear storage modulus (G'), loss modulus (G") and complex viscosity (η*) plotted against angular frequency for HYA600 pipes produced at 20 rpm with and without ultrasound.

Figure C-143: Dynamic shear storage modulus (G'), loss modulus (G") and complex viscosity (η*) plotted against angular frequency for HYA600/20 pipes produced at 14 rpm with and without ultrasound.

Figure C-144: Dynamic shear storage modulus (G'), loss modulus (G") and complex viscosity (η*) plotted against angular frequency for HYA600/20 pipes produced at 16 rpm with and without ultrasound.

309

Figure C-145: Dynamic shear storage modulus (G'), loss modulus (G") and complex viscosity (η*) plotted against angular frequency for HYA600/20 pipes produced at 18 rpm with and without ultrasound.

Figure C-146: Dynamic shear storage modulus (G'), loss modulus (G") and complex viscosity (η*) plotted against angular frequency for HYA600/20 pipes produced at 20 rpm with and without ultrasound.

Figure C-147: Dynamic shear storage modulus (G'), loss modulus (G") and complex viscosity (η*) plotted against angular frequency for HYA600/40 pipes produced at 14 rpm with and without ultrasound.

Figure C-148: Dynamic shear storage modulus (G'), loss modulus (G") and complex viscosity (η*) plotted against angular frequency for HYA600/40 pipes produced at 16 rpm with and without ultrasound.

Figure C-149: Dynamic shear storage modulus (G'), loss modulus (G") and complex viscosity (η*) plotted against angular frequency for HYA600/40 pipes produced at 18 rpm with and without ultrasound.

Figure C-150: Dynamic shear storage modulus (G'), loss modulus (G") and complex viscosity (η*) plotted against angular frequency for HYA600/40 pipes produced at 20 rpm with and without ultrasound.

312

Appendix D

I. Assembly of the ultrasonic Die
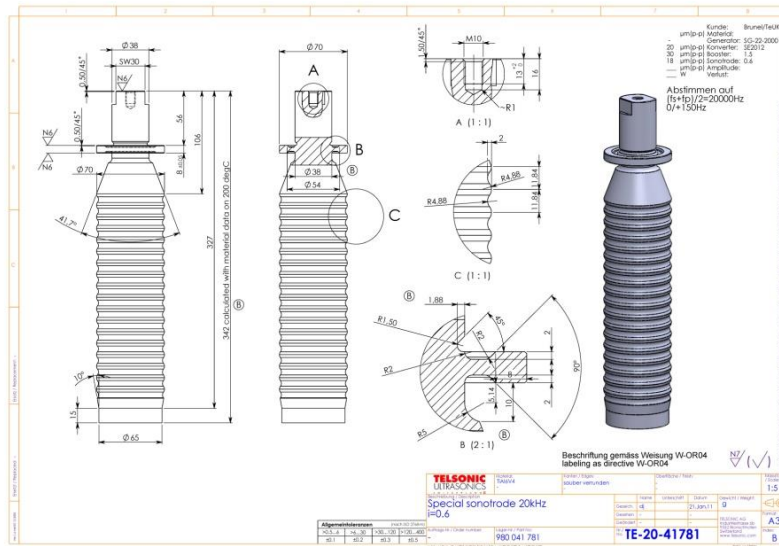
Figure D-1: Recommended dimensions of the third generation ultrasonic horn by Telsonic.
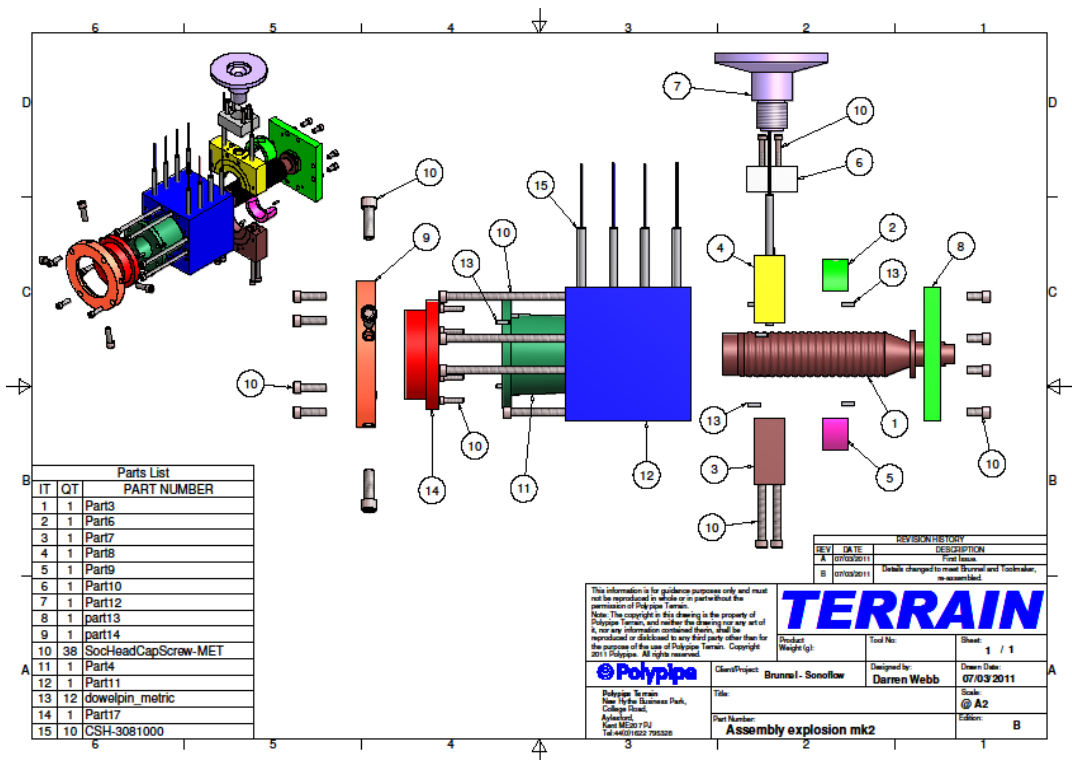
Figure D-2: Individual parts of the third generation ultrasonic die.
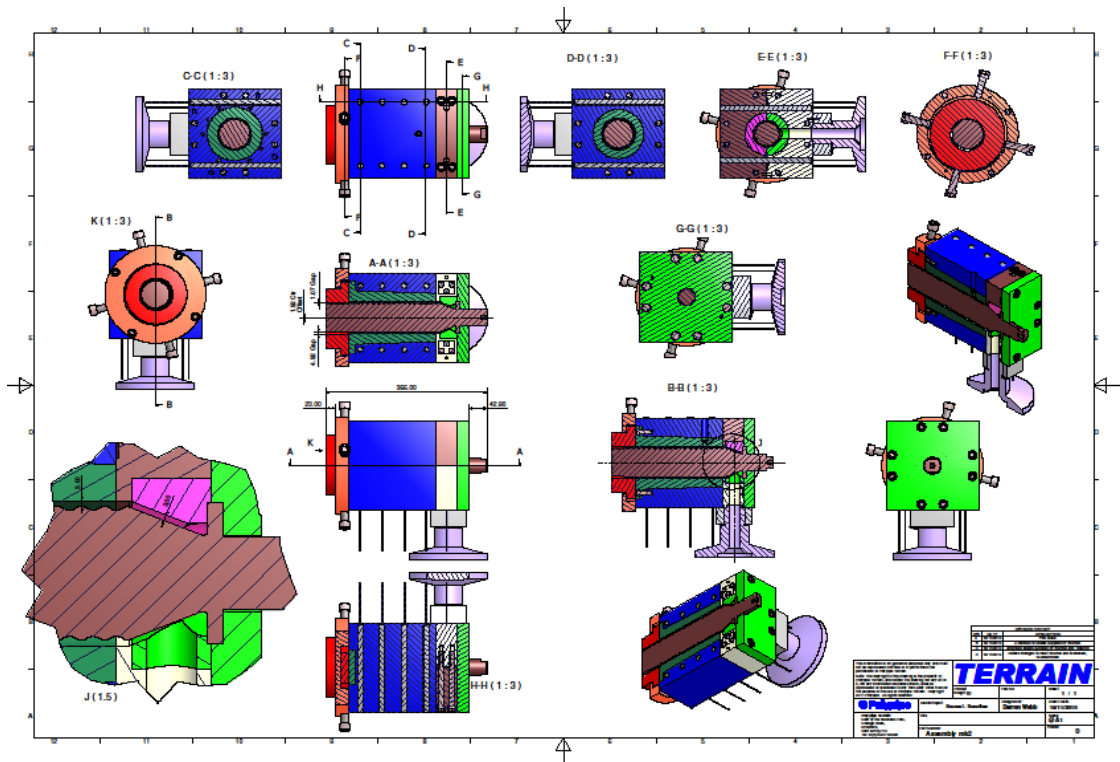
Figure D-3: Side views from components of the third generation ultrasonic die when fitted.
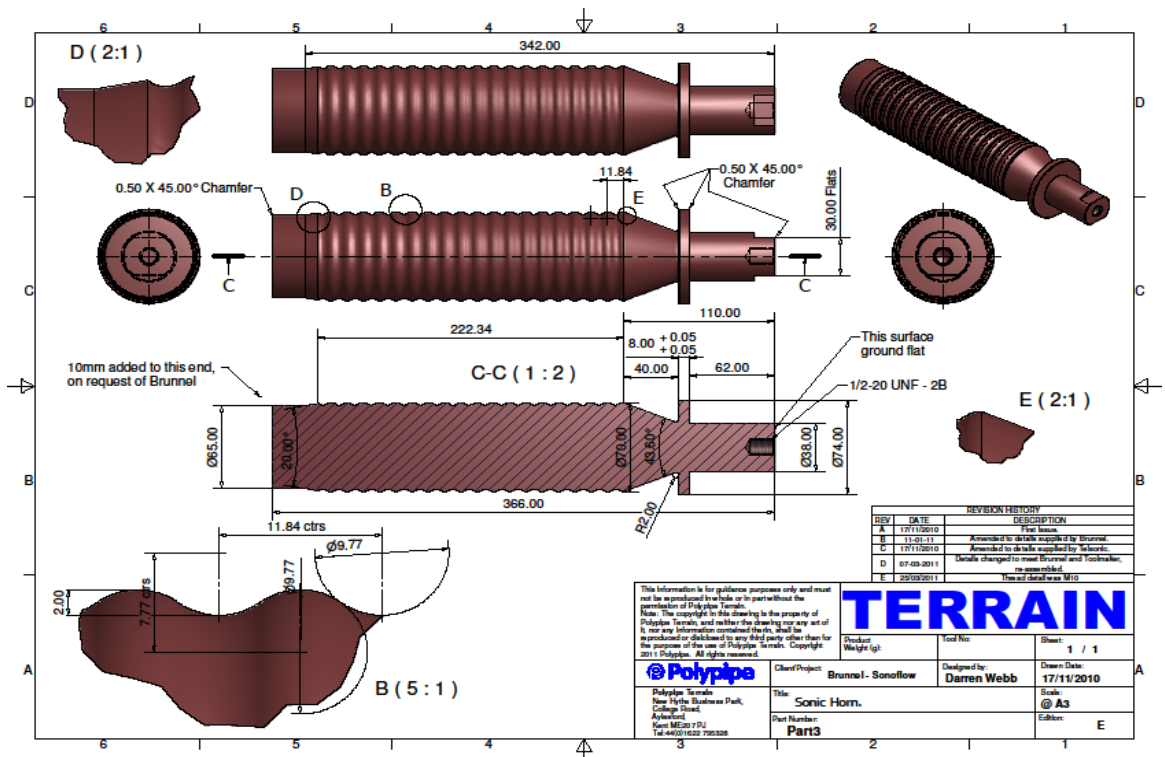
Figure D-4: Final design sheet of third generation ultrasonic horn.
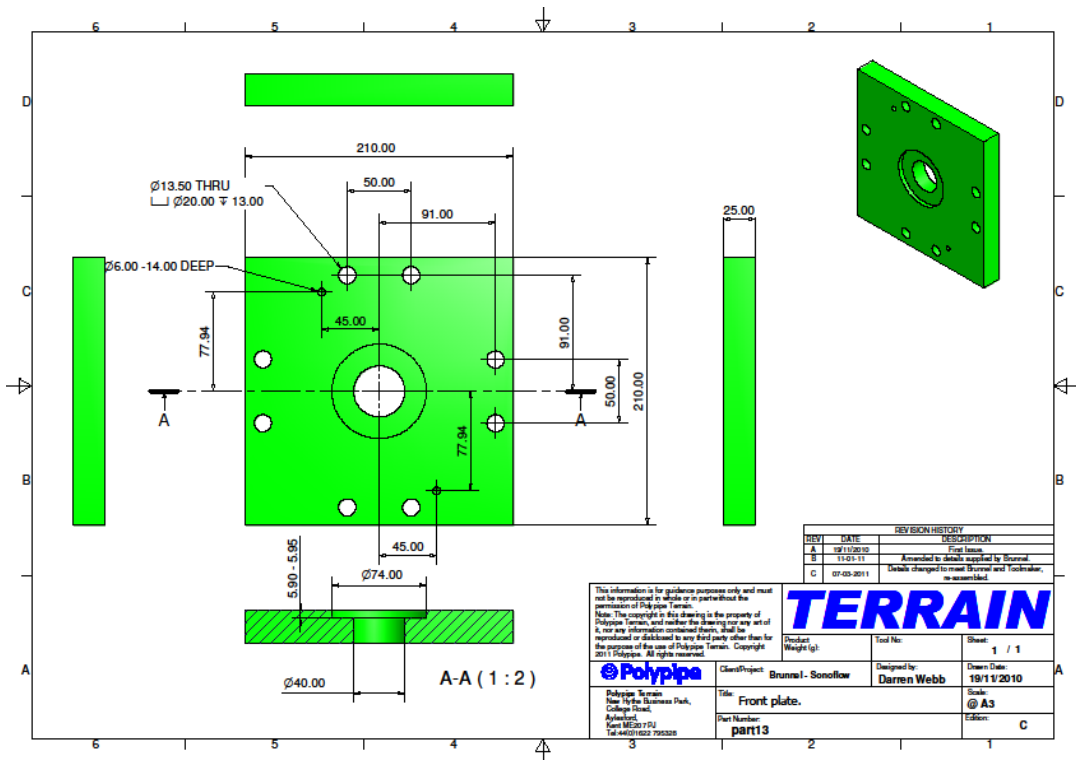
Figure D-5: Top plate design sheet for third generation ultrasonic die.
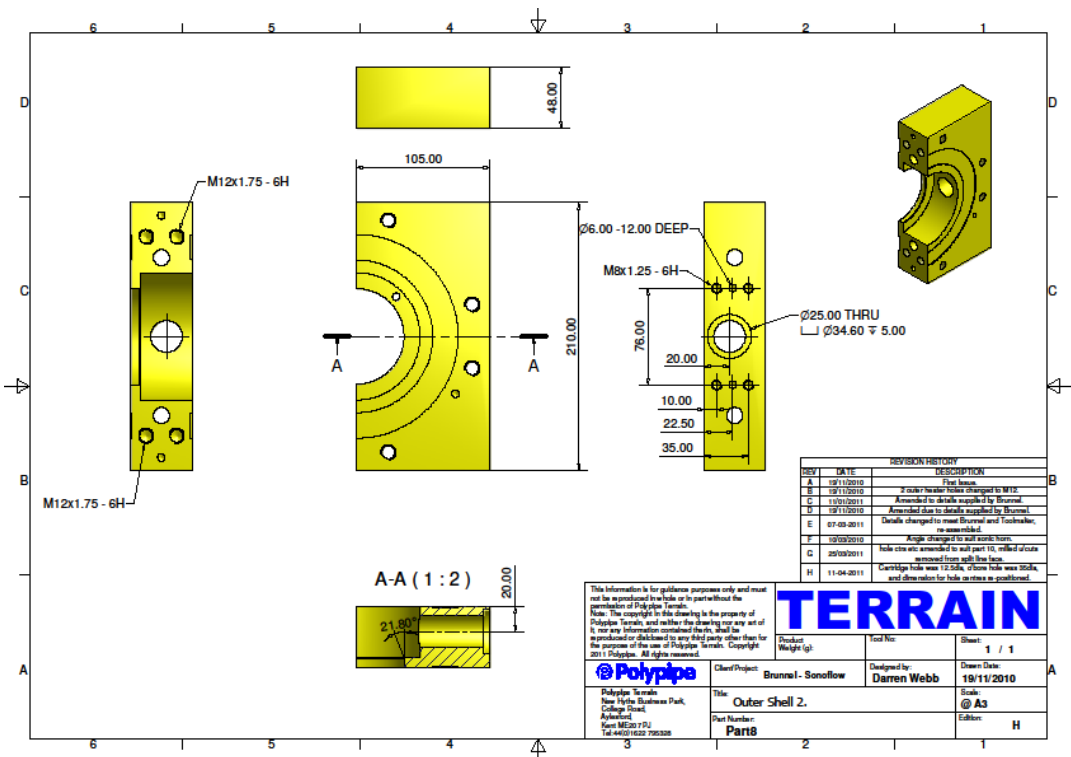
Figure D-6: Design sheet for the feed side of the mid plate.
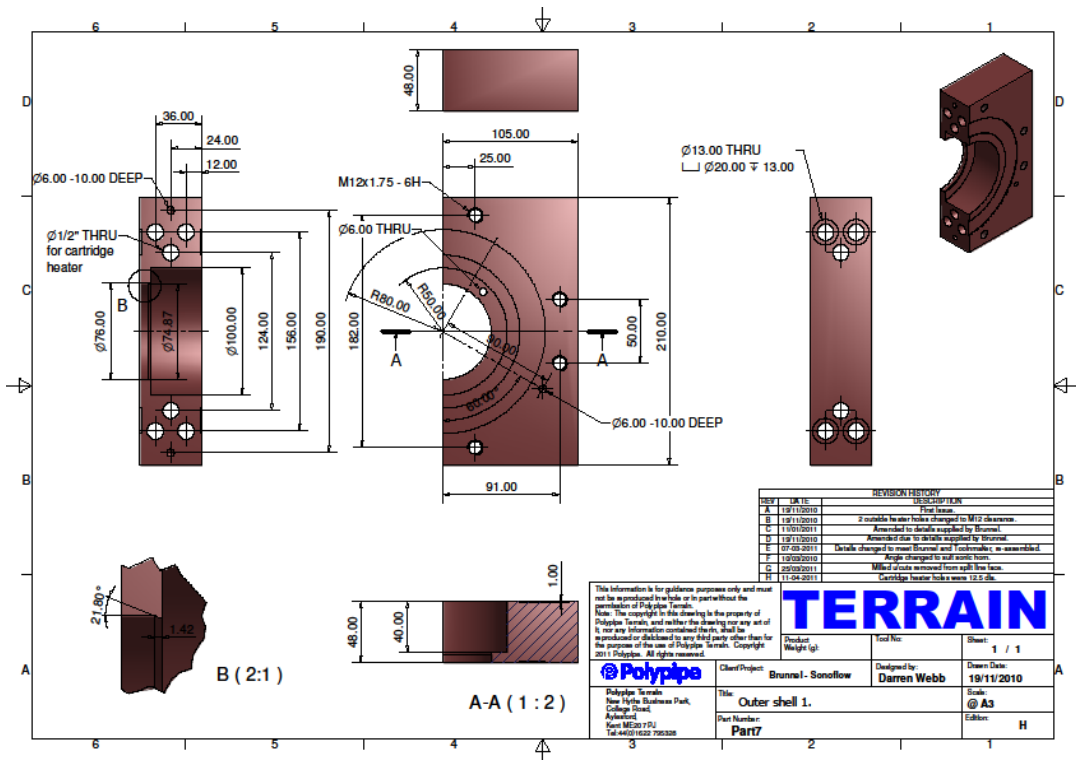
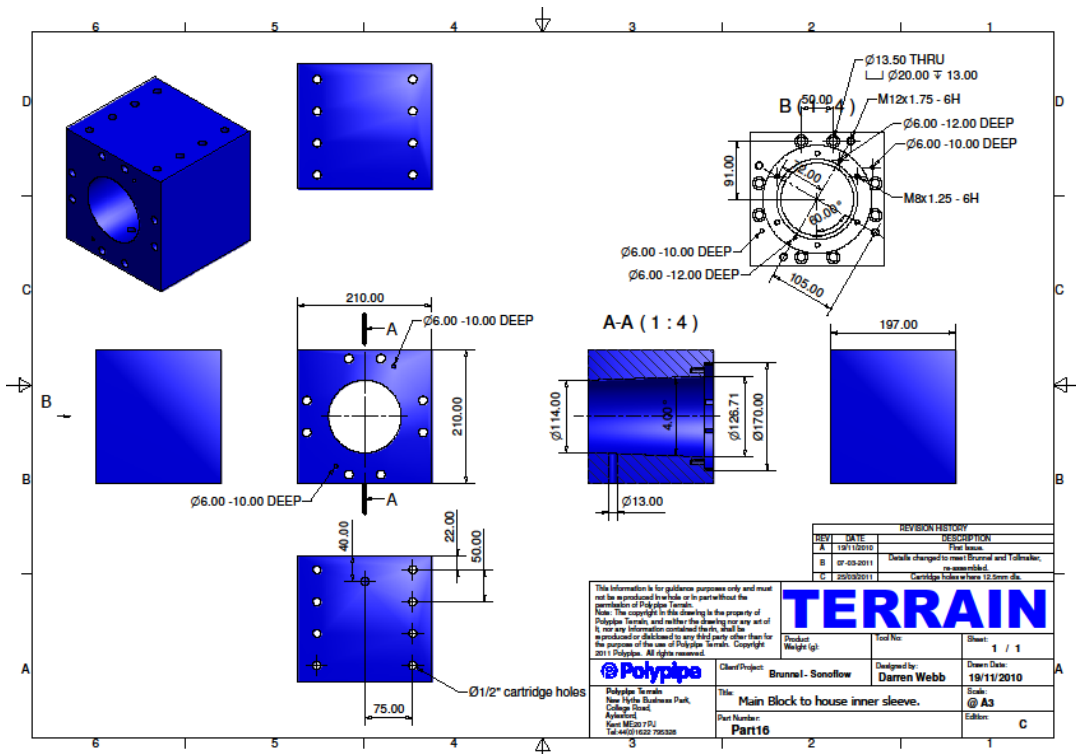**Figure D-7: Design sheet for the opposite side of the feed hole for the mid plate.**
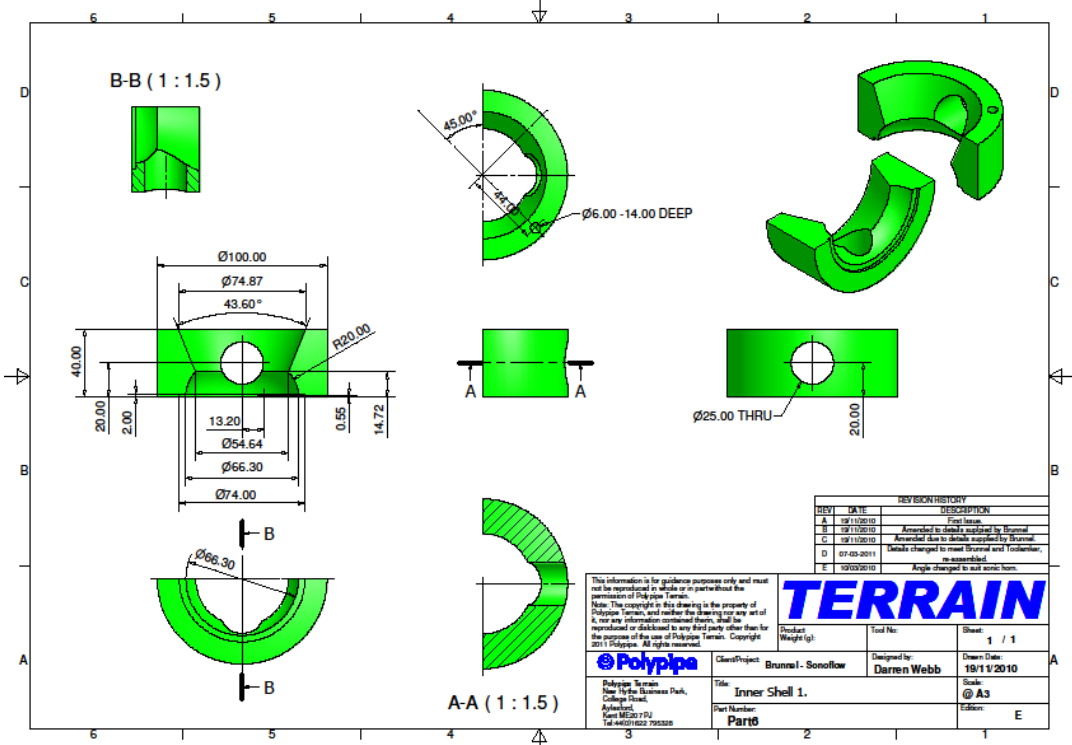
Figure D-8: Design sheet for the feed side of the ring gate.
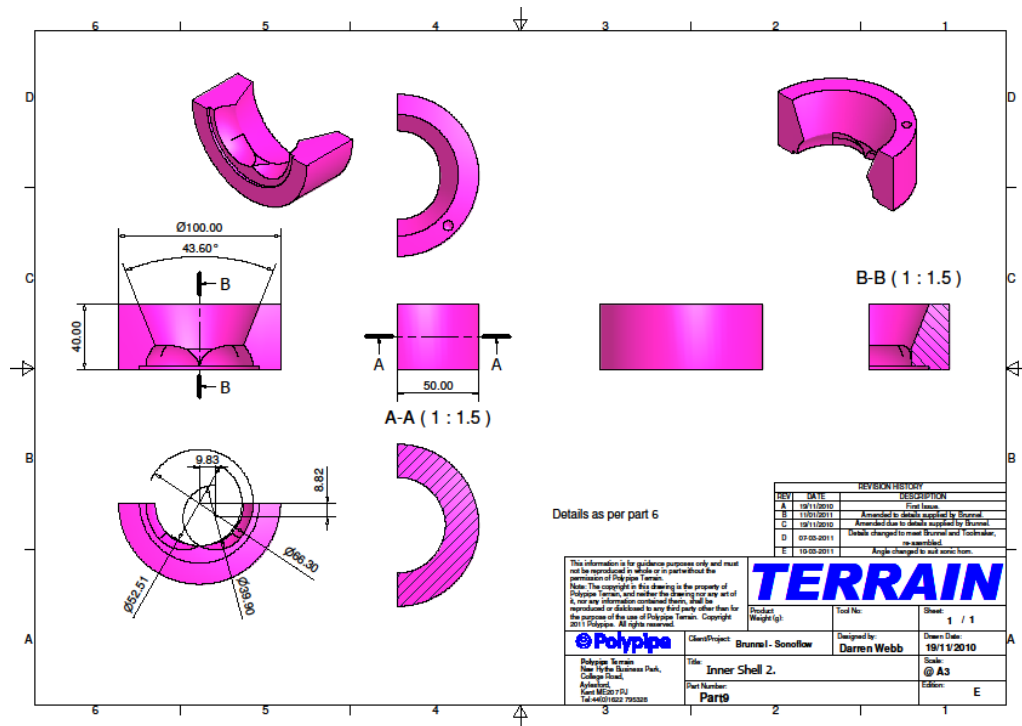
Figure D-9: Design sheet for the opposite side of the feed hole for the ring gate.

Figure D-10: Design sheet of the bottom block.
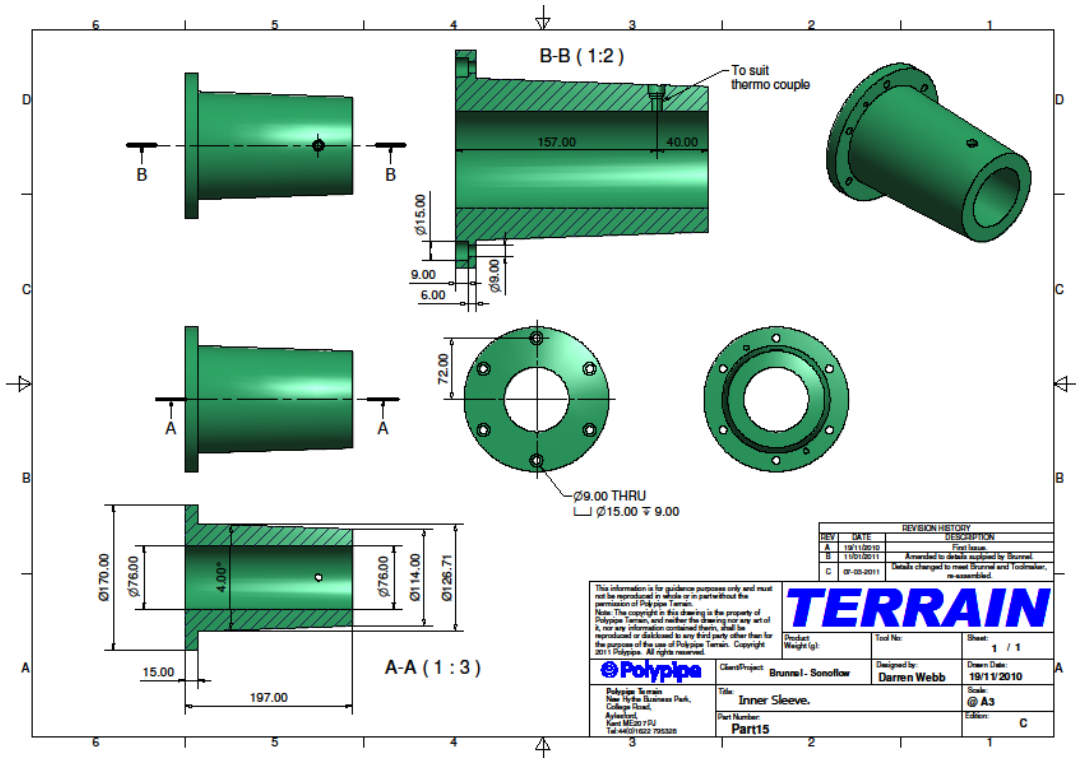
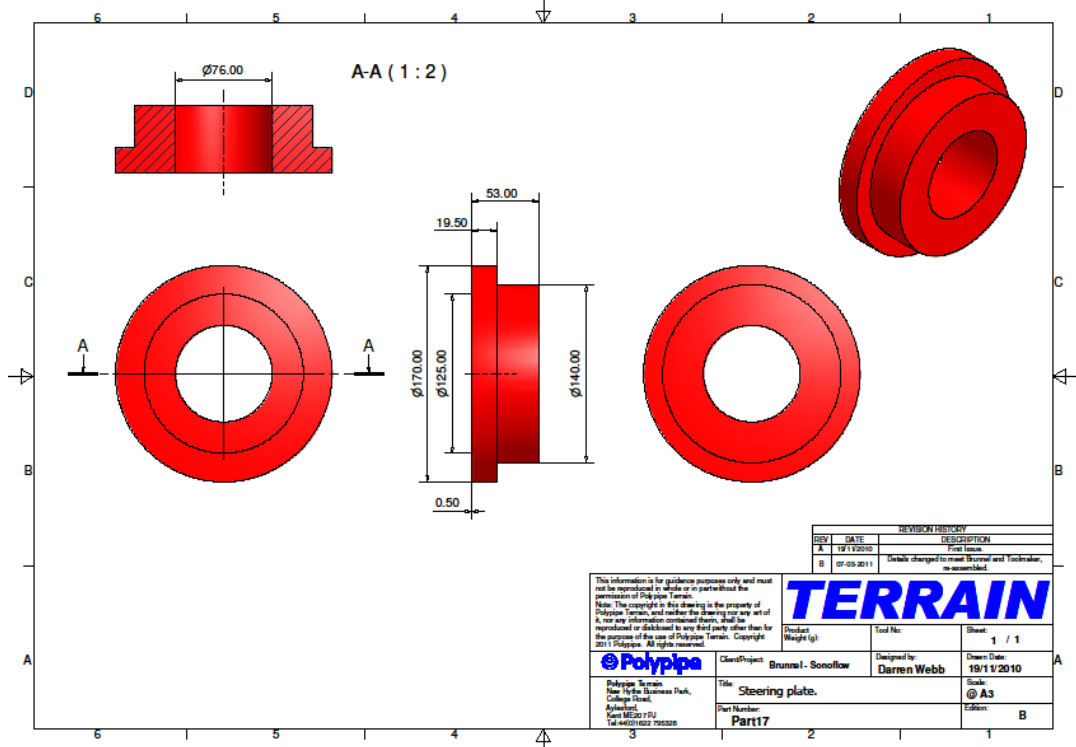**Figure D-11: Design sheet for the inner sleeve of the bottom block.**

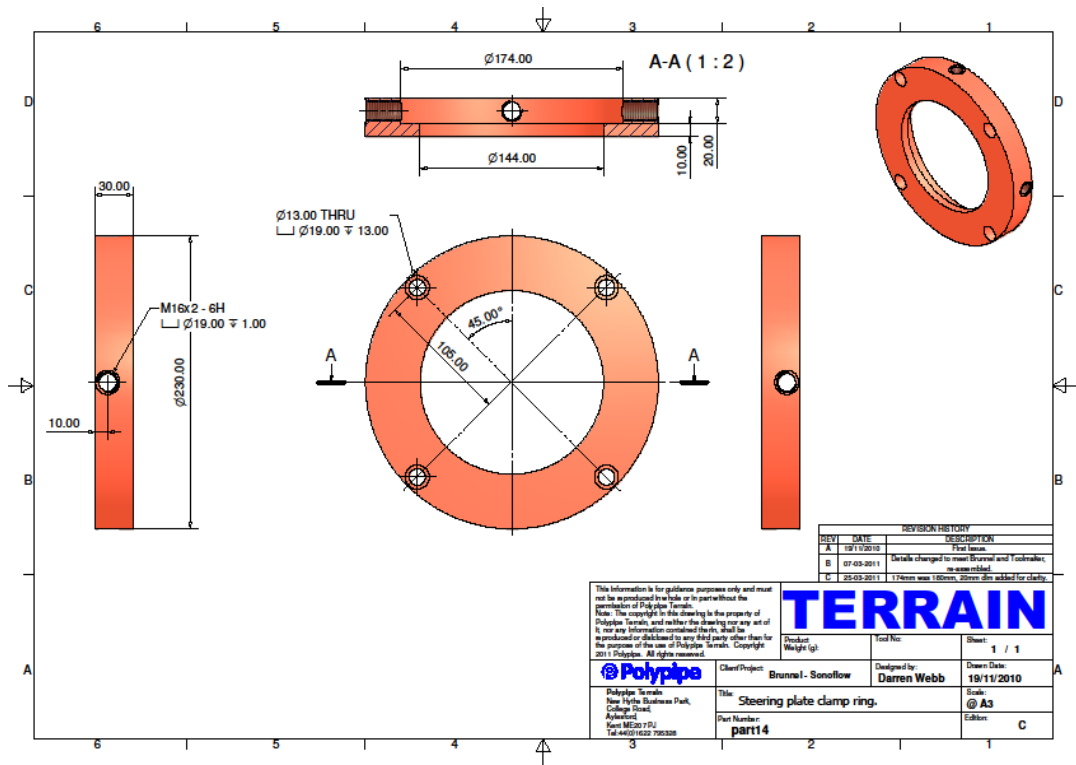**Figure D-12: Design sheet for the steering plate.**

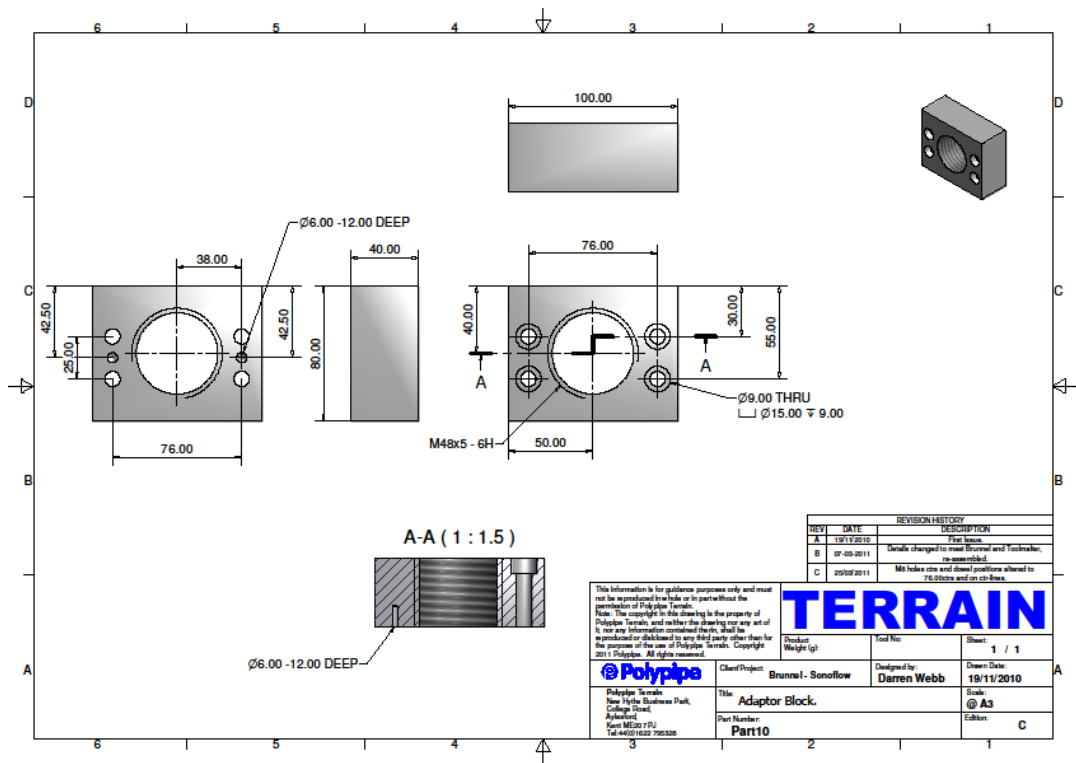**Figure D-13: Design sheet for the ring clamp of the steering plate.**

Figure D-14: Design sheet for the adaptor block for connection of ultrasonic horn to 50mm extruder.
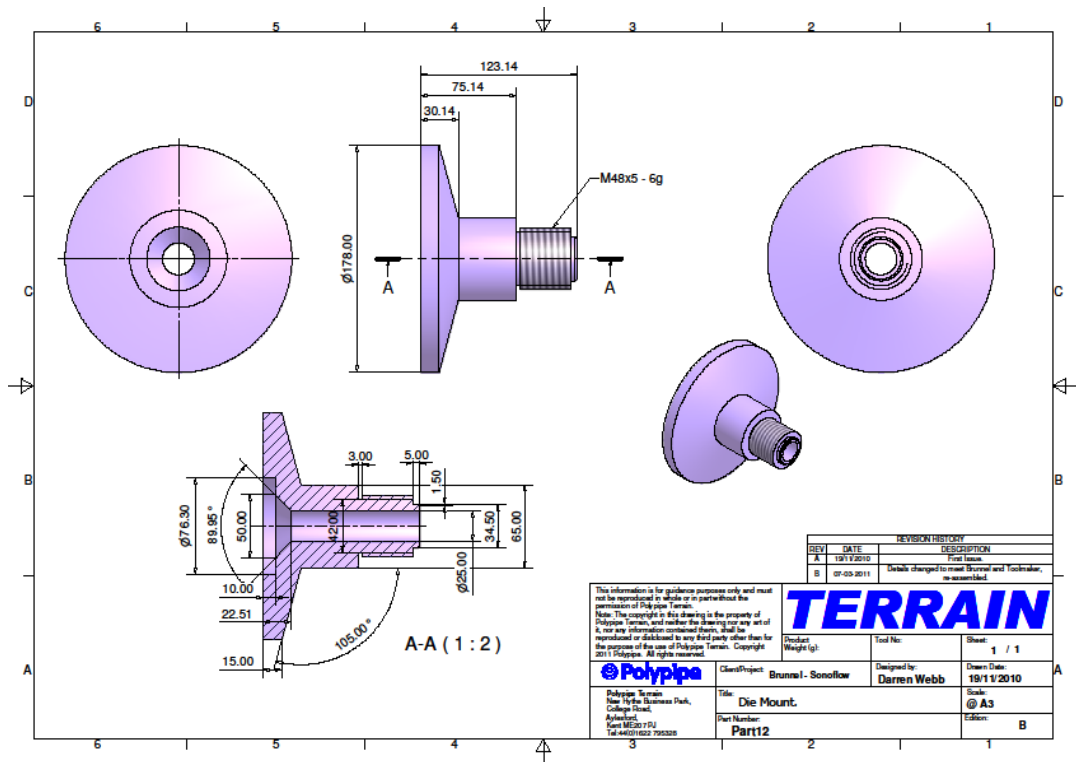
Figure D-15: Design sheet for the die mount for connecting the ultrasonic die to the 50mm extruder.